

**GOLD COMPLEXES BASED ON (N,C) AND (N,C,C)
CHELATING LIGANDS: LIGAND DESIGN AND
REACTIVITY STUDIES IN CROSS-COUPLING
CATALYSIS**

Pau Font Rubio



<http://creativecommons.org/licenses/by-nc/4.0/deed.ca>

Aquesta obra està subjecta a una llicència Creative Commons Reconeixement-NoComercial

Esta obra está bajo una licencia Creative Commons Reconocimiento-NoComercial

This work is licensed under a Creative Commons Attribution-NonCommercial licence



DOCTORAL THESIS

GOLD COMPLEXES BASED ON (N,C) AND (N,C,C)
CHELATING LIGANDS: LIGAND DESIGN AND
REACTIVITY STUDIES IN CROSS-COUPLING
CATALYSIS

Pau Font Rubio

2023



DOCTORAL THESIS

GOLD COMPLEXES BASED ON (N,C) AND (N,C,C)
CHELATING LIGANDS: LIGAND DESIGN AND
REACTIVITY STUDIES IN CROSS-COUPLING
CATALYSIS

Pau Font Rubio

2023

Doctoral programme in Chemistry

Supervised by: Prof. Dr. Xavi Ribas Salamaña

Tutor: Prof. Dr. Xavi Ribas Salamaña

Thesis submitted to the University of Girona for the degree of Doctor



Prof. Dr. Xavi Ribas Salamaña from Universitat de Girona,

I DECLARE:

That the thesis entitled “Gold complexes based on (N,C) and (N,C,C) chelating ligands: ligand design and reactivity studies in cross-coupling catalysis”, presented by Pau Font Rubio to obtain a doctoral degree, has been completed under my supervision and meets the requirements to opt for an International Doctorate.

For all intents and purposes, I hereby sign this document.

Prof. Dr. Xavi Ribas Salamaña

Girona, 27th July 2023

A la família i als amics,
perquè sempre hi he pogut comptar.

只要功夫深，
铁杵磨成针。

不怕慢，就怕站。

Zhǐyào gōngfu shēn, tiěchǔ móchéng zhēn.

As long as you work hard enough, an iron pestle can be ground down to a needle (Chinese proverb).

Bù pà màn, jiù pà zhàn.

Do not be afraid of going slow, just be afraid of stopping (Chinese proverb).

Full list of publications

This thesis is based on a compendium of the following publications:

Chapter III

“Hemilabile MIC^N ligands allow oxidant-free Au(I)/Au(III) arylation-lactonization of γ -alkenoic acids”

P. Font, H. Valdés,* G. Guisado-Barrios,* X. Ribas*

Chem. Sci. **2022**, *13*, 9351 – 9360. DOI: 10.1039/d2sc01966c

(Impact factor: 9.969; Chemistry (multidisciplinary), Q1)

Chapter IV

“Novel NHC-based Au(I) complexes as precursors of highly pure Au(0) nuggets under oxidative conditions”

P. Font, N. V. Tzouras, A. T. Papastavrou, G. C. Vougioukalakis,* X. Ribas*

Molecules **2023**, *28*, 2302. DOI: 10.3390/molecules28052302

(Impact factor: 4.927; Organometallic chemistry, Q2)

Annex 1

“Fundamental basis for implementing oxidant-free Au(I)/Au(III) catalysis”

P. Font, X. Ribas*

Eur. J. Inorg. Chem. **2021**, *2021*, 2556 – 2569. DOI: 10.1002/ejic.202100301

(Impact factor: 2.551; Inorganic chemistry, Q2)

Publications not included in this thesis:

“Cyclometalated gold(III) complexes: noticeable differences between (N,C) and (P,C) ligands in migratory insertion”

J. Serra, P. Font, E. D. Sosa Carrizo, S. Mallet-Ladeira, S. Massou, T. Parella, K. Miqueu, A. Amgoune, X. Ribas,* D. Bourissou*

Chem. Sci. **2018**, *9*, 3932 – 3940. DOI: 10.1039/C7SC04899H

“High-valent Cu, Ag, and Au coordination compounds”

X. Ribas, L. Capdevila, P. Font

In: *Comprehensive coordination chemistry III*; E. C. Constable, G. Parkin, L. Que Jr (eds); Volume 6, Elsevier, **2021**, pp 474 – 516. ISBN: 9780081026885.

DOI: 10.1016/B978-0-08-102688-5.00106-9

List of abbreviations

°C	Degree(s) Celsius
Å	Ångström(s)
Ac	Acetyl
Ac ^F	Trifluoroacetyl
Ar	Aryl
Bn	Benzyl
Bpin	Boronic acid pinacol ester
bpy	Bipyridine
CAAC	Cyclic Alkyl Amino Carbene
calcd	Calculated
cat.	Catalyst or catalytic
Cbz	Benzyloxycarbonyl
Conv.	Conversion
COSY	Correlation Spectroscopy
Cp*	Pentamethylcyclopentadiene
δ	Chemical shift
1,2-DCE	1,2-dichloroethane
DCM	dichloromethane
DFT	Density Functional Theory
Dipp	2,6-diisopropylphenyl
DMEDA	<i>N,N</i> -dimethylethylenediamine
DMF	<i>N,N</i> -dimethylformamide
DMS	Dimethylsulfide
DPCb	Carborane diphosphine
dppm	Bis(diphenylphosphino)methane
E ⁰	Standard oxidation potential
e ⁻	Electron(s)
EBX	Ethynylbenziodoxolone
EDX	Energy Dispersive Spectroscopy
ESI	Electrospray Ionization
Et	Ethyl
eq	Equivalent(s)
eV	Electronvolt(s)
h	Hour(s)
HFIP	1,1,1,3,3,3-hexafluoropropan-2-ol
HMBC	Heteronuclear Multiple Bond Correlation spectroscopy
HRMS	High Resolution Mass Spectrometry
HSQC	Heteronuclear Single Quantum Coherence spectroscopy
hν	The energy of photons
Hz	Hertz
ᐢr	Isopropyl
IPr	1,3-bis(2,6-diisopropylphenyl)imidazol-2-ylidene
IR	Infrared

K	Degree(s) Kelvin
kcal	Kilocalorie(s)
kJ	Kilojoule(s)
λ	Wavelength
L	Ligand
LED	Light-Emitting Diode
LUMO	Lowest Unoccupied Molecular Orbital
M	Molar / Metal (depending on the context)
Me	Methyl
MeDalphos	Di(1-adamantyl)-2-dimethylaminophenylphosphine
MHz	Megahertz
MIC	Mesoionic Carbene
min	Minute(s)
mL	Milliliter(s)
mm	Millimeter(s)
μm	Micrometer(s)
MOF	Metal-organic framework
MS	Mass Spectrometry
MW	Microwave
m/z	Mass/charge
NBS	<i>N</i> -bromosuccinimide
<i>n</i> Bu	<i>n</i> -butyl
NFSI	<i>N</i> -fluorobenzenesulfonimide
NHC	<i>N</i> -Heterocyclic Carbene
nm	Nanometer(s)
NMR	Nuclear Magnetic Resonance
NOESY	Nuclear Overhauser Effect Spectroscopy
Nuc	Nucleophile
OLED	Organic light-emitting diode
PC	Photocatalyst
Ph	Phenyl
ppm	Part(s) per million
ppy	2-phenylpyridine
py	Pyridine
pym	Pyrimidine
rt	Room temperature
$S_{\text{E}}\text{Ar}$	Electrophilic Aromatic Substitution
SEM	Scanning Electron Microscopy
SET	Single electron transfer
SHE	Standard Hydrogen Electrode
SIPr	1,3-bis(2,6-diisopropylphenyl)-4,5-dihydroimidazol-2-ylidene
t	Time
T	Temperature
TBA	Tetrabutylammonium cation
<i>t</i> Bu	<i>tert</i> -butyl
Tf	Triflyl
TFE	2,2,2-trifluoroethanol
THF	Tetrahydrofuran

TM	Transition Metal
TON	Turnover Number
tpy	2-(<i>p</i> -tolyl)pyridine
Ts	Tosyl
V	Volt(s) / Volume (depending on the context)
χ	Electronegativity
XRD	X-Ray Diffraction
Z	Atomic nuclear charge

Acknowledgements

This work would not have been possible without the following collaborations:

- Serveis Tècnics de Recerca (STR) from Universitat de Girona for technical support, with especial remark to Dr. Laura Gómez (HRMS), Anna Costa (MS), Xavi Fontrodona (XRD), Carme Carulla (SEM-EDX), and Dr. Lluïsa Matas and Dr. Sergio Gil (selected NMR experiments).
- Dr. Gregorio Guisado-Barrios, from Universidad de Zaragoza (Spain), for the collaboration in the study of gold complexes bearing hemilabile mesoionic carbene ligands.
- Prof. Dr. Georgios C. Vougioukalakis, and his coworkers, from University of Athens (Greece), for the collaboration in the study of gold complexes bearing hemilabile NHC ligands.
- Prof. Dr. Cristina Nevado, Dr. Jaime Martín, and coworkers, for hosting, supervising, and collaborative research in the synthesis of asymmetric (N,C,C) pincer ligands for Au(III) metalation, during my scientific visit at Universität Zürich (Switzerland).
- Financial support by:
 - Spanish Ministry of Universities: FPU/06047 PhD fellowship, EST19/00777 mobility grant.
 - MINECO-Spain: CTQ2016-77989-P, PID2019-104498GB-I00.
 - Generalitat de Catalunya: Grups Consolidats 2017SGR264 and 2021SGR00475.
 - X. Ribas ICREA Academia award 2015 and 2020.

Table of contents

Graphical abstract	1
List of figures.....	3
List of schemes.....	6
List of tables	10
Summary.....	11
Resum.....	12
Resumen.....	13
CHAPTER I. General Introduction	15
I.1. The recent growing interest in gold chemistry.....	17
I.2. Relativistic effects.....	19
I.3. Gold-mediated homogeneous catalysis.....	24
I.3.1. Redox-neutral catalysis: π -activation of C–C multiple bonds	26
I.3.2. Oxidative Au(I)/Au(III) cross-coupling catalysis.....	34
I.3.3. Oxidant-free Au(I)/Au(III) cross-coupling catalysis.....	39
I.3.3.1. Chelation assistance: rational design of substrates and ligands	40
I.3.3.2. Coupling partners with dual role.....	52
I.3.3.3. Dual gold photoredox catalysis for cross-coupling reactions.....	55
I.3.4. Other gold-based catalytic cycles: Au(III) complexes in catalysis	59
I.4. Elementary organometallic reactions at gold.....	62
I.4.1. Oxidative addition	63
I.4.1.1. Strain release to promote oxidative addition to Au(I)	64
I.4.1.2. Ligand design to promote oxidative addition to Au(I).....	65
I.4.1.3. Photochemical conditions to promote oxidative addition to Au(I)...	73
I.4.2. Reductive elimination.....	75
I.4.3. Transmetalation.....	79
I.4.4. Migratory insertion	83
I.4.5. β -Hydride elimination	88
I.5. References.....	91
CHAPTER II. Objectives.....	103

CHAPTER III. Hemilabile MIC^N Ligands Allow Oxidant-Free Au(I)/Au(III) Arylation-Lactonization of γ-Alkenoic Acids	107
CHAPTER IV. Novel NHC-Based Au(I) Complexes as Precursors of Highly Pure Au(0) Nuggets under Oxidative Conditions	119
CHAPTER V. Results and discussion	133
V.1. Hemilabile MIC ^N ligands allow oxidant-free Au(I)/Au(III) arylation-lactonization of γ -alkenoic acids	135
V.1.1. Synthesis of (MIC ^N)Au(I) complexes	135
V.1.2. Synthesis of (MIC ^N)Au(III) complexes with external oxidants	139
V.1.3. Reactivity of (MIC ^N)Au(I) complexes towards oxidative addition.....	140
V.1.4. Engaging (MIC ^N)Au(I) complexes in oxidant-free catalytic transformations	145
V.2. Novel NHC-based Au(I) complexes as precursors of highly pure Au(0) nuggets under oxidative conditions.....	152
V.2.1. Synthesis of NHC–Au(I) complexes.....	153
V.2.2. Reactivity of NHC–Au(I) complexes with oxidants	155
V.2.3. Characterization of the Au(0) nuggets	160
V.3. Boron-to-gold(III) transmetalation as a synthetic strategy to access (N ^C C)-biscyclometalated gold(III) complexes.....	162
V.3.1. Functionalization studies with a symmetric (N ^C C) scaffold.....	167
V.3.2. Functionalization studies with a non-symmetric (N ^C C) scaffold.....	171
V.4. References.....	175
CHAPTER VI. General conclusions	181
ANNEX. Supporting information.....	187
ANNEX 1. Fundamental Basis for Implementing Oxidant-Free Au(I)/Au(III) Catalysis	189
ANNEX 2. Supporting information Chapter III.....	207
ANNEX 3. Supporting information Chapter IV	297
ANNEX 4. Supporting information Chapter V.3	357

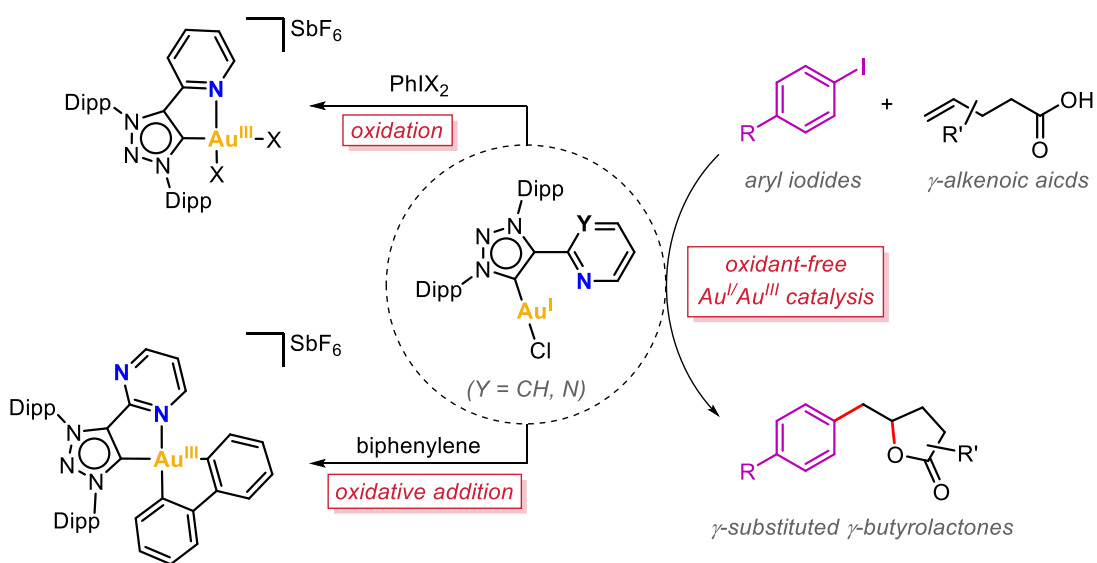
Graphical abstract

SUMMARY (p. 11)

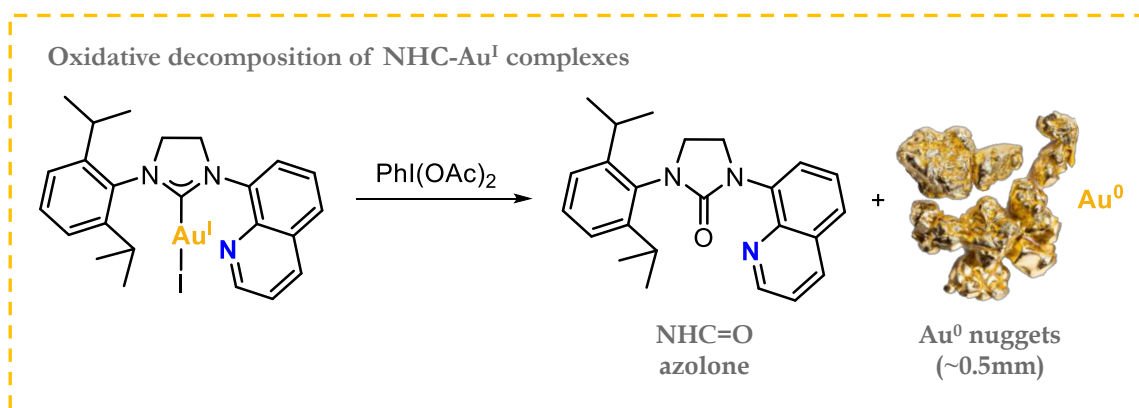
CHAPTER I. General introduction (p. 15)

CHAPTER II. Objectives (p. 103)

CHAPTER III. Hemilabile MIC^N Ligands Allow Oxidant-Free Au(I)/Au(III) Arylation-Lactonization of γ -Alkenoic Acids (p. 107)



CHAPTER IV. Novel NHC-Based Au(I) Complexes as Precursors of Highly Pure Au(0) Nuggets under Oxidative Conditions (p. 119)



CHAPTER V. Results and discussion (p. 133)

CHAPTER VI. General conclusions (p. 181)

ANNEX. Supporting information (p. 187)

List of figures

- Figure I.1.** Number of academic articles on gold compounds and gold catalysis (homogeneous and heterogeneous) published in the area of chemistry by year (period 1970-2022), according to “Scopus” database (December 2022)18
- Figure I.2.** Schematic energy-level diagram of gold’s valence shells without relativistic effects (left) and with relativistic effects (right)20
- Figure I.3.** Relativistic contraction of the 6s shell radii in the atomic ground states of the elements ranging from Z=55 (Cs) to Z=100 (Fm). (Figure taken from ref. 29, and originally published in ref. 31 with the numbers taken from the Dirac-Fock and Hartree-Fock calculations of Desclaux)21
- Figure I.4.** *d*-Orbital splitting diagrams for linear Au(I) and square-planar Au(III) complexes23
- Figure V.1.** a) Synthesis of Au(I) complexes **2a** and **2b**. b) Crystal structures of **2a** and **2b** (ellipsoids set at 50% probability and H atoms removed for clarity). Selected bond distances (Å): for **2a**, Au1–C3 1.982(6), Au1–Cl2 2.2854(17); for **2b**, Au1–C3 2.006(4), Au1–Cl2 2.2728(16)136
- Figure V.2.** a) Synthesis of dimeric Au(I) complexes **3a** and **3b** from complexes **2a** and **2b** upon chloride abstraction. b) Crystal structure of **3a** (ellipsoids set at 50% probability, H atoms and SbF₆⁻ anions removed for clarity). Selected bond distances (Å): Au1–Au2 2.8212(4), Au1–N44 2.078(6), Au1–C3 1.988(8), Au2–N9 2.069(6), Au2–C38 1.990(8) ...137
- Figure V.3.** ¹H NMR (400MHz, CD₂Cl₂, 298K) spectra of complexes **2b** (top) and **3b** (bottom), evidencing the desymmetrization of pyrimidine when it is coordinated to gold in complex **3b**138
- Figure V.4.** a) Reactivity of Au(I) complex **2a** towards oxidation by using hypervalent iodine oxidants. b) Crystal structures of **4a-Cl** and **4a-OAc** (ellipsoids set at 50% probability, H atoms and SbF₆⁻ anions removed for clarity). Selected bond distances (Å): for **4a-Cl**, Au1–C4 2.017(8), Au1–N10 2.089(6), Au1–Cl2 2.268(2), Au1–Cl3 2.302(2); for **4a-OAc**, Au1–C9 1.991(11), Au1–N2 2.052(11), Au1–O37 2.032(10), Au1–O41 1.998(9)140
- Figure V.5.** a) Study of the reaction conditions for the oxidative addition of a strained C(sp²)–C(sp²) bond to complex **2b**. b) Crystal structures of **3b·biphenylene**, **5b** and **6b**

(ellipsoids set at 50% probability, H atoms removed for clarity; in the case of **3b·biphenylene**, SbF₆⁻ anions are removed and the biphenylene molecule is painted in green for clarity). Selected bond distances (Å): for **3b·biphenylene**, Au1–Au1' 2.8768(10), Au1–N2 2.105(8), Au1–C9 2.027(10); for **5b**, Au1–C2 2.108(5), Au1–N8 2.254(5), Au1–C37 2.066(5), Au1–C44 2.019(5); for **6b**, Au1–C3 2.080(6), Au1–Cl2 2.376(3), Au1–C38 2.072(7), Au1–C49 2.057(7)141

Figure V.6. a) Reactivity of complexes **2a** and **2b** with aryl iodides (5 eq.) and AgSbF₆ (1.2 eq.), leading to the decomposition towards products **8-R**, **9** and **1**. b) Crystal structures of **8a-OMe**, **9a** and **8b-OMe** (ellipsoids set at 50% probability, H atoms removed for clarity; for **8a-OMe** and **9a**, SbF₆⁻ anion is removed for clarity; **8b-OMe** was obtained as a chloride salt)143

Figure V.7. a) Synthesis of **cis-7a-Cl** by oxidative addition at **2a** using blue LED irradiation ($\lambda = 447$ nm), and thermal reductive elimination from **cis-7a-Cl** to afford **8a-OMe**. b) Crystal structure of **cis-7a-Cl** (ellipsoids set at 50% probability, H atoms and BF₄⁻ anion are removed for clarity). Selected bond distances (Å): Au1–C10 2.009(7), Au1–N3 2.154(7), Au1–C38 2.006(8), Au1–Cl2 2.303(2)145

Figure V.8. Scope of the arylation-lactonization of alkenoic acids to afford products **10 – 16**, using catalysts **2a** and **2b** (NMR yields are displayed for each product). Crystal structure of **16** is shown (ellipsoids set at 50% probability, H atoms removed for clarity). *NMR yield using 20 mol% of [Au] is given in parenthesis148

Figure V.9. X-ray molecular structures of complexes **1**, **2**, **3** and **4** (ellipsoids set at 50% probability and H atoms removed for clarity). Selected bond distances (Å): for **1**, Au1–C11 2.007(13), Au1–I2 2.5580(10); for **2**, Au1–C1 1.981(9), Au1–I1 2.5467(8); for **3**, Au1–C10 2.000(3), Au1–I2 2.5516(2); for **4**, Au1–C3 1.966(6), Au1–Cl2 2.262(3). Selected angles (°): for **1**, C11–Au1–I2 177.4(4); for **2**, C1–Au1–I1 175.4(2); for **3**, C10–Au1–I2 178.38(8); for **4**, C3–Au1–Cl2 179.12(16)155

Figure V.10. Reaction of complex **2** with PhI(OAc)₂ and water or ¹⁸O-labeled water, and peaks of product **L2^{ox}** obtained by HRMS-ESI(+) in each case159

Figure V.11. a) Reaction outcome with Au(0) nuggets precipitated (left), and SEM image of the isolated Au(0) nuggets at x30 (right); b) EDX spectrum from a region of a gold grain set by SEM at x1000161

Figure V.12. Depiction of symmetric and non-symmetric (N[^]C[^]C) scaffolds166

Figure V.13. Synthesis of compounds **1^I** and **1^{Bpin}** from **1^H** as ligand precursors to access complex **1AuCl**, and crystal structure of **1^{Bpin}** (ellipsoids set at 50% probability and H atoms removed for clarity). Selected bond distances (Å): C8–B1 1.625(3), N1–B1 1.728(3)169

Figure V.14. Synthesis of compound **2^{Bpin}** and complex **2AuCl**, and crystal structure of **2^{Bpin}** (ellipsoids set at 50% probability and H atoms removed for clarity). Selected bond distances (Å): C21–B1 1.642(2), N10–B1 1.689(2)172

List of schemes

Scheme I.1. a) General depiction of a cross-coupling reaction and b) general mechanism operating in palladium-catalyzed cross-coupling reactions	25
Scheme I.2. General mechanism for gold-catalyzed nucleophilic addition to C–C multiple bonds	27
Scheme I.3. Works on gold(III)-catalyzed hydroamination (a) and hydration (b) of alkynes, by Utimoto	28
Scheme I.4. Works of Hashmi on gold(III) chloride-catalyzed a) cycloisomerization of terminal allenyl ketones, b) formation of spirocyclic compounds and c) intramolecular cycloisomerization of furans with a terminal alkyne moiety	29
Scheme I.5. Gold-catalyzed stereoselective cycloisomerizations of α -hydroxyallenes, α -aminoallenes and α -hydroxyallenes, reported by Krause	30
Scheme I.6. Gold(I)-catalyzed additions of a) O-nucleophiles, b) N-nucleophiles, and c) C-nucleophiles to non-activated olefins	31
Scheme I.7. Gold(I)-catalyzed skeletal rearrangements of 1,6-enynes and dienyne, by Echavarren	32
Scheme I.8. Evidence of a dual gold activation mechanism operating in gold(I)-catalyzed cyclization hydroarylation of diyne with benzene	33
Scheme I.9. a) General mechanism in Au(I)/Au(III) oxidative cross-coupling catalysis, featuring in red the alternative oxidative addition step that is circumvented by using external oxidants, to access Au(III) intermediates. b) Gold-catalyzed oxidative coupling reactions involving aryl C–H functionalization and c) involving nucleophilic addition	35
Scheme I.10. General Au(I)/Au(III)-catalyzed oxy- and aminoarylations of terminal alkenes. (a) Three-component oxyarylation of terminal olefins using arylsilanes and boronic acids as competent arylating agents. (b) Two-component oxyarylations and aminoarylations of terminal alkenes using arylboronic acids. (c) Aminoarylation of terminal alkenes via intramolecular C–C coupling	37
Scheme I.11. Different methodologies for the synthesis of biaryls by means of gold-catalyzed oxidative C(sp ²)-C(sp ²) cross-coupling	38

Scheme I.12. Intermolecular allylation of arylboronic acids catalyzed by a bimetallic Au(I) complex, proceeding through a Au(II)–Au(II) intermediate formed upon oxidative addition	40
Scheme I.13. General mechanism of ligand-enabled oxidant-free Au(I)/Au(III) catalytic transformations (DG = Directing Group)	41
Scheme I.14. Substrate chelation-enabled oxidant-free Au(I)/Au(III)-catalyzed halide exchange, C(sp ³)–N, and C(sp ³)–O cross-coupling transformations reported by Ribas	42
Scheme I.15. MeDalphos-enabled oxidant-free Au(I)/Au(III) cross-coupling catalysis ...	45
Scheme I.16. MeDalphos-enabled oxidant-free Au(I)/Au(III) cross-coupling catalysis merging oxidative addition and π -alkene activation	47
Scheme I.17. Enantioselective oxidant-free Au(I)/Au(III)-catalyzed aminoarylation and oxyarylation reactions of alkenes, achieved with chiral hemilabile (P,N) ligands	48
Scheme I.18. Gold complexes with hemilabile (N,C) ligands engaging and not engaging in ligand-enabled oxidant-free Au(I)/Au(III) cross-coupling catalysis	51
Scheme I.19. Selected examples of the use of EBX reagents as both coupling partners and oxidizing equivalents in Au(I)/Au(III) alkynylation couplings	53
Scheme I.20. Oxidant-free and photosensitizer-free Au(I)/Au(III)-catalyzed cross-coupling reactions using aryldiazonium salts as coupling partners, under light irradiation	55
Scheme I.21. General mechanism of dual gold photoredox cross-coupling catalysis using aryldiazonium salts of the type ArN ₂ BF ₄ . (Sub = substrate; Sub' = modified substrate, if modified, after Au(III)-mediated organometallic steps)	56
Scheme I.22. Selected examples of dual gold photoredox catalytic systems using aryldiazonium salts as coupling partners	58
Scheme I.23. Trifluoroacetoxylation of acetylene catalyzed by a (N [^] C)-cyclometalated gold(III) complex	60
Scheme I.24. Hydroarylation of alkynes catalyzed by (P [^] C)-cyclometalated gold(III) complexes	61
Scheme I.25. Dehydrogenation of formic acid catalyzed by a (N [^] C [^] C)-biscyclometalated gold(III) complex	62
Scheme I.26. General scheme of an oxidative addition process	63

Scheme I.27. Early examples of oxidative addition of disulfide bonds to Au(I). The NEt_4^+ cation in the X-ray structure of 108 has been omitted for clarity	64
Scheme I.28. Oxidative addition of the strained C–C bond in biphenylene to a cationic $[(\text{NHC})\text{Au}]^+$ fragment, disclosed by Toste. The SbF_6^- anion in the X-ray structure of 111 has been omitted for clarity	65
Scheme I.29. Examples of intramolecular chelation-assisted oxidative addition to Au(I) ...	67
Scheme I.30. Intermolecular oxidative addition to non-linear (DPCb)gold(I) complexes, reported by Bourissou. The anions in the X-ray structures are omitted for clarity	69
Scheme I.31. Intermolecular oxidative addition to (a,b) non-linear three-coordinate ($\text{N}^{\wedge}\text{N}$)gold(I) complexes, and to (c) a T-shaped gold(I) complex. The anions in the X-ray structures are omitted for clarity	70
Scheme I.32. Selected examples of hemilabile ligand-stabilized Au(III) complexes obtained via oxidative addition. The anions in the X-ray structures are omitted for clarity	72
Scheme I.33. Selected examples of arylgold(III) complexes obtained via oxidative addition promoted by photochemical conditions	74
Scheme I.34. General scheme of a reductive elimination process	75
Scheme I.35. Mechanism of a $\text{C}(\text{sp}^2)\text{--N}$ reductive elimination from a gold(III) complex ...	76
Scheme I.36. S-arylation of cysteine-containing peptides via $\text{C}(\text{sp}^2)\text{--S}$ reductive elimination from Au(III) complexes	77
Scheme I.37. Toste's studies on a) $\text{C}(\text{sp}^3)\text{--C}(\text{sp}^2)$ reductive elimination and b) borane-catalyzed $\text{C}(\text{sp}^3)\text{--CF}_3$ reductive elimination, both occurring at NHC-gold(III) complexes ...	78
Scheme I.38. $\text{C}(\text{sp}^2)\text{--C}(\text{sp})$ reductive elimination processes from ($\text{P}^{\wedge}\text{N}$)gold(III) fluoride complexes, reported by Nevado	79
Scheme I.39. Selected examples of boron-to-gold transmetalation reactions	81
Scheme I.40. a) Stoichiometric Zn-to-Au transmetalation, and b) catalytic Rh-to-Au transmetalation for the synthesis of (N,C)-cyclometalated gold(III) complexes	83
Scheme I.41. a) General migratory insertion of an unsaturated ligand at a transition-metal complex, and b) gold-mediated addition of nucleophiles to C–C multiple bonds	84
Scheme I.42. <i>Syn</i> insertion of a terminal alkyne into a Au(I)–Si bond	85

Scheme I.43. Migratory insertions at well-defined Au(III) complexes: a,b) Formation of norbornyl gold(III) complexes upon <i>syn</i> insertion of norbornene into Au–Me and Au–Ph bonds, and c) double insertion of ethylene into a Au–Ph bond	86
Scheme I.44. a) Migratory insertion of carbene ligands and b) migratory insertion of CO, both into Au(III)–C bonds, and c) migratory insertion step involved in a Au(I)/Au(III)-catalyzed Heck reaction	87
Scheme I.45. General scheme of a β -hydride elimination	88
Scheme I.46. Formation of cationic (P,C)-cyclometalated gold(III) alkyl complexes 202 and 204 and reaction outcomes upon β -hydride elimination/reinsertion pathways	90
Scheme II.1. Schematic representation of the objectives regarding the part of the thesis dealing with (N,C) hemilabile ligands (top: Chapter III, and bottom: Chapter IV)	106
Scheme II.2. Schematic representation of the objectives regarding the synthesis of non-symmetric borylated (N [^] C [^] C) ligands and the ensuing (N [^] C [^] C)-biscyclometalated Au(III) complexes	106
Scheme V.1. Proposed reaction mechanism for the gold-catalyzed arylation-lactonization of γ -alkenoic acids	150
Scheme V.2. Stoichiometric reaction of complex <i>cis-7a-Cl</i> towards the formation of product 10	150
Scheme V.3. Synthesis of complexes 1–4 from the respective imidazolium salts L1–L4	154
Scheme V.4. Synthesis of [Au(ppy)Cl ₂] from 2-phenylpyridine by C–H auration (top) and by transmetalation with an organomercury precursor (bottom)	163
Scheme V.5. General synthesis of κ^3 -[(N [^] C [^] C)AuF] complexes (top) and selected examples of such complexes (bottom)	165
Scheme V.6. Envisioned synthetic protocol to access non-symmetric (N [^] C [^] C)Au(III) complexes	167
Scheme V.7. Alternative approaches to the already reported microwave-assisted C(sp ²)–H activation to access the symmetric (N [^] C [^] C)Au(III) complex 1AuCl	168
Scheme V.8. Envisioned non-symmetric borylated ligand precursor (2^{Bpin}) and the corresponding (N [^] C [^] C)Au(III) target complex 2AuCl	171

List of tables

Table V.1. Yield of products 8-R , 9 , and 1 obtained from complexes 2a and 2b under the reaction conditions depicted in Figure V.6a (NMR yields calculated using 1,3,5-trimethoxybenzene as internal standard)	144
Table V.2. Optimization of the reaction conditions for the 2b -catalyzed synthesis of γ -benzyl- γ -butyrolactone product 10	147
Table V.3. Oxyarylation and 1,2-diarylation reactions of alkenes catalyzed by complex 2a	149
Table V.4. Reactivity of Au(I) complexes towards the formation of Au(0) nuggets and azolones (Lx^{ox})	157
Table V.5. Reaction conditions for the transmetalation of 1^{Bpin} towards 1AuCl	170
Table V.6. Reaction conditions applied to compound 2^H seeking the bromination towards compound 2^{Br}	173

Summary

Homogeneous reactions catalyzed by gold have mainly been developed in the past two decades, stemming from the proneness of Au(I) and Au(III) complexes to coordinate and activate carbon-carbon multiple bonds towards a wide range of transformations. However, and in contrast to classical cross-coupling methodologies based on catalytic cycles mediated by other late transition metals, two-electron Au(I)/Au(III) catalytic cycles have long remained elusively attainable. The rationale behind this fact is the high redox potential of the Au(I)/Au(III) pair that makes Au(I) especially reluctant to being oxidized to Au(III). Therefore, cycling between +1 and +3 oxidation states in gold-catalyzed cross-coupling reactions is far from trivial. Besides, compared to other transition metals, with emphasis on the metals of groups 9 and 10, there is still limited knowledge of the main elementary steps of organometallic chemistry in the case of gold complexes. Achieving and studying these fundamental steps is crucial to understand gold's reactivity and to provide mechanistic insight that would help in designing new gold-catalyzed transformations. In this regard, the projects presented in this dissertation aim to synthesize novel gold complexes using pre-designed ligands, as well as to carry out reactivity studies with them.

The first part of the thesis deals with Au(I) complexes bearing (N,C) hemilabile ligands. On one hand, gold complexes with mesoionic carbene (MIC) ligands were subjected to oxidative conditions and tested in oxidative addition to obtain (N,C)-cyclometalated gold(III) complexes, thereby confirming the suitability of the (N,C) ligands for chelating Au(III) centers. Then, we employed these Au(I) complexes as catalysts for the arylation-lactonization of γ -alkenoic acids, the mechanism of which was proposed to operate through an oxidant-free Au(I)/Au(III) catalytic cycle based on an oxidative addition/reductive elimination pathway. On the other hand, gold complexes bearing NHC ligands were subjected to oxidative conditions and, conversely, pure Au(0) nuggets were formed along with the oxidation of the ligand. Thus, these systems served to study the decomposition reaction of Au(I) complexes into Au(0), instead of obtaining (N,C)-cyclometalated gold(III) complexes.

The second part of the thesis focuses on developing a synthetic strategy to access non-symmetric borylated (N,C,C) ligands, which might be utilized for the synthesis of non-symmetric (N,C,C)-biscyclometalated Au(III) pincer complexes through boron-to-gold(III) transmetalation. With this metalation approach we overcome the limitations of other current methods that generate toxic waste or are limited to symmetric (N,C,C) platforms.

Resum

Les reaccions homogènies catalitzades per or han estat desenvolupades principalment al llarg de les dues últimes dècades, sorgint de la predisposició dels complexos d'Au(I) i Au(III) de coordinar i activar enllaços múltiples carboni-carboni en un ampli ventall de transformacions. Tanmateix, i en contrast amb els mètodes clàssics d'acoblament creuat basats en cicles catalítics promoguts per altres metalls de transició, els cicles catalítics de dos electrons d'Au(I)/Au(III) han romàs difícilment assolibles. La raó és l'elevat potencial redox del parell Au(I)/Au(III), que fa que l'Au(I) sigui especialment reticent a ser oxidat a Au(III). Conseqüentment, la ciclació entre els estats d'oxidació +1 i +3 en reaccions d'acoblament creuat catalitzades per or no és trivial. A més, en comparació amb altres metalls de transició, especialment els dels grups 9 i 10, el coneixement sobre els processos fonamentals en química organometàl·lica encara és limitat en el cas dels complexos d'or. Aconseguir dur a terme i estudiar aquests processos és clau per comprendre la reactivitat de l'or i proporcionar una perspectiva mecanística que ajudi a dissenyar noves reaccions catalitzades per or. En aquest context, els projectes presentats en aquesta tesi pretenen sintetitzar nous complexos d'or utilitzant lligands predissenyats, així com utilitzar-los en estudis de reactivitat.

La primera part de la tesi se centra en complexos d'Au(I) amb lligands hemilàbils (N,C). D'una banda, els complexos amb lligands de tipus carbè mesoiònic (MIC) van ser sotmesos a condicions oxidants i es van provar en addició oxidant per tal d'obtenir complexos d'or(III) (N,C)-ciclometal·lats, confirmant així la idoneïtat dels lligands (N,C) per quelar centres d'Au(III). Llavors, els complexos d'Au(I) es van utilitzar com a catalitzadors per a l'arilació-lactonització d'àcids γ -alquenoics, el mecanisme de la qual es va proposar a través d'un cicle catalític Au(I)/Au(III) lliure d'oxidants mitjançant una via d'addició oxidant/eliminació reductiva. D'altra banda, els complexos amb lligands NHC van ser sotmesos a condicions oxidants i, per contra, es van obtenir agregats d'Au(0) pur juntament amb l'oxidació del lligand. Així doncs, aquests sistemes van servir per estudiar la reacció de descomposició dels complexos d'Au(I) a Au(0), en lloc d'obtenir complexos d'or(III) (N,C)-ciclometal·lats.

La segona part de la tesi s'enfoca en el desenvolupament d'una estratègia sintètica per accedir a lligands (N,C,C) borilats no-simètrics, que es podrien utilitzar per a la síntesi de complexos d'Au(III) (N,C,C)-bisciclometal·lats no-simètrics tipus *pincer* mitjançant transmetal·lació de bor a or(III). Amb aquesta estratègia de metal·lació s'eviten limitacions que presenten altres mètodes que generen residus tòxics o que es limiten a plataformes (N,C,C) simètriques.

Resumen

Las reacciones homogéneas catalizadas por oro se han desarrollado principalmente a lo largo de las dos últimas décadas, surgiendo de la predisposición de los complejos de Au(I) y Au(III) de coordinar y activar enlaces múltiples carbono-carbono en un amplio abanico de transformaciones. No obstante, y a diferencia de los métodos clásicos de acoplamiento cruzado basados en ciclos catalíticos mediados por otros metales de transición, los ciclos catalíticos de dos electrones Au(I)/Au(III) han permanecido difícilmente alcanzables. La razón es el elevado potencial redox del par Au(I)/Au(III), que hace que el Au(I) sea especialmente reticente a ser oxidado a Au(III). Por eso, ciclar entre los estados de oxidación +1 y +3 en reacciones de acoplamiento cruzado catalizadas por oro no es trivial. Además, en comparación con otros metales de transición, especialmente los de los grupos 9 y 10, el conocimiento sobre los procesos fundamentales en química organometálica todavía es limitado en el caso de los complejos de oro. Conseguir llevar a cabo y estudiar dichos procesos es clave para comprender la reactividad del oro y proporcionar una perspectiva mecanística que ayude a diseñar nuevas reacciones catalizadas por oro. En este contexto, los proyectos presentados en esta tesis pretenden sintetizar nuevos complejos de oro utilizando ligandos prediseñados, así como utilizarlos en estudios de reactividad.

La primera parte de la tesis se centra en complejos de Au(I) con ligandos hemilábiles (N,C). Por un lado, los complejos con ligandos de tipo carbeno mesoiónico (MIC) fueron sometidos a condiciones oxidantes y se probaron en adición oxidante para obtener complejos de oro(III) (N,C)-ciclometalados, confirmando así la idoneidad de los ligandos (N,C) para quelar centros de Au(III). Luego, los complejos de Au(I) se utilizaron como catalizadores para la arilación-lactonización de ácidos γ -alquenoicos, el mecanismo de la cual se propuso a través de un ciclo catalítico Au(I)/Au(III) libre de oxidantes mediante una vía de adición oxidante/eliminación reductiva. Por otro lado, los complejos con ligandos NHC se sometieron a condiciones oxidantes y, por el contrario, se obtuvieron pepitas de Au(0) puro junto con la oxidación del ligando. Así pues, estos sistemas sirvieron para estudiar la reacción de descomposición de los complejos de Au(I) a Au(0), en lugar de obtener complejos de oro(III) (N,C)-ciclometalados.

La segunda parte de la tesis se enfoca en el desarrollo de una estrategia sintética para acceder a ligandos (N,C,C) borilados no-simétricos, que se podrían utilizar para la síntesis de complejos de Au(III) (N,C,C)-bisciclometalados no-simétricos tipo *pincer* mediante

transmetalación de boro a oro(III). Con esta estrategia de metalación se evitan limitaciones que presentan otros métodos que generan residuos tóxicos o que se limitan a plataformas (N,C,C) simétricas.

CHAPTER I. General Introduction

I.1. THE RECENT GROWING INTEREST IN GOLD CHEMISTRY

Gold has been known since the earliest human civilizations, as it occurs widespread in nature in its metallic form. The beauty of its bright yellow color, its durability, malleability, ductility, and good thermal and electrical conductivity have attracted the attention of all cultures around the world, which have used this precious metal for a wide scope of applications. For instance, gold has been employed with esthetic purposes in jewelry and in art pieces since ancient times, it is employed as currency and, very importantly nowadays, in electronics. In addition, gold has traditionally been charged with power and wealth symbolism, as it has always been deemed a valuable noble metal. This value attribution comes specially from the fact that, unlike other metals, it is highly durable due to its resistance towards getting oxidized by air and water. The scarcity of gold in the Earth's crust may have contributed as well to consider gold as special, thus valuable. Indeed, the admiration for gold was evidenced by alchemists, who pursued the goal of getting gold by transmutation of other metals, or by the several "gold rush" social movements that have historically been witnessed. On the other hand, the admiration for gold is quite a recent phenomenon within the chemical community.

The durability of gold, *a priori* related to a lack of reactivity, led the scientific community to, for a long time, consider gold species as chemically inert.¹ However, this perception started to change by the end of the 20th century when the carbophilicity of gold complexes emerged as a unique and powerful tool to build molecular complexity in organic synthesis.^{2,3} Indeed, gold complexes react as Lewis acids capable of activating C–C multiple bonds of olefins, alkynes and allenes towards nucleophiles.⁴⁻¹¹ The potential of using gold complexes as new homogeneous catalysts encouraged scientists to explore the reactivity behind such species. Thus, early this century, the interest in the field of organogold chemistry rose dramatically¹² entailing, consequently, a huge growth of the number of publications on this area (Figure I.1).

Along with the disclosure of the π -activation reactivity of gold, within the last two decades many studies have been devoted to gaining deeper insight into other aspects of gold chemistry, such as the coordination and fundamental organometallic properties of gold, the design of ligands and complexes, finding new reactivities of gold complexes beyond π -C–C activation catalysis, isolating and characterizing reaction intermediates for the understanding and rationalizing of reaction mechanisms, or seeking for applications of gold complexes in other fields besides organic and organometallic chemistry.

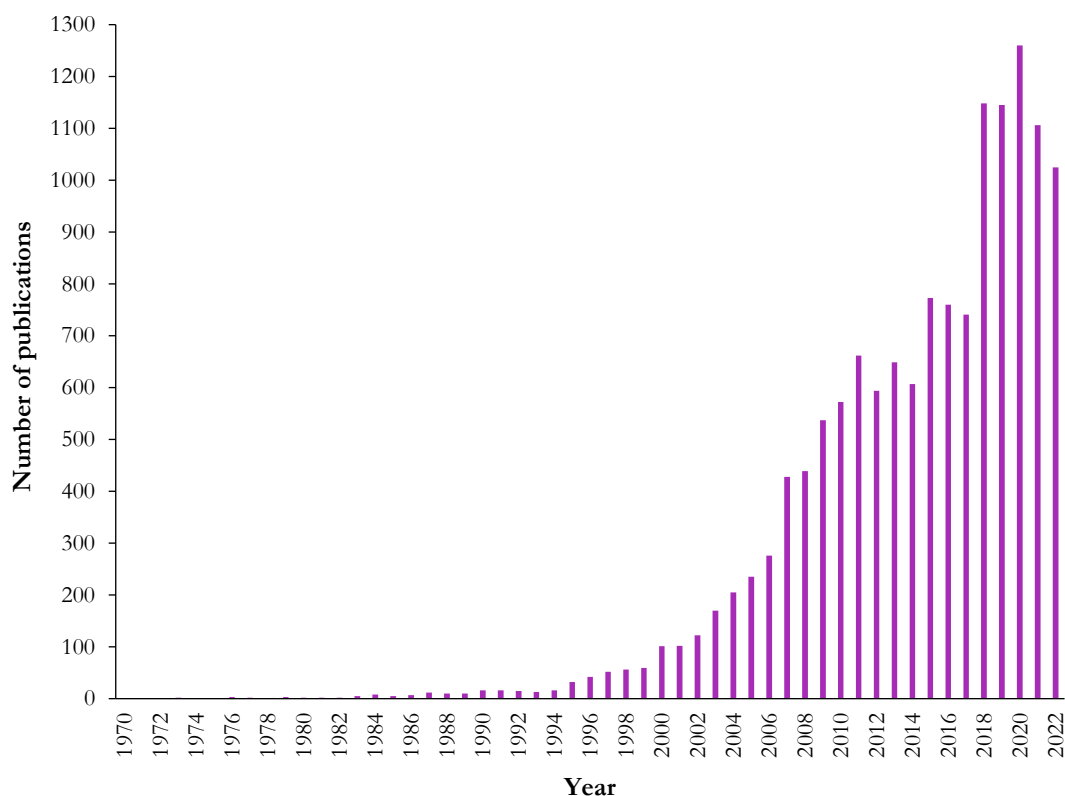


Figure I.1. Number of academic articles on gold compounds and gold catalysis (homogeneous and heterogeneous) published in the area of chemistry by year (period 1970-2022), according to “Scopus” database (December 2022).

Homogeneous gold catalysis experienced an outstanding development thanks to such extensive studies, and, in fact, it can still be regarded as a hot topic nowadays. Gold complexes can indeed engage in Au(I)/Au(III) catalytic cycles, showing reactivity beyond the initially reported π -bond activation catalytic processes.¹³ However, the high oxidation potential of the Au(I)/Au(III) redox couple makes it challenging to cycle between oxidation states +1 and +3. Therefore, many efforts have been put to find strategies to overcome this drawback and access Au(I)/Au(III) catalysis (see sections I.3.2 and I.3.3).

As stated, elementary organometallic reactions also needed to be explored because they had remained poorly investigated until then.^{14, 15} Among them, special emphasis was devoted to achieving oxidative addition from Au(I) to Au(III) complexes. Its achievement represented an important milestone as it triggered, later on, the rational design of homogeneous catalysts able to undergo Au(I)/Au(III) catalytic cycles via the traditional oxidative addition/reductive elimination pathway,¹⁶ so common in other transition-metal catalysis yet so new and challenging in the case of gold catalysis.

Gold chemistry has not only attracted attention in the fields of organic and organometallic chemistry, but also in a broad scope of other disciplines seeking for the development of innovative applications in a variety of areas. For instance, self-assembly supramolecular chemistry, material science, nanotechnology, and even medicinal chemistry also experienced a significant increase of the amount of works related to gold chemistry. Some of the applications found for gold complexes in these fields include their use in photoluminescent devices and as anticancer drugs.¹⁷⁻²⁷

Essentially, the rise of studies on organogold chemistry has provided valuable insights into the properties and reactivity of gold, highlighting that gold exhibits conspicuous differences compared to the other d-block elements. Certainly, gold's significant relativistic effects dictate, to a great extent, its "special" behavior in coordination and reactivity (see section I.2). The fascination with gold within the scientific community has established gold chemistry as a very active field of research, revealing that there is a huge scope of reactivities and applications yet to be discovered. Undeniably, gold chemistry has become a new world to be explored this century.

I.2. RELATIVISTIC EFFECTS

Gold ($Z=79$, $[\text{Xe}]4f^{14}5d^{10}6s^1$) is the third-row transition metal located in group 11 of the periodic table, along with the other coinage metals copper and silver. Although copper and silver are located above gold in the first and second row of the d-block, respectively, gold's properties are barely akin to theirs. In addition, the Au(I)/Au(III) couple does not interconvert between oxidation states as easily as its neighboring isoelectronic couples Pd(0)/Pd(II) and Pt(0)/Pt(II) do. Thus, the organometallic chemistry of gold is less well-established than that of gold's neighbors in the periodic table. Ultimately, these are consequences of the relativistic effects arising from gold's electronic structure, which give rise to the unique intrinsic properties in gold. In this section, the principal relativistic effects and their impact on gold's properties are discussed.

Essentially, the term "relativistic effects" refers to the phenomena resulting from the need to consider velocity as significant relative to the speed of light.^{28,29} The inner electrons of a given atom will orbit around the nucleus at a higher velocity as the atomic nuclear charge (Z) increases. Thus, since gold is a heavy element, inner electrons move at a substantially high velocity compared to those of lighter elements, approaching the speed of light and leading,

in turn, to a mass increase (Eq. 1) and to a smaller effective Bohr radius of such electrons (Eq. 2). Consequently, this results into a notorious contraction of the s and, to a lesser extent, p orbitals (Figure I.2).²⁹⁻³³ In fact, the average relativistic mass increase of the $1s$ electron in gold is about $1.23 \cdot m_0$ and the average radial contraction of the relativistic $1s$ atomic orbital is *ca.* 20%.³⁴

$$m = \frac{m_0}{\sqrt{1 - (v/c)^2}} \quad (\text{Eq. 1})$$

where m is the corrected mass, m_0 is the non-relativistic mass, v is the velocity, and c is the speed of light.

$$a_0 = \frac{4\pi\epsilon_0\hbar^2}{m_e \cdot e^2} \quad (\text{Eq. 2})$$

where a_0 is the Bohr radius, ϵ_0 is the vacuum permittivity, \hbar is the reduced Planck constant, m_e is the mass of the electron and e is the elementary charge.

The electrons in the contracted s and p orbitals shield better the outer electrons occupying the d and f orbitals. Hence, the latter see a weaker nuclear attraction and it translates into an expansion and destabilization of the d and f orbitals (Figure I.2).²⁹

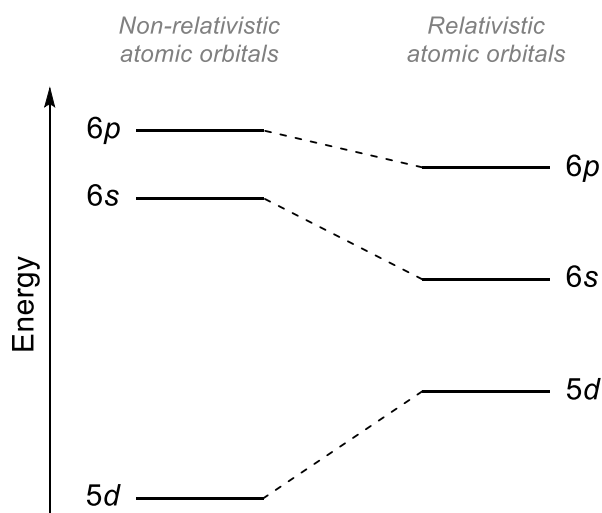


Figure I.2. Schematic energy-level diagram of gold's valence shells without relativistic effects (left) and with relativistic effects (right).³⁵

Moreover, the poor shielding of nuclear charge by $4f$ electrons enhances the contraction and stabilization of the $6s$ orbital. This phenomenon is known as lanthanide contraction. Remarkably, the “relativistic” triad Pt, Au, Hg ($Z = 78, 79$ and 80 , respectively) shows an “abnormal” lanthanide contraction since this effect gets more pronounced as the d -shell gets filled, and gold exhibits the maximum relativistic $6s$ orbital contraction (Figure I.3).^{31, 33}

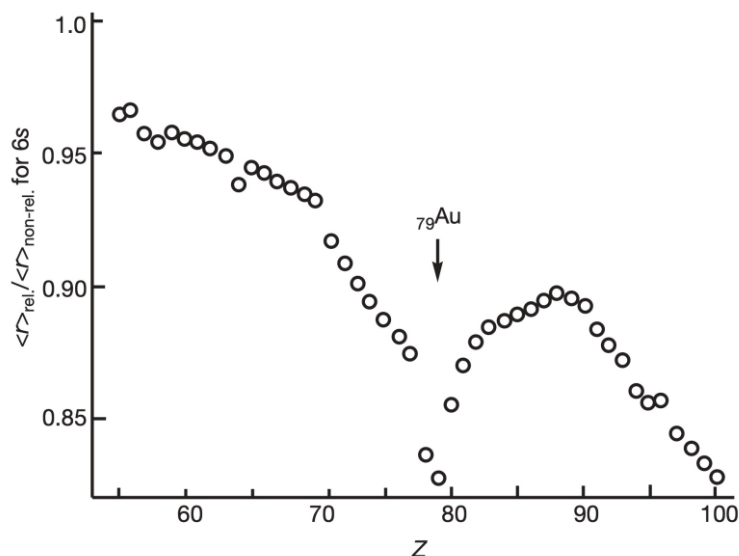


Figure I.3. Relativistic contraction of the $6s$ shell radii in the atomic ground states of the elements ranging from $Z=55$ (Cs) to $Z=100$ (Fm). (Figure taken from ref. 29, and originally published in ref. 31 with the numbers taken from the Dirac-Fock and Hartree-Fock calculations of Desclaux³⁶).

One consequence of raising the $5d$ and lowering the $6s$ energies (*i.e.* the decrement of the energetic gap between such levels) is the singular yellow color of metallic gold. Gold has an absorption beginning at ~ 2.4 eV associated with transitions from the $5d$ band to the Fermi level, which is essentially the $6s$ band. Thus, gold absorbs blue visible light and reflects yellow. Analogously, the absorption from the $4d$ band to the $5s$ band in silver is in the ultraviolet because the band gap is larger (~ 3.7 eV). Hence, it explains why silver is colorless.^{37, 38}

Also, relativistic effects result in a larger spin-orbit coupling phenomenon in heavy atoms like gold. This has a direct impact on the photoluminescent properties of the molecule that contains the gold center and, in this line, significant interest in Au(III) complexes has been put, as isoelectronic Ir(I) and Pt(II) complexes had been broadly used for photoluminescent applications. The spin-orbit coupling is the interaction between the spin and orbital angular momenta of electrons (s and l quantum numbers, respectively), resulting in states that are characterized by total angular momentum values (j ; $j = l + s$). That is, the spin-orbit

interaction splits a shell with a specific value of l into subshells with total angular momentum $j = l - 1/2$ and $j = l + 1/2$. Therefore, transitions between states of different spin multiplicities, which are otherwise spin-forbidden, can take place thanks to the spin-orbit coupling. It includes the population of excited triplet states by intersystem crossing ($S_1 \rightarrow T_1$) and phosphorescent emissions ($T_1 \rightarrow S_0$).^{31, 34, 39}

The relativistic effects have a remarkable influence on the coordination chemistry of gold. The contraction of the $6s$ orbital causes gold to have a small atomic size (covalent radii for Cu: 1.32 Å; Ag: 1.45 Å; and Au: 1.36 Å)⁴⁰ and to exhibit highly strengthened Au–L bonds (L = ligand). There is a relativistic bond-length contraction which pulls in the Au–L single-bond lengths to lengths that are similar to or shorter than those of the corresponding Ag–L bonds.^{29, 41}

The most common oxidation states for gold are 0, +1 and +3, although the occurrence of states -1, +2 and +5 has also been evidenced. Setting aside the metallic Au(0) occurring in nature, few examples of low-valent Au(-I) and Au(0) complexes are reported,⁴²⁻⁴⁶ and AuF₅ and AuF₆⁻ anion stand as the only examples of high-valent Au(V) compounds known to date.⁴⁷⁻⁵¹ Nevertheless, organogold chemistry is dominated by Au(I) and Au(III) as the valence electron arrangements of such species are more favorable.

Au(I) is by far the most common and well-studied oxidation state of the metal.^{38, 52} Au(I) complexes are d^{10} species ($[Xe]4f^{14}5d^{10}6s^0$) with, therefore, all the d orbitals doubly occupied (Figure I.4). Au(I) preferentially forms 14-electron dicoordinated complexes featuring a linear coordination. This stands in contrast to the other coinage metals, where tricoordinate and tetracoordinate Cu(I) and Ag(I) complexes prevail.^{29, 53}

The destabilization and expansion of the $5d$ orbitals allow gold to access the oxidation state +3, which, in contrast, is less frequent in copper and almost absent in silver. The reason why Au(III) complexes are thermodynamically more stable than Cu(III) and Ag(III) complexes is that, in gold, the expansion of the $5d$ shell makes the electron-electron repulsion of the $5d$ electrons to decrease. Thus, the $5d$ electrons feel an increased effective nuclear attraction and so are held with larger energy than the $3d$ electrons in copper and the $4d$ electrons in silver.^{29,}

⁵⁴ Despite that, the favorable Au(I)/Au(0), Au(III)/Au(I) and Au(III)/Au(0) reduction potentials (1.83, 1.36 and 1.52 V, respectively, under standard conditions, in 1 M aqueous acid, 25 °C) make the synthesis of stable Au(III) complexes difficult, as reduction products are often observed. Indeed, these potentials are much more positive than those of Pd(II)/Pd(0) and Pt(II)/Pt(0) redox couples (0.91 and 1.19 V, respectively). Hence, gold is

more easily reduced than palladium or platinum, to either Au(I) or Au(0).^{55, 56} Au(III) complexes are d^8 species ($[\text{Xe}]4f^{14}5d^86s^0$) with an empty d orbital. Thus, they are typically 16-electron tetracoordinated complexes with a square-planar geometry (Figure I.4).

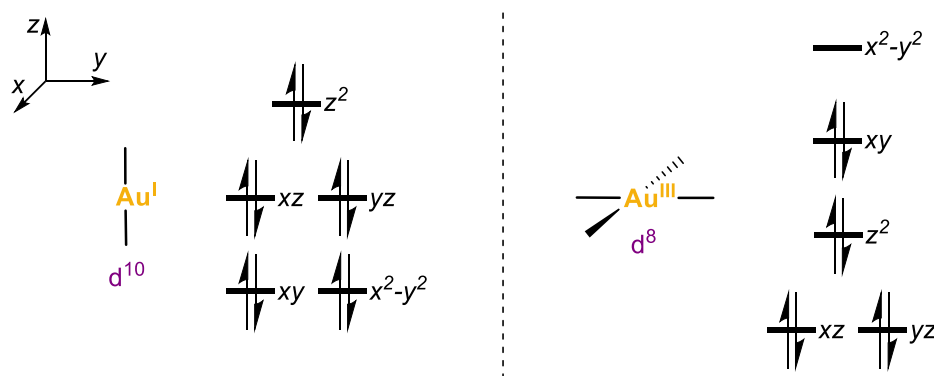


Figure I.4. d -Orbital splitting diagrams for linear Au(I) and square-planar Au(III) complexes.

Au(II) complexes are d^9 species ($[\text{Xe}]4f^{14}5d^96s^0$) with the dx^2-y^2 orbital singly occupied, featuring a square-planar geometry. Because of the electronic configuration, Au(II) complexes are prone to dimerize into $[\text{Au(II)}-\text{Au(II)}]^{4+}$ core species or disproportionate into mixed Au(I) and Au(III) species.⁵⁷⁻⁶¹ Consequently, mononuclear gold(II) complexes stand as very rare labile species and, generally, they have been postulated as transient intermediate species in homogeneous catalysis.⁶²⁻⁶⁸ Only scarce examples of the isolation and characterization of genuine mononuclear Au(II) complexes have been reported so far.^{57, 69-71} In this thesis, however, we will focus our attention on the study of Au(I) and Au(III) complexes.

Concerning reactivity, the relativistic contraction of s and p orbitals gives gold high ionization potentials (9.23/20.50 eV), high electron affinity (222.7 $\text{kJ}\cdot\text{mol}^{-1}$) and high electronegativity (2.54 *vs.* 1.93 for Ag).^{33, 37, 72} In fact, gold is the most electronegative metal of the periodic table, with a value comparable to that of carbon ($\chi = 2.55$).⁷² Consequently, all these characteristics make gold difficult to oxidize ($E^0 \text{Au(I)}/\text{Au(III)} = +1.41 \text{ V vs. SHE in water}$).⁷³ Moreover, due to the low electron-electron repulsion in the $5d$ shell and the increased effective nuclear attraction that these electrons feel, Au(I) complexes do not tend to undergo oxidative addition. Au(I) and Au(III) complexes do not readily cycle between oxidation states due to this gold's general reluctance to oxidation, and that explains why addressing Au(I)/Au(III) catalytic cycles in homogeneous catalysis is challenging.

On the other hand, gold presents aurophilicity.⁷⁴ This term was coined by Schmidbaur *et al* in 1988⁷⁵⁻⁷⁷ to describe the tendency of gold for Au–Au bonding, with a strength on the order of hydrogen bonds,^{41, 78} through London forces at distances of around 3 Å caused by the electrostatic interaction of the destabilized 5*d* orbitals in Au(I) complexes.^{29, 33}

Also, the contraction of the 6*s* orbital leaves the LUMO in a low-lying level of energy in comparison with the other coinage metals. In fact, the LUMO for Au(I) complexes ([Xe]4f¹⁴5d¹⁰6s⁰) is the stabilized 6*s* orbital. Therefore, gold features a significant Lewis acid character and an enhanced π -backbonding. This results in soft Au(I) cations⁷⁹ that are prone to activate soft nucleophiles, such as π -C–C bonds, by rendering gold π -complex species capable of withdrawing electron density. Indeed, the high catalytic performance of gold complexes and gold salts in activating C–C multiple bonds of alkynes, alkenes and allenes has been widely studied.⁴⁻¹⁰

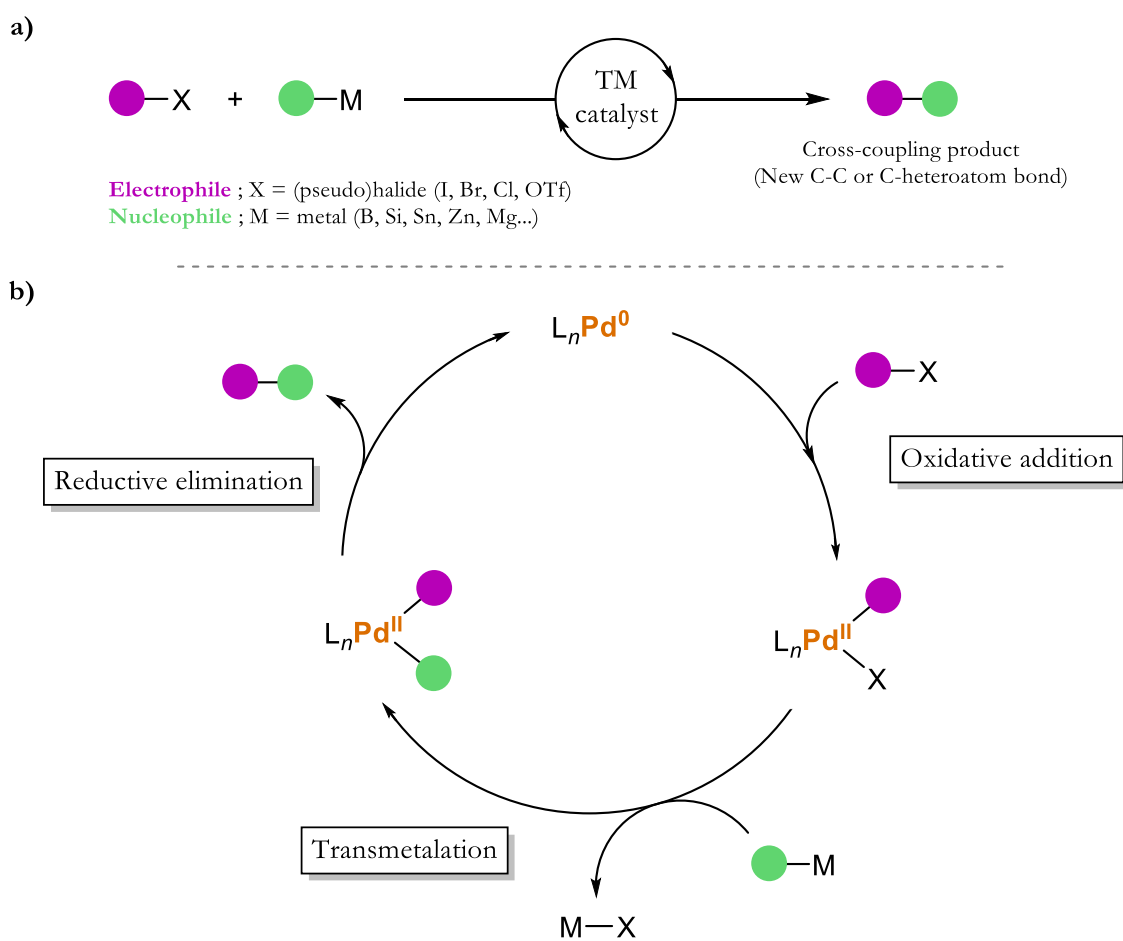
I.3. GOLD-MEDIATED HOMOGENEOUS CATALYSIS

Catalysis has radically revolutionized organic synthesis, as it allows transformations that would be otherwise difficult or even impossible to attain by means of traditional synthetic methodologies.⁸⁰⁻⁸³ Catalysis is, indubitably, the way to go to address the main concerns around the development of novel synthetic protocols; it seeks the enhancement of step and atom economy, efficiency, and selectivity in new reactions that build up molecular complexity. Therefore, catalytic processes can lead to a reduction of waste and side-products generated during the reactions, being more sustainable and environmentally friendly. Such an advantageous synthetic tool has clearly become a field of paramount interest in research and a very appealing approach for industrial applications.

The most widely used homogeneous catalysts are those based on transition metals. Thus, the interplay between organic, organometallic, and computational chemistry has become crucial to study the mechanisms operating in metal-mediated catalytic reactions and provide useful insight to further develop novel synthetic procedures. Indeed, studies where these disciplines work hand in hand have gained momentum in the recent years. Moreover, the use of molecular organometallic complexes as homogeneous catalysts is an extremely versatile approach when looking for new reactivities; the choice of the metal will influence on the reactivity (every metal has its own properties), as well as the ligands (they allow the

modulation of electronics, steric effects, chirality, etc.), the reagents, and conditions employed.

Cross-coupling reactions consist in the assembly of two coupling partners promoted by the action of a transition metal (Scheme I.1a). They stand as a very powerful kind of transformation to build up molecular complexity because ubiquitous bonds in organic molecules such as C–C and C–heteroatom bonds can be formed, allowing the synthesis of relevant complex molecules from rather simple coupling partners.



Scheme I.1. a) General depiction of a cross-coupling reaction and b) general mechanism operating in palladium-catalyzed cross-coupling reactions.

Although some cross-coupling transformations have been known for more than a century, they gained momentum in the seventies with the reports on the first reactions catalyzed by palladium,⁸⁴⁻⁸⁶ revolutionizing the field of organic synthesis and becoming relevant in industry.⁸⁷⁻⁹¹ Indeed, the importance of palladium-catalyzed couplings was recognized in 2010 by awarding R. F. Heck, E-I. Negishi, and A. Suzuki with the Nobel Prize in Chemistry for

their works on the coupling of aryl and vinyl halides with organometallic reagents to provide coupling products upon forming new C–C bonds.⁹² The general mechanism operating in palladium-catalyzed cross-coupling reactions (Scheme I.1b) starts with an oxidative addition step of the organic (pseudo)halide at the Pd(0) catalyst, it is followed by transmetalation of the second coupling partner to the Pd(II) catalyst and, finally, a reductive elimination step delivers the coupling product and regenerates the Pd(0) catalyst, so the catalytic cycle can restart.⁸⁶

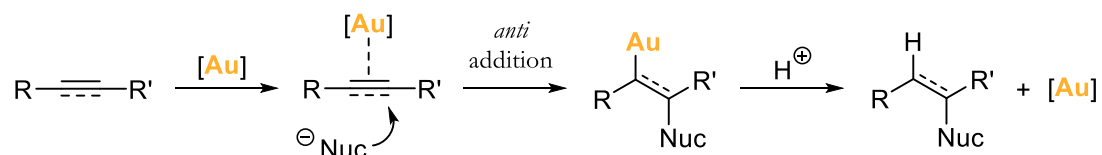
The field of cross-coupling chemistry has evolved over the years and, nowadays, many metals aside from palladium are known to catalyze cross-coupling reactions, such as manganese,⁹³ iron,⁹⁴ cobalt,⁹⁵ nickel,⁹⁶ copper,⁹⁷ rhodium,⁹⁸ and gold⁹⁹. In addition, the scope of couplings has broadened; nitrogen-, sulfide- and oxygen-based nucleophiles can be used besides organometallic reagents to access C–heteroatom couplings,¹⁰⁰⁻¹⁰² and direct cross-couplings of C–H bonds are also feasible, avoiding the prefunctionalization of the coupling partner.

Given the importance of catalysis in organic synthesis, the amount of works dedicated to finding applications in catalysis for gold complexes has been unstoppably growing since the first works disclosing that gold was not as inert as assumed. This section aims to provide a global overview on the evolution of the field of homogeneous gold catalysis, going from the early redox-neutral π -activation chemistry to the latest findings in oxidant-free Au(I)/Au(III) cross-coupling catalysis, whose development has been made possible thanks to the efforts devoted to triggering the oxidative addition at Au(I) complexes (section I.4.1). This field of investigation was already revised by us (see the review in Annex 1),¹⁰³ and an extended and updated version including recent publications (up to April 2023) is displayed herein.

I.3.1. Redox-neutral catalysis: π -activation of C–C multiple bonds

The catalytic potential of gold was discovered at the end of the 1990's, when gold complexes emerged as particular carbophilic Lewis acids able to activate unsaturated C–C bonds towards nucleophiles (Scheme I.2). Since then, the development of homogeneous gold catalysis for organic synthesis has been extremely fast, as this early mode of reactivity materialized a useful method to form new C–C and C–heteroatom bonds under catalytic and mild conditions. From a general mechanistic point of view, first, the gold complex π -coordinates the multiple C–C bond from the alkyne, alkene, or allene. Then, an *anti*-nucleophilic addition takes place on the gold-activated C–C bond to furnish a σ -complex,

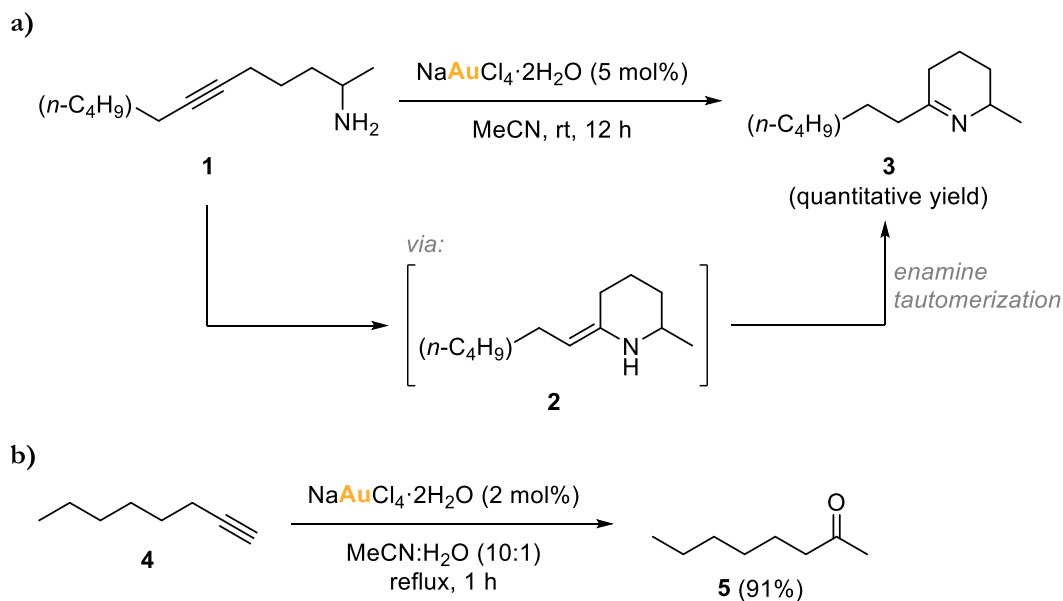
which, upon protodeauration, delivers the addition product (Scheme I.2). Also, the oxidation state of the gold center does not change throughout the catalytic cycle, standing in stark contrast to well-known cross-coupling reactions catalyzed by other late transition metals, which generally proceed through a two-electron mechanism.



Scheme I.2. General mechanism for gold-catalyzed nucleophilic addition to C–C multiple bonds.

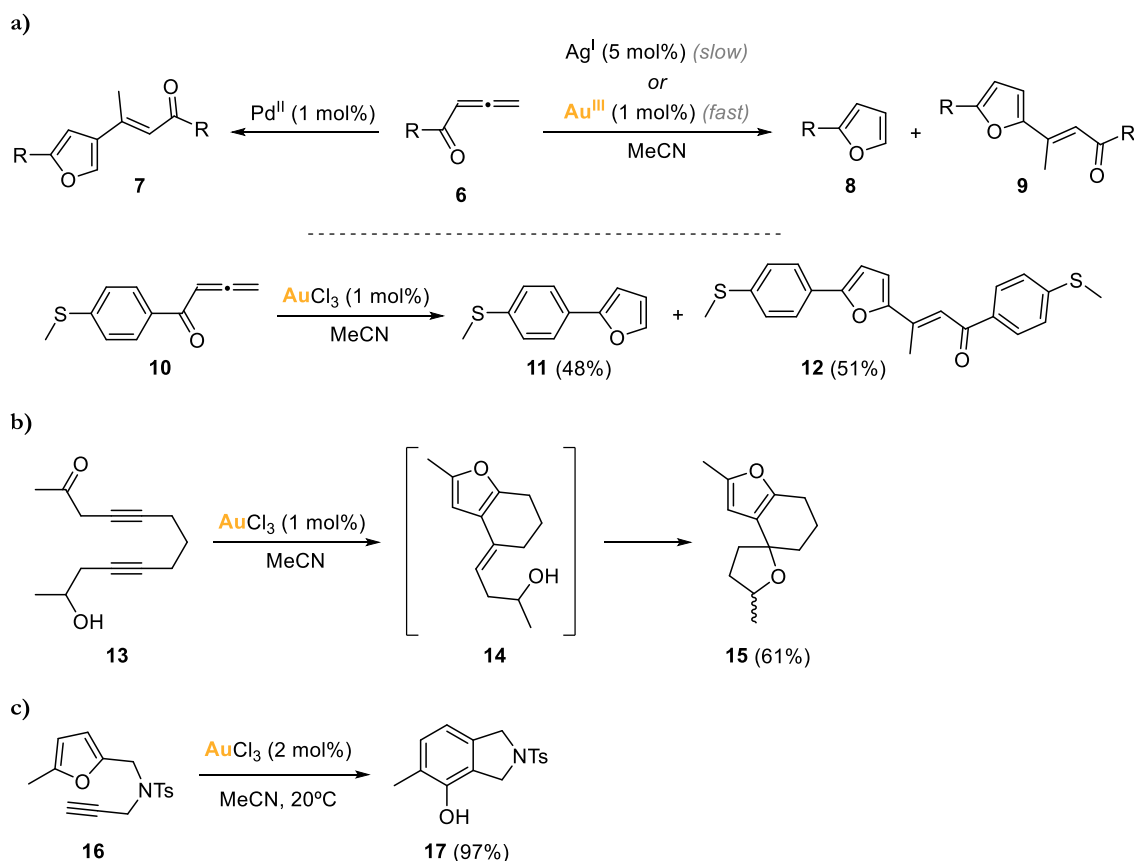
Among the wide literature on gold-mediated π -activation and functionalization of C–C multiple bonds, some works are highlighted herein to illustrate the vast scope of transformations achieved in this field.⁴⁻⁸

The pioneer reports were published intermittently between 1986 and 1998. The gold(I)-catalyzed asymmetric aldol reactions reported by Ito, Sawamura and Hayashi in 1986 can be considered the first application of Au(I) in homogeneous catalysis.¹⁰⁴ Later, in 1990, Togni and Pastor also contributed to explore this transformation.¹⁰⁵ Other relevant pioneer works are those of Utimoto reporting the gold(III)-catalyzed nucleophilic addition of N-nucleophiles to alkynes,^{3, 106} disclosed in 1987 (Scheme I.3a), and the gold(III)-catalyzed hydration of alkynes in 1990-1991 (Scheme I.3b).^{107, 108} Seven years later, in 1998, Teles upgraded the field of the addition of O-nucleophiles to alkynes by employing much more efficient gold(I) catalysts for the addition of alcohols to alkynes.² However, these initial studies did not generate much interest in the field of homogeneous gold catalysis.



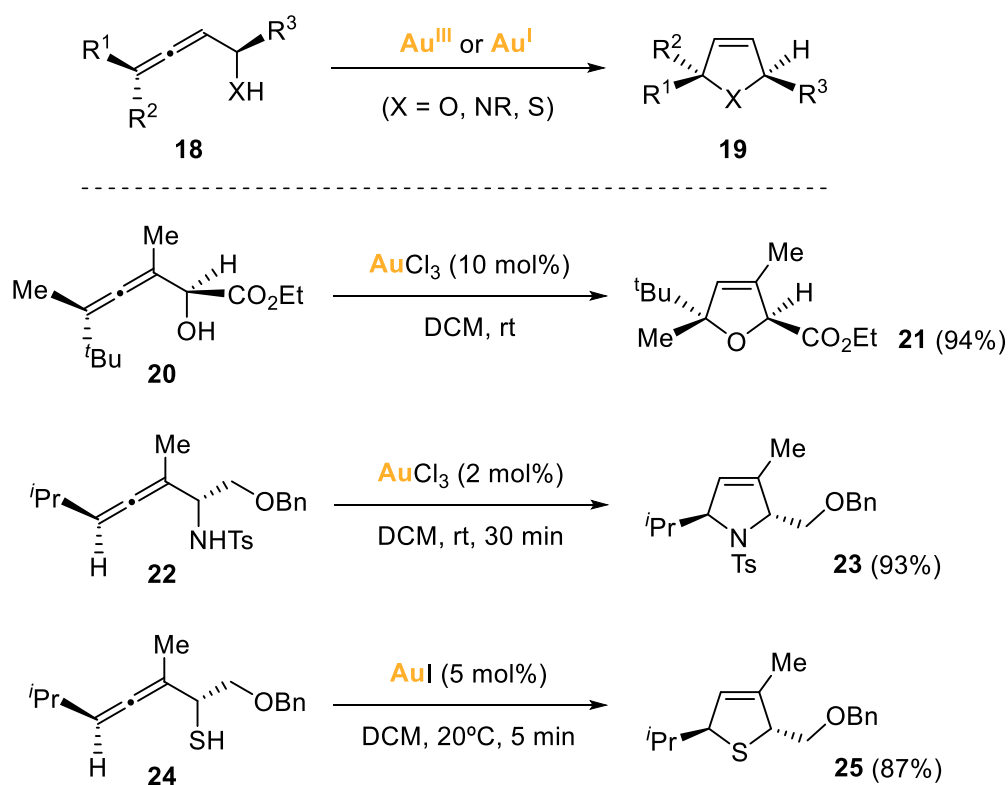
Scheme I.3. Works on gold(III)-catalyzed hydroamination (a) and hydration (b) of alkynes, by Utimoto.

Nevertheless, in 2000, the works of Hashmi^{109, 110} entailed a real breakthrough. Not only did they trigger a huge interest in the field, which has been increasing ever since, but also led to the expansion of gold-catalyzed unsaturated C–C bond functionalizations, extending the reactivity to an array of unsaturated substrates and nucleophiles.^{6, 7, 111-116} On one hand, Hashmi reported the selective cross cycloisomerization/dimerization of terminal allenyl ketones **6** and α,β -unsaturated ketones in the presence of catalytic AuCl_3 to afford furans **8** with higher kinetics than those of the analogous Pd(II) and Ag(I) catalysts (Scheme I.4a).¹⁰⁹ Also, the formation of spirocycles **15** was achieved via an intermediate **14** that undergoes intramolecular addition of an alcohol to an activated alkene (Scheme I.4b).¹⁰⁹ On the other hand, Hashmi also reported the Au(III) -catalyzed intramolecular synthesis of highly substituted phenols **17** from furans bearing a terminal alkyne **16** (Scheme I.4c).¹¹⁰ Interestingly, in 2006 the same group could synthesize phenols of the type **17** from the intermolecular reaction between an alkyne and a furan, using a dinuclear Au(I) catalyst.¹¹⁷



Scheme I.4. Works of Hashmi on gold(III) chloride-catalyzed a) cycloisomerization of terminal allenyl ketones, b) formation of spirocyclic compounds and c) intramolecular cycloisomerization of furans with a terminal alkyne moiety.

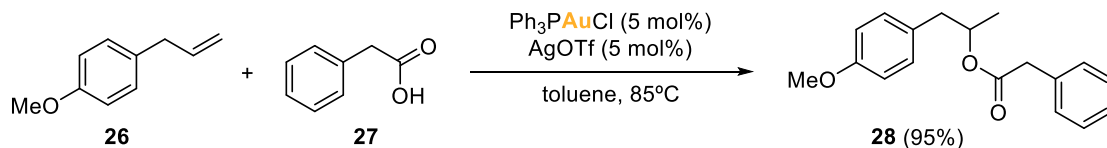
Analogously to Hashmi's work on the cycloisomerization of allenyl ketones,¹⁰⁹ between 2001 and 2006 the group of Krause investigated the gold-catalyzed stereoselective cycloisomerization of substituted α -hydroxyallenes **20**,¹¹⁸ α -aminoallenes **22**,¹¹⁹ and α -thioallenes **24**¹²⁰ to the corresponding 2,5-dihydrofurans **21**, 3-pyrrolines **23** and 2,5-dihydrothiophenes **25** (Scheme I.5).¹¹¹ In all cases, axis-to-center chirality transfer occurred, catalyzed by AuCl_3 . Interestingly, α -thioallenes **24** were converted to 2,5-dihydrothiophenes **25** in higher yields when gold(I) salts were employed instead of AuCl_3 , specifically AuCl and AuI , and this work stands as the first example of gold-catalyzed C–S bond formation.¹²⁰ Likewise, in 2006 Widenhoefer worked on the *exo*-hydroamination of N-allenyl carbamates, *exo*-hydroalkoxylation of allenyl alcohols, and *exo*-hydroarylation of 2-allenyl indoles, all in an intramolecular fashion, by using 5 mol% loading of $[\text{Au}\{\text{P}(t\text{-Bu})_2(o\text{-biphenyl})\}\text{Cl}]$ activated by either AgOTf or AgOTf s.¹²¹



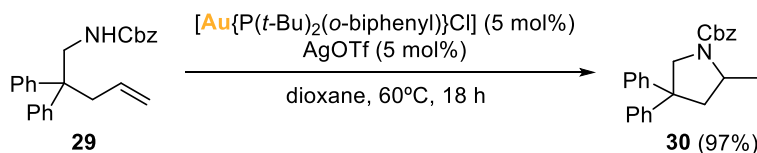
Scheme I.5. Gold-catalyzed stereoselective cycloisomerizations of α -hydroxyallenes, α -aminoallenes and α -hydroxyallenes, reported by Krause.

Regarding alkenes, He and Yang reported in 2005 the gold(I)-catalyzed intermolecular addition of weak nucleophiles like phenols and carboxylates **27** to unactivated terminal alkenes **26**, therefore generating new C–O bonds (Scheme I.6a).¹²² Widenhoefer also contributed to the functionalization of non-activated olefins by developing the intramolecular hydroamination of N-alkenyl carbamates **29** (Scheme I.6b)¹²³ and of N-alkenyl carboxamides,¹²⁴ thus forming new C–N bonds to render N-heterocycles **30**. Likewise, the generation of heterocycles via a gold(I)-mediated intramolecular addition to unactivated alkenes could also be achieved upon forming new C–C bonds, as reported by Che in 2007.¹²⁵ They employed β -ketoamides **31** as carbon nucleophiles, demonstrating that they could be intramolecularly added to unsaturated olefins to yield highly substituted lactams **32** with excellent regioselectivities and yields (Scheme I.6c).

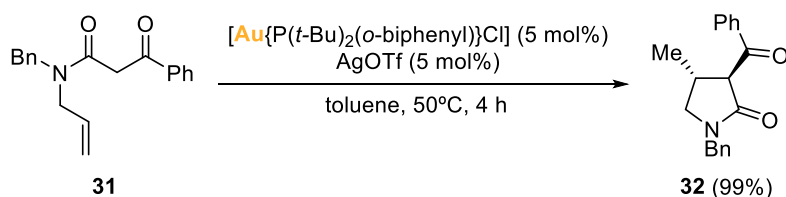
a) He (2005)



b) Widenhoefer (2006)



c) Che (2007)

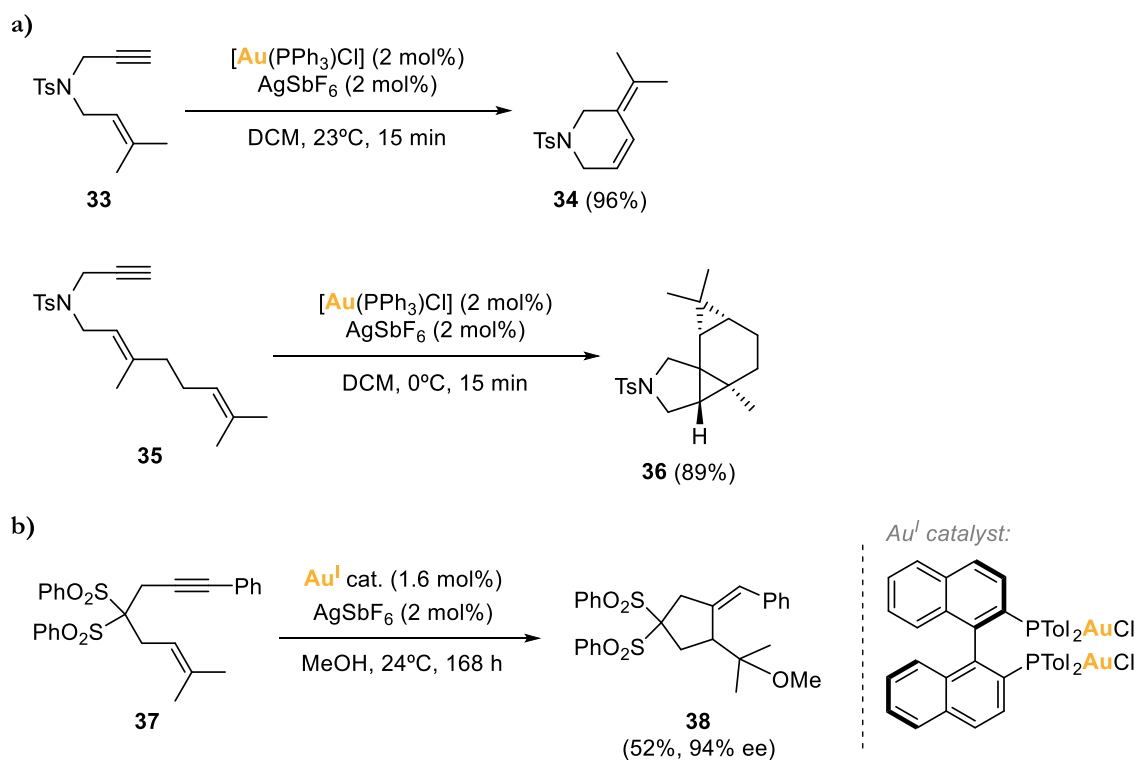


Scheme I.6. Gold(I)-catalyzed additions of a) O-nucleophiles, b) N-nucleophiles, and c) C-nucleophiles to non-activated olefins.

The field evolved toward more sophisticated transformations in terms of building up complex molecular architectures. Certainly, skeletal rearrangements including cycloadditions, cycloisomerizations, and other carbocyclization reactions of polyunsaturated molecules gained importance since the initial works of Hashmi.^{10, 126-132} In addition, there were efforts made to develop enantioselective versions of such reactions. Mechanistically, these reactions resemble hydrofunctionalizations in that they commence with the activation of a $\pi\text{-C-C}$ bond, but then the attack of another unsaturated C-C bond follows, leading to multiple rearrangement steps.

In this line, Echavarren reported in 2004 highly alkynophilic cationic gold(I) catalysts of the type $[\text{Au}(\text{PPh}_3)]^+\text{X}^-$ for skeletal rearrangements of enynes **33** and dienyne **35** (Scheme I.7a)¹³³ and, one year later, the same group employed chiral bis(phosphine)digold(I) catalysts with the aim to render this reactivity enantioselective, as these ligands provide gold centers with a suitable steric environment to exert chirality. Specifically, they employed these Au(I) catalysts in the enantioselective alkoxy cyclization of 1,6-enynes **37** (Scheme I.7b).¹³⁴ It is worth mentioning that other strategies were explored to induce chirality, like using other ligands or modifying the weakly coordinating ligand or counterion.¹³⁵ Gold(I)-catalyzed rearrangements of enynes was indeed widely explored by several groups, as enynes are substrates that showed to give access to a bunch of different reactivities¹³⁶⁻¹⁴⁰ Also, Echavarren's group studied the

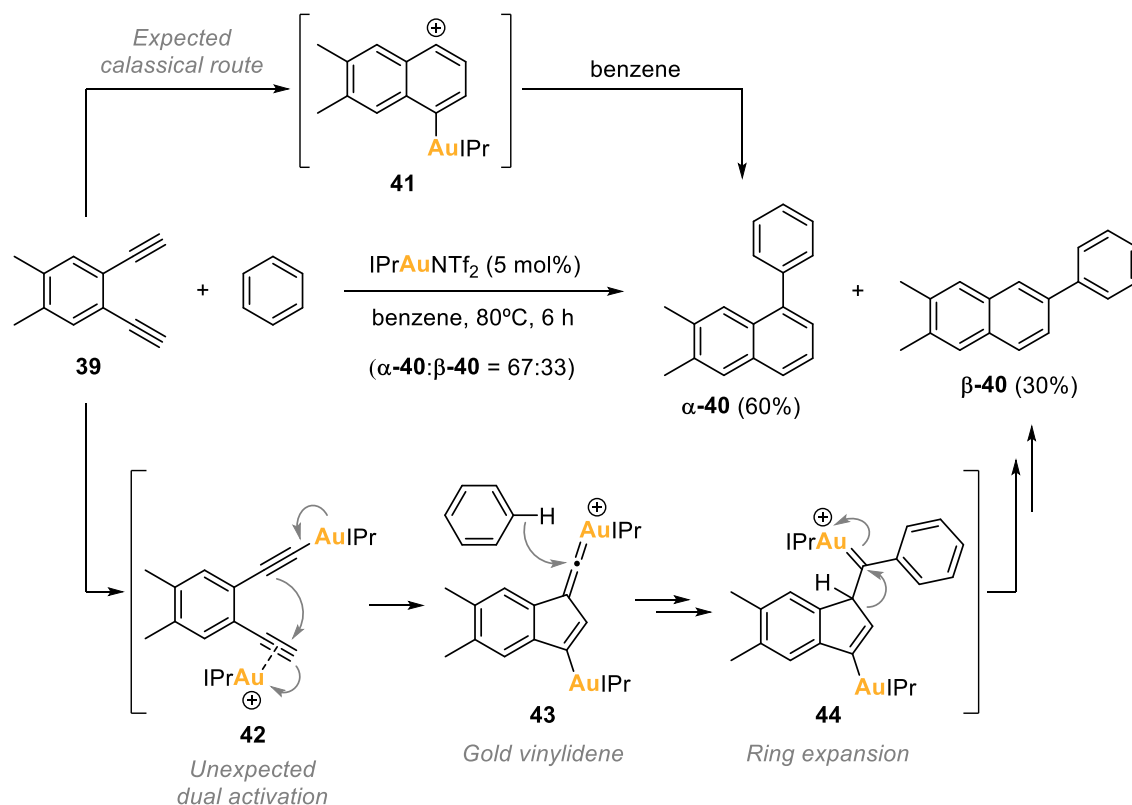
intramolecular [4+2] cycloadditions of arylalkynes or 1,3-enynes with alkenes, using cationic phosphine gold(I) catalysts,¹⁴¹ and in 2008, they reported the DFT studies on the mechanism of such reactions.¹⁴²



Scheme I.7. Gold(I)-catalyzed skeletal rearrangements of 1,6-enynes and diynes, by Echavarren.

Not only did enynes prove to be very versatile substrates, but also diynes did,¹⁴³ and, strikingly, an unprecedented mode of reactivity emerged in 2012 when Hashmi's group was exploring the gold(I)-catalyzed activation of diynes: the so-called dual gold catalysis.¹⁴⁴ This novel category of gold-catalyzed reactions is characterized by the simultaneous activation of the organic substrate by two gold centers; while one gold center is σ -bonded to a terminal alkynyl group of the substrate forming a gold(I) acetylide, the other gold center is π -coordinated to the substrate. In some cases, both gold centers can be found coordinated to the same alkynyl moiety forming a σ,π -digold(I) acetylide, although in most of the cases the reaction proceeds through an intermediate that has one alkyne σ -bonded to a gold complex and a different alkyne π -coordinated to the second gold complex.¹⁴⁵ Indeed, Hashmi's group observed in 2012 the formation of significant amount of the unexpected product β -40 from diyne 39 upon cyclization hydroarylation (Scheme I.8).¹⁴⁴ These were clear evidences of a different mechanism competing with the classical route that affords product α -40. After some

experimental and computational studies, the mechanism that was proposed to deliver product **β -40** proceeded via a dual activation of diyne **39**, with a gold complex σ -bonded to one alkyne and a π -coordinated gold complex on the other alkynyl moiety (intermediate **42**), that triggers the formation of a gold vinylidene intermediate **43**. Then, an insertion to the vinylidene moiety of a C–H bond of a benzene solvent molecule occurs, leading to several rearrangement steps that finally afford product **β -40** (Scheme I.8).^{144, 145}



Scheme I.8. Evidence of a dual gold activation mechanism operating in gold(I)-catalyzed cyclization hydroarylation of diynes with benzene.

Dual gold catalysis indeed emerged as a powerful mode of reactivity to access a wide scope of polycyclic products from diynes, as demonstrated by subsequent works.¹⁴⁶⁻¹⁵¹

All in all, the Lewis acidity of gold complexes and salts is a very versatile tool that allows a huge array of transformations in terms of building up molecular complexity from substrates with unsaturated bonds and, nowadays, it is still a continuously growing field of research. However, the study of homogeneous gold catalysis is not limited to π -activation chemistry. In parallel to the development of this kind of chemistry, studies were also devoted to achieve two-electron Au(I)/Au(III) homogeneous catalysis, seeking other novel modes of reactivity

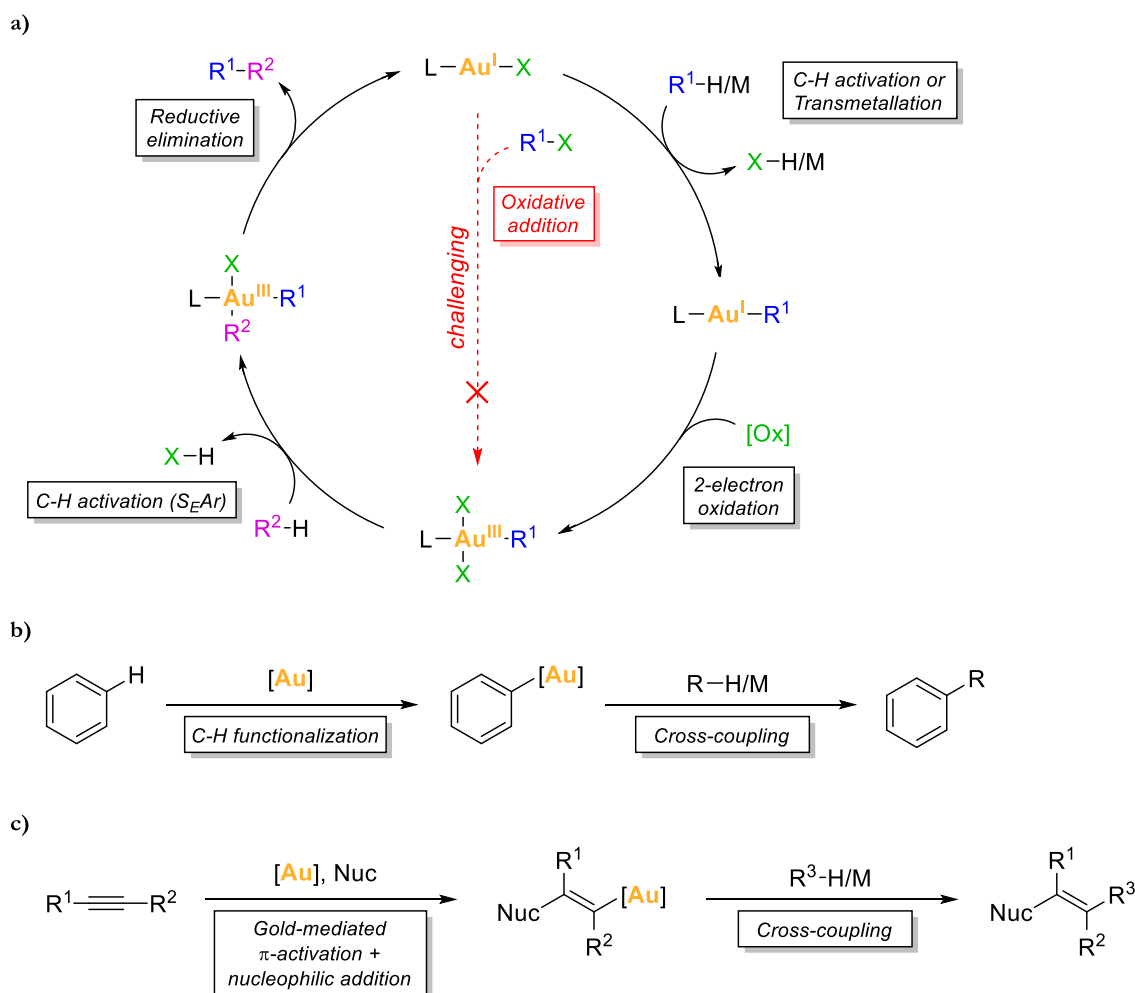
for gold, while trying to build catalytic cycles that resemble those well-studied for other late transition metals (Scheme I.1). Thus, the following sections I.3.2 and I.3.3 will deal with gold-catalyzed homogeneous cross-coupling reactions operating through Au(I)/Au(III) catalytic cycles.

I.3.2. Oxidative Au(I)/Au(III) cross-coupling catalysis

Transition metal-catalyzed cross-coupling transformations are usually based on catalytic cycles that comprise the interconversion between different oxidation states of the metallic atom, generally proceeding through M^n/M^{n+2} redox cycles. Thus, the transition metal undergoes a formal two-electron oxidation and reduction, achieved via two-electron redox steps, namely oxidative addition (Section I.4.1, Scheme I.26) and reductive elimination (Section I.4.2, Scheme I.34). Palladium has typically been the metal of choice for catalyzing a vast array of cross-coupling transformations, therefore countless Pd(0)/Pd(II)¹⁵²⁻¹⁵⁴ catalytic cycles have been reported to be the operating mechanisms in Pd-mediated couplings. Nevertheless, many other transition metals have also shown to be good catalysts in cross-coupling transformations. For instance, works on Ni(0)/Ni(II)-,^{155, 156} Co(I)/Co(III)-,¹⁵⁷ Cu(I)/Cu(III)-¹⁵⁸⁻¹⁶² and Au(I)/Au(III)-catalyzed cross-couplings can be found in the literature, among others.

The case of gold, however, can be regarded as special because, due to its strong relativistic effects, the Au(I)/Au(III) redox pair features an unusual high redox potential ($E^0 = 1.41$ V) compared to that of the isoelectronic Pd(0)/Pd(II) pair ($E^0 = 0.92$ V).⁷³ This peculiarity makes Au(I) specially reluctant to oxidative addition¹⁶³⁻¹⁶⁵ so, in order to build Au(I)/Au(III) catalytic cycles, the use of stoichiometric amounts of sacrificial external oxidants is the approach that has traditionally been applied to access the envisioned Au(III) intermediates. However, this implies a 2-electron oxidation step in the mechanism instead of an oxidative addition step (Scheme I.9a). In comparison with coupling reactions involving an oxidative addition step, where one coupling partner inherently comes from the organic halide, in these processes, both fragments coordinate to the metal by a redox-neutral “ligand exchange” step, such as transmetalation.¹³ Common sacrificial oxidants are F^+ donors, such as Selectfluor or *N*-fluorobenzenesulfonimide (NFSI), and hypervalent iodine reagents. Following this strategy, a wide assortment of Au(I)/Au(III)-catalyzed oxidative couplings exists,^{13, 166, 167} including C–C and C–X couplings at alkynes, alkenes, allenes and arenes.

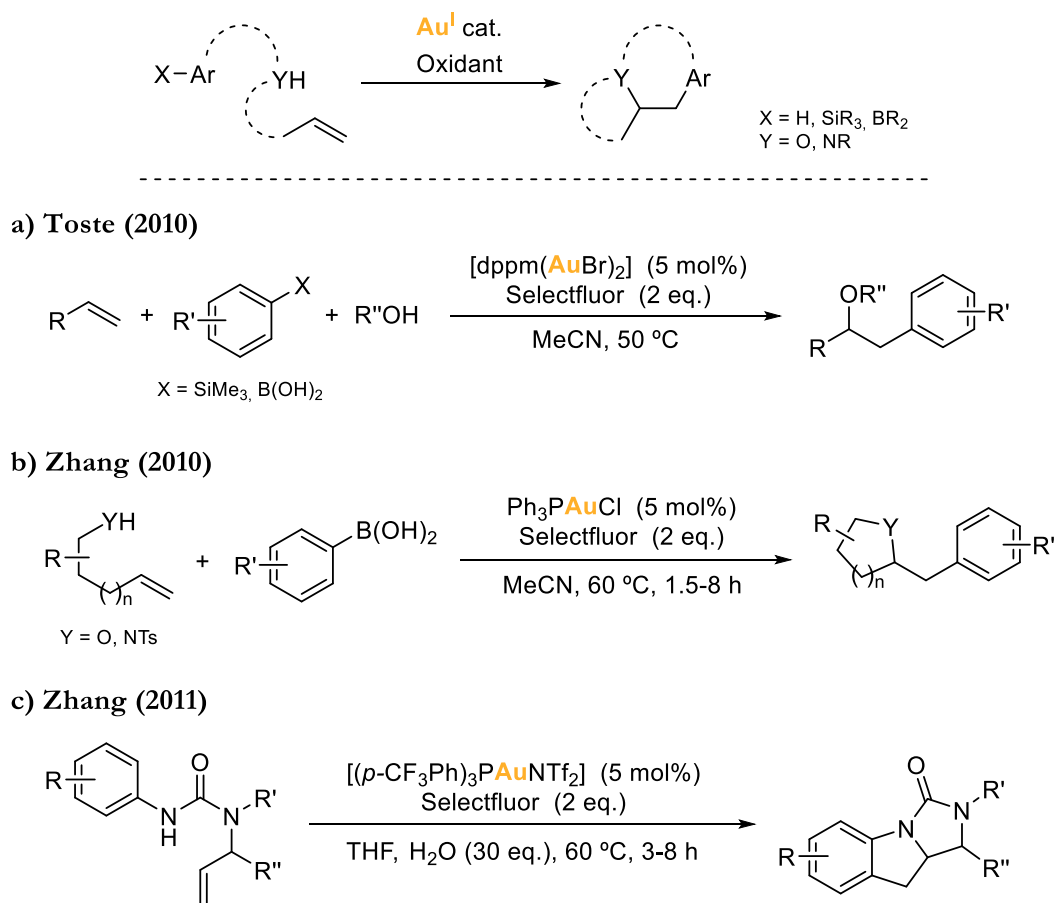
Taking advantage of the unique properties of gold, Au(I)/Au(III) oxidative couplings are usually combined with direct C–H bond functionalizations of arenes (Scheme I.9b) or with nucleophilic additions of C–C multiple bonds promoted by π -activation (Scheme I.9c). Indeed, it is well-established that gold(III) display selectivity for C–H activation of electron-rich arenes to afford arylgold(III) complexes, characteristic of an electrophilic aromatic substitution (S_EAr). Thus, arylation reactions can be done using simple arenes that do not require “pre-activation” by halogenation or metalation (Scheme I.9b).¹³ Alternatively, one unsaturated organic coupling partner may π -coordinate to gold, being followed by a nucleophilic attack onto the C–C multiple bond. In this case, the oxidative coupling replaces the protodeauration step typically observed in gold-catalyzed hydrofunctionalizations of alkynes, alkenes and allenes (Scheme I.9c, in comparison with Scheme I.2).¹³



Scheme I.9. a) General mechanism in Au(I)/Au(III) oxidative cross-coupling catalysis, featuring in red the alternative oxidative addition step that is circumvented by using external oxidants, to access Au(III) intermediates. b) Gold-catalyzed oxidative coupling reactions involving aryl C–H functionalization and c) involving nucleophilic addition.

In 2008, Tse and coworkers reported the first gold-catalyzed C–C homo-coupling of arenes to obtain biaryls, using 2 mol% HAuCl_4 and $\text{PhI}(\text{OAc})_2$ as a sacrificial oxidant.¹⁶⁸ In 2009, Zhang's group used propargylic acetates to develop the corresponding Au(I)/Au(III)-catalyzed oxidative dimerization as well as the oxidative coupling with arylboronic acids.^{169, 170} In both transformations, the formation of Au(III) intermediates was proposed to be promoted by Selectfluor.

From 2010 to 2012, several research groups reported independently numerous studies on gold-catalyzed oxy- and aminoarylation reactions at olefins (Scheme I.10). On one hand, Russell and Lloyd-Jones employed arylsilanes as coupling fragments in two- and three-component gold-catalyzed oxyarylation of terminal alkenes.¹⁷¹ In this work, the use of Selectfluor not only allowed the access to a Au(I)/Au(III) catalytic cycle but also avoided the need for adding a stoichiometric base as it provided a fluoride anion for silane activation. Likewise, two years later, the same group expanded the scope of compatible olefins to styrenes and mono- and gem-disubstituted olefins in gold-catalyzed three-component oxyarylations by employing iodosobenzoic acid as oxidant instead of Selectfluor.¹⁷² On the other hand, Toste and coworkers studied in parallel the three-component gold-catalyzed oxyarylation of terminal olefins employing the bimetallic gold(I) complex $[\text{dppm}(\text{AuBr})_2]$ ¹⁷³ and expanded the scope of the arylating fragment from arylsilanes to arylboronic acids (Scheme I.10a).¹⁷⁴ Moreover, they also developed the intramolecular aminoarylation of terminal alkenes using the same $[\text{dppm}(\text{AuBr})_2]$ complex, arylboronic acids as coupling partners and selectfluor as oxidant.¹⁷⁵ Simultaneously, the group of Zhang also worked in the use of arylboronic acids for both the oxyarylation and aminoarylation of olefins, employing Ph_3PAuCl and Selectfluor (Scheme I.10b).¹⁷⁶ In addition, Gouverneur and coworkers reported the intramolecular oxidative C–C cross-coupling of non-activated arenes to afford tricyclic dihydroindenofuranone-type products.¹⁷⁷ Similarly, in 2011 the group of Zhang combined the oxidative Au(I)/Au(III)-catalysis with C–H functionalization to yield tricyclic indolines as formal intramolecular [3+2] annulation products (Scheme I.10c).¹⁷⁸

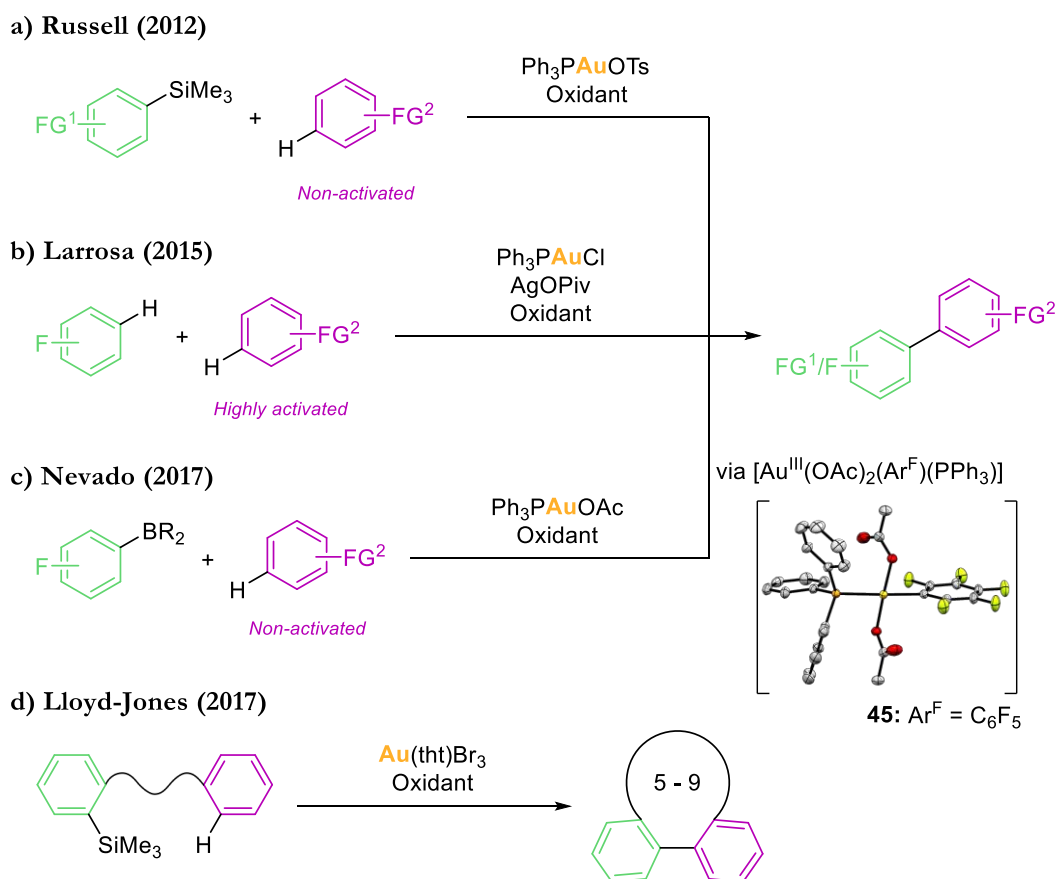


Scheme I.10. General Au(I)/Au(III)-catalyzed oxy- and aminoarylations of terminal alkenes. (a) Three-component oxyarylation of terminal olefins using arylsilanes and boronic acids as competent arylating agents. (b) Two-component oxyarylations and aminoarylations of terminal alkenes using arylboronic acids. (c) Aminoarylation of terminal alkenes via intramolecular C–C coupling.

Regarding couplings involving terminal alkynes, Nevado and de Haro reported in 2010 the gold-mediated oxidative C(sp)–C(sp²) coupling of arenes with electron-deprived terminal alkynes to yield arylacetylenes.¹⁷⁹ This work stands as the first ethynylation reaction of this kind occurring via a gold-catalyzed C–H activation of both aromatic and acetylenic counterparts. Also, Zhang and coworkers published an unprecedented gold-catalyzed Sonogashira cross-coupling of terminal alkynes with arylboronic acids.¹⁸⁰ In addition, the group of Shi reported the first example of the formation of unsymmetrical 1,3-diynes upon C(sp)–C(sp) coupling of two different terminal alkynes, in excellent heteroselectivity, under gold-catalyzed oxidative cross-coupling conditions.¹⁸¹ Crucial factors to promote this transformation were the use of PhI(OAc)₂ as oxidant and 1,10-phenanthroline as auxiliary ligand.

As to C(sp²)–C(sp²) couplings, in 2012 Lloyd-Jones and Russell synthesized biaryls by reacting arylsilanes with non-activated arenes, using a Au(I) catalyst and PhI(OAc)₂ as

oxidant under mild conditions (Scheme I.11a).¹⁸² Later, between 2014 and 2016, they reported the gold-catalyzed oxidative coupling of arylsilanes with arenes and heteroarenes, exploring other catalysts and oxidants.^{183, 184} Remarkably, Larrosa's group published in 2015 the first gold-catalyzed oxidative cross-coupling of arenes via double C–H activation (Scheme I.11b).¹⁸⁵ The biaryls obtained consisted of the coupling between highly activated (hetero)arenes and perfluorinated arenes. This strategy, however, required the employment of silver salts to help at the C–H activation of the electron-deficient arene counterpart. In 2017, Nevado and coworkers also contributed to the field of gold-catalyzed oxidative couplings to yield biaryls by providing a system in which strong electron-poor fluorinated aryl boronates coupled to arenes efficiently (Scheme I.11c).¹⁸⁶ Interestingly, the intermediacy of a Au(III) species of the type $[\text{Au}(\text{OAc})_2(\text{Ar}^{\text{F}})(\text{PPh}_3)]$ **45**, obtained upon $\text{PhI}(\text{OAc})_2$ -mediated oxidation, could be validated.



Scheme I.11. Different methodologies for the synthesis of biaryls by means of gold-catalyzed oxidative C(sp²)-C(sp²) cross-coupling.

Also in the same year, Lloyd-Jones and coworkers developed an intramolecular system for the gold-catalyzed arylation of arenes by aryl-trimethylsilanes.¹⁸⁷ The biaryl coupling afforded products featuring 5- to 9-membered rings. By tethering the arene to the arylsilane, the system was provided with the ability to tolerate a wide range of electron donating and electron withdrawing arene substituents (Scheme I.11d).

I.3.3. Oxidant-free Au(I)/Au(III) cross-coupling catalysis

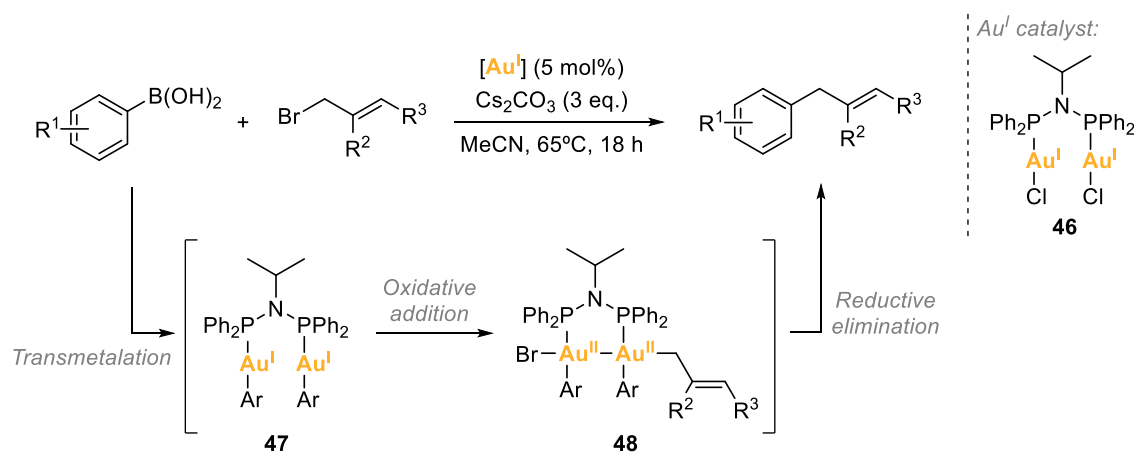
In sharp contrast to section I.3.2, this section focuses the attention on cross-coupling catalysis based on Au(I)/Au(III) cycles in the absence of external oxidants.^{99, 188, 189} The entry point to these catalytic cycles is an oxidative addition step, as it generally is in two-electron M^n/M^{n+2} redox cycles. Thus, typical oxidant-free Au(I)/Au(III) catalytic cycles are the combination of a first oxidative addition at gold(I) to provide a gold(III) intermediate, with subsequent organometallic transformations at gold(III) intermediates, and a final reductive elimination to release the cross-coupling product and regenerate the gold(I) catalyst.

However, these catalytic cycles are challenging to achieve due to the sluggish oxidative addition of alkyl and aryl halides to gold(I).¹⁶⁵ Although gold-catalyzed Suzuki and Sonogashira cross-couplings had been reported as early as 2006 and 2007,^{190, 191} intense debate was sparked by the involvement of Au(I)/Au(III) redox cycles in these processes. Palladium traces as a contaminant of gold were suggested to be responsible of the catalytic activity, according to a report by Espinet and Echavarren in 2010.^{163, 164} Also, the discovery of the thermal decomposition of Au(I) complexes to gold clusters led to suspect that gold nanoparticles could be the real catalysts.¹⁶⁴ In fact, these gold nanoparticles proved to be efficient heterogeneous catalysts in Suzuki and Sonogashira couplings,¹⁹²⁻¹⁹⁵ explaining why the reactivity was observed under strict palladium-free conditions.¹⁹⁶

Nonetheless, oxidative addition at gold(I) complexes to access gold(III) complexes can clearly be achieved if proper conditions are provided (see section I.4.1). Efforts pursuing oxidative addition at gold(I) are closely related to efforts seeking the development of oxidant-free gold-catalyzed cross-coupling protocols because these reactions rely on oxidative addition. So, by studying the oxidative addition at gold(I), the field of oxidant-free Au(I)/Au(III) catalysis could gain reliability and became feasible.

The field of Au(I)/Au(III) homogeneous catalysis without external oxidants has been growing continuously since the first example reported in 2014 by Toste and coworkers.¹⁹⁷

They used a bis(diphenylphosphino)amine ligand-supported bimetallic Au(I) complex **46** to catalyze the allylation of arylboronic acids (Scheme I.12).¹⁹⁷ Interestingly, the analogous monometallic aminophosphine Au(I) complex afforded the C(sp²)-C(sp³) coupling products in much lower yields, suggesting that the bimetallic catalyst's structure enhanced the catalytic activity. Mechanistically, a first transmetalation step was proposed to take place between the Au(I) catalyst **46** and the arylboronic acid, affording a bimetallic Au(I) intermediate **47**. Then, the oxidative addition of allyl bromides to the bimetallic Au(I) aryl complex **47** was suggested to be the key step of the catalytic cycle, and a bimetallic Au(II)-Au(II) species **48** was proposed to be formed rather than a discrete Au(III) species. Moreover, although the authors could not detect the putative intermediates, they supported the viability of the oxidative addition of the allylic C(sp³)-Br bond to Au(I) under intramolecular conditions (see Scheme I.29b).

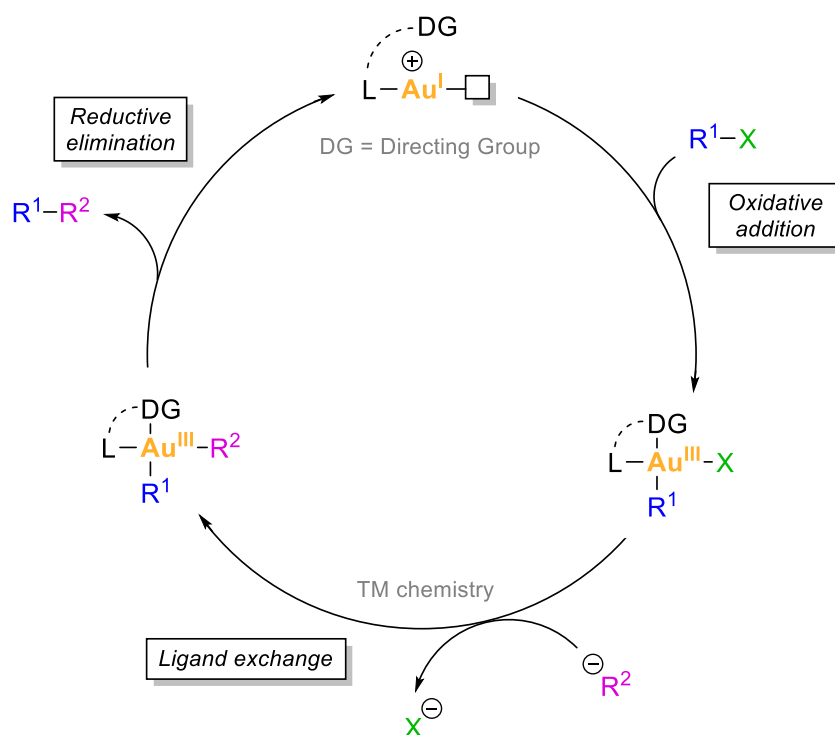


Scheme I.12. Intermolecular allylation of arylboronic acids catalyzed by a bimetallic Au(I) complex, proceeding through a Au(II)-Au(II) intermediate formed upon oxidative addition.

I.3.3.1. Chelation assistance: rational design of substrates and ligands

In order to trigger oxidative addition at Au(I) to subsequently attain oxidant-free Au(I)/Au(III) catalytic cycles, several approaches have proved fruitful. One of them is the rational design of substrates and ligands with the ability to chelate a metallic center. Basically, this strategy relies on the fact that either the substrate (coupling partner) or the ligand bears a hemilabile coordinating directing group that coordinates, therefore stabilizes, the Au(III) center of Au(III) intermediate species involved in the catalytic cycle. A general ligand-enabled Au(I)/Au(III) catalytic cycle is depicted in Scheme I.13. Generally, a vacant

site at the starting gold(I) catalyst must be created to trigger reactivity. Then, a gold(III) intermediate is formed upon oxidative addition of one organic coupling partner. It is stabilized by chelation of the ligand through the coordination of the pendant hemilabile directing group. Next, this intermediate undergoes whatever redox-neutral organometallic transformation to end up with the second organic coupling fragment coordinated to the Au(III) center (C–H functionalization, transmetalation, π -activation of C–C multiple bonds followed by nucleophilic addition, etc.). Finally, a reductive elimination step closes the cycle by regenerating the catalytically active Au(I) species and delivering the cross-coupling product (Scheme I.13). In the case of having the directing group attached to the substrate instead of to the ligand, the mechanism proceeds likewise. However, the stabilization of the gold(III) intermediate formed upon oxidative addition is provided by chelation of the coupling partner.

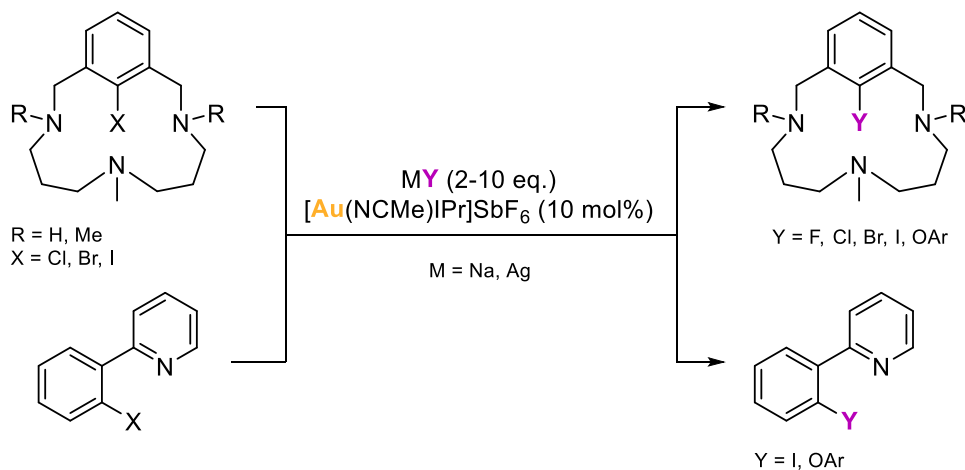


Scheme I.13. General mechanism of ligand-enabled oxidant-free Au(I)/Au(III) catalytic transformations (DG = Directing Group).

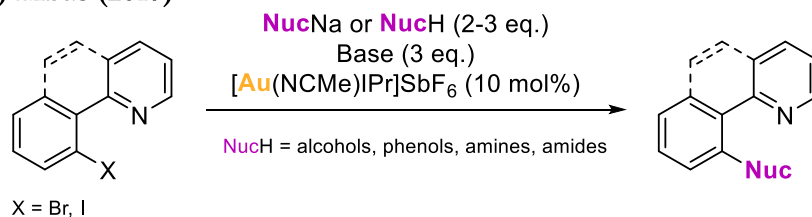
In 2015, Ribas and coworkers reported the halide exchange and C(sp²)-O bond-forming reactions employing a cationic NHC–Au(I) complex and model aryl halide triazamacrocyclic substrates, taking advantage of the chelation assistance of the substrate (Scheme I.14a).¹⁹⁸ These model substrates had previously demonstrated to be convenient substrates for the

stabilization of Cu(III) and Ag(III) intermediates obtained via oxidative addition in Cu(I)/Cu(III)- and Ag(I)/Ag(III)-catalyzed C–C and C–X bond-forming cross-couplings.^{158, 161, 162, 199} In this work, the authors also extrapolated the halide exchange and the C(sp²)-O coupling reactions to 2-(2-halophenyl)pyridines, *i.e.* substrates bearing a single chelating group (Scheme I.14a). The detection of Au(III) intermediates was not possible neither using the triazamacrocyclic substrates nor the 2-(2-halophenyl)pyridines. However, a Au(I)/Au(III) catalytic cycle was postulated and supported by DFT studies.¹⁹⁸ In 2017, the same group reported oxidant-free C(sp²)-O and C(sp²)-N coupling reactions catalyzed by the same cationic NHC–Au(I) complex employing 2-(2-halophenyl)pyridines as substrates (Scheme I.14b).²⁰⁰ Interestingly, this time the intermediacy of Au(III) species could be validated when using 10-iodobenzo[*b*]quinoline instead of 2-(2-halophenyl)pyridines, evidencing that a more rigid and flat chelating substrate stabilizes better the Au(III) intermediate formed upon oxidative addition (see Scheme I.29d). Both works were pioneer proofs of concept of the viability of oxidant-free Au(I)/Au(III) coupling catalysis, enabled by the chelation assistance of hemilabile amines and pyridines attached to the substrates (Scheme I.14).

a) Ribas (2015)



b) Ribas (2017)

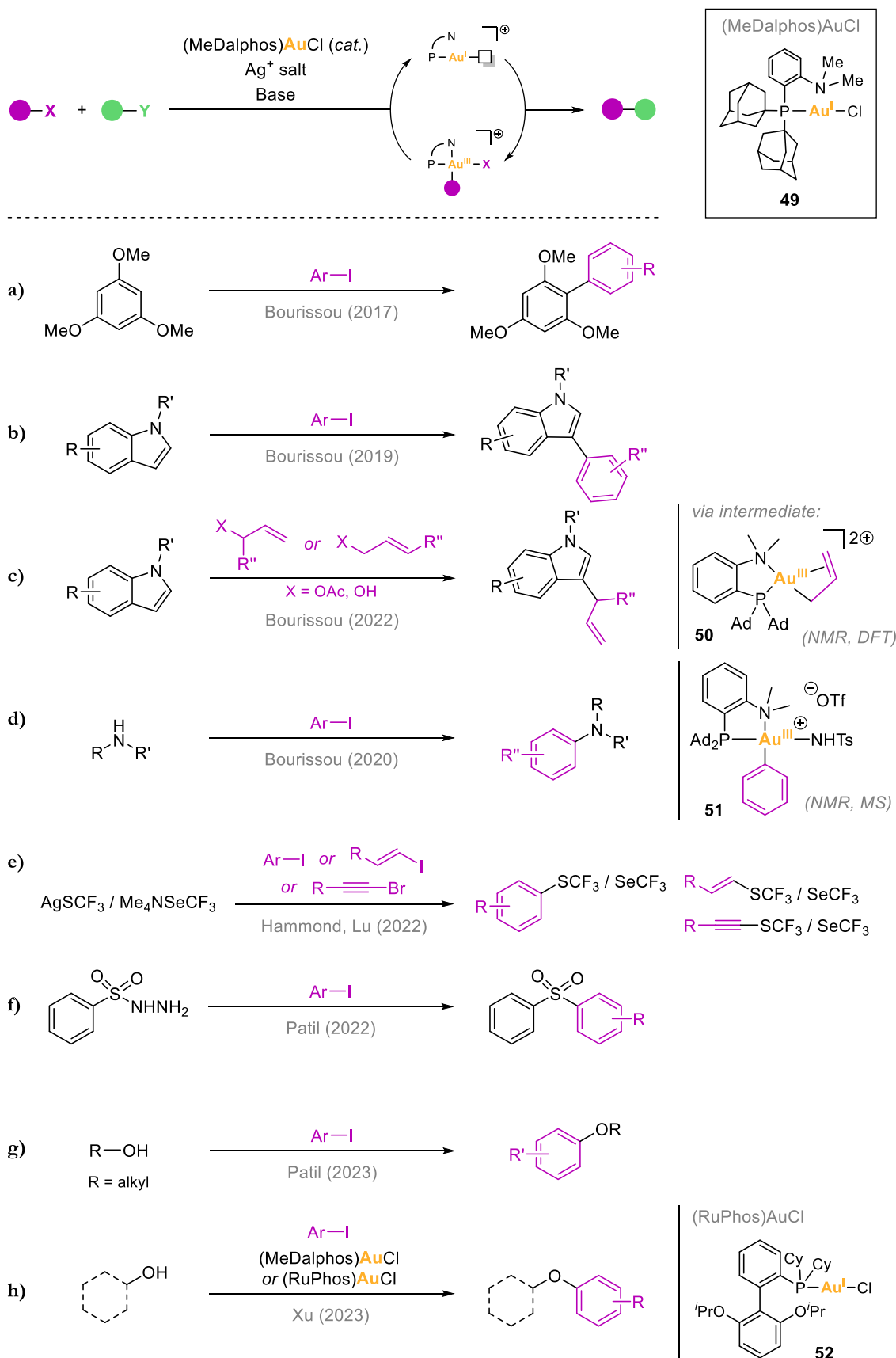


Scheme I.14. Substrate chelation-enabled oxidant-free Au(I)/Au(III)-catalyzed halide exchange, C(sp²)-N, and C(sp²)-O cross-coupling transformations reported by Ribas.

On the other hand, when ligands bear a hemilabile directing group, functionalizing the substrates with coordinating moieties is no longer required. Bidentate ligands are the most suitable platforms to design oxidant-free Au(I)/Au(III)-catalyzed cross-coupling reactions because the Au(III) intermediates will have two coordination sites in *cis* occupied by the ligand, and two coordination sites in *trans* intended to allow the cross-coupling reactivity (see Scheme I.13). The most relevant bidentate ligand in oxidant-free Au(I)/Au(III) cross-coupling catalysis is, so far, the so-called MeDalphos ligand **49**, a (P,N) phosphine ligand that has shown to be extraordinarily versatile in terms of allowing a wide array of catalytic transformations.

In 2017, Bourissou and coworkers employed the (P,N) bidentate MeDalphos ligand in homogeneous oxidant-free Au(I)/Au(III) catalysis for the first time (MeDalphos = di(1-adamantyl)-2-dimethylaminophenylphosphine). It allowed the synthesis of biaryls from the cross-coupling of aryl iodides and bromides with electron-rich arenes under mild conditions (Scheme I.15a).¹⁶ The catalytic cycle proceeded following the sequence C(sp²)-X oxidative addition / C(sp²)-H auration / reductive elimination. When (MeDalphos)AuCl was reacted with iodobenzene and a silver salt from -80°C to room temperature, the expected arylgold(III) oxidative addition product was obtained. Thus, the bottleneck oxidative addition step was evidenced, being indeed efficiently promoted by the ligand (see Scheme I.32b). The great performance of MeDalphos at stabilizing Au(III) intermediates paved the way to envision new Au(I)/Au(III) catalytic transformations using the gold(I) complex (MeDalphos)AuCl as catalyst. In this regard, Bourissou and coworkers reported in 2019 the regioselective C3 arylation of indoles, which is rarely observed by means of other transition metal-mediated catalysis. Moreover, it displayed a high functional group toleration at both the iodoarene and indole partners (Scheme I.15b).²⁰¹ Remarkably, three years later they expanded the reactivity of indoles to the coupling with allyl acetates and allyl alcohols. The transformation selectively afforded the branched C3-allylated products from both α - and γ -substituted allyl substrates (Scheme I.15c).²⁰² The C(sp²)-C(sp³) coupling proceeded via a Au(I)/Au(III) cycle involving a dicationic π -allyl Au(III) complex **50** as a key intermediate. In 2020, the same group used the (MeDalphos)AuCl catalyst in C(sp²)-N cross-coupling reactions. They developed a robust and mild methodology for coupling a wide scope of aryl iodides and N-nucleophiles under mild conditions. The reaction mechanism was thoroughly investigated, including the characterization of a key Au(III) intermediate **51** by NMR and MS. (Scheme I.15d).²⁰³ Patil and coworkers also contributed, independently, to the development of C(sp²)-N cross-coupling of aryl iodides with amines by means of MeDalphos-enabled Au(I)/Au(III)

catalysis.²⁰⁴ More recently, in 2022, Hammond and Lu used the MeDalphos ligand in the Au(I)/Au(III)-catalyzed thiolation and selenolation of organohalides. More specifically, they reported the first C–SCF₃ and C–SeCF₃ cross-coupling reactions using (MeDalphos)AuCl as catalyst, AgSCF₃ and Me₄NSeCF₃ as the nucleophilic SCF₃ and SeCF₃ sources, and aryl iodides, vinyl iodides, and alkynyl bromides as substrates (Scheme I.15e).²⁰⁵ Also in 2022, the group of Patil achieved the C(sp²)–S cross-coupling of aryl iodides with arylsulfonyl hydrazides (Scheme I.15f),²⁰⁶ and in 2023, they reported the synthesis of a wide scope of aryl alkyl ethers from the coupling of aryl iodides with aliphatic alcohols (Scheme I.15g).²⁰⁷ Strikingly, a very recent work from Xu’s group reports the C(sp²)–O coupling of (hetero)aryl iodides with primary and secondary alcohols, proceeding in both inter- and intramolecular ways. The reactions were catalyzed by either (MeDalphos)AuCl or (RuPhos)AuCl **52** in an efficient manner, being the first time that RuPhos ligand was applied to gold-catalyzed cross-couplings (Scheme I.15h).²⁰⁸

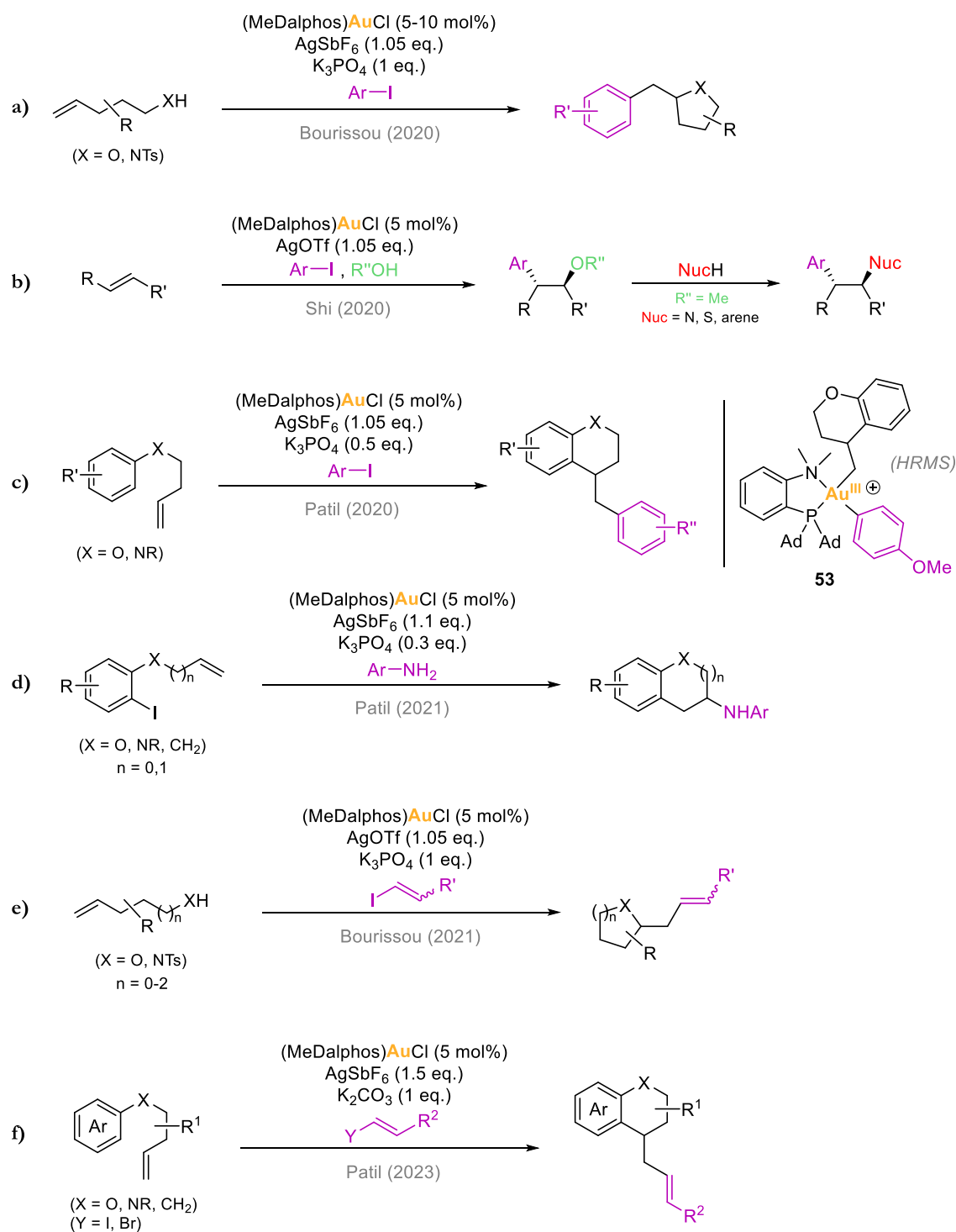


Scheme I.15. MeDalphos-enabled oxidant-free Au(I)/Au(III) cross-coupling catalysis.

Interestingly, the fact that cationic tricoordinate (P[^]N)-chelated gold(I) π -complexes could be obtained from (MeDalphos)AuCl^{209, 210} drove the attention towards the development of catalytic systems for cross-coupling reactions that merge two modes of reactivity of gold complexes: the idiosyncratic redox-neutral carbophilic π -activation of C–C multiple bonds with the two-electron redox chemistry based on oxidative addition / reductive elimination cycles (Scheme I.16).^{211, 212}

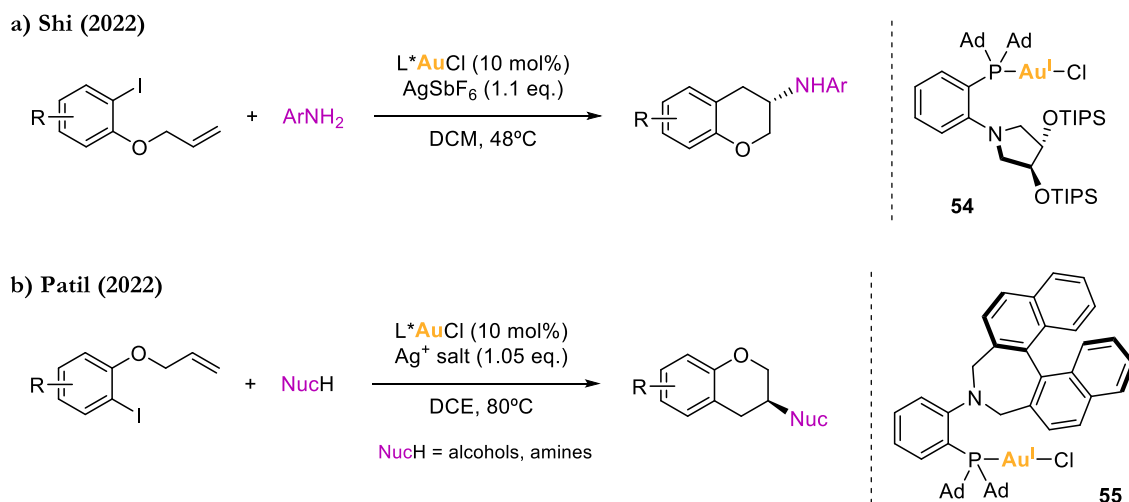
In this line, the group of Bourissou pioneered this new field by reporting in 2020 the oxy- and aminoarylation of alkenols and alkenamines with aryl iodides (Scheme I.16a).²¹³ This work showcased for the first time that (MeDalphos)AuCl could combine oxidative addition of aryl iodides and π -activation of alkenes. These transformations were robust and general, enabling the access to products with 5-, 6- and 7-membered rings, and were more efficient with electron-rich aryl substrates. Likewise, the group of Patil also employed the MeDalphos ligand to synthesize 1,2-oxy- and 1,2-aminoarylation products from the coupling of aryl iodides with alkenols and alkenamines.²¹⁴ Additionally, in the case of oxyarylations, two- and three-component reactions were reported, whereas aminoarylations were only carried out as two-component reactions. Simultaneously, the group of Shi also worked with the intermolecular three-component oxyarylation of alkenes. Interestingly, the products obtained upon the addition of methoxide could be further reacted converting the methoxy groups into other nucleophiles allowing the formation of C–N, C–S, and C–C bonds (Scheme I.16b).²¹⁵ In another work, Patil and coworkers disclosed the first ligand-enabled Au(I)/Au(III)-catalyzed 1,2-diarylation of alkenes by merging the oxidative addition of aryl iodides to Au(I) with π -activation of alkenes, reacting aryl iodides with arenes bearing an olefinic moiety (Scheme I.16c).²¹⁶ The mechanism was proposed to involve an aromatic electrophilic substitution (S_EAr) step for the carboauration of alkenes. The resulting Au(III)-aryl-alkyl intermediate **53** could be detected by means of mass spectrometry. Notably, the selective reactivity disclosed in this work avoids the formation of undesired Ar–Ar' and Heck-type byproducts observed in other transition metal catalysis. In 2021, the same group demonstrated that 1,2-aminoarylations of olefins also proceeded by reacting alkenes tethered to aryl iodide moieties with external amines (Scheme I.16d).²¹⁷ In parallel, the group of Bourissou validated the oxidative addition of vinyl and alkynyl iodides to (MeDalphos)AuCl (see Scheme I.32b).²¹⁸ So, they took advantage of such transformation to expand the applicability of the MeDalphos ligand in oxidant-free Au(I)/Au(III) cross-coupling catalysis, accessing oxy- and amino-vinylations by reacting alkenols and N-tosyl alkenamines with vinyl iodides (Scheme I.16e).²¹⁸ Very recently, Patil and coworkers used the MeDalphos system to

achieve the first ligand-enabled Au(I)/Au(III)-catalyzed aryl-alkenylation of unactivated alkenes with alkenyl iodides and bromides (Scheme I.16f).²¹⁹ Detailed mechanistic investigations concluded that a π -activation pathway was involved rather than a migratory insertion pathway.



Scheme I.16. MeDalphos-enabled oxidant-free Au(I)/Au(III) cross-coupling catalysis merging oxidative addition and π -alkene activation.

Undeniably, the design of MeDalphos is the key that unlocked the access to successful oxidant-free Au(I)/Au(III)-catalyzed cross-coupling reactions. Indeed, the gold(I) complex (MeDalphos)AuCl tolerates a broad scope of transformations exhibiting a great performance as catalyst. Based on this principle, attempts to render enantioselective ligand-enabled Au(I)/Au(III) catalysis have been made recently (Scheme I.17).²²⁰ In 2022, over a four-day period, the groups of Shi and Patil independently reported on the design of novel chiral hemilabile (P,N) phosphine ligands (see complexes **54** and **55**) for the enantioselective 1,2-difunctionalization of alkenes tethered to aryl iodide moieties, in an oxidant-free Au(I)/Au(III) catalytic regime. Whereas Shi and coworkers studied the enantioselective aminoarylation of alkenes (Scheme I.17a),²²¹ Patil and coworkers studied both the enantioselective oxyarylation and aminoarylation of alkenes (Scheme I.17b).²²²



Scheme I.17. Enantioselective oxidant-free Au(I)/Au(III)-catalyzed aminoarylation and oxyarylation reactions of alkenes, achieved with chiral hemilabile (P,N) ligands.

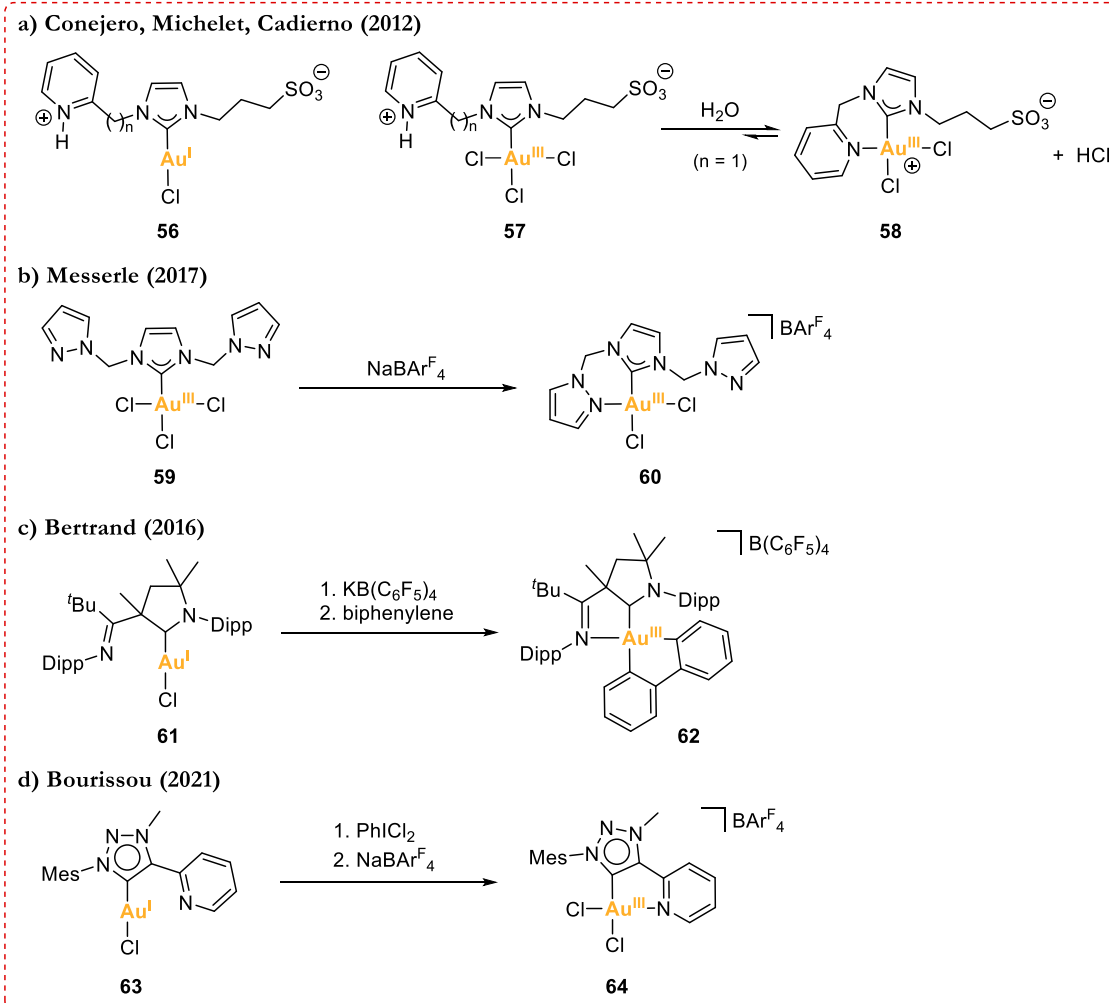
More recently, Patil and coworkers have reported an outstanding work on a ligand-enabled Au(I)/Au(III)-catalyzed Heck reaction (see Section I.4.4, Scheme I.44c). By employing (MeDalphos)AuCl as catalyst, they coupled aryl iodides with terminal alkenes offering a complementary regioselectivity compared to other transition metal catalysis, and, advantageously, mixtures of regioisomeric products were avoided as chain-walking processes did not take place.²²³ Remarkably, this work is the first one in which migratory insertion (Section I.4.4) and β -hydride elimination (Section I.4.5) steps are validated in Au(I)/Au(III) catalysis.

Besides the use of hemilabile (P,N) ligands to access ligand-enabled Au(I)/Au(III) cross-coupling catalysis, less common is the use of other type of ligands such as hemilabile (N,C) and (C,O) ligands. Nevertheless, and despite examples of (C,O) ligands are really scanty,²²⁴ the use of (N,C) ligands is flourishing.

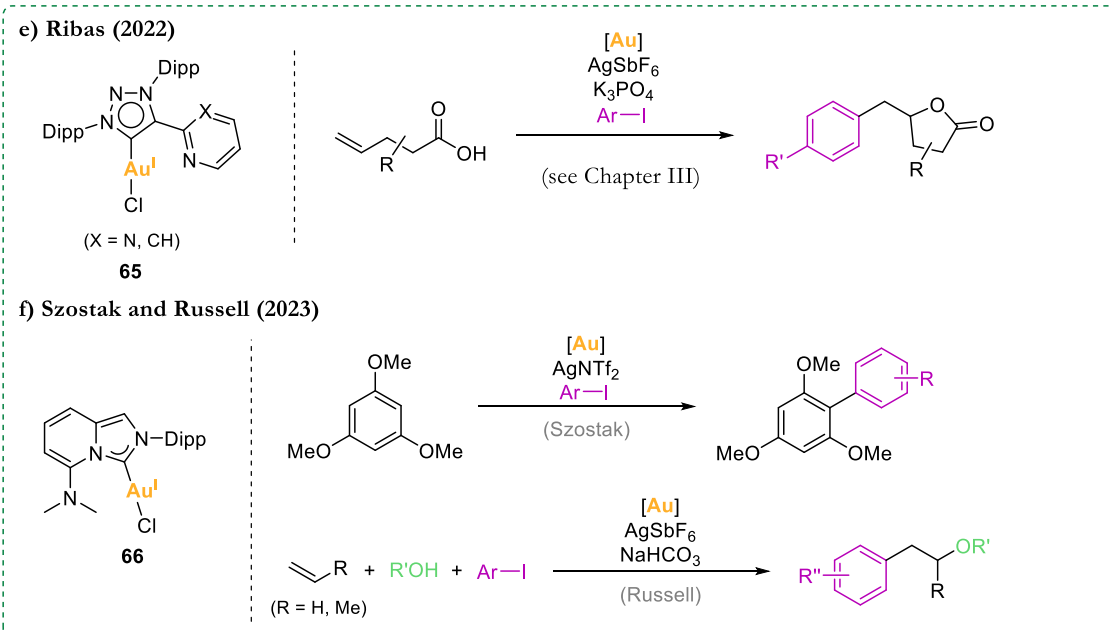
In 2012 and 2013, Conejero, Michelet and Cadierno reported water-soluble gold(I) **56** and gold(III) **57** complexes with N-heterocyclic carbene (NHC) ligands bearing a pendant hemilabile pyridine that proved to be suitable catalysts for the cycloisomerization of γ -alkynoic acids into enol-lactones (Scheme I.18a).^{225, 226} Therefore, the application of these Au(I) and Au(III) complexes in catalysis relied on the carbophilicity of gold towards alkynes. In aqueous media, the Au(III) complexes were found in equilibrium between [(NHC)AuCl₂] species **57** and [(NHC[^]N)AuCl₂] species **58**, proving that the pyridine moiety was indeed hemilabile, as confirmed by X-ray diffraction analysis of (C[^]N) chelated Au(III) complexes. Although it is important to test the ability of the ligand to chelate gold(III) centers in order to design ligand-enabled two-electron redox Au(I)/Au(III) catalytic cycles, the authors did not explore such reactivity. In fact, it is not surprising because the first studies on oxidative addition at gold and on oxidant-free Au(I)/Au(III) catalysis did not appear until 2014. Similarly, Messerle and coworkers reported in 2017 the dihydroalkoxylation and hydroamination of alkynes catalyzed by a Au(III) complex **59** bearing a NHC ligand with two pendant pyrazole arms (Scheme I.18b).²²⁷ Despite observing the coordination of the pyrazole moieties upon chloride abstraction, the catalysis also relied on the carbophilic activation of alkynes. On the other hand, a remarkable study on hemilabile cyclic (alkyl)(amino)carbene ligands (CAACs) and the ability of a (CAAC)gold(I) complex **61** to undergo oxidative addition of biphenylene was reported by Bertrand and coworkers in 2016.²²⁸ The carbene ligand had a hemilabile imine group that coordinated to the Au(III) center upon oxidative addition of biphenylene (Scheme I.18c, also see Scheme I.32a). Although this chelation-assisted oxidative addition is a crucial step to build up ligand-enabled Au(I)/Au(III) catalytic cycles, the authors only explored the catalytic activity of the (CAAC)gold(I) complex in the hydroarylation of olefins, a transformation that, again, relies on the Lewis acidity of gold to activate π -C=C bonds. In 2021, Bourissou and coworkers studied the reactivity of a gold(I) complex **63** with a mesoionic carbene ligand (MIC) bearing a pendant pyridine group (Scheme I.18d).²²⁹ The (MIC)gold(I) complex did not undergo oxidative addition towards iodobenzene, precluding its exploitation in oxidant-free Au(I)/Au(III) catalysis. However, a (MIC[^]N)Au(III) chelate complex **64** was obtained by reacting the (MIC)gold(I) complex **63** with an external oxidant and a halide scavenger to

abstract one chloride ligand. This demonstrated that the design of the ligand could potentially be a suitable platform for ligand-enabled oxidant-free Au(I)/Au(III) catalysis. Nevertheless, the group of Ribas independently reported in 2022 a related work in which, by employing a similar hemilabile MIC ligand with a pendant pyridine or pyrimidine group, the (MIC)gold(I) complexes **65** were engaged in oxidative addition and in oxidant-free two-electron Au(I)/Au(III) catalytic cycles for the catalytic arylation-lactonization of γ -alkenoic acids (Scheme I.18e).²³⁰ This study is part of the experimental work of this thesis, it is presented in Chapter III and discussed in Section V.1. Very recently, Szostak's group designed a rigid NHC ligand with a hemilabile amino group that allowed the oxidative addition of biphenylene at the (NHC)gold(I) complex **66**, affording the (N,C)Au(III) chelate complex (see **146** in Scheme I.32c). Moreover, the NHC–Au(I) complex **66** catalyzed efficiently the arylation of electron-rich arenes with aryl halides under mild conditions (Scheme I.18f).²³¹ Independently, the group of Russell also designed complex **66** to substantiate the oxidative addition of aryl iodides (see **147** in Scheme I.32c) and to use it as catalyst in the 1,2-oxyarylation of alkenes (Scheme I.18f).²³² The conformational lock of the ligand plays a key role in these transformations, as it prevents nitrogen from rotation and renders the pendant N atom at the closest position to gold, thus maximizing the stabilization of gold(III) centers. The design of this ligand resembles that of the MeDalphos ligand, allowing the reactivity to be transferred from (P,C) to (N,C) platforms. Definitely, (N,C)-ligand-enabled oxidant-free Au(I)/Au(III) catalysis surely is a burgeoning field within gold-catalyzed cross-coupling catalysis.

Gold complexes not engaging in hemilabile (N,C) ligand-enabled oxidant-free Au(I)/Au(III) catalysis



Gold complexes engaging in hemilabile (N,C) ligand-enabled oxidant-free Au(I)/Au(III) catalysis



Scheme I.18. Gold complexes with hemilabile (N,C) ligands engaging and not engaging in ligand-enabled oxidant-free Au(I)/Au(III) cross-coupling catalysis.

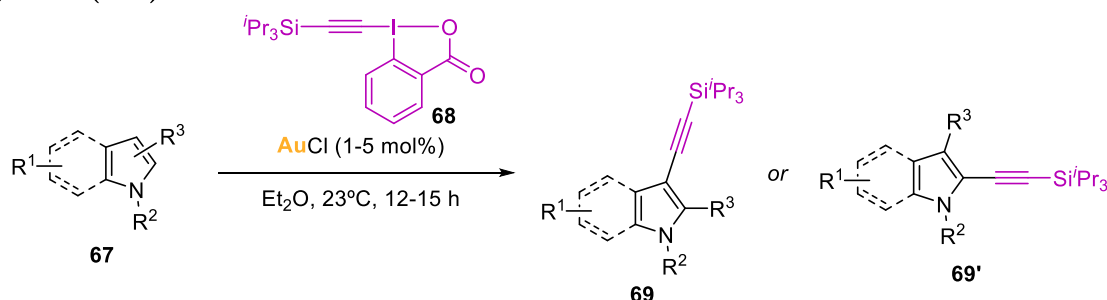
1.3.3.2. Coupling partners with dual role

Ethynylbenziodoxolone (EBX) reagents, which can be regarded as electrophilic alkyne surrogates, have been used as reagents that play a dual role as coupling partners and oxidants. Therefore, these iodine(III) compounds are an improvement over the use of external sacrificial oxidants such as Selectfluor or other hypervalent iodine (I^{3+}) compounds, as revised in section 1.3.2. In 2009, Waser and coworkers reported the regioselective alkylation of indoles and pyrroles **67**, using AuCl (5 mol%) and a EBX reagent **68**, in excellent yields under ambient conditions, proposing a Au(I)/Au(III) catalytic cycle (Scheme I.19a).²³³ In 2012, the same group improved the methodology for the gold-catalyzed direct alkylation of heterocycles, including thiophenes, by using modified EBX reagents²³⁴ and, one year later, they reported the domino cyclization/alkylation reaction of allenic ketones **70** with EBXs to afford C3-alkylated furans **71**, using a Au(III) catalyst (Scheme I.19b).²³⁵ Computational studies on the mechanism of this domino reaction revealed that the Au(III) catalyst was the precursor of the active Au(I) catalyst that initiates the Au(I)/Au(III) catalytic cycle.²³⁶ In 2017, Patil and coworkers reported the gold-catalyzed C(sp)-C(sp) alkylation of terminal alkynes **72** with EBXs to access unsymmetric 1,3-diynes **73**. They used Ph₃PAuCl as catalyst and catalytic amount of 1,10-phenanthroline as auxiliary ligand. (Scheme I.19c).²³⁷ Likewise, the group of Liu also used alkynyl hypervalent iodine reagents in the coupling with terminal alkynes for the synthesis of unsymmetrical 1,3-diynes.²³⁸

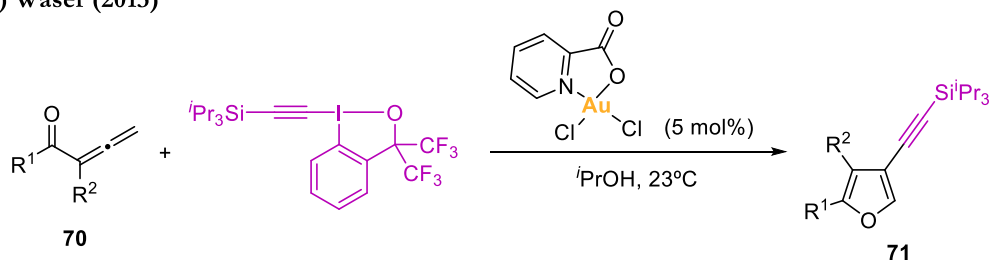
The use of diazonium salts, which also act dually as coupling partners and as oxidizing equivalents, has as well led to a wide scope of oxidant-free gold redox coupling catalysis. For instance, in 2015 Chen and Shi reported the C(sp)-C(sp²) and C(sp²)-C(sp²) cross-coupling of aryldiazonium salts with terminal alkynes or arylboronic acids. The addition of a bipyridine auxiliary ligand was key to assist nitrogen extrusion and coordinate the Au(III) intermediate species.²³⁹ In 2016, the same group reported the gold-catalyzed C-Br, C-S and C-P Sandmeyer couplings between aryldiazonium salts and the corresponding nucleophiles.²⁴⁰ Crucial to the success of this transformation was the nucleophile-assisted activation of aryldiazonium salts, which were then added to Au(I) to access Au(III) intermediates. In 2017, Shi and coworkers reported the Lewis base-assisted diazonium activation as a strategy to access gold oxidation and build a Au(I)/Au(III) catalytic cycle for the intramolecular oxy- and aminoarylation of alkenes, the arylation ring expansion of alkenes, the oxy- and aminoarylation of allenes, and the propargyl ester rearrangement of alkynes.²⁴¹ Additionally, in 2018 the group of Dughera reported the gold-catalyzed Heck and Suzuki couplings using arenediazonium *o*-benzenedisulfonimides as electrophilic coupling partners.²⁴² They

proposed a Au(I)/Au(III) catalytic cycle that did not require the presence of external oxidants since the *o*-benzenedisulfonimide anion was suggested to act as an electron transfer agent that promoted the gold oxidation via a radical pathway. Intriguingly, in 2018, Patil and coworkers reacted aryldiazonium salts with diverse organostannanes towards the formation of biaryls, vinyl arenes and arylacetylenes via Au(I)/Au(III) cross-coupling under mild conditions.²⁴³ In the same year, the group of Porcel showed that alkynoic acids could undergo arylative cyclization with arenediazonium salts, promoted by gold, to furnish ring enol lactones. The reaction was thermally induced, it could proceed in the absence of light, and mechanistic studies suggested the involvement of aryl radicals and arylgold(III) intermediates.²⁴⁴ In 2019, Shi and coworkers reported the cyclization-arylation of allylic oximes to access aryl functionalized 2-isoxazolines in good yields.²⁴⁵ The reaction occurred via chemical activation of the diazonium salt; the use of Li₂CO₃ as a base assisted the N₂ extrusion to promote the oxidation of Au(I) to Au(III) aryl species while slowing down the aryl radical generation, which otherwise would decompose the oxime substrate.

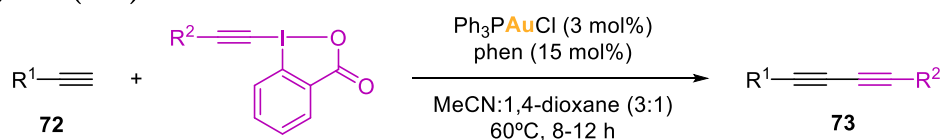
a) Waser (2009)



b) Waser (2013)



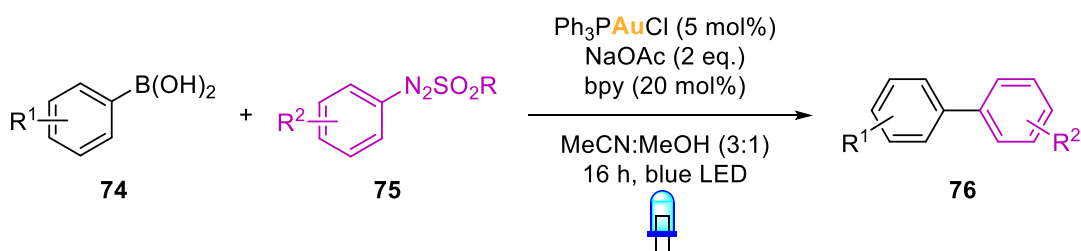
c) Patil (2017)



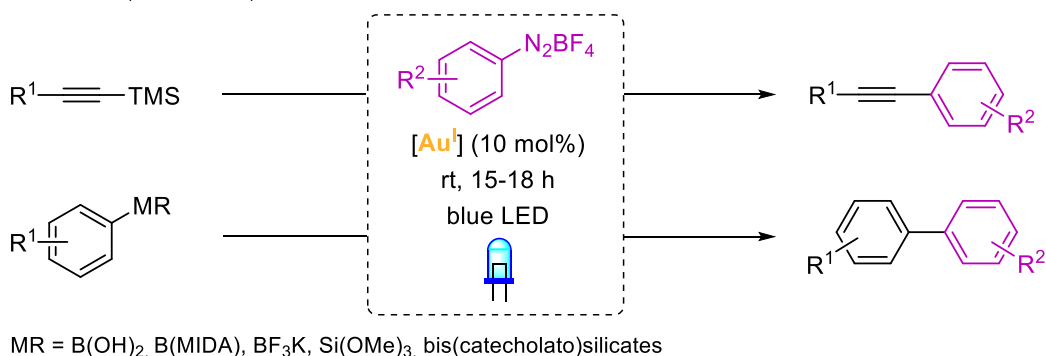
Scheme I.19. Selected examples of the use of EBX reagents as both coupling partners and oxidizing equivalents in Au(I)/Au(III) alkylation couplings.

Light irradiation, however, has proved useful to promote the activation of aryldiazonium salts, which can then add to Au(I) giving access to Au(I)/Au(III) catalytic cycles. Several groups have worked on the synthesis of (hetero)biaryls **76** by means of photosensitizer-free light-induced gold redox catalysis, such as Bandini, who worked on the Suzuki coupling of arylboronic acids **74** with arylazosulfones **75** (Scheme I.20a),²⁴⁶ or Hashmi, who worked on the coupling of aryldiazonium salts with organoboron and organosilicon reagents (Scheme I.20b).²⁴⁷⁻²⁴⁹ In 2016, Hashmi and coworkers reported the visible-light-mediated gold-catalyzed intermolecular 1,2-difunctionalization of alkynes with aryldiazonium salts in methanol to afford α -aryl ketones.⁶⁷ In 2017, the group of Wong reported the light-mediated gold-catalyzed *cis*-difunctionalization of silyl-substituted alkynes with quinoline-substituted aryldiazonium salts in high chemo- and regioselectivity.²⁵⁰ In 2020, Feng and coworkers reported the visible-light-promoted Au(I)/Au(III) catalysis for the regio- and stereoselective fluoroarylation of allenic esters **77**, using an aryldiazonium salt **78**, Et₃N·3HF as the fluorinating agent and Ph₃PAuCl as the catalyst (Scheme I.20c).²⁵¹

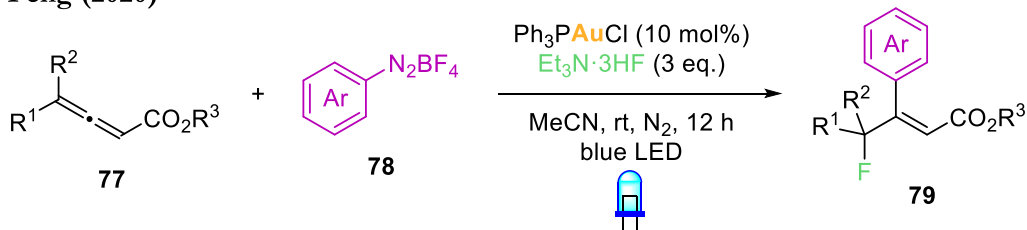
a) Bandini (2017)



b) Hashmi (2017-2018)



c) Feng (2020)

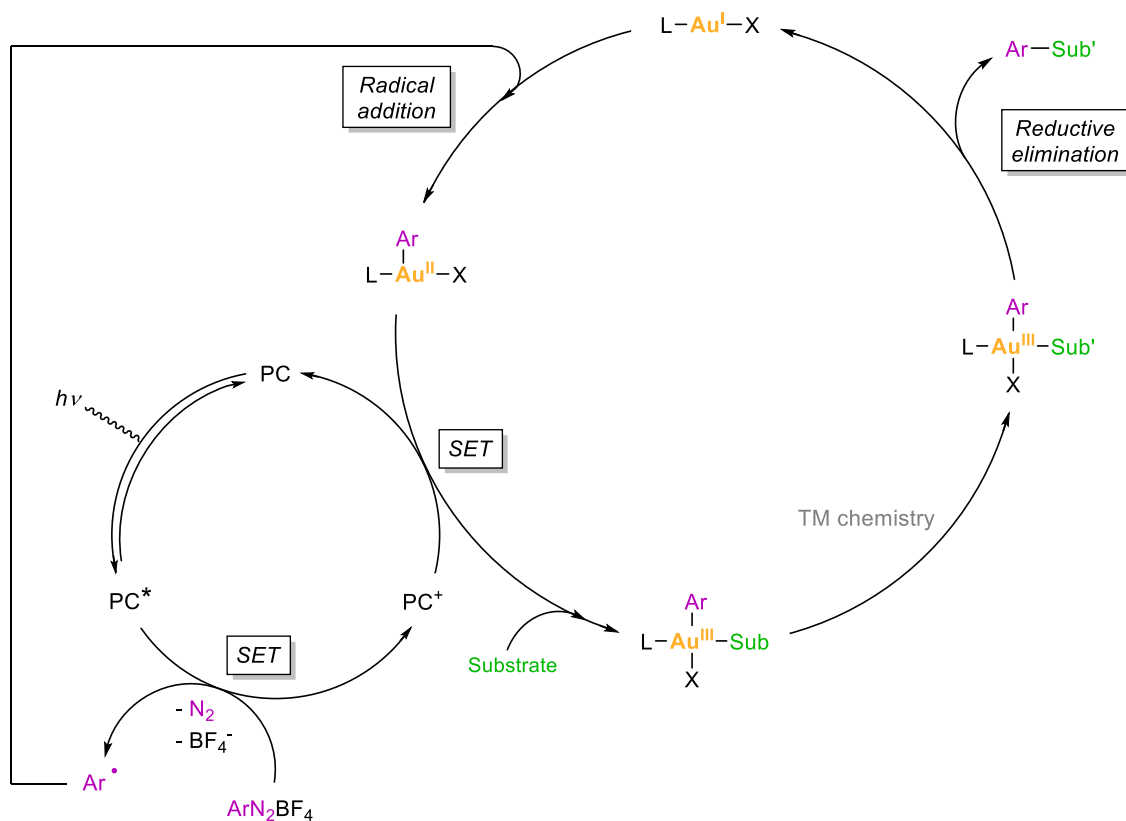


Scheme I.20. Oxidant-free and photosensitizer-free Au(I)/Au(III)-catalyzed cross-coupling reactions using aryldiazonium salts as coupling partners, under light irradiation.

I.3.3.3. Dual gold photoredox catalysis for cross-coupling reactions

Besides the abovementioned examples of photosensitizer-free Au(I)/Au(III)-catalyzed couplings of aryldiazonium salts occurring via chemical activation or light-assisted activation of the diazonium salts, many recent studies have focused on merging the burgeoning fields of visible-light photoredox catalysis and gold catalysis for driving selective organic transformations under mild conditions.^{68, 99, 252-254} The combination of homogeneous gold catalysis and photoredox catalysis consists, generally, of a ruthenium or iridium photocatalyst (PC) that, once excited by light irradiation (PC*), generates an organic radical (generally an aryl radical from aryldiazonium salts) via single electron transfer (SET) while getting itself oxidized (PC⁺). The organic radical can add to Au(I) to give a transient gold(II) species, which subsequently undergoes oxidation to Au(III) while regenerating the ground-state

photocatalyst (PC) via single electron transfer. Then, the substrate coordinates the Au(III) species, the Au(III) intermediate can undergo organometallic reactivity (π -activation and nucleophilic addition, cyclization, ring expansion, transmetalation, etc.) and finally, reductive elimination from Au(III) affords the coupling product and regenerates the Au(I) catalyst (Scheme I.21).

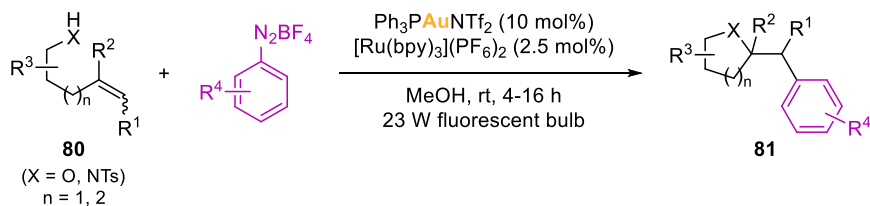


Scheme I.21. General mechanism of dual gold photoredox cross-coupling catalysis using aryl diazonium salts of the type ArN_2BF_4 . (Sub = substrate; Sub' = modified substrate, if modified, after Au(III)-mediated organometallic steps).

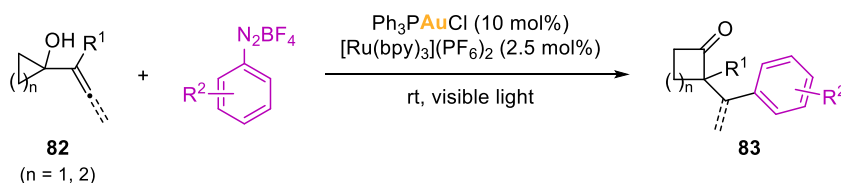
The pioneering examples of works that combined gold catalysis and photocatalysis emerged in 2013. Glorius and coworkers reported for the first time a dual gold photoredox catalytic system for the intramolecular oxy- and aminoarylation of alkenes **80** with aryl diazonium salts, at room temperature under the irradiation of a fluorescent light bulb, with the assistance of $[\text{Ru}(\text{bpy})_3](\text{PF}_6)_2$ as photocatalyst (Scheme I.22a).⁶² One year later, they underwent the oxyarylation of alkenes in an intermolecular three-component fashion. Interestingly, both aryl diazonium salts and diaryliodonium compounds could be employed as the source of the arene coupling partner.²⁵⁵ In 2014, Frei and Toste developed the arylation ring expansion of allenyl and alkenyl cycloalkanols **82** by coupling them with aryl diazonium salts at room

temperature, affording cyclic ketone products **83** (Scheme I.22b).⁶³ Mechanistic studies let the authors propose that an electrophilic Au(III)–aryl intermediate reacted towards the π -bonds of the substrates to undergo a ring expansion followed by a reductive elimination. Toste and coworkers, one year later, used a dual gold photoredox catalytic system for the C(sp²)–P coupling between aryldiazonium salts and H-phosphonates **84** under visible light irradiation at room temperature (Scheme I.22c).²⁵⁶ In addition, in 2016 Glorius and coworkers developed the arylation of terminal alkynes **86** using aryldiazonium salts. The reaction was mediated by visible light from a household bulb or sunlight at room temperature and was run in the absence of base. This work stands as the first example of achieving C–H activation by means of dual gold photoredox catalysis (Scheme I.22d).⁶⁶ Also, the group of Lee pioneered in reporting the first aryl-aryl cross-coupling of aryldiazonium salts with arenes via direct C–H activation in a dual gold photoredox catalytic fashion, under blue LED light irradiation.²⁵⁷ In 2016, independent groups reported tandem Meyer-Schuster/arylation reactions for the synthesis of α -arylated enones, under dual gold photoredox catalysis.^{258–260} The following year, a novel dual gold/photoredox-catalyzed enantioselective domino bis-arylation cyclization of chiral homopropargyl sulfonamides with aryldiazonium salts was reported by Ye and coworkers.²⁶¹ The reaction afforded highly functionalized 2,3-dihydropyrroles in good yields, under mild conditions and white LED irradiation, using Ph₃PAuCl as catalyst and [Ru(bpy)₃](PF₆)₂ as photocatalyst. Interestingly, Breher and coworkers recently developed novel heterobimetallic Au(I)/Ru(II) complexes **90** to be applied as catalysts in dual gold photoredox C(sp²)–P cross-coupling, under mild conditions, showing that the dinuclear complexes could outperform their monometallic counterparts. The heterobimetallic complexes **90** had the general formula *syn*- and *anti*-[AuCl](L1∩L2){Ru(bpy)₂}(PF₆)₂, where the ditopic bridging ligand L1∩L2 is a (P,N) hybrid ligand, and were tested in the P-arylation of H-phosphonates **88** with aryldiazonium salts to afford arylphosphonates **89** (Scheme I.22e).²⁶²

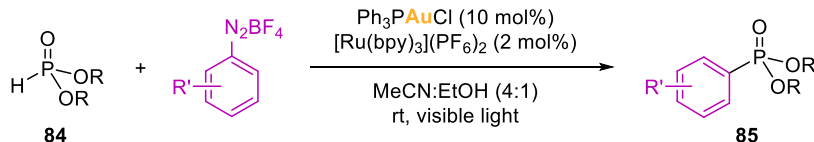
a) Glorius (2013)



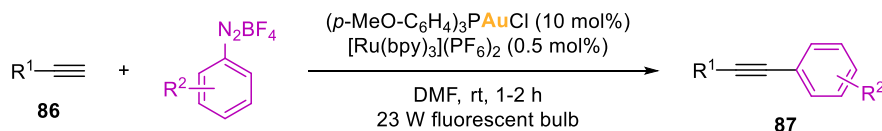
b) Toste (2014)



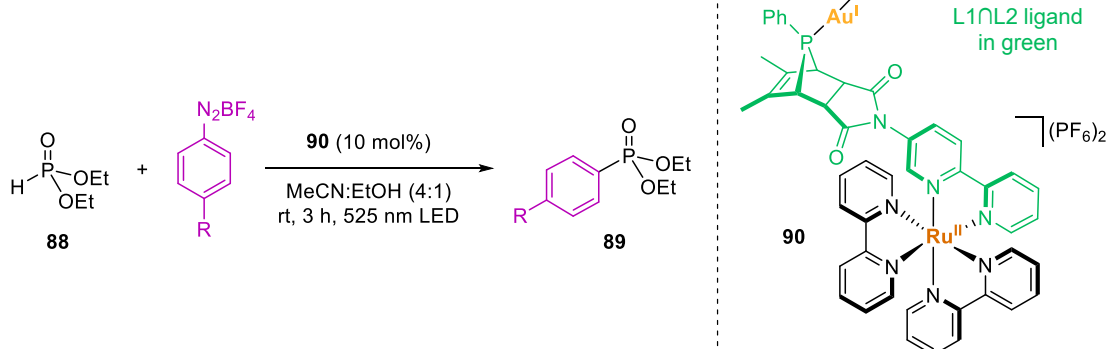
c) Toste (2015)



d) Glorius (2016)



e) Breher (2022)



Scheme I.22. Selected examples of dual gold photoredox catalytic systems using aryldiazonium salts as coupling partners.

The scope of compatible coupling partners in dual gold photoredox catalysis does not only rely on the employment of aryldiazonium salts. For instance, in 2017 the group of Xu aimed to expand the scope by reporting an unprecedented intermolecular thiosulfonylation of alkenes with excellent regio- and diastereoselectivity.²⁶³ They reacted styrenes with $\text{PhS}(\text{O})_2\text{SR}$ reagents, using $[(\text{IPr})\text{AuCl}]$ as catalyst, AgSbF_6 , and $[\text{Ru}(\text{bpy})_3]\text{Cl}_2$ as photocatalyst at room temperature under visible light irradiation. Another example is that reported by

Fensterbank's group in 2019, in which the alkynylative cyclization of *o*-alkynylphenols with iodoalkynes under visible light irradiation to access alkynylbenzofuran derivatives was developed.²⁶⁴ They claimed that the iridium(III) photocatalyst triggered the oxidative addition of the alkynyl iodide coupling partner onto an excited vinylgold(I) intermediate obtained by energy transfer from the excited iridium photocatalyst.

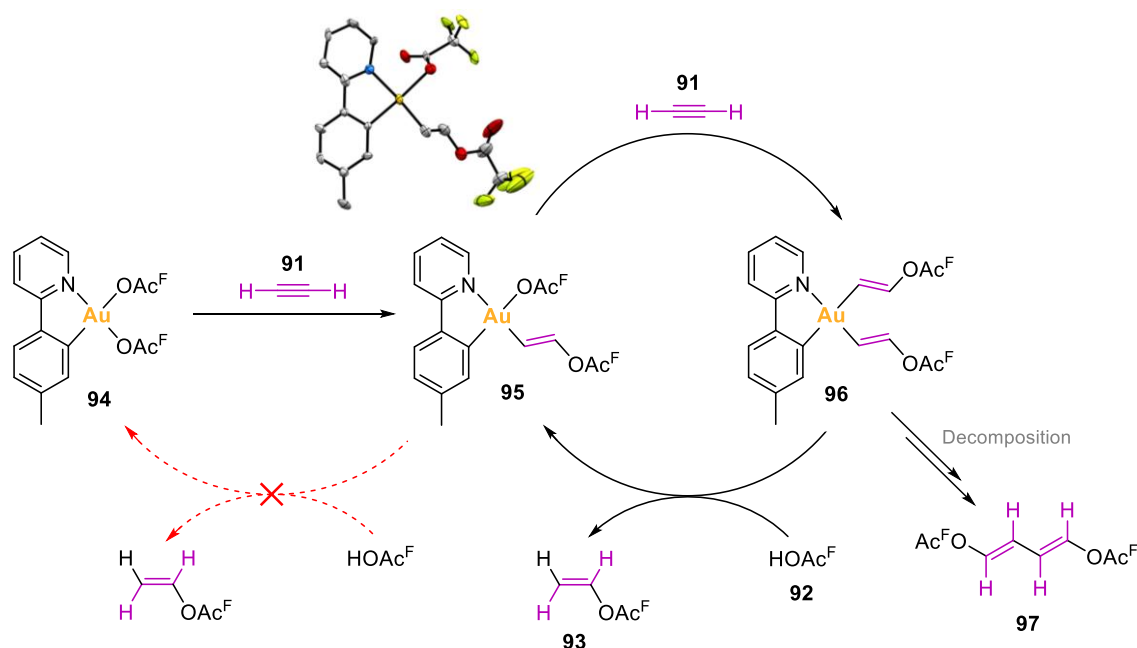
I.3.4. Other gold-based catalytic cycles: Au(III) complexes in catalysis

Gold(III) complexes remain way less developed than gold(I) complexes in catalysis, despite being valuable for the distinct properties and reactivity they offer.^{56, 265} Although several Au(III)-catalyzed transformations have been reported to date, very little is yet known about their reaction mechanisms, and very few Au(III) key intermediates have been substantiated. Experimentally, the subtle balance between stability and reactivity of Au(III) complexes compromises the study of reaction mechanisms. Therefore, N- and C-based cyclometalated ligands are usually employed, and labile ligands or vacant coordination sites at Au(III) most often lead to Au(I) or Au(0) species as a fast reduction decomposition pathway. In this section, selected examples of catalytic cycles using well-defined Au(III) complexes as catalysts will be presented.

In 2015, Toste and coworkers reported the stabilization of the [(IPr)Au(biphenyl)Cl] complex by oxidative addition (see **110** in Scheme I.28).²⁶⁶ Its activity as a hard Lewis-acid catalyst was explored in six different reactions of α,β -unsaturated or $\alpha,\beta,\gamma,\delta$ -diunsaturated aldehydes. Specifically, good yields and excellent selectivities were obtained for the expected products of Mukaiyama-Michael additions, nitronate Michael additions, thiol additions, Hantzsch ester reductions, Diels-Alder reactions and [2+2] cycloadditions. The selectivity obtained in these reactions was believed to be governed by the sterically defined binding pocket of the catalyst.^{266, 267}

On the other hand, Tilset's group has worked with 2-(*p*-tolyl)pyridine (tpy) ligands to synthesize (N,C)-cyclometalated Au(III) complexes. They reported in 2017 the catalytic formation of vinyl trifluoroacetate **93**, via *anti* addition of trifluoroacetic acid **92** to acetylene **91**, when acetylene was bubbled into a solution of [Au(tpy)(OAc^F)₂] **94** in trifluoroacetic acid (Scheme I.23).²⁶⁸ The mechanism of the acetylene trifluoroacetoxylation reaction starts with a first formal acetylene insertion at the site *trans* to tpy-N, forming the active catalyst vinylgold(III) complex **95**. Then, a second insertion of acetylene **91** is required at the site

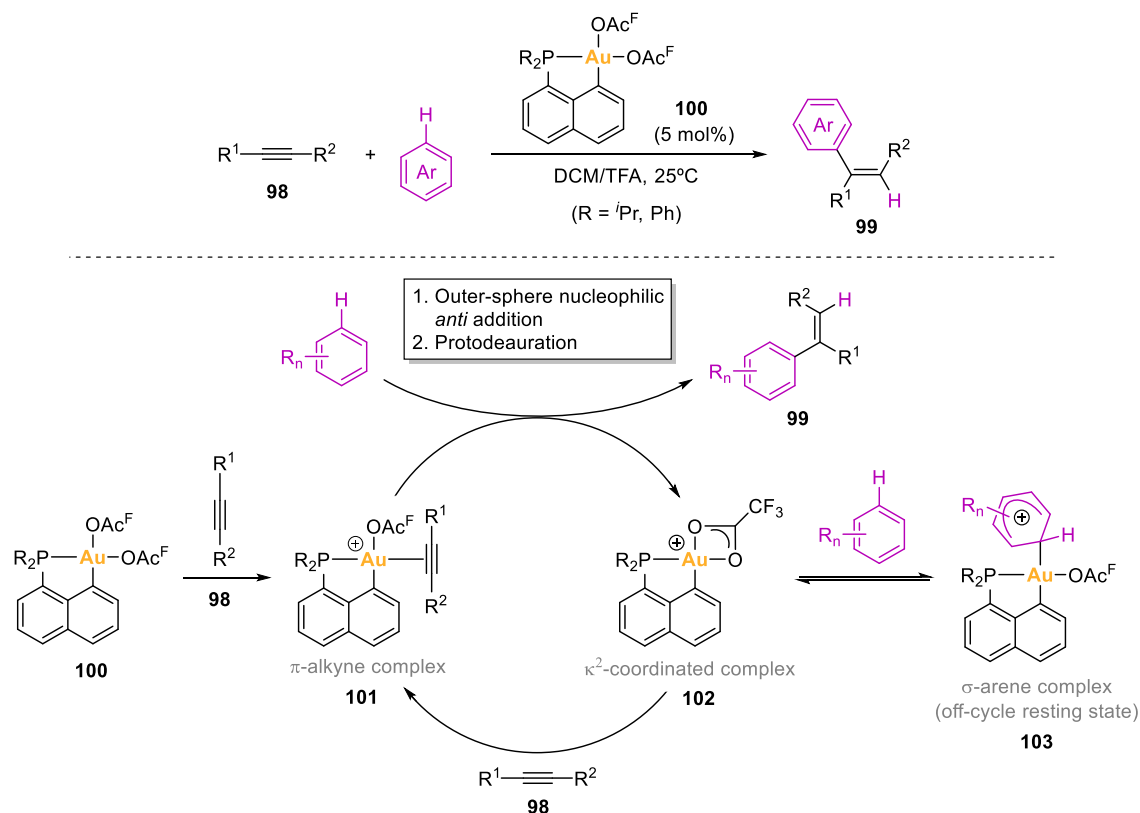
trans to tpy-C for the catalysis to proceed. Although the resulting divinylgold(III) species **96** was not detected, DFT calculations and isotopic labelling experiments supported the double insertion mechanism. In addition, the formation of the (1*E*,3*E*)-1,4-bis(trifluoroacetoxy)-1,3-butadiene byproduct **97** resulting from a catalyst decomposition pathway promoted by a competitive protolytic cleavage of the Au-tpy-C bond also supported the formation of the putative divinylgold(III) intermediate **96**.^{268, 269}



Scheme I.23. Trifluoroacetoxylation of acetylene catalyzed by a (N[^]C)-cyclometalated gold(III) complex.

In 2018, Amgoune, Bourissou and coworkers reported the Au(III)-catalyzed intermolecular hydroarylation of terminal and internal alkynes **98** employing well-defined (P,C)-cyclometalated Au(III) complexes of the type [(P,C)Au(OAc^F)₂] **100** (Scheme I.24).²⁷⁰ The catalytic performance of (P,C)-cyclometalated Au(III) complexes was better than that of (N,C)-cyclometalated Au(III) complexes and gold(III) salts, providing the styrene derivatives **99** in high yields under mild conditions. The mechanism was proposed to proceed following an outer-sphere pathway because the products were stereoselectively obtained from the *trans* addition of the aryl group and the H atom across the triple bond of the alkyne. In 2022, they studied thoroughly the mechanism by means of NMR, MS and DFT, confirming the outer-sphere mechanism but, more importantly, providing spectroscopic evidence of the Au(III) intermediates involved. While the π -alkyne gold(III) species **101** was detected by MS and

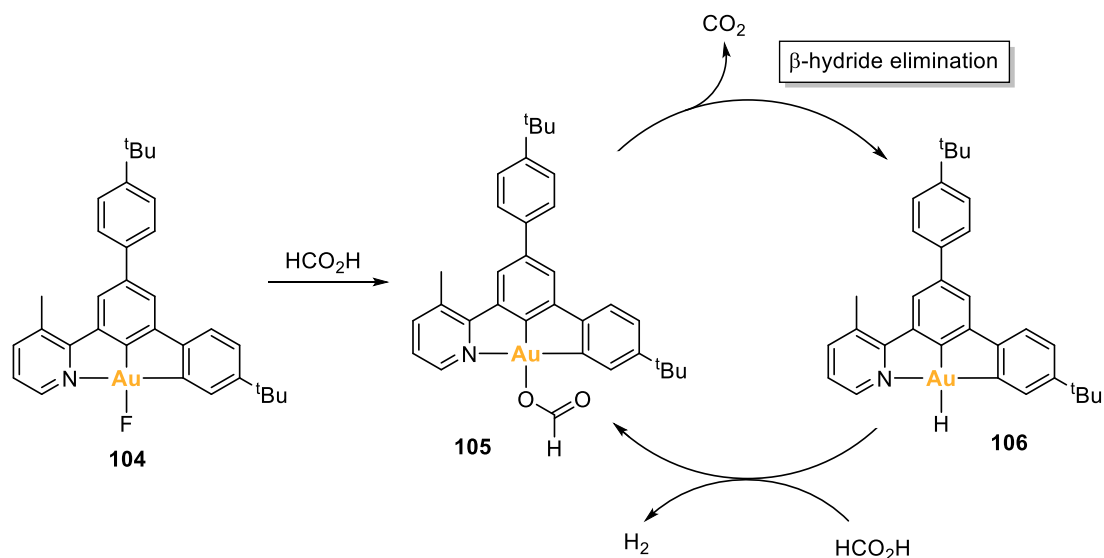
validated by DFT, species **102** and **103** were evidenced by NMR, MS and DFT (Scheme I.24).²⁷¹



Scheme I.24. Hydroarylation of alkynes catalyzed by (P^C)-cyclometalated gold(III) complexes.

Interestingly, Pápai, Fiksdahl, Erdélyi and coworkers also contributed to shed light into Au(III)-mediated transformations with mechanistic understanding based on NMR, XRD and DFT studies. They unveiled the mechanisms of the Au(III)-catalyzed alkoxy cyclization of 1,6-enynes using a gold(III) complex with a bidentate pyridine-oxazoline ligand,²⁷² and of the Au(III)-catalyzed cyclopropanation of styrene with propargyl esters using bis(pyridine)Au(III) complexes.²⁷³

The use of a (N,C,C) pincer ligand was key to stabilize the first Au(III) formate complex **105**, as reported by Nevado's group. When κ^3 -(N^CC)gold(III) complexes **104** or **105** were heated at 100°C in pure formic acid, a linear production of H₂ versus time was obtained. With experimental and DFT studies, the authors could depict a mechanism for the Au(III)-catalyzed dehydrogenation of formic acid; a β -hydride elimination step releases CO₂ from the formate ligand while leading to a (N^CC)-biscyclometalated gold(III) hydride intermediate **106**, which then rapidly reacts with formic acid to release H₂ and regenerate the formate complex **105** thereby closing the catalytic cycle (Scheme I.25).²⁷⁴



Scheme I.25. Dehydrogenation of formic acid catalyzed by a (N[^]C[^]C)-biscyclometalated gold(III) complex.

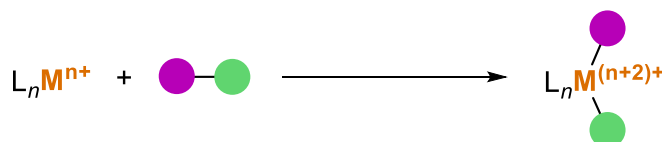
I.4. ELEMENTARY ORGANOMETALLIC REACTIONS AT GOLD

The properties of gold complexes barely mirror those of the other transition metals. This can be rationalized in terms of the relativistic effects governing gold's nature, as discussed in section I.2. Consequently, common elementary organometallic transformations have been much less evident in the case of gold and some of them are notably rare. However, these fundamental organometallic reactions have been studied in the recent years not only to gain deeper insight into the intrinsic behavior of gold, but also to provide useful knowledge for the design and understanding of reaction mechanisms in gold catalysis.^{14, 56, 275} Among them, oxidative addition has been studied with especial emphasis because it is a challenging transformation due to the high redox potential of the Au(I)/Au(III) pair. Furthermore, the substantiation of oxidative addition allowed the development of oxidant-free Au(I)/Au(III) catalysis (section I.3.3).

This section aims to provide a general overview concerning elementary organometallic reactions of gold complexes, focusing the attention on oxidative addition, and discussing more briefly reductive elimination, transmetalation, migratory insertion and β -hydride elimination.

I.4.1. Oxidative addition

Oxidative addition is the elementary organometallic process by which a metal center of a given complex cleaves a bond to form a complex with two additional ligands entailing an increase in the oxidation state of the metal by two units, that is, the metal center is oxidized by two electrons (Scheme I.26).

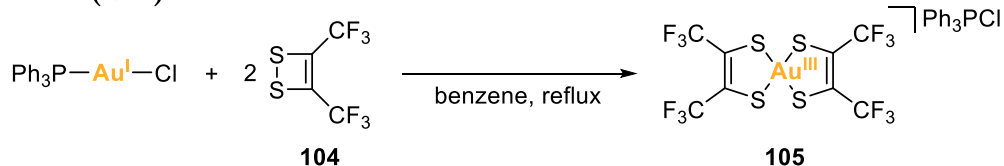


Scheme I.26. General scheme of an oxidative addition process.

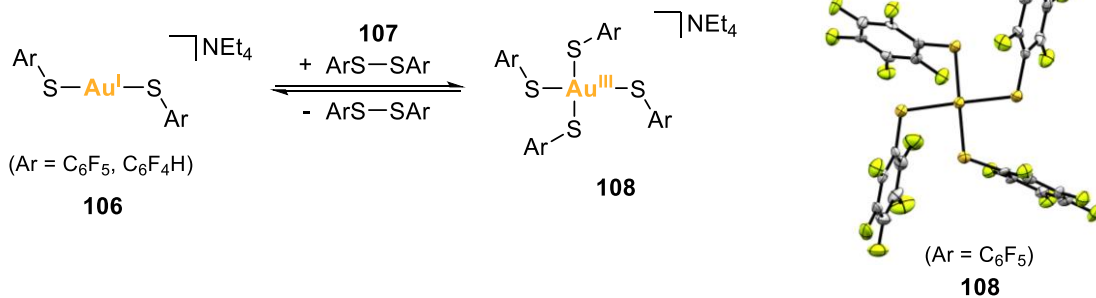
Oxidative addition is a pivotal step in organometallic chemistry as it is usually the entry point to most of homogeneous catalytic transformations operating via two-electron redox cycles, especially cross-coupling reactions. The ability of gold to undergo oxidative addition, in sharp contrast to other transition metals, remained elusive and scarcely investigated for a long time.¹⁶³⁻¹⁶⁵ However, many well-defined Au(III) complexes have been obtained to date via oxidative addition, isolated, and characterized. Strategies like strain release, ligand design and photochemistry have proven helpful in overcoming the high redox potential of the Au(I)/Au(III) pair and trigger the otherwise sluggish oxidative addition to Au(I).

To find the early works on oxidative addition to gold, we must go back to 1967, when Shawl and coworkers reported the reaction between *cis*-bis(trifluoromethyl)-1,2-dithietene **104** and Ph₃PAuCl (Scheme I.27a). A chlorotriphenylphosphonium tetrathiolatoaurate salt **105** was obtained via oxidative addition of two S–S disulfide bonds to Au(I).²⁷⁶ Its molecular structure was elucidated by Ibers soon after in 1968 by means of X-ray crystallography.²⁷⁷ Some independent studies done by Kochi, Puddephatt and Schmidbaur in the early 1970's showed how phosphine gold(I) methyl complexes reacted with methyl iodide to yield ethane and phosphine gold(I) iodide.²⁷⁸⁻²⁸⁰ Further studies on the mechanism revealed the oxidative addition of the C(sp³)–I bond to Au(I) and in certain cases the ensuing Au(III) complexes could be characterized, depending on the phosphine donor ligand.²⁸¹⁻²⁸³ Also, it is worth mentioning the work published in 2008 by Gray's group, where strongly activated disulfides **107** underwent facile and reversible oxidative addition to dithiolate Au(I) complexes **106** (Scheme I.27b).²⁸⁴ Despite these sporadic early studies, the investigations on the field of oxidative addition at gold(I) were not resumed until 2011, and experienced a dramatic growth from then on.

a) Shawl (1967)



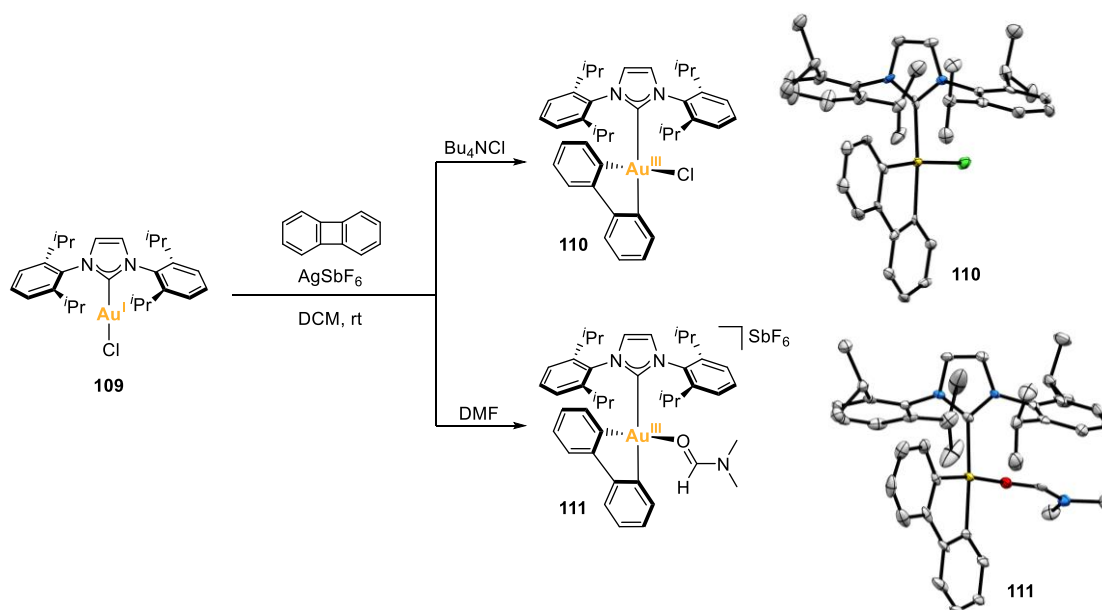
b) Gray (2008)



Scheme I.27. Early examples of oxidative addition of disulfide bonds to Au(I). The NEt₄⁺ cation in the X-ray structure of **108** has been omitted for clarity.

I.4.1.1. Strain release to promote oxidative addition to Au(I)

In 2015, Toste and coworkers reported the intermolecular oxidative addition of the strained C–C bond in biphenylene to the coordinatively unsaturated NHC–Au(I) cationic complex (NHC = IPr) formed upon chloride abstraction of the (IPr)AuCl **109** starting complex using AgSbF₆.^{266,267} The ensuing cationic Au(III) complex was trapped with *n*Bu₄NCl or with DMF to yield the corresponding tetracoordinate [(IPr)Au(biphenyl)Cl] **110** and [(IPr)Au(biphenyl)(DMF)]SbF₆ **111** complexes, which could be characterized by X-ray diffraction (Scheme I.28). This work outstands for being an example on how the oxidative addition of a substrate, biphenylene in this case, is driven by the energy release from a strained covalent bond. In fact, many other examples of oxidative addition of biphenylene to Au(I) complexes were reported in the following years, in combination with other strategies to trigger oxidative addition (see section I.4.1.2).



Scheme I.28. Oxidative addition of the strained C–C bond in biphenylene to a cationic $[(\text{NHC})\text{Au}]^+$ fragment, disclosed by Toste. The SbF_6^- anion in the X-ray structure of **111** has been omitted for clarity.

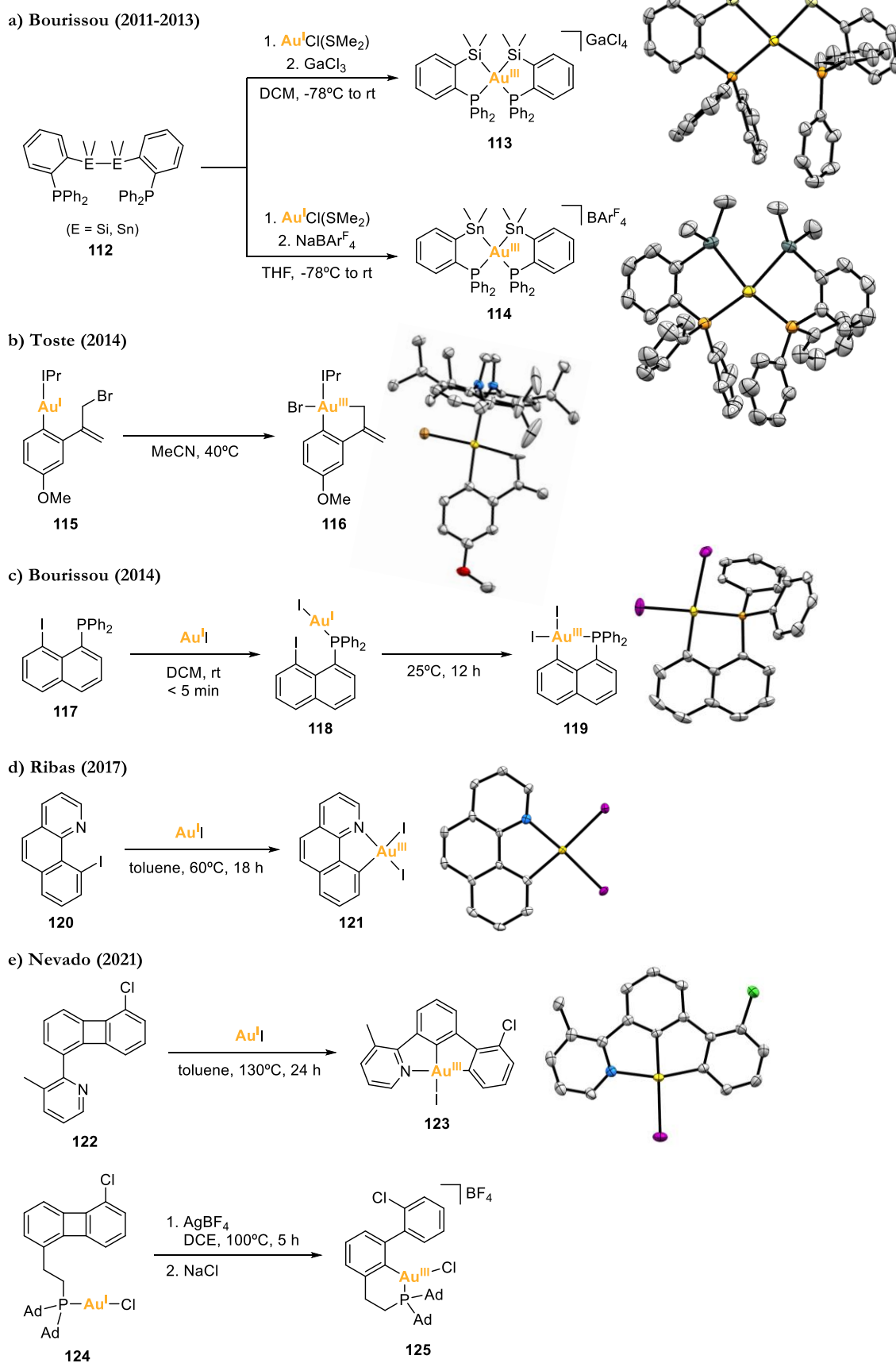
I.4.1.2. Ligand design to promote oxidative addition to Au(I)

On one hand, chelation-assisted strategy has proved fruitful in triggering the oxidative addition to Au(I). The chelation-assisted strategy is based on generating a Au(I) complex that is coordinated to a ligand that bears a functional moiety placed in the right position in close proximity to the metal center to become susceptible to undergo oxidative addition to the Au(I) atom. By means of this strategy, the oxidative addition of E–E apolar σ -bonds (E = Si, Sn) and polarized C–X bonds to Au(I) has been achieved.

From 2011 to 2014, Amgoune, Bourissou and coworkers reported on the spontaneous intramolecular oxidative addition of apolar σ -bonds to Au(I), using diphosphine ligands **112** bearing Si–Si and Sn–Sn bonds (Scheme I.29a).^{285–287} Remarkably, when using the corresponding monophosphine-disilane ligand, the oxidative addition of the σ -Si–Si bond to gold(I) also occurred.²⁸⁷ In all cases, the resulting bis(silyl)- and bis(stannyl)gold(III) complexes **113** and **114** were characterized. Furthermore, the oxidative addition of σ -Si–Si bonds could be expanded to an intermolecular regime by reacting phosphine gold(I) chloride complexes with disilanes in the presence of GaCl_3 at low temperature, as a proof of concept that oxidative addition of the σ -Si–Si bond can take place directly without requiring chelating

assistance. The resulting Au(III) complexes featured an unusual distorted Y shape and were unstable above -60°C or even -80°C depending on the phosphine.²⁸⁸

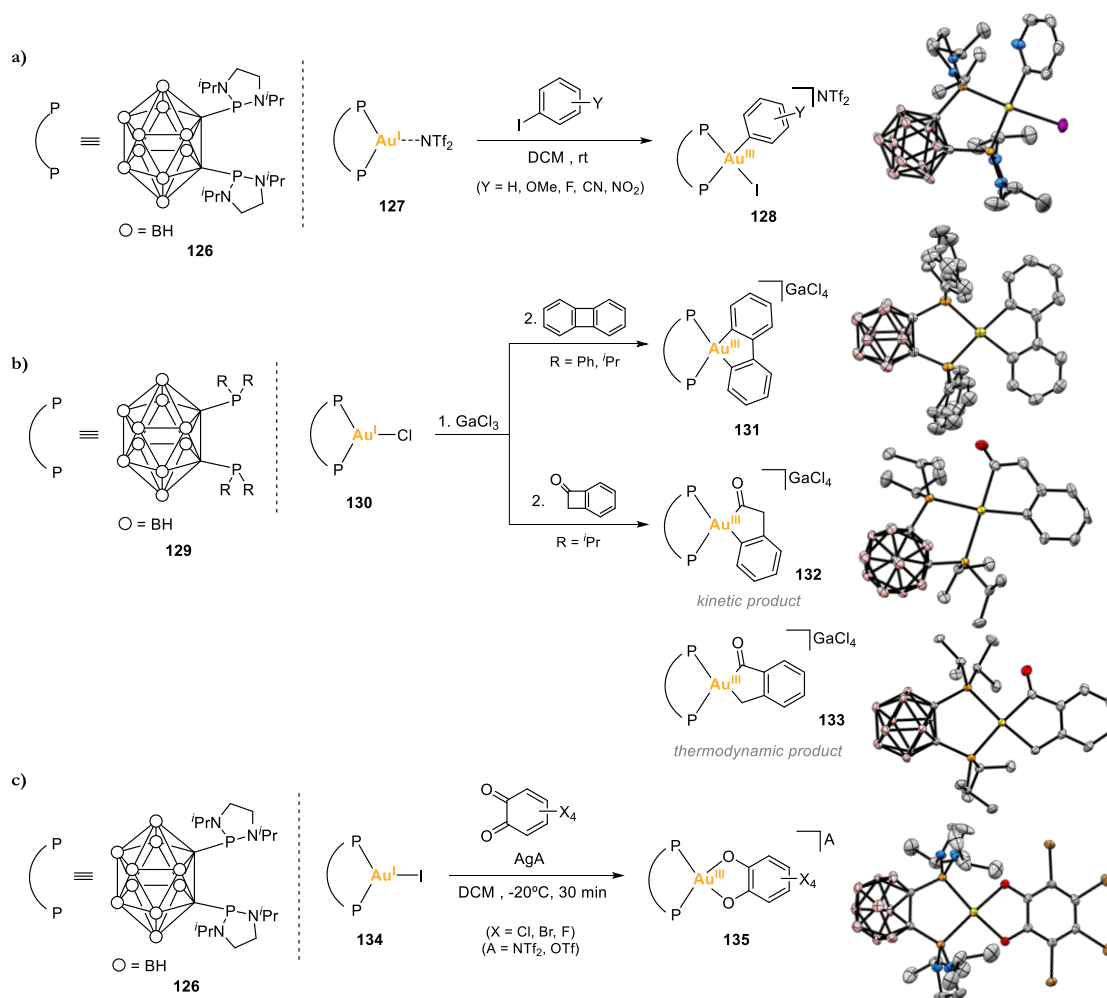
In 2014, the group of Toste designed an arylgold(I) complex **115** with a tethered allyl bromide arm that underwent intramolecular oxidative addition of the $\text{C}(\text{sp}^3)\text{-Br}$ bond to the Au(I) center under mild conditions (Scheme I.29b). The resulting Au(III) complex **116** served as a mechanistic proof for the oxidant-free gold-catalyzed allylation of arylboronic acids presented in the same work (see Scheme I.12).¹⁹⁷ Also in 2014, Amgoune, Bourissou and coworkers reported the intramolecular oxidative addition of $\text{C}(\text{sp}^2)\text{-X}$ bonds ($\text{X} = \text{Br}, \text{I}$) to Au(I). The design of 8-halonaphthyl phosphine ligands **117** suitably places the $\text{C}(\text{sp}^2)\text{-X}$ bond close to the Au(I) atom when it is coordinated to the phosphine moiety (see **118**), inducing the stabilization of the $(\text{P}^{\wedge}\text{C})$ -cyclometalated Au(III) products **119** obtained upon oxidative addition (Scheme I.29c).²⁸⁹ Additionally, the authors also prepared $(\text{P},\text{C},\text{P})$ pincer Au(III) complexes via oxidative addition of a $\text{C}(\text{sp}^2)\text{-Br}$ bond when employing a bromophenyl diphosphine ligand, by means of the same strategy.²⁸⁹ In 2017, Ribas and coworkers generated a $(\text{N}^{\wedge}\text{C})$ -cyclometalated Au(III) complex **121** via oxidative addition by reacting gold(I) iodide and 10-iodobenzo[*b*]quinoline **120** under moderate heating (Scheme I.29d). In this case, the pyridine coordination assisted the oxidative addition of the $(\text{Csp}^2)\text{-I}$ bond.²⁰⁰ More recently, in 2021, the group of Nevado designed biphenylene ligands functionalized with a coordinating group (a pyridine **122** or a phosphine **124**) to assist, by chelation, the oxidative addition of the strained C–C bond in biphenylene. In the case of the biphenylene functionalized with a pyridine **122**, a $(\text{N}^{\wedge}\text{C}^{\wedge}\text{C})$ -biscyclometalated Au(III) complex **123** was obtained, whereas in the case of the phosphine ligand **124**, the oxidative addition afforded a $(\text{P}^{\wedge}\text{C})$ -cyclometalated Au(III) complex **125** (Scheme I.29e).²⁹⁰



Scheme I.29. Examples of intramolecular chelation-assisted oxidative addition to Au(I).

On the other hand, the design of bidentate ligands featuring a bite angle smaller than 180° when chelating gold(I) centers has also showed efficiency at rendering Au(III) complexes via oxidative addition. The preorganization of the non-linear Au(I) complex reduces the deformation energy required to become a square-planar Au(III) complex, therefore the oxidative addition is more favored.

In this line, Amgoune, Bourissou and coworkers reported in 2014 the use of carborane diphosphine ligands (DPCb) **126** that chelate gold(I) centers with P–Au–P angles between 90° and 100° depending on the counterion. The authors could activate C(sp²)–I bonds from several aryl iodides at room temperature affording well-defined arylgold(III) complexes **128** that could be isolated and fully characterized (Scheme I.30a).²⁹¹ Intriguingly, the oxidative addition of *p*-substituted iodobenzenes occurred faster with more electron-rich arenes, featuring the opposite reactivity trend to that observed in isoelectronic L₂Pd(0) complexes undergoing oxidative addition of aryl halides.^{292–294} In 2015, the same group combined the use of bent [(DPCb)Au]^I complexes **130** with the strain release strategy to promote the oxidative addition of the strained C–C bonds in biphenylene and in benzocyclobutenone (Scheme I.30b).²⁹⁵ The oxidative addition of benzocyclobutenone afforded two acyl-gold(III) complexes upon selective activation of either the C(aryl)–C(O) bond (kinetic product **132**) or the C(alkyl)–C(O) bond (thermodynamic product **133**), by adjusting the reaction conditions. Remarkably, the oxidative addition of the C(aryl)–C(O) bond turned to be reversible since the isolated kinetic product, when in solution, evolved slowly back to the cationic Au(I) complex and, over time or upon heating, the thermodynamic acyl-Au(III) complex **133** was formed. In 2022, the same group used the DPCb ligand **126** to promote the oxidative addition of *o*-benzoquinones to bent (P[^]P)Au(I) complexes **134**. They obtained the expected (P[^]P)Au(III) catecholate complexes **135** quantitatively when using strongly oxidizing *o*-quinones such as *o*-chloranil and the related tetrabromo and tetrafluoro *o*-benzoquinones (Scheme I.30c).²⁹⁶

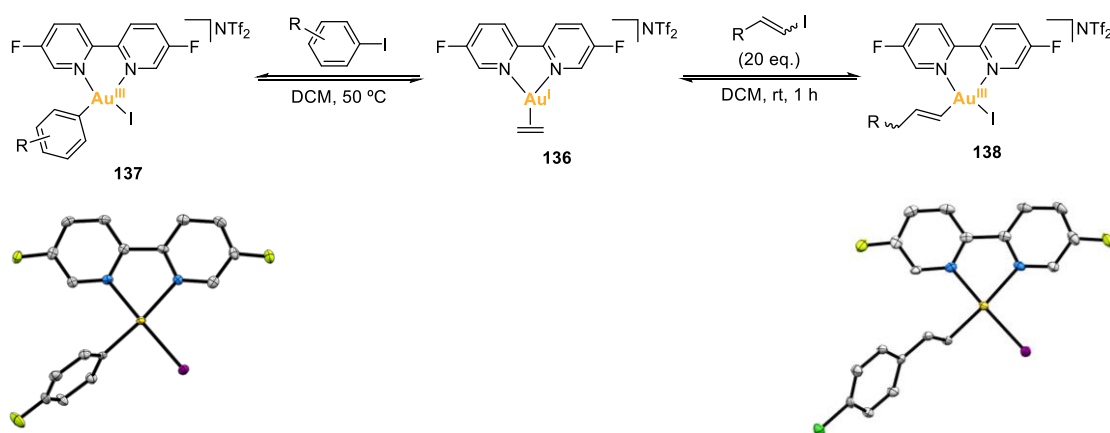


Scheme I.30. Intermolecular oxidative addition to non-linear (DPCb)gold(I) complexes, reported by Bourissou. The anions in the X-ray structures are omitted for clarity.

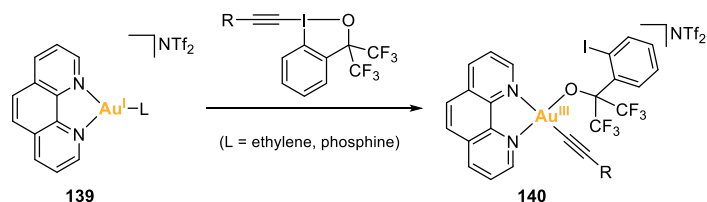
In 2018, Russell and coworkers reacted a three-coordinated 2,2'-bipyridyl-chelated gold(I) ethylene complex **136**, featuring a N–Au–N angle of 74.57°, towards the reversible oxidative addition of C(sp³)-I bonds in different aryl iodides to obtain the corresponding arylgold(III) complexes **137** (Scheme I.31a).²⁹⁷ Electron-rich aryl iodides reacted faster than electron-poor ones, showing a reactivity trend that agrees with the previously reported by Bourissou.²⁹¹ In 2020, Russell reported the first examples of intermolecular oxidative addition of alkenyl and alkynyl iodides to the same (N[^]N)Au(I) ethylene complex **136**. Subsequent alkenyl Au(III) complexes **138** were formed in a reversible and stereospecific manner, and alkynyl iodide oxidative addition generated bimetallic complexes containing both Au(I) and Au(III) centers in which the Au(III) center was formed upon oxidative addition and the Au(I) center was π-coordinated to the alkyne moiety (Scheme I.31a).²⁹⁸ Indeed, Hashmi's group showed that

non-linear tri- and tetracoordinated Au(I) complexes are prone to undergo oxidative addition of C(sp) centers using (N,N)-ligands (Scheme I.31b).^{299, 300} Regarding tricoordinated Au(I) complexes, in 2016 Bezuidenhout and coworkers developed nucleophilic T-shaped (LXL)Au(I)-pincer complexes **141** based on a carbazole framework flanked by two mesoionic carbenes (L = MIC, X = N). These complexes reacted with electrophiles and, interestingly, the corresponding chloromethyl gold(III) complex **142** could be obtained upon formal oxidative addition of dichloromethane (Scheme I.31c).³⁰¹

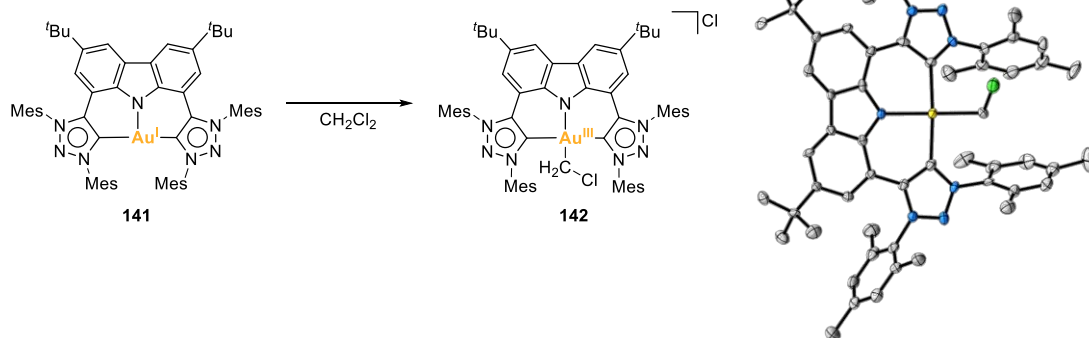
a) Russell (2018, 2020)



b) Hashmi (2019)



c) Bezuidenhout (2016)



Scheme I.31. Intermolecular oxidative addition to (a,b) non-linear three-coordinate (N[^]N)gold(I) complexes, and to (c) a T-shaped gold(I) complex. The anions in the X-ray structures are omitted for clarity.

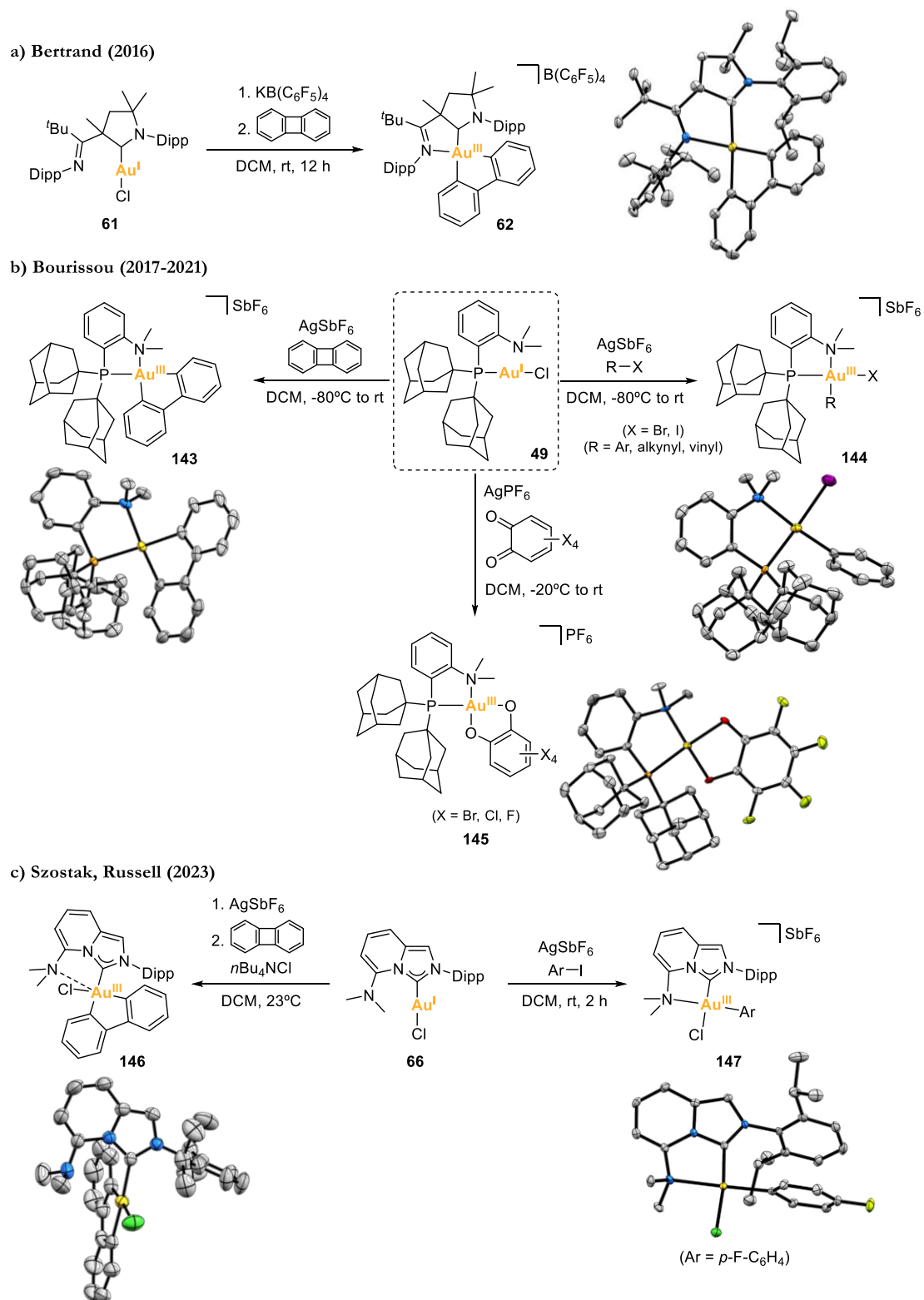
Further, hemilabile ligands are useful platforms to trigger oxidative addition of Au(I) complexes and stabilize the ensuing Au(III) centers by chelation.

In 2016, Bertrand and coworkers reported a (CAAC)AuCl complex **61** (CAAC = Cyclic Alkyl Amino Carbene) bearing a pendant hemilabile imine moiety that helped at stabilizing the Au(III) complex **62** obtained upon oxidative addition of the strained C–C bond in biphenylene (Scheme I.32a).²²⁸

One year later, Bourissou's group employed the MeDalphos ligand in (MeDalphos)AuCl **49** to stabilize the (P^N)-cyclometalated Au(III) complexes **143-144** resulting from the oxidative addition of the strained C–C bond in biphenylene and the C–X bonds in iodoaryls, bromoaryls, alkynyl iodides and vinyl iodides (Scheme I.32b).^{16, 218} The same group also showed that MeDalphos ligand excelled at triggering the oxidative addition of *o*-benzoquinones to yield (P^N)Au(III) catecholate complexes **145** (Scheme I.32b).²⁹⁶ Likewise, in 2021 the group of Nevado used different [(MeDalphos)Au(Ar)(I)]⁺ (P^N)gold(III) complexes obtained via oxidative addition to further synthesize the corresponding (P^N)gold(III) fluoride complexes and explore their performance in reductive elimination (see **165** in Scheme I.38). Interestingly, they included some variations at the ligand such as replacing the adamantyl substituents by *tert*-butyls, and replacing the dimethylamino group by a piperidinyl unit.³⁰² In addition, Spokoyny and coworkers also used (MeDalphos)AuCl to synthesize a wide library of (P^N)Au(III) complexes of the type [(MeDalphos)Au(Ar)(X)]SbF₆ (X = I, Cl) via oxidative addition.^{303, 304} These complexes served as robust arylation reagents in a general protocol for cysteine S-arylation of unprotected peptides and proteins. The same group also used the *tert*-butyl-substituted version of the MeDalphos ligand to develop (P,N)-gold(III) platforms that worked as efficient and selective cysteine arylation reagents, giving access to arylated bioconjugates of higher structural complexity including bicyclic peptides, stapled peptides and peptide-functionalized hybrid nanoclusters.³⁰⁵ Remarkably, in 2022 the same group prepared a robust MeDalphos-based (P^N)Au(III)-[¹⁸F]fluoroaryl complex through a fast oxidative addition of 4-[¹⁸F]fluoroiodobenzene. The ensuing gold(III) complex could be directly used in aqueous medium with peptides and thiosugars to furnish ¹⁸F-labeled conjugates via S-arylation under mild conditions, in excellent chemoselectivity, and with rapid reaction kinetics.³⁰⁶

Regarding hemilabile (N,C) ligands, the groups of Szostak and Russell independently reported this year 2023 the oxidative addition at gold(I) complex **66** (Scheme I.32c). On one hand, Szostak proved the ability of the ligand to stabilize the ensuing (N^C)gold(III) complex

146 formed upon oxidative addition of biphenylene.²³¹ On the other hand, Russell could isolate the (N[^]C)gold(III) complex **147** formed upon oxidative addition of aryl iodides.²³²



Scheme I.32. Selected examples of hemilabile ligand-stabilized Au(III) complexes obtained via oxidative addition. The anions in the X-ray structures are omitted for clarity.

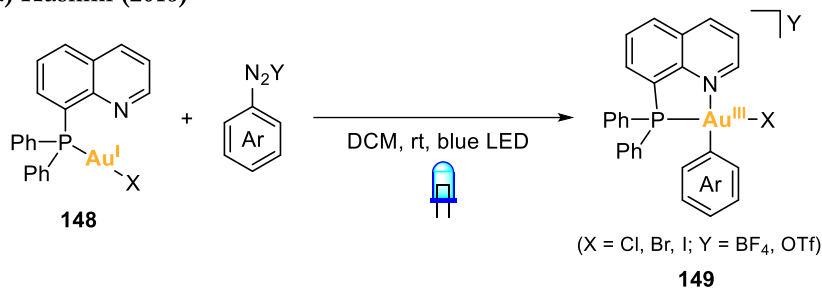
1.4.1.3. Photochemical conditions to promote oxidative addition to Au(I)

The oxidative addition at Au(I) complexes can be induced, as well, under photochemical conditions. Commonly, aryldiazonium salts are activated under irradiation leading to the formation of arylgold(III) complexes.

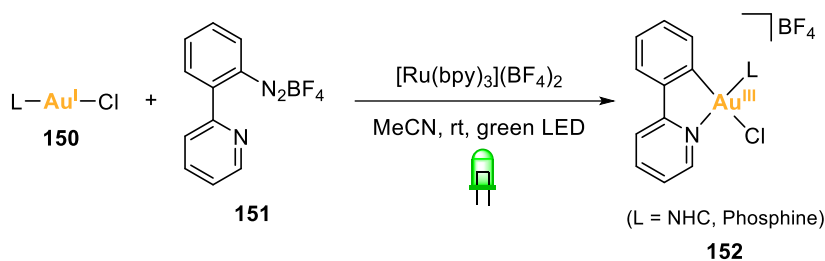
In 2016, the group of Hashmi reported the oxidative addition of aryldiazonium salts to phosphine–Au(I) and NHC–Au(I) complexes under irradiation of blue light LEDs. When using chelating (P,N) ligands, cationic five- and six-membered chelate gold(III) complexes **149** were obtained, whereas when using monodentate phosphine ligands and NHC ligands, the corresponding neutral Au(III) complexes were formed (Scheme I.33a).^{67, 307} Also in 2016, Glorius and coworkers developed a straightforward approach towards well-defined cationic (N⁺C)-cyclometalated Au(III) complexes **152**. The oxidative addition of aryldiazonium salts bearing a 2-(pyridin-2-yl) group **151** was achieved in gold(I) complexes **150** of the type LAuCl (L = phosphine or NHC), in the presence of a Ru(II) photocatalyst under irradiation of green LEDs at room temperature (Scheme I.33b).³⁰⁸ Alternatively, Porcel and coworkers employed *in situ* generated aryldiazonium salts as electrophiles that oxidatively added to LAuCl complexes (L = PPh₃ or SMe₂) under thermal conditions, without requiring photochemical conditions.³⁰⁹

In 2014, Toste and coworkers reported the oxidative addition of CF₃I to phosphine Au(I) aryl complexes **153** via a photoinitiated radical chain reaction. The use of near-ultraviolet light promoted the excitation of CF₃I to end up with Au(III) complexes **154** of the type [(PR₃)Au(aryl)(CF₃)(I)] that could be isolated and characterized (Scheme I.33c).⁶⁴ In 2019, the same group isolated Au(III) complexes from the photoredox-initiated arylation of (IPr)AuX complexes **155** (X = CF₃ or succinimide), using aryldiazonium salts, a Ru(II)-based photoredox catalyst and blue light LED irradiation.³¹⁰ The authors claimed a radical chain oxidative addition in which the ruthenium catalyst first generates an aryl radical that adds to the Au(I) complex. Then, the resulting arylgold(II) species undergoes a single electron oxidation by reacting with the aryldiazonium salt. This reaction generates an arylgold(III) species **156** that could be isolated in coordinating solvents (Scheme I.33d).

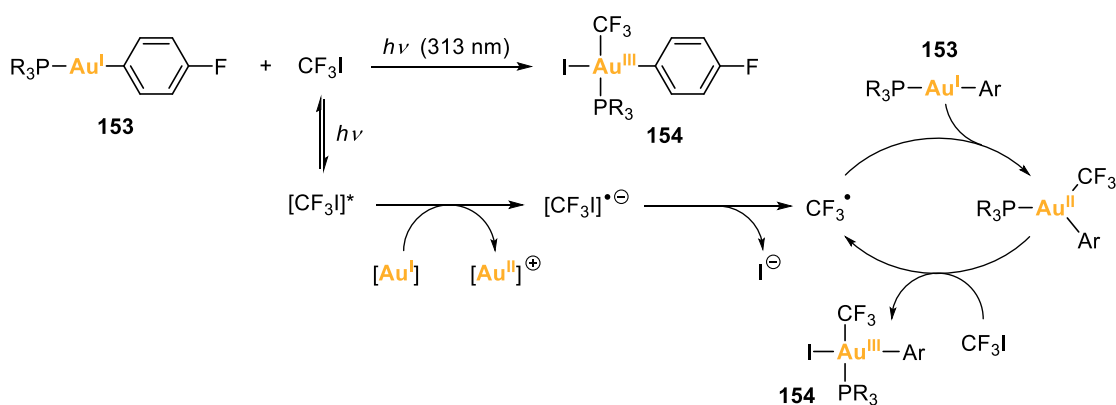
a) Hashmi (2016)



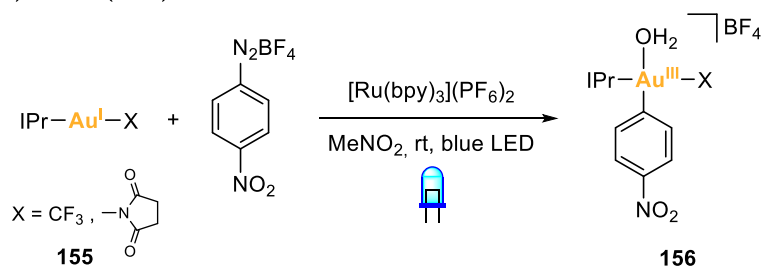
b) Glorius (2016)



c) Toste (2014)



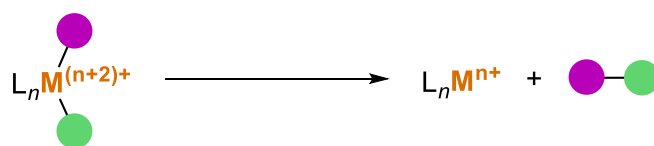
d) Toste (2019)



Scheme I.33. Selected examples of arylgold(III) complexes obtained via oxidative addition promoted by photochemical conditions.

I.4.2. Reductive elimination

Reductive elimination is the reverse process of oxidative addition. Consequently, the metal center of a given complex is reduced by two electrons and loses two ligands sitting in a relative *cis* position to generate a covalent bond between them (Scheme I.34). Therefore, reductive elimination is typically the product-forming step in catalytic processes, chiefly in cross-coupling transformations.

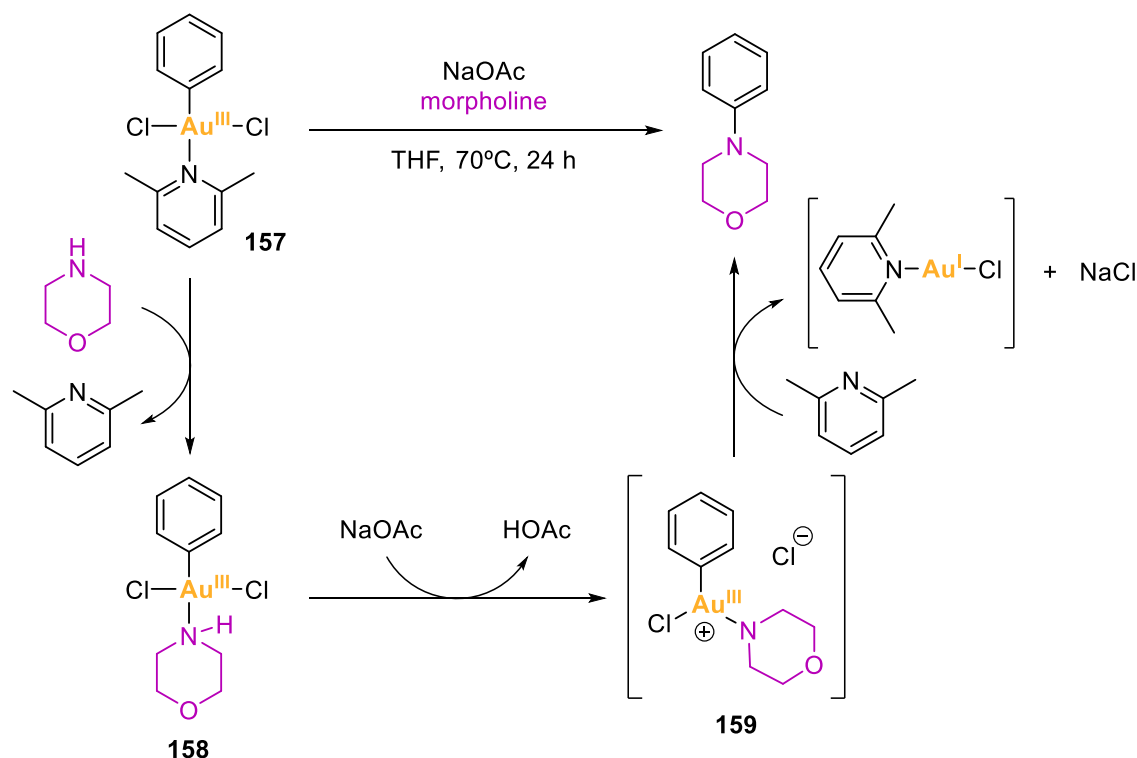


Scheme I.34. General scheme of a reductive elimination process.

In contrast to oxidative addition, reductive elimination at Au(III) was demonstrated experimentally much earlier and the viability of such process has never been questioned. In fact, the favorable reduction potential from Au(III) to Au(I) makes reductive elimination more attainable at gold than at other transition metals. Despite that, over the last years, studies on reductive elimination at well-defined gold(III) complexes have been done from a mechanistic point of view, in particular to gain mechanistic insights into gold-catalyzed cross-coupling reactions.

Amongst the early works on reductive elimination at gold(III) reported in the 20th century, examples of C(sp³)-Br,³¹¹ C(sp²)-Br,^{312, 313} C(sp³)-C(sp³),³¹⁴⁻³¹⁶ C(sp²)-C(sp²),^{317, 318} and C(sp²)-C(sp³)³¹⁹ bond-forming reductive eliminations can be highlighted.

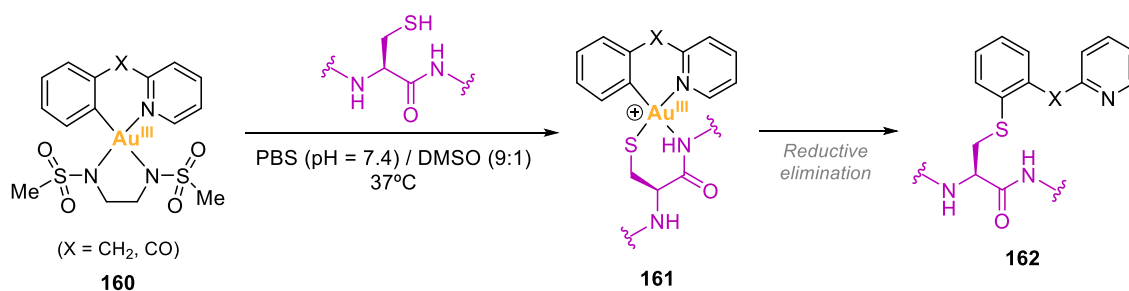
In 2010, Limbach and coworkers reported a stoichiometric C(sp²)-N reductive elimination when the dichloro(lutidine)phenylgold(III) complex **157** was reacted with N-nucleophiles in the presence of acetate. Mechanistically, the labile lutidine is first suggested to be exchanged by the N-nucleophile, as complex **158** was isolated and characterized when using morpholine as N-nucleophile. Then, the base deprotonates the nucleophile to give a putative T-shaped trigonal gold(III) complex **159**, and a subsequent C(sp²)-N reductive elimination takes place between the phenyl fragment and the N-ligand (Scheme I.35).³²⁰



Scheme I.35. Mechanism of a C(sp²)-N reductive elimination from a gold(III) complex.

In 2013, Rosenthal's group studied the C(sp²)-Cl reductive elimination at NHC-gold(III) complexes. Interestingly, two gold(I) complexes of the type [(IPr)Au(Ar)] (Ar = Ph, C₆F₅) were oxidized with PhICl₂ and, while the gold(III) complex *trans*-[(IPr)Au(Cl₂)(C₆F₅)] was isolable, the corresponding phenylgold(III) complex was not detected and chlorobenzene was obtained instead from the reductive elimination of the putative gold(III) complex *trans*-[(IPr)Au(Cl₂)Ph]. In contrast, *trans*-[(IPr)Au(Cl₂)(C₆F₅)] delivered C₆F₅Cl upon photoexcitation, thereby proving the C(sp²)-Cl reductive elimination.³²¹

In 2014, Wong and coworkers reported the C(sp²)-S reductive elimination from (N[^]C)-cyclometalated gold(III)-cysteine adducts **161** as an approach for chemoselective cysteine modification of peptides and proteins.³²² By using (N[^]C)-cyclometalated gold(III) complexes **160** of the type [Au(N[^]C)(msen)] (msen = N,N'-bis(methanesulfonyl)ethylenediamine), several cysteine-containing peptides afforded chemoselectively and quantitatively gold(III)-peptide adducts **161** that underwent C(sp²)-S reductive elimination to release the modified peptides **162** (Scheme I.36).



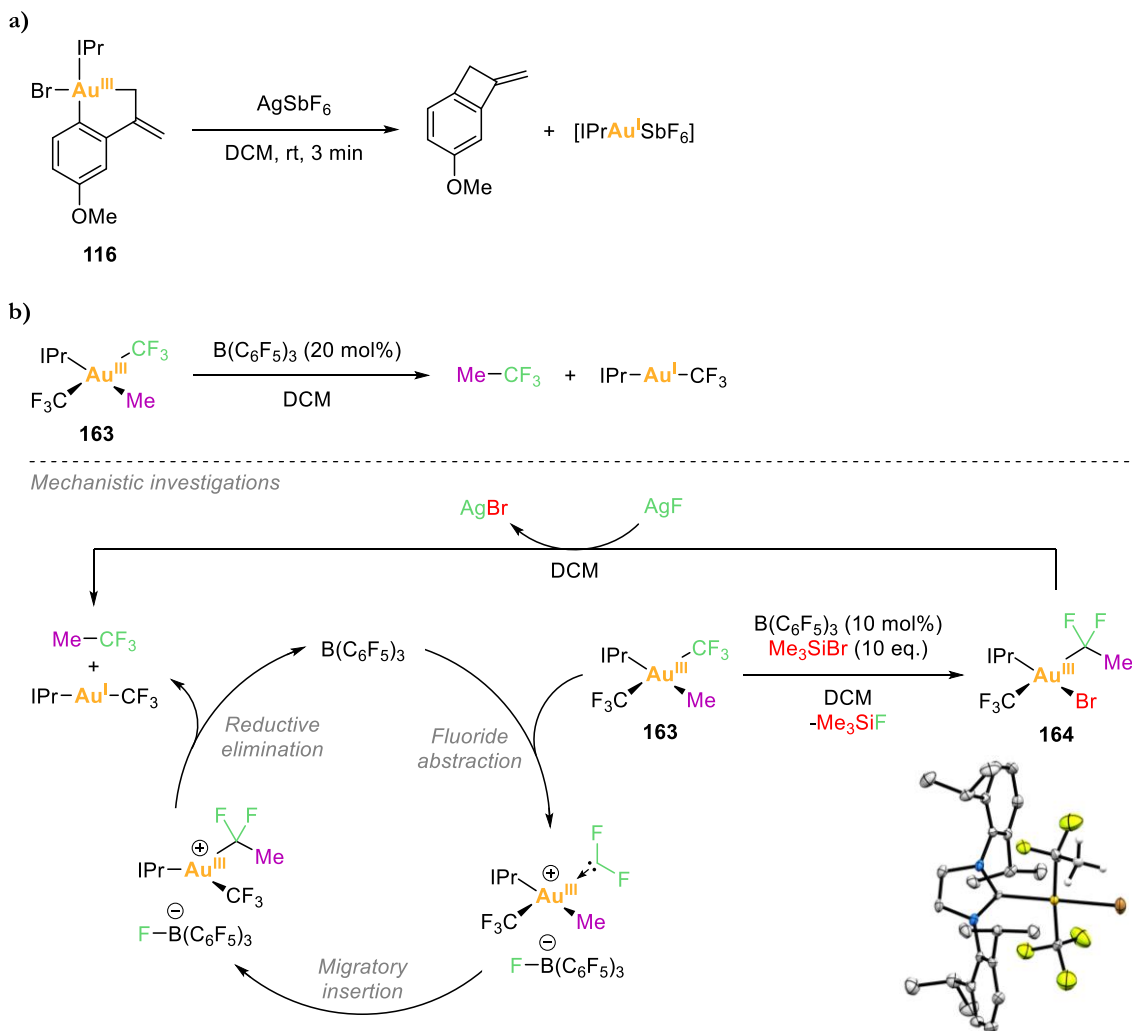
Scheme I.36. S-arylation of cysteine-containing peptides via C(sp²)-S reductive elimination from Au(III) complexes.

Toste's group outstands in the field, as they have provided several remarkable studies on reductive elimination at Au(III) complexes. In 2014, they reported the C(sp³)-C(sp²) reductive elimination from the stable cyclometalated gold(III) complex **116**.¹⁹⁷ By adding AgSbF₆, the bromide ligand was abstracted and the resulting putative cationic three-coordinate Au(III) intermediate underwent spontaneous intramolecular C(sp³)-C(sp²) reductive elimination (Scheme I.37a).

Also in 2014, they investigated very fast C(sp²)-C(sp²) reductive elimination rates from *cis*-bis(aryl)gold(III) complexes of the type *cis*-[Au(*p*-F-C₆H₄)₂Cl(PPh₃)].³²³ Interestingly, similar gold(III) complexes of the type *cis*-[Au(*p*-F-C₆H₄)Cl₂(PR₃)] underwent C(sp²)-P reductive elimination to afford phosphonium salts.³²⁴ Moreover, the [Au(aryl)(CF₃)(I)(PR₃)] gold(III) complexes (R = Ph, Cy) obtained by photochemical oxidative addition of CF₃I (discussed above in section I.4.1.3, Scheme I.33c) served to investigate the competitive C(sp²)-I and C(sp²)-CF₃ reductive elimination processes.⁶⁴ Also, they studied the halide dependence of C(sp²)-X and C(sp²)-CF₃ reductive elimination mechanisms at two series of Au(III) complexes: [Au(*p*-Me-C₆H₄)(CF₃)(X)(PPh₃)] and [Au(*p*-F-C₆H₄)(CF₃)(X)(PCy₃)] (X = I, Br, Cl, F).³²⁵ Thermolysis studies of these complexes to generate C(sp²)-X and/or C(sp²)-CF₃ reductive elimination products revealed that the selectivity for C(sp²)-CF₃ bond formation increases in the order X = I < Br < Cl < F, with exclusive C(sp²)-I bond formation when X = I, and exclusive C(sp²)-CF₃ bond formation when X = F.

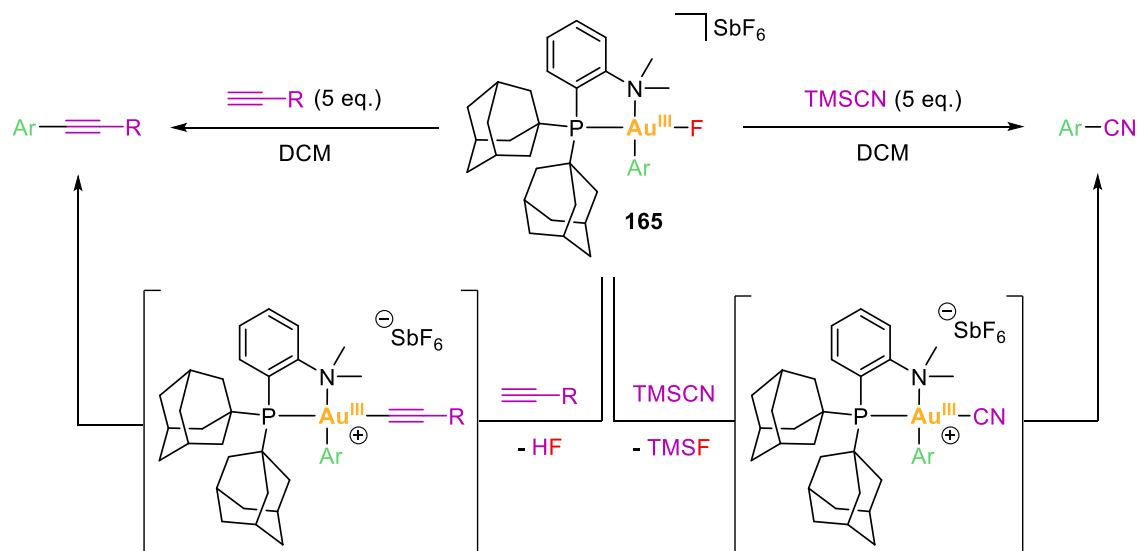
Strikingly, in 2017 Toste and coworkers reported the serendipitous discovery of a borane-catalyzed C(sp³)-CF₃ reductive elimination from [Au(R)(CF₃)₂(L)] gold(III) complexes **163** (R = alkyl, allyl, aryl; L = IPr, PCy₃).³²⁶ Mechanistic studies suggested that the reaction proceeded through a fluoride-rebound mechanism involving fluoride abstraction, migratory insertion, and reductive elimination steps (Scheme I.37b). This protocol tolerated a wide scope of functional groups and was useful to synthesize the antirheumatic Leflunomide and

the cannabinoid agonist BAY 59-3074. In addition, it enabled the radio synthesis of ^{18}F -labeled aliphatic CF_3 -containing compounds for their application in potential tracers in positron emission tomography (PET).



Scheme I.37. Toste's studies on a) $\text{C}(\text{sp}^3)\text{-C}(\text{sp}^2)$ reductive elimination and b) borane-catalyzed $\text{C}(\text{sp}^3)\text{-CF}_3$ reductive elimination, both occurring at NHC-gold(III) complexes.

Ligands that provide stable well-defined gold(III) complexes are good platforms to study reductive elimination from a mechanistic point of view. For instance, $(\text{C}^{\wedge}\text{N}^{\wedge}\text{C})\text{Au}(\text{III})$ pincer complexes allowed Bochmann and coworkers to study the C-C and C-S reductive elimination on platforms of this type,^{327, 328} and the group of Nevado employed $(\text{P}^{\wedge}\text{N})\text{arylgold}(\text{III})$ fluoride complexes **165** bearing the MeDalphos ligand, or slightly modified MeDalphos ligands. These complexes were able to activate $\text{C}(\text{sp})$ ligands, like terminal alkynes and TMSCN , and rendered the corresponding $\text{C}(\text{sp}^2)\text{-C}(\text{sp})$ reductive elimination products in high rates (Scheme I.38).³⁰²



Scheme I.38. C(sp²)-C(sp) reductive elimination processes from (P[^]N)gold(III) fluoride complexes, reported by Nevado.

I.4.3. Transmetalation

Transmetalation is the elementary reaction involving the transfer of an organic fragment from a coupling reagent (based on a metal or a metalloid) to a transition metal.¹⁴ In metal catalyzed cross-coupling reactions, transmetalation is a typical bridging step between the oxidative addition and reductive elimination steps.

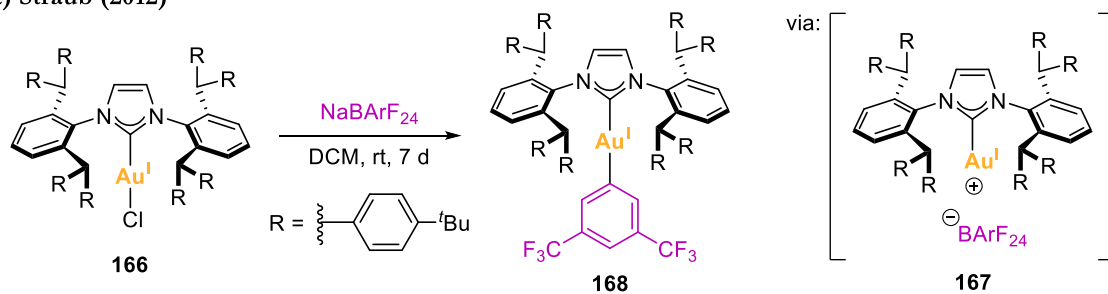
Many transmetalation events have been documented with gold, ranging from salt metathesis with gold halides and organolithium or Grignard reagents, to transmetalation involving p-block elements (boron,^{329, 330} silicon^{183, 331} and tin^{332, 333}), and involving a variety of other transition metals under stoichiometric and catalytic conditions.³³⁴⁻³⁴⁷ Noticeably, transmetalation allowed the development of bimetallic catalytic systems involving organogold co-catalysts in which organic fragments are transferred between gold and another transition metal.^{299, 348-354} Nonetheless, this section only covers the most relevant literature regarding transmetalation reactions, mainly being focused on typical boron-to-gold transmetalation.

In 1995, Schmidbaur and Fackler groups independently reported early evidence for transmetalation of an aryl group from boron to gold using NaBPh₄ and phosphine gold(I) complexes in a stoichiometric fashion.^{355, 356} A related reactivity was reported in 2012 by Straub and coworkers using NaBArF₂₄ and a sterically encumbered NHC-Au(I) chloride complex **166**. The corresponding transient cationic NHC-Au(I) complex **167** slowly

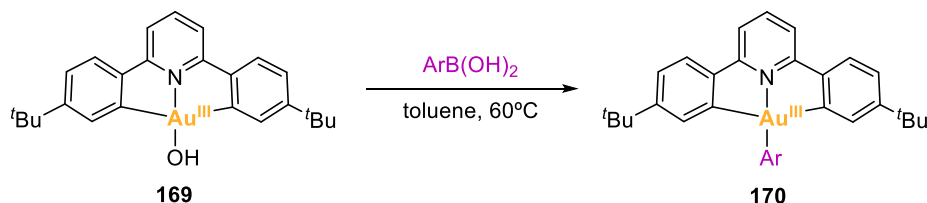
abstracted an aryl moiety from the weakly coordinating borate anion to afford the final arylgold(I) complex **168** (Scheme I.39a).³⁵⁷

Arylboronic acids have also been employed in boron-to-gold transmetalation. For instance, the group of Gray reacted LAuX gold(I) complexes (L = phosphine, NHC; X = Br, Cl) with arylboronic acids in the presence of a mild base, under heating or microwave irradiation, to obtain the corresponding LAuAr complexes.³⁵⁸⁻³⁶⁰ Interestingly, Nolan and coworkers improved the protocol using (IPr)AuCl and KOH as a base to achieve the transmetalation at room temperature. In this case, mechanistic studies postulated the involvement of a gold(I) hydroxide intermediate.³⁶¹ Regarding Au(III) complexes, boron-to-gold has also been substantiated by several groups. The group of Bochmann used a (C,N,C)-pincer gold(III) hydroxide complex **169** and different electron-rich and electron-poor arylboronic acids to obtain the corresponding (C[^]N[^]C)gold(III) aryl complexes **170** in the absence of base (Scheme I.39b).^{362, 363} Additionally, Nevado and coworkers reacted [Au(C₆F₅)Cl₂(PPh₃)] complexes with electron-deficient arylboronic acids to afford [Au(C₆F₅)(Ar^F)Cl(PPh₃)] products, without requiring external bases. However, the reaction occurred under harsh conditions (150°C) and was limited to electron-poor arylboronic acids.³³⁰ Shortly after, the group of Nevado provided experimental evidence for direct transmetalation of gold(III) fluoride complexes **172** with arylboronic acids. They synthesized (N,C)-cyclometalated gold(III) complexes **172** of the type [(N[^]C)AuF₂] and [(N[^]C)AuRF] (R = aryl, alkyl) to react them with arylboronic acids (Scheme I.39c).³⁶⁴ The corresponding transmetalation products **173** were obtained, and depending on the electronic and steric characteristics of these products, either intra- or intermolecular reductive elimination products could be also observed. This work supported the previously postulated Au(III)–F/B transmetalation step in the catalytic system reported by You, in which 2-(aryl)pyridine substrates reacted with Au(III) salts in the presence of NFSI as fluoride source and arylboronic acids to afford the corresponding C(sp²)–C(sp²) coupling products on biaryl (N[^]C)gold(III) intermediates.³⁶⁵ However, the authors did not give a clear mechanism on whether the fluoride source formed a Au(III)–F species that could undergo transmetalation or the fluoride source assisted the C–B bond cleavage by noncoordinated fluoride anions.

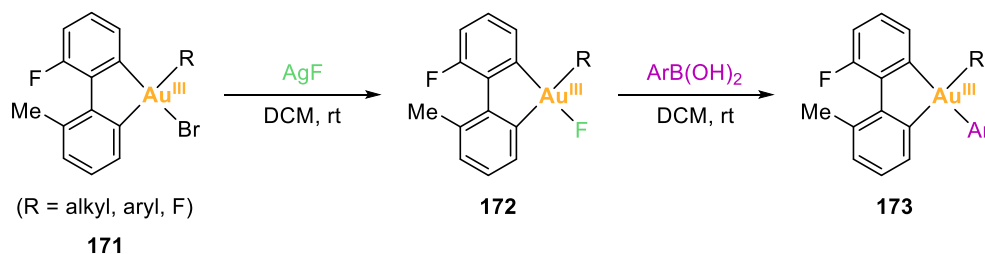
a) Straub (2012)



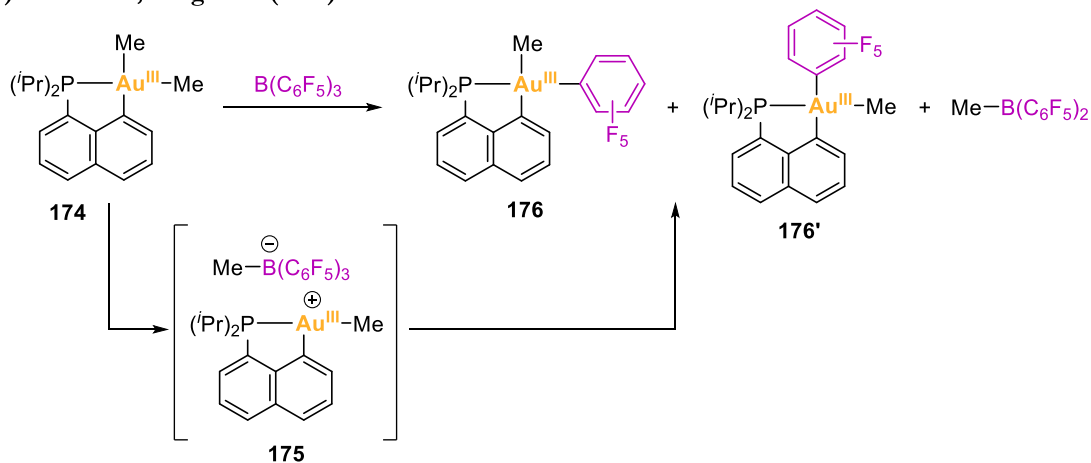
b) Bochmann (2012)



c) Nevado (2016)



d) Bourissou, Amgoune (2015)



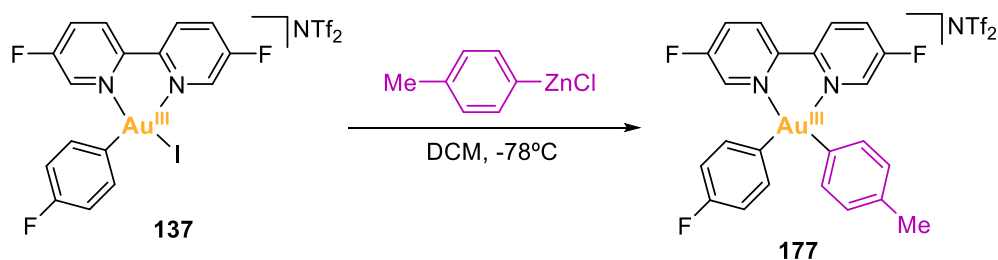
Scheme I.39. Selected examples of boron-to-gold transmetalation reactions.

The strong Lewis acid tris(pentafluorophenyl)borane $\text{B(C}_6\text{F}_5)_3$ has been used as a surrogate halide scavenger to silver salts to generate cationic gold species. Strikingly, Hansmann, Stephan, and Hashmi reacted L-Au(I) acetylides ($\text{L} = \text{phosphine, NHC}$) with $\text{B(C}_6\text{F}_5)_3$ to trigger the alkynyl abstraction by $\text{B(C}_6\text{F}_5)_3$.³²⁰ Indeed, the corresponding alkynyl borate species were formed and featured a π -coordination of the alkyne moiety to the $[(\text{L})\text{Au}]^+$

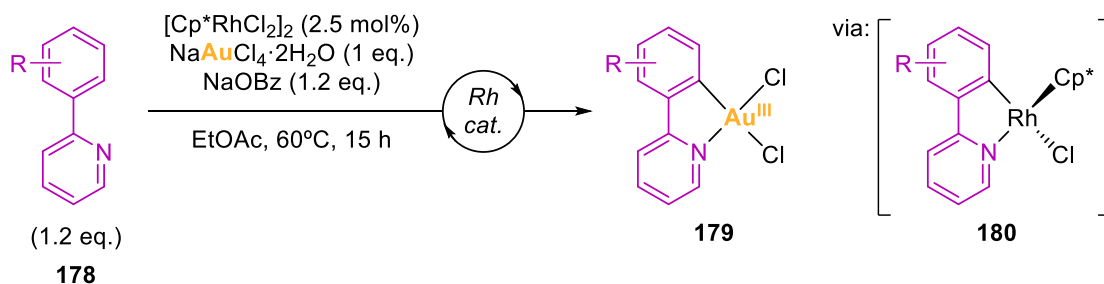
fragment. Then, these stable zwitterionic π -alkyne gold complexes underwent a slow C_6F_5 group transfer to the gold center upon heating at $60^\circ C$, thereby rendering $[(L)Au(C_6F_5)]$ complexes. Moreover, Bourissou, Amgoune, and coworkers reacted a (P,C)-cyclometalated gold(III) dimethyl complex **174** with $B(C_6F_5)_3$ to afford the corresponding $[(P^{\wedge}C)Au(Me)(C_6F_5)]$ isomers **176** and **176'** and $MeB(C_6F_5)_2$ by boron-to-gold aryl group transfer (Scheme I.39d).³⁶⁶ The outcome was postulated to be obtained via a tricoordinate cationic gold(III) methyl intermediate **175**.

Lastly, a couple of works are worth mentioning. On one hand, Russell and coworkers reported in 2018 a detailed study on elementary organometallic reactions from a three-coordinate 2,2'-bipyridyl-chelated gold(I) ethylene complex **136**.²⁹⁷ After isolating the oxidative addition gold(III) product **137** (see Section I.4.1.2, Scheme I.31a), they reacted it with *p*-tolylzinc chloride at low temperature toward the formation of the Zn-to-Au(III) transmetalation product **177** (Scheme I.40a). By variable temperature ^{19}F -NMR spectroscopy and ESI-HRMS, the identity of complex **177** was confirmed. Above $-40^\circ C$, complex **177** decomposed yielding the corresponding biaryl reductive elimination product. Indeed, this work was the first example of a Negishi cross-coupling at gold under stoichiometric conditions. On the other hand, the group of Nevado reported in 2022 the synthesis of (N,C)-cyclometalated gold(III) complexes via a catalytic and unprecedented Rh-to-Au(III) transmetalation.³⁴⁰ They reacted unfunctionalized $(N^{\wedge}C)$ ligands **178** with catalytic amounts of $[Cp^*RhCl_2]_2$ and stoichiometric amounts of $NaAuCl_4 \cdot 2H_2O$ and base, to afford the final $[(N^{\wedge}C)AuCl_2]$ complexes **179** via a catalytic rhodium-mediated $C(sp^2)-H$ bond activation followed by a catalytic Rh-to-Au(III) transmetalation (Scheme I.40b).

a) Russell (2018)



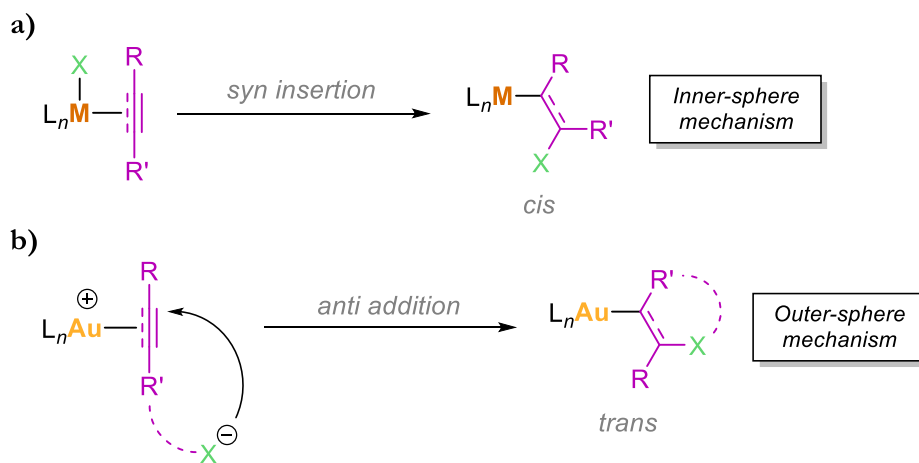
b) Nevado (2022)



Scheme I.40. a) Stoichiometric Zn-to-Au transmetalation, and b) catalytic Rh-to-Au transmetalation for the synthesis of (N,C)-cyclometalated gold(III) complexes.

I.4.4. Migratory insertion

Migratory insertion is an elementary organometallic reaction, known for all transition metals, in which an unsaturated substrate (alkenes, allenes, alkynes, ketones, CO, and related compounds) inserts into an adjacent M–X bond (X= ligand). The insertion operates via an inner-sphere mechanism in a *syn* manner, thus leaving the X ligand in a *cis* position to the metal (Scheme I.41a). Migratory *syn* insertions, however, remained elusive for gold complexes until 2015. Conversely, gold species activate C–C multiple bonds towards intra- or intermolecular nucleophilic attacks affording *trans* configured products, which is typical for outer-sphere *anti* selective additions (Scheme I.41b).¹⁴ Therefore, this section is focused on providing illustrative examples on migratory *syn* insertions at well-defined gold complexes.

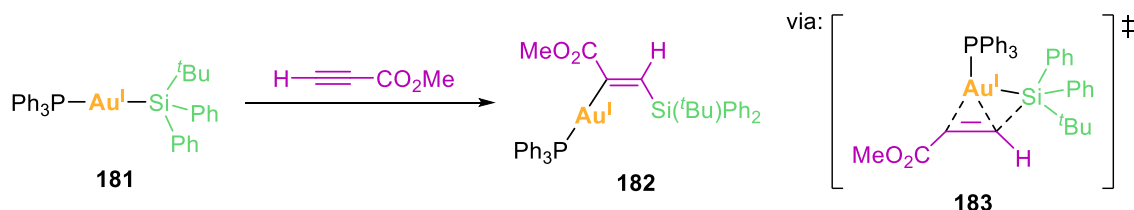


Scheme I.41. a) General migratory insertion of an unsaturated ligand at a transition-metal complex, and b) gold-mediated addition of nucleophiles to C–C multiple bonds.

Early studies on insertion reactions at well-defined gold(I) complexes resulted in *trans* configured products. For instance, when Sadighi and coworkers reacted NHC–Au(I) fluoride complexes with alkynes, they obtained vinylgold(I) complexes featuring a *trans* rearrangement of the gold center and the fluoride atom.³⁶⁷ This observation was in agreement with an outer-sphere mechanism in which the fluoride was displaced and subsequently added in *anti* to the π -coordinated alkyne. Also, when they reacted [(IPr)Au(H)] with electron-poor alkynes, the formal insertion of the alkyne into the Au–H bond resulted in the corresponding *trans* vinylgold(I) complex.³⁶⁸ No clear mechanistic understanding was provided though. Interestingly, after a theoretical and experimental study, Hashmi and Köppel stated that terminal and non-activated alkynes, ethylene, and norbornene are not prone to insert into the Au–H bond of [(IPr)Au(H)].³⁶⁹

The coordination of a third ligand to linear two-coordinate Au(I) complexes is unfavored owing to a high deformation energy. Consequently, the implementation of migratory *syn* insertions at Au(I) complexes is unlikely feasible. Instead, the d^8 configuration of Au(III) complexes makes them better candidates for the insertion of insaturations. In this line, numerous groups have synthesized well-defined Au(III) complexes with strongly chelating ligands to enhance their stability and enable the study of insertions at them. However, there is an exceptionally worth mentioning work by Bourissou, Amgoune and coworkers that disclosed the *syn* insertion of allenes, terminal, and internal alkynes into the Au–Si bonds of gold(I) complexes **181** of the type [(PPh₃)Au(SiPh₂R)].³⁷⁰ In all cases, β -silyl vinylgold(I) complexes **182** were obtained with a *cis* arrangement of the gold and silicon atoms. Further mechanistic studies underpinned that the insertions proceeded through an inner-sphere

pathway involving the intermediacy of a three-coordinate gold(I) π -complex **183** (Scheme I.42).³⁷¹



Scheme I.42. *Syn* insertion of a terminal alkyne into a Au(I)–Si bond.

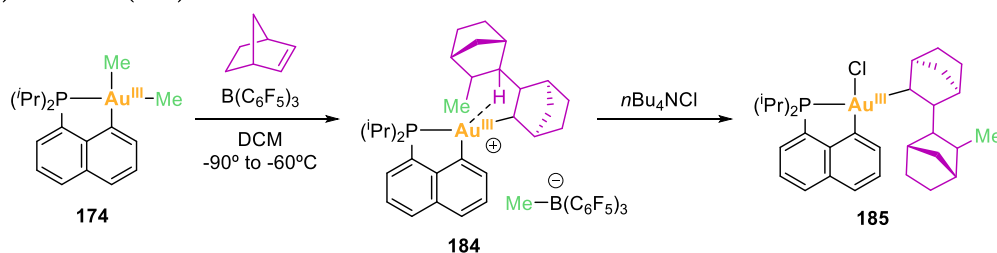
Although *anti* additions at gold(III) have been documented, particularly highlighting the studies of Bochmann^{61, 372} and Tilstet^{268, 373, 374} groups where they use (C,N,C)-pincer Au(III) complexes and (N,C)-cyclometalated Au(III) complexes respectively, as previously stated, *syn* insertions occur more readily at gold(III) complexes than at gold(I) complexes. Hence, relevant examples of *syn* insertions at gold(III) are presented hereunder.

The first evidence of olefin migratory *syn* insertions at Au(III) appeared in 2015, when Bourissou, Amgoune and coworkers disclosed the norbornene insertion into Au–methyl bonds of the (P,C)-cyclometalated gold(III) dimethyl complex **174** (Scheme I.43a).^{366, 375} Upon a first methide abstraction by B(C₆F₅)₃ to form a cationic intermediate **175** (see Section I.4.3, Scheme I.39d), norbornene inserts at -60°C into a Au–Me bond to yield a cationic norbornyl complex **184** that decomposes even at low temperature, despite its stabilization by a γ -CH agostic interaction.³⁷⁶ Therefore, the presence of pyridine or chloride helped at trapping the norbornylgold(III) species by rendering a thermally stable neutral four-coordinate complex **185**. The crystal structure of the chloride complex revealed that two norbornene units inserted on the *exo* face in a *syn* manner, which agreed with an inner-sphere mechanism. The striking double insertion of norbornene was rationalized with mechanistic studies that demonstrated the higher thermodynamic stability of the product.³⁷⁷

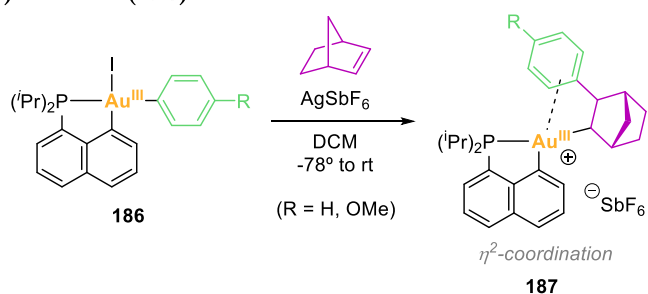
Later, the same (P,C) chelating ligand was used to study the norbornene and ethylene *syn* insertion in Au(III)–aryl bonds (Scheme I.43b).^{375, 378} In this case, both olefins were mono-inserted into the Au–aryl bond. While the insertion of ethylene led to a β -hydride elimination/reinsertion pathway (see Section I.4.5, Scheme I.46b), the insertion of norbornene did not. In both cases, the cationic products **187** and **205** were obtained since a η^2 -coordination of the remote phenyl ring to gold, substantiated spectroscopically, crystallographically and computationally, provided enhanced stability to the resulting complex. Interestingly, when a (N,C)-cyclometalated phenylgold(III) complex **188** was used

instead, a double insertion of ethylene into the Au(III)–Ph bond was obtained, as reported by Bourissou, Ribas and coworkers (Scheme I.43c).³⁷⁹ The different reactivity observed in ethylene migratory insertion when using a (P,C) system or a (N,C) system was attributed to the different electronic properties of the ancillary ligand.

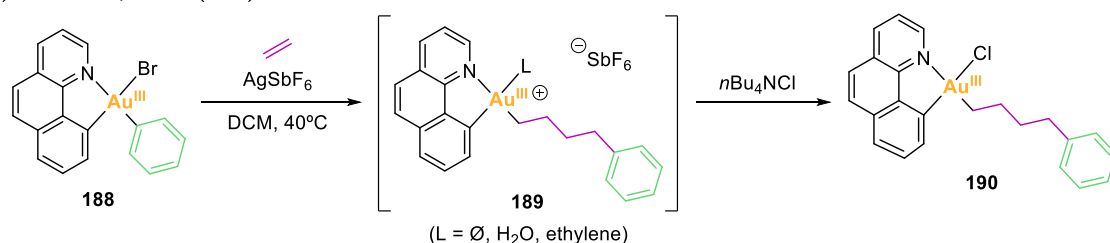
a) Bourissou (2015)



b) Bourissou (2017)



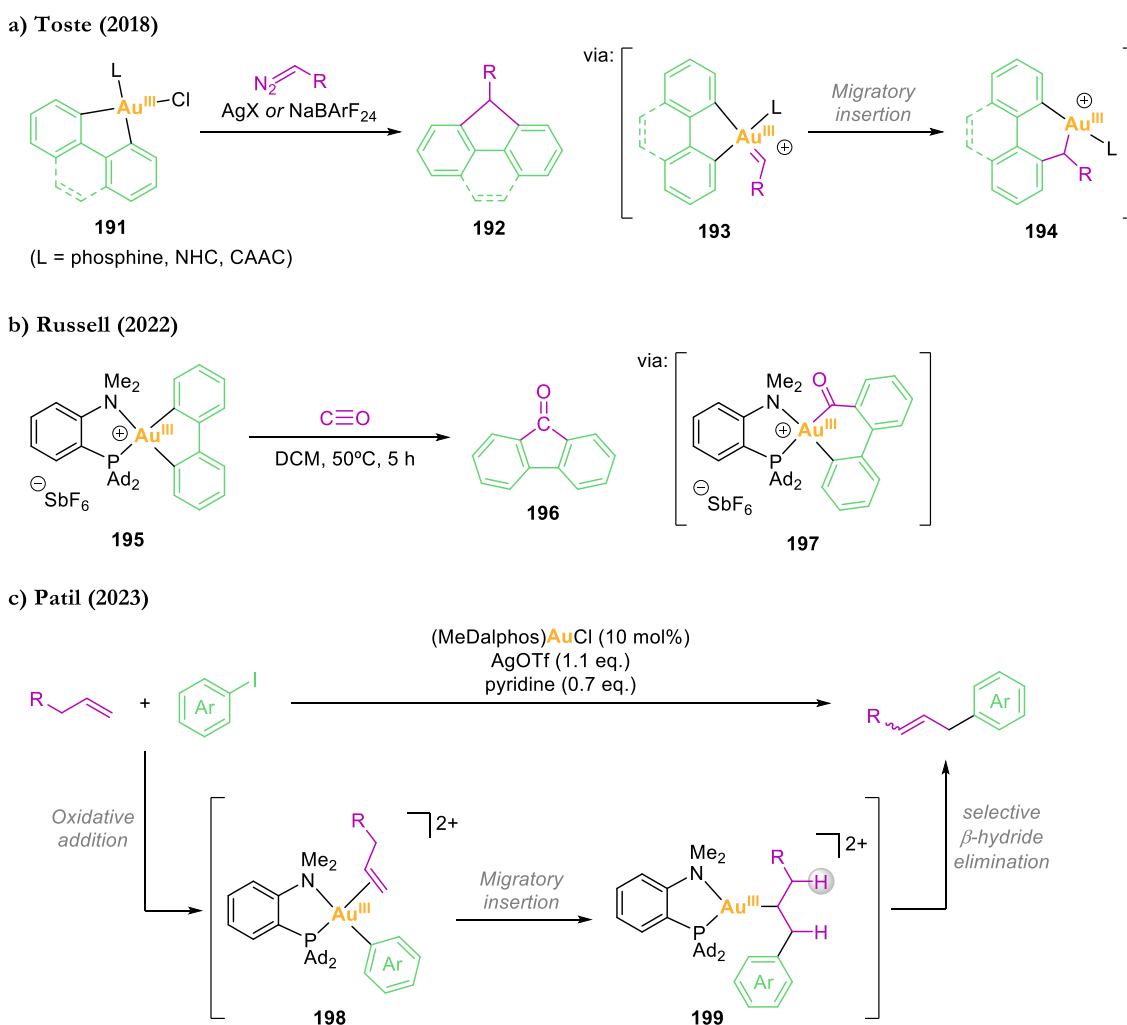
c) Bourissou, Ribas (2018)



Scheme I.43. Migratory insertions at well-defined Au(III) complexes: a,b) Formation of norbornyl gold(III) complexes upon *syn* insertion of norbornene into Au–Me and Au–Ph bonds, and c) double insertion of ethylene into a Au–Ph bond.

Regarding migratory insertions that have been evidenced to be involved in multistep transformations, four works can be highlighted. First, the work reported by Toste in 2018 on borane-catalyzed $C(sp^3)-CF_3$ reductive elimination from $[Au(R)(CF_3)_2(L)]$ gold(III) complexes **163** ($R = \text{alkyl, allyl, aryl}$; $L = iPr, PCy_3$), where a migratory insertion of a CF_2 carbene ligand occurred (see Section I.4.2, Scheme I.37b).³²⁶ Second, another work from Toste's group published in 2018, where fluorene derivatives **192** were obtained from gold(III) complexes **191** (Scheme I.44a).³⁸⁰ The reaction mechanism involved a migratory insertion of carbene ligands derived from diazoalkanes into Au(III)–C bonds, and a reductive elimination from **194** to release the fluorene derivative products **192**. The gold(III) complex **194** resulting

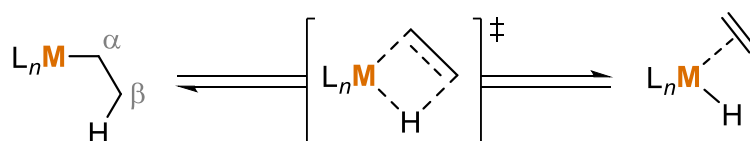
from the migratory insertion step could not be isolated due to the fast rate of the reaction even at -40°C . Third, in 2022 Russell and coworkers evidenced the migratory insertion of CO into a Au(III)–C bond of a MeDalphos-ligated aurafluorene complex **195** when they reacted this complex in CO to produce 9-fluorenone **196** (Scheme I.44b).³⁸¹ The reaction was suggested to operate via a migratory insertion followed by a reductive elimination step to release the fluorenone product. Last, Patil and coworkers reported very recently in 2023 a ligand-enabled gold-catalyzed Heck reaction. It included a migratory insertion step, followed by a selective β -hydride elimination, to render the coupling products in a complementary regioselectivity as compared to Heck reactions catalyzed by other transition metals (Scheme I.44c).²²³



Scheme I.44. a) Migratory insertion of carbene ligands and b) migratory insertion of CO, both into Au(III)–C bonds, and c) migratory insertion step involved in a Au(I)/Au(III)-catalyzed Heck reaction.

I.4.5. β -Hydride elimination

β -hydride elimination is the microscopic reverse of olefin insertion into M–H bonds, thus it is a process that occurs at metal alkyl complexes. It consists in the elimination of a hydrogen atom in β position of the metal that renders a metal hydride species and an olefin (Scheme I.45). Also, an open *cis* coordination site at the metal is required prior to the C–H bond cleavage, hence, coordinatively saturated metal alkyl complexes are reluctant to engage in such process.



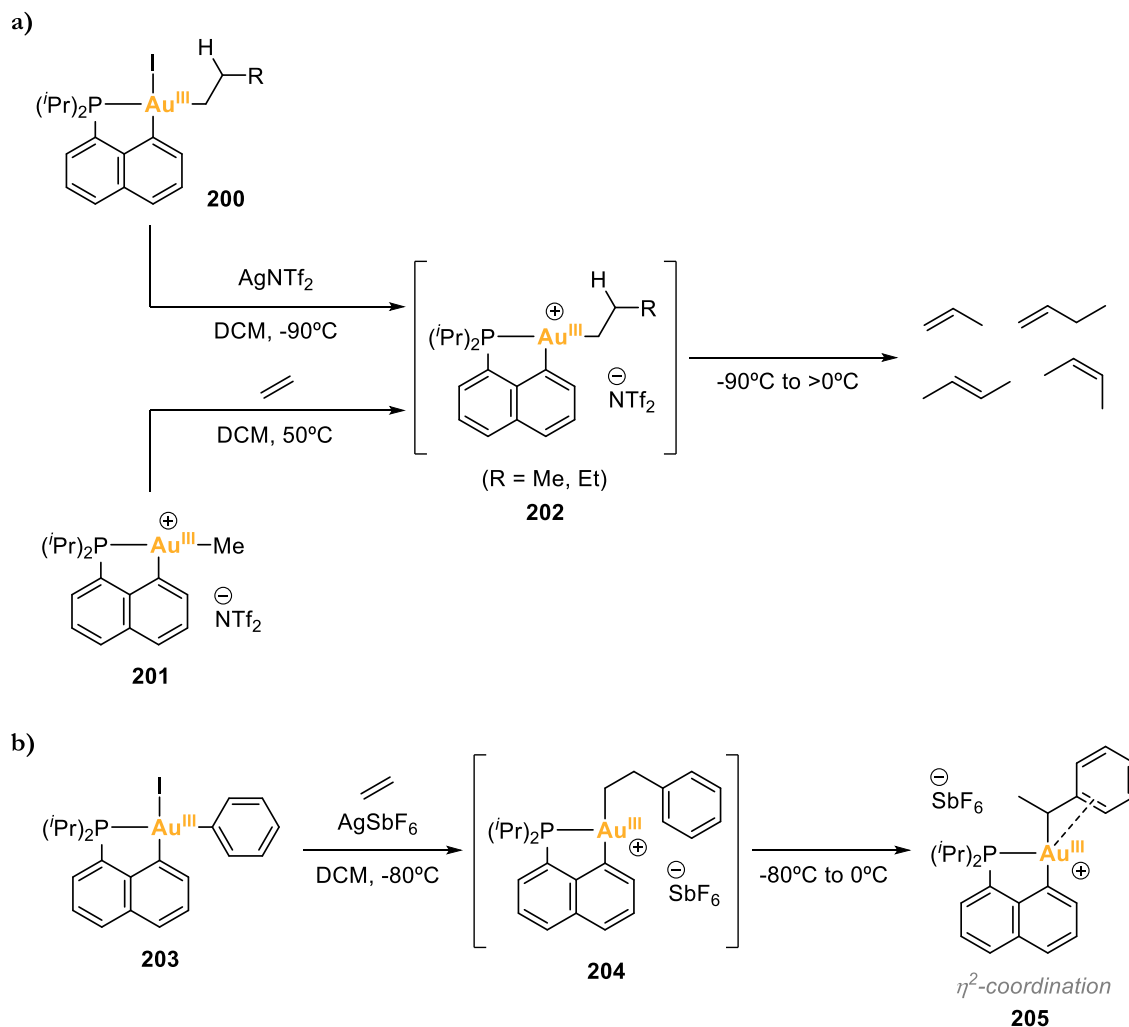
Scheme I.45. General scheme of a β -hydride elimination.

While the propensity of late transition metals to undergo β -hydride elimination is well established, gold alkyl complexes are highly reluctant to this transformation.³⁸² C–Au bonds are labile towards protodeauration but not susceptible to β -hydride elimination,⁶ which makes gold hydrides rare species that are difficult to access.

Gold(I) reluctance to engage in β -hydride elimination is indeed demonstrated by the isolation and thermal stability of several gold alkyl complexes. Consequently, Au(I)/Au(III) cycles including β -hydride elimination and migratory insertion steps at Au(I) are not feasible.^{369, 383} Köppel and coworkers studied experimentally and computationally the possibility of β -hydride elimination or migratory insertion in Au(I) alkyl or Au(I) hydride complexes, respectively.³⁶⁹ DFT calculations predicted a high barrier ($49.7 \text{ kcal}\cdot\text{mol}^{-1}$) for the β -hydride elimination of ethylene from [(IPr)Au(Et)], and, experimentally, the complex decomposed at 180°C presumably not via β -hydride elimination. The lack of reactivity was attributed to the filled $5d$ shell of Au(I) complexes, which hampers the required $\text{Au}\cdots\text{H}$ interaction for the elimination to occur. Nevertheless, Au(III) complexes feature empty $5d$ orbitals which might be available for $\text{Au}\cdots\text{H}$ interactions, thereby allowing β -hydride elimination.

Certainly, this hypothesis was supported by the work of Toste where NHC-alkylgold(III) fluoride complexes afforded alkenes as side-products, suggesting that a β -hydride elimination pathway was competing with the expected $\text{C}(\text{sp}^3)\text{–F}$ reductive elimination. However, the putative NHC-gold(III) hydride species was not detected.³⁸⁴

In 2016, the group of Bourissou provided the first comprehensive study of β -hydride elimination events at Au(III) complexes. Taking advantage of a phosphino-naphthyl (P,C) chelating ligand, they thoroughly investigated, both experimentally and computationally, the fate of a series of well-defined cationic cyclometalated gold(III) alkyl complexes **202**.³⁸⁵ From *n*-propyl and *n*-butyl Au(III) complexes **202**, propylene, 1-butene, and 2-butenes were formed, validating the decomposition of the complexes via a β -hydride elimination pathway (Scheme I.46a). The formation of both *cis* and *trans* isomers of 2-butene was rationalized by an olefin isomerization process based on sequential β -hydride elimination/reinsertion steps. In addition, when phenylgold(III) complex **203** was reacted with ethylene and a halide scavenger, the corresponding transient gold(III) alkyl complex **204** was formed via ethylene insertion, then it eliminated styrene via β -hydride elimination, and finally styrene reinserted into the Au–H bond to generate complex **205** (Scheme I.46b).³⁷⁸ Notably, the arene moiety of complex **205** featured a η^2 -coordination to the Au(III) center, disfavoring further β -hydride elimination of styrene from complex **205**.



Scheme I.46. Formation of cationic (P,C)-cyclometalated gold(III) alkyl complexes **202** and **204** and reaction outcomes upon β -hydride elimination/reinsertion pathways.

As aforementioned, the group of Nevado reported in 2017 the synthesis of a gold(III) formate complex **105** that participated in the catalytic dehydrogenation of formic acid (Section I.3.4, Scheme I.25).²⁷⁴ Although they did not experimentally detect the putative gold(III) hydride intermediate **106** formed via β -hydride elimination, its involvement in the catalytic cycle was evidenced. Additionally, the group of Patil reported in 2023 a gold-catalyzed Heck reaction involving a selective β -hydride elimination step from intermediate **199** that explains the regioselectivity observed in the coupling products (Section I.4.4, Scheme I.44c).²²³ These are examples of β -hydride elimination events at Au(III) species being part of a catalytic reaction.

I.5. REFERENCES

1. R. V. Parish, *Gold Bull.*, 1998, **31**, 14-21.
2. J. H. Teles, S. Brode and M. Chabanas, *Angew. Chem. Int. Ed.*, 1998, **37**, 1415-1418.
3. Y. Fukuda, K. Utimoto and H. Nozaki, *Heterocycles*, 1987, **25**, 297-300.
4. A. S. K. Hashmi, *Chem. Rev.*, 2007, **107**, 3180-3211.
5. C. Nevado, *CHIMLA*, 2010, **64**, 247.
6. A. Corma, A. Leyva-Pérez and M. J. Sabater, *Chem. Rev.*, 2011, **111**, 1657-1712.
7. M. Rudolph and A. S. K. Hashmi, *Chem. Commun.*, 2011, **47**, 6536-6544.
8. R. Dorel and A. M. Echavarren, *Chem. Rev.*, 2015, **115**, 9028-9072.
9. A. S. K. Hashmi, *Gold Bull.*, 2003, **36**, 3-9.
10. C. Obradors and A. M. Echavarren, *Acc. Chem. Res.*, 2014, **47**, 902-912.
11. A. S. K. Hashmi, in *Topics in Organometallic Chemistry*, ed. L. J. Gooßen, Springer Berlin Heidelberg, Berlin, Heidelberg, 2013, vol. 44, pp. 143-164.
12. H. G. Raubenheimer and H. Schmidbaur, *J. Chem. Educ.*, 2014, **91**, 2024-2036.
13. M. N. Hopkinson, A. D. Gee and V. Gouverneur, *Chem. Eur. J.*, 2011, **17**, 8248-8262.
14. M. Joost, A. Amgoune and D. Bourissou, *Angew. Chem. Int. Ed.*, 2015, **54**, 15022-15045.
15. R. T. Mertens and S. G. Awuah, in *Catalysis by Metal Complexes and Nanomaterials: Fundamentals and Applications*, American Chemical Society, 2019, vol. 1317, ch. 2, pp. 19-55.
16. A. Zeineddine, L. Estévez, S. Mallet-Ladeira, K. Miqueu, A. Amgoune and D. Bourissou, *Nat. Commun.*, 2017, **8**, 565.
17. M.-C. Daniel and D. Astruc, *Chem. Rev.*, 2004, **104**, 293-346.
18. V. W.-W. Yam, V. K.-M. Au and S. Y.-L. Leung, *Chem. Rev.*, 2015, **115**, 7589-7728.
19. X. He and V. W.-W. Yam, *Coord. Chem. Rev.*, 2011, **255**, 2111-2123.
20. M.-C. Tang, M.-Y. Chan and V. W.-W. Yam, *Chem. Rev.*, 2021, **121**, 7249-7279.
21. B. Bertrand, M. Bochmann, J. Fernandez-Cestau and L. Rocchigiani, in *Pincer Compounds*, ed. D. Morales-Morales, Elsevier, 2018, pp. 673-699.
22. J. H. Kim, S. Ofori, S. Parkin, H. Vekaria, P. G. Sullivan and S. G. Awuah, *Chem. Sci.*, 2021, **12**, 7467-7479.
23. L.-L. Yan, L.-Y. Yao, M. Ng, W. K. Tang, M.-Y. Leung and V. W.-W. Yam, *J. Am. Chem. Soc.*, 2022, **144**, 19748-19757.
24. J.-F. Longevial, K. El Cheikh, D. Aggad, A. Lebrun, A. van der Lee, F. Tielens, S. Clément, A. Morère, M. Garcia, M. Gary-Bobo and S. Richeter, *Chem. Eur. J.*, 2017, **23**, 14017-14026.
25. M. Üçüncü, E. Karakuş, E. Kurulgan Demirci, M. Sayar, S. Dartar and M. Emrullahoğlu, *Org. Lett.*, 2017, **19**, 2522-2525.
26. F.-H. Yu, X.-F. Song, G.-H. Liu, X. Chang, K. Li, Y. Wang, G. Cui and Y. Chen, *Chem. Eur. J.*, 2022, **28**, e202202439.
27. G. Moreno-Alcántar, P. Picchetti and A. Casini, *Angew. Chem. Int. Ed.*, 2023, e202218000.
28. P. Pyykkö, *Angew. Chem. Int. Ed.*, 2002, **41**, 3573-3578.
29. D. J. Gorin and F. D. Toste, *Nature*, 2007, **446**, 395-403.
30. K. S. Pitzer, *Acc. Chem. Res.*, 1979, **12**, 271-276.
31. P. Pyykko and J. P. Desclaux, *Acc. Chem. Res.*, 1979, **12**, 276-281.
32. P. Schwerdtfeger, *Heteroat. Chem*, 2002, **13**, 578-584.
33. A. Leyva-Pérez and A. Corma, *Angew. Chem. Int. Ed.*, 2012, **51**, 614-635.
34. N. Kaltsoyannis, *J. Chem. Soc., Dalton Trans.*, 1997, 1-12.
35. V. W.-W. Yam and E. C.-C. Cheng, *Chem. Soc. Rev.*, 2008, **37**, 1806-1813.
36. J. P. Desclaux, *At. Data Nucl. Data Tables*, 1973, **12**, 311-406.

37. N. Bartlett, *Gold Bull.*, 1998, **31**, 22-25.
38. M. C. Gimeno, in *Modern Supramolecular Gold Chemistry*, 2008, pp. 1-63.
39. J. M. López-de-Luzuriaga, M. Monge and M. E. Olmos, *Dalton Trans.*, 2017, **46**, 2046-2067.
40. B. Cordero, V. Gómez, A. E. Platero-Prats, M. Revés, J. Echeverría, E. Cremades, F. Barragán and S. Alvarez, *Dalton Trans.*, 2008, 2832-2838.
41. P. Pykkö, *Angew. Chem. Int. Ed.*, 2004, **43**, 4412-4456.
42. J. W. Taylor, A. McSkimming, M.-E. Moret and W. H. Harman, *Angew. Chem. Int. Ed.*, 2017, **56**, 10413-10417.
43. D. McIntosh and G. A. Ozin, *Inorg. Chem.*, 1977, **16**, 51-59.
44. D. F. McIntosh, G. A. Ozin and R. P. Messmer, *Inorg. Chem.*, 1981, **20**, 3640-3650.
45. N. Mézailles, N. Avarvari, N. Maigrot, L. Ricard, F. Mathey, P. Le Floch, L. Cataldo, T. Berclaz and M. Geoffroy, *Angew. Chem. Int. Ed.*, 1999, **38**, 3194-3197.
46. D. S. Weinberger, M. Melaimi, C. E. Moore, A. L. Rheingold, G. Frenking, P. Jerabek and G. Bertrand, *Angew. Chem. Int. Ed.*, 2013, **52**, 8964-8967.
47. I.-C. Hwang and K. Seppelt, *Angew. Chem. Int. Ed.*, 2001, **40**, 3690-3693.
48. K. Leary and N. Bartlett, *J. Chem. Soc., Chem. Commun.*, 1972, 903-904.
49. K. Leary, A. Zalkin and N. Bartlett, *J. Chem. Soc., Chem. Commun.*, 1973, 131-132.
50. K. Leary, A. Zalkin and N. Bartlett, *Inorg. Chem.*, 1974, **13**, 775-779.
51. F. Mohr, *Gold Bull.*, 2004, **37**, 164-169.
52. M. C. Gimeno and A. Laguna, *Gold Bull.*, 2003, **36**, 83-92.
53. M. A. Carvajal, J. J. Novoa and S. Alvarez, *J. Am. Chem. Soc.*, 2004, **126**, 1465-1477.
54. W. Nakanishi, M. Yamanaka and E. Nakamura, *J. Am. Chem. Soc.*, 2005, **127**, 1446-1453.
55. D.-A. Roşca, J. A. Wright and M. Bochmann, *Dalton Trans.*, 2015, **44**, 20785-20807.
56. L. Rocchigiani and M. Bochmann, *Chem. Rev.*, 2021, **121**, 8364-8451.
57. S. Preiß, C. Förster, S. Otto, M. Bauer, P. Müller, D. Hinderberger, H. Hashemi Haeri, L. Carella and K. Heinze, *Nat. Chem.*, 2017, **9**, 1249-1255.
58. A. A. Mohamed, H. E. Abdou and J. P. Fackler, *Coord. Chem. Rev.*, 2010, **254**, 1253-1259.
59. R. Usón, A. Laguna, M. Laguna, M. N. Fraile, P. G. Jones and G. M. Sheldrick, *J. Chem. Soc., Dalton Trans.*, 1986, 291-296.
60. H. Kitagawa, N. Kojima and T. Nakajima, *J. Chem. Soc., Dalton Trans.*, 1991, 3121-3125.
61. D.-A. Roşca, D. A. Smith, D. L. Hughes and M. Bochmann, *Angew. Chem. Int. Ed.*, 2012, **51**, 10643-10646.
62. B. Sahoo, M. N. Hopkinson and F. Glorius, *J. Am. Chem. Soc.*, 2013, **135**, 5505-5508.
63. X.-z. Shu, M. Zhang, Y. He, H. Frei and F. D. Toste, *J. Am. Chem. Soc.*, 2014, **136**, 5844-5847.
64. M. S. Winston, W. J. Wolf and F. D. Toste, *J. Am. Chem. Soc.*, 2014, **136**, 7777-7782.
65. S. Kim, J. Rojas-Martin and F. D. Toste, *Chem. Sci.*, 2016, **7**, 85-88.
66. A. Tlahuext-Aca, M. N. Hopkinson, B. Sahoo and F. Glorius, *Chem. Sci.*, 2016, **7**, 89-93.
67. L. Huang, M. Rudolph, F. Rominger and A. S. K. Hashmi, *Angew. Chem. Int. Ed.*, 2016, **55**, 4808-4813.
68. M. N. Hopkinson, A. Tlahuext-Aca and F. Glorius, *Acc. Chem. Res.*, 2016, **49**, 2261-2272.
69. A. J. Blake, J. A. Greig, A. J. Holder, T. I. Hyde, A. Taylor and M. Schröder, *Angew. Chem. Int. Ed.*, 1990, **29**, 197-198.
70. S. Seidel and K. Seppelt, *Science*, 2000, **290**, 117-118.
71. T. Drews, S. Seidel and K. Seppelt, *Angew. Chem. Int. Ed.*, 2002, **41**, 454-456.

72. A. L. Allred, *J. Inorg. Nucl. Chem.*, 1961, **17**, 215-221.
73. S. G. Bratsch, *J. Phys. Chem. Ref. Data*, 1989, **18**, 1-21.
74. H. Schmidbaur and A. Schier, *Chem. Soc. Rev.*, 2008, **37**, 1931-1951.
75. F. Scherbaum, A. Grohmann, B. Huber, C. Krüger and H. Schmidbaur, *Angew. Chem. Int. Ed.*, 1988, **27**, 1544-1546.
76. H. Schmidbaur, F. Scherbaum, B. Huber and G. Müller, *Angew. Chem. Int. Ed.*, 1988, **27**, 419-421.
77. H. Schmidbaur, *Gold Bull.*, 1990, **23**, 11-21.
78. P. Pykkö, *Chem. Rev.*, 1997, **97**, 597-636.
79. R. G. Pearson, *J. Am. Chem. Soc.*, 1963, **85**, 3533-3539.
80. G. Dyker, *Angew. Chem. Int. Ed.*, 1999, **38**, 1698-1712.
81. J. Hassan, M. Sévignon, C. Gozzi, E. Schulz and M. Lemaire, *Chem. Rev.*, 2002, **102**, 1359-1470.
82. B. M. Frost and L. C. Czabaniuk, *Angew. Chem. Int. Ed.*, 2014, **53**, 2826-2851.
83. B. Su, Z.-C. Cao and Z.-J. Shi, *Acc. Chem. Res.*, 2015, **48**, 886-896.
84. M. Kosugi, M. Kameyama and T. Migita, *Chem. Lett.*, 1983, **12**, 927-928.
85. S. L. Buchwald, *Acc. Chem. Res.*, 2008, **41**, 1439-1439.
86. J. F. Hartwig, *Nature*, 2008, **455**, 314-322.
87. B. Schlummer and U. Scholz, *Adv. Synth. Catal.*, 2004, **346**, 1599-1626.
88. J.-P. Corbet and G. Mignani, *Chem. Rev.*, 2006, **106**, 2651-2710.
89. S. L. Buchwald, C. Mauger, G. Mignani and U. Scholz, *Adv. Synth. Catal.*, 2006, **348**, 23-39.
90. J. Magano and J. R. Dunetz, *Chem. Rev.*, 2011, **111**, 2177-2250.
91. J. Yamaguchi, A. D. Yamaguchi and K. Itami, *Angew. Chem. Int. Ed.*, 2012, **51**, 8960-9009.
92. C. C. C. Johansson Seechurn, M. O. Kitching, T. J. Colacot and V. Snieckus, *Angew. Chem. Int. Ed.*, 2012, **51**, 5062-5085.
93. D. A. Valyaev, G. Lavigne and N. Lugan, *Coord. Chem. Rev.*, 2016, **308**, 191-235.
94. T. L. Mako and J. A. Byers, *Inorg. Chem. Front.*, 2016, **3**, 766-790.
95. C. Gosmini, J.-M. Bégouin and A. Moncomble, *Chem. Commun.*, 2008, 3221-3233.
96. B. M. Rosen, K. W. Quasdorf, D. A. Wilson, N. Zhang, A.-M. Resmerita, N. K. Garg and V. Percec, *Chem. Rev.*, 2011, **111**, 1346-1416.
97. G. Evano, N. Blanchard and M. Toumi, *Chem. Rev.*, 2008, **108**, 3054-3131.
98. D. A. Colby, R. G. Bergman and J. A. Ellman, *Chem. Rev.*, 2010, **110**, 624-655.
99. A. Nijamudheen and A. Datta, *Chem. Eur. J.*, 2020, **26**, 1442-1487.
100. J. P. Wolfe, S. Wagaw, J.-F. Marcoux and S. L. Buchwald, *Acc. Chem. Res.*, 1998, **31**, 805-818.
101. J. F. Hartwig, *Acc. Chem. Res.*, 1998, **31**, 852-860.
102. I. P. Beletskaya and V. P. Ananikov, *Chem. Rev.*, 2011, **111**, 1596-1636.
103. P. Font and X. Ribas, *Eur. J. Inorg. Chem.*, 2021, **2021**, 2556-2569.
104. Y. Ito, M. Sawamura and T. Hayashi, *J. Am. Chem. Soc.*, 1986, **108**, 6405-6406.
105. A. Togni and S. D. Pastor, *J. Org. Chem.*, 1990, **55**, 1649-1664.
106. Y. Fukuda and K. Utimoto, *Synthesis*, 1991, **1991**, 975-978.
107. Y. Fukuda and K. Utimoto, *J. Org. Chem.*, 1991, **56**, 3729-3731.
108. Y. Fukuda and K. Utimoto, *Bull. Chem. Soc. Jpn.*, 1991, **64**, 2013-2015.
109. A. S. K. Hashmi, L. Schwarz, J.-H. Choi and T. M. Frost, *Angew. Chem. Int. Ed.*, 2000, **39**, 2285-2288.
110. A. S. K. Hashmi, T. M. Frost and J. W. Bats, *J. Am. Chem. Soc.*, 2000, **122**, 11553-11554.
111. A. Hoffmann-Röder and N. Krause, *Org. Biomol. Chem.*, 2005, **3**, 387-391.
112. R. A. Widenhoefer and X. Han, *Eur. J. Org. Chem.*, 2006, **2006**, 4555-4563.

113. J. Muzart, *Tetrahedron*, 2008, **64**, 5815-5849.
114. Z. Li, C. Brouwer and C. He, *Chem. Rev.*, 2008, **108**, 3239-3265.
115. A. Arcadi, *Chem. Rev.*, 2008, **108**, 3266-3325.
116. E. Jiménez-Núñez and A. M. Echavarren, *Chem. Commun.*, 2007, 333-346.
117. A. S. K. Hashmi, M. C. Blanco, E. Kurpejović, W. Frey and J. W. Bats, *Adv. Synth. Catal.*, 2006, **348**, 709-713.
118. A. Hoffmann-Röder and N. Krause, *Org. Lett.*, 2001, **3**, 2537-2538.
119. N. Morita and N. Krause, *Org. Lett.*, 2004, **6**, 4121-4123.
120. N. Morita and N. Krause, *Angew. Chem. Int. Ed.*, 2006, **45**, 1897-1899.
121. Z. Zhang, C. Liu, R. E. Kinder, X. Han, H. Qian and R. A. Widenhoefer, *J. Am. Chem. Soc.*, 2006, **128**, 9066-9073.
122. C.-G. Yang and C. He, *J. Am. Chem. Soc.*, 2005, **127**, 6966-6967.
123. X. Han and R. A. Widenhoefer, *Angew. Chem. Int. Ed.*, 2006, **45**, 1747-1749.
124. C. F. Bender and R. A. Widenhoefer, *Chem. Commun.*, 2006, 4143-4144.
125. C.-Y. Zhou and C.-M. Che, *J. Am. Chem. Soc.*, 2007, **129**, 5828-5829.
126. M. Marín-Luna, O. Nieto Faza and C. Silva López, *Front. Chem.*, 2019, **7**, 296.
127. A. Fürstner and P. W. Davies, *Angew. Chem. Int. Ed.*, 2007, **46**, 3410-3449.
128. A. S. K. Hashmi, W. Yang and F. Rominger, *Angew. Chem. Int. Ed.*, 2011, **50**, 5762-5765.
129. A. S. K. Hashmi, W. Yang and F. Rominger, *Chem. Eur. J.*, 2012, **18**, 6576-6580.
130. M. Ackermann, J. Bucher, M. Rappold, K. Graf, F. Rominger and A. S. K. Hashmi, *Chem. Asian J.*, 2013, **8**, 1786-1794.
131. C. Hu, K. Farshadfar, M. C. Dietl, A. Cervantes-Reyes, T. Wang, T. Adak, M. Rudolph, F. Rominger, J. Li, A. Ariafard and A. S. K. Hashmi, *ACS Catal.*, 2021, **11**, 6510-6518.
132. C. Aubert, L. Fensterbank, P. Garcia, M. Malacria and A. Simonneau, *Chem. Rev.*, 2011, **111**, 1954-1993.
133. C. Nieto-Oberhuber, M. P. Muñoz, E. Buñuel, C. Nevado, D. J. Cárdenas and A. M. Echavarren, *Angew. Chem. Int. Ed.*, 2004, **43**, 2402-2406.
134. M. P. Muñoz, J. Adrio, J. C. Carretero and A. M. Echavarren, *Organometallics*, 2005, **24**, 1293-1300.
135. Y.-M. Wang, A. D. Lackner and F. D. Toste, *Acc. Chem. Res.*, 2014, **47**, 889-901.
136. N. Mézailles, L. Ricard and F. Gagosz, *Org. Lett.*, 2005, **7**, 4133-4136.
137. E. Jiménez-Núñez and A. M. Echavarren, *Chem. Rev.*, 2008, **108**, 3326-3350.
138. L. Zhang, J. Sun and S. A. Kozmin, *Adv. Synth. Catal.*, 2006, **348**, 2271-2296.
139. S. Ma, S. Yu and Z. Gu, *Angew. Chem. Int. Ed.*, 2006, **45**, 200-203.
140. A. M. Echavarren and E. Jiménez-Núñez, *Top. Catal.*, 2010, **53**, 924-930.
141. C. Nieto-Oberhuber, S. López and A. M. Echavarren, *J. Am. Chem. Soc.*, 2005, **127**, 6178-6179.
142. C. Nieto-Oberhuber, P. Pérez-Galán, E. Herrero-Gómez, T. Lauterbach, C. Rodríguez, S. López, C. Bour, A. Rosellón, D. J. Cárdenas and A. M. Echavarren, *J. Am. Chem. Soc.*, 2008, **130**, 269-279.
143. A. M. Asiri and A. S. K. Hashmi, *Chem. Soc. Rev.*, 2016, **45**, 4471-4503.
144. A. S. K. Hashmi, I. Braun, M. Rudolph and F. Rominger, *Organometallics*, 2012, **31**, 644-661.
145. A. S. K. Hashmi, *Acc. Chem. Res.*, 2014, **47**, 864-876.
146. M. Wietek, Y. Tokimizu, M. Rudolph, F. Rominger, H. Ohno, N. Fujii and A. S. K. Hashmi, *Chem. Eur. J.*, 2014, **20**, 16331-16336.
147. Y. Tokimizu, M. Wietek, M. Rudolph, S. Oishi, N. Fujii, A. S. K. Hashmi and H. Ohno, *Org. Lett.*, 2015, **17**, 604-607.

148. M. H. Larsen, K. N. Houk and A. S. K. Hashmi, *J. Am. Chem. Soc.*, 2015, **137**, 10668-10676.
149. S. Tšupova, M. M. Hansmann, M. Rudolph, F. Rominger and A. S. K. Hashmi, *Chem. Eur. J.*, 2016, **22**, 16286-16291.
150. S. Tšupova, M. Rudolph, F. Rominger and A. S. K. Hashmi, *Chem. Eur. J.*, 2017, **23**, 12259-12263.
151. X. Zhao, M. Rudolph and A. S. K. Hashmi, *Chem. Commun.*, 2019, **55**, 12127-12135.
152. X. Chen, K. M. Engle, D.-H. Wang and J.-Q. Yu, *Angew. Chem. Int. Ed.*, 2009, **48**, 5094-5115.
153. P. Ruiz-Castillo and S. L. Buchwald, *Chem. Rev.*, 2016, **116**, 12564-12649.
154. A. Biffis, P. Centomo, A. Del Zotto and M. Zecca, *Chem. Rev.*, 2018, **118**, 2249-2295.
155. L. Capdevila, T. H. Meyer, S. Roldán-Gómez, J. M. Luis, L. Ackermann and X. Ribas, *ACS Catal.*, 2019, **9**, 11074-11081.
156. C. A. Malapit, J. R. Bour, S. R. Laursen and M. S. Sanford, *J. Am. Chem. Soc.*, 2019, **141**, 17322-17330.
157. R. Mei, U. Dhawa, R. C. Samanta, W. Ma, J. Wencel-Delord and L. Ackermann, *ChemSusChem*, 2020, **13**, 3306-3356.
158. A. Casitas, A. E. King, T. Parella, M. Costas, S. S. Stahl and X. Ribas, *Chem. Sci.*, 2010, **1**, 326-330.
159. A. Casitas, M. Canta, M. Solà, M. Costas and X. Ribas, *J. Am. Chem. Soc.*, 2011, **133**, 19386-19392.
160. M. Font, T. Parella, M. Costas and X. Ribas, *Organometallics*, 2012, **31**, 7976-7982.
161. A. Casitas and X. Ribas, *Chem. Sci.*, 2013, **4**, 2301-2318.
162. X. Ribas and M. Devillard, *Chem. Eur. J.*, 2018, **24**, 1222-1230.
163. T. Lauterbach, M. Livendahl, A. Rosellón, P. Espinet and A. M. Echavarren, *Org. Lett.*, 2010, **12**, 3006-3009.
164. M. Livendahl, P. Espinet and A. M. Echavarren, *Platinum Met. Rev.*, 2011, **55**, 212-214.
165. M. Livendahl, C. Goehry, F. Maseras and A. M. Echavarren, *Chem. Commun.*, 2014, **50**, 1533-1536.
166. P. Garcia, M. Malacria, C. Aubert, V. Gandon and L. Fensterbank, *ChemCatChem*, 2010, **2**, 493-497.
167. H. A. Wegner and M. Auzias, *Angew. Chem. Int. Ed.*, 2011, **50**, 8236-8247.
168. A. Kar, N. Mangu, H. M. Kaiser, M. Beller and M. K. Tse, *Chem. Commun.*, 2008, 386-388.
169. L. Cui, G. Zhang and L. Zhang, *Bioorg. Med. Chem. Lett.*, 2009, **19**, 3884-3887.
170. G. Zhang, Y. Peng, L. Cui and L. Zhang, *Angew. Chem. Int. Ed.*, 2009, **48**, 3112-3115.
171. L. T. Ball, M. Green, G. C. Lloyd-Jones and C. A. Russell, *Org. Lett.*, 2010, **12**, 4724-4727.
172. L. T. Ball, G. C. Lloyd-Jones and C. A. Russell, *Chem. Eur. J.*, 2012, **18**, 2931-2937.
173. W. E. Brenzovich, J.-F. Brazeau and F. D. Toste, *Org. Lett.*, 2010, **12**, 4728-4731.
174. A. D. Melhado, W. E. Brenzovich, A. D. Lackner and F. D. Toste, *J. Am. Chem. Soc.*, 2010, **132**, 8885-8887.
175. W. E. Brenzovich Jr., D. Benitez, A. D. Lackner, H. P. Shunatona, E. Tkatchouk, W. A. Goddard III and F. D. Toste, *Angew. Chem. Int. Ed.*, 2010, **49**, 5519-5522.
176. G. Zhang, L. Cui, Y. Wang and L. Zhang, *J. Am. Chem. Soc.*, 2010, **132**, 1474-1475.
177. M. N. Hopkinson, A. Tessier, A. Salisbury, G. T. Giuffredi, L. E. Combettes, A. D. Gee and V. Gouverneur, *Chem. Eur. J.*, 2010, **16**, 4739-4743.
178. G. Zhang, Y. Luo, Y. Wang and L. Zhang, *Angew. Chem. Int. Ed.*, 2011, **50**, 4450-4454.
179. T. de Haro and C. Nevado, *J. Am. Chem. Soc.*, 2010, **132**, 1512-1513.

180. D. Qian and J. Zhang, *Beilstein J. Org. Chem.*, 2011, **7**, 808-812.
181. H. Peng, Y. Xi, N. Ronaghi, B. Dong, N. G. Akhmedov and X. Shi, *J. Am. Chem. Soc.*, 2014, **136**, 13174-13177.
182. L. T. Ball, G. C. Lloyd-Jones and C. A. Russell, *Science*, 2012, **337**, 1644-1648.
183. L. T. Ball, G. C. Lloyd-Jones and C. A. Russell, *J. Am. Chem. Soc.*, 2014, **136**, 254-264.
184. A. J. Cresswell and G. C. Lloyd-Jones, *Chem. Eur. J.*, 2016, **22**, 12641-12645.
185. X. C. Cambeiro, N. Ahlsten and I. Larrosa, *J. Am. Chem. Soc.*, 2015, **137**, 15636-15639.
186. M. Hofer, A. Genoux, R. Kumar and C. Nevado, *Angew. Chem. Int. Ed.*, 2017, **56**, 1021-1025.
187. T. J. A. Corrie, L. T. Ball, C. A. Russell and G. C. Lloyd-Jones, *J. Am. Chem. Soc.*, 2017, **139**, 245-254.
188. M. O. Akram, S. Banerjee, S. S. Saswade, V. Bedi and N. T. Patil, *Chem. Commun.*, 2018, **54**, 11069-11083.
189. S. Kramer, *Synthesis*, 2020, **52**, 2017-2030.
190. C. González-Arellano, A. Corma, M. Iglesias and F. Sánchez, *J. Catal.*, 2006, **238**, 497-501.
191. C. González-Arellano, A. Abad, A. Corma, H. García, M. Iglesias and F. Sánchez, *Angew. Chem. Int. Ed.*, 2007, **46**, 1536-1538.
192. J. Han, Y. Liu and R. Guo, *J. Am. Chem. Soc.*, 2009, **131**, 2060-2061.
193. G. Kyriakou, S. K. Beaumont, S. M. Humphrey, C. Antonetti and R. M. Lambert, *ChemCatChem*, 2010, **2**, 1444-1449.
194. V. K. Kanuru, G. Kyriakou, S. K. Beaumont, A. C. Papageorgiou, D. J. Watson and R. M. Lambert, *J. Am. Chem. Soc.*, 2010, **132**, 8081-8086.
195. S. K. Beaumont, G. Kyriakou and R. M. Lambert, *J. Am. Chem. Soc.*, 2010, **132**, 12246-12248.
196. A. Corma, R. Juárez, M. Boronat, F. Sánchez, M. Iglesias and H. García, *Chem. Commun.*, 2011, **47**, 1446-1448.
197. M. D. Levin and F. D. Toste, *Angew. Chem. Int. Ed.*, 2014, **53**, 6211-6215.
198. J. Serra, C. J. Whiteoak, F. Acuna-Pares, M. Font, J. M. Luis, J. Lloret-Fillol and X. Ribas, *J. Am. Chem. Soc.*, 2015, **137**, 13389-13397.
199. M. Font, F. Acuña-Parés, T. Parella, J. Serra, J. M. Luis, J. Lloret-Fillol, M. Costas and X. Ribas, *Nat. Commun.*, 2014, **5**:4373.
200. J. Serra, T. Parella and X. Ribas, *Chem. Sci.*, 2017, **8**, 946-952.
201. J. Rodriguez, A. Zeineddine, E. D. Sosa Carrizo, K. Miqueu, N. Saffon-Merceron, A. Amgoune and D. Bourissou, *Chem. Sci.*, 2019, **10**, 7183-7192.
202. J. Rodriguez, D. Vesseur, A. Tabey, S. Mallet-Ladeira, K. Miqueu and D. Bourissou, *ACS Catal.*, 2022, **12**, 993-1003.
203. J. Rodriguez, N. Adet, N. Saffon-Merceron and D. Bourissou, *Chem. Commun.*, 2020, **56**, 94-97.
204. M. O. Akram, A. Das, I. Chakrabarty and N. T. Patil, *Org. Lett.*, 2019, **21**, 8101-8105.
205. S. R. Mudshinge, Y. Yang, B. Xu, G. B. Hammond and Z. Lu, *Angew. Chem. Int. Ed.*, 2022, **61**, e202115687.
206. A. G. Tathe and N. T. Patil, *Org. Lett.*, 2022, **24**, 4459-4463.
207. A. Das and N. T. Patil, *ACS Catal.*, 2023, 3847-3853.
208. G. Chen and B. Xu, *ACS Catal.*, 2023, **13**, 1823-1829.
209. M. Navarro, A. Toledo, M. Joost, A. Amgoune, S. Mallet-Ladeira and D. Bourissou, *Chem. Commun.*, 2019, **55**, 7974-7977.
210. M. Navarro, A. Toledo, S. Mallet-Ladeira, E. D. Sosa Carrizo, K. Miqueu and D. Bourissou, *Chem. Sci.*, 2020, **11**, 2750-2758.
211. V. W. Bhoyare, A. G. Tathe, A. Das, C. C. Chintawar and N. T. Patil, *Chem. Soc. Rev.*, 2021, **50**, 10422-10450.

212. T. McCallum, *Org. Biomol. Chem.*, 2023, **21**, 1629-1646.
213. M. Rigoulet, O. Thillaye du Boullay, A. Amgoune and D. Bourissou, *Angew. Chem. Int. Ed.*, 2020, **59**, 16625-16630.
214. A. G. Tathe, C. C. Chintawar, V. W. Bhojare and N. T. Patil, *Chem. Commun.*, 2020, **56**, 9304-9307.
215. S. Zhang, C. Wang, X. Ye and X. Shi, *Angew. Chem. Int. Ed.*, 2020, **59**, 20470-20474.
216. C. C. Chintawar, A. K. Yadav and N. T. Patil, *Angew. Chem. Int. Ed.*, 2020, **59**, 11808-11813.
217. A. G. Tathe, Urvashi, A. K. Yadav, C. C. Chintawar and N. T. Patil, *ACS Catal.*, 2021, **11**, 4576-4582.
218. J. Rodriguez, A. Tabey, S. Mallet-Ladeira and D. Bourissou, *Chem. Sci.*, 2021, **12**, 7706-7712.
219. A. Kumar, A. Das and N. T. Patil, *Org. Lett.*, 2023.
220. C. C. Chintawar and N. T. Patil, *Gold Bull.*, 2022, **55**, 161-168.
221. X. Ye, C. Wang, S. Zhang, Q. Tang, L. Wojtas, M. Li and X. Shi, *Chem. Eur. J.*, 2022, e202201018.
222. C. C. Chintawar, V. W. Bhojare, M. V. Mane and N. T. Patil, *J. Am. Chem. Soc.*, 2022, **144**, 7089-7095.
223. V. W. Bhojare, E. D. Sosa Carrizo, C. C. Chintawar, V. Gandon and N. T. Patil, *J. Am. Chem. Soc.*, 2023.
224. T. Shibata, R. Nagai, S. Okazaki, S. Nishibe and M. Ito, *Bull. Chem. Soc. Jpn.*, 2022, **95**, 700-706.
225. E. Tomás-Mendivil, P. Y. Toullec, J. Díez, S. Conejero, V. Michelet and V. Cadierno, *Org. Lett.*, 2012, **14**, 2520-2523.
226. E. Tomás-Mendivil, P. Y. Toullec, J. Borge, S. Conejero, V. Michelet and V. Cadierno, *ACS Catal.*, 2013, **3**, 3086-3098.
227. A. G. Nair, R. T. McBurney, M. R. D. Gatus, S. C. Binding and B. A. Messerle, *Inorg. Chem.*, 2017, **56**, 12067-12075.
228. J. Chu, D. Munz, R. Jazzar, M. Melaimi and G. Bertrand, *J. Am. Chem. Soc.*, 2016, **138**, 7884-7887.
229. M. Navarro, A. Tabey, G. Szalóki, S. Mallet-Ladeira and D. Bourissou, *Organometallics*, 2021, **40**, 1571-1576.
230. P. Font, H. Valdés, G. Guisado-Barrios and X. Ribas, *Chem. Sci.*, 2022, **13**, 9351-9360.
231. P. Gao, J. Xu, T. Zhou, Y. Liu, E. Bisz, B. Dziuk, R. Lalancette, R. Szostak, D. Zhang and M. Szostak, *Angew. Chem. Int. Ed.*, 2023, **62**, e202218427.
232. S. C. Scott, J. A. Cadge, G. Boden, J. Bower and C. A. Russell, *Angew. Chem. Int. Ed.*, 2023, e202301526.
233. J. P. Brand, J. Charpentier and J. Waser, *Angew. Chem. Int. Ed.*, 2009, **48**, 9346-9349.
234. J. P. Brand, C. Chevalley, R. Scopelliti and J. Waser, *Chem. Eur. J.*, 2012, **18**, 5655-5666.
235. Y. Li, J. P. Brand and J. Waser, *Angew. Chem. Int. Ed.*, 2013, **52**, 6743-6747.
236. H. Ghari, Y. Li, R. Roohzadeh, P. Caramenti, J. Waser and A. Ariafard, *Dalton Trans.*, 2017, **46**, 12257-12262.
237. S. Banerjee and N. T. Patil, *Chem. Commun.*, 2017, **53**, 7937-7940.
238. X. Li, X. Xie, N. Sun and Y. Liu, *Angew. Chem. Int. Ed.*, 2017, **56**, 6994-6998.
239. R. Cai, M. Lu, E. Y. Aguilera, Y. Xi, N. G. Akhmedov, J. L. Petersen, H. Chen and X. Shi, *Angew. Chem. Int. Ed.*, 2015, **54**, 8772-8776.
240. H. Peng, R. Cai, C. Xu, H. Chen and X. Shi, *Chem. Sci.*, 2016, **7**, 6190-6196.
241. B. Dong, H. Peng, S. E. Motika and X. Shi, *Chem. Eur. J.*, 2017, **23**, 11093-11099.
242. M. Barbero and S. Dughera, *Tetrahedron*, 2018, **74**, 5758-5769.

243. M. O. Akram, P. S. Shinde, C. C. Chintawar and N. T. Patil, *Org. Biomol. Chem.*, 2018, **16**, 2865-2869.
244. U. A. Carrillo-Arcos and S. Porcel, *Org. Biomol. Chem.*, 2018, **16**, 1837-1842.
245. A. A. Jimoh, S. Hosseyni, X. Ye, L. Wojtas, Y. Hu and X. Shi, *Chem. Commun.*, 2019, **55**, 8150-8153.
246. C. Sauer, Y. Liu, A. De Nisi, S. Protti, M. Fagnoni and M. Bandini, *ChemCatChem*, 2017, **9**, 4456-4459.
247. S. Witzel, J. Xie, M. Rudolph and A. S. K. Hashmi, *Adv. Synth. Catal.*, 2017, **359**, 1522-1528.
248. S. Witzel, K. Sekine, M. Rudolph and A. S. K. Hashmi, *Chem. Commun.*, 2018, **54**, 13802-13804.
249. J. Xie, K. Sekine, S. Witzel, P. Krämer, M. Rudolph, F. Rominger and A. S. K. Hashmi, *Angew. Chem. Int. Ed.*, 2018, **57**, 16648-16653.
250. J.-R. Deng, W.-C. Chan, N. Chun-Him Lai, B. Yang, C.-S. Tsang, B. Chi-Bun Ko, S. Lai-Fung Chan and M.-K. Wong, *Chem. Sci.*, 2017, **8**, 7537-7544.
251. H.-J. Tang, X. Zhang, Y.-F. Zhang and C. Feng, *Angew. Chem. Int. Ed.*, 2020, **59**, 5242-5247.
252. M. Zidan, S. Rohe, T. McCallum and L. Barriault, *Catal. Sci. Technol.*, 2018, **8**, 6019-6028.
253. S. Witzel, A. S. K. Hashmi and J. Xie, *Chem. Rev.*, 2021, **121**, 8868-8925.
254. A. Y. Chan, I. B. Perry, N. B. Bissonnette, B. F. Buksh, G. A. Edwards, L. I. Frye, O. L. Garry, M. N. Lavagnino, B. X. Li, Y. Liang, E. Mao, A. Millet, J. V. Oakley, N. L. Reed, H. A. Sakai, C. P. Seath and D. W. C. MacMillan, *Chem. Rev.*, 2022, **122**, 1485-1542.
255. M. N. Hopkinson, B. Sahoo and F. Glorius, *Adv. Synth. Catal.*, 2014, **356**, 2794-2800.
256. Y. He, H. Wu and F. D. Toste, *Chem. Sci.*, 2015, **6**, 1194-1198.
257. V. Gauchot, D. R. Sutherland and A. L. Lee, *Chem. Sci.*, 2017, **8**, 2885-2889.
258. A. Tlahuext-Aca, M. N. Hopkinson, R. A. Garza-Sanchez and F. Glorius, *Chem. Eur. J.*, 2016, **22**, 5909-5913.
259. J. Um, H. Yun and S. Shin, *Org. Lett.*, 2016, **18**, 484-487.
260. B. Alcaide, P. Almendros, E. Busto and A. Luna, *Adv. Synth. Catal.*, 2016, **358**, 1526-1533.
261. Z.-S. Wang, T.-D. Tan, C.-M. Wang, D.-Q. Yuan, T. Zhang, P. Zhu, C. Zhu, J.-M. Zhou and L.-W. Ye, *Chem. Commun.*, 2017, **53**, 6848-6851.
262. L. Bayer, B. S. Birenheide, F. Krämer, S. Lebedkin and F. Breher, *Chem. Eur. J.*, 2022, **28**, e202201856.
263. H. Li, C. Shan, C.-H. Tung and Z. Xu, *Chem. Sci.*, 2017, **8**, 2610-2615.
264. Z. Xia, V. Corcé, F. Zhao, C. Przybylski, A. Espagne, L. Jullien, T. Le Saux, Y. Gimbert, H. Dossmann, V. Mouriès-Mansuy, C. Ollivier and L. Fensterbank, *Nat. Chem.*, 2019, **11**, 797-805.
265. C. C. Chintawar, A. K. Yadav, A. Kumar, S. P. Sancheti and N. T. Patil, *Chem. Rev.*, 2021, **121**, 8478-8558.
266. C.-Y. Wu, T. Horibe, C. B. Jacobsen and F. D. Toste, *Nature*, 2015, **517**, 449-454.
267. J. H. Teles, *Angew. Chem. Int. Ed.*, 2015, **54**, 5556-5558.
268. M. S. M. Holmsen, A. Nova, D. Balcels, E. Langseth, S. Øien-Ødegaard, R. H. Heyn, M. Tilset and G. Laurenczy, *ACS Catal.*, 2017, **7**, 5023-5034.
269. M. S. M. Holmsen, A. Nova, K. Hylland, D. S. Wragg, S. Øien-Ødegaard, R. H. Heyn and M. Tilset, *Chem. Commun.*, 2018, **54**, 11104-11107.
270. C. Blons, S. Mallet-Ladeira, A. Amgoune and D. Bourissou, *Angew. Chem. Int. Ed.*, 2018, **57**, 11732-11736.

271. M. S. M. Holmsen, C. Blons, A. Amgoune, M. Regnacq, D. Lesage, E. D. Sosa Carrizo, P. Lavedan, Y. Gimbert, K. Miqueu and D. Bourissou, *J. Am. Chem. Soc.*, 2022, **144**, 22722-22733.
272. A. C. Reiersølmoen, D. Csókás, I. Pápai, A. Fiksdahl and M. Erdélyi, *J. Am. Chem. Soc.*, 2019, **141**, 18221-18229.
273. A. C. Reiersølmoen, D. Csókás, S. Øien-Ødegaard, A. Vanderkooy, A. K. Gupta, A.-C. C. Carlsson, A. Orthaber, A. Fiksdahl, I. Pápai and M. Erdélyi, *J. Am. Chem. Soc.*, 2020, **142**, 6439-6446.
274. R. Kumar, J.-P. Krieger, E. Gómez-Bengoa, T. Fox, A. Linden and C. Nevado, *Angew. Chem. Int. Ed.*, 2017, **56**, 12862-12865.
275. B. Huang, M. Hu and F. D. Toste, *Trends Chem.*, 2020, **2**, 707-720.
276. A. Davison, D. V. Howe and E. T. Shawl, *Inorg. Chem.*, 1967, **6**, 458-463.
277. J. H. Enemark and J. A. Ibers, *Inorg. Chem.*, 1968, **7**, 2636-2642.
278. A. Tamaki and J. K. Kochi, *J. Organomet. Chem.*, 1972, **40**, C81-C84.
279. A. Johnson and R. J. Puddephatt, *Inorg. Nucl. Chem. Lett.*, 1973, **9**, 1175-1177.
280. A. Shiotani and H. Schmidbaur, *J. Organomet. Chem.*, 1972, **37**, C24-C26.
281. A. Tamaki and J. K. Kochi, *J. Organomet. Chem.*, 1974, **64**, 411-425.
282. A. Johnson and R. J. Puddephatt, *J. Organomet. Chem.*, 1975, **85**, 115-121.
283. A. Tamaki and J. K. Kochi, *J. Chem. Soc., Dalton Trans.*, 1973, 2620-2626.
284. R. E. Bachman, S. A. Bodolosky-Bettis, C. J. Pyle and M. A. Gray, *J. Am. Chem. Soc.*, 2008, **130**, 14303-14310.
285. N. Lassauque, P. Gualco, S. Mallet-Ladeira, K. Miqueu, A. Amgoune and D. Bourissou, *J. Am. Chem. Soc.*, 2013, **135**, 13827-13834.
286. P. Gualco, S. Ladeira, K. Miqueu, A. Amgoune and D. Bourissou, *Organometallics*, 2012, **31**, 6001-6004.
287. P. Gualco, S. Ladeira, K. Miqueu, A. Amgoune and D. Bourissou, *Angew. Chem. Int. Ed.*, 2011, **50**, 8320-8324.
288. M. Joost, P. Gualco, Y. Coppel, K. Miqueu, C. E. Kefalidis, L. Maron, A. Amgoune and D. Bourissou, *Angew. Chem. Int. Ed.*, 2014, **53**, 747-751.
289. J. Guenther, S. Mallet-Ladeira, L. Estevez, K. Miqueu, A. Amgoune and D. Bourissou, *J. Am. Chem. Soc.*, 2014, **136**, 1778-1781.
290. H. Beucher, J. Schörghener, E. Merino and C. Nevado, *Chem. Sci.*, 2021, **12**, 15084-15089.
291. M. Joost, A. Zeineddine, L. Estévez, S. Mallet-Ladeira, K. Miqueu, A. Amgoune and D. Bourissou, *J. Am. Chem. Soc.*, 2014, **136**, 14654-14657.
292. J.-F. Fauvarque, F. Pflüger and M. Troupel, *J. Organomet. Chem.*, 1981, **208**, 419-427.
293. K. C. Lam, T. B. Marder and Z. Lin, *Organometallics*, 2007, **26**, 758-760.
294. A. K. d. K. Lewis, S. Caddick, F. G. N. Cloke, N. C. Billingham, P. B. Hitchcock and J. Leonard, *J. Am. Chem. Soc.*, 2003, **125**, 10066-10073.
295. M. Joost, L. Estévez, K. Miqueu, A. Amgoune and D. Bourissou, *Angew. Chem. Int. Ed.*, 2015, **54**, 5236-5240.
296. G. Szalóki, J. Babinot, V. Martin-Diaconescu, S. Mallet-Ladeira, Y. García-Rodeja, K. Miqueu and D. Bourissou, *Chem. Sci.*, 2022, **13**, 10499-10505.
297. M. J. Harper, C. J. Arthur, J. Crosby, E. J. Emmett, R. L. Falconer, A. J. Fensham-Smith, P. J. Gates, T. Leman, J. E. McGrady, J. F. Bower and C. A. Russell, *J. Am. Chem. Soc.*, 2018, **140**, 4440-4445.
298. J. A. Cadge, H. A. Sparkes, J. F. Bower and C. A. Russell, *Angew. Chem. Int. Ed.*, 2020, **59**, 6617-6621.
299. Y. Yang, P. Antoni, M. Zimmer, K. Sekine, F. F. Mulks, L. Hu, L. Zhang, M. Rudolph, F. Rominger and A. S. K. Hashmi, *Angew. Chem. Int. Ed.*, 2019, **58**, 5129-5133.

300. Y. Yang, L. Eberle, F. F. Mulks, J. F. Wunsch, M. Zimmer, F. Rominger, M. Rudolph and A. S. K. Hashmi, *J. Am. Chem. Soc.*, 2019, **141**, 17414-17420.
301. G. Kleinhans, M. M. Hansmann, G. Guisado-Barrios, D. C. Liles, G. Bertrand and D. I. Bezuidenhout, *J. Am. Chem. Soc.*, 2016, **138**, 15873-15876.
302. A. Genoux, M. Biedrzycki, E. Merino, E. Rivera-Chao, A. Linden and C. Nevado, *Angew. Chem. Int. Ed.*, 2021, **60**, 4164-4168.
303. M. S. Messina, J. M. Stauber, M. A. Waddington, A. L. Rheingold, H. D. Maynard and A. M. Spokoyny, *J. Am. Chem. Soc.*, 2018, **140**, 7065-7069.
304. J. M. Stauber, E. A. Qian, Y. Han, A. L. Rheingold, P. Král, D. Fujita and A. M. Spokoyny, *J. Am. Chem. Soc.*, 2020, **142**, 327-334.
305. J. M. Stauber, A. L. Rheingold and A. M. Spokoyny, *Inorg. Chem.*, 2021, **60**, 5054-5062.
306. J. W. McDaniel, J. M. Stauber, E. A. Doud, A. M. Spokoyny and J. M. Murphy, *Org. Lett.*, 2022, **24**, 5132-5136.
307. L. Huang, F. Rominger, M. Rudolph and A. S. K. Hashmi, *Chem. Commun.*, 2016, **52**, 6435-6438.
308. A. Tlahuext-Aca, M. N. Hopkinson, C. G. Daniliuc and F. Glorius, *Chem. Eur. J.*, 2016, **22**, 11587-11592.
309. E. O. Asomoza-Solís, J. Rojas-Ocampo, R. A. Toscano and S. Porcel, *Chem. Commun.*, 2016, **52**, 7295-7298.
310. S. Kim and F. D. Toste, *J. Am. Chem. Soc.*, 2019, **141**, 4308-4315.
311. A. Burawoy and C. S. Gibson, *J. Chem. Soc.*, 1934, 860-864.
312. M. Aresta and G. Vasapollo, *J. Organomet. Chem.*, 1973, **50**, C51-C53.
313. R. Uson, A. Laguna and J. Vicente, *J. Organomet. Chem.*, 1975, **86**, 415-421.
314. A. Tamaki, S. A. Magennis and J. K. Kochi, *J. Am. Chem. Soc.*, 1974, **96**, 6140-6148.
315. S. Komiya, T. A. Albright, R. Hoffmann and J. K. Kochi, *J. Am. Chem. Soc.*, 1976, **98**, 7255-7265.
316. S. Komiya and J. K. Kochi, *J. Am. Chem. Soc.*, 1976, **98**, 7599-7607.
317. J. Vicente, M. Dolores Bermudez and J. Escribano, *Organometallics*, 1991, **10**, 3380-3384.
318. J. Vicente, M. D. Bermúdez, J. Escribano, M. P. Carrillo and P. G. Jones, *J. Chem. Soc., Dalton Trans.*, 1990, 3083-3089.
319. J. Vicente, M. D. Bermúdez and F. J. Carrión, *Inorg. Chim. Acta*, 1994, **220**, 1-3.
320. S. Lavy, J. J. Miller, M. Pažický, A.-S. Rodrigues, F. Rominger, C. Jäkel, D. Serra, N. Vinokurov and M. Limbach, *Adv. Synth. Catal.*, 2010, **352**, 2993-3000.
321. M. J. Ghidui, A. J. Pistner, G. P. A. Yap, D. A. Lutterman and J. Rosenthal, *Organometallics*, 2013, **32**, 5026-5029.
322. K. K.-Y. Kung, H.-M. Ko, J.-F. Cui, H.-C. Chong, Y.-C. Leung and M.-K. Wong, *Chem. Commun.*, 2014, **50**, 11899-11902.
323. W. J. Wolf, M. S. Winston and F. D. Toste, *Nat. Chem.*, 2014, **6**, 159-164.
324. H. Kawai, W. J. Wolf, A. G. DiPasquale, M. S. Winston and F. D. Toste, *J. Am. Chem. Soc.*, 2016, **138**, 587-593.
325. M. S. Winston, W. J. Wolf and F. D. Toste, *J. Am. Chem. Soc.*, 2015, **137**, 7921-7928.
326. M. D. Levin, T. Q. Chen, M. E. Neubig, C. M. Hong, C. A. Theulier, I. J. Kobylanski, M. Janabi, J. P. O'Neil and F. D. Toste, *Science*, 2017, **356**, 1272-1276.
327. L. Rocchigiani, J. Fernandez-Cestau, P. H. M. Budzelaar and M. Bochmann, *Chem. Eur. J.*, 2018, **24**, 8893-8903.
328. L. Currie, L. Rocchigiani, D. L. Hughes and M. Bochmann, *Dalton Trans.*, 2018, **47**, 6333-6343.
329. M. M. Hansmann, F. Rominger, M. P. Boone, D. W. Stephan and A. S. K. Hashmi, *Organometallics*, 2014, **33**, 4461-4470.
330. M. Hofer, E. Gomez-Bengoa and C. Nevado, *Organometallics*, 2014, **33**, 1328-1332.

331. S. Dupuy, A. M. Z. Slawin and S. P. Nolan, *Chem. Eur. J.*, 2012, **18**, 14923-14928.
332. W. Feuerstein, C. Holzer, X. Gui, L. Neumeier, W. Klopper and F. Breher, *Chem. Eur. J.*, 2020, **26**, 17156-17164.
333. Y. Chen, M. Chen and Y. Liu, *Angew. Chem. Int. Ed.*, 2012, **51**, 6181-6186.
334. M. Contel, M. Stol, M. A. Casado, G. P. M. van Klink, D. D. Ellis, A. L. Spek and G. van Koten, *Organometallics*, 2002, **21**, 4556-4559.
335. Y. Shi and S. A. Blum, *Organometallics*, 2011, **30**, 1776-1779.
336. D. Serra, M.-E. Moret and P. Chen, *J. Am. Chem. Soc.*, 2011, **133**, 8914-8926.
337. M. H. Pérez-Temprano, J. A. Casares, Á. R. de Lera, R. Álvarez and P. Espinet, *Angew. Chem. Int. Ed.*, 2012, **51**, 4917-4920.
338. T. P. Cornell, Y. Shi and S. A. Blum, *Organometallics*, 2012, **31**, 5990-5993.
339. K. Klauke, S. Werner and F. Mohr, *Eur. J. Inorg. Chem.*, 2018, **2018**, 1053-1056.
340. J. Martín, E. Gómez-Bengoia, A. Genoux and C. Nevado, *Angew. Chem. Int. Ed.*, 2022, **61**, e202116755.
341. Y. Shi, S. D. Ramgren and S. A. Blum, *Organometallics*, 2009, **28**, 1275-1277.
342. K.-H. Wong, K.-K. Cheung, M. C.-W. Chan and C.-M. Che, *Organometallics*, 1998, **17**, 3505-3511.
343. M. N. Peñas-Defrutos, C. Bartolomé, M. García-Melchor and P. Espinet, *Angew. Chem. Int. Ed.*, 2019, **58**, 3501-3505.
344. M. M. Hansmann, M. Pernpointner, R. Döpp and A. S. K. Hashmi, *Chem. Eur. J.*, 2013, **19**, 15290-15303.
345. A. S. K. Hashmi and L. Molinari, *Organometallics*, 2011, **30**, 3457-3460.
346. A. S. K. Hashmi, R. Döpp, C. Lothschütz, M. Rudolph, D. Riedel and F. Rominger, *Adv. Synth. Catal.*, 2010, **352**, 1307-1314.
347. A. S. K. Hashmi, C. Lothschütz, R. Döpp, M. Rudolph, T. D. Ramamurthi and F. Rominger, *Angew. Chem. Int. Ed.*, 2009, **48**, 8243-8246.
348. J. J. Hirner, Y. Shi and S. A. Blum, *Acc. Chem. Res.*, 2011, **44**, 603-613.
349. A. S. K. Hashmi, C. Lothschütz, R. Döpp, M. Ackermann, J. De Buck Becker, M. Rudolph, C. Scholz and F. Rominger, *Adv. Synth. Catal.*, 2012, **354**, 133-147.
350. M. H. Pérez-Temprano, J. A. Casares and P. Espinet, *Chem. Eur. J.*, 2012, **18**, 1864-1884.
351. J. delPozo, D. Carrasco, M. H. Pérez-Temprano, M. García-Melchor, R. Álvarez, J. A. Casares and P. Espinet, *Angew. Chem. Int. Ed.*, 2013, **52**, 2189-2193.
352. P. García-Domínguez and C. Nevado, *J. Am. Chem. Soc.*, 2016, **138**, 3266-3269.
353. W. Li, D. Yuan, G. Wang, Y. Zhao, J. Xie, S. Li and C. Zhu, *J. Am. Chem. Soc.*, 2019, **141**, 3187-3197.
354. R. A. Daley, A. S. Morrenzin, S. R. Neufeldt and J. J. Topczewski, *ACS Catal.*, 2021, **11**, 9578-9587.
355. A. Sladek, S. Hofreiter, M. Paul and H. Schmidbaur, *J. Organomet. Chem.*, 1995, **501**, 47-51.
356. J. M. Forward, J. P. Fackler, Jr. and R. J. Staples, *Organometallics*, 1995, **14**, 4194-4198.
357. S. G. Weber, D. Zahner, F. Rominger and B. F. Straub, *Chem. Commun.*, 2012, **48**, 11325-11327.
358. D. V. Partyka, M. Zeller, A. D. Hunter and T. G. Gray, *Angew. Chem. Int. Ed.*, 2006, **45**, 8188-8191.
359. H. K. Lenker, T. G. Gray and R. A. Stockland, *Dalton Trans.*, 2012, **41**, 13274-13276.
360. D. V. Partyka, M. Zeller, A. D. Hunter and T. G. Gray, *Inorg. Chem.*, 2012, **51**, 8394-8401.
361. S. Dupuy, L. E. Crawford, M. Bühl, A. M. Z. Slawin and S. P. Nolan, *Adv. Synth. Catal.*, 2012, **354**, 2380-2386.
362. D.-A. Roşca, D. A. Smith and M. Bochmann, *Chem. Commun.*, 2012, **48**, 7247-7249.

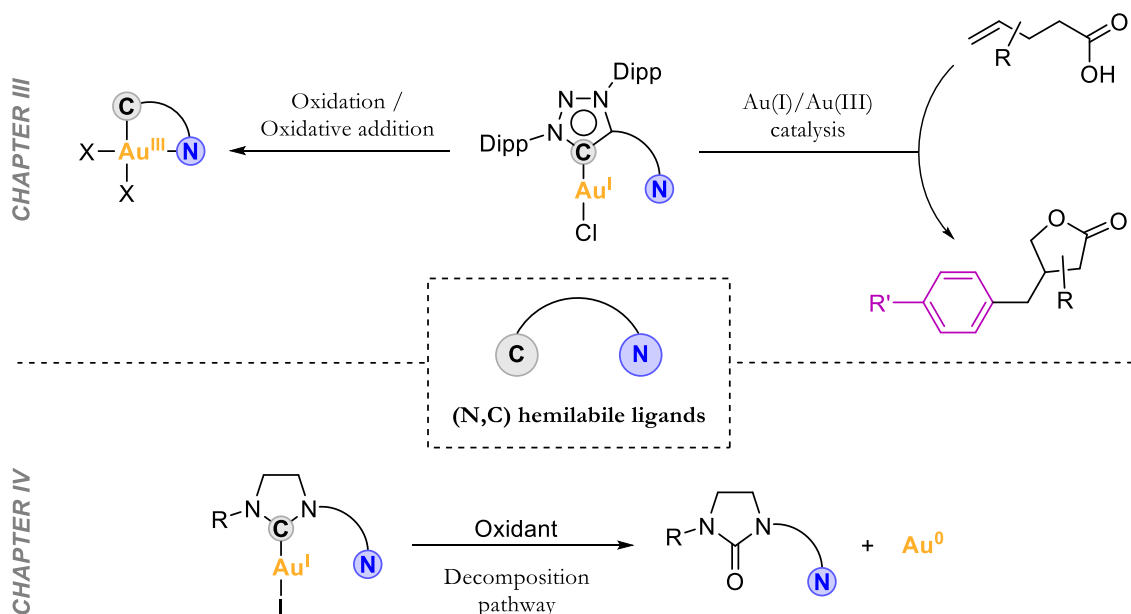
363. D. A. Smith, D.-A. Roşca and M. Bochmann, *Organometallics*, 2012, **31**, 5998-6000.
364. R. Kumar, A. Linden and C. Nevado, *J. Am. Chem. Soc.*, 2016, **138**, 13790-13793.
365. Q. Wu, C. Du, Y. Huang, X. Liu, Z. Long, F. Song and J. You, *Chem. Sci.*, 2015, **6**, 288-293.
366. F. Rekhroukh, R. Brousses, A. Amgoune and D. Bourissou, *Angew. Chem. Int. Ed.*, 2015, **54**, 1266-1269.
367. J. A. Akana, K. X. Bhattacharyya, P. Müller and J. P. Sadighi, *J. Am. Chem. Soc.*, 2007, **129**, 7736-7737.
368. E. Y. Tsui, P. Müller and J. P. Sadighi, *Angew. Chem. Int. Ed.*, 2008, **47**, 8937-8940.
369. G. Klatt, R. Xu, M. Pernpointner, L. Molinari, T. Quang Hung, F. Rominger, A. S. K. Hashmi and H. Köppel, *Chem. Eur. J.*, 2013, **19**, 3954-3961.
370. M. Joost, P. Gualco, S. Mallet-Ladeira, A. Amgoune and D. Bourissou, *Angew. Chem. Int. Ed.*, 2013, **52**, 7160-7163.
371. M. Joost, L. Estevez, S. Mallet-Ladeira, K. Miqueu, A. Amgoune and D. Bourissou, *J. Am. Chem. Soc.*, 2014, **136**, 10373-10382.
372. N. Savjani, D.-A. Roşca, M. Schormann and M. Bochmann, *Angew. Chem. Int. Ed.*, 2013, **52**, 874-877.
373. E. Langseth, A. Nova, E. A. Tråseth, F. Rise, S. Øien, R. H. Heyn and M. Tilset, *J. Am. Chem. Soc.*, 2014, **136**, 10104-10115.
374. M. S. M. Holmsen, F. S. Ihlefeldt, S. Øien-Ødegaard, E. Langseth, Y. Wencke, R. H. Heyn and M. Tilset, *Organometallics*, 2018, **37**, 1937-1947.
375. C. Blons, A. Amgoune and D. Bourissou, *Dalton Trans.*, 2018, **47**, 10388-10393.
376. F. Rekhroukh, L. Estévez, C. Bijani, K. Miqueu, A. Amgoune and D. Bourissou, *Angew. Chem. Int. Ed.*, 2016, **55**, 3414-3418.
377. F. Rekhroukh, L. Estevez, C. Bijani, K. Miqueu, A. Amgoune and D. Bourissou, *Organometallics*, 2016, **35**, 995-1001.
378. F. Rekhroukh, C. Blons, L. Estévez, S. Mallet-Ladeira, K. Miqueu, A. Amgoune and D. Bourissou, *Chem. Sci.*, 2017, **8**, 4539-4545.
379. J. Serra, P. Font, E. D. Sosa Carrizo, S. Mallet-Ladeira, S. Massou, T. Parella, K. Miqueu, A. Amgoune, X. Ribas and D. Bourissou, *Chem. Sci.*, 2018, **9**, 3932-3940.
380. A. V. Zhukhovitskiy, I. J. Kobylanskii, C.-Y. Wu and F. D. Toste, *J. Am. Chem. Soc.*, 2018, **140**, 466-474.
381. J. A. Cadge, P. J. Gates, J. F. Bower and C. A. Russell, *J. Am. Chem. Soc.*, 2022, **144**, 19719-19725.
382. B. Alcaide, P. Almendros, T. M. del Campo and I. Fernández, *Chem. Commun.*, 2011, **47**, 9054-9056.
383. K. E. Roth and S. A. Blum, *Organometallics*, 2011, **30**, 4811-4813.
384. N. P. Mankad and F. D. Toste, *Chem. Sci.*, 2012, **3**, 72-76.
385. F. Rekhroukh, L. Estevez, S. Mallet-Ladeira, K. Miqueu, A. Amgoune and D. Bourissou, *J. Am. Chem. Soc.*, 2016, **138**, 11920-11929.

CHAPTER II. Objectives

As the general introduction underscores, since the rise of gold chemistry about two decades ago, a myriad of studies have been devoted to comprehending deeply the fundamental aspects governing the reactivity of gold complexes. Indeed, still nowadays there is the need of exploring elementary reactions at gold, such as oxidative addition or migratory insertion, to understand gold's behavior from a mechanistic point of view and tame it toward desired reactivities in homogeneous catalysis. The insufficient knowledge on the reactivity of gold complexes relies on the challenging access to Au(III) species involved in catalytic cycles, especially those operating under an oxidant-free regime. In this context, the projects presented in this dissertation deal with the synthesis of novel gold complexes and reactivity studies.

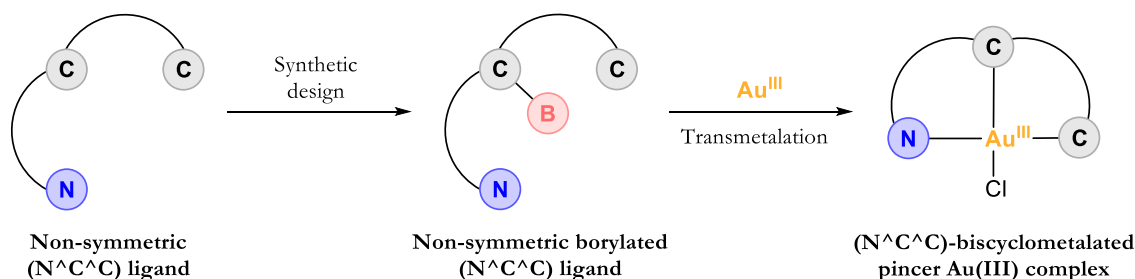
The first part of this thesis (Chapter III and IV) has aimed to employ (N,C) hemilabile ligands to access gold(I) complexes that can potentially become (N,C)-cyclometalated gold(III) complexes. In Chapter III, we envisioned the design of mesoionic carbene ligands (MIC) bearing a hemilabile N-donor atom to create suitable scaffolds to chelate Au(III) centers by forming a 5-membered auracycle. Two ligands are designed; one with a hemilabile pyridine moiety and another one with a hemilabile pyrimidine. From the corresponding Au(I) chloride complexes, oxidation and oxidative addition reactions will be tested with the aim of getting the expected (N,C)-cyclometalated gold(III) complexes, thereby demonstrating the desired functionality of the ligands. If successfully achieved, we will proceed to develop oxidant-free (N,C) ligand-enabled Au(I)/Au(III) cross-coupling catalysis (Scheme II.1, top). As far as we are concerned, this catalytic approach remained unprecedented for (N,C) hemilabile systems, even though it resembles the widely explored MeDalphos (P,C) ligand-enabled Au(I)/Au(III) catalysis. Therefore, our goal is to shed light into this new catalytic approach to widen the scope of hemilabile ligands that can be used in oxidant-free Au(I)/Au(III) cross-coupling catalysis. We envisioned that the arylation-lactonization of γ -alkenoic acids using aryl iodides and catalytic amounts of our gold(I) complexes would be an attainable reaction to produce γ -substituted γ -butyrolactones.

In Chapter IV, we will work with Au(I) complexes based on NHC ligands having a pyridine or a quinoline hemilabile group. We will study their reactivity with oxidants and the decomposition pathways of these (N,C) systems towards the formation of azolones and Au(0) nuggets (Scheme II.1, bottom).



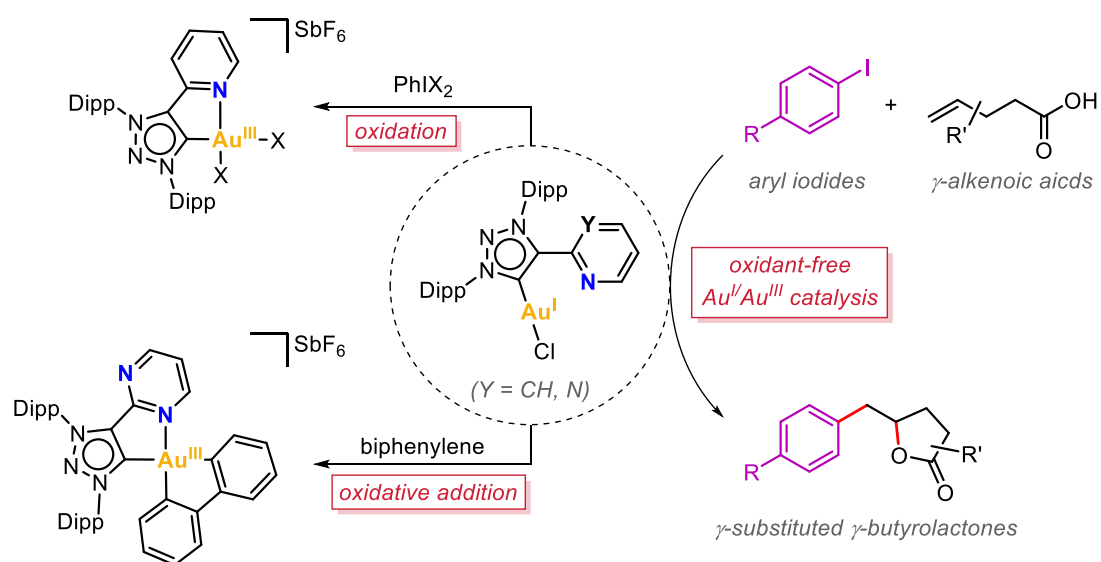
Scheme II.1. Schematic representation of the objectives regarding the part of the thesis dealing with (N,C) hemilabile ligands (top: Chapter III, and bottom: Chapter IV).

In Chapter V, Section V.3, we will strive to find a metalation strategy for non-symmetric ($N^{\wedge}C^{\wedge}C$) architectures to generate ($N^{\wedge}C^{\wedge}C$)-biscyclometalated pincer gold(III) complexes. To this end, we envisioned that boron-to-gold(III) transmetalation would be a suitable approach to overcome the limitations of other current metalation strategies. For instance, transmetalation from organomercury complexes generates toxic waste, and the microwave-assisted C–H metalation is limited to symmetric ($N^{\wedge}C^{\wedge}C$) scaffolds. Hence, the objective of this project is to design borylated ligands that can potentially undergo transmetalation to gold(III) salts and obtain the desired ($N^{\wedge}C^{\wedge}C$)-biscyclometalated gold(III) complexes (Scheme II.2).



Scheme II.2. Schematic representation of the objectives regarding the synthesis of non-symmetric borylated ($N^{\wedge}C^{\wedge}C$) ligands and the ensuing ($N^{\wedge}C^{\wedge}C$)-biscyclometalated $Au(III)$ complexes.

CHAPTER III. Hemilabile MIC[^]N Ligands Allow Oxidant-Free Au(I)/Au(III) Arylation-Lactonization of γ -Alkenoic Acids



This chapter corresponds to the following publication:

Pau Font, Hugo Valdés*, Gregorio Guisado-Barrios*, Xavi Ribas*. Reprinted with permission from *Chem. Sci.* **2022**, *13*, 9351 – 9360.

Cite this: *Chem. Sci.*, 2022, 13, 9351

All publication charges for this article have been paid for by the Royal Society of Chemistry

Received 5th April 2022

Accepted 8th July 2022

DOI: 10.1039/d2sc01966c

rsc.li/chemical-science

Hemilabile MIC^{AN} ligands allow oxidant-free Au(I)/Au(III) arylation-lactonization of γ -alkenoic acids†

Pau Font,^a Hugo Valdés,^a Gregorio Guisado-Barrios^{*b} and Xavi Ribas^{*a}

Oxidant-free Au-catalyzed reactions are emerging as a new synthetic tool for innovative organic transformations. Still, a deeper mechanistic understanding is needed for a rational design of these processes. Here we describe the synthesis of two Au(I) complexes bearing bidentated hemilabile MIC^{AN} ligands, [Au(MIC^{AN})Cl], and their ability to stabilize square-planar Au(III) species (MIC = mesoionic carbene). The presence of the hemilabile N-ligand contributed to stabilize the ensuing Au(III) species acting as a five-membered ring chelate upon its coordination to the metal center. The Au(III) complexes can be obtained either by using external oxidants or, alternatively, by means of feasible oxidative addition with strained biphenylene C_{sp²}-C_{sp²} bonds as well as with aryl iodides. Based on the fundamental knowledge gained on the redox properties on these Au(I)/Au(III) systems, we successfully develop a novel Au(I)-catalytic procedure for the synthesis of γ -substituted γ -butyrolactones through the arylation-lactonization reaction of the corresponding γ -alkenoic acid. The oxidative addition of the aryl iodide, which in turn is allowed by the hemilabile nature of the MIC^{AN} ligand, is an essential step for this transformation.

Introduction

Gold catalysis has been dominated by the Lewis acidity of gold towards activation of alkenes and alkynes for nucleophilic attacks.^{1–6} On the other hand, redox Au(I)/Au(III) catalysis has been less explored and mainly achieved in the presence of sacrificial external oxidants,^{7–17} especially due to the reluctance of Au(I) to undergo oxidative addition.^{18–21} In this regard, several strategies have been explored to overcome this limitation,^{22–46} among which the chelation-assisted strategy in pre-designed ligands^{30–34} or the oxidative addition using strained molecules such as biphenylene stand out.³⁵ Bourissou pioneered in 2014 the intramolecular oxidative addition of C_{sp²}-X bonds (X = Br, I) at Au(I) by utilizing rigid 8-halonaphthyl phosphine model substrates, which suitably place the C_{sp²}-X bond close to the Au(I) atom upon coordination

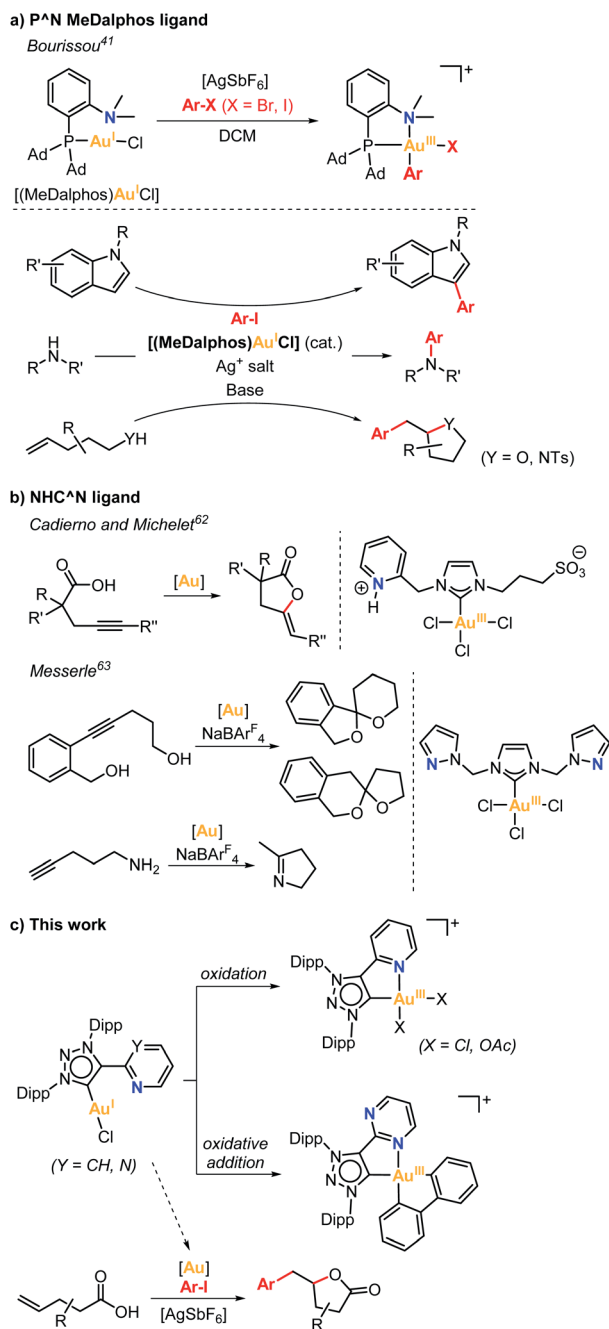
to the phosphine moiety. In this manner, facile stabilization of the (P,C)-cyclometalated Au(III) products is obtained *via* oxidative addition.³² In the same line, Hashmi and Hermange used a similar strategy taking advantage of pendant pyridine groups in monophosphine ligands to stabilize Au(III) systems upon reaction of Au(I) complexes with aryldiazonium salts.^{47,48} In these examples, the subtle change from linear to square-planar geometry is crucial for the facile reactivity of Au(I) species towards a key oxidative addition process. Noteworthy, P^{AN} MeDalpos ligand showed great performance at promoting the oxidative addition of aryl halides at Au(I), as well as at stabilizing Au(III) intermediates, which paved the way to Au(I)/Au(III) catalytic transformations using the (MeDalpos)AuCl catalyst (Scheme 1a).⁴¹ For instance, in 2019 Bourissou and coworkers reported the regioselective Au(I)/Au(III)-catalyzed C3 arylation of indoles, which is rarely attained by other transition metals (Scheme 1a),⁴⁹ additionally they described the Au(I)/Au(III) catalyzed C3 allylation of indoles using allyl alcohols or allyl acetates.⁵⁰ Significantly, two independent reports by the groups of Patil⁵¹ and Bourissou⁵² disclosed the C_{sp²}-N cross-coupling reactions of aryl iodides with amines mediated by the MeDalpos-enabled Au(I)/Au(III) catalysis (Scheme 1a). In 2020, Bourissou and Patil groups independently showed that the oxidative addition of aryl iodides and π -activation of olefins can be merged by the Au(I)/Au(III) platform using (MeDalpos)AuCl as catalyst, which involves the oxy- and aminoarylation reactions of alkenols and alkenamines (Scheme 1a).^{53,54} The 1,2-heteroarylation of alkenes was also achieved using external alcohols and amines.^{54–56} Interestingly, (MeDalpos)AuCl catalyst has proven to

^aInstitut de Química Computacional i Catàlisi (IQCC) and Departament de Química, Universitat de Girona, Campus de Montilivi, Girona E-17003, Catalonia, Spain. E-mail: hugo.valdes@udg.edu; xavi.ribas@udg.edu

^bDepartamento de Química Inorgánica, Instituto de Síntesis Química y Catálisis Homogénea (ISQCH), Universidad de Zaragoza-CSIC, Zaragoza 50009, Spain. E-mail: ggusado@unizar.es

† Electronic supplementary information (ESI) available: For materials, instrumentation, experimental procedures and spectroscopic characterization of all compounds. CCDC 2163608 (4a-OAc), 2163609 (2a), 2163610 (2b), 2163611 (4a-Cl), 2163612 (8a-OMe), 2163613 (3b-biphenylene), 2163614 (5b), 2163615 (6b), 2163616 (8b-OMe), 2163617 (3a), 2163877 (16) and 2176932 (cis-7a-Cl) contain the supplementary crystallographic data for this paper. For ESI and crystallographic data in CIF or other electronic format see <https://doi.org/10.1039/d2sc01966c>





Scheme 1 (a) Oxidative addition of aryl halides to a Au(I) complex bearing the hemilabile P[^]N MeDalphos ligand, and selected examples of its catalytic activity. (b) Selected examples of gold complexes bearing hemilabile NHC[^]N ligands. (c) Ability of hemilabile MIC[^]N ligands to stabilize Au(III) complexes obtained from Au(I) via oxidation or via oxidative addition, and application of the (MIC[^]N)Au(I) complexes to the arylation-lactonization reaction of γ -alkenoic acids.

be a key factor in the development of other transformations such as 1,2-diarylation of alkenes,⁵⁷ or trifluoromethylthiolation and trifluoromethyl-selenolation of organohalides.⁵⁸ Very recently, Shi and Patil groups developed new chiral-hemilabile P[^]N-ligands to access enantioselective Au(I)/Au(III) catalysis.^{59,60}

In contrast to the well-known P[^]N ligands, the use of bidentate C[^]N or C[^]O ligands⁶¹ remains scarcely explored, and

the few representative examples are depicted in Scheme 1b. Cadierno and Michelet studied the catalytic activity of a (NHC[^]N)Au(III) complex containing a *N*-heterocyclic carbene ligand (NHC) with a pyridinium side arm in the cyclization of γ -alkynoic acids (Scheme 1b),⁶² while Messerle and coworkers explored the dihydroalkoxylation and hydroamination catalyzed by a Au(III) complex bearing a NHC ligand with two pendant pyrazole arms (Scheme 1b).⁶³ Alternatively, Bertrand and coworkers showed that a hemilabile bidentate cyclic (alkyl)(amino)carbene (CAAC) Au(I) complex undergoes oxidative addition of biphenylene.⁴⁰

More recently, Bourissou and coworkers reported the reactivity of a Au(I) complex containing a N3-alkylated mesoionic 1,2,3-triazol-5-ylidene bearing a pendant pyridine group.⁶⁴ However, the complex did not undergo oxidative addition towards iodobenzene, thus precluding its exploitation in oxidant-free reactivity. In fact, the formation of a dimeric Au(I) species was observed instead of the formation of the oxidative addition Au(III) product. On the other hand, the Au(I) complex was reactive towards a strong oxidant such as PhICl₂, forming a mononuclear square-planar Au(III) species. The latter experiment demonstrated that mesoionic carbene ligands bearing *N*-based hemilabile groups (MIC[^]N) can potentially be suitable platforms to stabilize Au(III) species.

Based on the abovementioned, we herein explore the reactivity of two new (MIC[^]N)Au(I) complexes bearing hemilabile pyridine (py) or pyrimidine (pym) pendant groups, their ability to stabilize (MIC[^]N)Au(III) species and their performance in oxidant-free oxidative addition of aryl halides and strained C–C bonds. After proving the successful ability to sustain oxidant-free Au(I)/Au(III) redox processes, we further extended its application to arylation-lactonization reactions of γ -alkenoic acids (Scheme 1c).

Results and discussion

Synthesis and characterization of (MIC[^]N)Au(I) complexes

Initially, two 1,2,3-triazolium ligand salt precursors (MIC[^]N) bearing 2,6-diisopropylphenyl substituents (Dipp) at the outer nitrogens of the azolium ring and either a pyridine (**1a**) or a pyrimidine (**1b**) side arm were prepared by following an adapted method reported in the literature (Fig. 1a).⁶⁵ We reacted 1,3-bis(2,6-diisopropylphenyl)triaz-1-ene with 2-ethynylpyridine or 2-ethynylpyrimidine in the presence of *tert*-butyl hypochlorite (*t*BuOCl) and anhydrous potassium hexafluorophosphate (KPF₆), affording the desired products in high and moderate yield (99% for **1a** and 67% for **1b**). In order to obtain the corresponding (MIC[^]N)Au(I) complexes, we attempted the Au(I) coordination through a transmetalation reaction to Ag(I) species. For this purpose, we reacted the corresponding triazolium salts with silver oxide (Ag₂O) in the presence of cesium carbonate (Cs₂CO₃) and potassium chloride (KCl) as halide source. Then, the addition of dimethylsulfide gold(I) chloride [AuCl(SMe₂)] immediately produced the precipitation of the silver halide. After purification, the desired Au(I) complexes **2a** and **2b** were obtained in 32% and 35% yield, respectively. The ¹H NMR spectra of the complexes showed the absence of the acidic proton of the triazolium salts, indicating that the



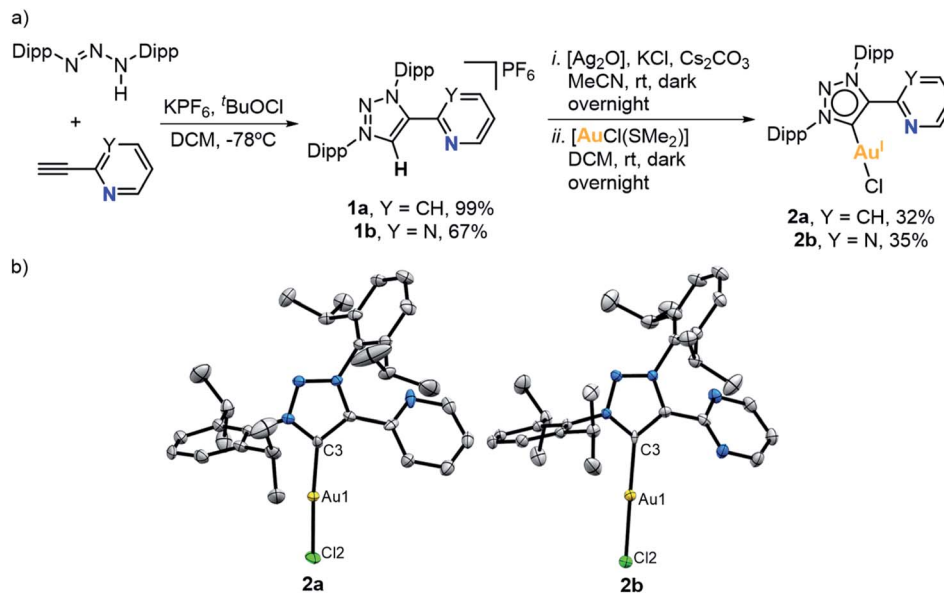


Fig. 1 (a) Synthesis of Au(I) complexes **2a** and **2b**. (b) Crystal structures of **2a** and **2b** (ellipsoids set at 50% probability and H atoms removed for clarity). Selected bond distances (Å): for **2a**, Au1–C3 1.982(6), Au1–Cl2 2.2854(17); for **2b**, Au1–C3 2.006(4), Au1–Cl2 2.2728(16).

coordination to gold had occurred. The ¹³C{¹H} NMR spectrum of **2a** showed the characteristic signal of the metalated carbon at 162.1 ppm, while in the case of the pyrimidine derivative **2b**, such signal was slightly shifted downfield, appearing at 165.3 ppm. Furthermore, the molecular structure of both Au(I) complexes **2a** and **2b** was unambiguously determined by X-ray diffraction analyses (Fig. 1b). Both complexes are isostructural, showing the mesoionic carbene ligand coordinated to an Au(I) atom, and a chlorine ligand completing the linear coordination sphere around the metal (C–Au–Cl angle is 174.31(18)° for **2a** and 179.30(9)° for **2b**). Noticeably, no coordination of the hemilabile pyridine or pyrimidine moieties at Au(I) was observed.

Then, Au(I) complexes **2a** and **2b** were reacted with silver hexafluoroantimonate (AgSbF₆) in CD₂Cl₂ at room temperature (Fig. 2a), seeking the engagement of the pendant pyrimidine or pyridine groups in the coordination to Au(I). The ¹H NMR spectra of the corresponding complexes showed some changes in the aromatic and aliphatic region. In particular, the signals of the pyridine or pyrimidine fragments were shifted due to gold coordination. The most significant change was observed in the ¹³C{¹H} NMR spectra. The signal of the carbenic carbon was shifted from 162.1 to 157.2 ppm in the case of the pyridine derivative (**3a**), and from 165.3 to 161.3 ppm in the case of the pyrimidine derivative (**3b**).

X-ray diffraction analysis of complex **3a** showed a head-to-tail dimeric Au(I) species where each ligand is bridging two metals (Fig. 2). The Au(I) centers adopted a linear dicoordinate arrangement, showing an aurophilic interaction (Au...Au length of 2.8212(4) Å). Analogously to Bourissou's (MIC[^]N)Au(I) complex,⁶⁴ the formation of a dimeric Au(I) species was favored rather than a mononuclear Au(I) having both the MIC and py or pym pendant groups coordinated.

Reactivity of (MIC[^]N)Au(I) complexes with external oxidants and towards oxidative addition

In order to promote the coordination of the side arms of our MIC[^]N ligands, we attempted the 2 e⁻ chemical oxidation of the Au(I) complexes to mononuclear Au(III). To that end, we studied the reactivity of complex **2a** against a 2 e⁻ oxidant, namely PhIX₂ (X = Cl or OAc) (Fig. 2a). The reaction was performed at low temperature, from -80 °C to rt, in the presence of AgSbF₆ as halogen scavenger. Gratifyingly, the oxidation of Au(I) to Au(III) took place, with the concomitant coordination of the pendant N-moiety to gold. The ¹³C{¹H} NMR spectra of the resulting complexes **4a-Cl** and **4a-OAc** showed the characteristic signal of the carbenic carbon at higher field when compared to the Au(I) analogue **2a** (147.3 ppm for **4a-Cl** and 137.1 ppm for **4a-OAc** vs. 162.1 ppm for **2a**). The molecular structures of complexes **4a-Cl** and **4a-OAc** were elucidated by X-ray diffraction analyses (Fig. 2b). Both complexes showed a similar arrangement, *i.e.* the bidentate MIC[^]N ligand coordinated to Au(III), and two chlorides or acetates completing its tetracoordinated Au(III) center, which featured a slightly distorted square planar geometry. The C_{carbene}–Au(III) lengths were slightly longer than those found in the Au(I) analogue (2.017(8) Å for **4a-Cl** and 1.991(11) Å for **4a-OAc** vs. 1.982(6) Å for **2a**).

At this point, we had demonstrated that these MIC[^]N ligands are indeed suitable platforms to stabilize Au(III) species. Thus, we were encouraged to explore the possibility of obtaining Au(III) complexes *via* oxidative addition. With this aim, we first attempted the oxidative addition of complex **2b** towards the strained C_{sp}²–C_{sp}² bond of biphenylene, by mixing equimolar amount of **2b** and biphenylene in dichloromethane, in the presence of a halide scavenger, from -80 °C to room temperature for 10 minutes (Fig. 3a). Unfortunately, we did not observe the desired Au(III) center with a biphenyl moiety but,



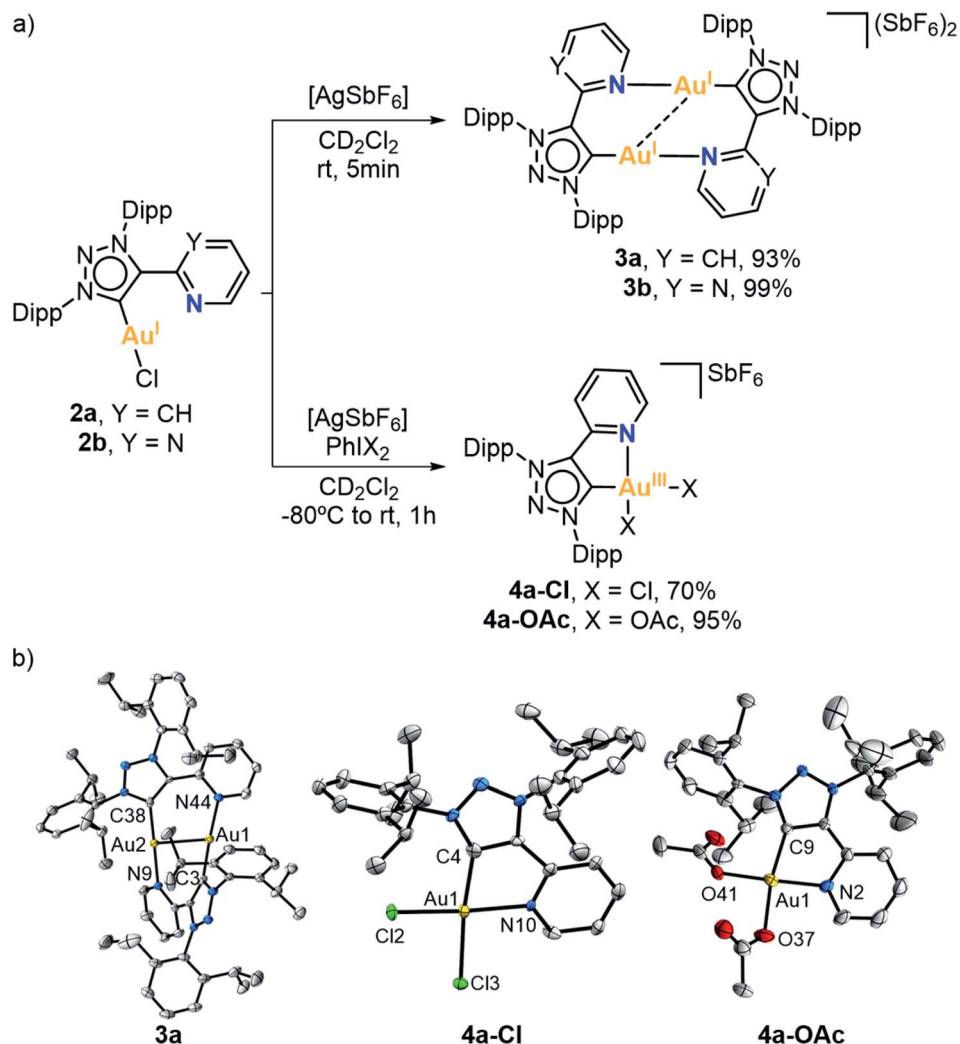


Fig. 2 (a) Reactivity of Au(I) complexes **2a** and **2b** towards halogen scavengers and strong oxidants. (b) Crystal structures of **3a**, **4a-Cl** and **4a-OAc** (ellipsoids set at 50% probability, H atoms and SbF_6^- anions removed for clarity). Selected bond distances (Å): for **3a**, Au1–Au2 2.8212(4), Au1–N44 2.078(6), Au1–C3 1.988(8), Au2–N9 2.069(6), Au2–C38 1.990(8); for **4a-Cl**, Au1–C4 2.017(8), Au1–N10 2.089(6), Au1–Cl2 2.268(2), Au1–Cl3 2.302(2); for **4a-OAc**, Au1–C9 1.991(11), Au1–N2 2.052(11), Au1–O37 2.032(10), Au1–O41 1.998(9).

interestingly, crystallization of the reaction mixture revealed the co-crystallization of the dimeric complex **3b** with intact biphenylene (**3b**·biphenylene) (Fig. 3b). Even after 5 hours at 50 °C, the outcome of the reaction remained the same. To our delight, when the reaction was heated at 90 °C for 2 hours in 1,2-dichloroethane, the Au(I) center underwent oxidative addition of the strained biphenylene $\text{C}_{\text{sp}^2}\text{--C}_{\text{sp}^2}$ bond, forming the expected Au(III) complex **5b** (Fig. 3a). Notably, the presence of a chloride source (such as KCl or tetrabutylammonium chloride) displaced the hemilabile pyrimidine, affording a neutral Au(III) species, **6b**. By adding AgSbF_6 as halide scavenger, we could reversibly form complex **5b**, also reinforcing the hemilabile character of the pyrimidine moiety. Indeed, the NMR spectra of **5b** showed a dynamic behaviour of the pyrimidine pendant arm, even at 248 K, as indicated by ^1H , ^1H -NOESY experiment (Fig. S49[†]). Both the cationic **5b** and the neutral **6b** Au(III) species were characterized by X-ray diffraction analyses (Fig. 3b), confirming the weak coordination of the

pyrimidine moiety with a long Au(III)–N_{pyrimidine} bond of 2.254 Å for **5b**. The carbene resonance signals were downfield shifted to 182.8 and 180.1 ppm for **5b** and **6b**, respectively.

We then explored the possibility of Au(I) complexes **2a** and **2b** to undergo oxidative addition of $\text{C}_{\text{sp}^2}\text{--I}$ bonds (Fig. 4a). For this purpose, we reacted the Au(I) complexes with *para*-substituted iodoaryls (R = OMe, Me, F) in the presence of AgSbF_6 , in 1,2-dichloroethane and heating at 120 °C overnight. Unexpectedly, no Au-containing compounds were isolated, but on the contrary, the ^1H NMR and mass spectra were consistent with the full conversion to three triazolium salts (**8a-R**, **9a**, and **1a** when **2a** was used, and **8b-R**, **9b** and **1b** when **2b** was used; R = OMe, Me, F) (see yields in Fig. 4a). When using **2a** with 4-iodoanisole, the triazolium salts **8a-OMe** and **9a** were unambiguously characterized by X-ray diffraction. Both species co-crystallized, and the single crystal X-ray analysis revealed the presence of **8a-OMe** and **9a** in a 0.89 : 0.11 ratio (Fig. 4b). Likewise, when **2b** was reacted with 4-iodoanisole, the major product was **8b-OMe** with



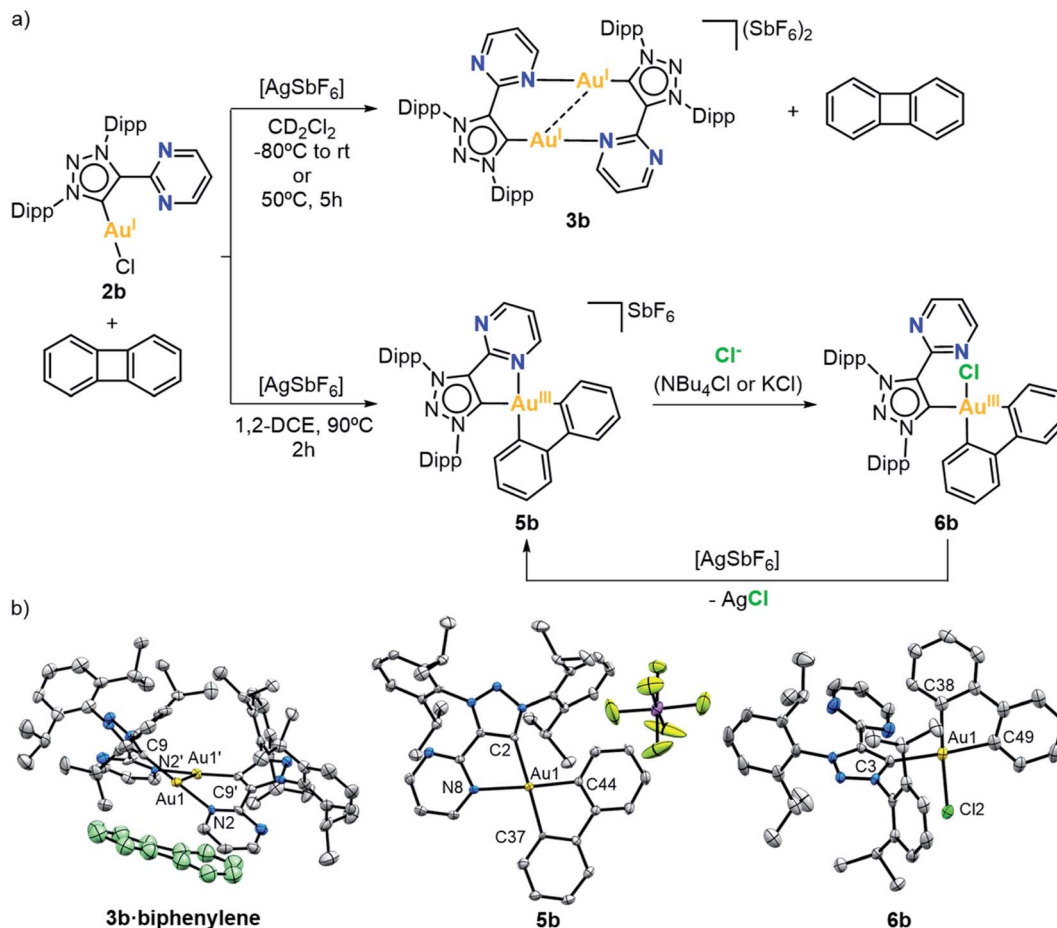


Fig. 3 (a) Study of the reaction conditions for the oxidative addition of a strained $C_{sp^2}-C_{sp^2}$ bond to complex **2b**. (b) Crystal structures of **3b-biphenylene**, **5b** and **6b** (ellipsoids set at 50% probability, H atoms removed for clarity; in the case of **3b-biphenylene** the SbF_6^- anions have been removed and the biphenylene molecule is painted in green for clarity). Selected bond distances (Å): for **3b-biphenylene**, Au1–Au1' 2.8768(10), Au1–N2 2.105(8), Au1–C9 2.027(10); for **5b**, Au1–C2 2.108(5), Au1–N8 2.254(5), Au1–C37 2.066(5), Au1–C44 2.019(5); for **6b**, Au1–C3 2.080(6), Au1–Cl2 2.376(3), Au1–C38 2.072(7), Au1–C49 2.057(7).

a 65% NMR yield, whereas **9b** and **1b** were both obtained in 16% NMR yield. In this case, **8b-OMe** could be isolated and characterized by 1H NMR, HRMS and X-ray diffraction (Fig. 4b). The formation of such compounds suggested that gold(i) compounds underwent oxidative addition of the aryl iodide followed by a fast reductive elimination of the mesoionic carbene ligand either with the aryl or the iodide moiety coordinated in *cis*, respectively (Fig. 4a). Interestingly, products **8a-R/8b-R** were obtained in higher yields than **9a/9b**, indicating that after the oxidative addition the major product is the one with the aryl ligand in *cis* (**cis-7a-I** or **cis-7b-I**), probably due to the *trans* effect of the NHC ligand. By an alternative route,⁴⁷ the analogous complex **cis-7a-Cl** was synthesized through the oxidative addition of an aryldiazonium salt promoted by blue LED irradiation ($\lambda = 447$ nm). This methodology has the advantage to occur at 25 °C, allowing the isolation and fully characterization of the Au(III) species **cis-7a-Cl** (see XRD in Fig. 4b). When **cis-7a-Cl** was heated at 120 °C overnight in 1,2-DCE, product **8a-OMe** was formed in 96% yield. This reaction supports that the formation of **8a-R/8b-R** and **9a/9b** from Au(i)

complexes **2a/2b** proceeds *via* an oxidative addition/reductive elimination pathway. We hypothesize that the hemilabile character of the nitrogen atom and the fast decomposition of Au(III) at high temperatures promote the reductive elimination process, which has only been observed, to our knowledge, for a 1,2,3-triazol-5-ylidene based palladium complex.^{66–68} Nevertheless, our observations sharply contrasted with the lack of reactivity described by Bourissou for a similar (MIC[^]N)Au(i) system with aryl iodides.⁶⁴

Arylation-lactonization of γ -alkenoic acids

Based on the successful catalytic application of the P[^]N hemilabile ligand strategy, we envisioned that our hemilabile (MIC[^]N)Au(i) complexes may also mediate a cascade reaction involving the key oxidative addition step. Recently, Bourissou and coworkers described the coupling/cyclization reaction of aryl iodides with alkenol and alkenamine compounds catalyzed by a hemilabile P[^]N MeDalPhos/Au(i) system.⁵³ Additionally, in 2017, Shi and coworkers reported a system that afforded coupling/cyclization products upon reacting aryldiazonium



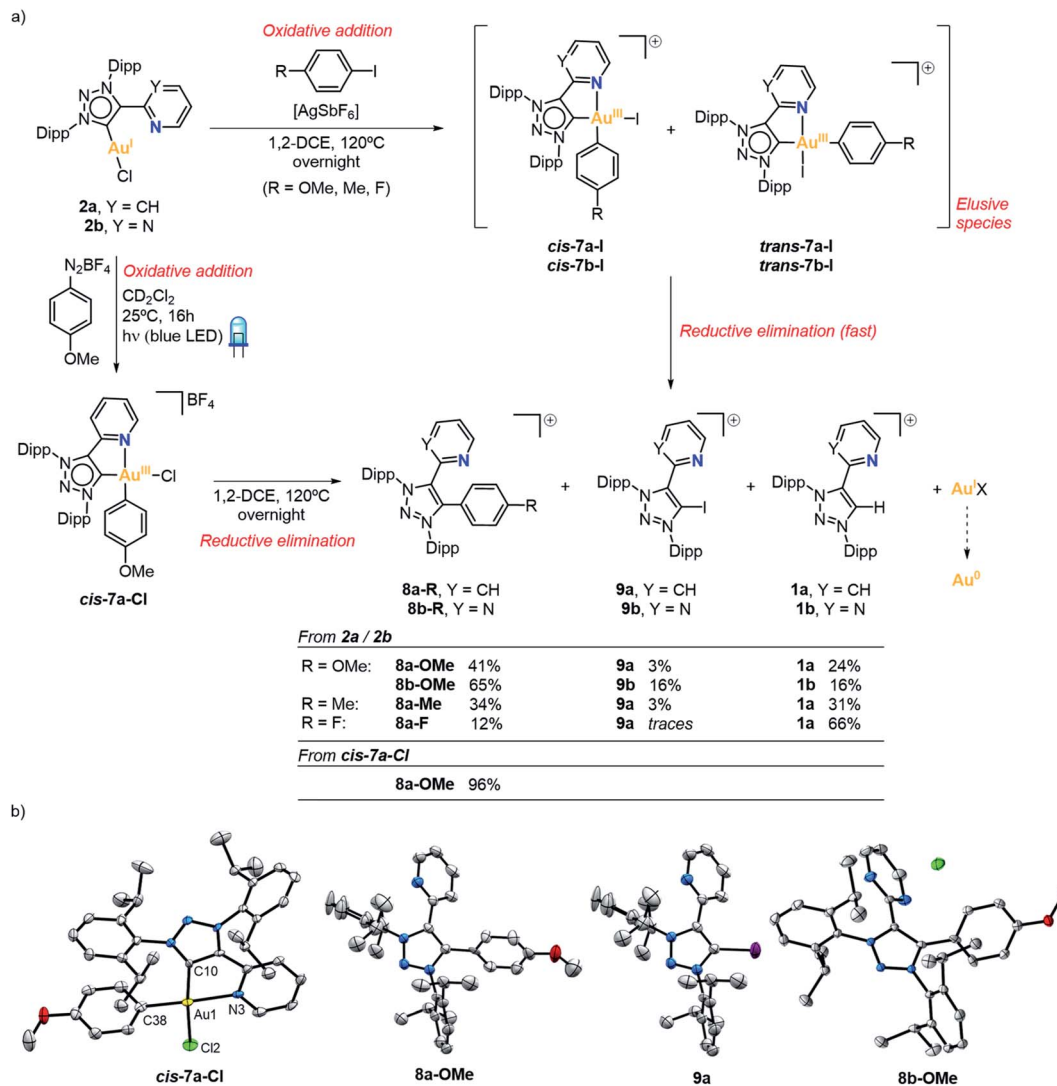


Fig. 4 (a) Reactivity towards aryl iodides and decomposition route of Au(I) species **2a** and **2b**, and synthesis of **cis-7a-Cl** by oxidative addition of an aryldiazonium salt. NMR yield of the reactions calculated using 1,3,5-trimethoxybenzene as internal standard. (b) Crystal structures of **cis-7a-Cl**, **8a-OMe**, **9a** and **8b-OMe** (ellipsoids set at 50% probability, H atoms removed for clarity; for **cis-7a-Cl**, BF_4^- anion is removed for clarity; for **8a-OMe** and **9a**, SbF_6^- anion is not shown for clarity). Selected bond distances for **cis-7a-Cl** (Å): Au1–C10 2.009(7), Au1–N3 2.154(7), Au1–C38 2.006(8), Au1–Cl2 2.303(2).

salts with either alkenamines, alkenols or alkenoic acids, using $[(\text{Ph}_3\text{P})\text{AuCl}]$ under photo-free conditions.⁶⁹ Thus, we envisioned that our MIC^{^N}/Au(I) system should afford γ -benzyl- γ -butyrolactone products when reacting aryl iodides with γ -alkenoic acids, *via* coupling/lactonization, provided the oxidative addition step takes place (see reaction scheme embedded in Table 1). Our first attempts consisted in a stoichiometric reaction between 4-iodoanisole, 4-pentenoic acid, complex **2b**, K_3PO_4 , and AgSbF_6 at 80 °C. When the reactions were carried out in the presence of an excess of base or AgSbF_6 , we did not observe any conversion, probably due to the rapid decomposition of the Au(I) complex. We also found that by using chlorinated solvents such as 1,2-dichloroethane, the conversion reached up to 49% (Table S3†). We determined by ^1H NMR analysis that the catalyst decomposes under the reaction conditions, forming the triazolium salt **1b**. Interestingly, the

conversion was significantly higher using 2,2,2-trifluoroethanol (TFE) (up to 92%) instead of 1,2-dichloroethane (Table 1 and S3†). When the reaction was carried out at 100 °C, the conversion was quantitative, but the yield was very similar to that found at 80 °C (67% yield at 100 °C *vs.* 63% yield at 80 °C, entries 1–2 in Table 1), and we also observed the formation of the triazolium salt **8b-OMe**. This was a strong indication that complex **2b** underwent an oxidative addition of the C_{sp^2} -I bond, but rapid reductive elimination to form the coupling product **8b-OMe** occurred.

With these results in hand, we explored the possibility to perform the catalytic version of the arylation-lactonization of γ -alkenoic acids. Thus, we carried out the reaction decreasing the loading of **2b**, first using substoichiometric 70 mol% of the gold complex. Product **10** was obtained in 65% yield (entry 3), so effectively a quantitative transformation was achieved with

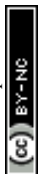



Table 1 Synthesis of γ -benzyl- γ -butyrolactone **10** promoted by complex **2b**^a


Entry	[Ag] (eq.)	[Au] mol%	K ₃ PO ₄ (eq.)	Solvent	Conversion% (yield%)
1 ^b	2.8	100	1.0	TFE	92(63)
2 ^{b,c}	2.6	100	1.2	TFE	>99(67)
3 ^d	2.2	70	1.2	TFE	81(65)
4 ^d	2.0	40	1.1	TFE	79(44)
5 ^b	1.5	10	1.0	TFE	51(28)
6	1.5	10	0.5	TFE	51(24)
7 ^d	1.5	10	1.1	TFE	54(15)
8 ^d	1.1	1	0.5	TFE	38(1.6)
9	1.5	10	1.0	HFIP	56(29)

^a Reaction conditions: [Ar-I] = 0.08 M, [4-pentenoic acid] = 0.08 M, 80 °C, 16 h. V = 0.55 – 1.40 mL (¹H NMR yield obtained with 1,3,5-trimethoxybenzene as internal standard). ^b [Ar-I] = 0.02 M, [4-pentenoic acid] = 0.1 M, V = 1 mL. ^c T = 100 °C. ^d Reaction time = 24 h.

respect to Au loading. By using 40 mol% of Au(I) complex the yield was 44%, reaching about 1 TON (entry 4). Interestingly, using a lower amount of **2b** (10 mol%) the yield was around 28% (~3 TON, entry 5). Similarly, by using hexafluoro-2-propanol (HFIP) the yield was 29% (~3 TON, entry 9); therefore, the best optimized results were obtained with fluorinated alcohols.

To exclude the possibility of oxidizing Au(I) to Au(III) in the presence of Ag(I), complex **2a** (1 eq.) was reacted with AgSbF₆ (15 eq.) in HFIP at 80 °C for 16 hours. Quantitative formation of the Au(I) dimer **3a** was observed by NMR, confirming the role of silver as halide scavenger (see Scheme S12[†]).

The scope of the reaction was examined with different aryl halides and γ -alkenoic acids (Fig. 5). The arylation-lactonization using iodobenzene and complex **2b** reached 50% yield (~5 TON) in product **11**. As expected, by increasing the catalyst loading to 20 mol%, the yield of **11** increased up to 87%, thus maintaining the turnover number (~4–5 TON). Gratifyingly, the best yields were reached using 4-iodotoluene, obtaining product **12** in 60% yield using **2a** (~6 TON) and 81% yield using **2b** (~8 TON). However, the presence of the strong electron-withdrawing group CF₃ in the *para*-position of the iodoaryl produced product **13** in a lower yield (~13%). Following this trend,^{36,38} 1-iodo-4-nitrobenzene produced a more dramatic drop of the yield of the corresponding product **14** (1%).

Interestingly, the γ -alkenoic acid with α -methyl groups reacted smoothly, yielding 37% of **15** using **2a** and 41% of **15** using **2b**. Also, complexes **2a** and **2b** performed very similar, except in the case of using iodobenzene and 4-pentenoic acid, yet complex **2b** is almost two-fold more active than **2a** (31% vs. 50% yield of compound **11**, for **2a** and **2b**, respectively). The molecular structure of compound **16** was determined by X-ray diffraction analysis and revealed the formation of the (*R*)-enantiomer by spontaneous resolution.

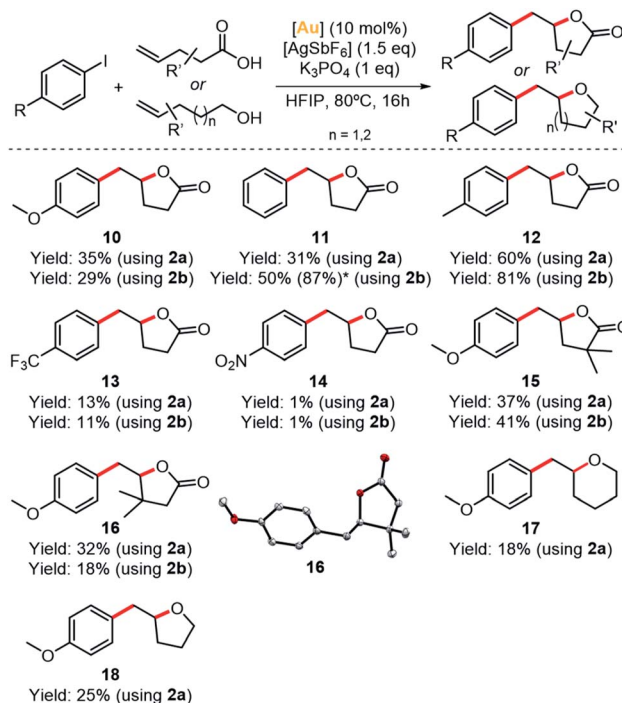


Fig. 5 Scope of the arylation-lactonization of alkenoic acids (**10–16**) and oxyarylation of alkenes (**17–18**). *NMR yield using 20% of [Au] is shown in parenthesis. Crystal structure of **16** is shown (ellipsoids set at 50% probability, H atoms removed for clarity).

Finally, in order to broaden the scope of these (MIC^N)Au(I) complexes, we tested complex **2a** in the oxyarylation of alkenols and 1,2-diarylation of alkenes under the same catalytic conditions (Scheme S11[†]). The oxyarylation products **17** and **18** were obtained in low but significant yields (18–25%, ~2 TON) (Fig. 5 and Table S6[†]). On the contrary, the 1,2-diarylation reaction was unsuccessful.

Based on the fundamental understanding of the redox behaviour of complexes **2a** and **2b**, and the previously reported gold-catalyzed processes combining aryl halide oxidative addition and π -activation of alkenes,⁵³ a mechanistic proposal is depicted in Fig. 6. First, the oxidative addition of the C_{sp²}-I bond into a cationic gold(I) species occurs, affording a cationic aryl-gold(III) species. Then, the silver salt abstracts the iodide from this Au(III) species to generate a vacant site that can be occupied by the π -coordination of the olefin. Subsequent intramolecular γ -lactonization is enabled by the presence of base and the π -activation of the alkene produced by the gold center, to yield an alkylaryl gold(III) intermediate. The latter is proposed to undergo a reductive elimination step that affords the γ -benzyl- γ -butyrolactone product and closes the catalytic cycle by regenerating the initial catalytically active hemilabile [Au^I(-MIC^N)]⁺ species.

To gain mechanistic insight, the stoichiometric reaction of **cis-7a-Cl** with AgSbF₆ (1.2 eq.), 4-pentenoic acid (1.3 eq.) and K₃PO₄ (1.0 eq.) was carried out in HFIP at 80 °C. After 16 hours, γ -benzyl- γ -butyrolactone **10** was obtained in 73% yield (Scheme S13[†]). Therefore, it is plausible to propose the formation of an



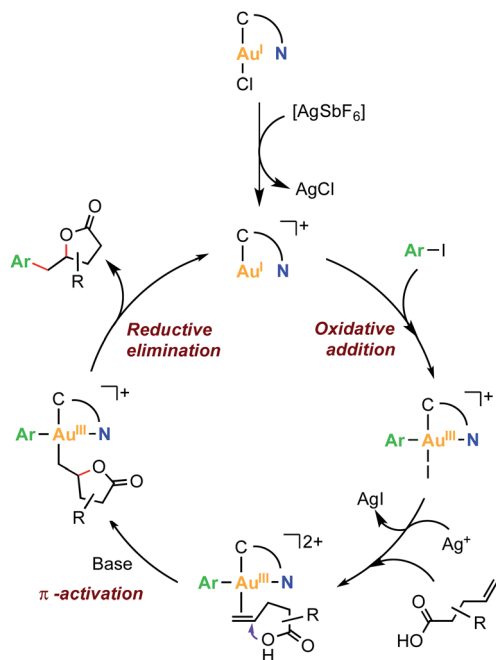


Fig. 6 Proposed reaction mechanism for the Au(I)/Au(III)-mediated arylation-lactonization of alkenoic acids.

arylgold(III) intermediate formed by an oxidative addition reaction of the C_{sp^2} -I bond to Au(I).

Conclusions

We synthesized two Au(I) complexes bearing bidentate hemilabile MIC[^]N ligands, [Au^I(MIC[^]N)Cl], **2a** and **2b**, and explored their redox reactivity. The formation of the Au(III) complexes **4a-Cl** and **4a-OAc** was achieved by using 2 e⁻ oxidants of the type PhIX₂ (X = Cl, OAc), demonstrating a suitable design of the MIC[^]N ligand to stabilize Au(III) centers. Next, we showed that effective oxidative addition of a strained C_{sp^2} - C_{sp^2} bond was obtained when reacting **2b** with biphenylene in the presence of a halide scavenger and heating at 90 °C. In this case, complex **5b** was obtained as the desired ensuing Au(III) species.

On the other hand, the oxidative addition of aryl iodides to Au(I) required a temperature of 120 °C, and under these conditions the reductive elimination reaction of Au(III) species is also favored, yielding a series of triazolium salts (**8a-R/8b-R**, **9a/9b** and **1a/1b**). Although the expected Au(III) complexes were not directly detected, we independently synthesized the analogous Au(III) complex **cis-7a-Cl**, which after heating produced the same triazolium product (**8a-OMe**), thus supporting the oxidative addition/reductive elimination pathway for aryl iodides.

Finally, we combined all the redox knowledge gained with this system to develop a novel reaction for the synthesis of γ -benzyl- γ -butyrolactones upon arylation-lactonization of γ -alkenoic acids. The reaction was catalyzed by **2a** and **2b** (10 mol% catalyst loading), obtaining up to 8 TON. The catalytic activity shown by MIC[^]N/Au system is significant because it shows that readily available hemilabile C[^]N ligands are a real alternative to

hemilabile P[^]N ligands, where MeDalphos system stands out among catalytic examples of oxidant-free oxidative addition of aryl halides allowed by the presence of pendant N-groups. Current efforts are devoted to extending the application of these hemilabile [Au^I(MIC[^]N)Cl] complexes to novel catalytic transformations.

Data availability

Data for this work, including experimental procedures, NMR spectra and crystallographic data, are provide in the ESI.†

Author contributions

P. F., H. V. and G. G.-B. performed the experiments. All authors discussed the results and wrote the manuscript.

Conflicts of interest

There are no conflicts to declare.

Acknowledgements

We acknowledge financial support from MINECO of Spain for projects CTQ2016-77989-P, PID2019-104498GB-I00, RTI2018-098903-J-100 and PID2021-122900NB-I00 (financed by MICIN/AEI/10.13039/501100011033/FEDER “Una manera de hacer Europa”), and for a FPU PhD grant to P. F. We also thank the Generalitat de Catalunya for project 2017SGR264 to X. R. and for a Beatriu de Pinós contract to H. V. (Beatriu de Pinós, 2019-BP-0080). X. R. is grateful for an ICREA Acadèmia award. G. G.-B gratefully acknowledges (RYC2019-026693-I/AEI/10.13039/501100011033) “El Fondo Social Europeo invierte en tu futuro”. Gobierno de Aragón/FEDER, UE (GA/FEDER, Reactividad y catálisis en química inorgánica, Group E50_20D). The authors would like to acknowledge the ‘Servicio General de Apoyo a la Investigación-SAI, Universidad de Zaragoza’, and the STR-UdG for technical support.

Notes and references

- 1 R. Dorel and A. M. Echavarren, *Chem. Rev.*, 2015, **115**, 9028–9072.
- 2 A. S. K. Hashmi, *Chem. Rev.*, 2007, **107**, 3180–3211.
- 3 A. Fürstner and P. W. Davies, *Angew. Chem., Int. Ed.*, 2007, **46**, 3410–3449.
- 4 J. H. Teles, S. Brode and M. Chabanas, *Angew. Chem., Int. Ed.*, 1998, **37**, 1415–1418.
- 5 Y. Fukuda and K. Utimoto, *J. Org. Chem.*, 1991, **56**, 3729–3731.
- 6 A. S. K. Hashmi, T. M. Frost and J. W. Bats, *J. Am. Chem. Soc.*, 2000, **122**, 11553–11554.
- 7 M. N. Hopkinson, A. D. Gee and V. Gouverneur, *Chem. – Eur. J.*, 2011, **17**, 8248–8262.
- 8 A. Nijamudheen and A. Datta, *Chem. – Eur. J.*, 2020, **26**, 1442–1487.



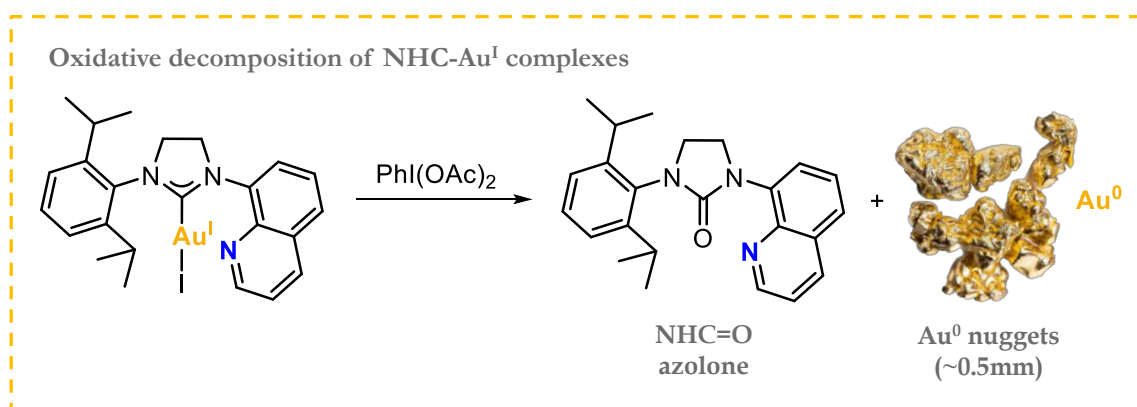
- 9 A. Kar, N. Mangu, H. M. Kaiser, M. Beller and M. K. Tse, *Chem. Commun.*, 2008, 386–388.
- 10 L. T. Ball, M. Green, G. C. Lloyd-Jones and C. A. Russell, *Org. Lett.*, 2010, **12**, 4724–4727.
- 11 L. T. Ball, G. C. Lloyd-Jones and C. A. Russell, *Chem. – Eur. J.*, 2012, **18**, 2931–2937.
- 12 G. Zhang, L. Cui, Y. Wang and L. Zhang, *J. Am. Chem. Soc.*, 2010, **132**, 1474–1475.
- 13 T. de Haro and C. Nevado, *J. Am. Chem. Soc.*, 2010, **132**, 1512–1513.
- 14 T. Ball Liam, C. Lloyd-Jones Guy and A. Russell Christopher, *Science*, 2012, **337**, 1644–1648.
- 15 L. T. Ball, G. C. Lloyd-Jones and C. A. Russell, *J. Am. Chem. Soc.*, 2014, **136**, 254–264.
- 16 X. C. Cambeiro, N. Ahlsten and I. Larrosa, *J. Am. Chem. Soc.*, 2015, **137**, 15636–15639.
- 17 M. Hofer, A. Genoux, R. Kumar and C. Nevado, *Angew. Chem., Int. Ed.*, 2017, **56**, 1021–1025.
- 18 M. Livendahl, P. Espinet and A. M. Echavarren, *Platinum Met. Rev.*, 2011, **55**, 212–214.
- 19 T. Lauterbach, M. Livendahl, A. Rosellón, P. Espinet and A. M. Echavarren, *Org. Lett.*, 2010, **12**, 3006–3009.
- 20 M. Livendahl, C. Goehry, F. Maseras and A. M. Echavarren, *Chem. Commun.*, 2014, **50**, 1533–1536.
- 21 D. J. Gorin and F. D. Toste, *Nature*, 2007, **446**, 395–403.
- 22 M. Joost, A. Amgoune and D. Bourissou, *Angew. Chem., Int. Ed.*, 2015, **54**, 15022–15045.
- 23 B. Huang, M. Hu and F. D. Toste, *Trends Chem.*, 2020, **2**, 707–720.
- 24 P. Font and X. Ribas, *Eur. J. Inorg. Chem.*, 2021, **2021**, 2556–2569.
- 25 M. N. Hopkinson, A. Tlahuext-Aca and F. Glorius, *Acc. Chem. Res.*, 2016, **49**, 2261–2272.
- 26 S. Banerjee, V. W. Bhojare and N. T. Patil, *Chem. Commun.*, 2020, **56**, 2677–2690.
- 27 M. O. Akram, S. Banerjee, S. S. Saswade, V. Bedi and N. T. Patil, *Chem. Commun.*, 2018, **54**, 11069–11083.
- 28 J. Miró and C. del Pozo, *Chem. Rev.*, 2016, **116**, 11924–11966.
- 29 V. W. Bhojare, A. G. Tathe, A. Das, C. C. Chintawar and N. T. Patil, *Chem. Soc. Rev.*, 2021, **50**, 10422–10450.
- 30 N. Lassauque, P. Gualco, S. Mallet-Ladeira, K. Miqueu, A. Amgoune and D. Bourissou, *J. Am. Chem. Soc.*, 2013, **135**, 13827–13834.
- 31 P. Gualco, S. Ladeira, K. Miqueu, A. Amgoune and D. Bourissou, *Angew. Chem., Int. Ed.*, 2011, **50**, 8320–8324.
- 32 J. Guenther, S. Mallet-Ladeira, L. Estevez, K. Miqueu, A. Amgoune and D. Bourissou, *J. Am. Chem. Soc.*, 2014, **136**, 1778–1781.
- 33 J. Serra, T. Parella and X. Ribas, *Chem. Sci.*, 2017, **8**, 946–952.
- 34 H. Beucher, J. Schörghener, E. Merino and C. Nevado, *Chem. Sci.*, 2021, **12**, 15084–15089.
- 35 C.-Y. Wu, T. Horibe, C. B. Jacobsen and F. D. Toste, *Nature*, 2015, **517**, 449–454.
- 36 M. Joost, A. Zeineddine, L. Estévez, S. Mallet-Ladeira, K. Miqueu, A. Amgoune and D. Bourissou, *J. Am. Chem. Soc.*, 2014, **136**, 14654–14657.
- 37 M. Joost, L. Estévez, K. Miqueu, A. Amgoune and D. Bourissou, *Angew. Chem., Int. Ed.*, 2015, **54**, 5236–5240.
- 38 M. J. Harper, C. J. Arthur, J. Crosby, E. J. Emmett, R. L. Falconer, A. J. Fensham-Smith, P. J. Gates, T. Leman, J. E. McGrady, J. F. Bower and C. A. Russell, *J. Am. Chem. Soc.*, 2018, **140**, 4440–4445.
- 39 J. A. Cadge, H. A. Sparkes, J. F. Bower and C. A. Russell, *Angew. Chem., Int. Ed.*, 2020, **59**, 6617–6621.
- 40 J. Chu, D. Munz, R. Jazzar, M. Melaimi and G. Bertrand, *J. Am. Chem. Soc.*, 2016, **138**, 7884–7887.
- 41 A. Zeineddine, L. Estévez, S. Mallet-Ladeira, K. Miqueu, A. Amgoune and D. Bourissou, *Nat. Commun.*, 2017, **8**, 565.
- 42 J. Rodriguez, A. Tabey, S. Mallet-Ladeira and D. Bourissou, *Chem. Sci.*, 2021, **12**, 7706–7712.
- 43 D. Mendoza-Espinosa, D. Rendon-Nava, A. Alvarez-Hernandez, D. Angeles-Beltran, G. E. Negron-Silva and O. R. Suarez-Castillo, *Chem.-Asian J.*, 2017, **12**, 203–207.
- 44 G. Kleinhans, M. M. Hansmann, G. Guisado-Barrios, D. C. Liles, G. Bertrand and D. I. Bezuidenhout, *J. Am. Chem. Soc.*, 2016, **138**, 15873–15876.
- 45 G. Kleinhans, A. K. Chan, M. Y. Leung, D. C. Liles, M. A. Fernandes, V. W. Yam, I. Fernandez and D. I. Bezuidenhout, *Chem. – Eur. J.*, 2020, **26**, 6993–6998.
- 46 R. P. Herrera and M. C. Gimeno, *Chem. Rev.*, 2021, **121**, 8311–8363.
- 47 L. Huang, F. Rominger, M. Rudolph and A. S. K. Hashmi, *Chem. Commun.*, 2016, **52**, 6435–6438.
- 48 A. Tabey, M. Berlande, P. Hermange and E. Fouquet, *Chem. Commun.*, 2018, **54**, 12867–12870.
- 49 J. Rodriguez, A. Zeineddine, E. D. Sosa Carrizo, K. Miqueu, N. Saffon-Merceron, A. Amgoune and D. Bourissou, *Chem. Sci.*, 2019, **10**, 7183–7192.
- 50 J. Rodriguez, D. Vesseur, A. Tabey, S. Mallet-Ladeira, K. Miqueu and D. Bourissou, *ACS Catal.*, 2022, **12**, 993–1003.
- 51 M. O. Akram, A. Das, I. Chakrabarty and N. T. Patil, *Org. Lett.*, 2019, **21**, 8101–8105.
- 52 J. Rodriguez, N. Adet, N. Saffon-Merceron and D. Bourissou, *Chem. Commun.*, 2020, **56**, 94–97.
- 53 M. Rigoulet, O. Thillaye du Boullay, A. Amgoune and D. Bourissou, *Angew. Chem., Int. Ed.*, 2020, **59**, 16625–16630.
- 54 A. G. Tathe, C. C. Chintawar, V. W. Bhojare and N. T. Patil, *Chem. Commun.*, 2020, **56**, 9304–9307.
- 55 S. Zhang, C. Wang, X. Ye and X. Shi, *Angew. Chem., Int. Ed.*, 2020, **59**, 20470–20474.
- 56 A. G. Tathe, Urvashi, A. K. Yadav, C. C. Chintawar and N. T. Patil, *ACS Catal.*, 2021, **11**, 4576–4582.
- 57 C. C. Chintawar, A. K. Yadav and N. T. Patil, *Angew. Chem., Int. Ed.*, 2020, **59**, 11808–11813.
- 58 S. R. Mudshinge, Y. Yang, B. Xu, G. B. Hammond and Z. Lu, *Angew. Chem., Int. Ed.*, 2022, **61**, e202115687.
- 59 X. Ye, C. Wang, S. Zhang, Q. Tang, L. Wojtas, M. Li and X. Shi, *Chem. – Eur. J.*, 2022, e202201018.
- 60 C. C. Chintawar, V. W. Bhojare, M. V. Mane and N. T. Patil, *J. Am. Chem. Soc.*, 2022, **144**, 7089–7095.
- 61 T. Shibata, R. Nagai, S. Okazaki, S. Nishibe and M. Ito, *Bull. Chem. Soc. Jpn.*, 2022, **95**, 700–706.



- 62 E. Tomás-Mendivil, P. Y. Toullec, J. Borge, S. Conejero, V. Michelet and V. Cadierno, *ACS Catal.*, 2013, **3**, 3086–3098.
- 63 A. G. Nair, R. T. McBurney, M. R. D. Gatus, S. C. Binding and B. A. Messerle, *Inorg. Chem.*, 2017, **56**, 12067–12075.
- 64 M. Navarro, A. Tabey, G. Szalóki, S. Mallet-Ladeira and D. Bourissou, *Organometallics*, 2021, **40**, 1571–1576.
- 65 G. Guisado-Barrios, M. Soleilhavoup and G. Bertrand, *Acc. Chem. Res.*, 2018, **51**, 3236–3244.
- 66 J. Lorkowski, P. Żak, M. Kubicki, C. Pietraszuk, D. Jędrzkiewicz and J. Ejfler, *New J. Chem.*, 2018, **42**, 10134–10141.
- 67 K. J. Cavell and A. T. Normand, in *N-Heterocyclic Carbenes in Transition Metal Catalysis and Organocatalysis*, ed. C. S. J. Cazin, Springer, Dordrecht, 2010, vol. 32, pp. 299–314.
- 68 C. M. Crudden and D. P. Allen, *Coord. Chem. Rev.*, 2004, **248**, 2247–2273.
- 69 B. Dong, H. Peng, S. E. Motika and X. Shi, *Chem. – Eur. J.*, 2017, **23**, 11093–11099.



CHAPTER IV. Novel NHC-Based Au(I) Complexes as Precursors of Highly Pure Au(0) Nuggets under Oxidative Conditions







This chapter corresponds to the following publication:

Pau Font, Nikolaos V. Tzouras, Argyro T. Papastavrou, Georgios C. Vougioukalakis*, Xavi Ribas*. Reprinted with permission from *Molecules* **2023**, *28*, 2302.

Article

Novel NHC-Based Au(I) Complexes as Precursors of Highly Pure Au(0) Nuggets under Oxidative Conditions

Pau Font ¹, Nikolaos V. Tzouras ², Argyro T. Papastavrou ², Georgios C. Vougioukalakis ^{2,*}
and Xavi Ribas ^{1,*}

¹ Institut de Química Computacional i Catàlisi and Departament de Química, Universitat de Girona, Campus Montilivi, E-17003 Girona, Catalonia, Spain

² Department of Chemistry, National and Kapodistrian University of Athens, Panepistimiopolis, 15771 Athens, Greece

* Correspondence: vougiouk@chem.uoa.gr (G.C.V.); xavi.ribas@udg.edu (X.R.); Tel.: +30-210-7274230 (G.C.V.); +34-683376923 (X.R.)

Abstract: The Lewis-acidic character and robustness of NHC-Au(I) complexes enable them to catalyze a large number of reactions, and they are enthroned as the catalysts of choice for many transformations among polyunsaturated substrates. More recently, Au(I)/Au(III) catalysis has been explored either by utilizing external oxidants or by seeking oxidative addition processes with catalysts featuring pendant coordinating groups. Herein, we describe the synthesis and characterization of N-heterocyclic carbene (NHC)-based Au(I) complexes, with and without pendant coordinating groups, and their reactivity in the presence of different oxidants. We demonstrate that when using iodosylbenzene-type oxidants, the NHC ligand undergoes oxidation to afford the corresponding NHC=O azolone products concomitantly with quantitative gold recovery in the form of Au(0) nuggets ~0.5 mm in size. The latter were characterized by SEM and EDX-SEM showing purities above 90%. This study shows that NHC-Au complexes can follow decomposition pathways under certain experimental conditions, thus challenging the believed robustness of the NHC-Au bond and providing a novel methodology to produce Au(0) nuggets.

Keywords: NHC-Au(I) complexes; pendant ligands; iodosylbenzene-type oxidants; oxidized NHC=O compounds; Au(0) nuggets



Citation: Font, P.; Tzouras, N.V.; Papastavrou, A.T.; Vougioukalakis, G.C.; Ribas, X. Novel NHC-Based Au(I) Complexes as Precursors of Highly Pure Au(0) Nuggets under Oxidative Conditions. *Molecules* **2023**, *28*, 2302. <https://doi.org/10.3390/molecules28052302>

Academic Editor: Cristina Tubaro

Received: 1 February 2023

Revised: 14 February 2023

Accepted: 24 February 2023

Published: 1 March 2023



Copyright: © 2023 by the authors. Licensee MDPI, Basel, Switzerland. This article is an open access article distributed under the terms and conditions of the Creative Commons Attribution (CC BY) license (<https://creativecommons.org/licenses/by/4.0/>).

1. Introduction

Fundamental comprehension of the intrinsic reactivity of NHC-based gold complexes is needed to evaluate their success in different fields, such as in the biological sector [1–5] or in catalysis. NHC ligands are typically described as strongly σ -donating, which form very stable NHC-metal bonds throughout a catalytic cycle [6,7]. Complexes of transition metals with N-heterocyclic carbene (NHC) ligands are commonly applied as catalysts for a variety of C-C and C-heteroatom bond formations, C-H functionalizations, cross-couplings, atom-economic additions, olefin metathesis, and many other transformations [8–12]. Moreover, there is high variability of the steric and electronic parameters of NHC ligands, which allows effective tuning of the catalyst activity [13].

Focusing on gold catalysis, a large number of NHC-Au complexes have been successfully used in Lewis acid catalysis for the cyclization and rearrangements of polyunsaturated substrates [14,15]. However, in order to further expand the scope of applications of these complexes, it is necessary to explore experimental conditions where NHC-gold complexes might suffer from instability. For instance, the exploration of Au(I)/Au(III) catalysis using external oxidants or oxidant-free catalysis with ligands featuring pendant coordinating groups has become prominent in the last decade, but the intrinsic decomposition of gold complexes is underexplored. In a related work, Ananikov reported the unusual role of

bases in the deactivation of NHC–metal catalysts (metal = Ni(II), Pd(II) and Pt(II)), undergoing metal reduction to M(0) and formation of NHC=O coupling azolone products (Figure 1a) [8]. In their study it is demonstrated that a base-mediated azolone NHC=O coupling reaction is integrated into the catalytic M/NHC systems and metal-free NHC derivatives are present in the catalytic mixture. A proposed mechanism of the revealed transformation includes NHC-OR reductive elimination, as implied by a series of mechanistic studies including $^{18}\text{OH}^-$ labeling experiments. Similar decomposition pathways were reported on triazolylidene Cu(I) complexes, which decompose into mesoionic oxides in the presence of CsOH [16]. Almost no reports exist for a detailed description of NHC-Au(I) decomposition pathways [17].

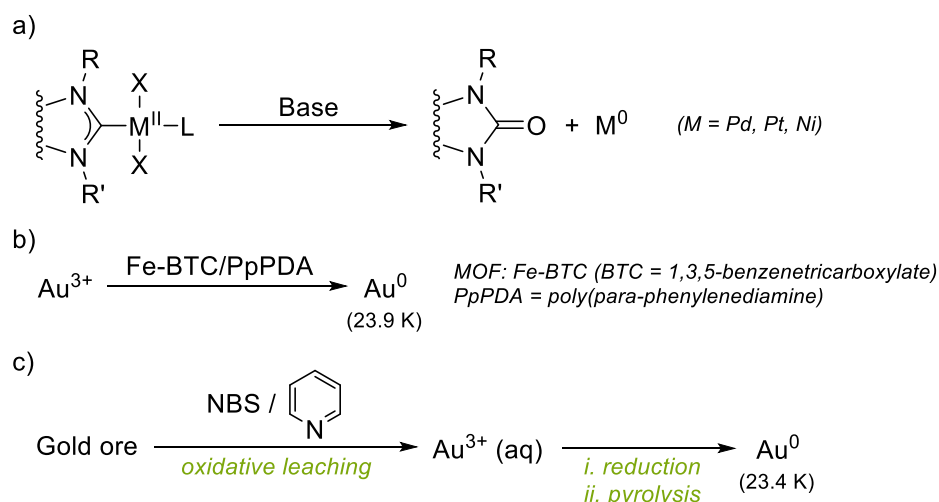


Figure 1. (a) Examples of azolone decomposition pathways of NHC-M, and (b,c) strategies to recover highly pure Au(0) (>23 karats).

Herein, we show how distinct NHC-Au(I) complexes undergo a controlled decomposition pathway towards the formation of the oxidized NHC=O azolone counterpart, together with the formation of naked eye-observable Au(0) nuggets. The NHC-Au(I) complexes studied under oxidative conditions cover various types, from typical IPrAuCl to novel (NHC-hemilabile)Au(I) complexes. Indeed, the ability of related triazolylidene ligands to bear pendant pyridine or pyrimidine groups for Au(I)/Au(III) redox processes has recently been studied [18]. We show that only typical NHC-Au(I) complexes such as IPr-Au-Cl and SIPr-Au-Cl are robust and remain intact after exposure to oxidants, and the gold complexes with NHC-hemilabile ligands or other NHC derivatives undergo the azolone/Au(0) nugget decomposition pathway. The origin of the O-atom in the azolone-products obtained is discussed. Remarkably, a straightforward and reliable chemical methodology to produce Au(0) nuggets from Au complexes is not available, and the main source of gold(0) nuggets are, like natural ores, hypogenic in origin.¹⁹ Native gold grains are usually small in size (10–500 nm), with a composition of 5 to <30% Ag, typical of hypogene gold, although Ag can be less than 1% depending on the goldfield of origin [19]. Supergene gold biomineralization has also been studied [20,21]. Recently, an Fe-based MOF/polymer composite (Fe-BTC/PpPDA) has been reported as a selective and efficient methodology to extract trace amounts of gold from water up to high purities (23.9 karats (K); >99%) (Figure 1b) [22]. Reduction of Au^{3+} to Au(0), mediated by the MOF-polymer composite, is proposed. On the other hand, recovery of Au(0) from ores or waste electronic materials entails stepwise tedious processes such as reduction with metallic Zn, HCl treatment, centrifugation and pyrolysis (Figure 1c) [23]. The decomposition to Au(0) observed in our systems could be used as a methodology to obtain metallic gold more easily, as we show that Au(0) nuggets of up to ~500 μm can be afforded in one step by treatment of NHC-Au(I) complexes with external oxidants.

2. Results and Discussion

2.1. Synthesis of Novel NHC-Au(I) Complexes (1–4)

The synthesis of imidazolium salts **L1**, **L2**, **L3** and **L4** was achieved by standard procedures [24,25]. **L1–L3** contain a pendant pyridine or quinoline whereas **L4** contains a non-coordinating arene moiety (Figure 2).

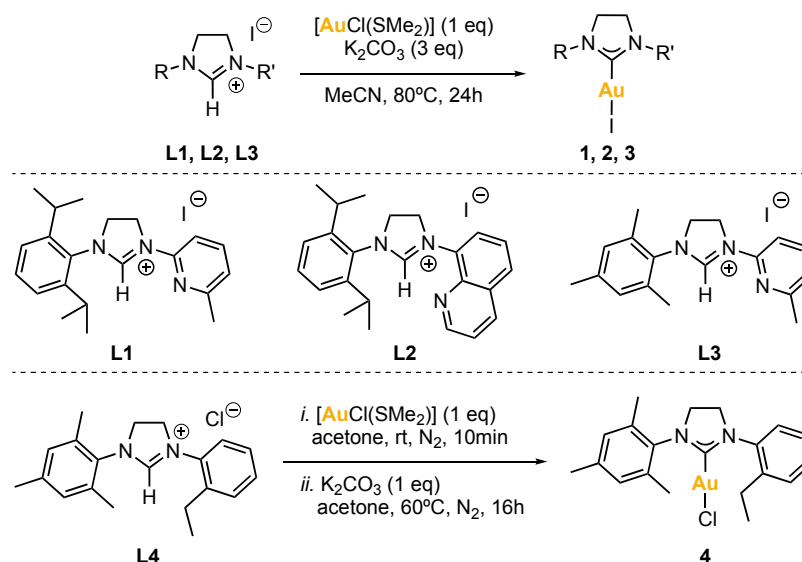


Figure 2. Synthesis of complexes 1–4 from the respective imidazolium salt ligand precursors **L1–L4**.

The synthesis of NHC-Au(I) complexes was based on previously reported works [26,27]. Complexes **1**, **2** and **3** were obtained by reacting the corresponding imidazolium salt **L1**, **L2** or **L3** (1 eq), chloro(dimethylsulfide)gold(I) (1 eq), and potassium carbonate (3 eq), in acetonitrile for 24 h at 80°C . After this time, the reaction mixture was filtered over Celite[®] and all volatiles were removed under vacuum. The product was purified by column chromatography. The fractions that contained the product were combined, and the solvent was removed under vacuum to afford the gold(I) complexes as solids. Complex **4** was obtained analogously from imidazolium salt **L4** (Figure 2).

X-ray molecular structures of complexes **1**, **2**, **3** and **4** were obtained (Figure 3). In complexes **1–3**, the pendant coordinating arm did not show any interaction with the metal center, and the linear coordination for the Au(I) center was confirmed in all cases, since the angle formed between the carbenic carbon, the gold center and the halide atom was close to 180° (for **1**, $177.4(4)^\circ$; for **2**, $175.4(2)^\circ$; for **3**, $178.38(8)^\circ$; for **4**, $179.12(16)^\circ$). No H-bonding network was observed with the non-coordinating pendant groups.

Complexes **1–4** were asymmetrical; therefore, the two methylenes of the imidazolidine ring appeared at different ^1H NMR chemical shifts: for complexes **1** and **3**, the two $-\text{NCH}_2-$ appeared as multiplets at 4.54 and 3.90 ppm, respectively, and for complex **2**, at 4.68 and 4.08 ppm. For complex **4**, the two $-\text{NCH}_2-$ appeared at 4.22 and 3.96 ppm. On the other hand, the characteristic ^{13}C NMR peak of the $\text{C}_{\text{carbene}}-\text{Au}$ appeared at 201.0, 203.7, 192.2 and 195.5 ppm for **1**, **2**, **3** and **4**, respectively.

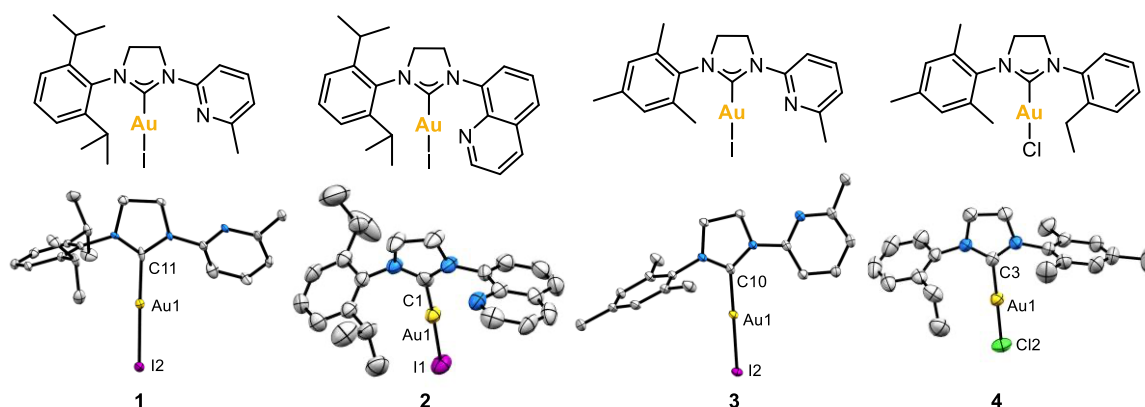


Figure 3. X-ray molecular structures of complexes **1**, **2**, **3** and **4** (ellipsoids set at 50% probability and H atoms removed for clarity). Selected bond distances (Å): for **1**, Au1–C11 2.007(13), Au1–I2 2.5580(10); for **2**, Au1–C1 1.981(9), Au1–I1 2.5467(8); for **3**, Au1–C10 2.000(3), Au1–I2 2.5516(2); for **4**, Au1–C3 1.966(6), Au1–Cl2 2.262(3). Selected angles (°): for **1**, C11–Au1–I2 177.4(4); for **2**, C1–Au1–I1 175.4(2); for **3**, C10–Au1–I2 178.38(8); for **4**, C3–Au1–Cl2 179.12(16).

2.2. Reactivity of Novel NHC–Au(I) Complexes (1–4) with External Oxidants

Complexes **1–3** were reacted with external oxidants in order to stabilize the NHC–Au(III) species, taking advantage of the pendant coordinating arms (pyridine-type for **1** and **3**, and quinoline-type for **2**). The external oxidants used were $\text{PhI}(\text{OAc})_2$, $\text{PhI}(\text{Cl})_2$, H_2O_2 , XeF_2 , $\text{CH}_3\text{CO}_3\text{H}$ under different solvents and temperatures (Table 1). However, the expected NHC–Au(III) species could not be stabilized in any case, and the mixture underwent a decomposition pathway involving the formation of a) the corresponding NHC=O azolones and b) Au(0) nuggets.

The formation of the NHC=O azolone products **L1^{ox}**, **L2^{ox}**, **L3^{ox}**, **L4^{ox}** was monitored by HRMS, and **L2^{ox}** and **L3^{ox}** were fully characterized by 1D and 2D NMR. In some reactions, the NHC–Au(I) complexes were treated with silver salts (as halide scavengers) and the oxidant. The aim of using a silver salt as additive was to promote the halide abstraction from the gold(I) starting complex and generate a reactive species that, hopefully, would evolve to a gold(III) complex in the presence of an oxidant, expecting the hemilabile N-donor arm to be coordinated to gold in the case of using complexes **1–3**. In addition, the halide abstraction could likely induce the formation of head-to-tail dimeric Au(I) species with the C[∞]N ligand bridging two metals [18,28,29]. However, the synthesis of such dimeric species was not the focus of our interest.

When complex **1** was reacted with $\text{PhI}(\text{OAc})_2$, regardless whether AgOAc was added or not, Au(0) nuggets and azolones **L1^{ox}** and **L1^{ox}-I** were formed (entries 1,2). The azolones were detected by ESI-MS and, in the case of the reaction in entry 3, the **L1^{ox}-I** product was isolated in 53% yield. When the oxidant was changed to H_2O_2 , the outcome of the reaction in presence of AgOAc was mainly the starting complex **1**, whereas in the absence of AgOAc , **L1^{ox}-I** could be detected by ESI-MS as well. **L1^{ox}-I** was also detected in the reaction of **1** with $\text{PhI}(\text{Cl})_2$ at room temperature. Intriguingly, the formation of azolones that underwent a C–H iodination on the most activated position of the heteroaromatic system of the ligand was also observed. In this manner, products **L1^{ox}-I** and **L2^{ox}-I** were isolated and characterized. Indeed, the 2D NMR experiments revealed that the iodination occurred at the para position to the imidazolinone substituent (see Supplementary Material, Sections S5.7 and S5.9). The selective C–H halogenation at the para position to N-substituted positions and C5-halogenation of 8-aminoquinolines is a reactivity pattern that has already been reported [30–34]. Neither the reactions with H_2O_2 nor that with $\text{PhI}(\text{Cl})_2$ afforded Au(0) nuggets (entries 4–6). A blank experiment was conducted with complex **2**; without oxidant and additives, the complex was recovered after being heated at 100 °C overnight (entry 7). When using $\text{PhI}(\text{OAc})_2$, Au(0) nuggets were obtained in high yields (56–91%), and **L2^{ox}** and **L2^{ox}-I** products were detected by ESI-MS in all cases (entries 8–11). The isolation

of both **L2^{ox}** and **L2^{ox}-I** azolones allowed their full characterization. When complex **2** was reacted with CH₃CO₃H as oxidant (entry 12), Au(0) nuggets were formed in moderate yield (34%) and NMR revealed the presence of complex **2** and **L2^{ox}**.

Table 1. Reactivity of gold(I) complexes towards the formation of gold(0) nuggets and azolones (**Lx^{ox}**).

Entry	Complex	Oxidant	Additive	Solvent	T (°C)	Yield % Au(0)	NHC=O (yield %)*
1	1	PhI(OAc) ₂	AgOAc	1,2-DCE	90	75	Detected MS
2	1	PhI(OAc) ₂	-	1,2-DCE	90	46	Detected MS
3	1	PhI(OAc) ₂	-	MeCN	90	60	L1^{ox}-I (53)
4	1	H ₂ O ₂	AgOAc	1,2-DCE	90	0	0
5	1	H ₂ O ₂	-	1,2-DCE	90	0	Detected MS
6	1	PhI(Cl) ₂	-	DCM	rt	0	Detected MS
7	2	-	-	1,2-DCE	100	0	0
8	2	PhI(OAc) ₂	AgOAc	1,2-DCE	90	85	Detected MS
9	2	PhI(OAc) ₂	-	1,2-DCE	90	90	L2^{ox} (22) and L2^{ox}-I (17)
10	2	PhI(OAc) ₂	AgOAc	DCM	70	91	Detected MS
11	2	PhI(OAc) ₂	-	MeCN	90	56	L2^{ox} (34)
12	2	CH ₃ CO ₃ H	-	1,2-DCE	90	34	Detected NMR
13	3	PhI(OAc) ₂	AgOAc	1,2-DCE	90	>99	L3^{ox} (60)
14	3	XeF ₂	-	CDCl ₃	rt	0	Detected MS
15	4	PhI(OAc) ₂	-	DCM	rt	0	0
16 ^a	4	PhI(OAc) ₂	-	DCM	100	97	Detected MS
17	4	PhI(OAc) ₂	-	1,2-DCE	90	32	Detected MS
18	IPrAuCl	PhI(OAc) ₂	AgOAc	1,2-DCE	90	0	0
19	IPrAuCl	PhI(OAc) ₂	-	1,2-DCE	90	0	0
20	SIPrAuCl	PhI(OAc)	AgOAc	1,2-DCE	90	0	0
21	SIPrAuCl	PhI(OAc)	-	1,2-DCE	90	11	6
22 ^b	2	PhI(OAc) ₂	H ₂ O	MeCN	90	88	L2^{ox} (48)
23 ^b	2	PhI(OAc) ₂	H ₂ ¹⁸ O	MeCN	90	97	L2^{ox} (41)

* Isolated yield; ^a 5 h of reaction; ^b 60 equivalents of additive.

The reaction of complex **3** with PhI(OAc)₂ and AgOAc yielded Au(0) quantitatively, and azolone **L3^{ox}** was isolated in 60% yield and characterized (entry 13). On the contrary, when the oxidant XeF₂ was tested with complex **3** at room temperature, no Au(0) nuggets were formed (entry 14). However, the formation of azolone **L3^{ox}** was detected by ESI-MS.

Complex **4** was employed to search for contrast with the complexes that contained a hemilabile pendant arm. The reaction with PhI(OAc)₂ in DCM at room temperature did not provide Au(0) nuggets nor azolone, as the starting complex was recovered (entry 15). However, by heating at 100 °C for 5 h, the mixture decomposed, affording Au(0) nuggets in a 97% yield, and the corresponding **L4^{ox}** azolone was detected by ESI-MS (entry 16). When **4** was reacted with PhI(OAc)₂ in 1,2-DCE at 90 °C, Au(0) nuggets were obtained in a 32% yield (entry 17).

Interestingly, the commercial IPrAuCl was also reacted with PhI(OAc)₂ under the same experimental conditions as **1-4**, and in this case, neither azolone product nor Au(0) nuggets were formed, and the complex was recovered after the reaction time (entries 18–19). Additionally, when the commercial saturated SIPrAuCl analog complex was reacted with

PhI(OAc)₂, a very low 11% conversion to Au(0) nuggets was obtained along with a 6% conversion to the corresponding azolone, as determined by NMR, according to the reported description of the azolone (entries 20,21) [35]. The stability of these well-known complexes is remarkable compared to that of 1–4, showing that when a structural modification of the most typical NHC ligands, such as IPr and SIPr, is performed, a sharp change in reactivity occurs. Additionally, it is worth mentioning that there are examples of unsaturated NHC–Au(I) complexes bearing a hemilabile pyridine moiety that could be oxidized with PhI(Cl)₂ to the corresponding NHC–Au(III) complexes without observing decomposition [36,37].

The origin of the O-atom in azolones was investigated by reacting complex 2, with PhI(OAc)₂ as the oxidant and water as the additive, under nitrogen atmosphere (Table 1, entries 22,23, and Figure 4). In order to track the origin of the O-atom, a control reaction was carried out using distilled H₂O, and another using 97% labeled ¹⁸O-water (see Supporting Material, Section S6). The reaction crudes were analyzed by ESI-HRMS. For the control experiment, a major peak at *m/z* = 374.2 was obtained, corresponding to the NHC=¹⁶O azolone L2^{ox}, whereas for the reaction with H₂¹⁸O two major peaks were obtained at *m/z* = 374.2 and *m/z* = 376.2, corresponding to the NHC=¹⁶O and NHC=¹⁸O azolones L2^{ox}, respectively. According to the isotopic pattern of such peaks, a 35% of ¹⁸O incorporation was obtained, suggesting that the O-atom in the azolones obtained in the reaction outcomes may come from adventitious water. The low ¹⁸O incorporation from water suggests that an oxygen-transferring mechanism may exist, and that at some point of the mechanism, water might react with the oxidant to deliver a ¹⁸O-labeled reactive intermediate. Further investigations would be needed to elucidate the mechanism; at this stage, the alternative possibility of considering acetate to be the O-atom source cannot be ruled out [38].

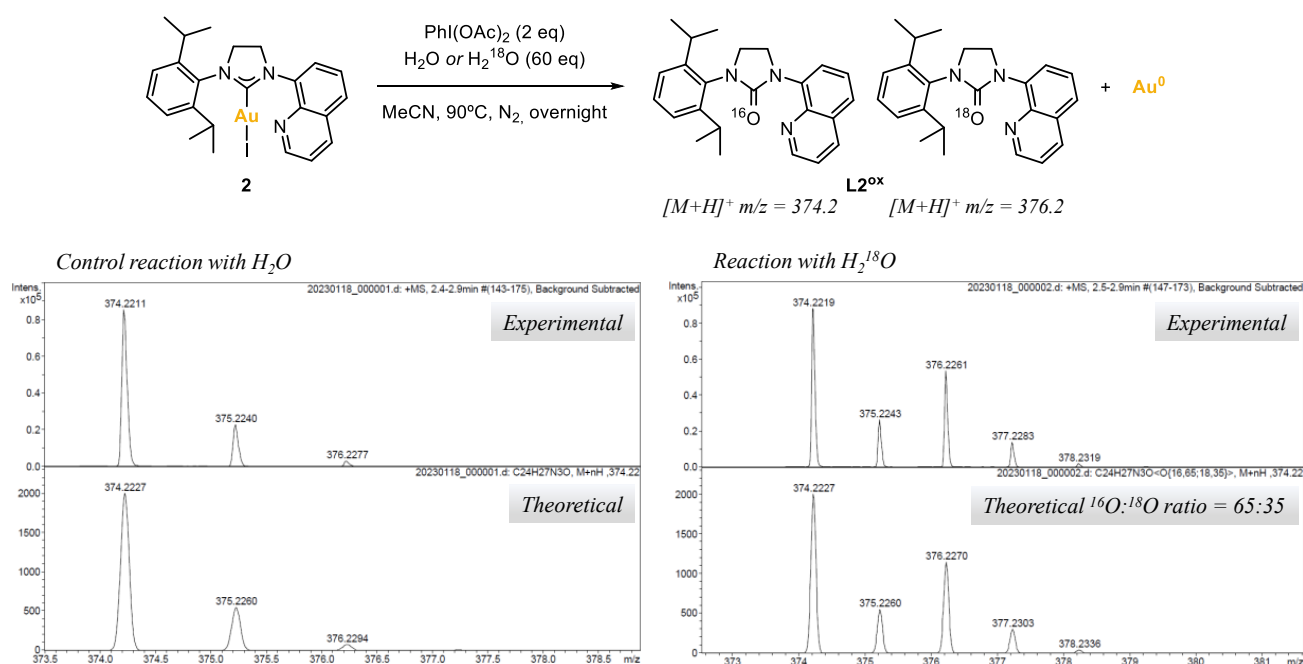


Figure 4. Reaction of complex 2 with PhI(OAc)₂ (2 eq) and water or ¹⁸O-labeled water (60 eq), and peaks of L2^{ox} obtained by ESI-HRMS(+).

2.3. Characterization and Reactivity of the Au(0) Nuggets

On the other hand, the formation of large Au(0) nuggets was naked-eye evident (Figure 5). The metallic gold grains were easily filtered/decanted and represented quantitative recovery (up to 90%) of all the Au(I) into Au(0) nuggets. The Au(0) nuggets were characterized by SEM and SEM-EDX, showing grains of 0.4–0.5 mm diameter mean size and purity up to 90% by EDX (only C and N impurities from the carbon tape support).

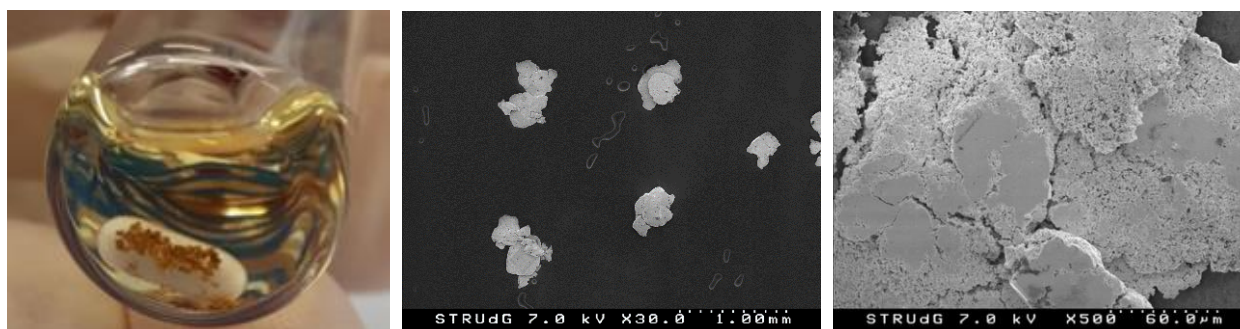


Figure 5. Reaction outcome with Au(0) precipitate (**left**), and SEM images of the isolated Au(0) nuggets at $\times 30$ and $\times 500$ (**middle** and **right**), from the reaction employing complex **1** (1 eq), AgOAc (1 eq) and $\text{PhI}(\text{OAc})_2$ (2 eq) in 1,2-DCE, at 90°C overnight, under N_2 atmosphere in the absence of light (Table 1, entry 1).

The Au(0) nuggets were tested as a heterogeneous catalyst for transformations typically catalyzed by gold complexes, such as Sonogashira, A3 and Glaser couplings [39–43]. None of these attempts resulted in effective coupling, which is in line with the macroscopic size of the Au(0) nuggets and the absence of more reactive Au(0) nanoparticles.

3. Materials and Methods

All reagents and solvents were purchased from Sigma Aldrich-Merck (Madrid, Spain), Fischer Scientific (Madrid, Spain), TCI (Windrush, Belgium) or Fluorophen (Glossip, United Kingdom) and were used without further purification. NMR spectra were recorded at 298 K unless otherwise specified, on Bruker spectrometers (Billerica, MA, USA) operating at 400 MHz (^1H NMR) and 101 MHz ($^{13}\text{C}\{^1\text{H}\}$ NMR), or on a Varian Mercury 200 MHz spectrometer (Palo Alto, CA, USA), and referenced to residual solvent (δ in ppm and J in hertz). High resolution mass spectra (HRMS) were recorded on a Bruker Microsoft-Q IITM or a QTOF maxis Impact (Bruker) spectrometer using ESI source at Servais Tècnics de Recerca, University of Girona, or at the National and Kapodistrian University of Athens. For reactions carried out under inert atmosphere, a N_2 drybox with O_2 and H_2O concentrations <1 ppm was employed, or standard Schlenk techniques were followed. SEM images of the Au(0) nuggets were carried out with a scanning electron microscope FE-SEM Hitachi S-4100 (Hitachi, Chiyoda City, Japan). Digital images were collected and processed by Quarz PCI program. SEM-EDX analysis was performed with a scanning electron microscope Zeiss DSM 960 Germany (EDX Bruker, Quantax Esprit Spectrometer SVE III, Billerica, MA, USA).

Synthesis of complexes 1–3. For the synthesis of NHC-Au(I) complexes **1**, **2** and **3**, the corresponding imidazolium salt **L1**, **L2** or **L3** (1 eq), chloro(dimethylsulfide)gold(I) (1 eq), and potassium carbonate (3 eq), were reacted in acetonitrile for 24 h at 80°C . After this time, the reaction mixture was filtered over Celite[®] and all volatiles were removed under vacuum. The product was purified by column chromatography. The fractions that contained the product were combined, and the solvent was removed under vacuum to afford the gold(I) complexes as solids.

Complex 1. The imidazolium iodide salt **L1** (102.4 mg, 0.23 mmol, 1.0 eq.), K_2CO_3 (126.7 mg, 0.92 mmol, 4.0 eq.) and $[\text{AuCl}(\text{SMe}_2)]$ (87.2 mg, 0.30 mmol, 1.3 eq.) were reacted in acetonitrile (1 mL). The product was purified by column chromatography using DCM:hexane (4:1). By slow diffusion of pentane into a concentrated solution of complex **1** in chloroform, pale yellow crystals suitable for X-ray diffraction analysis were obtained (59.3 mg, 40% yield). ^1H NMR (400 MHz, CDCl_3) δ 8.58 (d, $J = 8.3$ Hz, 1H, CH_{py}), 7.63 (t, $J = 7.8$ Hz, 1H, CH_{py}), 7.43 (t, $J = 7.8$ Hz, 1H, CH_{Ar}), 7.24 (d, $J = 7.8$ Hz, 2H, CH_{Ar}), 7.02 (d, $J = 7.5$ Hz, 1H, CH_{py}), 4.59–4.52 (m, 2H, NCH_2), 3.95–3.87 (m, 2H, NCH_2), 2.97 (hept, $J = 6.8$ Hz, 2H, $\text{CH}(\text{CH}_3)_2$), 2.53 (s, 3H, CH_3), 1.39 (d, $J = 6.8$ Hz, 6H, $\text{CH}(\text{CH}_3)_2$), 1.26 (d, $J = 6.9$ Hz, 6H, $\text{CH}(\text{CH}_3)_2$). $^{13}\text{C}\{^1\text{H}\}$ NMR (101 MHz, CDCl_3) δ 201.0 ($\text{C}_{\text{carbene-Au}}$), 157.3 (C_{py}), 151.9 (C_{py}), 146.2 (C_{Ar} , 2C), 138.3 (CH_{py}), 134.7 (C_{Ar}), 130.3 (CH_{Ar}), 124.8 (CH_{Ar} , 2C),

120.5 (CH_{py}), 111.4 (CH_{py}), 53.1 (NCH₂), 48.7 (NCH₂), 28.7 (CH(CH₃)₂, 2C), 25.0 (CH(CH₃)₂, 2C), 24.6 (CH(CH₃)₂, 2C), 24.4 (CH₃). HRMS (ESI+): calcd. for C₂₁H₂₇AuN₃ [M + H]⁺: *m/z* 646.0988; found: *m/z* 646.0984; [M + Na]⁺: *m/z* 668.0807; found: 668.0840; [2M – I]⁺: *m/z* 1163.2780; found: 1163.2804.

Complex 2. The imidazolium iodide salt **L2** (180.0 mg, 0.37 mmol, 1.0 eq.), K₂CO₃ (261.2 mg, 1.89 mmol, 5.1 eq.) and [AuCl(SMe₂)] (139.1 mg, 0.47 mmol, 1.3 eq.) were reacted in acetonitrile (2 mL). After the filtration over Celite[®], the product was purified by filtering the residue over a pad of silica using DCM. The solvent was removed to obtain a yellow solid. It was washed with hexane and diethyl ether to afford complex **2** as a white solid (105.8 mg, 42% yield). ¹H NMR (400 MHz, CDCl₃) δ 8.96 (dd, *J* = 4.2, 1.7 Hz, 1H, CH_{Quin}), 8.23 (dd, *J* = 8.3, 1.7 Hz, 1H, CH_{Quin}), 8.10 (dd, *J* = 7.3, 1.4 Hz, 1H, CH_{Quin}), 7.87 (dd, *J* = 8.2, 1.4 Hz, 1H, CH_{Quin}), 7.60 (dd, *J* = 8.3, 7.4 Hz, 1H, CH_{Quin}), 7.50 (dd, *J* = 8.3, 4.2 Hz, 1H, CH_{Quin}), 7.42 (t, *J* = 7.8 Hz, 1H, CH_{Ar}), 7.25 (d, *J* = 7.8 Hz, 2H, CH_{Ar}), 4.72–4.64 (m, 2H, NCH₂), 4.12–4.04 (m, 2H, NCH₂), 3.23 (hept, *J* = 6.9 Hz, 2H, CH(CH₃)₂), 1.43 (d, *J* = 6.8 Hz, 6H, CH(CH₃)₂), 1.39 (d, *J* = 6.8 Hz, 6H, CH(CH₃)₂). ¹³C{¹H} NMR (101 MHz, CDCl₃) δ 203.7 (C_{carbene}-Au), 150.4 (CH_{Quin}), 146.8 (C_{Ar}, 2C), 144.1 (C_{Quin}), 137.6 (C_{Quin}), 136.6 (CH_{Quin}), 134.6 (C_{Ar}), 130.0 (CH_{Ar}), 129.6 (C_{Quin}), 128.8 (CH_{Quin}), 128.3 (CH_{Quin}), 126.4 (CH_{Quin}), 124.7 (CH_{Ar}, 2C), 122.0 (CH_{Quin}), 54.4 (NCH₂), 53.0 (NCH₂), 28.7 (CH(CH₃)₂, 2C), 25.3 (CH(CH₃)₂, 2C), 24.6 (CH(CH₃)₂, 2C). HRMS (ESI+): calcd. for C₂₄H₂₇AuN₃ [M + H]⁺: *m/z* 682.0988; found: *m/z* 682.0974; [2M – I]⁺: *m/z* 1235.2780; found: 1235.2746.

Complex 3. The imidazolium iodide salt **L3** (67.5 mg, 0.17 mmol, 1.0 eq.), K₂CO₃ (91.1 mg, 0.66 mmol, 4.0 eq.) and [AuCl(SMe₂)] (63.8 mg, 0.22 mmol, 1.3 eq.) were reacted in acetonitrile (1 mL). The product was purified by column chromatography using DCM. By slow diffusion of pentane into a concentrated solution of complex **3** in chloroform, crystals suitable for X-ray diffraction analysis were obtained (32.9 mg, 33% yield). ¹H NMR (400 MHz, CDCl₃) δ 8.54 (d, *J* = 8.2 Hz, 1H, CH_{py}), 7.62 (t, *J* = 7.9 Hz, 1H, CH_{py}), 7.02 (d, *J* = 7.5 Hz, 1H, CH_{py}), 6.94 (s, 2H, CH_{Ar}), 4.57–4.48 (m, 2H, NCH₂), 3.94–3.85 (m, 2H, NCH₂), 2.52 (s, 3H, CH_{3py}), 2.30 (s, 3H, CH_{3Ar}), 2.27 (s, 6H, CH_{3Ar}). ¹³C{¹H} NMR (101 MHz, CDCl₃) δ 192.2 (C_{carbene}-Au), 157.3 (C_{py}), 151.9 (C_{py}), 139.3 (C_{Ar}), 138.3 (CH_{py}), 135.5 (C_{Ar}), 135.1 (C_{Ar}, 2C), 130.0 (CH_{Ar}, 2C), 120.6 (CH_{py}), 112.0 (CH_{py}), 50.3 (NCH₂), 48.8 (NCH₂), 24.3 (CH_{3py}), 21.2 (CH_{3Ar}), 18.2 (CH_{3Ar}, 2C). HRMS (ESI+): calcd. for C₁₈H₂₁AuN₃ [M + Na]⁺: *m/z* 626.0338; found: *m/z* 626.0336; [(C₁₈H₂₁N₃)₂Au]⁺: *m/z* 755.3131; found: 755.3150; [2M – I]⁺: *m/z* 1079.1841; found: 1079.1830.

Complex 4. For the synthesis of NHC-Au(I) complex **4**, imidazolium salt **L4** (60.1 mg, 0.18 mmol, 1.0 eq) and chloro(dimethylsulfide)gold(I) (54.8 mg, 0.19 mmol, 1.0 eq) were mixed in acetone (0.6 mL), under nitrogen atmosphere, and stirred at room temperature for 10 min. Then, potassium carbonate (27.6 mg, 0.20 mmol, 1.1 eq) was added and the mixture was stirred and heated at 60 °C for 16 h. After this time, the reaction mixture was cooled down to room temperature, then the solvent was removed under reduced pressure, and DCM was added. The mixture was filtered over a pad of silica, which was washed with more DCM, and the resulting solution was concentrated to the minimal volume. Next, pentane was added to precipitate the desired product. It was washed with more pentane, and it was dried under vacuum. Complex **4** was obtained as a white solid (75.5 mg, 67% yield). ¹H NMR (400 MHz, CDCl₃) δ 7.40–7.24 (m, 4H, CH_{Ar}), 6.94 (d, *J* = 0.7 Hz, 2H, CH_{Ar}), 4.11 (t, *J* = 9.6 Hz, 2H, NCH₂), 3.96 (td, *J* = 10.4, 1.7 Hz, 2H, NCH₂), 2.76 (q, *J* = 7.6 Hz, 2H, CH₂CH₃), 2.31 (s, 6H, CH₃), 2.30 (s, 3H, CH₃), 1.35 (t, *J* = 7.6 Hz, 3H, CH₂CH₃). ¹³C{¹H} NMR (101 MHz, CDCl₃) δ 195.0 (C_{carbene}-Au), 141.2 (C_{Ar}), 139.1 (C_{Ar}), 138.4 (C_{Ar}), 135.6 (C_{Ar}, 2C), 134.8 (C_{Ar}), 129.9 (CH_{Ar}, 2C), 129.9 (CH_{Ar}), 129.5 (CH_{Ar}), 128.4 (CH_{Ar}), 127.5 (CH_{Ar}), 53.3 (NCH₂), 51.0 (NCH₂), 24.4 (CH₂CH₃), 21.2 (CH₃), 18.1 (CH₃, 2C), 15.0 (CH₂CH₃). HRMS (ESI+): calcd. for C₂₀H₂₄AuClN₂ [M + Na]⁺: *m/z* 547.1186; found: *m/z* 547.1181; [2M + Na]⁺: *m/z* 1071.2479; found: 1071.2438; [2M – Cl]⁺: *m/z* 1013.2899; found: 1013.2865.

Compound L1^{ox}-I. ¹H NMR (400 MHz, 228K, CDCl₃) δ 7.91–7.83 (m, 2H, CH_{py}), 7.38 (t, *J* = 7.7 Hz, 1H, CH_{Ar}), 7.23 (d, *J* = 7.6 Hz, 2H, CH_{Ar}), 4.23 (t, *J* = 8.2 Hz, 2H, NCH₂), 3.71

(t, $J = 8.2$ Hz, 2H, NCH₂), 2.98 (hept, $J = 6.8$ Hz, 2H, CH(CH₃)₂), 2.63 (s, 3H, CH₃), 1.23 (d, $J = 6.9$ Hz, 6H, CH(CH₃)₂), 1.20 (d, $J = 6.6$ Hz, 6H, CH(CH₃)₂). ¹³C{¹H} NMR (101 MHz, CDCl₃) δ 157.7 (C_{py}), 156.2 (C=O), 152.1 (C_{py}), 148.0 (C_{Ar}, 2C), 147.3 (CH_{py}), 132.8 (C_{Ar}), 129.2 (CH_{Ar}), 124.3 (CH_{Ar}, 2C), 112.2 (CH_{py}), 86.2 (C_{py-I}), 45.7 (NCH₂), 41.7 (NCH₂), 28.9 (CH(CH₃)₂, 2C), 28.8 (CH₃), 24.6 (CH(CH₃)₂, 2C), 24.4 (CH(CH₃)₂, 2C). HRMS (ESI+): calcd for C₂₁H₂₆IN₃O [M + H]⁺: m/z 464.1193; found: m/z 464.1193; [M + Na]⁺: m/z 486.1013; found: m/z 486.1012; [2M + Na]⁺: m/z 949.2133; found: m/z 949.2141.

Compound L2^{ox}. ¹H NMR (400 MHz, CDCl₃) δ 8.93 (dd, $J = 4.2, 1.8$ Hz, 1H, CH_{Ar}), 8.17 (dd, $J = 8.3, 1.8$ Hz, 1H, CH_{Ar}), 7.93 (dd, $J = 7.5, 1.4$ Hz, 1H, CH_{Ar}), 7.71 (dd, $J = 8.2, 1.4$ Hz, 1H, CH_{Ar}), 7.56 (dd, $J = 8.2, 7.5$ Hz, 1H, CH_{Ar}), 7.42 (dd, $J = 8.3, 4.1$ Hz, 1H, CH_{Ar}), 7.35 (dd, $J = 8.3, 7.1$ Hz, 1H, CH_{Ar}), 7.23 (d, $J = 7.7$ Hz, 2H, CH_{Ar}), 4.45–4.40 (m, 2H, NCH₂), 3.90–3.84 (m, 2H, NCH₂), 3.32 (hept, $J = 6.9$ Hz, 2H, CH(CH₃)₂), 1.32 (d, $J = 6.9$ Hz, 6H, CH(CH₃)₂), 1.30 (d, $J = 6.8$ Hz, 6H, CH(CH₃)₂). ¹³C{¹H} NMR (101 MHz, CDCl₃) δ 159.5 (C=O), 149.3 (CH_{Quin}), 148.5 (C_{Ar}, 2C), 144.3 (C_{Quin}), 138.3 (C_{Quin}), 136.5 (CH_{Quin}), 133.8 (C_{Ar}), 129.7 (C_{Quin}), 128.8 (CH_{Ar}), 127.5 (CH_{Quin}), 126.7 (CH_{Quin}), 126.1 (CH_{Quin}), 124.2 (CH_{Ar}, 2C), 121.3 (CH_{Quin}), 47.4 (NCH₂), 47.0 (NCH₂), 28.8 (CH(CH₃)₂, 2C), 24.8 (CH(CH₃)₂, 2C), 24.5 (CH(CH₃)₂, 2C). HRMS (ESI+): calcd. for C₂₄H₂₇N₃O [M + H]⁺: m/z 374.2227; found: m/z 374.2211; [M + Na]⁺: m/z 396.2046; found: 396.2036; [2M + Na]⁺: m/z 769.4200; found: m/z 769.4164.

Compound L2^{ox-I}. ¹H NMR (400 MHz, CDCl₃) δ 8.88 (dd, $J = 4.1, 1.6$ Hz, 1H, CH_{Quin}), 8.39 (dd, $J = 8.5, 1.6$ Hz, 1H, CH_{Quin}), 8.13 (d, $J = 8.1$ Hz, 1H, CH_{Quin}), 7.69 (d, $J = 8.0$ Hz, 1H, CH_{Quin}), 7.49 (dd, $J = 8.6, 4.1$ Hz, 1H, CH_{Quin}), 7.35 (dd, $J = 8.3, 7.1$ Hz, 1H, CH_{Ar}), 7.23 (d, $J = 7.4$ Hz, 2H, CH_{Ar}), 4.46–4.39 (m, 2H, NCH₂), 3.89–3.83 (m, 2H, NCH₂), 3.28 (hept, $J = 6.9$ Hz, 2H, CH(CH₃)₂), 1.32 (d, $J = 6.9$ Hz, 6H, CH(CH₃)₂), 1.29 (d, $J = 6.8$ Hz, 6H, CH(CH₃)₂). ¹³C{¹H} NMR (101 MHz, CDCl₃) δ 159.2 (C=O), 149.9 (CH_{Quin}), 148.4 (C_{Ar}, 2C), 144.8 (C_{Quin}), 140.9 (CH_{Quin}), 139.4 (C_{Quin}), 137.7 (CH_{Quin}), 133.5 (C_{Ar}), 131.2 (C_{Quin}), 129.0 (CH_{Ar}), 128.5 (CH_{Quin}), 124.2 (CH_{Ar}, 2C), 122.9 (CH_{Quin}), 95.3 (C_{Quin-I}), 47.4 (NCH₂), 47.0 (NCH₂), 28.8 (CH(CH₃)₂, 2C), 24.8 (CH(CH₃)₂, 2C), 24.5 (CH(CH₃)₂, 2C). HRMS (ESI+): calcd. for C₂₄H₂₆IN₃O [M + H]⁺: m/z 500.1193; found: m/z 500.1184; [M + Na]⁺: m/z 522.1013; found: 522.0999.

Compound L3^{ox}. ¹H NMR (400 MHz, CDCl₃) δ 8.11 (d, $J = 8.4$ Hz, 1H, CH_{py}), 7.51 (t, $J = 7.9$ Hz, 1H, CH_{py}), 6.93 (s, 2H, CH_{Ar}), 6.78 (d, $J = 7.3$ Hz, 1H, CH_{py}), 4.31–4.23 (m, 2H, NCH₂), 3.74–3.67 (m, 2H, NCH₂), 2.47 (s, 3H, CH_{3py}), 2.29 (s, 3H, CH_{3Ar}), 2.25 (s, 6H, CH_{3Ar}). ¹³C{¹H} NMR (101 MHz, CDCl₃) δ 156.3 (C_{py}), 155.9 (C=O), 152.4 (C_{py}), 138.0 (C_{Ar}), 137.7 (CH_{py}), 137.0 (C_{Ar}, 2C), 133.1 (C_{Ar}), 129.5 (CH_{Ar}, 2C), 116.8 (CH_{py}), 109.9 (CH_{py}), 43.2 (NCH₂), 42.0 (NCH₂), 24.5 (CH_{3py}), 21.1 (CH_{3Ar}), 18.0 (CH_{3Ar}, 2C). HRMS (ESI+): calcd. for C₁₈H₂₁N₃O [M + H]⁺: m/z 296.1757; found: m/z 296.1774; [M + Na]⁺: m/z 318.1577; found: 318.1595; [2M + Na]⁺: m/z 613.3261; found: m/z 613.3278.

4. Conclusions

In summary, novel NHC-Au(I) complexes (1–4) were synthesized and thoroughly characterized, and their reactivity in front external oxidants was analyzed. In contrast to the stability shown by commercial IPr- and SIPr-Au(I) complexes, complexes 1–4 underwent a controlled decomposition pathway to form oxidized NHC=O azolones as the main organic product, and quantitative conversion of all the Au(I) contained in complexes into macroscopic Au(0) nuggets (~0.4–0.5 mm). Azolones and M(0) have previously been described as decomposition products of NHC-metal complexes (M = Pd(II), Pt(II), Ni(II)), and we show herein a singular case of gold transforming this decomposition pathway, representing a good strategy to recover gold nuggets of high purity from soluble gold species (as NHC-Au(I)).

Supplementary Materials: The following supporting information can be downloaded at: <https://www.mdpi.com/article/10.3390/molecules28052302/s1>, Figure S1–S80, Table S1–S6, Schemes S1–S8. CCDC 2238757 (1), 2238754 (2), 2238755 (3), 2238756, (4) contain the supplementary crystallographic data for this paper [44].

Author Contributions: Conceptualization, G.C.V. and X.R.; methodology and formal analysis, P.F., A.T.P. and N.V.T.; writing—original draft preparation and editing, P.F., N.V.T., G.C.V. and X.R.; funding acquisition, G.C.V. and X.R. All authors have read and agreed to the published version of the manuscript.

Funding: The research project was supported by MINECO-Spain, PID2019-104498GB-I00 to X.R., as well as by the Hellenic Foundation for Research and Innovation (H.F.R.I.) under the “1st Call for H.F.R.I. Research Projects to support Faculty Members & Researchers and the procurement of high-cost research equipment grant” (Project Number: 16).

Institutional Review Board Statement: Not applicable.

Informed Consent Statement: Not applicable.

Data Availability Statement: Data is contained within the article or supplementary material.

Acknowledgments: X.R. is grateful for an ICREA-Acadèmia award. Athanasios Zarkadoulas is acknowledged for carrying out the catalytic activity evaluation experiments. We also thank L. Capdevila and STR-UdG for technical support.

Conflicts of Interest: The authors declare no conflict of interest.

Sample Availability: Samples of the compounds 1–4 are available from the authors.

References

1. Hemmert, C.; Gornitzka, H. Luminescent bioactive NHC–metal complexes to bring light into cells. *Dalton Trans.* **2016**, *45*, 440–447. [[CrossRef](#)] [[PubMed](#)]
2. Karaaslan, M.G.; Aktaş, A.; Gürses, C.; Gök, Y.; Ateş, B. Chemistry, structure, and biological roles of Au-NHC complexes as TrxR inhibitors. *Bioorganic Chem.* **2020**, *95*, 103552. [[CrossRef](#)] [[PubMed](#)]
3. Mora, M.; Gimeno, M.C.; Visbal, R. Recent advances in gold–NHC complexes with biological properties. *Chem. Soc. Rev.* **2019**, *48*, 447–462. [[CrossRef](#)] [[PubMed](#)]
4. Long, Y.; Cao, B.; Xiong, X.; Chan, A.S.C.; Sun, R.W.; Zou, T. Bioorthogonal Activation of Dual Catalytic and Anti-Cancer Activities of Organogold(I) Complexes in Living Systems. *Angew. Chem. Int. Ed.* **2021**, *60*, 4133–4141. [[CrossRef](#)] [[PubMed](#)]
5. Porchia, M.; Pellei, M.; Marinelli, M.; Tisato, F.; Del Bello, F.; Santini, C. New insights in Au-NHCs complexes as anticancer agents. *Eur. J. Med. Chem.* **2018**, *146*, 709–746. [[CrossRef](#)] [[PubMed](#)]
6. Zhao, Q.; Meng, G.; Nolan, S.P.; Szostak, M. N-Heterocyclic Carbene Complexes in C–H Activation Reactions. *Chem. Rev.* **2020**, *120*, 1981–2048. [[CrossRef](#)] [[PubMed](#)]
7. Collado, A.; Nelson, D.J.; Nolan, S.P. Optimizing Catalyst and Reaction Conditions in Gold(I) Catalysis–Ligand Development. *Chem. Rev.* **2021**, *121*, 8559–8612. [[CrossRef](#)] [[PubMed](#)]
8. Chernyshev, V.M.; Khazipov, O.V.; Shevchenko, M.A.; Chernenko, A.Y.; Astakhov, A.V.; Eremin, D.B.; Pasyukov, D.V.; Kashin, A.S.; Ananikov, V.P. Revealing the unusual role of bases in activation/deactivation of catalytic systems: O–NHC coupling in M/NHC catalysis. *Chem. Sci.* **2018**, *9*, 5564–5577. [[CrossRef](#)]
9. Fortman, G.C.; Nolan, S.P. N-Heterocyclic carbene (NHC) ligands and palladium in homogeneous cross-coupling catalysis: A perfect union. *Chem. Soc. Rev.* **2011**, *40*, 5151–5169. [[CrossRef](#)]
10. Peris, E. Smart N-Heterocyclic Carbene Ligands in Catalysis. *Chem. Rev.* **2018**, *118*, 9988–10031. [[CrossRef](#)]
11. Danopoulos, A.A.; Simler, T.; Braunstein, P. N-Heterocyclic Carbene Complexes of Copper, Nickel, and Cobalt. *Chem. Rev.* **2019**, *119*, 3730–3961. [[CrossRef](#)] [[PubMed](#)]
12. Vougioukalakis, G.C.; Grubbs, R.H. Ruthenium-Based Heterocyclic Carbene-Coordinated Olefin Metathesis Catalysts. *Chem. Rev.* **2010**, *110*, 1746–1787. [[CrossRef](#)] [[PubMed](#)]
13. Chernyshev, V.M.; Denisova, E.A.; Eremin, D.B.; Ananikov, V.P. The key role of R–NHC coupling (R = C, H, heteroatom) and M–NHC bond cleavage in the evolution of M/NHC complexes and formation of catalytically active species. *Chem. Sci.* **2020**, *11*, 6957–6977. [[CrossRef](#)] [[PubMed](#)]
14. Dorel, R.; Echavarren, A.M. Gold(I)-Catalyzed Activation of Alkynes for the Construction of Molecular Complexity. *Chem. Rev.* **2015**, *115*, 9028–9072. [[CrossRef](#)] [[PubMed](#)]
15. Hashmi, A.S.K. Gold-Catalyzed Organic Reactions. *Chem. Rev.* **2007**, *107*, 3180–3211. [[CrossRef](#)]
16. Petronilho, A.; Müller-Bunz, H.; Albrecht, M. Mesoionic oxides: Facile access from triazolium salts or triazolylidene copper precursors, and catalytic relevance. *Chem. Commun.* **2012**, *48*, 6499–6501. [[CrossRef](#)]

17. Nandy, A.; Samanta, T.; Mallick, S.; Mitra, P.; Seth, S.K.; Saha, K.D.; Al-Deyab, S.S.; Dinda, J. Synthesis of gold(iii) ← gold(i)-NHC through disproportionation: The role of gold(i)-NHC in the induction of apoptosis in HepG2 cells. *New J. Chem.* **2016**, *40*, 6289–6298. [[CrossRef](#)]
18. Font, P.; Valdés, H.; Guisado-Barrios, G.; Ribas, X. Hemilabile MIC^N ligands allow oxidant-free Au(i)/Au(iii) arylation-lactonization of γ -alkenoic acids. *Chem. Sci.* **2022**, *13*, 9351–9360. [[CrossRef](#)]
19. Hough, R.M.; Butt, C.R.M.; Reddy, S.M.; Verrall, M. Gold nuggets: Supergene or hypogene? *Aust. J. Earth. Sci.* **2007**, *54*, 959–964. [[CrossRef](#)]
20. Bütöf, L.; Wiesemann, N.; Herzberg, M.; Altschnner, M.; Holleitner, A.; Reith, F.; Nies, D.H. Synergistic gold–copper detoxification at the core of gold biomineralisation in *Cupriavidus metallidurans*. *Metallomics* **2018**, *10*, 278–286. [[CrossRef](#)]
21. Reith, F.; Rogers, S.L.; McPhail, D.C.; Webb, D. Biomineralization of Gold: Biofilms on Bacterioform Gold. *Science* **2006**, *313*, 233–236. [[CrossRef](#)]
22. Sun, D.T.; Gasilova, N.; Yang, S.; Oveisi, E.; Queen, W.L. Rapid, Selective Extraction of Trace Amounts of Gold from Complex Water Mixtures with a Metal–Organic Framework (MOF)/Polymer Composite. *J. Am. Chem. Soc.* **2018**, *140*, 16697–16703. [[CrossRef](#)]
23. Yue, C.; Sun, H.; Liu, W.-J.; Guan, B.; Deng, X.; Zhang, X.; Yang, P. Environmentally Benign, Rapid, and Selective Extraction of Gold from Ores and Waste Electronic Materials. *Angew. Chem. Int. Ed.* **2017**, *56*, 9331–9335. [[CrossRef](#)]
24. Papastavrou, A.T.; Pauze, M.; Gómez-Bengoá, E.; Vougioukalakis, G.C. Unprecedented Multicomponent Organocatalytic Synthesis of Propargylic Esters via CO₂ Activation. *ChemCatChem* **2019**, *11*, 5379–5386. [[CrossRef](#)]
25. Liori, A.A.; Stamatopoulos, I.K.; Papastavrou, A.T.; Pinaka, A.; Vougioukalakis, G.C. A Sustainable, User-Friendly Protocol for the Pd-Free Sonogashira Coupling Reaction. *Eur. J. Org. Chem.* **2018**, *2018*, 6134–6139. [[CrossRef](#)]
26. Collado, A.; Gómez-Suárez, A.; Martín, A.R.; Slawin, A.M.Z.; Nolan, S.P. Straightforward synthesis of [Au(NHC)X] (NHC = N-heterocyclic carbene, X = Cl, Br, I) complexes. *Chem. Commun.* **2013**, *49*, 5541–5543. [[CrossRef](#)]
27. Visbal, R.; Laguna, A.; Gimeno, M.C. Simple and efficient synthesis of [MCl(NHC)] (M = Au, Ag) complexes. *Chem. Commun.* **2013**, *49*, 5642–5644. [[CrossRef](#)]
28. Catalano, V.J.; Moore, A.L. Mono-, Di-, and Trinuclear Luminescent Silver(I) and Gold(I) N-Heterocyclic Carbene Complexes Derived from the Picolyl-Substituted Methylimidazolium Salt: 1-Methyl-3-(2-pyridinylmethyl)-1H-imidazolium Tetrafluoroborate. *Inorg. Chem.* **2005**, *44*, 6558–6566. [[CrossRef](#)]
29. Navarro, M.; Tabey, A.; Szalóki, G.; Mallet-Ladeira, S.; Bourissou, D. Stable Au(III) Complexes Bearing Hemilabile P^N and C^N Ligands: Coordination of the Pendant Nitrogen upon Oxidation of Gold. *Organometallics* **2021**, *40*, 1571–1576. [[CrossRef](#)]
30. Reddy, K.S.K.; Narender, N.; Rohitha, C.N.; Kulkarni, S.J. Iodination of Aromatic Compounds Using Potassium Iodide and Hydrogen Peroxide. *Synth. Commun.* **2008**, *38*, 3894–3902. [[CrossRef](#)]
31. Manke, D.R.; Golen, J.A.; Stennett, C.R.; Naeem, M.; Javier-Jimenez, D.R.; Power, P.P. Reusing meta-terphenyl ligands: Synthesis, metalation and recycling of 5-pyrrolidino-m-terphenyl. *Polyhedron* **2022**, *222*, 115947. [[CrossRef](#)]
32. Fernandes, R.A.; Choudhary, P. Ni-Catalyzed Regioselective C-5 Halogenation of 8-Aminoquinoline and Co-Catalyzed Chelation Assisted C–H Iodination of Aromatic Sulfonamides with Molecular Iodine. *Chem. Asian J.* **2022**, *17*, e202200874. [[CrossRef](#)]
33. Motati, D.R.; Uredi, D.; Watkins, E.B. A general method for the metal-free, regioselective, remote C–H halogenation of 8-substituted quinolines. *Chem. Sci.* **2018**, *9*, 1782–1788. [[CrossRef](#)]
34. Chen, J.; Wang, T.; Liu, Y.; Wang, T.; Lin, A.; Yao, H.; Xu, J. Metal-free C5-selective halogenation of quinolines under aqueous conditions. *Org. Chem. Front.* **2017**, *4*, 622–626. [[CrossRef](#)]
35. Zeng, W.; Wang, E.; Qiu, R.; Sohail, M.; Wu, S.; Chen, F.-X. Oxygen-atom insertion of NHC–copper complex: The source of oxygen from N,N-dimethylformamide. *J. Organomet. Chem.* **2013**, *743*, 44–48. [[CrossRef](#)]
36. Tomás-Mendivil, E.; Toullec, P.Y.; Borge, J.; Conejero, S.; Michelet, V.; Cadierno, V. Water-Soluble Gold(I) and Gold(III) Complexes with Sulfonated N-Heterocyclic Carbene Ligands: Synthesis, Characterization, and Application in the Catalytic Cycloisomerization of γ -Alkynoic Acids into Enol-Lactones. *ACS Catal.* **2013**, *3*, 3086–3098. [[CrossRef](#)]
37. Tomás-Mendivil, E.; Toullec, P.Y.; Díez, J.; Conejero, S.; Michelet, V.; Cadierno, V. Cycloisomerization versus Hydration Reactions in Aqueous Media: A Au(III)-NHC Catalyst That Makes the Difference. *Org. Lett.* **2012**, *14*, 2520–2523. [[CrossRef](#)]
38. Ghavami, Z.S.; Anneser, M.R.; Kaiser, F.; Altmann, P.J.; Hofmann, B.J.; Schlagintweit, J.F.; Grivani, G.; Kühn, F.E. A bench stable formal Cu(iii) N-heterocyclic carbene accessible from simple copper(ii) acetate. *Chem. Sci.* **2018**, *9*, 8307–8314. [[CrossRef](#)]
39. Shi, Q.; Qin, Z.; Xu, H.; Li, G. Heterogeneous Cross-Coupling over Gold Nanoclusters. *Nanomaterials* **2019**, *9*, 838. [[CrossRef](#)]
40. Chen, Z.; Shen, R.; Chen, C.; Li, J.; Li, Y. Synergistic effect of bimetallic PdAu nanocrystals on oxidative alkyne homocoupling. *Chem. Commun.* **2018**, *54*, 13155–13158. [[CrossRef](#)]
41. Kidwai, M.; Bansal, V.; Kumar, A.; Mozumdar, S. The first Au-nanoparticles catalyzed green synthesis of propargylamines via a three-component coupling reaction of aldehyde, alkyne and amine. *Green Chem.* **2007**, *9*, 742–745. [[CrossRef](#)]
42. Li, Q.; Das, A.; Wang, S.; Chen, Y.; Jin, R. Highly efficient three-component coupling reaction catalysed by atomically precise ligand-protected Au₃₈(SC₂H₄Ph)₂₄ nanoclusters. *Chem. Commun.* **2016**, *52*, 14298–14301. [[CrossRef](#)]

43. Kyriakou, G.; Beaumont, S.K.; Humphrey, S.M.; Antonetti, C.; Lambert, R.M. Sonogashira Coupling Catalyzed by Gold Nanoparticles: Does Homogeneous or Heterogeneous Catalysis Dominate? *ChemCatChem* **2010**, *2*, 1444–1449. [[CrossRef](#)]
44. Prasad, B.; Gilbertson, S. One-Pot Synthesis of N-Heterocyclic Carbene Ligands From a N-(2-iodoethyl)arylamine salts. *Org. Lett.* **2009**, *11*, 3710–3713. [[CrossRef](#)]

Disclaimer/Publisher's Note: The statements, opinions and data contained in all publications are solely those of the individual author(s) and contributor(s) and not of MDPI and/or the editor(s). MDPI and/or the editor(s) disclaim responsibility for any injury to people or property resulting from any ideas, methods, instructions or products referred to in the content.

CHAPTER V. Results and discussion

V.1. HEMILABILE MIC^N LIGANDS ALLOW OXIDANT-FREE Au(I)/Au(III) ARYLATION-LACTONIZATION OF γ -ALKENOIC ACIDS

Homogeneous gold catalysis has been dominated by the Lewis acidic mode of reactivity in which gold is prone to activate C–C multiple bonds (see Section I.3.1). However, redox Au(I)/Au(III) catalysis emerged later, and can be achieved in the presence of sacrificial external oxidants (see Section I.3.2) to overcome the reluctance of Au(I) to become Au(III), or, more interestingly, it can be achieved in the absence of oxidants (see Section I.3.3) by strategically triggering oxidative addition to cyclize between Au(I) and Au(III) species. Indeed, the chelation-assisted strategy using pre-designed ligands has allowed the successful development of oxidant-free Au(I)/Au(III)-catalyzed cross-coupling catalysis, as demonstrated by the widely used MeDalphos (P^N) bidentate hemilabile ligand (see Section I.3.3.1).¹⁻¹⁷ Conversely, hemilabile (N^C) carbene-based bidentate ligands have been scarcely explored in this regard.

Although there were published works focused on studying the oxidative addition at hemilabile (N^C)Au(I) complexes^{18, 19} when we envisioned this project, the implementation of (N^C)Au(I) systems in oxidant-free cross-coupling catalysis was lacking. Hence, we aimed at designing hemilabile (N^C) ligands that could stabilize Au(III) centers by chelation upon oxidative addition, and seek a catalytic application for the (N^C)Au(I) complexes in Au(I)/Au(III) cross-coupling catalysis. To this end, we believed that mesoionic carbene ligands (MIC) bearing a N-donor atom with hemilabile character could be suitable architectures to tackle our goals.

Remarkably, the group of Bourissou independently reported a gold(I) complex, bearing a N3-alkylated mesoionic 1,2,3-triazol-5-ylidene ligand, aiming at obtaining the corresponding (N^C)-cyclometalated Au(III) complex in oxidation reactions.¹⁹ However, they did not find the oxidant-free conditions to access the expected gold(III) complex via oxidative addition of iodobenzene.

V.1.1. Synthesis of (MIC^N)Au(I) complexes

In collaboration with the group of Dr. Guisado-Barríos, we designed two 1,2,3-triazolium salts with 2,6-diisopropylphenyl (Dipp) substituents at N1 and N3 positions of the triazolium ring: one bearing a pyridine side arm (**1a**), and one bearing a pyrimidine side arm (**1b**). Both triazolium salts were prepared by following an adapted method reported in the literature,^{20, 21}

by reacting 1,3-bis(2,6-diisopropylphenyl)triaz-1-ene with 2-ethynylpyridine or 2-ethynylpyrimidine in the presence of *tert*-butyl hypochlorite and anhydrous potassium hexafluorophosphate. The corresponding (MIC)Au(I) complexes **2a** and **2b** were obtained through transmetalation to Ag(I). For this purpose, we first reacted the corresponding triazolium salts **1a** and **1b** with silver oxide, in the presence of cesium carbonate as a base and potassium chloride as a halide source. Then, the addition of dimethylsulfide gold(I) chloride immediately produced the precipitation of silver chloride and the expected gold(I) complexes **2a** and **2b** (Figure V.1a). Upon purification, complexes **2a** and **2b** were obtained in 32% and 35% yield, respectively, and were characterized by NMR, HRMS and XRD. The ^1H NMR spectra of the complexes did not show the acidic proton of the triazolium salts, indicating that the coordination to gold had indeed occurred. On the other hand, in both cases the carbenic carbon could be identified by $^{13}\text{C}\{^1\text{H}\}$ NMR as the most downfield shifted signal. The spectrum of **2a** showed this characteristic signal at 162.1 ppm (Annex 2, Figure S12), whereas **2b** featured such signal at 165.3 ppm (Annex 2, Figure S17).

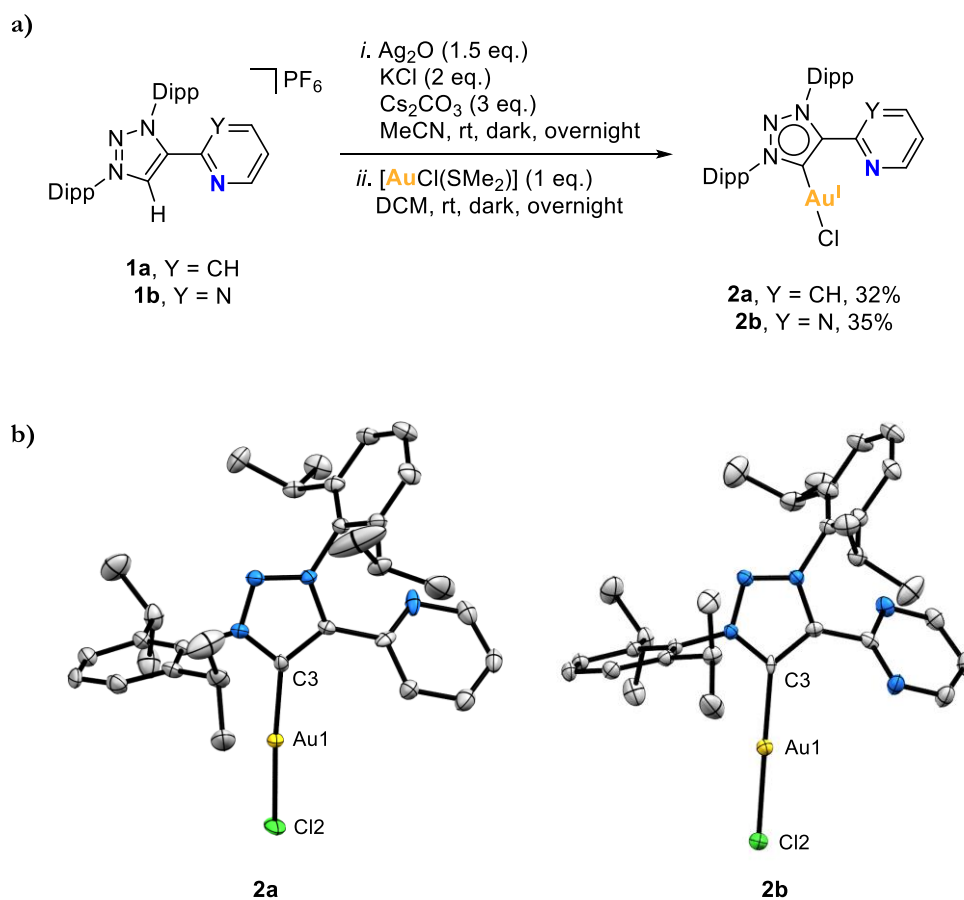


Figure V.1. a) Synthesis of Au(I) complexes **2a** and **2b**. b) Crystal structures of **2a** and **2b** (ellipsoids set at 50% probability and H atoms removed for clarity). Selected bond distances (\AA): for **2a**, Au1–C3 1.982(6), Au1–Cl2 2.2854(17); for **2b**, Au1–C3 2.006(4), Au1–Cl2 2.2728(16).

Moreover, the molecular structure of both Au(I) complexes was unambiguously determined by X-ray diffraction analyses (Figure V.1b). As expected, both complexes are isostructural, bearing the mesoionic carbene ligand coordinated to a Au(I) atom, and a chloride ligand completing the linear coordination sphere around the metal (C–Au–Cl angle is $174.31(18)^\circ$ for **2a** and $179.30(9)^\circ$ for **2b**). Noticeably, no coordination of the hemilabile pyridine or pyrimidine moieties at Au(I) was observed.

Next, we reacted complexes **2a** and **2b** with silver hexafluoroantimonate in CD_2Cl_2 at room temperature (Figure V.2a), seeking the chloride removal and the engagement of the pendant hemilabile groups in the coordination to Au(I). After 5 minutes, the reaction outcomes were filtered to remove the silver chloride and were analyzed. Indeed, the ^1H NMR spectra showed significant changes in the signals corresponding to the protons of the pyridine and pyrimidine fragments, suggesting effective gold coordination. Also, the number of signals and their integrals matched with the formation of complexes **3a** and **3b**, *i.e.* head-to-tail dimeric Au(I) complexes where each ligand is bridging two metals (Figure V.2).

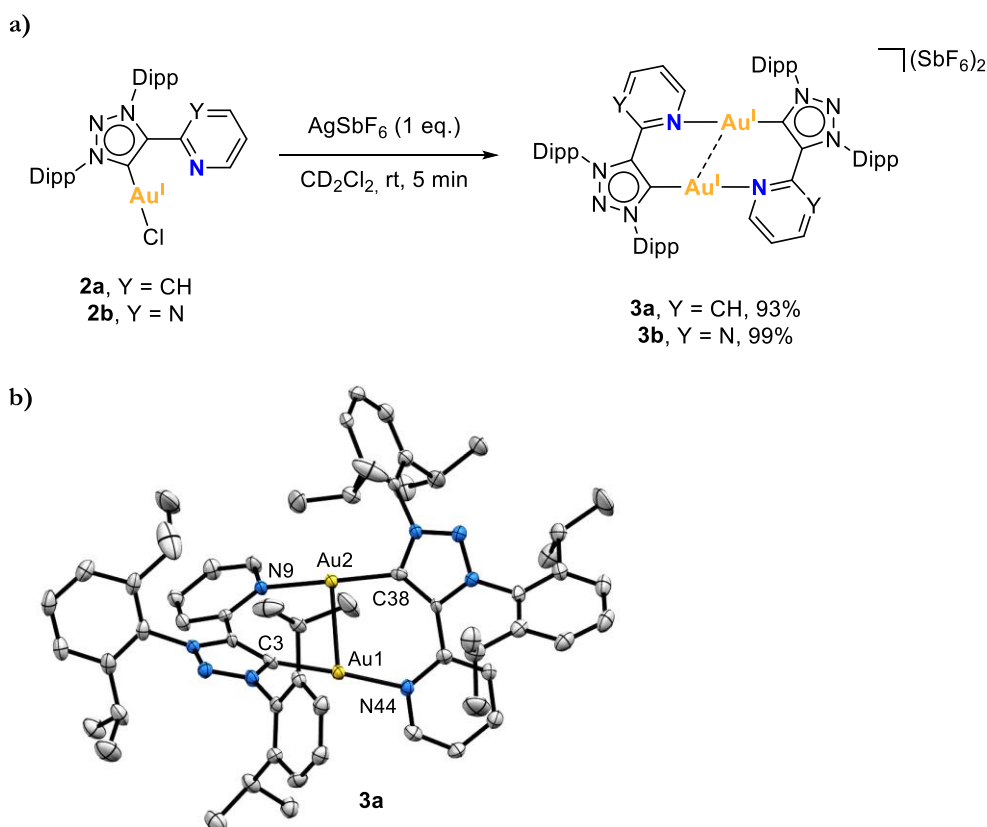


Figure V.2. a) Synthesis of dimeric Au(I) complexes **3a** and **3b** from complexes **2a** and **2b** upon chloride abstraction. b) Crystal structure of **3a** (ellipsoids set at 50% probability, H atoms and SbF_6^- anions removed for clarity). Selected bond distances (\AA): Au1–Au2 2.8212(4), Au1–N44 2.078(6), Au1–C3 1.988(8), Au2–N9 2.069(6), Au2–C38 1.990(8).

The X-ray diffraction analysis of complex **3a** indeed confirmed the head-to-tail dimeric structure of this compound (Figure V.2b). Both Au(I) centers adopted a linear dicoordinate arrangement, showing an aurophilic interaction of a Au \cdots Au length of 2.8212(4) Å. Thus, upon halide abstraction, the formation of a dimeric Au(I) species is favored rather than a mononuclear Au(I) species chelated by the carbenic carbon and the nitrogen atom of the pyridine or pyrimidine pendant arm. For both **3a** and **3b**, the integrals of the ^1H NMR spectra revealed that the complexes were symmetric. Complex **3a** had the same number of signals than **2a**, supporting the symmetry of **3a**. Interestingly, **3b** featured an extra signal compared to **2b** because the coordination to gold caused the desymmetrization of the pyrimidine moiety (Figure V.3). Regarding the $^{13}\text{C}\{^1\text{H}\}$ NMR spectra, the signals of the carbenic carbons were shifted upfield when compared to those of **2a** and **2b**. The signal of the carbenic carbon was shifted from 162.1 to 157.2 ppm in the case of **3a**, and from 165.3 to 161.3 ppm in the case of **3b** (Annex 2, Figures S22 and S27).

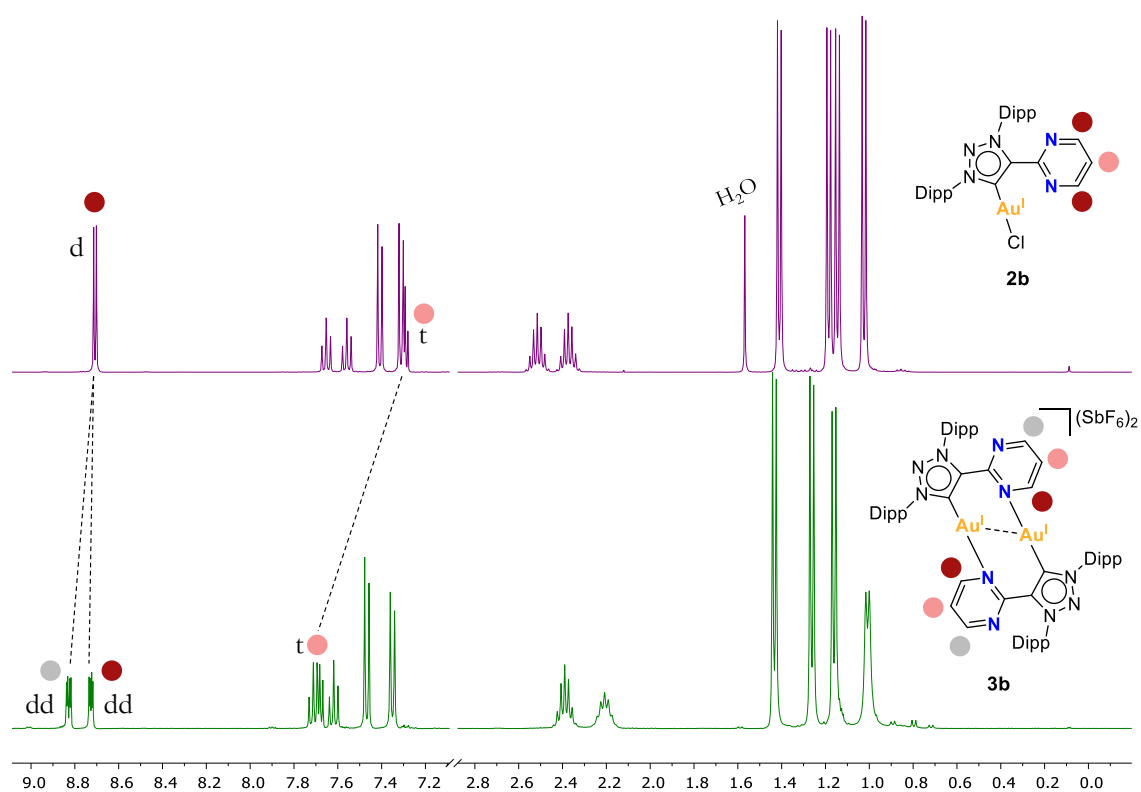


Figure V.3. ^1H NMR (400MHz, CD_2Cl_2 , 298K) spectra of complexes **2b** (top) and **3b** (bottom), evidencing the desymmetrization of pyrimidine when it is coordinated to gold in complex **3b**.

V.1.2. Synthesis of (MIC[^]N)Au(III) complexes with external oxidants

To promote the coordination of the side arms of the MIC[^]N ligands, we next attempted the two-electron chemical oxidation of gold(I) complex **2a** to get mononuclear (N[^]C)-cyclometalated gold(III) complexes. To this end, we reacted **2a** with 2 e⁻ oxidants, namely hypervalent iodine oxidants PhIX₂ (X = Cl or OAc) (Figure V.4a). The reactions were performed at low temperature in the presence of AgSbF₆ as halogen scavenger to abstract the chloride ligand from **2a** and favor the formation of a square-planar (N[^]C)-cyclometalated Au(III) complex with two X ligands coming from the oxidant. Gratifyingly, the reactions afforded the expected gold(III) complexes **4a-Cl** and **4a-OAc** when PhICl₂ and PhI(OAc)₂ oxidants were employed, respectively (Figure V.4a). Notably, the ¹³C{¹H} NMR spectra of the resulting complexes **4a-Cl** and **4a-OAc** displayed the signal of the carbenic carbon at significantly higher fields than that of the initial Au(I) complex **2a** (147.3 ppm for **4a-Cl** and 137.1 ppm for **4a-OAc** *vs.* 162.1 ppm for **2a**). The molecular structures of complexes **4a-Cl** and **4a-OAc** were elucidated by X-ray diffraction analyses (Figure V.4b). Both of them showed a similar arrangement, *i.e.* the tetracoordinated Au(III) center featured a slightly distorted square-planar geometry, and was coordinated to the bidentate MIC[^]N ligand and to two chlorides or acetates to complete its coordination sphere. Up to that point, we had demonstrated that these MIC[^]N ligands were indeed suitable platforms to stabilize Au(III) complexes by forming a 5-membered auracycle.

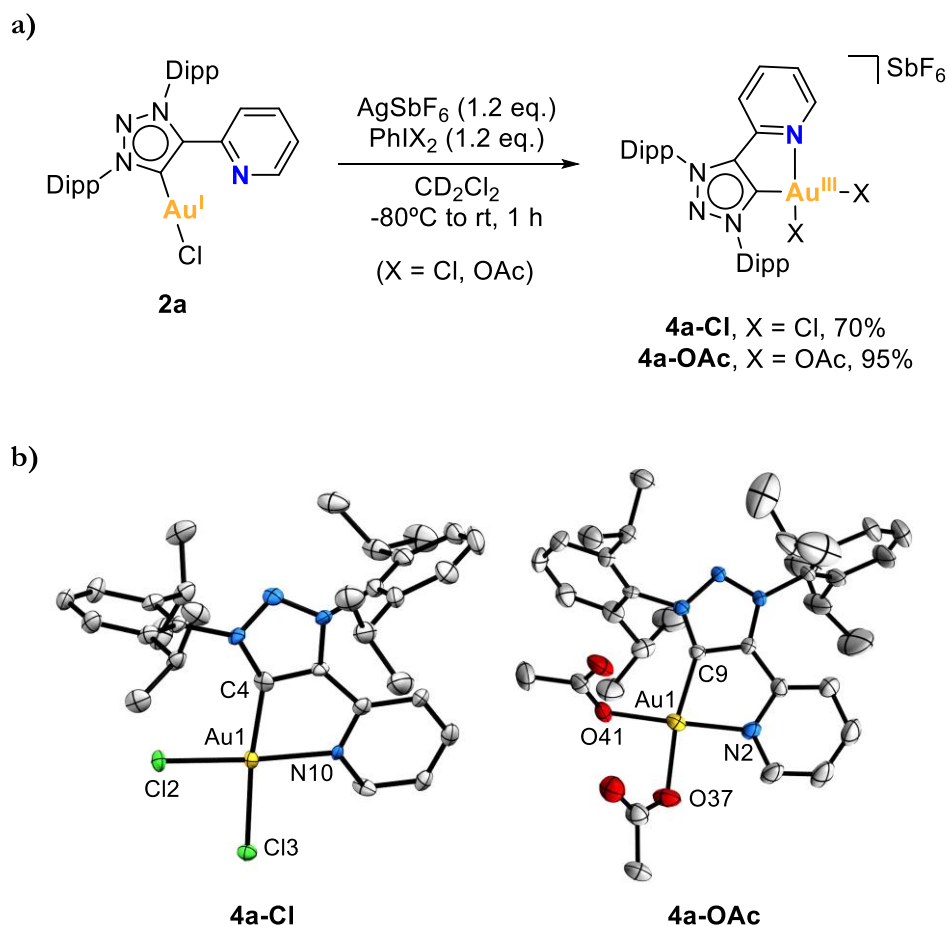


Figure V.4. a) Reactivity of Au(I) complex **2a** towards oxidation by using hypervalent iodine oxidants. b) Crystal structures of **4a-Cl** and **4a-OAc** (ellipsoids set at 50% probability, H atoms and SbF_6^- anions removed for clarity). Selected bond distances (\AA): for **4a-Cl**, Au1–C4 2.017(8), Au1–N10 2.089(6), Au1–Cl2 2.268(2), Au1–Cl3 2.302(2); for **4a-OAc**, Au1–C9 1.991(11), Au1–N2 2.052(11), Au1–O37 2.032(10), Au1–O41 1.998(9).

V.1.3. Reactivity of (MIC[^]N)Au(I) complexes towards oxidative addition

These results prompted us to explore the possibility of obtaining (N[^]C)-cyclometalated Au(III) complexes via oxidative addition instead of by using two-electron oxidants. With this aim, we first studied the oxidative addition of the strained C(sp²)–C(sp²) bond of biphenylene and then the oxidative addition of aryl iodides.

Complex **2b** was chosen to study the oxidative addition of biphenylene. Our first attempt consisted in mixing **2b** with 5 equivalents of biphenylene in dichloromethane, in the presence of one equivalent of AgSbF_6 as halide scavenger to remove the chloride, from -80°C to room temperature for 10 minutes (Figure V.5a). Unfortunately, we did not observe the desired Au(III) complex but, interestingly, crystallization of the reaction mixture revealed the co-crystallization of the dimeric complex **3b** with intact biphenylene in a 1:1 ratio

(**3b**·biphenylene) (Figure V.5b). Even after 5 hours at 50°C, the outcome of the reaction remained unchanged.

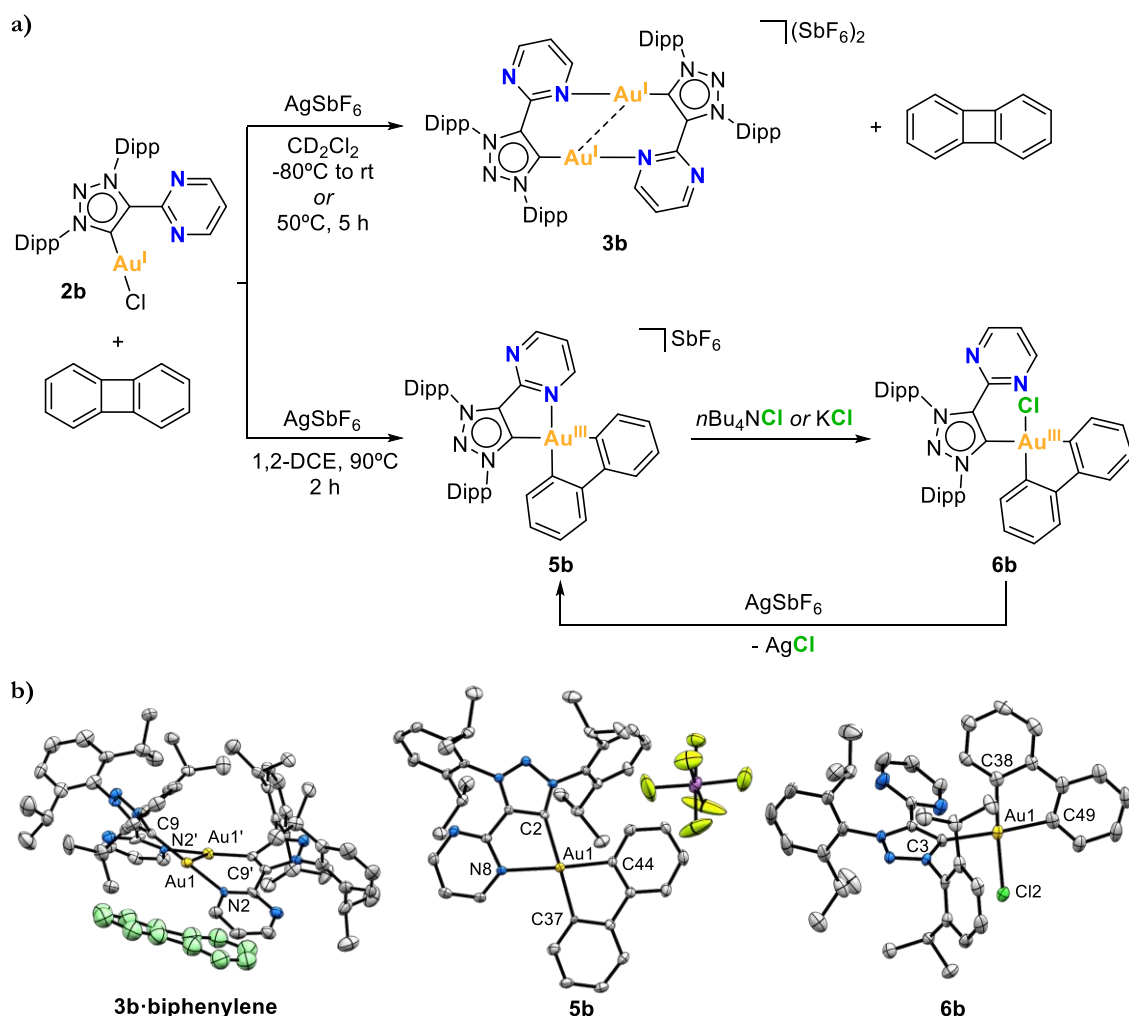


Figure V.5. a) Study of the reaction conditions for the oxidative addition of a strained C(sp²)–C(sp²) bond to complex **2b**. b) Crystal structures of **3b**·biphenylene, **5b** and **6b** (ellipsoids set at 50% probability, H atoms removed for clarity; in the case of **3b**·biphenylene, SbF₆⁻ anions are removed and the biphenylene molecule is painted in green for clarity). Selected bond distances (Å): for **3b**·biphenylene, Au1–Au1' 2.8768(10), Au1–N2 2.105(8), Au1–C9 2.027(10); for **5b**, Au1–C2 2.108(5), Au1–N8 2.254(5), Au1–C37 2.066(5), Au1–C44 2.019(5); for **6b**, Au1–C3 2.080(6), Au1–Cl2 2.376(3), Au1–C38 2.072(7), Au1–C49 2.057(7).

Nonetheless, when the reaction was heated up to 90°C for 2 hours in 1,2-dichloroethane, the Au(I) center underwent oxidative addition of the strained biphenylene C(sp²)–C(sp²) bond, forming the desired Au(III) complex **5b** (Figure V.5a). By adding a chloride source in the reaction mixture, such as potassium or tetrabutylammonium chloride, the hemilabile pyrimidine ligand was displaced to afford the neutral Au(III) complex **6b**. Whereas *n*Bu₄NCl afforded **6b** readily, the reaction mixture was heated at 40°C for 12 hours when using KCl.

Next, by adding AgSbF_6 to **6b**, we could reversibly form complex **5b** thereby reinforcing the hemilabile character of the pyrimidine moiety (Figure V.5a). Both the cationic **5b** and the neutral **6b** Au(III) species were characterized by XRD analyses (Figure V.5b). The long Au(III)–N bond in **5b** (2.254 Å) confirmed the weak coordination of the pyrimidine moiety. Interestingly, the $^1\text{H}, ^1\text{H}$ -NOESY NMR spectra of **5b** showed a dynamic behavior of the pyrimidine pendant arm, even at 248K (Annex 2, Figure S49). Regarding ^{13}C NMR, the carbene resonance signals were shifted downfield to 182.8 and 180.1 ppm for **5b** and **6b**, respectively.

With these results in hand, we then moved on to the oxidative addition of $\text{C}(\text{sp}^2)\text{--I}$ bonds of aryl iodides at Au(I) complexes **2a** and **2b**. Like in the case of biphenylene, a first attempt was carried out at low temperature. Complex **2a** was chosen to be reacted with one equivalent of AgSbF_6 and 5 equivalents of an aryl iodide (iodobenzene and 4-iodoanisole were tested), from -80°C to room temperature. In both cases, complex **3a** was obtained along with the unreacted aryl iodide. Hence, we decided to run the reaction at higher temperature to trigger the oxidative addition. To this end, we reacted the Au(I) complexes **2a** and **2b** with *para*-substituted iodoaryls ($\text{R} = \text{OMe}, \text{Me}, \text{F}$) in the presence of AgSbF_6 , in 1,2-dichloroethane and heating at 120°C overnight (Figure V.6a). Unexpectedly, the desired arylgold(III) complexes were not detected, but instead, the ^1H NMR and mass spectra were consistent with the formation of three triazolium salts (**8a-R**, **9a**, and **1a** when **2a** was used, and **8b-R**, **9b** and **1b** when **2b** was used; $\text{R} = \text{OMe}, \text{Me}, \text{F}$). Also, decomposition to Au(0) nanoparticles was observed.

When **2a** was reacted with 4-iodoanisole, the triazolium salts **8a-OMe** and **9a** were unambiguously characterized by X-ray diffraction. Both species co-crystallized, and the single crystal X-ray analysis revealed the presence of **8a-OMe** and **9a** in a 0.89:0.11 ratio (Figure V.6b). Likewise, **2b** afforded **8b-OMe** as the major product (65% NMR yield) when reacted with 4-iodoanisole, and **9b** and **1b** were both obtained in 16% NMR yield (Table V.1, entry 2). In this case, **8b-OMe** could be isolated and characterized by ^1H NMR, HRMS and X-ray diffraction (Figure V.6b). The formation of compounds of the type **8** and **9** suggested that gold(I) complexes **2a** and **2b** underwent oxidative addition of the aryl iodides, as expected, forming transient Au(III) species of the type **7**. However, the oxidative addition should be followed by a reductive elimination step to bond the MIC ligand with the ligand sitting in *cis* (the aryl ligand in *cis-7a-I* and *cis-7b-I*, leading to products **8a-R** and **8b-R**; or the iodide ligand in *trans-7a-I* and *trans-7b-I*, leading to products **9a** and **9b**) (Figure V.6a).

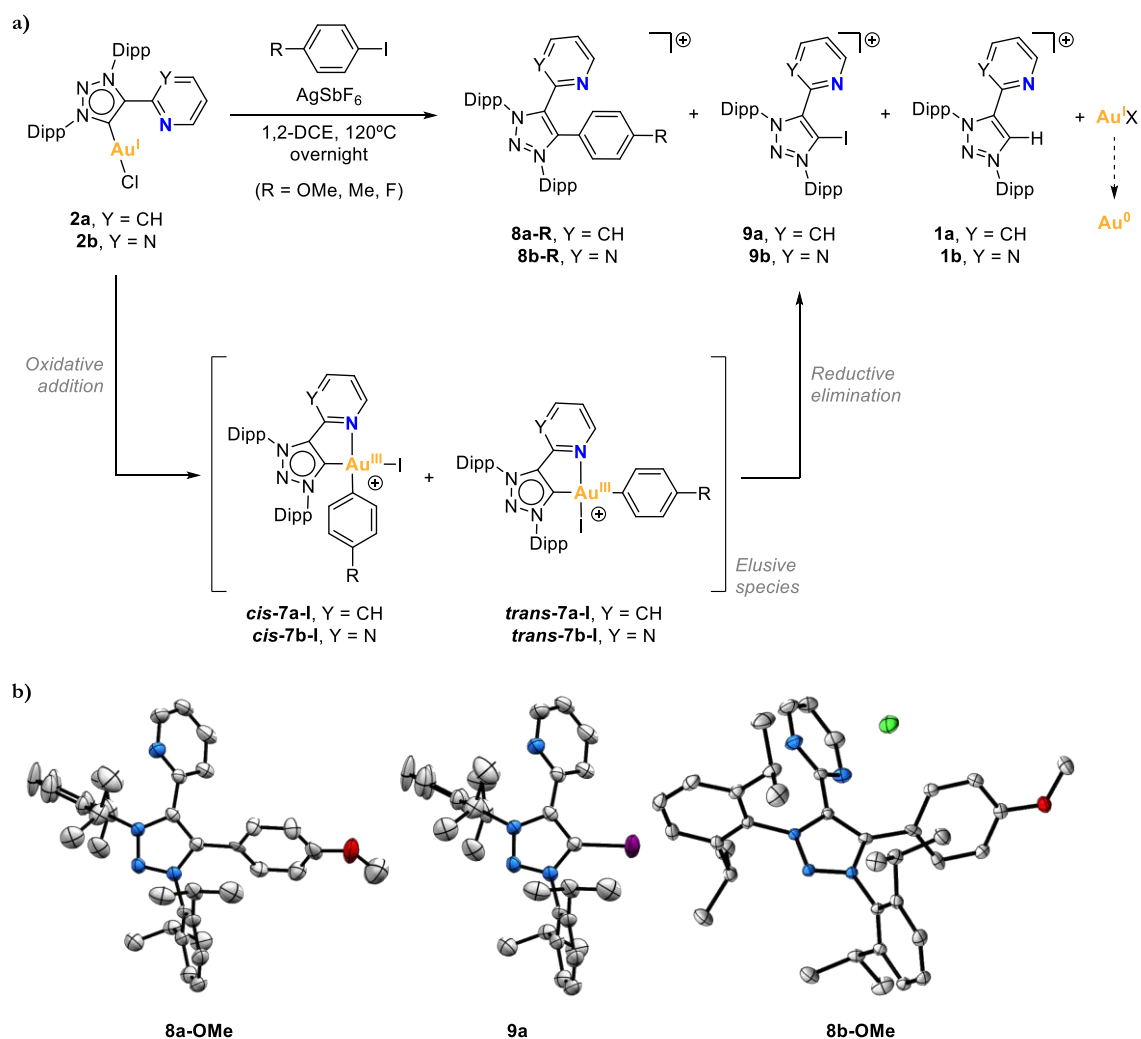


Figure V.6. a) Reactivity of complexes **2a** and **2b** with aryl iodides (5 eq.) and AgSbF_6 (1.2 eq.), leading to the decomposition towards products **8-R**, **9** and **1**. b) Crystal structures of **8a-OMe**, **9a** and **8b-OMe** (ellipsoids set at 50% probability, H atoms removed for clarity; for **8a-OMe** and **9a**, SbF_6^- anion is removed for clarity; **8b-OMe** was obtained as a chloride salt).

Interestingly, products **8a-R** and **8b-R** were generally obtained in higher yields than **9a** and **9b** (Table V.1), indicating that the oxidative addition generates preferentially the Au(III) species with the aryl ligand in *cis* to the carbene ligand (*cis-7a-I* or *cis-7b-I*) over the Au(III) species with the iodide ligand in *cis* and the aryl ligand in *trans* to the carbene ligand (*trans-7a-I* or *trans-7b-I*). This fact can be rationalized by the *trans* effect exerted by the carbene and the pyridine or pyrimidine ligands of the MIC^N chelates.

Table V.1. Yield of products **8-R**, **9**, and **1** obtained from complexes **2a** and **2b** under the reaction conditions depicted in Figure V.6a (NMR yields calculated using 1,3,5-trimethoxybenzene as internal standard).

Entry	R	Product 8-R	Product 9	Product 1
1	OMe	8a-OMe 41%	9a 3%	1a 24%
2	OMe	8b-OMe 65%	9b 16%	1b 16%
3	Me	8a-Me 34%	9a 3%	1a 31%
4	F	8a-F 12%	9a traces	1a 66%

By following an alternative route,²² we synthesized complex **cis-7a-Cl**, a Au(III) complex analogous to **cis-7a-I** differing only in the halide ligand. Complex **cis-7a-Cl** was obtained upon oxidative addition of 4-methoxybenzenediazonium tetrafluoroborate to complex **2a**, promoted by blue LED irradiation ($\lambda = 447$ nm) at 25°C (Figure V.7a). It was isolated and fully characterized, including XRD analysis (Figure V.7b). In order to support the involvement of a C(sp²)-I oxidative addition and a reductive elimination in the formation of products **8a-R/8b-R** and **9a/9b** from complexes **2a/2b**, we subjected the isolated complex **cis-7a-Cl** to the same reaction conditions (120°C, overnight, in 1,2-DCE), aiming at obtaining the **8a-OMe** product. To our delight, **8a-OMe** was indeed obtained in 96% yield from the reductive elimination between the carbene and the aryl ligands (Figure V.7a). Also, decomposition to Au(0) was obtained, and AuCl₂⁻ and AuCl₄⁻ species were detected by MS-ESI(-) (Annex 2, Scheme S8 and Figure S74).

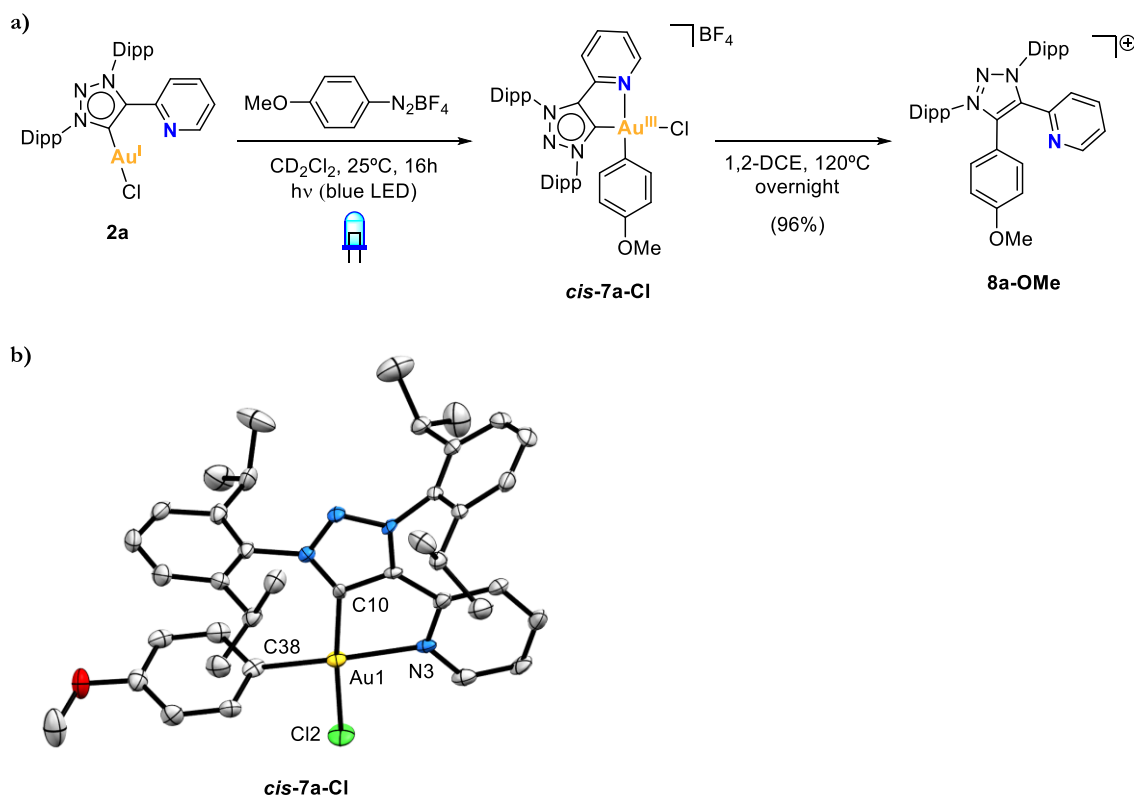


Figure V.7. a) Synthesis of **cis-7a-Cl** by oxidative addition at **2a** using blue LED irradiation ($\lambda = 447 \text{ nm}$), and thermal reductive elimination from **cis-7a-Cl** to afford **8a-OMe**. b) Crystal structure of **cis-7a-Cl** (ellipsoids set at 50% probability, H atoms and BF_4^- anion are removed for clarity). Selected bond distances (\AA): Au1–C10 2.009(7), Au1–N3 2.154(7), Au1–C38 2.006(8), Au1–Cl2 2.303(2).

Therefore, these results supported an oxidative addition/reductive elimination pathway for the formation of products **8a-R/8b-R** and **9a/9b** from complexes **2a/2b**. We hypothesize that the hemilabile character of the nitrogen atom and the fast decomposition of the arylgold(III) species at high temperatures promoted the reductive elimination process instead of leading to the stabilization of the (N \wedge C)-cyclometalated arylgold(III) complexes. To the best of our knowledge, this reductive elimination process had only been observed to a 1,2,3-triazol-5-ylidene based palladium complex.²³⁻²⁵

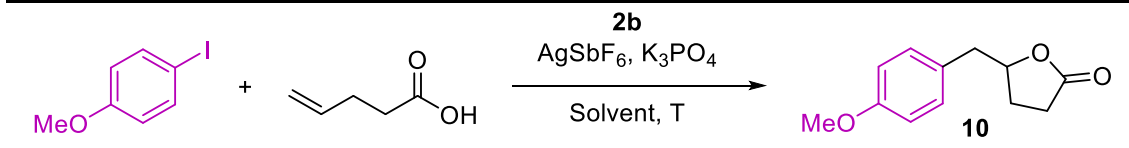
V.1.4. Engaging (MIC \wedge N)Au(I) complexes in oxidant-free catalytic transformations

With these results in hand and based on the successful catalytic applications enabled by the MeDalphos hemilabile (P \wedge N) ligand, we postulated that (MIC \wedge N)Au(I) complexes **2a** and **2b** may also have potential as catalysts in cross-coupling reactions involving the key oxidative addition step. Recent works described the coupling/cyclization reaction of aryl iodides with

alkenols and alkenamines catalyzed by (MeDalphos)AuCl.^{5,6} Additionally, in 2017, Shi and coworkers had reported a system that afforded coupling/cyclization products by reacting aryldiazonium salts with either alkenols, alkenamines, or alkenoic acids, using (Ph₃P)AuCl under photo-free conditions.²⁶ Thus, we sought the catalytic performance of our MIC^N/Au(I) systems in affording γ -benzyl- γ -butyrolactone products when reacting aryl iodides with γ -alkenoic acids (Table V.2 and Figure V.8). We envisioned this coupling/lactonization transformation to proceed via a catalytic cycle that merges the oxidative addition of aryl iodides with gold's π -activation mode of reactivity, as supported by previous studies.⁵⁻¹⁰

We started by carrying out the stoichiometric reaction between 4-iodoanisole, 4-pentenoic acid, complex **2b**, K₃PO₄, and AgSbF₆ at 80°C. In the presence of an excess of base or AgSbF₆ (Annex 2, Table S3), we did not observe any conversion, probably due to a rapid decomposition of the gold complex. We also found that by using chlorinated solvents such as 1,2-DCE, the conversion reached up to 49% (Annex 2, Table S3). By ¹H NMR analysis, we detected that the catalyst decomposes under the reaction conditions, forming the triazolium salt **1b**. However, the conversion was significantly higher (up to 92%) using 2,2,2-trifluoroethanol (TFE) instead of 1,2-DCE (Table V.2 entry 1, and Annex 2 Table S3). When the reaction was carried out at 100°C, the conversion was quantitative but the yield was very similar to that found at 80°C (67% yield at 100°C *vs.* 63% yield at 80°C, entries 1-2 in Table V.2), and we also observed the formation of the triazolium salt **8b-OMe**. This was a strong indication that complex **2b** underwent the C(sp²)-I oxidative addition, but rapid reductive elimination to form the undesired coupling product **8b-OMe** also occurs at this temperature.

Next, we explored the possibility to perform the catalytic version of the arylation-lactonization of γ -alkenoic acids. With a substoichiometric 70 mol% loading of **2b**, product **10** was obtained in 65% yield (Table V.2, entry 3), so a quantitative transformation was achieved with respect to Au loading. By using 40 mol% of Au(I) complex, the yield was 44% reaching about 1 TON (Table V.2, entry 4). Interestingly, using a lower amount of **2b** (10 mol%) the yield was around 28% (~3 TON, entry 5). Similarly, by using hexafluoro-2-propanol (HFIP) the yield was 29% (~3 TON, entry 9); therefore, the best optimized results were obtained with fluorinated alcohols with HFIP featuring a slightly better result.

Table V.2. Optimization of the reaction conditions for the **2b**-catalyzed synthesis of γ -benzyl- γ -butyrolactone product **10**.


Entry	[Au] mol%	AgSbF ₆ (eq.)	K ₃ PO ₄ (eq.)	Solvent	Conv. % (yield %)
1^a	100	2.8	1.0	TFE	92 (63)
2^{a,b}	100	2.6	1.2	TFE	>99 (67)
3^c	70	2.2	1.2	TFE	81 (65)
4^c	40	2.0	1.1	TFE	79 (44)
5^a	10	1.5	1.0	TFE	51 (28)
6	10	1.5	0.5	TFE	51 (24)
7^c	10	1.5	1.1	TFE	54 (15)
8^c	1	1.1	0.5	TFE	38 (1.6)
9	10	1.5	1.0	HFIP	56 (29)

General reaction conditions: [Ar-I] = 0.08 M, [4-pentenoic acid] = 0.08 M, 80°C, 16 h. V = 0.55 – 1.40 mL. NMR yields obtained using 1,3,5-trimethoxybenzene as internal standard. ^a[Ar-I] = 0.02 M, [4-pentenoic acid] = 0.10 M, V = 1 mL. ^bT = 100°C. ^ct = 24h.

To exclude the possibility that Ag(I) oxidizes Au(I) to Au(III), complex **2a** (1 eq.) was reacted with AgSbF₆ (15 eq.) in HFIP at 80°C for 16 hours. Quantitative formation of the Au(I) dimer **3a** was observed by NMR, thereby confirming the role of silver as halide scavenger and not as oxidant (Annex 2, Scheme S12).

The scope of the reaction was examined with different aryl halides and γ -alkenoic acids (Figure V.8). The arylation-lactonization using iodobenzene and complex **2b** reached 50% yield (~5 TON) in product **11**. By doubling the catalyst loading to 20 mol%, the yield of **11** increased up to 87%, thus maintaining the turnover number (~4-5 TON). The best yields were reached using 4-iodotoluene, obtaining product **12** in 60% yield when using catalyst **2a** (~6 TON) and 81% yield when using catalyst **2b** (~8 TON). However, the presence of the strong electron-withdrawing group CF₃ in the *para*-position in 4-CF₃-iodobenzene produced product **13** in a lower yield (~13%). Following this trend,^{27, 28} 4-NO₂-iodobenzene afforded only traces of the corresponding product **14** (1%). In addition, the γ -alkenoic acid with α -methyl groups reacted smoothly, yielding 37% of **15** when using **2a**, and 41% of **15** when using **2b**. Also, the γ -alkenoic acid with β -methyl groups afforded product **16** in 32% yield

when using **2a** and in 18% when using **2b**. The molecular structure of compound **16** was determined by X-ray diffraction analysis, revealing the crystallization of the (*R*)-enantiomer by spontaneous resolution.

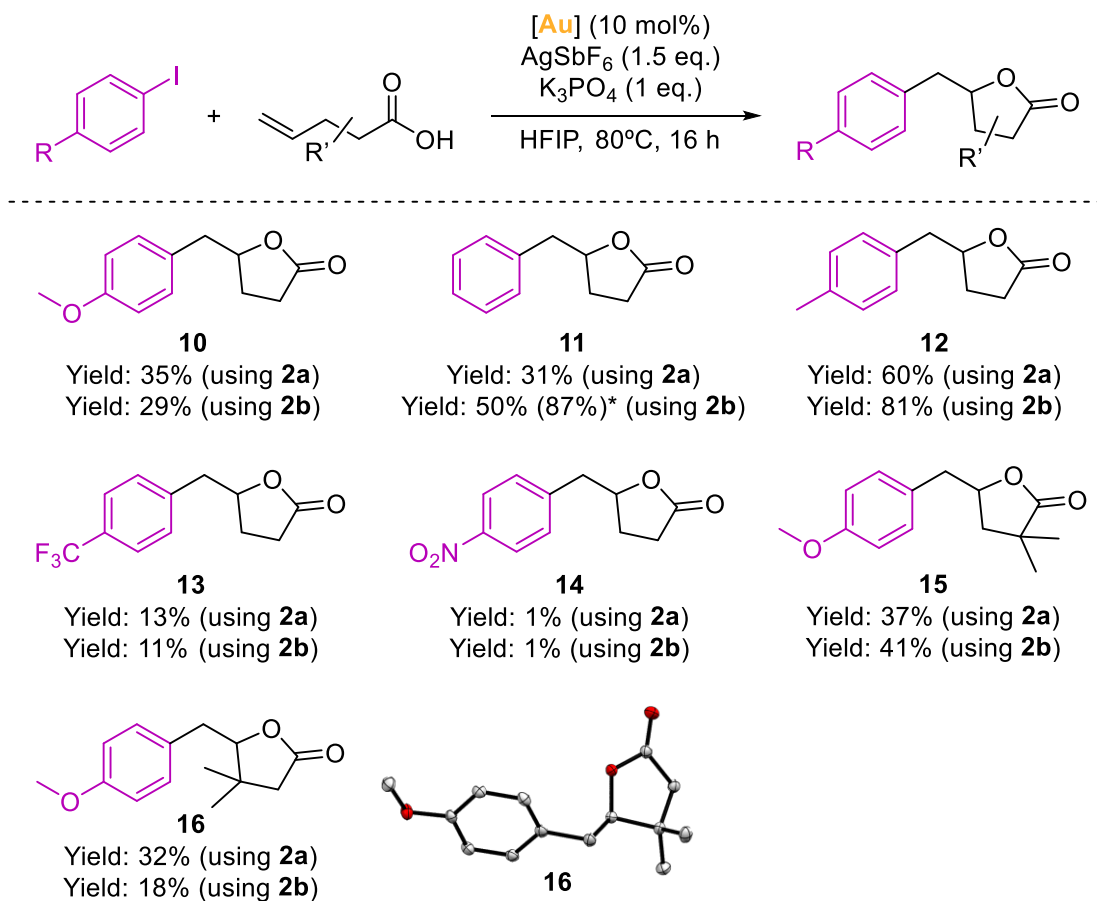


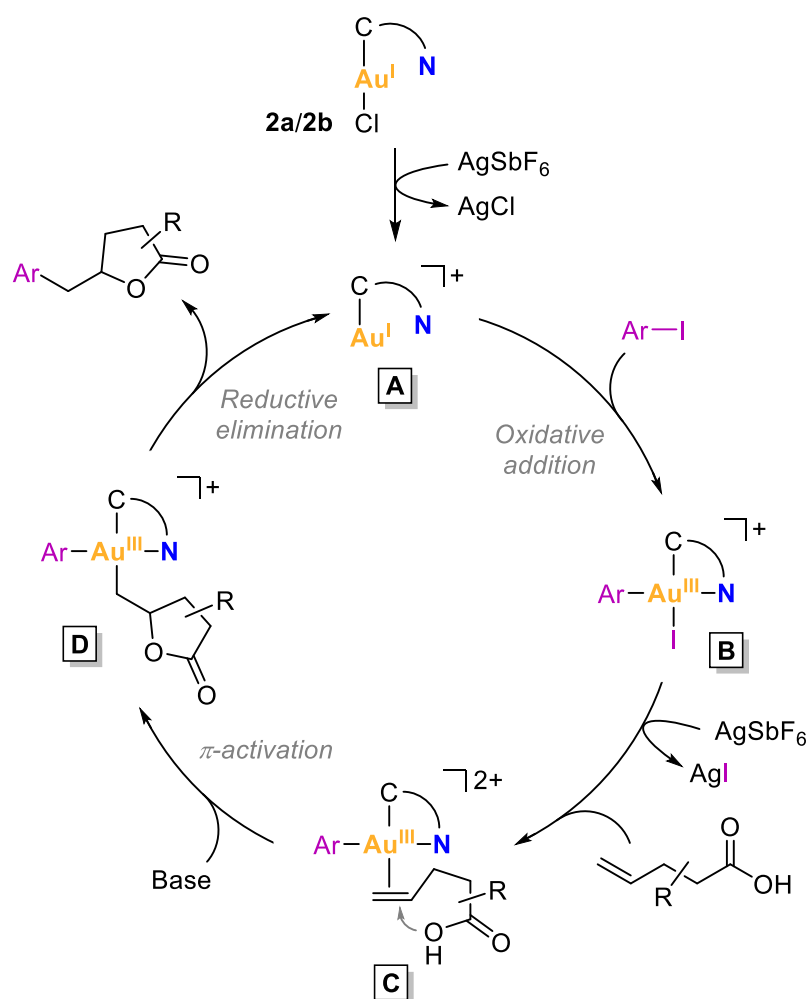
Figure V.8. Scope of the arylation-lactonization of alkenoic acids to afford products **10** – **16**, using catalysts **2a** and **2b** (NMR yields are displayed for each product). Crystal structure of **16** is shown (ellipsoids set at 50% probability, H atoms removed for clarity). *NMR yield using 20 mol% of [Au] is given in parenthesis.

Finally, to broaden the scope of the gold(I) catalysts, we tested complex **2a** in the oxyarylation^{5,6} and 1,2-diarylation⁸ of alkenes under the same catalytic conditions (Table V.3). The oxyarylation products **17** and **18** were obtained in low but significant yields (18% and 25% yield respectively, ~2 TON). On the contrary, the 1,2-diarylation reaction was unsuccessful.

Table V.3. Oxyarylation and 1,2-diarylation reactions of alkenes catalyzed by complex **2a**.

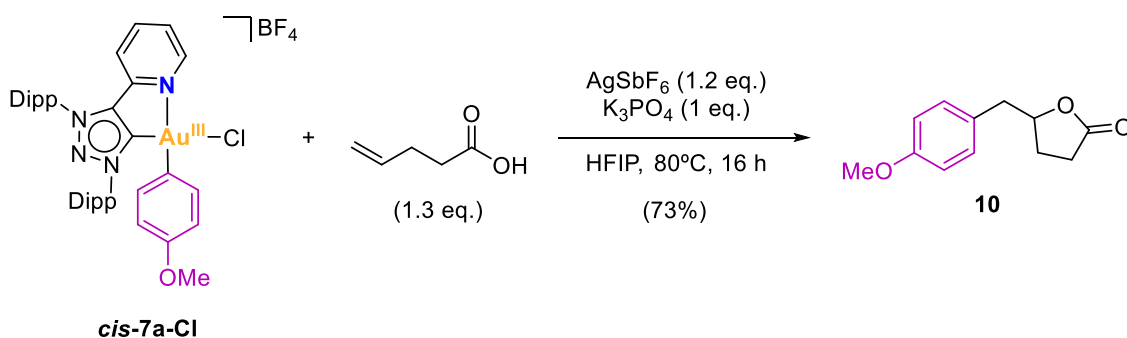
Entry	Alkene	Product	Yield (%)
1			18
2			25
3			5
4			0

Based on the fundamental understanding of the redox behavior of complexes **2a** and **2b**, and the previously reported gold-catalyzed processes merging aryl halide oxidative addition and π -activation of alkenes,⁵⁻¹⁰ the following reaction mechanism is proposed (Scheme V.1). First, the oxidative addition of the C(sp²)-I bond into a catalytically active cationic gold(I) species **A** occurs, affording a cationic arylgold(III) intermediate species **B**. Then, the silver salt abstracts the iodide ligand from this gold(III) species to generate a vacant site that can be occupied by the π -coordination of the olefin (species **C**). Then, the presence of base and the π -activation of the alkene produced by the gold center lead to an intramolecular γ -lactonization, rendering an alkylarylgold(III) intermediate **D**. Finally, the latter undergoes a reductive elimination step that affords the γ -benzyl- γ -butyrolactone product and closes the catalytic cycle by regenerating the initial catalytically active gold(I) species **A**.



Scheme V.1. Proposed reaction mechanism for the gold-catalyzed arylation-lactonization of γ -alkenoic acids.

To provide additional mechanistic insight, we also performed the stoichiometric reaction of **cis-7a-Cl** with AgSbF_6 , 4-pentenoic acid, and K_3PO_4 in HFIP at 80°C . After 16 hours, the γ -benzyl- γ -butyrolactone product **10** was obtained in 73% NMR yield (Scheme V.2).



Scheme V.2. Stoichiometric reaction of complex **cis-7a-Cl** towards the formation of product **10**.

Therefore, the connection between **cis-7a-Cl** and **10** implies that an arylgold(III) intermediate **B**, formed by C(sp²)-I oxidative addition, is plausibly involved in the catalytic cycle of the arylation-lactonization reaction of γ -alkenoic acids (Scheme V.1).

To sum up, we have prepared two gold(I) complexes (**2a** and **2b**) based on hemilabile MIC^N ligands; *i.e.*, mesoionic carbene ligands bearing a N-donor hemilabile group. The design of such ligands has allowed us to obtain (N^C)-cyclometalated Au(III) complexes by 2 e⁻ oxidation and by C(sp²)-C(sp²) oxidative addition of biphenylene, thereby proving the hemilabile character of the ligands. Although we could not detect or isolate gold(III) complexes resulting from the oxidative addition of C(sp²)-I bonds, the feasibility of such process was supported by the formation of products **8a-R/8b-R** and **9a/9b**, and further evidenced by the evolution of the analogous complex **cis-7a-Cl** to product **8a-OMe**. This reactivity prompted us to utilize complexes **2a** and **2b** as catalysts for the arylation-lactonization of γ -alkenoic acids, employing aryl iodides as coupling partners. The reaction mechanism was proposed to operate through an oxidant-free Au(I)/Au(III) catalytic cycle that merges the oxidative addition of C(sp²)-I bonds with the π -activation mode of reactivity of gold complexes. Even though the catalytic approach afforded the products in low to moderate yields, the significance of these results relies on showing that hemilabile (N,C) ligands can be a real alternative to hemilabile (P,N) ligands, among which MeDalphos ligand stands out in oxidant-free Au(I)/Au(III) cross-coupling catalysis. In fact, our work paved the way for the development of more catalytically efficient hemilabile (N^C)Au(I) systems in oxidant-free Au(I)/Au(III) catalysis.^{29,30}

V.2. NOVEL NHC-BASED Au(I) COMPLEXES AS PRECURSORS OF HIGHLY PURE Au(0) NUGGETS UNDER OXIDATIVE CONDITIONS

Fundamental comprehension of the intrinsic reactivity of NHC-based gold complexes (NHC = *N*-heterocyclic carbene) is needed to evaluate their success in different fields, such as in the biological sector³¹⁻³⁵ or in catalysis. NHC ligands are typically described as strongly σ -donating, therefore, they form very stable NHC–metal bonds which make them robust ligands in catalytic cycles.^{36, 37} Indeed, transition metal complexes bearing NHC ligands are commonly applied as catalysts for a variety of C–C and C–heteroatom bond forming reactions, cross-couplings, C–H functionalizations, atom-economic additions, olefin metathesis, and many other transformations.³⁸⁻⁴¹ Moreover, NHC ligands allow a high variability of their steric and electronic parameters, leading to effective tuning of the catalyst activity.⁴²

Regarding gold catalysis, a large number of NHC–gold complexes have been successfully employed in Lewis acid catalysis for the cyclization and rearrangements of polyunsaturated substrates.^{43, 44} However, to further expand the scope of applications of these complexes, it is also necessary to explore experimental conditions where NHC–gold complexes might suffer from instability. For instance, Au(I)/Au(III) catalysis using external oxidants or oxidant-free catalysis with ligands featuring pendant coordinating groups has become prominent in the last decade, yet the intrinsic decomposition of gold complexes remains underexplored.

There are some remarkable works on the decomposition of NHC-based complexes.^{42, 45} For example, Ananikov and coworkers reported the unusual role of bases in the deactivation of NHC–metal catalysts (metal = Ni(II), Pd(II), and Pt(II)), undergoing metal reduction to M(0) and formation of NHC=O azolone coupling products.⁴⁵ In their study, a base-mediated NHC=O coupling reaction is demonstrated to be integrated into the catalytic M/NHC systems, and metal-free NHC derivatives are present in the catalytic mixture. A proposed mechanism of such transformation includes NHC–OR reductive elimination, as implied by a series of mechanistic studies including ¹⁸O labeling experiments. In addition, similar decomposition pathways were reported on triazolylidene Cu(I) complexes, which decompose into mesoionic oxides in the presence of CsOH.⁴⁶ However, almost no reports exist for a detailed description of NHC–Au(I) decomposition pathways.⁴⁷

Moreover, a straightforward and reliable chemical methodology to produce Au(0) nuggets from gold complexes is not available. The main source of gold nuggets is, like natural ores,

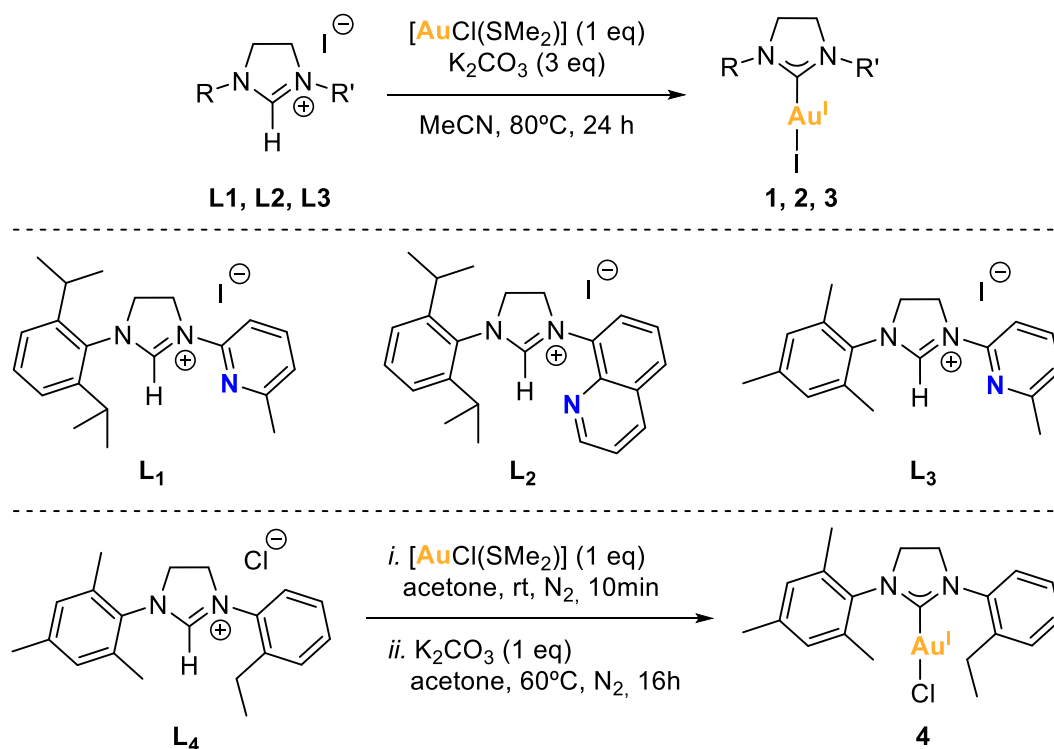
hypogenic in origin. Native gold grains are usually small in size (10–500 μm), with a composition of 5 to <30% Ag, typical of hypogene gold, although Ag contents can be less than 1% depending on the goldfield of origin.⁴⁸ The recovery of Au(0) from ores or waste electronic materials entails stepwise tedious processes such as reduction with metallic Zn, HCl treatment, centrifugation, and pyrolysis.⁴⁹ Alternatively, gold biomineralization has been studied as a method to obtain gold grains from Au(I/III)-complexes by the action of bacteria.^{50, 51} Also, material science can help in developing MOF/polymer composites that are able to efficiently extract trace amounts of gold from water.⁵²

Following the synthesis and reactivity studies of hemilabile (N[^]C)Au(I) complexes (Section V.1), in this project we aim at synthesizing gold(I) complexes based on NHC ligands having a hemilabile N-donor group, and subjecting them to oxidative conditions to study whether we are able to access the corresponding (N,C)-cyclometalated gold(III) complexes or, instead, we can study a controlled decomposition pathway towards the formation of oxidized ligands (NHC=O azolone-type products) and naked eye-observable Au(0) nuggets.

V.2.1. Synthesis of NHC–Au(I) complexes

In collaboration with the group of Prof. Vougioukalakis, we designed four imidazolium salts (**L1**, **L2**, **L3** and **L4**) as NHC ligand precursors, which were synthesized by standard procedures.^{53, 54} Imidazolium salts **L1–L3** contain a pendant pyridine or quinoline group, whereas **L4** contains a non-coordinating arene moiety (Scheme V.3).

The synthesis of the corresponding NHC–Au(I) complexes (**1**, **2**, **3**, and **4**) was based on previously reported works.^{55, 56} On one hand, complexes **1**, **2**, and **3** were obtained by reacting the imidazolium salt **L1**, **L2** or **L3** with chloro(dimethylsulfide)gold(I) and potassium carbonate, in acetonitrile at 80°C for 24 hours. After this time, the reaction mixture was filtered over Celite®, all volatiles were removed under vacuum, and the gold(I) complexes were purified by column chromatography. On the other hand, complex **4** was obtained from the reaction of imidazolium salt **L4** with chloro(dimethylsulfide)gold(I) and potassium carbonate, in acetone at 60°C for 16 hours (Scheme V.3).



Scheme V.3. Synthesis of complexes **1–4** from the respective imidazolinium salts **L1–L4**.

Complexes **1**, **2**, **3** and **4** were unequivocally characterized by XRD (Figure V.9). In complexes **1–3**, the pendant coordinating arm did not show any interaction with the metal center. No H-bonding network was observed with the non-coordinating pendant groups. The linear coordination was confirmed for the Au(I) center in all cases, as the angle formed by the carbenic carbon, the gold center, and the halide atom was close to 180° (for **1**, $177.4(4)^{\circ}$; for **2**, $175.4(2)^{\circ}$; for **3**, $178.38(8)^{\circ}$; for **4**, $179.12(16)^{\circ}$). Complexes **1–4** were asymmetrical; hence, the two methylene units of the imidazolidine ring appeared at different ^1H NMR chemical shifts. The two $-\text{NCH}_2-$ signals appeared as multiplets at 4.54 and 3.90 ppm for complexes **1** and **3** (Annex 3, Figures S7 and S22), at 4.68 and 4.08 ppm for complex **2** (Annex 3, Figure S15), and at 4.22 and 3.96 ppm for complex **4** (Annex 3, Figure S28). On the other hand, the characteristic ^{13}C NMR signal of the $\text{C}_{\text{carbene}}-\text{Au}$ appeared at 201.0, 203.7, 192.2, and 195.5 ppm for complexes **1**, **2**, **3** and **4**, respectively (Annex 3, Figures S8, S16, S23 and S29).

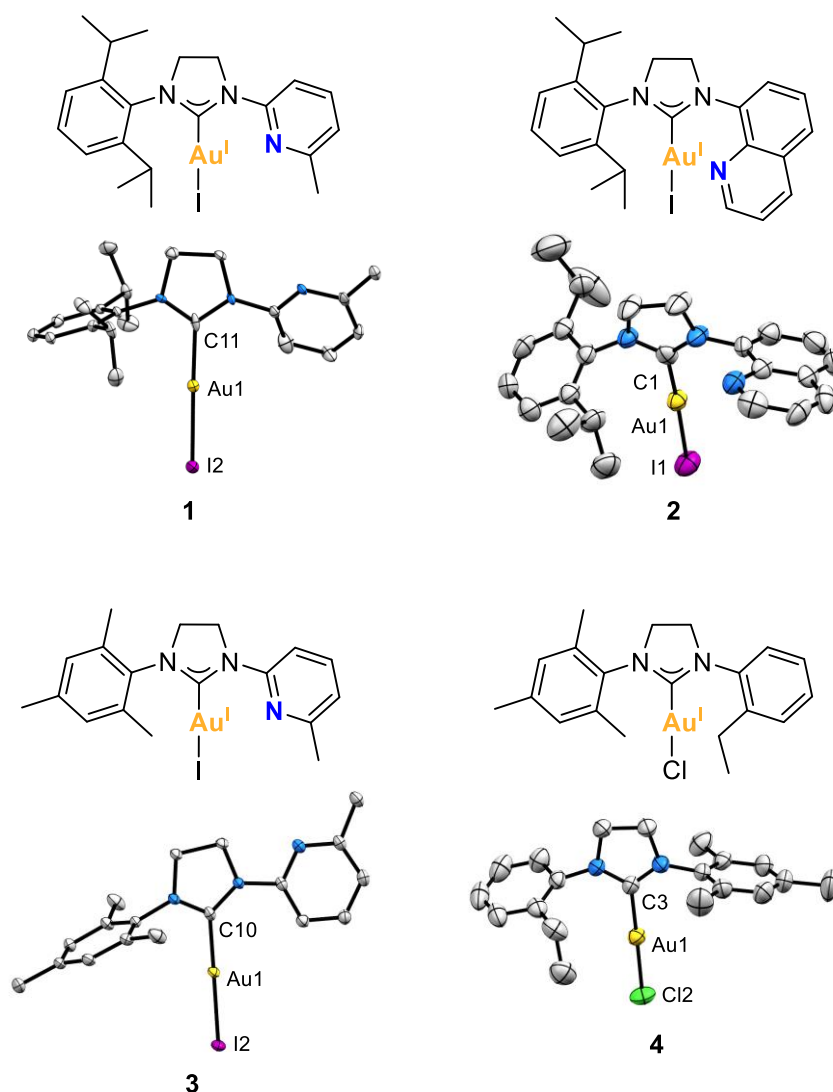


Figure V.9. X-ray molecular structures of complexes **1**, **2**, **3** and **4** (ellipsoids set at 50% probability and H atoms removed for clarity). Selected bond distances (Å): for **1**, Au1-C11 2.007(13), Au1-I2 2.5580(10); for **2**, Au1-C1 1.981(9), Au1-I1 2.5467(8); for **3**, Au1-C10 2.000(3), Au1-I2 2.5516(2); for **4**, Au1-C3 1.966(6), Au1-Cl2 2.262(3). Selected angles (°): for **1**, C11-Au1-I2 177.4(4); for **2**, C1-Au1-I1 175.4(2); for **3**, C10-Au1-I2 178.38(8); for **4**, C3-Au1-Cl2 179.12(16).

V.2.2. Reactivity of NHC–Au(I) complexes with oxidants

Complexes **1–3** were reacted with external oxidants seeking the stabilization of cyclometalated NHC–Au(III) species, taking advantage of the pendant coordinating arms (pyridine-type for **1** and **3**, and quinoline-type for **2**). The external oxidants used were $\text{PhI}(\text{OAc})_2$, PhICl_2 , H_2O_2 , XeF_2 , and $\text{CH}_3\text{CO}_3\text{H}$ under different solvents and temperatures (Table V.4). Nevertheless, the expected NHC–Au(III) species could not be stabilized in any case, and the mixture underwent a decomposition pathway involving the formation of a) the corresponding NHC=O azolones, and b) Au(0) nuggets.

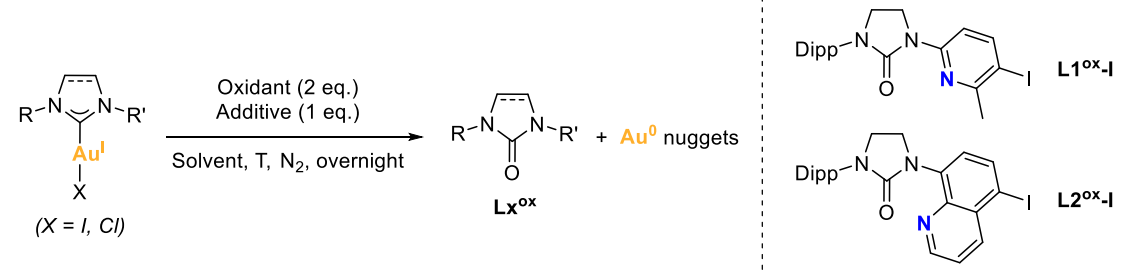
The formation of the azolone products **L1^{ox}**, **L2^{ox}**, **L3^{ox}**, **L4^{ox}** was monitored by HRMS, and **L2^{ox}** and **L3^{ox}** were fully characterized by 1D and 2D NMR. Intriguingly, we also observed the formation of azolones that underwent a C–H iodination on the most activated position of the pendant heteroaromatic system of the ligand. Indeed, products **L1^{ox}–I** and **L2^{ox}–I** were isolated and characterized. The 2D NMR experiments revealed that the iodination occurred at the *para* position to the imidazolinone substituent (see Annex 3, Sections 5.7 and 5.9). The selective C–H halogenation at the *para* position to N-substituted positions, and C5-halogenation of 8-aminoquinolines, is a reactivity pattern that has already been reported.⁵⁷⁻⁶¹

In some reactions, the NHC–Au(I) complexes were reacted with a silver salt and an oxidant. The use of silver salts as additives was intended to promote the halide abstraction from the gold(I) starting complexes, thereby generating a reactive species that, hopefully, would evolve to a gold(III) complex in the presence of an oxidant, expecting the coordination of the hemilabile N-donor arm to the gold center in the case of using complexes **1–3**. In addition, the halide abstraction could likely induce the formation of head-to-tail dimeric Au(I) species with the (N,C) ligand bridging two metals,^{19, 62, 63} as previously described in Section V.1 (see analogy in Figure V.2). However, the synthesis of such dimeric species was not the focus of our interest.

When complex **1** was reacted with PhI(OAc)₂ in 1,2-DCE, regardless AgOAc was added, Au(0) nuggets and azolones **L1^{ox}** and **L1^{ox}–I** were formed (Table V.4, entries 1 and 2). The azolones were detected by MS-ESI and, in MeCN (entry 3), the **L1^{ox}–I** product was isolated in 53% yield. When changing the oxidant to H₂O₂ or PhICl₂, no reaction afforded Au(0) nuggets (entries 4–6). By using H₂O₂, the reaction outcome in presence of AgOAc was mainly the starting complex **1**, whereas in the absence of AgOAc, **L1^{ox}–I** could be detected by MS-ESI as well (entries 4 and 5). By using PhICl₂ at room temperature, **L1^{ox}–I** was also detected by MS-ESI (entry 6).

A blank experiment was conducted with complex **2**; without oxidant and additives, the complex was recovered after being heated in 1,2-DCE at 100°C overnight (entry 7). Instead, decomposition was observed when using PhI(OAc)₂, as Au(0) nuggets were formed in high yields (56–91%) and **L2^{ox}** and **L2^{ox}–I** products were detected by MS-ESI in all cases (entries 8–11). The isolation of both **L2^{ox}** and **L2^{ox}–I** azolones allowed their full characterization. When complex **2** was reacted with CH₃CO₃H as oxidant (entry 12), Au(0) nuggets were obtained in moderate yield (34%) and NMR revealed the presence of the starting complex **2** and product **L2^{ox}**.

Table V.4. Reactivity of Au(I) complexes towards the formation of Au(0) nuggets and azolones (Lx^{ox}).



Entry	[Au]	Oxidant	Additive	Solvent	T (°C)	Au(0) yield (%)	NHC=O (yield %)*
1	1	PhI(OAc) ₂	AgOAc	1,2-DCE	90	75	Detected MS
2	1	PhI(OAc) ₂	-	1,2-DCE	90	46	Detected MS
3	1	PhI(OAc) ₂	-	MeCN	90	60	L1^{ox}-I (53)
4	1	H ₂ O ₂	AgOAc	1,2-DCE	90	0	0
5	1	H ₂ O ₂	-	1,2-DCE	90	0	Detected MS
6	1	PhICl ₂	-	DCM	rt	0	Detected MS
7	2	-	-	1,2-DCE	100	0	0
8	2	PhI(OAc) ₂	AgOAc	1,2-DCE	90	85	Detected MS
9	2	PhI(OAc) ₂	-	1,2-DCE	90	90	L2^{ox} (22) and L2^{ox}-I (17)
10	2	PhI(OAc) ₂	AgOAc	DCM	70	91	Detected MS
11	2	PhI(OAc) ₂	-	MeCN	90	56	L2^{ox} (34)
12	2	CH ₃ CO ₃ H	-	1,2-DCE	90	34	Detected NMR
13	3	PhI(OAc) ₂	AgOAc	1,2-DCE	90	>99	L3^{ox} (60)
14	3	XeF ₂	-	CDCl ₃	rt	0	Detected MS
15	4	PhI(OAc) ₂	-	DCM	rt	0	0
16 ^a	4	PhI(OAc) ₂	-	DCM	100	97	Detected MS
17	4	PhI(OAc) ₂	-	1,2-DCE	90	32	Detected MS
18	IPrAuCl	PhI(OAc) ₂	AgOAc	1,2-DCE	90	0	0
19	IPrAuCl	PhI(OAc) ₂	-	1,2-DCE	90	0	0
20	SIPrAuCl	PhI(OAc) ₂	AgOAc	1,2-DCE	90	0	0
21	SIPrAuCl	PhI(OAc) ₂	-	1,2-DCE	90	11	6
22 ^b	2	PhI(OAc) ₂	H ₂ O	MeCN	90	88	L2^{ox} (48)
23 ^b	2	PhI(OAc) ₂	H ₂ ¹⁸ O	MeCN	90	97	L2^{ox} (41)

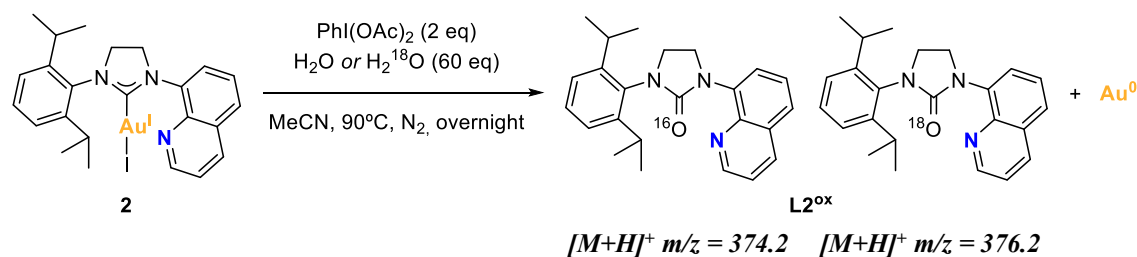
V = 0.5 – 1.6 mL. [complex] = 0.03 M. * Isolated yield. ^a 5h reaction. ^b 60 eq. additive, [complex] = 0.02 M.

The reaction of complex **3** with $\text{PhI}(\text{OAc})_2$ and AgOAc yielded $\text{Au}(0)$ quantitatively, and azolone **L3^{ox}** was isolated in 60% yield and characterized (entry 13). Conversely, when the oxidant XeF_2 was used at room temperature, no $\text{Au}(0)$ nuggets were formed (entry 14) although azolone **L3^{ox}** was detected by MS-ESI. Complex **4** was employed to search for contrast with the complexes that contained a hemilabile N-donor group in the ligand. The reaction of **4** with $\text{PhI}(\text{OAc})_2$ in DCM at room temperature did not provide $\text{Au}(0)$ nuggets nor azolone, as the starting complex was recovered (entry 15). However, by heating at 100°C for 5 hours, the mixture decomposed affording $\text{Au}(0)$ nuggets in 97% yield, and azolone **L4^{ox}** was detected by MS-ESI (entry 16). When **4** was reacted with $\text{PhI}(\text{OAc})_2$ in 1,2-DCE at 90°C , $\text{Au}(0)$ nuggets were obtained in 32% yield (entry 17).

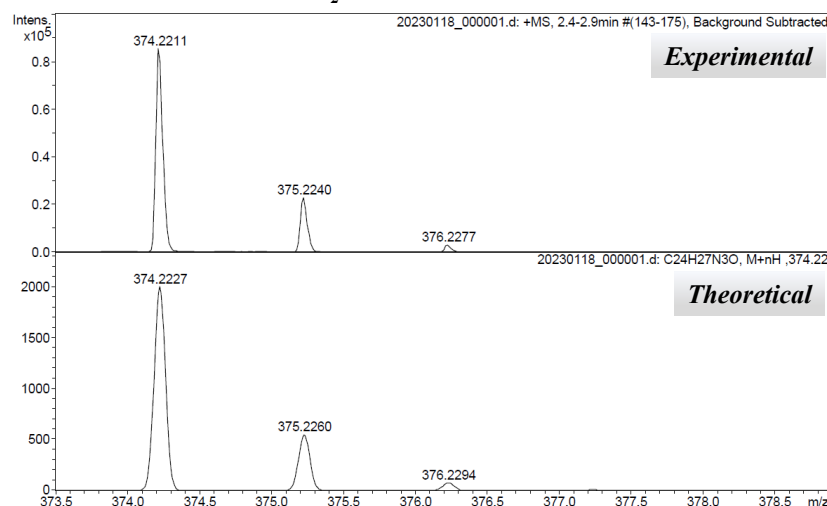
Interestingly, the commercial IPrAuCl was reacted with $\text{PhI}(\text{OAc})_2$ in 1,2-DCE, with and without AgOAc , and, in either case, neither azolone product nor $\text{Au}(0)$ nuggets were formed, and IPrAuCl was recovered after the reaction time (entries 18 and 19). Additionally, when the commercial saturated analog complex SIPrAuCl was reacted with $\text{PhI}(\text{OAc})_2$, a very low 11% conversion to $\text{Au}(0)$ nuggets was obtained along with a 6% conversion to the corresponding azolone, as determined by NMR, according to the reported description of the azolone⁶⁴ (entries 20 and 21). The stability of these well-known complexes is remarkable compared to that of complexes **1–4**, showing that when a structural modification of the most typical NHC ligands, such as IPr and SIPr , is performed, reactivity changes sharply. However, it is worth mentioning that there are examples of unsaturated NHC–Au(I) complexes bearing a hemilabile pyridine moiety that could be oxidized with PhICl_2 to the corresponding NHC–Au(III) complexes without observing decomposition.^{65, 66}

The origin of the O-atom in azolones was investigated by taking complex **2** as case study. It was reacted with $\text{PhI}(\text{OAc})_2$ as the oxidant and water as the additive, under nitrogen atmosphere (Table V.4, entries 22 and 23, and Figure V.10). To track the origin of the O-atom, a control reaction was carried out using distilled H_2O , and another one was carried out using 97% labeled ^{18}O -water (see Annex 3, Section 6). Then, the reaction crudes were analyzed by HRMS-ESI(+) to compare the isotopic pattern of the **L2^{ox}** product. For the control experiment, a major peak at $m/z = 374.2$ was obtained, corresponding to the $\text{NHC}=\text{}^{16}\text{O}$ azolone **L2^{ox}**, whereas for the reaction with H_2^{18}O two major peaks were obtained at $m/z = 374.2$ and $m/z = 376.2$, corresponding to the $\text{NHC}=\text{}^{16}\text{O}$ and $\text{NHC}=\text{}^{18}\text{O}$ azolones **L2^{ox}**, respectively (Figure V.10). According to the isotopic pattern, a 35% of ^{18}O incorporation was obtained, suggesting that the O-atom in the azolone products found in the reaction outcomes might have come from adventitious water. Also, the low ^{18}O

incorporation from labeled water suggests that an oxygen-transferring mechanism may exist, and that at some point of the mechanism, water should react with the oxidant to deliver a ^{18}O -labeled reactive intermediate species. With this information, the alternative possibility of considering acetate to be the O-atom source cannot be ruled out, as it would be supported by previous studies.⁶⁷



Control reaction with H_2O



Reaction with H_2^{18}O

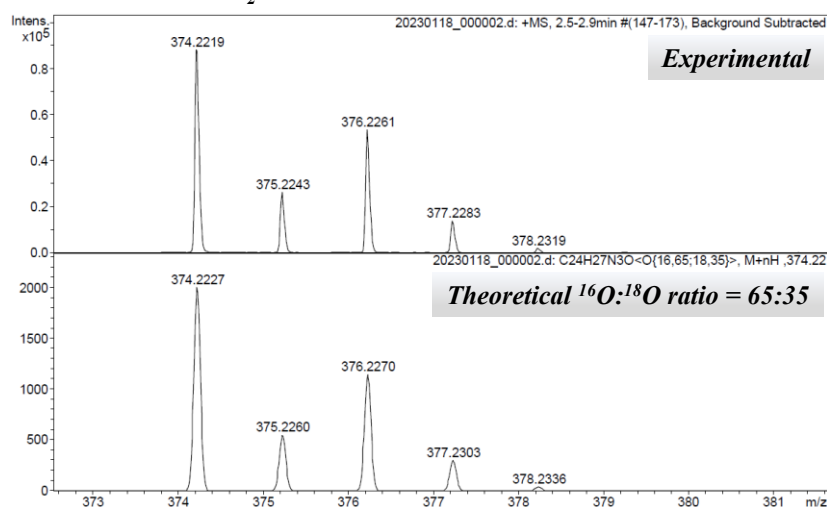


Figure V.10. Reaction of complex **2** with PhI(OAc)_2 and water or ^{18}O -labeled water, and peaks of product L2^{ox} obtained by HRMS-ESI(+) in each case.

V.2.3. Characterization of the Au(0) nuggets

The formation of Au(0) nuggets was naked-eye evident (Figure V.11a). The amount of gold obtained mostly represented the quantitative recovery of all the Au(I) into Au(0) nuggets. The grains were large enough to easily isolate them for analysis. Thus, they were decanted from the reaction mixture, thoroughly washed, and dried. The Au(0) nuggets obtained from the reaction described in Table V.4, entry 1, were chosen to be characterized by SEM and SEM-EDX. The morphological characterization was done by SEM analysis. It revealed that the diameter mean size of the grains was about 0.4–0.5 mm (Figure V.11a). The elemental composition was analyzed by SEM-EDX, obtaining purities of about 90% (only C and N impurities were detected, which were attributed to the carbon tape support) (Figure V.11b). The Au(0) nuggets were then tested as heterogeneous catalyst for transformations typically catalyzed by gold complexes, such as Sonogashira, A3, and Glaser couplings.⁶⁸⁻⁷² However, none of these attempts resulted in effective coupling, being in line with the macroscopic size of the Au(0) nuggets and the absence of more reactive Au(0) nanoparticles.

In summary, we have synthesized and characterized novel NHC–Au(I) complexes **1–4**, with and without pendant coordinating groups. Their reactivity under oxidative conditions has been explored. When using iodosylbenzene-type oxidants, complexes **1–4** underwent a controlled decomposition pathway to afford azolones as the main organic product, concomitantly with conversion of the Au(I) contained in complexes into Au(0) nuggets (~0.4–0.5 mm). On the contrary, commercial IPrAuCl and SIPrAuCl complexes are robust and remain intact after exposure to PhI(OAc)₂. We show that NHC–Au(I) complexes **1–4** can follow decomposition pathways under certain experimental conditions, thus challenging the believed general robustness of the NHC–Au bond. Also, we provide a novel methodology to easily recover Au(0) nuggets of high purity in one step, from the treatment of soluble NHC–Au(I) species with external oxidants. Azolones and M(0) have previously been described as decomposition products of NHC–M complexes (M = Ni(II), Pd(II), Pt(II), Cu(I)),^{45, 46, 64} but we have shown the singular case of gold undergoing this decomposition pathway.

a) Au(0) nuggets



b) SEM-EDX analysis

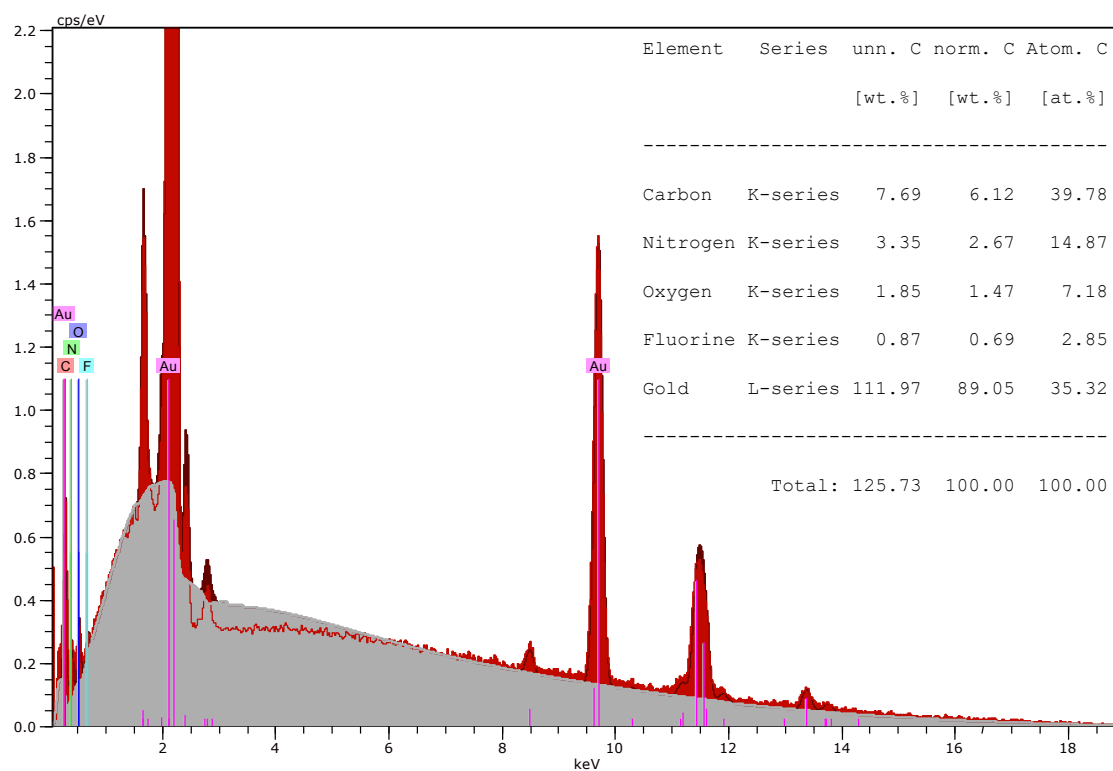


Figure V.11. a) Reaction outcome with Au(0) nuggets precipitated (left), and SEM image of the isolated Au(0) nuggets at x30 (right); b) EDX spectrum from a region of a gold grain set by SEM at x1000.

V.3. BORON-TO-GOLD(III) TRANSMETALATION AS A SYNTHETIC STRATEGY TO ACCESS (N[^]C[^]C)-BISCYCLOMETALATED GOLD(III) COMPLEXES

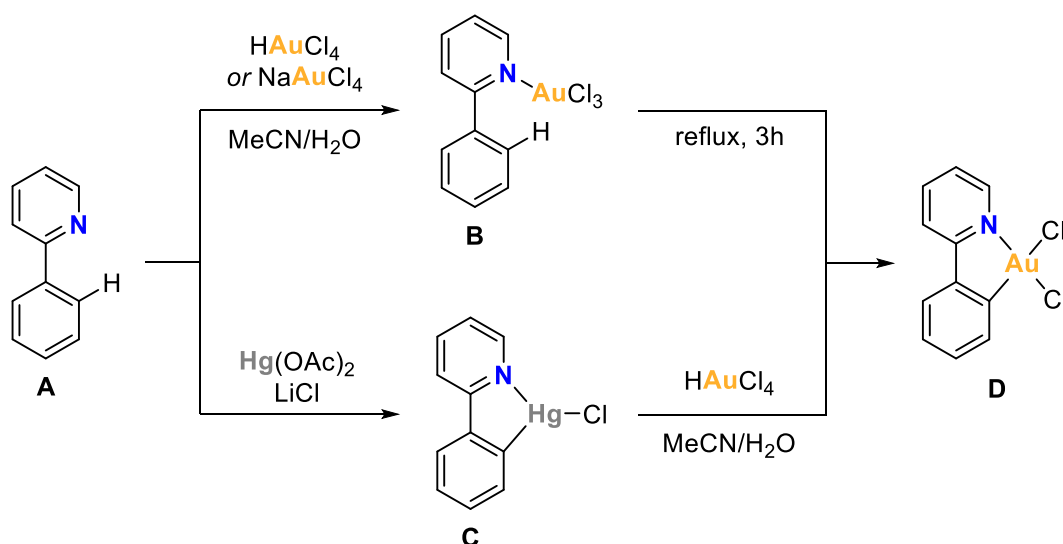
The exploration of gold(III) complexes in the field of organometallic chemistry is limited due to the tendency of Au(III) to get reduced to either Au(I) or Au(0), and due to the challenges associated with their synthesis.⁷³⁻⁷⁵ Nonetheless, a strategy to circumvent these limitations relies on the use of ligands that stabilize Au(III) centers in the form of cyclometalated complexes. In this regard, common cyclometalating ligands are those that afford five-membered auracycles and, less frequently, six-membered rings, upon cycloauration reactions. The balance between stabilization and reactivity of these d⁸-square planar Au(III) cyclometalated systems has led to the development of novel gold(III) complexes featuring interesting properties in multiple disciplines, such as catalysis, material science, and medicinal chemistry.⁷⁶⁻⁷⁸

Noticeably, two fields of research are gaining prominence concerning the exploration of applications for cyclometalated Au(III) complexes. On one hand, the luminescent properties of Au(III) complexes, which have been underutilized compared to isoelectronic Pd(II) and Ir(III) species, have led to the application of such complexes as additives to enhance the efficiency of OLEDs.^{77, 79, 80} (C[^]N[^]C) pincer ligands based on dianionic 2,6-diphenylpyridine architectures and (N[^]C) phenylpyridine ligands proved to be excellent platforms to stabilize Au(III) centers in this context, resulting in gold(III) complexes with good emissive properties, as demonstrated by Yam, Che, and Bochmann.⁸¹⁻⁸³ On the other hand, the potential antitumoral activity of cyclometalated Au(III) complexes has attracted the attention in medicinal chemistry. The square planar geometry of Au(III) species has been related by analogy to that of cisplatin, *cis*-[PtCl₂(NH₃)₂], assuming a similar mechanism of action for the Au(III) species.^{78, 84} In this context, cyclometalating ligands play a crucial role in stabilizing the Au(III) centers in intracellular media.

Numerous cyclometalated gold(III) complexes have been disclosed in the last decades, generally containing a Au(III)–aryl bond. Among these, (N[^]C),⁸⁵⁻⁸⁷ (P[^]C)^{88, 89} and rarer (C[^]C)^{90, 91} chelates, as well as (C[^]N[^]C),^{83, 92} (N[^]C[^]C),^{76, 79} (N[^]C[^]N),^{93, 94} and (N[^]N[^]C)⁹⁵⁻⁹⁷ pincer ligands, are the prevalent templates that are used to study mono- and biscyclometalated Au(III) complexes.^{73, 80}

The first example of arene activation with gold was reported by Kharasch and Isabell in 1931. They observed that the mixture of gold(III) chloride with benzene promoted the activation

of benzene to access gold(III)-aryl compounds.⁹⁸ The direct auration of arenes is generally thought to proceed via a $S_{\text{E}}\text{Ar}$ reaction where the electron-rich arene attacks the electrophilic gold(III) center, releasing hydrogen chloride (as gold(III) chloride salts are commonly employed). About a half century later, in 1989, Constable and Leese developed a general methodology to synthesize ($\text{N}^{\wedge}\text{C}$)-cycloaurated gold(III) complexes. Starting from 2-phenylpyridine **A**, they prepared the cyclometalated $[\text{Au}(\text{ppy})\text{Cl}_2]$ complex **D** (ppy = 2-phenylpyridine) either via direct C–H auration using HAuCl_4 or NaAuCl_4 under thermal conditions (through **B**), or via transmetalation of HAuCl_4 with the $[\text{Hg}(\text{ppy})\text{Cl}]$ organomercury compound **C**.⁹⁹ This work paved the way to access ($\text{N}^{\wedge}\text{C}$)-cyclometalated gold(III) complexes by means of these synthetic strategies.¹⁰⁰⁻¹⁰⁴



Scheme V.4. Synthesis of $[\text{Au}(\text{ppy})\text{Cl}_2]$ from 2-phenylpyridine by C–H auration (top) and by transmetalation with an organomercury precursor (bottom).

Indeed, the preparation of gold(III) complexes by transmetalation involving organomercury(II) precursors became popular, and, in the attempt to improve the stability of the ensuing gold(III) complexes, this methodology was transferred to systems based on pincer ligands that afford biscyclometalated gold(III) complexes. In 1998, Che and coworkers reported the first example of ($\text{C}^{\wedge}\text{N}_{\text{py}}^{\wedge}\text{C}$) $\text{Au}(\text{III})$ complexes obtained by reacting the corresponding organomercury(II) compound with KAuCl_4 in MeCN under reflux.¹⁰⁵ This contribution gave rise to the appearance of many works in which ($\text{C}^{\wedge}\text{N}^{\wedge}\text{C}$) $\text{Au}(\text{III})$ complexes were synthesized by means of transmetalation with organomercury species. Among these, the works of Che,^{82, 92, 106, 107} Yam¹⁰⁸ and Bochmann¹⁰⁹ stand out.

The main drawback of using the abovementioned transmetalation approach is the toxicity of the generated Hg-containing waste. Therefore, other mercury-free synthetic methodologies to access Au(III) pincer complexes are highly desirable. In fact, it has been demonstrated that cyclometalated Au(III) complexes can indeed be achieved through different alternative approaches, which are briefly surveyed below.

A mercury-free approach based on the same principle is the transmetalation of gold(III) with organotin(IV) precursors. For instance, (C[^]C)Au(III) complexes have been obtained by transmetalation of the corresponding (C[^]C)Sn(IV) compounds, as reported in the works of Chicote, Mohr, and Che.^{90, 110, 111} However, Sn-containing waste is as well toxic, therefore, this methodology is not a desirable alternative to avoid organomercury and HgCl₂ waste.

Another approach relies on the use of microwave heating to trigger the C–H auration step, instead of classical heating conditions. Illustrative examples are those disclosed by the group of Tilset where they prepared (N[^]C) and even (N[^]C(sp²)[^]C(sp³)) cyclometalated gold(III) complexes.^{86, 112-115}

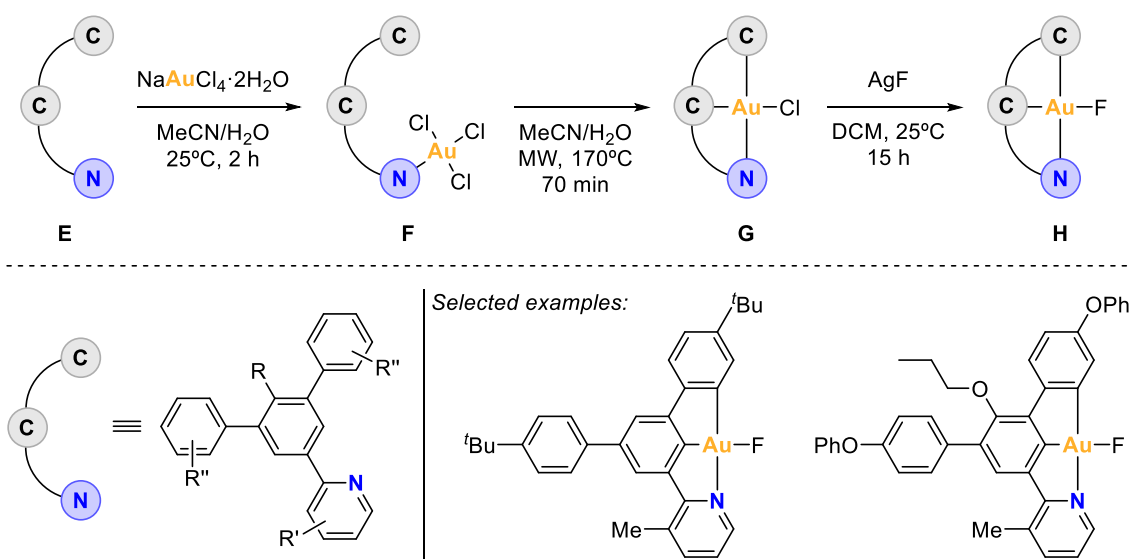
An interesting metalation surrogate was reported recently by Nevado and coworkers. They used catalytic amounts of rhodium to activate the C(sp²)–H bond of unfunctionalized (N[^]C) ligands, and to subsequently undergo a catalytic transmetalation to gold(III) to access (N[^]C)-cyclometalated Au(III) complexes of the type [(N[^]C)AuCl₂] under mild conditions (see Scheme I.40b).¹¹⁶

Since diazonium salts can oxidize Au(I) species, the group of Hashmi designed the synthesis of biscyclometalated gold(III) complexes through oxidative addition instead of transmetalation or direct C–H activation. To this end, the ligand precursor was prefunctionalized as a diazonium salt, and was reacted with [Au(DMS)Cl] at room temperature under the irradiation of blue LEDs. By this means, they accessed (C[^]N[^]C)¹¹⁷,¹¹⁸ and (N[^]C[^]N)¹¹⁹ gold(III) pincer complexes.

The synthesis of cyclometalated Au(III) complexes through alternative approaches like chelation-assisted oxidative addition and oxidative addition under photochemical conditions is not surveyed herein, as these strategies have already been revised in sections I.4.1.2 and I.4.1.3 respectively.

Hereafter we will focus on synthetic approaches to access (N[^]C[^]C)Au(III) complexes, as it is in part a subject of investigation of this thesis. The group of Nevado outstands in using (N[^]C[^]C) pincer ligands to render biscyclometalated Au(III) complexes under microwave

heating. In 2015, the group reported for the first time the novel ($\text{N}^{\wedge}\text{C}^{\wedge}\text{C}$) scaffolds **E**, which allowed the stabilization of electron-deprived gold(III) species and enabled the preparation of the corresponding κ^3 -[($\text{N}^{\wedge}\text{C}^{\wedge}\text{C}$)AuF] complexes **H** (Scheme V.5).⁷⁹ The unfunctionalized ($\text{N}^{\wedge}\text{C}^{\wedge}\text{C}$) platforms **E** were reacted with $\text{NaAuCl}_4 \cdot 2\text{H}_2\text{O}$ in $\text{MeCN}/\text{H}_2\text{O}$ at room temperature to afford [(L)AuCl₃] complexes **F** (L = ligand) upon gold coordination to the pyridine unit. Then, by subjecting these complexes to microwave heating, two $\text{C}(\text{sp}^2)\text{-H}$ auration reactions occurred, yielding the corresponding biscyclometalated gold(III) chloride complexes κ^3 -[($\text{N}^{\wedge}\text{C}^{\wedge}\text{C}$)AuCl] **G**. The latter could further be converted, upon ligand exchange, to the corresponding fluoride complexes **H**, which presented improved photophysical properties compared to classical pincer ($\text{C}^{\wedge}\text{N}^{\wedge}\text{C}$)–Au systems.



Scheme V.5. General synthesis of κ^3 -[($\text{N}^{\wedge}\text{C}^{\wedge}\text{C}$)AuF] complexes (top) and selected examples of such complexes (bottom).

The diversification from the κ^3 -[($\text{N}^{\wedge}\text{C}^{\wedge}\text{C}$)AuCl] complexes, obtained under microwave conditions, led the group to carry out studies on the applications of ($\text{N}^{\wedge}\text{C}^{\wedge}\text{C}$)–Au(III) complexes to OLEDs^{79, 120, 121} and as potential catalysts for the water-gas shift reaction.^{76, 122} However, the synthesis of such complexes was limited to symmetric ligands, *i.e.*, ($\text{N}^{\wedge}\text{C}^{\wedge}\text{C}$) architectures in which the central aryl ring has two equal substituents in *meta* position to the pyridine substituent (Figure V.12). Hence, the microwave-assisted cyclometalation is non-general and limited in scope, thus, a versatile synthetic strategy that allows the cyclometalation of non-symmetric ($\text{N}^{\wedge}\text{C}^{\wedge}\text{C}$) platforms is lacking. In addition, the development of such a strategy entails the intrinsic challenge of having to control the

regioselectivity of the cyclometalation reaction. Whereas symmetric ligands will provide only one ($\text{N}^{\wedge}\text{C}^{\wedge}\text{C}$)Au(III) complex, non-symmetric ligands can, *a priori*, provide different ($\text{N}^{\wedge}\text{C}^{\wedge}\text{C}$) complexes (depicted with an arrow and a “gold atom” in Figure V.12).

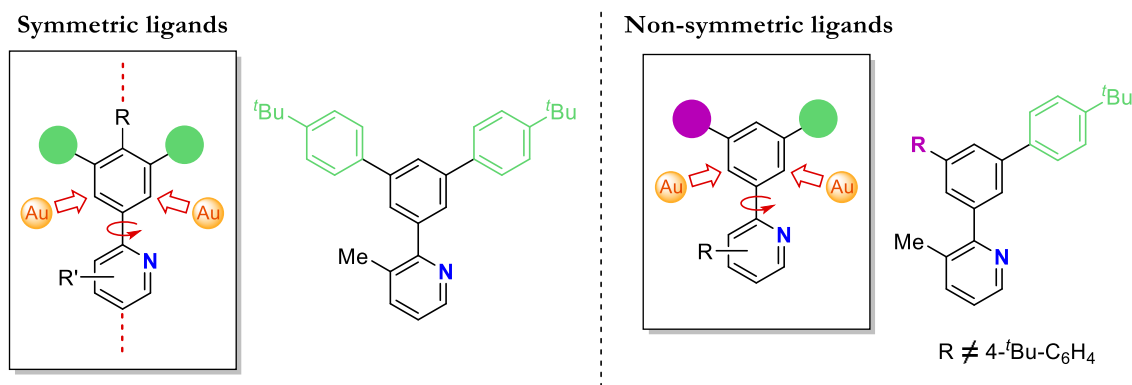


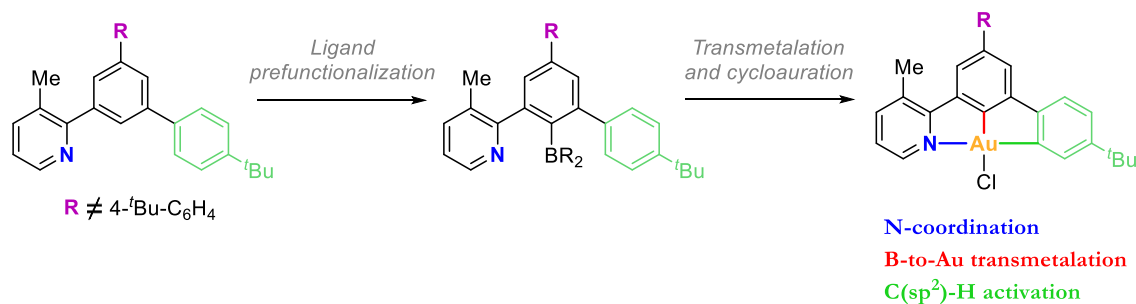
Figure V.12. Depiction of symmetric and non-symmetric ($\text{N}^{\wedge}\text{C}^{\wedge}\text{C}$) scaffolds.

In the context of seeking alternative approaches to the microwave-assisted cyclometalation, Nevado and coworkers reported in 2021 a new entry towards ($\text{N}^{\wedge}\text{C}^{\wedge}\text{C}$)-biscyclometalated gold(III) species, relying on the chelation-assisted oxidative addition of gold(I) into the $\text{C}(\text{sp}^3)\text{--}\text{C}(\text{sp}^3)$ bond of biphenylene.¹²³ The presence of a pyridine group in the biphenylene unit allowed the straightforward formation of the ensuing ($\text{N}^{\wedge}\text{C}^{\wedge}\text{C}$) complex (see Scheme I.29e). Although this strategy avoids the two C–H activation reactions, it is limited to a prefunctionalization of the biphenylene unit prior to the cyclometalation reaction, which can become a poorly versatile and tedious process to obtain non-symmetric ($\text{N}^{\wedge}\text{C}^{\wedge}\text{C}$) ligands.

Besides the group of Nevado, the groups of Yam and Breher also reported on the synthesis of ($\text{N}^{\wedge}\text{C}^{\wedge}\text{C}$)Au(III) complexes. On one hand, Yam accessed the complexes via mercury(II)-to-gold(III) transmetalation,¹²⁴ and Breher did it via tin(IV)-to-gold(III) transmetalation.¹²⁵ However, both approaches generate toxic waste and, therefore, can be considered unattractive alternative strategies to the microwave-assisted cyclometalation.

With all these precedents in mind, in collaboration with the group of Nevado, we envisioned that non-symmetric ($\text{N}^{\wedge}\text{C}^{\wedge}\text{C}$) scaffolds functionalized with a boronate group on the center ring might be suitable precursors to access non-symmetric biscyclometalated ($\text{N}^{\wedge}\text{C}^{\wedge}\text{C}$)Au(III) complexes via boron-to-gold transmetalation, N-coordination, and a $\text{C}(\text{sp}^3)\text{--}\text{H}$ activation (Scheme V.6). Plus, the installation of the boronate functionality would help driving the regioselectivity of the cyclometalation reaction. In fact, Flower and coworkers reported in

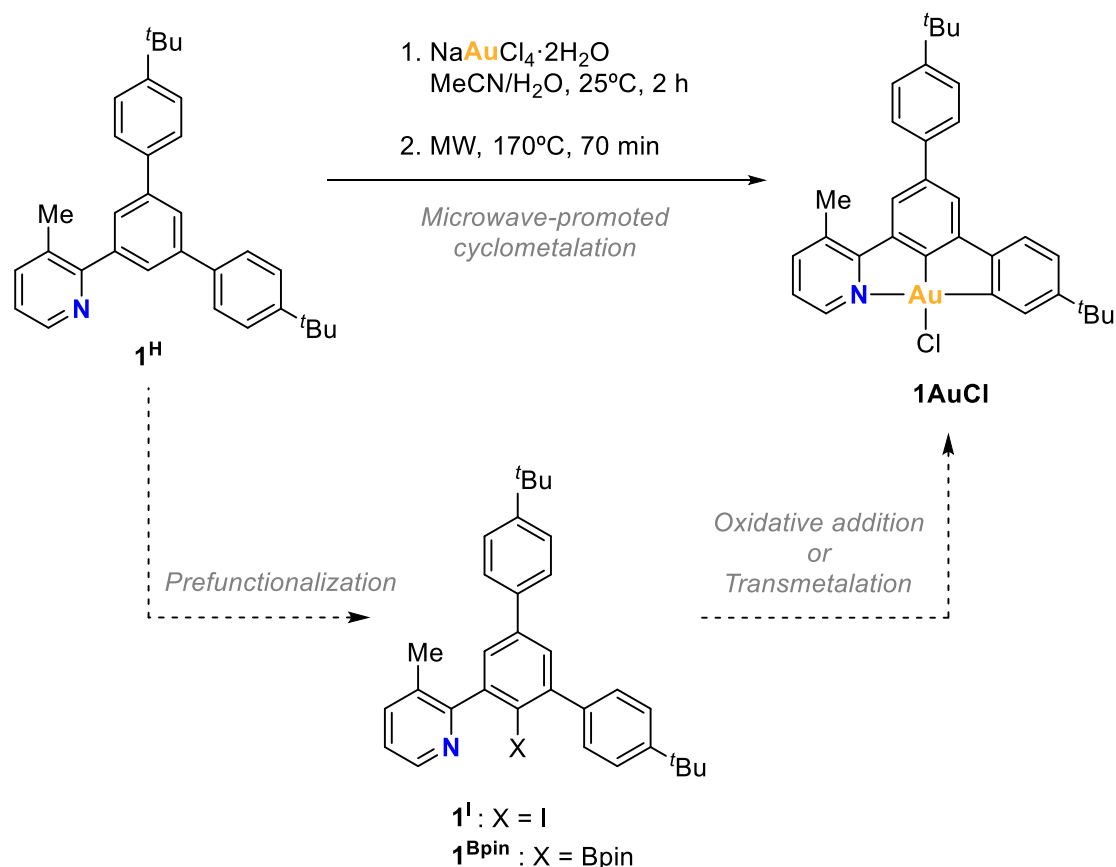
2011 the first example of the formation of gold(III) complexes by transmetalation from boroxines, where a N-coordination also took place to render (N[^]C) cyclometalated gold(III) complexes.¹²⁶ Thus, the objective of our project was to design a synthetic route towards the borylated precursors and test the boron-to-gold transmetalation (Scheme V.6).



Scheme V.6. Envisioned synthetic protocol to access non-symmetric (N[^]C[^]C)Au(III) complexes.

V.3.1. Functionalization studies with a symmetric (N[^]C[^]C) scaffold

Before moving to the synthesis of non-symmetric platforms, we employed the previously reported and widely used **1^H** (N[^]C[^]C) architecture^{76, 79, 120-122} to explore two different ligand functionalization methods that might allow the access to (N[^]C[^]C)Au(III) complex **1AuCl** by alternative routes to the microwave-promoted C(sp²)-H activation (Scheme V.7). On one hand, we aimed to test the metalation by C(sp²)-I oxidative addition of Au(I) to a pre-iodinated (N[^]C[^]C) platform **1^I**, and on the other hand, we aimed to test the metalation by boron-to-gold(III) transmetalation with an arylboronic ester (N[^]C[^]C) platform **1^{Bpin}** (Scheme V.7).



Scheme V.7. Alternative approaches to the already reported microwave-assisted C(sp²)–H activation to access the symmetric (N[^]C[^]C)Au(III) complex **1AuCl**.

Product **1^H** was synthesized following the literature procedure.⁷⁹ The synthesis of products **1^I** and **1^{Bpin}** was achieved from **1^H** through product **1^{Br}** (Figure V.13). A first bromination reaction was done to generate a versatile synthon (**1^{Br}**) that could lead to different further functionalizations. The reaction conditions for the bromination reaction were modified from reported procedures,¹²⁷ and relied on the Cu-assisted pyridine-*ortho*-directed C(sp²)–H bromination of substrates. Following this strategy, the corresponding di-brominated product that could potentially be formed was not detected, and the desired mono-brominated product **1^{Br}** was obtained in 82% yield (Figure V.13).

From **1^{Br}**, compound **1^I** was obtained in 63% yield upon Cu-catalyzed halide exchange reaction (Figure V.13).^{128, 129} Interestingly, the carbon atom in C(sp²)–X bond (X = Br, I) was diagnostic to identify the formation of **1^I** from **1^{Br}** by ¹³C{¹H} NMR, as the corresponding signal shifted from 121.5 ppm in **1^{Br}** to 100.6 ppm in **1^I** (spectra recorded in CDCl₃ at 298 K). On the other hand, compound **1^{Bpin}** was obtained by reacting **1^{Br}** with *n*BuLi in THF at low temperature to lithiate the targeted position, followed by the addition of ^tPrOBpin. Product **1^{Bpin}** was obtained in 63% yield, and its identity was confirmed by X-ray diffraction

analysis. The crystal structure revealed a dative bond between the nitrogen atom and the boron atom (Figure V.13). Although intramolecular directed C(sp²)-H borylation reactions are well studied,^{130, 131} we did not attempt the pyridine-directed borylation straight from compound **1^H**.

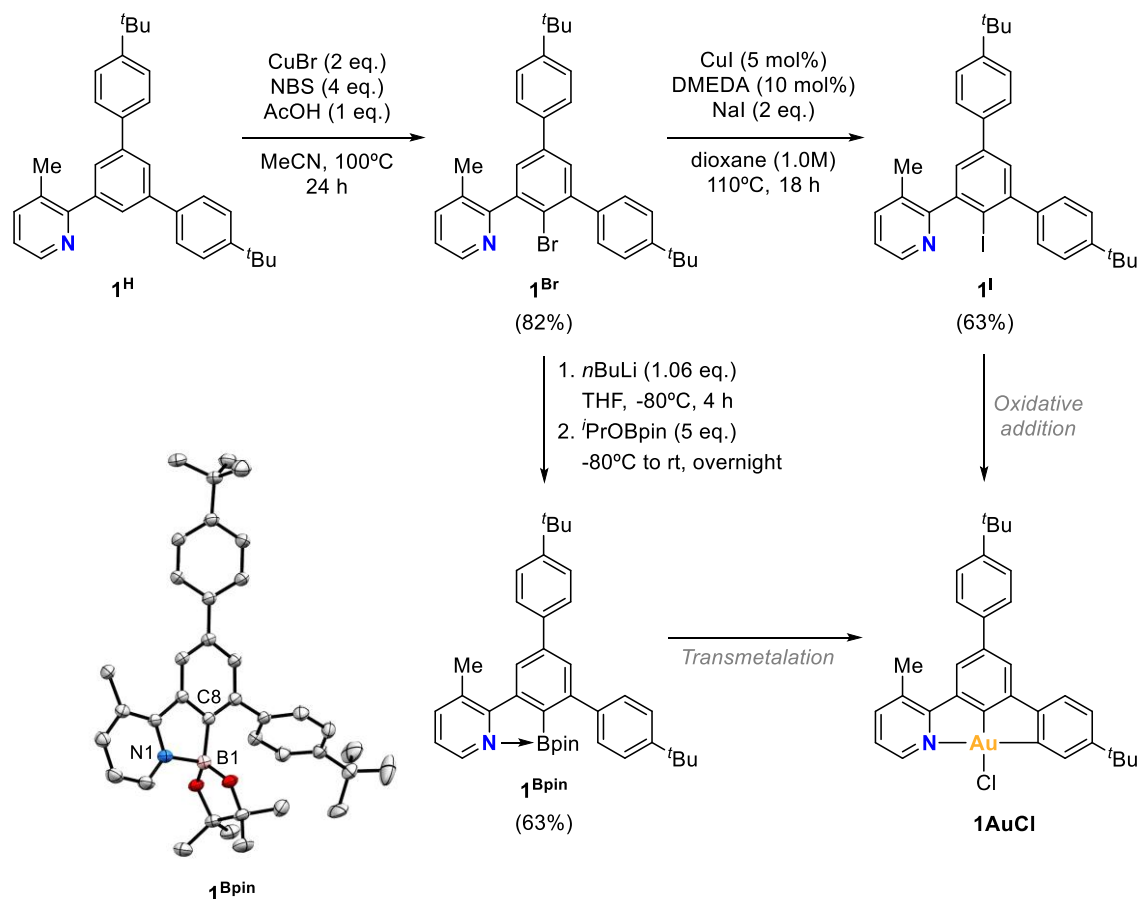
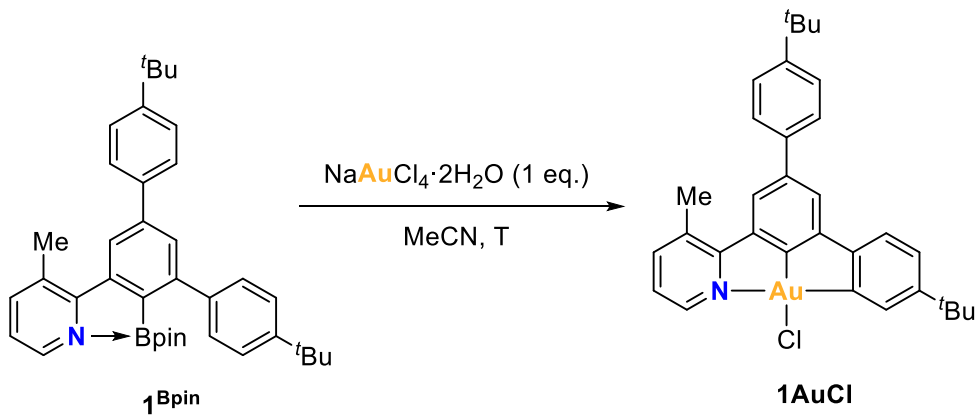


Figure V.13. Synthesis of compounds **1^I** and **1^{Bpin}** from **1^H** as ligand precursors to access complex **1AuCl**, and crystal structure of **1^{Bpin}** (ellipsoids set at 50% probability and H atoms removed for clarity). Selected bond distances (Å): C8–B1 1.625(3), N1–B1 1.728(3).

Next, we aimed to obtain complex **1AuCl** from **1^I** and **1^{Bpin}**. When we attempted the oxidative addition using **1^I**, we screened AuI and [Au(DMS)Cl] as the gold source in different solvents, heating at different temperatures, up to 140°C, overnight. In some cases, decomposition to Au(0) was observed, and the best results were obtained from the reaction with [Au(DMS)Cl] in toluene at 140°C, as complex **1AuCl** was obtained in a low 24% isolated yield. Thus, we explored the transmetalation approach from **1^{Bpin}** (Table V.5).

Table V.5. Reaction conditions for the transmetalation of **1^{Bpin}** towards **1AuCl**.


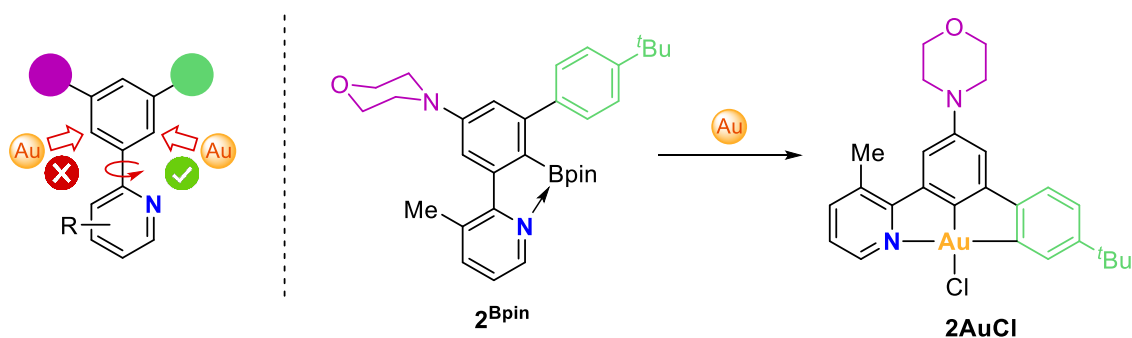
Entry	T (°C)	[1^{Bpin}] (M)	NMR yield (%)
1^a	90	0.06	46
2^b	100	0.06	65
3	120	0.06	51
4^c	120	0.10	49
5^c	120	0.20	54
6^d	120	0.06	63

General reaction conditions: **1^{Bpin}** (1 eq.), NaAuCl₄·2H₂O (1 eq.), overnight, V = 0.35 mL. Reaction run in a 3-mL Schlenk. NMR yields of **1AuCl** obtained using mesitylene as internal standard. ^aReflux, V = 1 mL. ^bReaction run in a sealed vial. ^ct = 24h. ^dLutidine (2 eq.) added as a base.

When **1^{Bpin}** was reacted with NaAuCl₄·2H₂O under reflux (entry 1), complex **1AuCl** was obtained in 46% yield. When the reactions were performed in a sealed vial or in a Schlenk (entries 2–5), complex **1AuCl** was obtained in moderate yields (49–65%) and the role of the concentration had no impact. Interestingly, when two equivalents of lutidine were added as a base (entry 6), the yield of the reaction increased slightly (63%). We suggested that the presence of base could help assisting the C(sp²)-H activation step. The transmetalation approach provided better results than the oxidative addition approach, encouraging us to test the viability of B-to-Au transmetalation in non-symmetric (N[^]C[^]C) systems.

V.3.2. Functionalization studies with a non-symmetric ($N^{\wedge}C^{\wedge}C$) scaffold

Having seen that complex **1AuCl** could be formed from ligand precursor **1^{Bpin}**, we aimed to transfer this reactivity to non-symmetric scaffolds. To this end, we envisioned compound **2^{Bpin}** as an interesting non-symmetric ($N^{\wedge}C^{\wedge}C$) platform to be metalated, as the electron-donating morpholine substituent in *para* to gold would stabilize the electron-deficient gold(III) center in **2AuCl**. However, the synthesis of **2^{Bpin}** should consider that the targeted borylated position must be that in *para* to morpholine and *ortho* to 4-*t*Bu-C₆H₄ substituent in order to get a ($N^{\wedge}C^{\wedge}C$)Au(III) complex (Scheme V.8). Otherwise, a borylated position in *para* to 4-*t*Bu-C₆H₄ substituent and *ortho* to morpholine would not give a ($N^{\wedge}C^{\wedge}C$)Au(III) complex. This consideration was not taken into account when synthesizing the symmetric **1^{Bpin}** from **1^H** because the pyridine-directed bromination would brominate equivalent positions.



Scheme V.8. Envisioned non-symmetric borylated ligand precursor (**2^{Bpin}**) and the corresponding ($N^{\wedge}C^{\wedge}C$)Au(III) target complex **2AuCl**.

The synthetic route is depicted in Figure V.14. Starting with 2-bromo-3-methylpyridine, two consecutive Suzuki couplings were performed to obtain 2-(4'-(*tert*-butyl)-5-chloro-[1,1'-biphenyl]-3-yl)-3-methylpyridine. Then, it was reacted with morpholine to create a C(sp²)-N bond through a Buchwald-Hartwig coupling, yielding the desired non-symmetric ($N^{\wedge}C^{\wedge}C$) scaffold **2^H**. Interestingly, ¹H NMR revealed that the proton signals of the morpholine appeared as two multiplets at 3.89 ppm and 3.27 ppm, integrating 4 protons each. Also, the proton sitting in the position to be further functionalized appeared as a singlet at 7.21 ppm (spectrum recorded in CDCl₃ at 298 K).

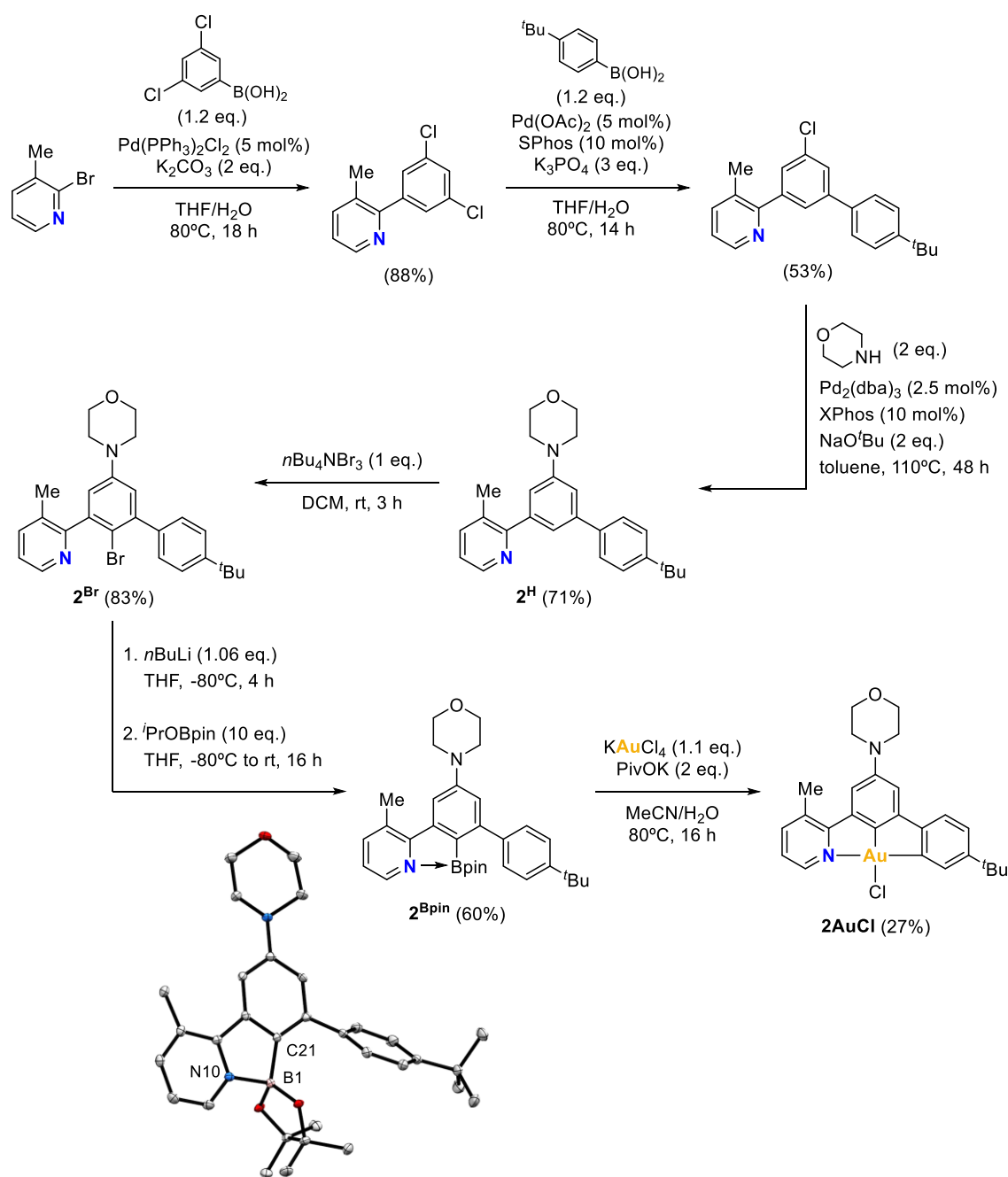
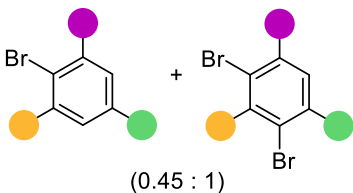
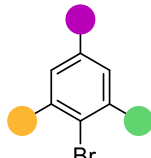


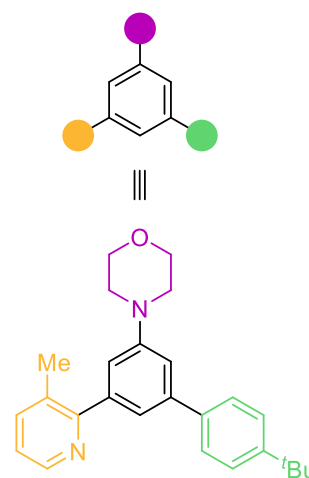
Figure V.14. Synthesis of compound **2^{Bpin}** and complex **2^{AuCl}**, and crystal structure of **2^{Bpin}** (ellipsoids set at 50% probability and H atoms removed for clarity). Selected bond distances (Å): C21–B1 1.642(2), N10–B1 1.689(2).

In order to brominate **2^H** in the desired position, different approaches were carried out (Table V.6). First, we tested the same conditions as in the bromination of **1^H** (entry 1). In this case, however, the pyridine-directed Cu-mediated bromination yielded an intractable messy outcome. MS-ESI of the crude revealed the presence of mono- and di-brominated products, among many other species, and NMR indeed confirmed the obtention of a complicated

mixture of species. Therefore, we moved on trying other bromination strategies. We tested the reaction conditions reported by Crousse and coworkers to obtain regioselective mono-brominated arenes using one equivalent of NBS in HFIP at room temperature (entry 2).¹³² Surprisingly, the reaction was so clean that only two products were detected by means of NMR and MS-ESI, corresponding to a mono-brominated product and a di-brominated product. ¹H and 2D NMR experiments let us determine the nature of both species (entry 2), obtained in a (mono : di = 0.45 : 1) ratio. However, the target product **2^{Br}** was not formed. Next, we applied the reaction conditions that Power and coworkers used to selectively brominate a similar scaffold to **2^H** (entry 3).⁵⁸ By using 5-pyrrolidino-*m*-terphenyl, the authors brominated only the *para* position to the N-donating pyrrolidinyl substituent. To our delight, the same reactivity could be transferred to our system **2^H** to provide exclusively product **2^{Br}**, which was obtained in 83% yield without needing chromatographic techniques for its purification.

Table V.6. Reaction conditions applied to compound **2^H** seeking the bromination towards compound **2^{Br}**.

Entry	Reaction conditions	Outcome
1	NBS (4 eq.) CuBr (2 eq.) AcOH (1 eq.) MeCN N ₂ , 100°C, overnight	Messy mixture
2	NBS (1 eq.) HFIP under air, rt, 3 h	 (0.45 : 1)
3	<i>n</i> Bu ₄ NBr ₃ (1 eq.) DCM under air, rt, 3 h	



In contrast, product **1^H** was not brominated to **1^{Br}** using TBABr₃, and all **1^H** was recovered, evidencing that systems **1^H** and **2^H** present different reactivity and that the presence of a *para* N-donor substituent is key for the bromination to proceed. Indeed, the bromination of compound **2^H** relied on electronics whereas, conversely, compound **1^H** relied on the pyridine coordination to copper to drive the bromination to the desired position.

The borylation step to produce **2^{Bpin}** from **2^{Br}** was done under the same conditions as the borylation of **1^{Br}**. Product **2^{Bpin}** was isolated in 60% yield as a yellow solid and suitable crystals for X-ray diffraction analysis were obtained. The crystal structure revealed, like in **1^{Bpin}**, a dative bond between the nitrogen atom and the boron atom (Figure V.14). Interestingly, compound **2^{Bpin}** emits fluorescence under irradiation at $\lambda = 365$ nm.

For the transmetalation step we employed KAuCl₄ as the gold(III) source. The attempts we carried out were all performed in a MeCN/water mixture and heating at 60°C or 80°C. When KAuCl₄ was reacted alone with **2^{Bpin}**, compound **2^H** was mainly obtained along with other byproducts, as detected by NMR and MS-ESI. Then, we ran the reaction in presence of a base to assist the C(sp²)-H activation step of the biscyclometalation. By using 2,6-di-*tert*-butylpyridine or K₂CO₃, the expected **2AuCl** was not detected, and in the case of using K₂CO₃, decomposition to Au(0) was observed. However, when we reacted **2^{Bpin}** with one equivalent of KAuCl₄ and two equivalents of potassium pivalate in MeCN/water at 80°C for 16 hours, we detected the formation of the expected complex (Figure V.14). We could isolate in 27% yield a yellow solid that emitted orange fluorescence under irradiation at $\lambda = 365$ nm whose NMR and HRMS-ESI data were in agreement with complex **2AuCl**.

To summarize, we first employed the widely used (N[^]C[^]C) scaffold **1^H** to functionalize it and demonstrate that complex **1AuCl** could be obtained by means of an alternative strategy to the standard microwave-assisted C(sp²)-H activation. Therefore, we synthesized compounds **1^I** and **1^{Bpin}**. Although the oxidative addition from **1^I** barely worked out, the transmetalation from **1^{Bpin}** led to complex **1AuCl** in moderate yields. This served as a proof-of-concept that biscyclometalated gold(III) complexes can be obtained through the envisioned mechanism involving a boron-to-gold(III) transmetalation, N-coordination, and a C(sp²)-H activation. With these results in hand, we designed a borylated non-symmetric (N[^]C[^]C) scaffold, **2^{Bpin}**, from which we could obtain complex **2AuCl** via boron-to-gold transmetalation. Hence, we demonstrated that, by prefunctionalizing the ligand precursor, it is possible to access non-symmetric (N[^]C[^]C) gold(III) complexes, thereby overcoming the microwave limitations.

V.4. REFERENCES

1. A. Zeineddine, L. Estévez, S. Mallet-Ladeira, K. Miqueu, A. Amgoune and D. Bourissou, *Nat. Commun.*, 2017, **8**, 565.
2. J. Rodriguez, A. Zeineddine, E. D. Sosa Carrizo, K. Miqueu, N. Saffon-Merceron, A. Amgoune and D. Bourissou, *Chem. Sci.*, 2019, **10**, 7183-7192.
3. M. O. Akram, A. Das, I. Chakrabarty and N. T. Patil, *Org. Lett.*, 2019, **21**, 8101-8105.
4. J. Rodriguez, N. Adet, N. Saffon-Merceron and D. Bourissou, *Chem. Commun.*, 2020, **56**, 94-97.
5. M. Rigoulet, O. Thillaye du Boullay, A. Amgoune and D. Bourissou, *Angew. Chem. Int. Ed.*, 2020, **59**, 16625-16630.
6. A. G. Tathe, C. C. Chintawar, V. W. Bhojare and N. T. Patil, *Chem. Commun.*, 2020, **56**, 9304-9307.
7. S. Zhang, C. Wang, X. Ye and X. Shi, *Angew. Chem. Int. Ed.*, 2020, **59**, 20470-20474.
8. C. C. Chintawar, A. K. Yadav and N. T. Patil, *Angew. Chem. Int. Ed.*, 2020, **59**, 11808-11813.
9. A. G. Tathe, Urvashi, A. K. Yadav, C. C. Chintawar and N. T. Patil, *ACS Catal.*, 2021, **11**, 4576-4582.
10. J. Rodriguez, A. Tabey, S. Mallet-Ladeira and D. Bourissou, *Chem. Sci.*, 2021, **12**, 7706-7712.
11. J. Rodriguez, D. Vesseur, A. Tabey, S. Mallet-Ladeira, K. Miqueu and D. Bourissou, *ACS Catal.*, 2022, **12**, 993-1003.
12. S. R. Mudshinge, Y. Yang, B. Xu, G. B. Hammond and Z. Lu, *Angew. Chem. Int. Ed.*, 2022, **61**, e202115687.
13. A. G. Tathe and N. T. Patil, *Org. Lett.*, 2022, **24**, 4459-4463.
14. A. Das and N. T. Patil, *ACS Catal.*, 2023, 3847-3853.
15. G. Chen and B. Xu, *ACS Catal.*, 2023, **13**, 1823-1829.
16. A. Kumar, A. Das and N. T. Patil, *Org. Lett.*, 2023.
17. V. W. Bhojare, E. D. Sosa Carrizo, C. C. Chintawar, V. Gandon and N. T. Patil, *J. Am. Chem. Soc.*, 2023.
18. J. Chu, D. Munz, R. Jazzar, M. Melaimi and G. Bertrand, *J. Am. Chem. Soc.*, 2016, **138**, 7884-7887.
19. M. Navarro, A. Tabey, G. Szalóki, S. Mallet-Ladeira and D. Bourissou, *Organometallics*, 2021, **40**, 1571-1576.
20. J. Bouffard, B. K. Keitz, R. Tonner, G. Guisado-Barrios, G. Frenking, R. H. Grubbs and G. Bertrand, *Organometallics*, 2011, **30**, 2617-2627.
21. G. Guisado-Barrios, M. Soleilhavoup and G. Bertrand, *Acc. Chem. Res.*, 2018, **51**, 3236-3244.
22. L. Huang, F. Rominger, M. Rudolph and A. S. K. Hashmi, *Chem. Commun.*, 2016, **52**, 6435-6438.
23. J. Lorkowski, P. Žak, M. Kubicki, C. Pietraszuk, D. Jędrzkiewicz and J. Ejfler, *New J. Chem.*, 2018, **42**, 10134-10141.
24. C. M. Crudden and D. P. Allen, *Coord. Chem. Rev.*, 2004, **248**, 2247-2273.
25. K. J. Cavell and A. T. Normand, in *N-Heterocyclic Carbenes in Transition Metal Catalysis and Organocatalysis*, ed. C. S. J. Cazin, Springer, Dordrecht, 2010, vol. 32, pp. 299-314.
26. B. Dong, H. Peng, S. E. Motika and X. Shi, *Chem. Eur. J.*, 2017, **23**, 11093-11099.
27. M. Joost, A. Zeineddine, L. Estévez, S. Mallet-Ladeira, K. Miqueu, A. Amgoune and D. Bourissou, *J. Am. Chem. Soc.*, 2014, **136**, 14654-14657.
28. M. J. Harper, C. J. Arthur, J. Crosby, E. J. Emmett, R. L. Falconer, A. J. Fensham-Smith, P. J. Gates, T. Leman, J. E. McGrady, J. F. Bower and C. A. Russell, *J. Am. Chem. Soc.*, 2018, **140**, 4440-4445.

29. P. Gao, J. Xu, T. Zhou, Y. Liu, E. Bisz, B. Dziuk, R. Lalancette, R. Szostak, D. Zhang and M. Szostak, *Angew. Chem. Int. Ed.*, 2023, **62**, e202218427.
30. S. C. Scott, J. A. Cadge, G. Boden, J. Bower and C. A. Russell, *Angew. Chem. Int. Ed.*, 2023, e202301526.
31. C. Hemmert and H. Gornitzka, *Dalton Trans.*, 2016, **45**, 440-447.
32. M. G. Karaaslan, A. Aktaş, C. Gürses, Y. Gök and B. Ateş, *Bioorg. Chem.*, 2020, **95**, 103552.
33. M. Mora, M. C. Gimeno and R. Visbal, *Chem. Soc. Rev.*, 2019, **48**, 447-462.
34. Y. Long, B. Cao, X. Xiong, A. S. C. Chan, R. W.-Y. Sun and T. Zou, *Angew. Chem. Int. Ed.*, 2021, **60**, 4133-4141.
35. M. Porchia, M. Pelli, M. Marinelli, F. Tisato, F. Del Bello and C. Santini, *Eur. J. Med. Chem.*, 2018, **146**, 709-746.
36. Q. Zhao, G. Meng, S. P. Nolan and M. Szostak, *Chem. Rev.*, 2020, **120**, 1981-2048.
37. A. Collado, D. J. Nelson and S. P. Nolan, *Chem. Rev.*, 2021, **121**, 8559-8612.
38. G. C. Fortman and S. P. Nolan, *Chem. Soc. Rev.*, 2011, **40**, 5151-5169.
39. E. Peris, *Chem. Rev.*, 2018, **118**, 9988-10031.
40. A. A. Danopoulos, T. Simler and P. Braunstein, *Chem. Rev.*, 2019, **119**, 3730-3961.
41. G. C. Vougioukalakis and R. H. Grubbs, *Chem. Rev.*, 2010, **110**, 1746-1787.
42. V. M. Chernyshev, E. A. Denisova, D. B. Eremin and V. P. Ananikov, *Chem. Sci.*, 2020, **11**, 6957-6977.
43. R. Dorel and A. M. Echavarren, *Chem. Rev.*, 2015, **115**, 9028-9072.
44. A. S. K. Hashmi, *Chem. Rev.*, 2007, **107**, 3180-3211.
45. V. M. Chernyshev, O. V. Khazipov, M. A. Shevchenko, A. Y. Chernenko, A. V. Astakhov, D. B. Eremin, D. V. Pasyukov, A. S. Kashin and V. P. Ananikov, *Chem. Sci.*, 2018, **9**, 5564-5577.
46. A. Petronilho, H. Müller-Bunz and M. Albrecht, *Chem. Commun.*, 2012, **48**, 6499-6501.
47. A. Nandy, T. Samanta, S. Mallick, P. Mitra, S. K. Seth, K. D. Saha, S. S. Al-Deyab and J. Dinda, *New J. Chem.*, 2016, **40**, 6289-6298.
48. R. M. Hough, C. R. M. Butt, S. M. Reddy and M. Verrall, *Aust. J. Earth Sci.*, 2007, **54**, 959-964.
49. C. Yue, H. Sun, W.-J. Liu, B. Guan, X. Deng, X. Zhang and P. Yang, *Angew. Chem. Int. Ed.*, 2017, **56**, 9331-9335.
50. L. Bütof, N. Wiesemann, M. Herzberg, M. Altzschner, A. Holleitner, F. Reith and D. H. Nies, *Metallomics*, 2018, **10**, 278-286.
51. F. Reith, S. L. Rogers, D. C. McPhail and D. Webb, *Science*, 2006, **313**, 233-236.
52. D. T. Sun, N. Gasilova, S. Yang, E. Oveisi and W. L. Queen, *J. Am. Chem. Soc.*, 2018, **140**, 16697-16703.
53. A. T. Papastavrou, M. Pauze, E. Gómez-Bengoia and G. C. Vougioukalakis, *ChemCatChem*, 2019, **11**, 5379-5386.
54. A. A. Liori, I. K. Stamatopoulos, A. T. Papastavrou, A. Pinaka and G. C. Vougioukalakis, *Eur. J. Org. Chem.*, 2018, **2018**, 6134-6139.
55. A. Collado, A. Gómez-Suárez, A. R. Martin, A. M. Z. Slawin and S. P. Nolan, *Chem. Commun.*, 2013, **49**, 5541-5543.
56. R. Visbal, A. Laguna and M. C. Gimeno, *Chem. Commun.*, 2013, **49**, 5642-5644.
57. K. S. K. Reddy, N. Narender, C. N. Rohitha and S. J. Kulkarni, *Synth. Commun.*, 2008, **38**, 3894-3902.
58. D. R. Manke, J. A. Golen, C. R. Stennett, M. Naeem, D. R. Javier-Jimenez and P. P. Power, *Polyhedron*, 2022, **222**, 115947.
59. R. A. Fernandes and P. Choudhary, *Chem. Asian J.*, 2022, **17**, e202200874.
60. D. R. Motati, D. Uredi and E. B. Watkins, *Chem. Sci.*, 2018, **9**, 1782-1788.

61. J. Chen, T. Wang, Y. Liu, T. Wang, A. Lin, H. Yao and J. Xu, *Org. Chem. Front.*, 2017, **4**, 622-626.
62. V. J. Catalano and A. L. Moore, *Inorg. Chem.*, 2005, **44**, 6558-6566.
63. P. Font, H. Valdés, G. Guisado-Barrios and X. Ribas, *Chem. Sci.*, 2022, **13**, 9351-9360.
64. W. Zeng, E. Wang, R. Qiu, M. Sohail, S. Wu and F.-X. Chen, *J. Organomet. Chem.*, 2013, **743**, 44-48.
65. E. Tomás-Mendivil, P. Y. Toullec, J. Borge, S. Conejero, V. Michelet and V. Cadierno, *ACS Catal.*, 2013, **3**, 3086-3098.
66. E. Tomás-Mendivil, P. Y. Toullec, J. Díez, S. Conejero, V. Michelet and V. Cadierno, *Org. Lett.*, 2012, **14**, 2520-2523.
67. Z. S. Ghavami, M. R. Anneser, F. Kaiser, P. J. Altmann, B. J. Hofmann, J. F. Schlagintweit, G. Grivani and F. E. Kühn, *Chem. Sci.*, 2018, **9**, 8307-8314.
68. Q. Shi, Z. Qin, H. Xu and G. Li, in *Nanomaterials*, 2019, vol. 9.
69. Z. Chen, R. Shen, C. Chen, J. Li and Y. Li, *Chem. Commun.*, 2018, **54**, 13155-13158.
70. M. Kidwai, V. Bansal, A. Kumar and S. Mozumdar, *Green Chem.*, 2007, **9**, 742-745.
71. Q. Li, A. Das, S. Wang, Y. Chen and R. Jin, *Chem. Commun.*, 2016, **52**, 14298-14301.
72. G. Kyriakou, S. K. Beaumont, S. M. Humphrey, C. Antonetti and R. M. Lambert, *ChemCatChem*, 2010, **2**, 1444-1449.
73. R. Kumar and C. Nevado, *Angew. Chem. Int. Ed.*, 2017, **56**, 1994-2015.
74. H. Schmidbaur and A. Schier, *Arab. J. Sci. Eng.*, 2012, **37**, 1187-1225.
75. D.-A. Roşca, J. A. Wright and M. Bochmann, *Dalton Trans.*, 2015, **44**, 20785-20807.
76. R. Kumar, J.-P. Krieger, E. Gómez-Bengoa, T. Fox, A. Linden and C. Nevado, *Angew. Chem. Int. Ed.*, 2017, **56**, 12862-12865.
77. M.-C. Tang, M.-Y. Chan and V. W.-W. Yam, *Chem. Rev.*, 2021, **121**, 7249-7279.
78. B. Bertrand, M. R. M. Williams and M. Bochmann, *Chem. Eur. J.*, 2018, **24**, 11840-11851.
79. R. Kumar, A. Linden and C. Nevado, *Angew. Chem. Int. Ed.*, 2015, **54**, 14287-14290.
80. C. Bronner and O. S. Wenger, *Dalton Trans.*, 2011, **40**, 12409-12420.
81. V. W.-W. Yam, K. M.-C. Wong, L.-L. Hung and N. Zhu, *Angew. Chem. Int. Ed.*, 2005, **44**, 3107-3110.
82. W.-P. To, G. S.-M. Tong, W. Lu, C. Ma, J. Liu, A. L.-F. Chow and C.-M. Che, *Angew. Chem. Int. Ed.*, 2012, **51**, 2654-2657.
83. D.-A. Roşca, D. A. Smith and M. Bochmann, *Chem. Commun.*, 2012, **48**, 7247-7249.
84. E. R. T. Tiekink, *Gold Bull.*, 2003, **36**, 117-124.
85. W. Henderson, in *Adv. Organomet. Chem.*, eds. R. West and A. F. Hill, Academic Press, 2006, vol. 54, pp. 207-265.
86. E. Langseth, C. H. Görbitz, R. H. Heyn and M. Tilset, *Organometallics*, 2012, **31**, 6567-6571.
87. V. K.-M. Au, K. M.-C. Wong, N. Zhu and V. W.-W. Yam, *Chem. Eur. J.*, 2011, **17**, 130-142.
88. J. Guenther, S. Mallet-Ladeira, L. Estevez, K. Miqueu, A. Amgoune and D. Bourissou, *J. Am. Chem. Soc.*, 2014, **136**, 1778-1781.
89. L. C. Wilkins, Y. Kim, E. D. Litle and F. P. Gabbaï, *Angew. Chem. Int. Ed.*, 2019, **58**, 18266-18270.
90. B. David, U. Monkowius, J. Rust, C. W. Lehmann, L. Hyzak and F. Mohr, *Dalton Trans.*, 2014, **43**, 11059-11066.
91. L. T. Ball, G. C. Lloyd-Jones and C. A. Russell, *J. Am. Chem. Soc.*, 2014, **136**, 254-264.
92. W.-P. To, D. Zhou, G. S. M. Tong, G. Cheng, C. Yang and C.-M. Che, *Angew. Chem. Int. Ed.*, 2017, **56**, 14036-14041.
93. G. Alesso, M. A. Cinellu, S. Stoccoro, A. Zucca, G. Minghetti, C. Manassero, S. Rizzato, O. Swang and M. K. Ghosh, *Dalton Trans.*, 2010, **39**, 10293-10304.

94. A. Herbst, C. Bronner, P. Dechambenoit and O. S. Wenger, *Organometallics*, 2013, **32**, 1807-1814.
95. V. K.-M. Au, W. H. Lam, W.-T. Wong and V. W.-W. Yam, *Inorg. Chem.*, 2012, **51**, 7537-7545.
96. C.-W. Chan, W.-T. Wong and C.-M. Che, *Inorg. Chem.*, 1994, **33**, 1266-1272.
97. M. A. Cinellu, A. Zucca, S. Stoccoro, G. Minghetti, M. Manassero and M. Sansoni, *J. Chem. Soc., Dalton Trans.*, 1996, 4217-4225.
98. M. S. Kharasch and H. S. Isbell, *J. Am. Chem. Soc.*, 1931, **53**, 3053-3059.
99. E. C. Constable and T. A. Leese, *J. Organomet. Chem.*, 1989, **363**, 419-424.
100. M. A. Cinellu, A. Zucca, S. Stoccoro, G. Minghetti, M. Manassero and M. Sansoni, *J. Chem. Soc., Dalton Trans.*, 1995, 2865-2872.
101. Y. Fuchita, H. Ieda and M. Yasutake, *J. Chem. Soc., Dalton Trans.*, 2000, 271-274.
102. R. V. Parish, J. P. Wright and R. G. Pritchard, *J. Organomet. Chem.*, 2000, **596**, 165-176.
103. Q. Wu, C. Du, Y. Huang, X. Liu, Z. Long, F. Song and J. You, *Chem. Sci.*, 2015, **6**, 288-293.
104. B. Y.-W. Wong, H.-L. Wong, Y.-C. Wong, V. K.-M. Au, M.-Y. Chan and V. W.-W. Yam, *Chem. Sci.*, 2017, **8**, 6936-6946.
105. K.-H. Wong, K.-K. Cheung, M. C.-W. Chan and C.-M. Che, *Organometallics*, 1998, **17**, 3505-3511.
106. W.-P. To, K. T. Chan, G. S. M. Tong, C. Ma, W.-M. Kwok, X. Guan, K.-H. Low and C.-M. Che, *Angew. Chem. Int. Ed.*, 2013, **52**, 6648-6652.
107. W.-P. To, G. S. M. Tong, C.-W. Cheung, C. Yang, D. Zhou and C.-M. Che, *Inorg. Chem.*, 2017, **56**, 5046-5059.
108. K. M.-C. Wong, L.-L. Hung, W. H. Lam, N. Zhu and V. W.-W. Yam, *J. Am. Chem. Soc.*, 2007, **129**, 4350-4365.
109. J. Fernandez-Cestau, B. Bertrand, M. Blaya, G. A. Jones, T. J. Penfold and M. Bochmann, *Chem. Commun.*, 2015, **51**, 16629-16632.
110. R. Usón, J. Vicente, J. A. Cirac and M. T. Chicote, *J. Organomet. Chem.*, 1980, **198**, 105-112.
111. K. T. Chan, G. S. M. Tong, Q. Wan, G. Cheng, C. Yang and C.-M. Che, *Chem. Asian J.*, 2017, **12**, 2104-2120.
112. A. P. Shaw, M. Tilset, R. H. Heyn and S. Jakobsen, *J. Coord. Chem.*, 2011, **64**, 38-47.
113. S. Witzel, M. S. M. Holmsen, M. Rudolph, M. C. Dietl, S. Øien-Ødegaard, F. Rominger, M. Tilset and A. S. K. Hashmi, *Organometallics*, 2020, **39**, 2830-2837.
114. M. S. M. Holmsen, A. Nova, K. Hylland, D. S. Wragg, S. Øien-Ødegaard, R. H. Heyn and M. Tilset, *Chem. Commun.*, 2018, **54**, 11104-11107.
115. K. T. Hylland, I. L. Schmidtke, D. S. Wragg, A. Nova and M. Tilset, *Dalton Trans.*, 2022, **51**, 5082-5097.
116. J. Martín, E. Gómez-Bengoa, A. Genoux and C. Nevado, *Angew. Chem. Int. Ed.*, 2022, **61**, e202116755.
117. D. Eppel, M. Rudolph, F. Rominger and A. S. K. Hashmi, *ChemSusChem*, 2020, **13**, 1986-1990.
118. D. Eppel, A. Eryiğit, M. Rudolph, M. Brückner, F. Rominger, A. M. Asiri and A. S. K. Hashmi, *Angew. Chem. Int. Ed.*, 2021, **60**, 13636-13640.
119. D. Eppel, P. Penert, J. Stemmer, C. Bauer, M. Rudolph, M. Brückner, F. Rominger and A. S. K. Hashmi, *Chem. Eur. J.*, 2021, **27**, 8673-8677.
120. H. Beucher, S. Kumar, E. Merino, W.-H. Hu, G. Stemmler, S. Cuesta-Galisteo, J. A. González, J. Jagielski, C.-J. Shih and C. Nevado, *Chem. Mater.*, 2020, **32**, 1605-1611.

121. H. Beucher, S. Kumar, R. Kumar, E. Merino, W.-H. Hu, G. Stemmler, S. Cuesta-Galisteo, J. A. González, L. Bezinge, J. Jagielski, C.-J. Shih and C. Nevado, *Chem. Eur. J.*, 2020, **26**, 17604-17612.
122. H. Beucher, E. Merino, A. Genoux, T. Fox and C. Nevado, *Angew. Chem. Int. Ed.*, 2019, **58**, 9064-9067.
123. H. Beucher, J. Schörghumer, E. Merino and C. Nevado, *Chem. Sci.*, 2021, **12**, 15084-15089.
124. W.-K. Kwok, M.-C. Tang, S.-L. Lai, W.-L. Cheung, L.-K. Li, M. Ng, M.-Y. Chan and V. W.-W. Yam, *Angew. Chem. Int. Ed.*, 2020, **59**, 9684-9692.
125. W. Feuerstein, C. Holzer, X. Gui, L. Neumeier, W. Klopffer and F. Breher, *Chem. Eur. J.*, 2020, **26**, 17156-17164.
126. G. A. Price, K. R. Flower, R. G. Pritchard, A. K. Brisdon and P. Quayle, *Dalton Trans.*, 2011, **40**, 11696-11697.
127. Z.-J. Du, L.-X. Gao, Y.-J. Lin and F.-S. Han, *ChemCatChem*, 2014, **6**, 123-126.
128. A. Klapars and S. L. Buchwald, *J. Am. Chem. Soc.*, 2002, **124**, 14844-14845.
129. J. Serra, T. Parella and X. Ribas, *Chem. Sci.*, 2017, **8**, 946-952.
130. S. A. Iqbal, J. Pahl, K. Yuan and M. J. Ingleson, *Chem. Soc. Rev.*, 2020, **49**, 4564-4591.
131. O. Sadek, A. Le Gac, N. Hidalgo, S. Mallet-Ladeira, K. Miqueu, G. Bouhadir and D. Bourissou, *Angew. Chem. Int. Ed.*, 2022, **61**, e202110102.
132. R.-J. Tang, T. Milcent and B. Crousse, *J. Org. Chem.*, 2018, **83**, 930-938.

CHAPTER VI. General conclusions

The field of homogeneous gold catalysis has been dominated by gold(I)-mediated transformations involving the Lewis-acidic activation of unsaturated organic substrates. However, in the last decade the field has also evolved to the development of oxidant-free Au(I)/Au(III) catalytic cycles in which gold(I) species convert to gold(III) intermediates through an oxidative addition step. This otherwise sluggish step can be promoted by different strategies, among which rational ligand design stands out. Indeed, the use of hemilabile (P[^]N) bidentate ligands has gained prominence in this regard, allowing access to a wide scope of gold-catalyzed cross-coupling reactions. Thus, in this thesis we endeavored further development of this burgeoning field by designing novel hemilabile (N[^]C) carbene-based bidentate ligands that would allow (N[^]C)gold(I) complexes to engage in Au(I)/Au(III) catalytic cycles. In fact, with this approach we intended to deal with an underexplored topic, thereby paving the way for future development of oxidant-free Au(I)/Au(III) catalysis employing hemilabile (N[^]C) ligands. In this context, we designed mesoionic carbene ligands and NHC ligands with pendant N-donor hemilabile groups. In the course of our investigations, however, unexpected findings were disclosed when using NHC–Au(I) complexes. The decomposition of such complexes into azolones and Au(0) nuggets in the presence of oxidants shifted our attention towards investigating this decomposition pathway, previously observed with other transition metals but not with gold.

Also, we wanted to contribute to the field of the synthesis of gold(III) complexes bearing pincer ligands, which have demonstrated to be gold species with remarkable potential applications in catalysis, material science, and medicinal chemistry. We focused on biscyclometalated (N[^]C[^]C)Au(III) systems because their standard preparation relies on a microwave-assisted metalation that is limited to symmetric (N[^]C[^]C) scaffolds. Therefore, we intended to seek green alternative synthetic approaches that would overcome this limitation by allowing access to non-symmetric (N[^]C[^]C)Au(III) complexes.

In Chapter III we describe the preparation of two gold(I) complexes (**2a** and **2b**) bearing hemilabile MIC[^]N ligands and their reactivity in oxidation, oxidative addition, and catalysis. The design of the MIC[^]N ligands allowed us to obtain the desired (N[^]C)-cyclometalated Au(III) complexes by 2 e⁻ oxidation using hypervalent iodine(III) oxidants, and by C(sp²)–C(sp²) oxidative addition of biphenylene, thereby proving the hemilabile character of the ligands. When we attempted the oxidative addition of C(sp²)–I bonds, we did not detect the resulting gold(III) complexes. Instead, we obtained organic products (**8a-R/8b-R** and **9a/9b**) that suggested that their formation should occur through C(sp²)–I oxidative addition followed by a reductive elimination step. Finally, we aimed to apply such reactivity in oxidant-

free gold-catalyzed cross-coupling reactions using complexes **2a** and **2b** as catalysts. By using aryl iodides and γ -alkenoic acids as coupling partners, we developed the gold-catalyzed arylation-lactonization of γ -alkenoic acids, the mechanism of which was proposed to operate through a Au(I)/Au(III) catalytic cycle that merges the oxidative addition of C(sp²)-I bonds with the π -activation intrinsic mode of reactivity of gold. Even though the catalytic approach afforded the products in low to moderate yields, the significance of these results relies on showing that hemilabile (N[^]C) ligands can be a real alternative to hemilabile (P[^]N) ligands. Hence, this can be considered a seminal work in the field of oxidant-free Au(I)/Au(III) cross-coupling catalysis using hemilabile (N[^]C) ligands that will help in the future development of more catalytically efficient hemilabile (N[^]C)Au(I) systems. This work is a proof-of-concept that ligand design is a useful tool to develop oxidant-free gold-catalyzed cross-coupling reactions by chelation assistance of the ligand, expanding beyond the already disclosed hemilabile (P[^]N) ligands. Indeed, gold complexes bearing hemilabile (N[^]C) rigid ligands have recently been revealed to have enhanced catalytic performance, compared to our work, in oxidant-free Au(I)/Au(III) cross-coupling reactions.

In Chapter IV we explore the reactivity of NHC–Au(I) complexes with oxidants to study the decomposition into azolones and Au(0) nuggets. In the context of developing hemilabile (N[^]C)Au(I) complexes, we also envisioned the use of NHC[^]N ligands. Thus, we synthesized and characterized novel NHC–Au(I) complexes **1–4**, with (**1–3**) and without (**4**) pendant coordinating groups. However, when we attempted to get (N[^]C)-cyclometalated Au(III) complexes by oxidation, we observed that when we employed iodosylbenzene-type oxidants the gold(I) complexes underwent a controlled decomposition pathway to afford azolones as the main organic product, concomitantly with conversion of the Au(I) contained in complexes into Au(0) nuggets (~0.4–0.5 mm). In contrast, commercial IPrAuCl and SIPrAuCl complexes were robust and remained intact after exposure to PhI(OAc)₂. The decomposition of complexes **1–4** questioned the believed general robustness of the NHC–Au bond and added complementary insight to previous studies on the decomposition of NHC–M complexes into azolones and M(0) (M = Ni(II), Pd(II), Pt(II), Cu(I)). This reactivity can be employed as a methodology to obtain Au(0) nuggets of high purity in one simple step from NHC–Au(I) complexes.

In Chapter V.3 we turned our attention to designing a novel synthetic methodology for (N[^]C[^]C)Au(III) pincer complexes, given that the standard microwave protocol to prepare them is limited to symmetric (N[^]C[^]C) scaffolds. In order to avoid harmful methodologies such as mercury or tin transmetalation, we envisioned that boron-to-gold transmetalation

would be a suitable strategy. Before using non-symmetric (N[^]C[^]C) platforms though, we tested our proposals with the symmetric scaffold **1^H**. We functionalized **1^H** to get products **1^I** and **1^{Bpin}** from which we tested the oxidative addition and the boron-to-gold transmetalation, respectively, as alternative routes towards the biscyclometalated (N[^]C[^]C)Au(III) complex **1AuCl**. The low yields of **1AuCl** from oxidative addition led us to dismiss this approach and implement the boron transmetalation approach in non-symmetric (N[^]C[^]C) platforms. As a non-symmetric (N[^]C[^]C) scaffold we used ligand precursor **2^{Bpin}**, which has a morpholine N-donor substituent in *para* position to the borylated position. The corresponding (N[^]C[^]C)Au(III) complex **2AuCl** could be obtained from **2^{Bpin}**, although in low yield. However, we demonstrated that, by pre-functionalizing the ligand precursor with a boronate group, it is possible to access non-symmetric biscyclometalated (N[^]C[^]C)Au(III) complexes upon boron-to-gold transmetalation, thereby overcoming the microwave limitations. This work is a first step in seeking a general synthetic method for the preparation of biscyclometalated (N[^]C[^]C)Au(III) complexes. Hopefully, it is an ongoing study that will eventually shed light, or at least provide knowledge, on general and greener synthetic alternatives to access a variety of novel pincer gold complexes, demonstrating that there is room for improvement in terms of overcoming current synthetic limitations while avoiding harmful protocols.

ANNEX. Supporting information

ANNEX 1. Fundamental Basis for Implementing Oxidant-Free Au(I)/Au(III) Catalysis

This chapter corresponds to the following publication:

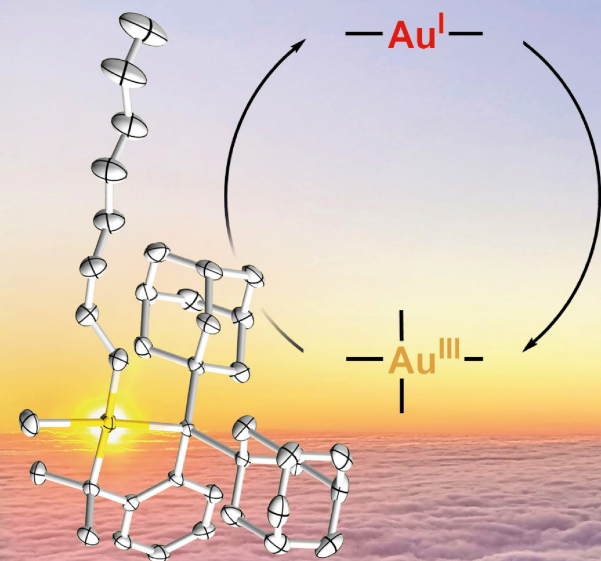
Pau Font, Xavi Ribas*. Reprinted with permission from *Eur. J. Inorg. Chem.* **2021**, 2556 – 2569.

Front Cover:*P. Font and X. Ribas*

Fundamental Basis for Implementing Oxidant-Free Au(I)/Au(III) Catalysis

IT'S GOLDEN HOUR!

-In search of new horizons in gold catalysis-



The Front Cover shows the first sunrise of 2020, spotted from the sanctuary of Rocacorba, built at the top of a cliff on the Rocacorba mountain range (Girona). That New Year's "golden hour" awakened amazement, reflection, and future projection, as this Minireview also intends to. The X-ray structure of a gold complex bearing the MeDalphos ligand highlights the employment of this ligand as an efficient state-of-the-art strategy to develop oxidant-free Au(I)/Au(III) cross-coupling catalysis.

VIP Very Important Paper

Fundamental Basis for Implementing Oxidant-Free Au(I)/Au(III) Catalysis

Pau Font^[a] and Xavi Ribas^{*[a]}

Oxidant-free Au(I)/Au(III) catalysis can still be regarded as a young and promising chemistry. Because the first examples of gold catalysis were limited to the activation and functionalization of π -C–C bonds and very little was known on fundamental organometallic transformations at gold, countless works during the past 15 years have been devoted to disclosing the elementary reactivity of gold and implementing it in catalysis. Remarkably, great emphasis on triggering oxidative addition at Au(I) has been placed, as the high redox potential of the Au(I)/Au(III) pair disfavors this reaction. In fact, different strategies

such as strain release, ligand design and photochemistry have been proven successful at allowing the bottleneck oxidative addition to occur. These approaches have led to the rational development of oxidant-free Au(I)/Au(III) redox catalysis, particularly catalytic cycles in cross-coupling transformations where oxidative addition is usually the entry point to the cycle. Herein, the background story, the development process, and relevant examples of oxidant-free gold-catalyzed cross-coupling reactions are reviewed.

1. The Early Years of Homogeneous Gold Catalysis

The field of homogeneous gold chemistry has experienced a large development the past 25 years, from the late 90's until present. Gold had previously been regarded as a chemically inert metal due to its remarkable air and moisture stability and because scarce examples of gold-mediated transformations were known by that time.^[1] Thus, the disclosure by the end of the 20th century of the so-called π -activation chemistry, in which gold complexes reacted as carbophilic Lewis acids capable of activating π -C–C bonds of alkenes, alkynes and allenes toward nucleophilic attacks, was a breakthrough in gold chemistry (Figure 1).^[2] Since then, huge research efforts were devoted to exploit this chemistry, emerging as a very useful method for organic synthesis, as new C–heteroatom and C–C bond couplings could be selectively formed by means of homogeneous catalysis under mild conditions.

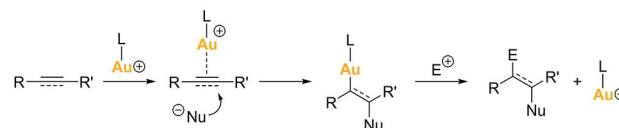


Figure 1. General scheme of gold-catalyzed π -activation and functionalization of multiple C–C bonds.

1.1. Redox-Neutral Gold Catalysis: π -Activation of C–C Multiple Bonds

In π -activation, the oxidation state of the gold center does not change throughout the process, fact that stands in stark contrast to well-known cross-couplings catalyzed by other late transition metals. Typically, Au(I) complexes or Au(III) salts are employed as catalysts. Among the wide literature on gold-mediated activation and functionalization of C–C multiple π -bonds, some works can be highlighted as examples to illustrate the vast variety of transformations that can be achieved.^[2–3] In this line, additions of O- and N-nucleophiles to alkynes,^[4] hydroamination of alkynes, allenes and alkenes (Figure 2a),^[5] cyclization of allenyl ketones, α,β -unsaturated ketones and alcohols,^[6] intermolecular addition of phenols and carboxylates to terminal alkenes (Figure 2b),^[7] and intramolecular rearrangements (Figure 2c),^[8] among other transformations, were demonstrated to afford the corresponding products through the above-described general gold-catalyzed π -activation mechanism.

1.2. Au(I)/Au(III)-Catalyzed Oxidative Couplings

Transition-metal-catalyzed cross-coupling transformations are usually based on catalytic cycles that comprise the interconver-

[a] P. Font, Dr. X. Ribas
QBIS-CAT group, Institut de Química Computacional i Catalàlisi (IQCC) and Departament de Química,
Universitat de Girona,
Campus Montilivi, Girona, 17003, Catalonia, Spain
E-mail: xavi.ribas@udg.edu
http://iqcc.udg.edu/

Part of the "RSEQ-GEQO Prize Winners" Special Collection.

© 2021 The Authors. European Journal of Inorganic Chemistry published by Wiley-VCH GmbH. This is an open access article under the terms of the Creative Commons Attribution Non-Commercial NoDerivs License, which permits use and distribution in any medium, provided the original work is properly cited, the use is non-commercial and no modifications or adaptations are made.

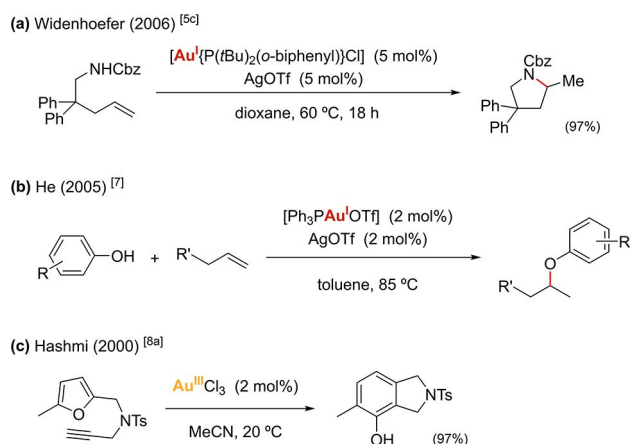


Figure 2. (a) Gold-catalyzed intramolecular hydroamination of a terminal olefin. (b) Gold-catalyzed intermolecular addition of phenols to olefins. (c) Gold-catalyzed intramolecular cycloisomerization of a furan with a terminal alkyne moiety.

sion between different oxidation states of the metallic atom which is generally achieved via two-electron redox steps, namely oxidative addition and reductive elimination.^[9] Palladium has typically been the metal of choice for catalyzing a vast array of cross-coupling transformations, therefore countless Pd(0)/Pd(II)^[10] and Pd(II)/Pd(IV)^[11] catalytic cycles have been reported to be the operating mechanisms in Pd-mediated couplings. Nevertheless, many other transition metals have also shown to be good candidates as catalysts in cross-coupling transformations. Thus, examples of Ni(0)/Ni(II)-,^[12] Ni(I)/Ni(III)-,^[13] Ni(II)/Ni(IV)-,^[14] Co(I)/Co(III)-,^[15] Cu(I)/Cu(III)-^[16] and Au(I)/Au(III)-catalyzed cross-couplings can be found out there in the literature, among others. The case of gold, however, can be regarded as special since, due to its strong relativistic effects,^[17] the Au(I)/Au(III) pair features an unusual high redox potential ($E^0 = 1.41$ V vs. SHE in water) compared to that of the isoelectronic Pd(0)/Pd(II) pair ($E^0 = 0.92$ V).^[18] This peculiarity is precisely what makes Au(I) especially reluctant to oxidative addition^[19] so, in order to build Au(I)/Au(III) catalytic cycles, stoichiometric amounts of external oxidants have traditionally been employed to promote, via a 2-electron oxidation instead of oxidative addition, the formation of the envisioned key Au(III) intermediates (Figure 3) Typical sacrificial oxidants are F^+ donors, such as Selectfluor or N-Fluorobenzenesulfonimide (NFSI), and hypervalent iodine reagents. Following this strategy, a wide

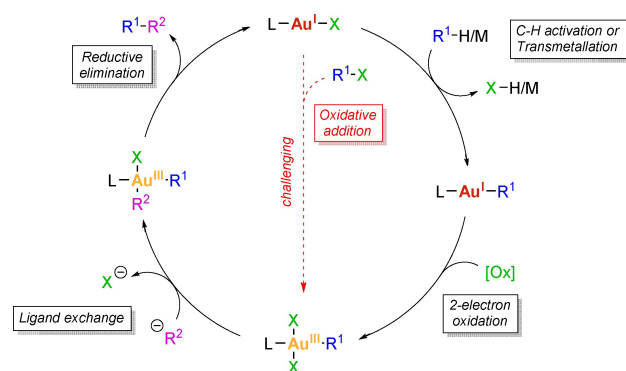


Figure 3. Mechanistic proposal for Au(I)/Au(III)-catalyzed oxidative cross-coupling reactions.

assortment of Au(I)/Au(III)-catalyzed oxidative couplings exists,^[3b,20] including C–C and C–X couplings at alkenes, allenes, alkynes and arenes. In 2008, Tse and coworkers published the first gold-catalyzed C–C coupling to yield biaryls, using 2 mol% HAuCl₄ and PhI(OAc)₂ as a sacrificial oxidant.^[21] In 2009, Zhang and coworkers used propargylic acetates to develop the corresponding Au(I)/Au(III)-catalyzed oxidative dimerization as well as the oxidative coupling with arylboronic acids.^[22] In both transformations, the Au(III) intermediate species were proposed to be formed from the Selectfluor-promoted oxidation of the corresponding Au(I) species.

From 2010 to 2012, several research groups reported independently numerous studies on gold-catalyzed oxy- and aminoarylation reactions at olefins (Figure 4). Russell and Lloyd-Jones employed arylsilanes as coupling fragments in two- and three-component gold-catalyzed oxyarylation of terminal alkenes.^[23] In this work, the use of Selectfluor not only allowed the access to a Au(I)/Au(III) catalytic cycle but also avoided the need for adding a stoichiometric base as it provided a fluoride anion for silane activation. In the same line, two years later, the same group expanded the scope of compatible olefins to styrenes and mono- and gem-disubstituted olefins in Au-catalyzed three-component oxyarylations by employing iodosobenzoic acid (IBA) as oxidant instead of Selectfluor.^[24] In parallel, the group of Toste also studied the three-component gold-catalyzed oxyarylation of terminal olefins employing the bimetallic gold(I) complex [dppm(AuBr)₂]^[25] and could expand the scope of the arylating fragment from arylsilanes to arylboronic acids (Figure 4a).^[26] In addition, they developed the



Pau Font completed his Master's degree in Advanced Catalysis and Molecular Modelling at the University of Girona in 2017. Then, he joined the QBIS-CAT research group, also at the University of Girona, to develop his PhD studies on the field of gold-catalyzed cross-coupling reactions, under the supervision of Dr. Xavi Ribas.



Xavi Ribas obtained his PhD in Chemistry in 2001 at the University of Girona. His research interests are broad, from organometallics catalysis to supramolecular chemistry. He received several ICREA Academia awards, and in 2018 he got the RSEQ Excellence in Research Award. He has published more than 130 papers (h index = 45).

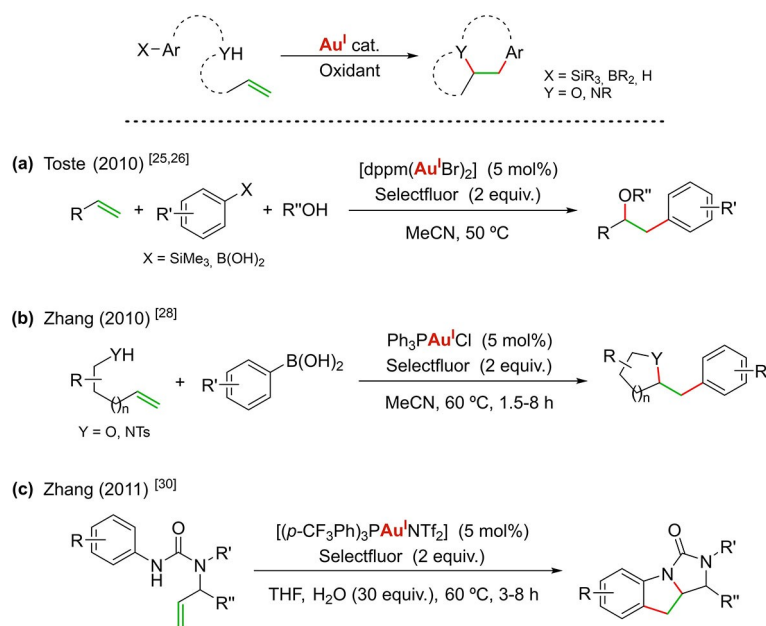


Figure 4. General Au(I)/Au(III)-catalyzed oxy- and aminoarylations of terminal alkenes. (a) Three-component oxyarylation of terminal olefins using arylsilanes and boronic acids as competent arylating agents. (b) Two-component oxyarylations and aminoarylations of terminal alkenes using arylboronic acids. (c) Aminoarylation of terminal alkenes via intramolecular C–C coupling.

intramolecular aminoarylation of terminal alkenes using the same $[dppm(AuBr)_2]$ complex, arylboronic acids as coupling partners and Selectfluor as oxidant.^[27] Simultaneously, Zhang and coworkers also worked in the use of arylboronic acids for both the oxyarylation and aminoarylation of olefins, employing Ph_3PAuCl and Selectfluor (Figure 4b).^[28] In addition, Gouverneur and coworkers reported the intramolecular oxidative C–C cross-coupling of non-activated arenes to yield tricyclic dihydroindole-nofuranone-type products.^[29] Similarly, in 2011 the group of Zhang combined the oxidative Au(I)/Au(III)-catalysis with C–H functionalization to yield tricyclic indolines as formal intramolecular [3 + 2] annulation products (Figure 4c).^[30] Nevado and de Haro reported in 2010 the gold-mediated oxidative C(sp)–C(sp²) coupling of arenes with electron-deprived terminal alkynes to yield arylacetylenes (Figure 5a).^[31] This work stands as the first ethynylation reaction of this kind occurring via a gold-catalyzed C–H activation of both aromatic and acetylenic counterparts. Additionally, the group of Zhang published an unprecedented gold-catalyzed Sonogashira cross-coupling of terminal alkynes with arylboronic acids.^[32] The group of Shi reported the formation of unsymmetrical 1,3-diynes by reacting two different terminal alkynes under gold-catalyzed oxidative cross-coupling conditions (Figure 5b).^[33] Lloyd-Jones and Russell synthesized biaryls by reacting arylsilanes with non-activated arenes, using a Au(I) catalyst and $PhI(OAc)_2$ as oxidant under mild conditions (Figure 5c).^[34] In 2015, the group of Larrosa published the first gold-catalyzed oxidative cross-coupling of arenes via double C–H activation (Figure 5c).^[35] The biaryls obtained consisted of the coupling between highly activated (hetero)arenes and perfluorinated arenes. This strategy, how-

ever, required the employment of silver salts to help at the C–H activation of the electron-deficient arene counterpart.

Later, Nevado and coworkers also contributed to the field of gold-catalyzed oxidative couplings to yield biaryls by providing a system in which strong electron-poor fluorinated aryl boronates coupled to arenes efficiently (Figure 5c).^[36] The intermediacy of Au(III) species of the type $[Au(OAc)_2(Ar^F)(PPh_3)]$ obtained upon $PhI(OAc)_2$ -mediated oxidation could be validated. Interestingly, in 2017, Lloyd-Jones and coworkers developed an intramolecular system for the gold-catalyzed arylation of arenes by aryl-trimethylsilanes.^[37] The biaryl coupling generated products featuring 5- to 9-membered rings. Tethering of the arene to the arylsilane provided the system with the ability to tolerate a wide range of electron donating and electron withdrawing arene substituents.

2. Synthesis of Well-Defined Au(III) Complexes via Oxidative Addition

In parallel with the development of gold-catalyzed oxidative cross-couplings, increasing interest arose on studying the behavior of gold complexes towards fundamental organometallic transformations and their involvement in catalytic cycles.^[38] Oxidative addition is a pivotal step in organometallic chemistry as it is the entry point to most of the catalytic transformations, especially cross-coupling reactions. The ability of gold to undergo oxidative addition, in sharp contrast to other transition metals, remained elusive and scarcely investigated for a long time (see Figure 3).^[18–19] However, stunning

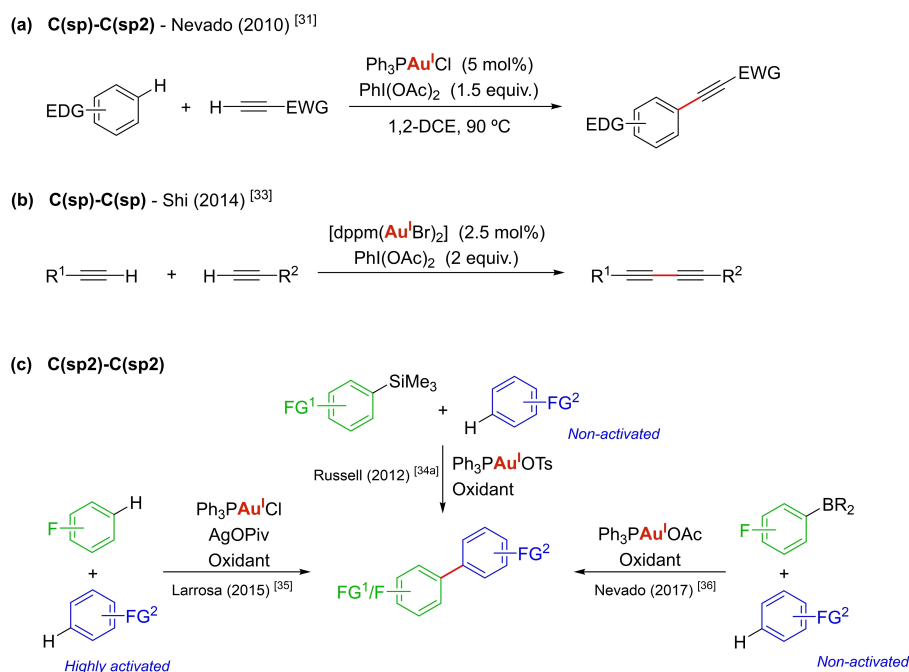


Figure 5. (a) Au(I)/Au(III)-catalyzed ethynylation of arenes occurring via double C–H bond activation. (b) Au(I)/Au(III)-catalyzed oxidative C(sp)–C(sp) coupling for the formation of unsymmetrical 1,3-diyne. (c) Different protocols for the synthesis of biaryls by means of gold-catalyzed oxidative C(sp²)–C(sp²) cross-coupling strategies.

advances in homogeneous gold redox chemistry have been achieved over the past 7 years, demonstrating that gold is, indeed, much less inert than previously thought two decades ago. In fact, to date, many well-defined Au(III) complexes have been obtained via oxidative addition, isolated, and characterized. Strategies like strain release, ligand design and photochemistry have been proven helpful in overcoming the high redox potential of the Au(I)/Au(III) pair and trigger the otherwise sluggish oxidative addition to Au(I).

In 1967, Davison and coworkers reported the reaction between *cis*-bis(trifluoromethyl)-1,2-dithietene and Ph₃PAuCl to yield a chlorotriphenylphosphonium tetrathiolatoaurate salt, a Au(III) species obtained via oxidative addition of two S–S disulfide bonds to Au(I) (Figure 6a).^[39] Its molecular structure was elucidated by Ibers soon after in 1968 by means of X-ray crystallography.^[40] Some independent studies done by Kochi, Puddephatt and Schmidbaur in the early 1970's showed how

phosphine gold(I) methyl complexes reacted with methyl iodide to yield ethane and phosphine gold(I) iodide.^[1a,b, 41] Further studies on the mechanism revealed the oxidative addition of the C(sp³)–I bond to Au(I) and in certain cases the ensuing Au(III) complexes could be characterized, depending on the phosphine donor ligand.^[1c,d,42]

Despite these early studies published from 1967 to 1975, the investigations on the field of oxidative addition at gold(I) were not resumed until 2011, and experienced a dramatic growth from then on. It is worth mentioning the work published in 2008 by Gray and coworkers, where strongly activated disulfides underwent facile and reversible oxidative addition to dithiolate Au(I) complexes (Figure 6b).^[43]

2.1. Strain Release to Promote Oxidative Addition at Au(I)

In 2015, Toste and coworkers reported the intermolecular oxidative addition of the strained C–C bond in biphenylene to the coordinatively unsaturated NHC–Au(I) cationic complex formed upon chloride abstraction of the (NHC)AuCl starting complex (NHC=IPr) using AgSbF₆.^[44] The ensuing cationic Au(III) complex was trapped either with *n*Bu₄NCl or with DMF to yield the corresponding tetracoordinate [(IPr)Au(III)(biphenyl)Cl] and [(IPr)Au(III)(biphenyl)(DMF)]SbF₆ complexes, which could be characterized by X-ray crystallography (Figure 7). This work outstands for being an example on how the oxidative addition of a bidentate substrate is favored because it is driven by the energy release from a strained covalent bond and because the

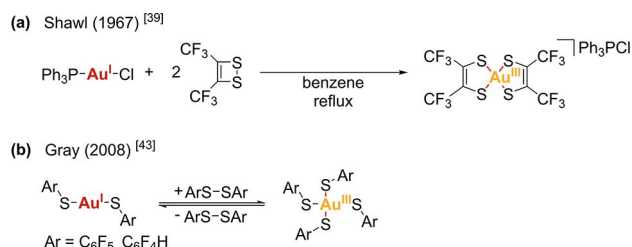


Figure 6. Early reported examples of oxidative addition of disulfide bonds to Au(I).

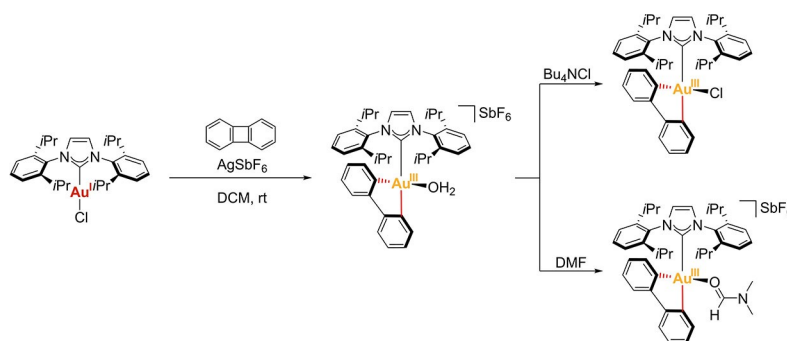


Figure 7. Oxidative addition of the strained C–C bond in biphenylene to a cationic [(NHC)Au(I)]⁺ fragment disclosed by Toste.^[44a]

substrate, once coordinated, stabilizes the gold(III) center by providing it with a proper coordination geometry.

2.2. Ligand Design to Promote Oxidative Addition at Au(I)

Chelation-assisted strategy. The chelation-assisted strategy is based on generating a Au(I) complex that is coordinated to a ligand that bears a functional moiety in a right position and in close proximity to the metal center, which becomes susceptible to undergo oxidative addition to the Au(I) atom. By means of this strategy, the oxidative addition of apolar σ -bonds (E–E, where E=Si, Sn) and polarized C–X bonds to Au(I) has been achieved.

From 2011 to 2014, Amgoune, Bourissou and coworkers worked on the spontaneous intramolecular oxidative addition of apolar σ -bonds to Au(I), using diphosphine ligands bearing Si–Si and Sn–Sn bonds (Figure 8a).^[45] Remarkably, when using the corresponding monophosphine-disilane ligand, the oxidative addition of the σ -Si–Si bond at gold(I) also occurred.^[45c] In all cases, the resulting bis(silyl)- and bis(stannyl)gold(III) complexes were characterized. In addition, the oxidative addition of σ -Si–Si bonds could be expanded to an intermolecular regime by reacting phosphine gold(I) chloride complexes with disilanes in the presence of GaCl₃ at low temperature, as a proof of concept that oxidative addition of the σ -Si–Si bond can take place directly at Au(I) without requiring chelating assistance (Figure 8b). The resulting Au(III) complexes featured an unusual, distorted Y shape and were unstable above –60 °C or even –80 °C depending on the phosphine.^[46] In 2014, the group of Toste designed a Au(I)-aryl complex with a tethered allyl bromide arm that underwent oxidative addition of the C(sp²)-Br bond to the Au(I) center under mild conditions (Figure 8c). The resulting Au(III) complex served as a mechanistic proof for the oxidant-free gold-catalyzed allylation of arylboronic acids presented in the same work.^[47] Also in 2014, Amgoune, Bourissou and coworkers reported the intramolecular oxidative addition of C(sp²)-X bonds (X=Br, I) to Au(I). The design of the 8-halonaphthyl phosphine ligands suitably places the C(sp²)-X bond close to the Au(I) atom when it is coordinated to the phosphine moiety, inducing the stabilization of the (P,C)-cyclometalated Au(III) products obtained upon

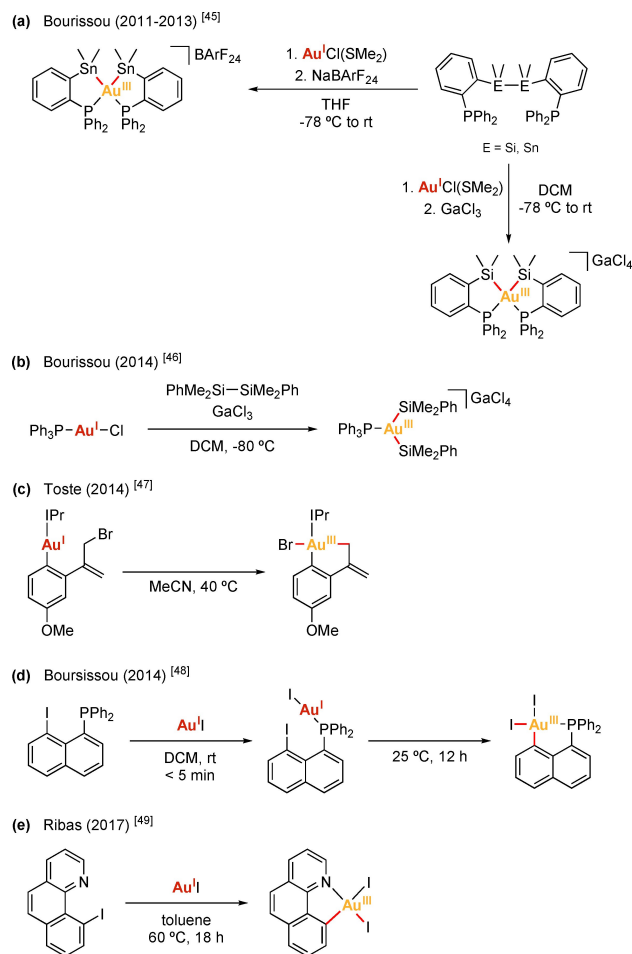


Figure 8. Selected examples of intramolecular chelation-assisted oxidative addition at Au(I) (a, c–e), and intermolecular oxidative addition of disilanes at a phosphine gold(I) chloride complex (b).

oxidative addition (Figure 8d).^[48] Additionally, the authors also prepared PCP-pincer Au(III) complexes via oxidative addition of a C(sp²)-Br bond when employing a bromophenyl diphosphine ligand, by means of the same strategy. In 2017, Ribas and coworkers generated a (N,C)-cyclometalated Au(III) complex via oxidative addition by reacting gold(I) iodide and 10-iodobenzo[h]quinoline under moderate heating (Figure 8e).^[49]

Bidentate ligands with small bite angles. The design of bidentate ligands featuring a bite angle smaller than 180° when chelating gold(I) centers has also showed efficiency at rendering Au(III) species via oxidative addition. The preorganization of the non-linear Au(I) complex reduces the deformation energy required to become a square-planar Au(III) complex.

In 2014, Amgoune, Bourissou and coworkers applied this strategy using carborane diphosphine ligands (DPCb) that chelate the gold(I) atom with P–Au–P angles between 90° and 100° depending on the counterion. The authors could activate C(sp²)-I bonds from several aryl iodides at room temperature affording well-defined aryl-Au(III) complexes that could be isolated and fully characterized (Figure 9a).^[50] Intriguingly, the oxidative addition of *p*-substituted iodobenzenes occurred faster with more electron-rich arenes, featuring the opposite reactivity trend to the one observed in isoelectronic L₂Pd(0) complexes undergoing oxidative addition of aryl halides.^[51] In 2015, the same group combined the use of bent [(DPCb)Au(I)]⁺ complexes with the strain release strategy to promote the oxidative addition of the strained C–C bonds in biphenylene and in benzocyclobutenone (Figure 9b).^[52] The oxidative addition of benzocyclobutenone afforded two acyl-gold(III) complexes upon selective activation of either the C(aryl)-C(O) bond (kinetic product) or the C(alkyl)-C(O) bond (thermodynamic product), by adjusting the reaction conditions. Remarkably, the oxidative addition of the C(aryl)-C(O) bond turned to be

reversible since the isolated kinetic product, when in solution, evolved slowly back to the cationic Au(I) complex and, over time or upon heating, the thermodynamic acyl-Au(III) complex was formed.

In 2018, Russell and coworkers reacted a three-coordinated 2,2'-bipyridyl-chelated gold(I) ethylene complex, featuring a N–Au–N angle of 74.57° , towards the reversible oxidative addition of C(sp²)-I bonds in different aryl iodides (Figure 9c).^[53] Electron-rich aryl iodides reacted faster than electron-poor ones, showing a reactivity trend that agrees with the previously reported by Bourissou.^[50] In 2020, Russell reported the first examples of intermolecular oxidative addition of alkenyl and alkynyl iodides to the same Au(I) complex, forming alkenyl Au(III) complexes in a reversible and stereospecific manner for the former (Figure 9c).^[54]

Hemilabile ligands. In 2016, Bertrand and coworkers reported a (CAAC)AuCl complex (CAAC=Cyclic Alkyl Amino Carbene) bearing a pendant hemilabile imine moiety that helped at stabilizing the Au(III) complex obtained upon oxidative addition of the strained C–C bond in biphenylene (Figure 10a).^[55] One year later, the group of Bourissou employed the di(1-adamantyl)-2-dimethylaminophenylphosphine (MeDalphos) ligand in (MeDalphos)AuCl, a phosphine ligand with a hemilabile tertiary amine, to stabilize the (P,N)-cyclometalated Au(III) species resulting from the oxidative addition of the strained C–C bond in biphenylene and the C–X bonds in

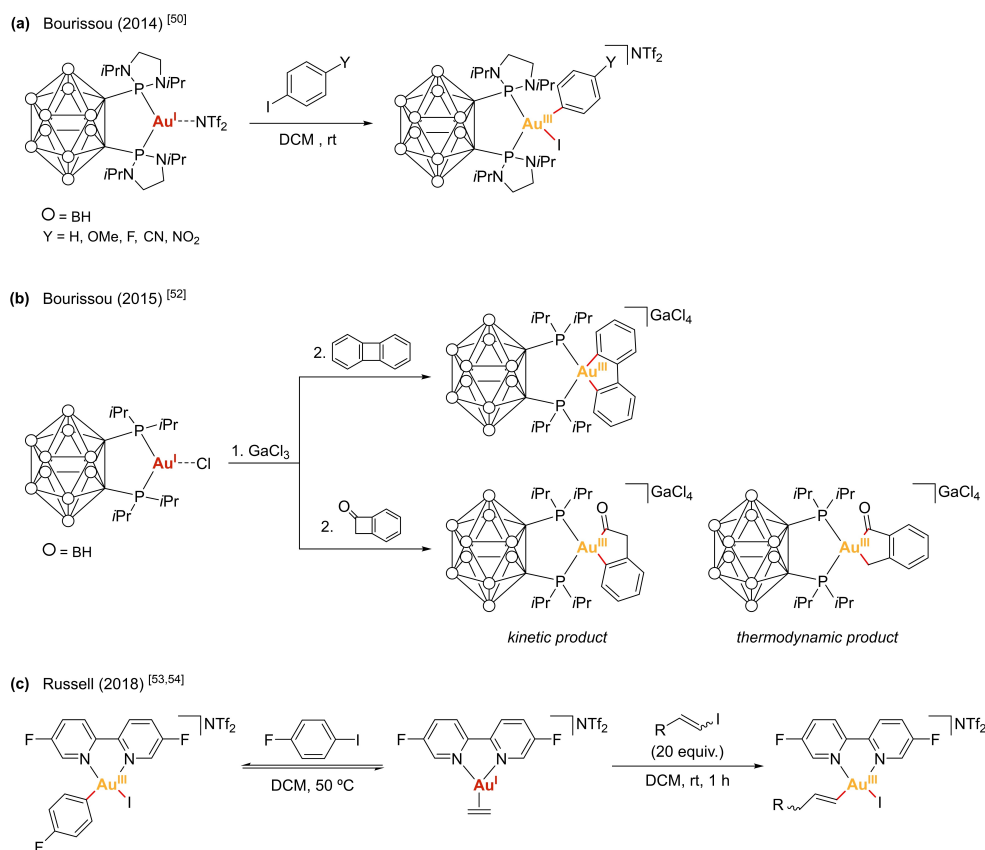


Figure 9. Selected examples of non-linear gold(I) complexes that are preorganized to undergo oxidative addition under mild conditions.

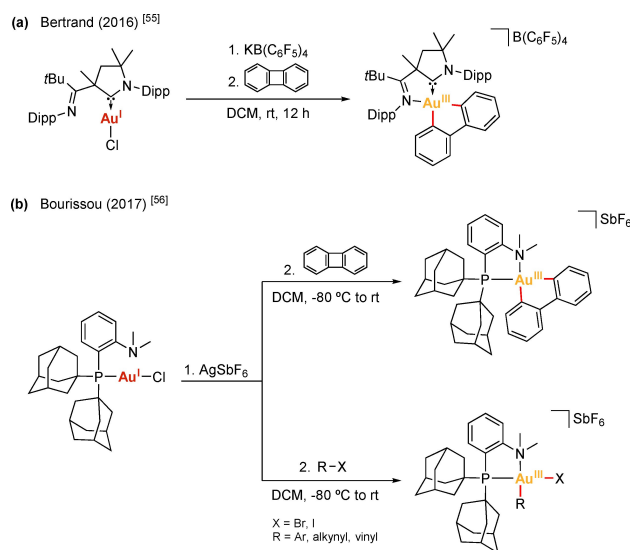


Figure 10. Selected examples of hemilabile ligand-stabilized aryl-Au(III) complexes obtained via oxidative addition.

iodoaryls, bromoaryls, alkynyl iodides and vinyl iodides (Figure 10b).^[56] In line with these works, in 2021, the group of Nevado used different (P,N)-[(MeDalphos)Au(III)(Ar)(I)]⁺ complexes, obtained via oxidative addition, to further explore their chemistry and included some variations at the ligand, such as replacing the adamantyl substituents by *tert*-butyls and replacing the dimethylamino group by a piperidinyll unit.^[57] In addition, Spokoyny and coworkers also used (MeDalphos)AuCl to synthesize a wide library of Au(III) complexes of the type (P,N)-[(MeDalphos)Au(III)(Ar)(X)]SbF₆ (X=I, Cl) via oxidative addition.^[58] These complexes served as robust arylation reagents in a general protocol for cysteine S-arylation of unprotected peptides and proteins. Further, in 2021 the same group used the *tert*-butyl-substituted version of the MeDalphos ligand to develop (P,N)-gold(III) platforms that work as efficient and selective cysteine arylation reagents, giving access to arylated bioconjugates of higher structural complexity including bicyclic peptides, stapled peptides and peptide-functionalized hybrid nanoclusters.^[59]

2.3. Photochemical Conditions to Promote Oxidative Addition at Au(I)

A surrogate strategy to access Au(III) species within Au(I)/Au(III) catalytic cycles avoiding external oxidants is the use of photochemical conditions that allow the oxidative addition, generally of diazonium salts, under mild conditions to obtain well-defined aryl-Au(III) complexes.

In 2016, the group of Hashmi reported the oxidative addition of aryldiazonium salts to phosphine- and NHC-gold(I) complexes promoted by the irradiation with blue light LEDs.^[60] When using chelating (P,N)-ligands, cationic five- and six-membered chelate gold(III) complexes were obtained, whereas when using monodentate phosphine ligands and NHC ligands,

the corresponding neutral Au(III) complexes were formed. Also in 2016, Glorius and coworkers developed a straightforward approach towards well-defined cationic (N,C)-cyclometalated Au(III) complexes via photoredox-promoted oxidative addition of aryldiazonium salts to LAuCl complexes (L=phosphine or NHC), in the presence of a Ru photocatalyst under irradiation of green LEDs at room temperature (Figure 11a).^[61] Alternatively, Porcel and coworkers employed in situ generated aryldiazonium salts as electrophiles that oxidatively added to LAuCl complexes (L=PPh₃ or SMe₂) under thermal conditions, without requiring photochemical conditions.^[62] The ensuing arylgold(III) complexes could be isolated and characterized.

In 2014, Toste and coworkers reported the oxidative addition of CF₃I to phosphine Au(I) aryl complexes via a photoinitiated radical chain reaction. The use of near-ultraviolet light promoted the excitation of CF₃I to end up with Au(III) complexes of the type (PR₃)Au(aryl)(CF₃)(I) that could be isolated and characterized (Figure 11b).^[63] In 2019, the same group isolated Au(III) complexes from the photoredox-initiated arylation of (IPr)AuX complexes (X=CF₃ or succinimide), using aryldiazonium salts, a Ru-based photoredox catalyst and blue light LED irradiation (Figure 11c).^[64] The authors claimed a radical chain oxidative addition in which the ruthenium catalyst first generates an aryl radical that adds to the Au(I) complex. Then, the resulting arylgold(II) species undergoes a single electron oxidation by reacting with the aryldiazonium salt. This reaction generates an arylgold(III) species that could be isolated in coordinating solvents.

3. Oxidant-Free Au(I)/Au(III) Cross-coupling Catalysis

Oxidative addition at gold(I) can unequivocally be achieved if proper conditions are provided, as revised in the approaches described in sections 2.1 - 2.3. The combination of oxidative addition with other fundamental organometallic transformations is key for designing synthetic methodologies proceeding through oxidant-free two-electron redox Au(I)/Au(III) catalytic cycles. In this section, the attention will be focused on cross-coupling catalysis operating via Au(I)/Au(III) cycles in the absence of external oxidants.^[65]

3.1. Substrate and Ligand Design for the Development of Au(I)/Au(III) Catalytic Cycles

In 2014, Toste and coworkers used a bis(diphenylphosphino) amine ligand-supported bimetallic Au(I) complex to catalyze the allylation of arylboronic acids.^[47] Interestingly, the analogous monometallic aminophosphine Au(I) complex afforded the C(sp²)-C(sp³) coupling products in much lower yields, suggesting that the bimetallic catalyst structure enhances the catalytic activity. The oxidative addition of allyl bromides to the bimetallic Au(I) aryl complex was suggested to be the key step of the catalytic cycle, and a bimetallic Au(II)-Au(II) species was

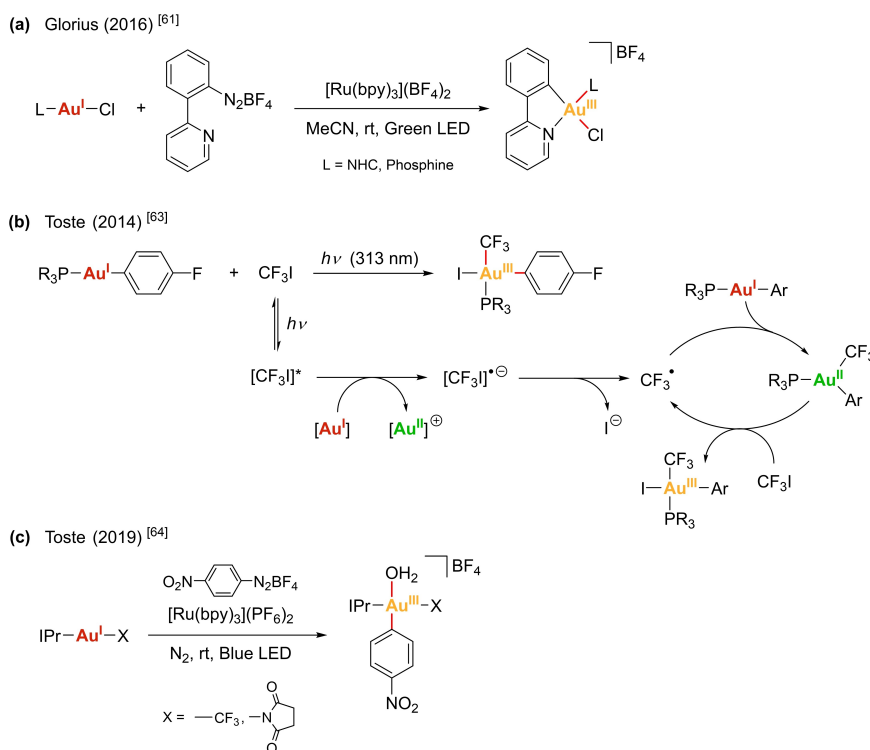


Figure 11. Selected examples of aryl-Au(III) complexes obtained via oxidative addition promoted by photochemical conditions.

proposed to be formed rather than discrete Au(III). They supported the viability of the oxidative addition of the allylic C(sp³)-Br bond to Au(I) under intramolecular conditions (see Figure 8c).

The group of Ribas designed Au(I)/Au(III)-catalyzed cross-coupling transformations taking advantage of the chelation-assisted strategy. In 2015, they reported the halide exchange and C(sp²)-O bond-forming reactions employing a cationic NHC-Au(I) complex and model aryl halide triazamacrocyclic substrates.^[66] The latter had previously demonstrated to be convenient substrates for the stabilization of Cu(III) and Ag(III) intermediates obtained via oxidative addition in Cu(I)/Cu(III)- and Ag(I)/Ag(III)-catalyzed C-C and C-X bond-forming cross-couplings.^[16a,d,e,67] In this work, the authors also could extrapolate the halide exchange and the C(sp²)-O coupling reactions to 2-(2-halophenyl)pyridines, i.e. substrates bearing a single chelating group. The detection of Au(III) intermediates was not possible neither using the triazamacrocyclic substrates nor the 2-(2-halophenyl)pyridines. However, a Au(I)/Au(III) catalytic cycle was postulated and supported by DFT studies.^[66] In 2017, the same group reported oxidant-free C(sp²)-O and C(sp²)-N coupling reactions catalyzed by the same cationic NHC-Au(I) complex employing 2-(2-halophenyl)pyridines as substrates.^[49] Interestingly, the intermediacy of Au(III) species could be validated when using 10-iodobenzo[h]quinoline, evidencing that a more rigid and flat chelating substrate stabilizes better the Au(III) species formed upon oxidative addition (Figure 12).

In line with the use of hemilabile bidentate ligands, Bourissou and coworkers employed the (P,N)-MeDalphos ligand

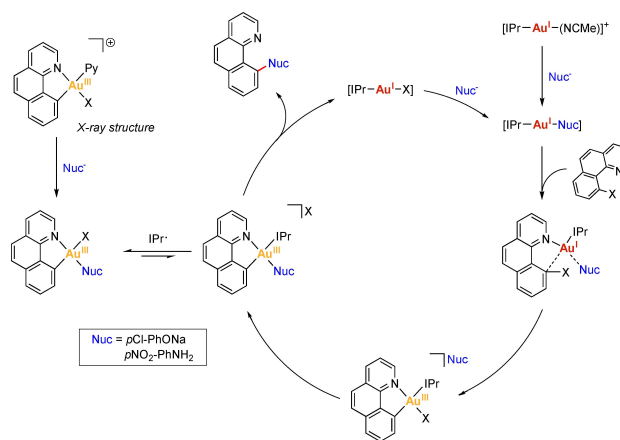


Figure 12. Proposed mechanism for the oxidant-free Au(I)/Au(III)-catalyzed C(sp²)-O and C(sp²)-N cross-coupling reported by Ribas and coworkers.^[49]

to develop the Au(I)/Au(III)-catalyzed cross-coupling between aryl halides and electron-rich arenes to afford biaryls under mild conditions (Figure 13a).^[56a] The catalytic cycle was shown to proceed following the C(sp²)-X oxidative addition/C(sp²)-H auration/reductive elimination sequence. The great performance of MeDalphos ligand at stabilizing Au(III) intermediates paved the way to envision new Au(I)/Au(III) catalytic transformations using the (MeDalphos)AuCl catalyst. In this regard, in 2019 Bourissou and coworkers reported the regioselective C3 arylation of indoles, which is rarely observed by means of other transition metal-mediated catalysis (Figure 13b).^[68] Moreover, it

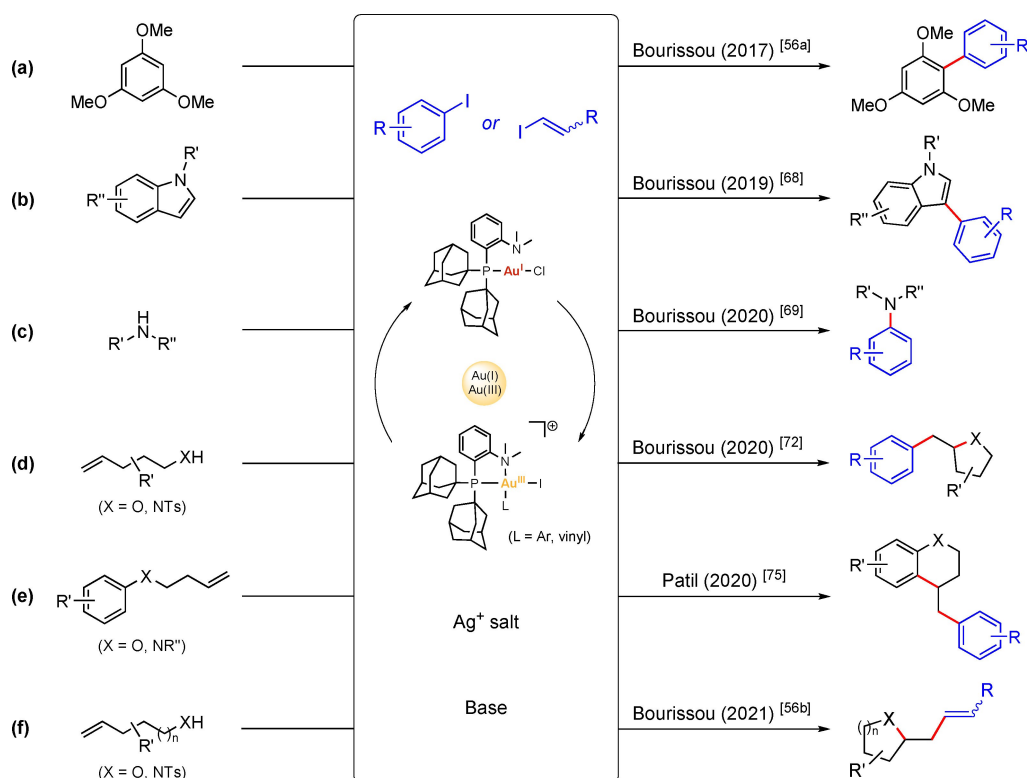


Figure 13. Au(I)/Au(III) cross-coupling catalysis enabled by MeDalphos ligand.

displayed a high functional group tolerance at both the iodoarene and indole partners. In 2020, the same group used the (MeDalphos)AuCl catalyst in C(sp²)-N cross-coupling reactions (Figure 13c).^[69] They developed a robust and mild methodology for coupling a wide scope of aryl iodides and N-nucleophiles under mild conditions. The reaction mechanism was thoroughly investigated, including the characterization of a key Au(III) intermediate. Patil and coworkers also contributed, independently, to the development of C(sp²)-N cross-coupling of aryl iodides with amines mediated by the MeDalphos-enabled Au(I)/Au(III) catalysis.^[70]

Further, Bourissou and coworkers had already demonstrated the ability of MeDalphos ligand to stabilize gold(I) π -complexes,^[71] besides its capability to promote Au(I)/Au(III) two-electron redox transformations. Therefore, the same group took advantage of the great performance of MeDalphos ligand to develop the oxy- and aminoarylation of alkenols and alkenamines by means of Au(I)/Au(III) catalysis that combines oxidative addition of aryl iodides with π -activation of olefins (Figure 13d).^[72] This strategy proved suitable to access products with 5-, 6- and 7-membered rings and electron-rich aryl substrates reacted readily. Likewise, the group of Patil also employed the MeDalphos ligand to synthesize 1,2-oxy- and 1,2-aminoarylation products from the coupling of aryl iodides with alkenes.^[73] In the case of oxyarylations, two- and three-component reactions were reported, whereas aminoarylations were only carried out as two-component reactions. The 1,2-aminoarylations of alkenes were also shown to proceed by

reacting alkenes tethered to aryl iodide moieties with external amines.^[74] The use of MeDalphos ligand allowed the same group to develop, as well, the first ligand-enabled Au(I)/Au(III)-catalyzed 1,2-diarylation of alkenes by merging the oxidative addition of aryl iodides to Au(I) with π -activation of alkenes (Figure 13e).^[75] In this case, the mechanism was proposed to involve an aromatic electrophilic substitution (S_EAr) step for the carboarylation of alkenes. The resulting Au(III)-aryl-alkyl intermediate could be detected by means of mass spectrometry. Notably, the selective reactivity disclosed in this work avoids the formation of undesired Ar-Ar' and Heck-type byproducts observed in other transition metal catalysis. More recently, the group of Bourissou applied the oxidative addition of vinyl iodides to (MeDalphos)AuCl in catalysis, in combination with π -activation, to develop oxy- and amino-vinylation reactions using alkenols and N-tosyl alkenamines, respectively (Figure 13f).^[56b]

3.2. Coupling Partners with Dual Role

The use of diazonium salts, which act dually as coupling partners and as oxidizing equivalents, has led to a wide scope of oxidant-free gold redox coupling catalysis. For instance, in 2015 Chen, Shi and coworkers reported the C(sp)-C(sp²) and C(sp²)-C(sp²) cross-coupling between aryldiazonium salts and terminal alkynes or arylboronic acids, respectively. In this case, the addition of a bipyridine auxiliary ligand was key to assist nitrogen extrusion.^[76] In 2016, the same group reported the

gold-catalyzed C–Br, C–S and C–P Sandmeyer couplings between aryldiazonium salts and the corresponding nucleophiles.^[77] Crucial to the success of this transformation was the nucleophile-assisted activation of aryldiazonium salts, which were then added to Au(I) to yield Au(III) intermediates. In 2017, Shi reported the Lewis base-assisted diazonium activation as a strategy to access gold oxidation and build a Au(I)/Au(III) catalytic cycle for the intramolecular oxy- and aminoarylation of alkenes, the arylative ring expansion of alkenes, the oxy- and aminoarylation of allenes, and the propargyl ester rearrangement of alkynes.^[78] Additionally, in 2018 the group of Dughera reported the gold-catalyzed Heck and Suzuki-Miyaura couplings using arenediazonium *o*-benzenedisulfonimides as electrophilic partners.^[79] They proposed a Au(I)/Au(III) catalytic cycle that did not require the presence of external oxidants since the *o*-benzenedisulfonimide anion was suggested to act as an electron transfer agent that promoted the oxidation to Au(III) intermediate species via a radical pathway. Intriguingly, in 2018, Patil and coworkers reacted aryldiazonium salts with diverse organostannanes towards the formation of biaryls, vinyl arenes and arylacetylenes via Au(I)/Au(III) cross-coupling at mild conditions.^[80] In 2019, Shi and coworkers reported the cyclization-arylation of allylic oximes to access aryl functionalized 2-isoxazolines in good yields.^[81] The reaction occurred via chemical activation of the diazonium salt. The use of Li₂CO₃ as a base assisted the N₂ extrusion to promote the oxidation of Au(I) to Au(III) aryl species while slowing down the aryl radical generation, which otherwise decomposed the oxime substrate.

Light irradiation, however, has proved useful to promote the activation of aryldiazonium salts, which can then add to Au(I) giving access to Au(I)/Au(III) catalytic cycles. Several groups have worked on the synthesis of (hetero)biaryls by means of photosensitizer-free light-induced gold redox catalysis, such as Bandini, who worked on the Suzuki coupling of arylboronic acids with arylazosulfones (Figure 14a),^[82] or Hashmi, who worked on the coupling of aryldiazonium salts with organoboron and organosilicon reagents (Figure 14b).^[83] In 2016, Hashmi and coworkers reported the visible-light-mediated gold-catalyzed intermolecular 1,2-difunctionalization of alkynes with aryldiazonium salts in methanol to afford α -aryl ketones.^[84] In 2017, the group of Wong reported the light-

mediated gold-catalyzed *cis*-difunctionalization of silyl-substituted alkynes with quinoline-substituted aryldiazonium salts in high chemo- and regioselectivity.^[85] Interestingly, in 2019, Hashmi and coworkers reported a study in which the Au-catalyzed reaction of *o*-alkynylphenols with aryldiazonium salts led to different outcome depending on whether blue LED light was applied or not, under the same reaction conditions.^[86] Under blue LED irradiation, N₂ extrusion from the diazonium salt was promoted and arylated benzofurans were formed, whereas in the absence of a light source, the N₂ unit was retained and azobenzofurans were obtained. In 2020, Feng and coworkers reported the visible-light-promoted gold redox catalysis for the regio- and stereoselective fluoroarylation of allenic esters.^[87]

Ethynylbenziodoxolone reagents (EBX), which can be regarded as electrophilic alkyne surrogates, have also been used as reagents that play the dual role as coupling partners and oxidants. In 2013, Waser and coworkers reported the domino cyclization/alkynylation reaction of allenic ketones with EBXs to afford C3-alkynylated furans, employing a Au(III) catalyst (Figure 15a).^[88] Computational studies on the mechanism of this domino reaction revealed that the Au(III) catalyst was the precursor of the active Au(I) catalyst that initiates the Au(I)/Au(III) catalytic cycle.^[89] In 2017, Patil and coworkers reported the gold-catalyzed C(sp)–C(sp) alkynylation of terminal alkynes with EBXs to access unsymmetric 1,3-diynes (Figure 15b).^[90] They used Ph₃PAuCl as catalyst and catalytic amount of 1,10-phenanthroline as auxiliary ligand. Likewise, the group of Liu also used alkynyl hypervalent iodine reagents in the coupling with terminal alkynes for the synthesis of unsymmetrical 1,3-diynes.^[91]

3.3. Photoredox-Gold Dual Catalysis

Despite the abovementioned examples of gold-catalyzed couplings under photosensitizer-free conditions or operating via light-assisted activation of aryldiazonium salts, many studies have relied on dual photoredox-gold catalytic systems to develop a wide array of synthetic strategies.^[92] The combination of homogeneous gold catalysis and photoredox catalysis consists of a photocatalyst that, once excited by light irradiation, generates an organic radical (generally an aryl

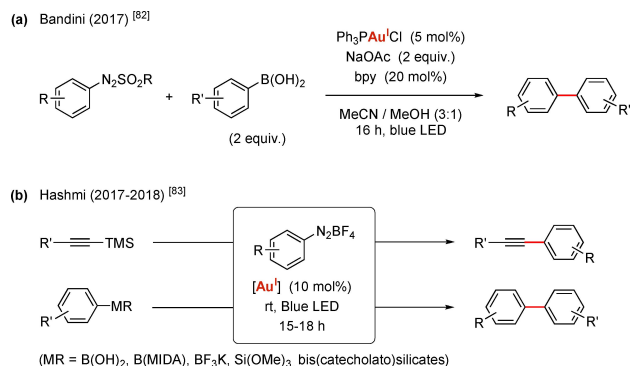


Figure 14. Au(I)/Au(III) cross-coupling catalysis of aryldiazonium salts with organoboron and organosilicon reagents under light irradiation.

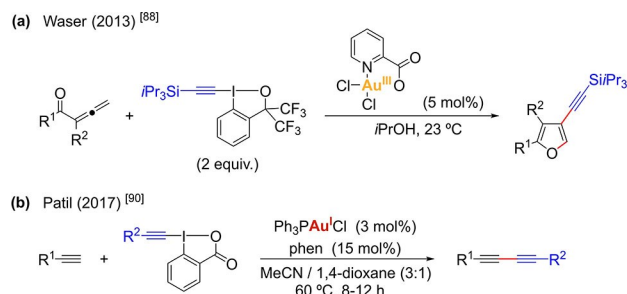


Figure 15. Selected examples of Au(I)/Au(III) cross-coupling catalysis involving EBX reagents as coupling partners.

radical from aryldiazonium salts) via single electron transfer while getting itself oxidized (Figure 16a). The organic radical can add to Au(I) to give a transient gold(II) species which subsequently undergoes oxidation to Au(III) while regenerating the ground-state photocatalyst via single electron transfer. Finally, reductive elimination from Au(III) affords the coupling product and Au(I).

In 2013, Glorius and coworkers reported for the first time a dual photoredox gold catalytic system for the intramolecular oxy- and aminoarylation of alkenes with aryldiazonium salts, at

room temperature under the irradiation of a fluorescent light bulb, with the assistance of the $[\text{Ru}(\text{bpy})_3](\text{PF}_6)_2$ photocatalyst (Figure 16b).^[93] Frei and Toste developed the aryliative ring expansion of alkenyl and allenyl cycloalkanols by coupling them with aryldiazonium salts, to afford cyclic ketones (Figure 16c).^[94] The reaction was promoted by visible light photoredox catalysis and gold catalysis at room temperature. Mechanistic studies let the authors propose that the electrophilic Au(III)-aryl intermediate reacted towards the π -bonds of the substrates to undergo ring expansion and reductive

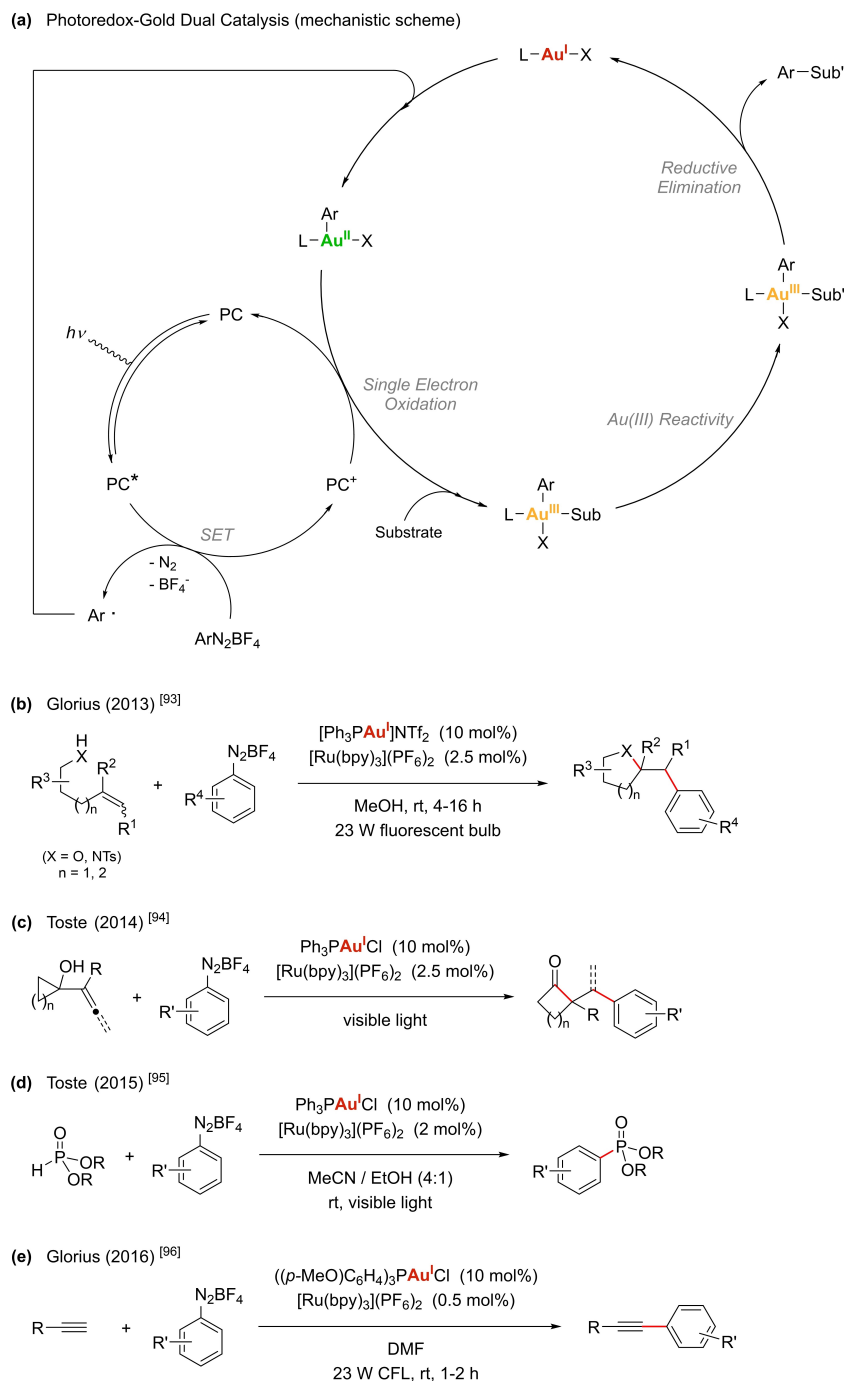


Figure 16. General mechanistic scheme of photoredox-gold dual catalysis and selected examples using aryldiazonium salts as coupling partners.

elimination. Toste and coworkers, one year later, used the dual photoredox gold catalysis approach to develop the C(sp²)–P coupling between aryldiazonium salts and H-phosphonates under visible light irradiation at room temperature (Figure 16d).^[95] Glorius and coworkers developed the arylation of terminal alkynes using aryldiazonium salts. The reaction was mediated by visible light from a household bulb or sunlight at room temperature and was run in the absence of base. Thus, it stands as the first example of achieving C–H activation by means of dual gold photoredox Au(I)/Au(III) catalysis (Figure 16e).^[96] The group of Lee reported the first aryl-aryl cross-coupling via direct C–H activation under a dual photoredox gold catalytic fashion under blue LED light irradiation.^[97] In 2016, independent groups reported tandem Meyer-Schuster/arylation reactions for the synthesis of α -arylated enones, under dual photoredox gold catalysis.^[98] Kim and Toste, more recently, provided mechanistic support for the formation of Au(III) intermediates in dual photoredox gold processes.^[64] Particularly, they validated the formation of Au(III) species via photoredox-initiated arylation of (IPr)Au(I)–CF₃ and (IPr)Au(I)–succinimide using 10 mol% [Ru(bpy)₃](PF₆)₂ (see Figure 11c) and confirmed that C(sp²)–CF₃ and C(sp²)–N coupling products were obtained via subsequent reductive elimination.

The scope of compatible coupling partners in dual photoredox gold catalysis does not only rely on the employment of aryldiazonium salts. In 2017, the group of Xu aimed to expand the scope by reporting an unprecedented intermolecular thiosulfonylation of alkenes with excellent regio- and diastereoselectivity (Figure 17a).^[99] They reacted styrenes with PhSO₂SR reagents, using (IPr)AuCl as catalyst, AgSbF₆, and [Ru(bpy)₃]Cl₂ as photocatalyst at room temperature under visible light. In 2019, Fensterbank and coworkers reported the alkynylative cyclization of *o*-alkynylphenols with iodoalkynes under visible light irradiation to access alkynylbenzofuran derivatives (Figure 17b).^[100] They claimed that the iridium(III) photocatalyst triggered the oxidative addition of the alkynyl iodide coupling partner onto an excited vinylgold(I) intermediate obtained by energy transfer from the excited iridium photocatalyst. The C(sp²)–C(sp) coupling products were obtained via subsequent reductive elimination.

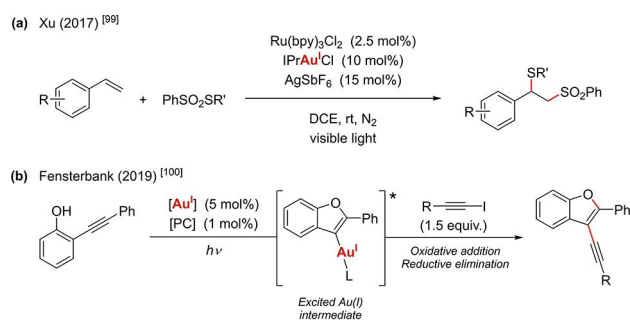


Figure 17. Dual photoredox gold-catalysis for (a) the thiosulfonylation of alkenes and (b) photosensitized oxidative addition to Au(I) in the alkynylative cyclization of *o*-alkynylphenols with iodoalkynes.

4. Conclusions

Gold catalysis is entering a new dimension through the development of external oxidant-free Au(I)/Au(III) catalytic protocols for C–C and C-heteroatom cross coupling reactions. The dedicated design of hemilabile ligands excels among other strategies to achieve the stabilization of Au(III) intermediate species upon oxidative addition with aryl halides, and the desired catalytic turnover. In this line, the P,N bidentate MeDalphos ligand stands as the most successful example. Moreover, the use of diazonium salts coupled with light irradiation in the absence or presence of photosensitizers is another successful strategy at front line of Au(I)/Au(III) that does not require external oxidants. We envision a bright and shiny golden future for this line of research.

Acknowledgements

We acknowledge financial support from MINECO-Spain for projects PID2019-104498GB-I00 and a FPU PhD grant to P.F. Generalitat de Catalunya is also acknowledged for project 2017SGR264. X.R. is thankful for an ICREA Acadèmia award.

Conflict of Interest

The authors declare no conflict of interest.

Keywords: Gold · Au(I)/Au(III) · Cross coupling · Oxidant-free · Catalysis

- [1] a) A. Tamaki, J. K. Kochi, *J. Organomet. Chem.* **1972**, *40*, C81–C84; b) A. Johnson, R. J. Puddephatt, *Inorg. Nucl. Chem. Lett.* **1973**, *9*, 1175–1177; c) A. Tamaki, J. K. Kochi, *J. Organomet. Chem.* **1974**, *64*, 411–425; d) A. Johnson, R. J. Puddephatt, *J. Organomet. Chem.* **1975**, *85*, 115–121; e) A. Burawoy, C. S. Gibson, *J. Chem. Soc.* **1934**, 860–864; f) M. Aresta, G. Vasapollo, *J. Organomet. Chem.* **1973**, *50*, C51–C53; g) R. Uson, A. Laguna, J. Vicente, *J. Organomet. Chem.* **1975**, *86*, 415–421; h) A. Tamaki, S. A. Magennis, J. K. Kochi, *J. Am. Chem. Soc.* **1974**, *96*, 6140–6148; i) S. Komiya, T. A. Albright, R. Hoffmann, J. K. Kochi, *J. Am. Chem. Soc.* **1976**, *98*, 7255–7265; j) S. Komiya, J. K. Kochi, *J. Am. Chem. Soc.* **1976**, *98*, 7599–7607; k) J. Vicente, M. D. Bermúdez, J. Escribano, M. P. Carrillo, P. G. Jones, *J. Chem. Soc. Dalton Trans.* **1990**, 3083–3089; l) J. Vicente, M. Dolores Bermudez, J. Escribano, *Organometallics* **1991**, *10*, 3380–3384; m) J. Vicente, M. D. Bermúdez, F. J. Carrión, *Inorg. Chim. Acta* **1994**, *220*, 1–3.
- [2] a) R. Dorel, A. M. Echavarren, *Chem. Rev.* **2015**, *115*, 9028–9072; b) A. S. K. Hashmi, *Chem. Rev.* **2007**, *107*, 3180–3211.
- [3] a) M. Rudolph, A. S. K. Hashmi, *Chem. Commun.* **2011**, *47*, 6536–6544; b) C. Nevado, *Chimia* **2010**, *64*, 247–251.
- [4] J. H. Teles, S. Brode, M. Chabanas, *Angew. Chem. Int. Ed.* **1998**, *37*, 1415–1418; *Angew. Chem.* **1998**, *110*, 1475–1478.
- [5] a) R. A. Widenhoefer, X. Han, *Eur. J. Org. Chem.* **2006**, *2006*, 4555–4563; b) J. C. Timmerman, S. Laulhé, R. A. Widenhoefer, *Org. Lett.* **2017**, *19*, 1466–1469; c) X. Han, R. A. Widenhoefer, *Angew. Chem. Int. Ed.* **2006**, *45*, 1747–1749; *Angew. Chem.* **2006**, *118*, 1779–1781.
- [6] A. S. K. Hashmi, L. Schwarz, J.-H. Choi, T. M. Frost, *Angew. Chem. Int. Ed.* **2000**, *39*, 2285–2288; *Angew. Chem.* **2000**, *112*, 2382–2385.
- [7] C.-G. Yang, C. He, *J. Am. Chem. Soc.* **2005**, *127*, 6966–6967.
- [8] a) A. S. K. Hashmi, T. M. Frost, J. W. Bats, *J. Am. Chem. Soc.* **2000**, *122*, 11553–11554; b) A. S. K. Hashmi, M. C. Blanco, E. Kurpejović, W. Frey, J. W. Bats, *Adv. Synth. Catal.* **2006**, *348*, 709–713; c) N. Morita, N. Krause,

- Org. Lett.* **2004**, *6*, 4121–4123; d) C. Nieto-Oberhuber, M. P. Muñoz, E. Buñuel, C. Nevado, D. J. Cárdenas, A. M. Echavarren, *Angew. Chem. Int. Ed.* **2004**, *43*, 2402–2406; *Angew. Chem.* **2004**, *116*, 2456–2460; e) A. S. K. Hashmi, I. Braun, M. Rudolph, F. Rominger, *Organometallics* **2012**, *31*, 644–661; f) M. Marín-Luna, O. Nieto Faza, C. Silva López, *Front. Chem.* **2019**, *7*, 296.
- [9] K. Kang, S. Liu, C. Xu, Z. Lu, S. Liu, X. Leng, Y. Lan, Q. Shen, *Organometallics* **2021**, DOI: 10.1021/acs.organomet.0c00784.
- [10] a) A. Biffis, P. Centomo, A. Del Zotto, M. Zecca, *Chem. Rev.* **2018**, *118*, 2249–2295; b) P. Ruiz-Castillo, S. L. Buchwald, *Chem. Rev.* **2016**, *116*, 12564–12649; c) X. Chen, K. M. Engle, D.-H. Wang, J.-Q. Yu, *Angew. Chem. Int. Ed.* **2009**, *48*, 5094–5115; *Angew. Chem.* **2009**, *121*, 5196–5217.
- [11] a) T. Furuya, D. Benitez, E. Tkatchouk, A. E. Strom, P. Tang, W. A. Goddard, T. Ritter, *J. Am. Chem. Soc.* **2010**, *132*, 3793–3807; b) M. H. Pérez-Temprano, J. M. Racowski, J. W. Kampf, M. S. Sanford, *J. Am. Chem. Soc.* **2014**, *136*, 4097–4100; c) E. Abada, P. Y. Zavalij, A. N. Vedernikov, *J. Am. Chem. Soc.* **2017**, *139*, 643–646.
- [12] a) C. A. Malapit, J. R. Bour, S. R. Laursen, M. S. Sanford, *J. Am. Chem. Soc.* **2019**, *141*, 17322–17330; b) L. Capdevila, T. H. Meyer, S. Roldán-Gómez, J. M. Luis, L. Ackermann, X. Ribas, *ACS Catal.* **2019**, *9*, 11074–11081.
- [13] J. R. Bour, N. M. Camasso, E. A. Meucci, J. W. Kampf, A. J. Canty, M. S. Sanford, *J. Am. Chem. Soc.* **2016**, *138*, 16105–16111.
- [14] a) E. Chong, J. W. Kampf, A. Ariafard, A. J. Canty, M. S. Sanford, *J. Am. Chem. Soc.* **2017**, *139*, 6058–6061; b) J. W. Schultz, K. Fuchigami, B. Zheng, N. P. Rath, L. M. Mirica, *J. Am. Chem. Soc.* **2016**, *138*, 12928–12934; c) J. R. Bour, D. M. Ferguson, E. J. McClain, J. W. Kampf, M. S. Sanford, *J. Am. Chem. Soc.* **2019**, *141*, 8914–8920.
- [15] a) G. Cahiez, A. Moyeux, *Chem. Rev.* **2010**, *110*, 1435–1462; b) T. Yamakawa, N. Yoshikai, *Org. Lett.* **2013**, *15*, 196–199; c) L. Grigorjeva, O. Daugulis, *Org. Lett.* **2014**, *16*, 4688–4690; d) L. Grigorjeva, O. Daugulis, *Org. Lett.* **2014**, *16*, 4684–4687.
- [16] a) A. Casitas, X. Ribas, *Chem. Sci.* **2013**, *4*, 2301–2318; b) M. Font, T. Parella, M. Costas, X. Ribas, *Organometallics* **2012**, *31*, 7976–7982; c) A. Casitas, M. Canta, M. Solà, M. Costas, X. Ribas, *J. Am. Chem. Soc.* **2011**, *133*, 19386–19392; d) A. Casitas, A. E. King, T. Parella, M. Costas, S. S. Stahl, X. Ribas, *Chem. Sci.* **2010**, *1*, 326–330; e) X. Ribas, M. Devillard, *Chem. Eur. J.* **2018**, *24*, 1222–1230.
- [17] a) P. Pyykko, J. P. Desclaux, *Acc. Chem. Res.* **1979**, *12*, 276–281; b) D. J. Gorin, F. D. Toste, *Nature* **2007**, *446*, 395–403; c) P. Pyykko, *Angew. Chem. Int. Ed.* **2004**, *43*, 4412–4456; *Angew. Chem.* **2004**, *116*, 4512–4557.
- [18] S. G. Bratsch, *J. Phys. Chem. Ref. Data* **1989**, *18*, 1–21.
- [19] a) M. Livendahl, P. Espinet, A. M. Echavarren, *Platinum Met. Rev.* **2011**, *55*, 212–214; b) T. Lauterbach, M. Livendahl, A. Rosellón, P. Espinet, A. M. Echavarren, *Org. Lett.* **2010**, *12*, 3006–3009; c) M. Livendahl, C. Goehry, F. Maseras, A. M. Echavarren, *Chem. Commun.* **2014**, *50*, 1533–1536.
- [20] a) P. Garcia, M. Malacria, C. Aubert, V. Gandon, L. Fensterbank, *ChemCatChem* **2010**, *2*, 493–497; b) M. N. Hopkinson, A. D. Gee, V. Gouverneur, *Chem. Eur. J.* **2011**, *17*, 8248–8262; c) H. A. Wegner, M. Auzias, *Angew. Chem. Int. Ed.* **2011**, *50*, 8236–8247; *Angew. Chem.* **2011**, *123*, 8386–8397.
- [21] A. Kar, N. Mangu, H. M. Kaiser, M. Beller, M. K. Tse, *Chem. Commun.* **2008**, 386–388.
- [22] a) L. Cui, G. Zhang, L. Zhang, *Bioorg. Med. Chem. Lett.* **2009**, *19*, 3884–3887; b) G. Zhang, Y. Peng, L. Cui, L. Zhang, *Angew. Chem. Int. Ed.* **2009**, *48*, 3112–3115; *Angew. Chem.* **2009**, *121*, 3158–3161.
- [23] L. T. Ball, M. Green, G. C. Lloyd-Jones, C. A. Russell, *Org. Lett.* **2010**, *12*, 4724–4727.
- [24] L. T. Ball, G. C. Lloyd-Jones, C. A. Russell, *Chem. Eur. J.* **2012**, *18*, 2931–2937.
- [25] W. E. Brenzovich, J.-F. Brazeau, F. D. Toste, *Org. Lett.* **2010**, *12*, 4728–4731.
- [26] A. D. Melhado, W. E. Brenzovich, A. D. Lackner, F. D. Toste, *J. Am. Chem. Soc.* **2010**, *132*, 8885–8887.
- [27] W. E. Brenzovich Jr., D. Benitez, A. D. Lackner, H. P. Shunatona, E. Tkatchouk, W. A. Goddard III, F. D. Toste, *Angew. Chem. Int. Ed.* **2010**, *49*, 5519–5522; *Angew. Chem.* **2010**, *122*, 5651–5654.
- [28] G. Zhang, L. Cui, Y. Wang, L. Zhang, *J. Am. Chem. Soc.* **2010**, *132*, 1474–1475.
- [29] M. N. Hopkinson, A. Tessier, A. Salisbury, G. T. Giuffredi, L. E. Combettes, A. D. Gee, V. Gouverneur, *Chem. Eur. J.* **2010**, *16*, 4739–4743.
- [30] G. Zhang, Y. Luo, Y. Wang, L. Zhang, *Angew. Chem. Int. Ed.* **2011**, *50*, 4450–4454; *Angew. Chem.* **2011**, *123*, 4542–4546.
- [31] T. de Haro, C. Nevado, *J. Am. Chem. Soc.* **2010**, *132*, 1512–1513.
- [32] D. Qian, J. Zhang, *Beilstein J. Org. Chem.* **2011**, *7*, 808–812.
- [33] H. Peng, Y. Xi, N. Ronaghi, B. Dong, N. G. Akhmedov, X. Shi, *J. Am. Chem. Soc.* **2014**, *136*, 13174–13177.
- [34] a) L. T. Ball, G. C. Lloyd-Jones, C. A. Russell, *Science* **2012**, *337*, 1644–1648; b) L. T. Ball, G. C. Lloyd-Jones, C. A. Russell, *J. Am. Chem. Soc.* **2014**, *136*, 254–264; c) A. J. Cresswell, G. C. Lloyd-Jones, *Chem. Eur. J.* **2016**, *22*, 12641–12645.
- [35] X. C. Cambeiro, N. Ahlsten, I. Larrosa, *J. Am. Chem. Soc.* **2015**, *137*, 15636–15639.
- [36] M. Hofer, A. Genoux, R. Kumar, C. Nevado, *Angew. Chem. Int. Ed.* **2017**, *56*, 1021–1025; *Angew. Chem.* **2017**, *129*, 1041–1045.
- [37] T. J. A. Corrie, L. T. Ball, C. A. Russell, G. C. Lloyd-Jones, *J. Am. Chem. Soc.* **2017**, *139*, 245–254.
- [38] a) M. Joost, A. Amgoune, D. Bourissou, *Angew. Chem. Int. Ed.* **2015**, *54*, 15022–15045; *Angew. Chem.* **2015**, *127*, 15234–15258; b) L. Rocchigiani, M. Bochmann, *Chem. Rev.* **2020**, DOI: 10.1021/acs.chemrev.0c00552; c) B. Huang, M. Hu, F. D. Toste, *Trends Chem.* **2020**, *2*, 707–720.
- [39] A. Davison, D. V. Howe, E. T. Shaw, *Inorg. Chem.* **1967**, *6*, 458–463.
- [40] J. H. Enemark, J. A. Ibers, *Inorg. Chem.* **1968**, *7*, 2636–2642.
- [41] A. Shiotani, H. Schmidbaur, *J. Organomet. Chem.* **1972**, *37*, C24-C26.
- [42] A. Tamaki, J. K. Kochi, *J. Chem. Soc. Dalton Trans.* **1973**, 2620–2626.
- [43] R. E. Bachman, S. A. Bodolosky-Bettis, C. J. Pyle, M. A. Gray, *J. Am. Chem. Soc.* **2008**, *130*, 14303–14310.
- [44] a) C.-Y. Wu, T. Horibe, C. B. Jacobsen, F. D. Toste, *Nature* **2015**, *517*, 449–454; b) J. H. Teles, *Angew. Chem. Int. Ed.* **2015**, *54*, 5556–5558; *Angew. Chem.* **2015**, *127*, 5648–5650.
- [45] a) N. Lassauque, P. Gualco, S. Mallet-Ladeira, K. Miqueu, A. Amgoune, D. Bourissou, *J. Am. Chem. Soc.* **2013**, *135*, 13827–13834; b) P. Gualco, S. Ladeira, K. Miqueu, A. Amgoune, D. Bourissou, *Organometallics* **2012**, *31*, 6001–6004; c) P. Gualco, S. Ladeira, K. Miqueu, A. Amgoune, D. Bourissou, *Angew. Chem. Int. Ed.* **2011**, *50*, 8320–8324; *Angew. Chem.* **2011**, *123*, 8470–8474.
- [46] M. Joost, P. Gualco, Y. Coppel, K. Miqueu, C. E. Kefalidis, L. Maron, A. Amgoune, D. Bourissou, *Angew. Chem. Int. Ed.* **2014**, *53*, 747–751; *Angew. Chem.* **2014**, *126*, 766–770.
- [47] M. D. Levin, F. D. Toste, *Angew. Chem. Int. Ed.* **2014**, *53*, 6211–6215; *Angew. Chem.* **2014**, *126*, 6325–6329.
- [48] J. Guenther, S. Mallet-Ladeira, L. Estevez, K. Miqueu, A. Amgoune, D. Bourissou, *J. Am. Chem. Soc.* **2014**, *136*, 1778–1781.
- [49] J. Serra, T. Parella, X. Ribas, *Chem. Sci.* **2017**, *8*, 946–952.
- [50] M. Joost, A. Zeineddine, L. Estévez, S. Mallet-Ladeira, K. Miqueu, A. Amgoune, D. Bourissou, *J. Am. Chem. Soc.* **2014**, *136*, 14654–14657.
- [51] a) J.-F. Fauvarque, F. Pflüger, M. Troupel, *J. Organomet. Chem.* **1981**, *208*, 419–427; b) K. C. Lam, T. B. Marder, Z. Lin, *Organometallics* **2007**, *26*, 758–760; c) A. K. d. K. Lewis, S. Caddick, F. G. N. Cloke, N. C. Billingham, P. B. Hitchcock, J. Leonard, *J. Am. Chem. Soc.* **2003**, *125*, 10066–10073.
- [52] M. Joost, L. Estévez, K. Miqueu, A. Amgoune, D. Bourissou, *Angew. Chem. Int. Ed.* **2015**, *54*, 5236–5240; *Angew. Chem.* **2015**, *127*, 5325–5329.
- [53] M. J. Harper, C. J. Arthur, J. Crosby, E. J. Emmett, R. L. Falconer, A. J. Fensham-Smith, P. J. Gates, T. Leman, J. E. McGrady, J. F. Bower, C. A. Russell, *J. Am. Chem. Soc.* **2018**, *140*, 4440–4445.
- [54] J. A. Cadge, H. A. Sparkes, J. F. Bower, C. A. Russell, *Angew. Chem. Int. Ed.* **2020**, *59*, 6617–6621; *Angew. Chem.* **2020**, *132*, 6679–6683.
- [55] J. Chu, D. Munz, R. Jazzar, M. Melaimi, G. Bertrand, *J. Am. Chem. Soc.* **2016**, *138*, 7884–7887.
- [56] a) A. Zeineddine, L. Estévez, S. Mallet-Ladeira, K. Miqueu, A. Amgoune, D. Bourissou, *Nat. Commun.* **2017**, *8*, 565; b) J. Rodriguez, A. Tabey, S. Mallet-Ladeira, D. Bourissou, *Chem. Sci.* **2021**, DOI: 10.1039/D1SC01483H.
- [57] A. Genoux, M. Biedrzycki, E. Merino, E. Rivera-Chao, A. Linden, C. Nevado, *Angew. Chem. Int. Ed.* **2021**, *60*, 4164–4168; *Angew. Chem.* **2021**, *133*, 4210–4214.
- [58] M. S. Messina, J. M. Stauber, M. A. Waddington, A. L. Rheingold, H. D. Maynard, A. M. Spokoynny, *J. Am. Chem. Soc.* **2018**, *140*, 7065–7069.
- [59] J. M. Stauber, A. L. Rheingold, A. M. Spokoynny, *Inorg. Chem.* **2021**, *60*, 5054–5062.
- [60] L. Huang, F. Rominger, M. Rudolph, A. S. K. Hashmi, *Chem. Commun.* **2016**, *52*, 6435–6438.
- [61] A. Tlhuexet-Aca, M. N. Hopkinson, C. G. Daniliuc, F. Glorius, *Chem. Eur. J.* **2016**, *22*, 11587–11592.
- [62] E. O. Asomoza-Solis, J. Rojas-Ocampo, R. A. Toscano, S. Porcel, *Chem. Commun.* **2016**, *52*, 7295–7298.

- [63] M. S. Winston, W. J. Wolf, F. D. Toste, *J. Am. Chem. Soc.* **2014**, *136*, 7777–7782.
- [64] S. Kim, F. D. Toste, *J. Am. Chem. Soc.* **2019**, *141*, 4308–4315.
- [65] a) M. O. Akram, S. Banerjee, S. S. Saswade, V. Bedi, N. T. Patil, *Chem. Commun.* **2018**, *54*, 11069–11083; b) A. Nijamudheen, A. Datta, *Chem. Eur. J.* **2020**, *26*, 1442–1487; c) S. Kramer, *Synthesis* **2020**, *52*, 2017–2030.
- [66] J. Serra, C. J. Whiteoak, F. Acuna-Pares, M. Font, J. M. Luis, J. Lloret-Fillol, X. Ribas, *J. Am. Chem. Soc.* **2015**, *137*, 13389–13397.
- [67] M. Font, F. Acuña-Parés, T. Parella, J. Serra, J. M. Luis, J. Lloret-Fillol, M. Costas, X. Ribas, *Nat. Commun.* **2014**, *5*:4373.
- [68] J. Rodriguez, A. Zeineddine, E. D. Sosa Carrizo, K. Miqueu, N. Saffon-Merceron, A. Amgoune, D. Bourissou, *Chem. Sci.* **2019**, *10*, 7183–7192.
- [69] J. Rodriguez, N. Adet, N. Saffon-Merceron, D. Bourissou, *Chem. Commun.* **2020**, *56*, 94–97.
- [70] M. O. Akram, A. Das, I. Chakrabarty, N. T. Patil, *Org. Lett.* **2019**, *21*, 8101–8105.
- [71] a) M. Navarro, A. Toledo, M. Joost, A. Amgoune, S. Mallet-Ladeira, D. Bourissou, *Chem. Commun.* **2019**, *55*, 7974–7977; b) M. Navarro, A. Toledo, S. Mallet-Ladeira, E. D. Sosa Carrizo, K. Miqueu, D. Bourissou, *Chem. Sci.* **2020**, *11*, 2750–2758.
- [72] M. Rigoulet, O. Thillaye du Boullay, A. Amgoune, D. Bourissou, *Angew. Chem. Int. Ed.* **2020**, *59*, 16625–16630; *Angew. Chem.* **2020**, *132*, 16768–16773.
- [73] A. G. Tathe, C. C. Chintawar, V. W. Bhojare, N. T. Patil, *Chem. Commun.* **2020**, *56*, 9304–9307.
- [74] A. G. Tathe, Urvashi, A. K. Yadav, C. C. Chintawar, N. T. Patil, *ACS Catal.* **2021**, *11*, 4576–4582.
- [75] C. C. Chintawar, A. K. Yadav, N. T. Patil, *Angew. Chem. Int. Ed.* **2020**, *59*, 11808–11813; *Angew. Chem.* **2020**, *132*, 11906–11911.
- [76] R. Cai, M. Lu, E. Y. Aguilera, Y. Xi, N. G. Akhmedov, J. L. Petersen, H. Chen, X. Shi, *Angew. Chem. Int. Ed.* **2015**, *54*, 8772–8776; *Angew. Chem.* **2015**, *127*, 8896–8900.
- [77] H. Peng, R. Cai, C. Xu, H. Chen, X. Shi, *Chem. Sci.* **2016**, *7*, 6190–6196.
- [78] B. Dong, H. Peng, S. E. Motika, X. Shi, *Chem. Eur. J.* **2017**, *23*, 11093–11099.
- [79] a) M. Barbero, S. Dughera, *Org. Biomol. Chem.* **2018**, *16*, 295–301; b) M. Barbero, S. Dughera, *Tetrahedron* **2018**, *74*, 5758–5769.
- [80] M. O. Akram, P. S. Shinde, C. C. Chintawar, N. T. Patil, *Org. Biomol. Chem.* **2018**, *16*, 2865–2869.
- [81] A. A. Jimoh, S. Hosseyni, X. Ye, L. Wojtas, Y. Hu, X. Shi, *Chem. Commun.* **2019**, *55*, 8150–8153.
- [82] C. Sauer, Y. Liu, A. De Nisi, S. Protti, M. Fagnoni, M. Bandini, *ChemCatChem* **2017**, *9*, 4456–4459.
- [83] a) S. Witzel, J. Xie, M. Rudolph, A. S. K. Hashmi, *Adv. Synth. Catal.* **2017**, *359*, 1522–1528; b) J. Xie, K. Sekine, S. Witzel, P. Krämer, M. Rudolph, F. Rominger, A. S. K. Hashmi, *Angew. Chem. Int. Ed.* **2018**, *57*, 16648–16653; *Angew. Chem.* **2018**, *130*, 16890–16895; c) S. Witzel, K. Sekine, M. Rudolph, A. S. K. Hashmi, *Chem. Commun.* **2018**, *54*, 13802–13804.
- [84] L. Huang, M. Rudolph, F. Rominger, A. S. K. Hashmi, *Angew. Chem. Int. Ed.* **2016**, *55*, 4808–4813; *Angew. Chem.* **2016**, *128*, 4888–4893.
- [85] J.-R. Deng, W.-C. Chan, N. Chun-Him Lai, B. Yang, C.-S. Tsang, B. Chi-Bun Ko, S. Lai-Fung Chan, M.-K. Wong, *Chem. Sci.* **2017**, *8*, 7537–7544.
- [86] S. Taschinski, R. Döpp, M. Ackermann, F. Rominger, F. de Vries, M. F. S. J. Menger, M. Rudolph, A. S. K. Hashmi, J. E. M. N. Klein, *Angew. Chem. Int. Ed.* **2019**, *58*, 16988–16993; *Angew. Chem.* **2019**, *131*, 17144–17149.
- [87] H.-J. Tang, X. Zhang, Y.-F. Zhang, C. Feng, *Angew. Chem. Int. Ed.* **2020**, *59*, 5242–5247; *Angew. Chem.* **2020**, *132*, 5280–5285.
- [88] Y. Li, J. P. Brand, J. Waser, *Angew. Chem. Int. Ed.* **2013**, *52*, 6743–6747; *Angew. Chem.* **2013**, *125*, 6875–6879.
- [89] H. Ghari, Y. Li, R. Roohzadeh, P. Caramenti, J. Waser, A. Ariafard, *Dalton Trans.* **2017**, *46*, 12257–12262.
- [90] S. Banerjee, N. T. Patil, *Chem. Commun.* **2017**, *53*, 7937–7940.
- [91] X. Li, X. Xie, N. Sun, Y. Liu, *Angew. Chem. Int. Ed.* **2017**, *56*, 6994–6998; *Angew. Chem.* **2017**, *129*, 7098–7102.
- [92] a) M. N. Hopkinson, A. Tlahuext-Aca, F. Glorius, *Acc. Chem. Res.* **2016**, *49*, 2261–2272; b) M. Zidan, S. Rohe, T. McCallum, L. Barriault, *Catal. Sci. Technol.* **2018**, *8*, 6019–6028; c) S. Witzel, A. S. K. Hashmi, J. Xie, *Chem. Rev.* **2021**, DOI: 10.1021/acs.chemrev.0c00841.
- [93] B. Sahoo, M. N. Hopkinson, F. Glorius, *J. Am. Chem. Soc.* **2013**, *135*, 5505–5508.
- [94] X.-z. Shu, M. Zhang, Y. He, H. Frei, F. D. Toste, *J. Am. Chem. Soc.* **2014**, *136*, 5844–5847.
- [95] Y. He, H. Wu, F. D. Toste, *Chem. Sci.* **2015**, *6*, 1194–1198.
- [96] A. Tlahuext-Aca, M. N. Hopkinson, B. Sahoo, F. Glorius, *Chem. Sci.* **2016**, *7*, 89–93.
- [97] V. Gauchot, D. R. Sutherland, A. L. Lee, *Chem. Sci.* **2017**, *8*, 2885–2889.
- [98] a) A. Tlahuext-Aca, M. N. Hopkinson, R. A. Garza-Sanchez, F. Glorius, *Chem. Eur. J.* **2016**, *22*, 5909–5913; b) J. Um, H. Yun, S. Shin, *Org. Lett.* **2016**, *18*, 484–487; c) B. Alcaide, P. Almendros, E. Busto, A. Luna, *Adv. Synth. Catal.* **2016**, *358*, 1526–1533.
- [99] H. Li, C. Shan, C.-H. Tung, Z. Xu, *Chem. Sci.* **2017**, *8*, 2610–2615.
- [100] Z. Xia, V. Corcé, F. Zhao, C. Przybylski, A. Espagne, L. Jullien, T. Le Saux, Y. Gimbert, H. Dossmann, V. Mouriès-Mansuy, C. Ollivier, L. Fensterbank, *Nat. Chem.* **2019**, *11*, 797–805.

Manuscript received: April 15, 2021
Revised manuscript received: May 14, 2021
Accepted manuscript online: May 19, 2021

ANNEX 2. Supporting information Chapter III

SUPPORTING INFORMATION

Hemilabile MIC[^]N ligands allow oxidant-free Au(I)/Au(III) arylation-lactonization of γ -alkenoic acids

Pau Font,[†] Hugo Valdés,^{†,*} Gregorio Guisado-Barrios,^{‡,*} Xavi Ribas^{†,*}

Table of Contents

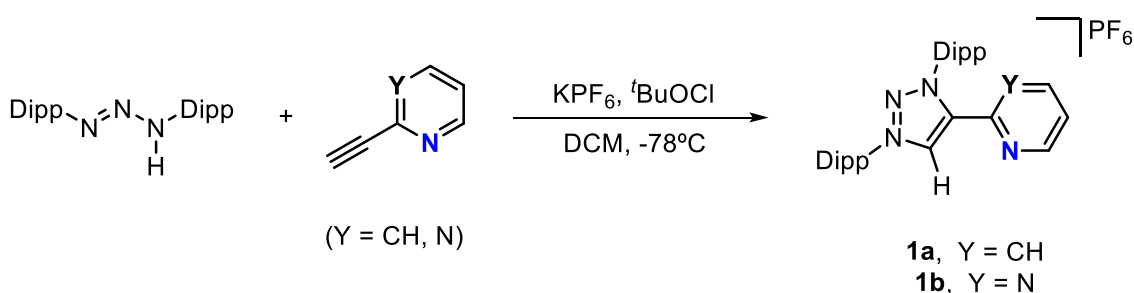
1. General considerations	3
2. Synthesis of triazolium salts 1a and 1b	3
3. Synthesis and reactivity of gold MIC complexes	5
3.1 General procedure for the synthesis of gold(I) complexes 2a and 2b.....	5
3.2 General procedure for the synthesis of dimeric gold(I) complexes 3a and 3b	6
3.3 General procedure for the synthesis of gold(III) complexes 4a-Cl and 4a-OAc via oxidation	8
3.4 Synthesis of gold(III) complexes 5b and 6b via oxidative addition.....	9
3.5 Synthesis of gold(III) complex cis-7a-Cl via oxidative addition	11
3.6 General procedure for the reactivity of gold(I) complexes 2a and 2b towards aryl halides.....	12
3.7 Reductive elimination from cis-7a-Cl to 8a-OMe	14
4. Optimization of the arylation-lactonization reaction of γ-alkenoic acids.....	15
5. Scope of the arylation-lactonization reaction of γ-alkenoic acids.....	18
6. Au(I)-catalyzed oxyarylation and 1,2-diarylation reactions of alkenes	20
7. Mechanistic studies	21
7.1 Role of the silver salt	21
7.2 Stoichiometric reaction from complex cis-7a-Cl to product 10	22
8. NMR and HRMS-ESI spectra	23
8.1 NMR and HRMS-ESI Spectra of triazolium salt 1a	23

8.2 NMR and HRMS-ESI Spectra of triazolium salt 1b	24
8.3 NMR Spectra of complex 2a	26
8.4 NMR Spectra of complex 2b	29
8.5 NMR Spectra of complex 3a	32
8.6 NMR Spectra of complex 3b	35
8.7 NMR and HRMS-ESI Spectra of complex 4a-Cl	38
8.8 NMR and HRMS-ESI Spectra of complex 4a-OAc	41
8.9 NMR and HRMS-ESI Spectra of complex 5b	45
8.10 NMR and HRMS-ESI Spectra of complex 6b	49
8.11 NMR and HRMS-ESI Spectra of complex cis-7a-Cl	52
8.12 NMR and HRMS-ESI Spectra of compound 8b-OMe	56
8.13 NMR and HRMS-ESI Spectra of compound 8a-Me	57
8.14 NMR and HRMS-ESI Spectra of compound 8a-OMe	58
8.15 NMR Spectra of compound 10	62
8.16 NMR and HRMS-ESI Spectra of compound 15	63
8.17 NMR and HRMS-ESI Spectra of compound 16	66
9. X-Ray structures and crystallographic data	69
9.1 Complex 2a	69
9.2 Complex 2b	70
9.3 Complex 3a	72
9.4 Complex 3b-biphenylene	73
9.5 Complex 4a-Cl	75
9.6 Complex 4a-OAc	76
9.7 Complex 5b	78
9.8 Complex 6b	79
9.9 Complex cis-7a-Cl	81
9.10 Compounds 8a-OMe and 9a	82
9.11 Compound 8b-OMe	84
9.12 Compound 16	85
10. References	87

1. General considerations

All reagents and solvents were purchased from Sigma Aldrich, Fischer Scientific, TCI or Fluorochem and were used without further purification. *Tert*-butyl hypochlorite¹ and 1,3-bis(2,6-diisopropylphenyl)triaz-1-ene² were prepared following reported methods. NMR spectra were recorded on Bruker spectrometers operating at 400 MHz (¹H NMR) and 101 MHz (¹³C{¹H} NMR), and referenced to residual solvent, (δ in ppm and J in hertz). ¹H NMR spectra recorded in CD₂Cl₂ are referenced at 5.32 ppm and those recorded in CDCl₃, at 7.26 ppm. Quantification of reaction yields was done by integration of the NMR signals, using an internal standard. High resolution mass spectra (HRMS) were recorded on a Bruker MicroTOF-Q IITM instrument using ESI source at Serveis Tècnics de Recerca, University of Girona. For reactions carried out under inert atmosphere, a N₂ drybox with O₂ and H₂O concentrations <1 ppm was employed. The reaction carried out under blue LED irradiation was performed in an in-house created photoreactor, which consists in an aluminum block with 16 holes for 20 mL vials, at the bottom of each hole is located a LED irradiation source. The aluminum block is over an orbital shaker and is also equipped with a refrigeration system to control the temperature of the photoreactor.

2. Synthesis of triazolium salts **1a** and **1b**



Scheme S1. Synthesis of triazolium salts **1a** and **1b**.

The triazolium salts were prepared by adapting a reported method in the literature.³

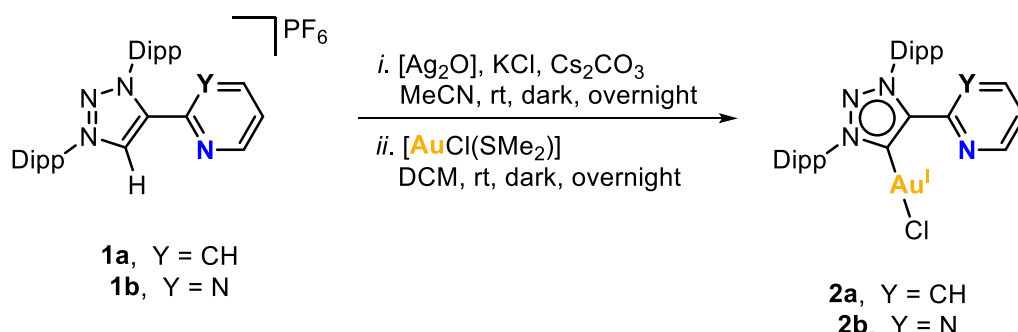
Synthesis of 1a. To a stirred suspension of 1,3-bis(2,6-diisopropylphenyl)triaz-1-ene (2.84 g, 7.8 mmol, 1.3 eq) and anhydrous potassium hexafluorophosphate (1.64 g, 9 mmol, 1.5 eq) in dry dichloromethane (30 mL) in the dark at -78°C was added *tert*-butyl hypochlorite (0.9 mL, 8 mmol, 1.3 eq) upon which the mixture instantly darkens. Stirring at -78°C, 2-ethynylpyridine (0.6 mL, 6 mmol, 1 eq) was added. The mixture was stirred overnight and was slowly allowed to warm to room temperature. The resulting red-brown solution was filtered using a frit funnel to remove a fine precipitate. The volatiles were then removed under reduced pressure to afford a light greenish powder, which was washed several times with diethyl ether followed by tetrahydrofuran and pentane to afford a white powder. Yield: 3.63 g (99%). ¹H NMR (400 MHz, CD₂Cl₂): δ 9.91 (s, 1H, CH_{trz}),

8.53 (ddd, $J = 4.8, 1.7, 0.9$ Hz, 1H, CH_{Ar}), 7.91 (td, $J = 7.8, 1.8$, Hz, 1H, CH_{Ar}), 7.77-7.70 (m, 3H, CH_{Ar}), 7.50 (d, $J = 7.9$ Hz, 2H, CH_{Ar}), 7.48 (dd, $J = 3.0, 1.1$ Hz, 1H, CH_{Ar}), 7.45 (d, $J = 7.9$ Hz, 2H, CH_{Ar}), 2.38 (hept, $J = 6.8$ Hz, 2H, $CH(CH_3)_2$), 2.27 (hept, $J = 6.8$ Hz, 2H, $CH(CH_3)_2$), 1.36 (d, $J = 6.8$ Hz, 6H, $CH(CH_3)_2$), 1.21 (dd, $J = 6.8$ Hz, 12H, $CH(CH_3)_2$), 1.06 (d, $J = 6.8$ Hz, 6H, $CH(CH_3)_2$). ^{13}C NMR (101 MHz, CD_2Cl_2): δ 151.1 (CH_{Ar}), 145.6 (C_{Ar}), 145.6 (C_{Ar}), 145.1 (C_{Ar}), 141.8 (C_{trz}), 138.7 (CH_{Ar}), 134.1 (CH_{Ar}), 133.7 (CH_{Ar}), 132.3 (CH_{trz}), 131.1 (C_{Ar}), 131.0 (C_{Ar}), 127.3 (CH_{Ar}), 125.6 (CH_{Ar}), 125.0 (CH_{Ar}), 30.3 ($CH(CH_3)_2$), 30.0 ($CH(CH_3)_2$), 25.1 ($CH(CH_3)_2$), 25.0 ($CH(CH_3)_2$), 23.8 ($CH(CH_3)_2$), 23.1 ($CH(CH_3)_2$). **HRMS (ESI+)**: calculated for $C_{31}H_{39}F_6N_4P$ $[M-PF_6]^+$: m/z 467.3175; found: m/z 467.3172.

Synthesis of 1b. To a stirred suspension of 1,3-bis(2,6-diisopropylphenyl)triaz-1-ene (4.58 g, 9.6 mmol, 1 eq) and anhydrous potassium hexafluorophosphate (2.65 g, 14.4 mmol, 1.5 eq) in dry dichloromethane (30 mL) in the dark at $-78^\circ C$ was added *tert*-butyl hypochlorite (1.45 mL, 12.9 mmol, 1.3 eq) upon which the mixture instantly darkens. Stirring was pursued at $-78^\circ C$ for 30 min and 2-ethynylpyrimidine (1 g, 9.6 mmol, 1 eq) was added. The mixture was stirred overnight and was slowly allowed to warm to room temperature. The resulting dark solution was filtered using a frit funnel, and the solid residue was washed with dichloromethane. The filtrate was collected, and the volatiles were removed under reduced pressure to afford a dark green foam, which was washed several times with diethyl ether, followed by tetrahydrofuran and pentane to afford a white powder. Yield: 3.94 g (67 %). 1H NMR (400 MHz, CD_2Cl_2): δ 9.24 (s, 1H, CH_{trz}), 8.80 (d, $J = 5.0$ Hz, 2H, CH_{pym}), 7.77 (t, $J = 7.9$ Hz, 1H, CH_{Ar}), 7.72 (t, $J = 7.8$ Hz, 1H, CH_{Ar}), 7.55 – 7.49 (m, 3H: 1H CH_{pym} and 2H CH_{Ar}), 7.44 (d, $J = 7.9$ Hz, 2H, CH_{Ar}), 2.37 (hept, $J = 6.8$ Hz, 2H, $CH(CH_3)_2$), 2.23 (hept, $J = 6.7$ Hz, 2H, $CH(CH_3)_2$), 1.36 (d, $J = 6.8$ Hz, 6H, $CH(CH_3)_2$), 1.21 (dd, $J = 14.2, 6.9$ Hz, 12H, $CH(CH_3)_2$), 1.06 (d, $J = 6.8$ Hz, 6H, $CH(CH_3)_2$). ^{13}C NMR (101 MHz, CD_2Cl_2): δ 158.8 (CH_{Ar}), 152.8 (C_{Ar}), 145.6 (C_{Ar}), 145.3 (C_{Ar}), 144.0 (C_{trz}), 134.3 (CH_{Ar}), 134.2 (CH_{Ar}), 133.6 (CH_{trz}), 131.3 (C_{Ar}), 130.8 (C_{Ar}), 125.7 (CH_{Ar}), 125.4 (CH_{Ar}), 123.8 (CH_{Ar}), 30.3 ($CH(CH_3)_2$), 30.1 ($CH(CH_3)_2$), 25.1 ($CH(CH_3)_2$), 24.9 ($CH(CH_3)_2$), 23.9 ($CH(CH_3)_2$), 23.2 ($CH(CH_3)_2$). **HRMS (ESI+)**: calculated for $C_{31}H_{39}F_6N_4P$ $[M-PF_6]^+$: m/z 468.3127; found: m/z 468.3117.

3. Synthesis and reactivity of gold MIC complexes

3.1 General procedure for the synthesis of gold(I) complexes **2a** and **2b**



Scheme S2. Synthesis of gold(I)-MIC complexes **2a** and **2b**.

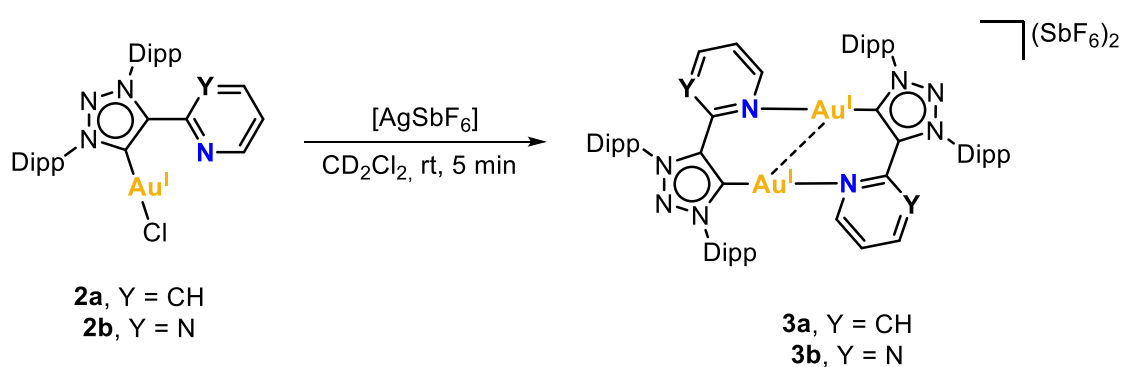
For the synthesis of Au(I) MIC complexes we followed a similar procedure to that reported in the literature.⁴ A solution of the corresponding triazolium salt (1 eq), silver(I) oxide (1.5 eq), potassium chloride (2 eq) and cesium carbonate (3 eq) in anhydrous acetonitrile was stirred overnight at room temperature under exclusion of light. After this time, the solution was filtered over Celite® and all volatiles were removed under vacuum. The obtained residue was dissolved in anhydrous dichloromethane, followed by the addition in one portion of dimethylsulfide gold(I) chloride. The resulting reaction mixture was stirred overnight at room temperature under exclusion of light. Then, the solution was filtered over Celite®, and all the volatiles were removed under vacuum. The product was purified by chromatographic column, using silica gel as stationary phase and dichloromethane as mobile phase. After the column, the fractions that contained the product were combined, and the solvent was reduced to the minimal portion. The addition of diethyl ether affords a white-off solid that contained the desired product. The gold complexes can be further crystallized by slow diffusion of diethyl ether into a concentrated solution of the complex in dichloromethane.

Synthesis of 2a. For the synthesis of **2a** was employed the triazolium salt **1a** (418.2 mg, 0.68 mmol, 1.0 eq), Ag₂O (256.9 mg, 1.11 mmol, 1.6 eq), KCl (121.2 mg, 1.63 mmol, 2.4 eq) and Cs₂CO₃ (678.0 mg, 2.08 mmol, 3.0 eq) in acetonitrile (55 mL), and [AuCl(SMe₂)] (197.3 mg, 0.67 mmol, 1.0 eq) in dichloromethane (55 mL). Yield: 154.7 mg (32%). ¹H NMR (400 MHz, CD₂Cl₂): δ 8.65 (dt, *J* = 8.0, 1.1 Hz, 1H, CH_{py}), 8.30 (ddd, *J* = 4.8, 1.8, 1.0 Hz, 1H, CH_{py}), 7.84 (td, *J* = 7.8, 1.8 Hz, 1H, CH_{py}), 7.65 (t, *J* = 7.8 Hz, 1H, CH_{Ar}), 7.54 (t, *J* = 7.8 Hz, 1H, CH_{Ar}), 7.41 (d, *J* = 7.9 Hz, 2H, CH_{Ar}), 7.29–7.26 (m, 3H: 2H CH_{Ar} and 1H CH_{py}), 2.51 (hept, *J* = 6.9 Hz, 2H, CH(CH₃)₂), 2.36 (hept, *J* = 6.9 Hz, 2H, CH(CH₃)₂), 1.41 (d, *J* = 6.8 Hz, 6H, CH(CH₃)₂), 1.19 (d, *J* = 6.9 Hz, 6H, CH(CH₃)₂), 1.14 (d, *J* = 6.9 Hz, 6H, CH(CH₃)₂), 1.01 (d, *J* = 6.8 Hz, 6H, CH(CH₃)₂). ¹³C NMR (101 MHz, CD₂Cl₂): δ 162.1 (C_{carbene}-Au), 149.7 (CH_{py}), 147.3 (C_{trz}), 146.5 (C_{py}), 145.8 (C_{Ar}, 2C), 145.7 (C_{Ar}, 2C), 137.4 (CH_{py}), 135.7 (C_{Ar}), 132.9 (C_{Ar}), 132.2 (CH_{Ar}),

131.9 (CH_{Ar}), 125.0 (CH_{py}), 125.0 (CH_{Ar} , 2C), 124.9 (CH_{py}), 124.4 (CH_{Ar} , 2C), 30.0 ($\text{CH}(\text{CH}_3)_2$), 29.6 ($\text{CH}(\text{CH}_3)_2$), 25.1 ($\text{CH}(\text{CH}_3)_2$), 24.7 ($\text{CH}(\text{CH}_3)_2$), 24.5 ($\text{CH}(\text{CH}_3)_2$), 23.0 ($\text{CH}(\text{CH}_3)_2$). **HRMS (ESI+)**: calcd for $\text{C}_{31}\text{H}_{38}\text{N}_4\text{AuCl}$ [$\text{M}+\text{Na}$] $^+$: m/z 721.2343; found: m/z 721.2322.

Synthesis of 2b. For the synthesis of **2b** was employed the azolium salt **1b** (499.7 mg, 0.81 mmol, 1.0 eq), Ag_2O (290.5 mg, 1.25 mmol, 1.5 eq), KCl (126.1 mg, 1.69 mmol, 2.1 eq) and Cs_2CO_3 (808.6 mg, 2.48 mmol, 3.0 eq) in acetonitrile (65 mL), and $[\text{AuCl}(\text{SMe}_2)]$ (243.6 mg, 0.83 mmol, 1.0 eq) in dichloromethane (65 mL). Yield: 199.7 mg (35%). **^1H NMR** (400 MHz, CD_2Cl_2): δ 8.71 (d, $J = 4.9$ Hz, 2H, CH_{pym}), 7.65 (t, $J = 7.8$ Hz, 1H, CH_{Ar}), 7.56 (t, $J = 7.8$ Hz, 1H, CH_{Ar}), 7.41 (d, $J = 7.8$ Hz, 2H, CH_{Ar}), 7.32 – 7.28 (m, 3H: 2H CH_{Ar} and 1H CH_{pym}), 2.52 (hept, $J = 6.8$ Hz, 2H, $\text{CH}(\text{CH}_3)_2$), 2.37 (hept, $J = 6.8$ Hz, 2H, $\text{CH}(\text{CH}_3)_2$), 1.41 (d, $J = 6.8$ Hz, 6H, $\text{CH}(\text{CH}_3)_2$), 1.19 (d, $J = 6.9$ Hz, 6H, $\text{CH}(\text{CH}_3)_2$), 1.15 (d, $J = 6.9$ Hz, 6H, $\text{CH}(\text{CH}_3)_2$), 1.02 (d, $J = 6.8$ Hz, 6H, $\text{CH}(\text{CH}_3)_2$). **^{13}C NMR** (101 MHz, CD_2Cl_2): δ 165.3 ($\text{C}_{\text{carbene-Au}}$), 157.8 (CH_{pym} , 2C), 156.5 (C_{pym}), 146.5 (C_{trz}), 145.8 (C_{Ar} , 2C), 145.7 (C_{Ar} , 2C), 135.7 (C_{Ar}), 132.7 (C_{Ar}), 132.3 (CH_{Ar}), 132.1 (CH_{Ar}), 125.0 (CH_{Ar} , 2C), 124.6 (CH_{Ar} , 2C), 121.5 (CH_{pym}), 29.9 ($\text{CH}(\text{CH}_3)_2$), 29.6 ($\text{CH}(\text{CH}_3)_2$), 25.1 ($\text{CH}(\text{CH}_3)_2$), 24.7 ($\text{CH}(\text{CH}_3)_2$), 24.4 ($\text{CH}(\text{CH}_3)_2$), 23.2 ($\text{CH}(\text{CH}_3)_2$). **HRMS (ESI+)**: calcd for $\text{C}_{30}\text{H}_{37}\text{N}_5\text{AuCl}$ [$\text{M}+\text{Na}$] $^+$: m/z 722.2295; found: m/z 722.2273.

3.2 General procedure for the synthesis of dimeric gold(I) complexes **3a** and **3b**



Scheme S3. Synthesis of dimeric gold(I)-MIC complexes **3a** and **3b**.

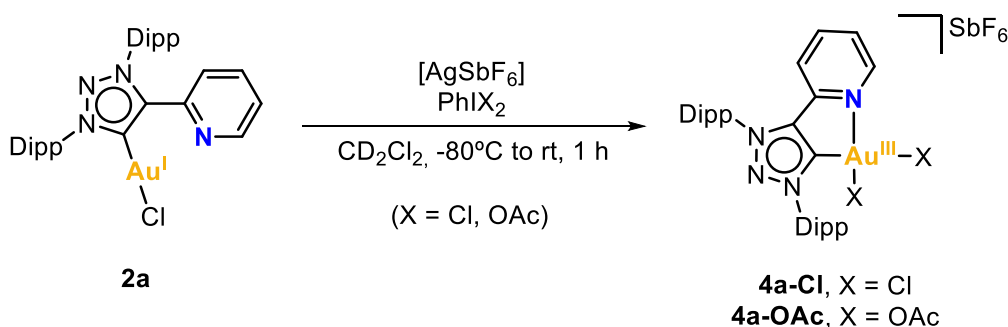
This procedure was carried out under nitrogen atmosphere using glovebox techniques. To a solution of $[\text{AgSbF}_6]$ in CD_2Cl_2 (0.2 mL) was added a solution of **2a** or **2b** in CD_2Cl_2 (0.5 mL). The resulting reaction mixture was stirred at room temperature for 5 min, then filtered through a micro filter and evaporated under vacuum. The resulting dimeric gold(I) complexes were obtained as white solids. For the case of **3a**, diethyl ether was slowly

diffused into a solution of the complex in dichloromethane, obtaining crystals that were suitable for X-ray diffraction.

Synthesis of 3a. 14.6 mg of **2a** (0.02 mmol, 1.0 eq) were mixed with 7.2 mg of [AgSbF₆] (0.02 mmol, 1.0 eq). Yield: 17.5 mg (93%). ¹H NMR (400 MHz, CD₂Cl₂) δ 8.65 (dd, *J* = 5.7, 1.6 Hz, 2H, CH_{py}), 7.94 (td, *J* = 8.0, 1.7 Hz, 2H, CH_{py}), 7.75 – 7.66 (m, 6H: 2H CH_{py} and 4H CH_{Ar}), 7.49 (d, *J* = 7.9 Hz, 4H, CH_{Ar}), 7.41 (d, *J* = 7.9 Hz, 4H, CH_{Ar}), 7.31 (dd, *J* = 8.3, 1.3 Hz, 2H, CH_{py}), 2.42 (hept, *J* = 6.8 Hz, 4H, CH(CH₃)₂), 2.25 (br s, 4H, CH(CH₃)₂), 1.45 (d, *J* = 6.7 Hz, 12H, CH(CH₃)₂), 1.26 (d, *J* = 6.8 Hz, 12H, CH(CH₃)₂), 1.16 (d, *J* = 6.8 Hz, 12H, CH(CH₃)₂), 0.95 (br s, 12H, CH(CH₃)₂). ¹³C NMR (101 MHz, CD₂Cl₂): δ 157.2 (C_{carbene}-Au), 154.5 (CH_{py}), 147.0 (C_{trz}), 145.5 – 145.2 (C_{Ar} and C_{py}), 141.7 (CH_{py}), 135.0 (C_{Ar}), 134.3 (CH_{Ar}), 133.4 (CH_{Ar}), 130.4 (CH_{py}), 130.1 (C_{Ar}), 128.7 (CH_{py}), 126.4 (CH_{Ar}), 125.5 (CH_{Ar}), 30.1 (CH(CH₃)₂), 30.0 (CH(CH₃)₂), 26.0 (CH(CH₃)₂), 24.9 (CH(CH₃)₂), 24.7 (CH(CH₃)₂), 22.7 (CH(CH₃)₂). **HRMS (ESI+):** calcd for C₃₁H₃₈AuN₄ [(MIC^{N^{py}})Au+MeCN]⁺: *m/z* 704.3027; found: *m/z* 704.3025.

Synthesis of 3b. 14.8 mg of **2b** (0.02 mmol, 1.0 eq) were mixed with 8.0 mg of [AgSbF₆] (0.02 mmol, 1.1 eq). Yield: 18.9 mg (99%). ¹H NMR (400 MHz, CD₂Cl₂) δ 8.83 (dd, *J* = 5.8, 2.2 Hz, 2H, CH_{pym}), 8.73 (dd, *J* = 4.8, 2.2 Hz, 2H, CH_{pym}), 7.73 – 7.67 (m, 4H: 2H CH_{Ar} and 2H CH_{pym}), 7.62 (t, *J* = 7.9 Hz, 2H, CH_{Ar}), 7.47 (d, *J* = 7.9 Hz, 4H, CH_{Ar}), 7.35 (d, *J* = 7.9 Hz, 4H, CH_{Ar}), 2.39 (hept, *J* = 6.6 Hz, 4H, CH(CH₃)₂), 2.26 – 2.15 (m, 4H, CH(CH₃)₂), 1.43 (d, *J* = 6.8 Hz, 12H, CH(CH₃)₂), 1.26 (d, *J* = 6.8 Hz, 12H, CH(CH₃)₂), 1.16 (d, *J* = 6.8 Hz, 12H, CH(CH₃)₂), 1.01 (d, *J* = 6.7 Hz, 12H, CH(CH₃)₂). ¹³C NMR (101 MHz, CD₂Cl₂) δ 161.3 (CH_{pym}), 160.4 (CH_{pym}), 157.2 (C_{carbene}-Au), 154.8 (C_{pym}), 145.8 (C_{trz}), 145.5 (br s, C_{Ar}), 134.8 (C_{Ar}), 133.5 (CH_{Ar}), 133.3 (CH_{Ar}), 131.7 (C_{Ar}), 125.6 (CH_{Ar}), 125.2 (CH_{Ar}), 123.9 (CH_{pym}), 30.4 (CH(CH₃)₂), 29.9 (CH(CH₃)₂), 25.3 (CH(CH₃)₂), 25.1 (CH(CH₃)₂), 24.6 (CH(CH₃)₂), 23.2 (CH(CH₃)₂). **HRMS (ESI+):** calcd for C₃₀H₃₇AuN₅ [(MIC^{N^{pym}})Au+MeCN]⁺: *m/z* 705.2980; found: *m/z* 705.2991.

3.3 General procedure for the synthesis of gold(III) complexes **4a-Cl** and **4a-OAc** via oxidation



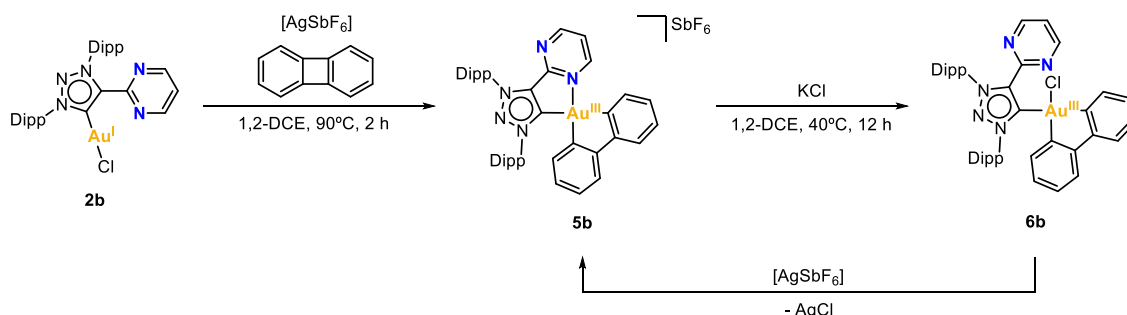
Scheme S4. Synthesis of gold(III)-MIC complexes **4a-Cl** and **4a-OAc**.

Under nitrogen atmosphere, a vial was charged with **2a** in CD_2Cl_2 (0.15 mL) and cooled to -80°C . Afterwards, $[\text{AgSbF}_6]$ in CD_2Cl_2 (0.3 mL) and PhICl_2 or $\text{PhI}(\text{OAc})_2$ in CD_2Cl_2 (0.3 mL) were added. The PhICl_2 used was freshly prepared following a reported procedure.⁵ Then, the reaction mixture was stirred and slowly warmed up to room temperature. During this time, an intense yellow color was observed with the concomitant formation of a grey solid. After 1h at room temperature, the reaction mixture was filtered over Celite®, obtaining a yellow solution. The ^1H NMR of the reaction mixture revealed that complex **2a** was quantitatively consumed. Slow diffusion of diethyl ether into this latter solution afforded crystals of the desired product.

Synthesis of 4a-Cl. 20.1 mg of **2a** (0.03 mmol, 1.0 eq) were mixed with 11.4 mg of AgSbF_6 (0.03 mmol, 1.2 eq) and 9.2 mg of PhICl_2 (0.03 mmol, 1.2 eq). **4a-Cl** was obtained as pale-yellow needles. Yield: 19.6 mg (70%). ^1H NMR (400 MHz, CD_2Cl_2) δ 9.83 (dd, $J = 6.0, 1.4$ Hz, 1H, CH_{py}), 8.27 (td, $J = 7.9, 1.4$ Hz, 1H, CH_{py}), 7.96 (ddd, $J = 7.7, 6.0, 1.5$ Hz, 1H, CH_{py}), 7.89 (t, $J = 7.9$ Hz, 1H, CH_{Ar}), 7.72 (t, $J = 7.9$ Hz, 1H, CH_{Ar}), 7.62 (d, $J = 7.9$ Hz, 2H, CH_{Ar}), 7.44 (d, $J = 7.9$ Hz, 2H, CH_{Ar}), 6.83 (ddd, $J = 8.0, 1.6, 0.6$ Hz, 1H, CH_{py}), 2.40 – 2.25 (m, 4H, $\text{CH}(\text{CH}_3)_2$), 1.36 (d, $J = 6.7$ Hz, 6H, $\text{CH}(\text{CH}_3)_2$), 1.21 – 1.17 (m, 18H, $\text{CH}(\text{CH}_3)_2$). ^{13}C NMR (101 MHz, CD_2Cl_2): δ 152.0 (CH_{py}), 149.0 (C_{trz}), 147.3 ($\text{C}_{\text{carbene-Au}}$), 145.9 (C_{Ar}), 145.9 (CH_{py}), 145.7 (C_{Ar}), 143.7 (C_{py}), 135.3 (CH_{Ar}), 133.7 (CH_{Ar}), 132.1 (C_{Ar}), 130.1 (CH_{py}), 128.6 (C_{Ar}), 126.8 (CH_{Ar}), 125.1 (CH_{Ar}), 123.8 (CH_{py}), 30.2 ($\text{CH}(\text{CH}_3)_2$), 30.1 ($\text{CH}(\text{CH}_3)_2$), 25.6 ($\text{CH}(\text{CH}_3)_2$), 25.3 ($\text{CH}(\text{CH}_3)_2$), 23.4 ($\text{CH}(\text{CH}_3)_2$), 23.4 ($\text{CH}(\text{CH}_3)_2$). **HRMS (ESI+)**: calcd for $\text{C}_{31}\text{H}_{38}\text{AuCl}_2\text{F}_6\text{N}_4\text{Sb}$ $[\text{M-SbF}_6]^+$: m/z 733.2134; found: m/z 733.2132.

Synthesis of 4a-OAc. 20.0 mg of **2a** (0.03 mmol, 1.0 eq) were mixed with 11.8 mg of AgSbF₆ (0.03 mmol, 1.2 eq) and 10.9 mg of PhI(OAc)₂ (0.03 mmol, 1.2 eq). **4a-OAc** was obtained as yellow blocks. Yield: 27.5 mg (95%). ¹H NMR (400 MHz, CD₂Cl₂) δ 8.88 (dd, *J* = 5.9, 1.4 Hz, 1H, CH_{py}), 8.30 (td, *J* = 7.9, 1.4 Hz, 1H, CH_{py}), 7.95 – 7.87 (m, 2H: 1H CH_{py} and 1H CH_{Ar}), 7.71 (t, *J* = 7.8 Hz, 1H, CH_{Ar}), 7.62 (d, *J* = 7.9 Hz, 2H, CH_{Ar}), 7.48 (d, *J* = 7.9 Hz, 2H, CH_{Ar}), 6.82 (dd, *J* = 8.0, 1.4 Hz, 1H, CH_{py}), 2.45 (hept, *J* = 6.9 Hz, 2H, CH(CH₃)₂), 2.26 (hept, *J* = 6.8 Hz, 2H, CH(CH₃)₂), 2.14 (s, 3H, CH₃COO *cis* to py), 1.45 (d, *J* = 6.7 Hz, 6H, CH(CH₃)₂), 1.36 (s, 3H, CH₃COO *trans* to py), 1.21 – 1.15 (m, 18H, CH(CH₃)₂). ¹³C NMR (101 MHz, CD₂Cl₂): δ 176.7 (COOCH₃ *cis* to py), 174.9 (COOCH₃ *trans* to py), 151.8 (CH_{py}), 148.5 (C_{trz}), 146.3 (CH_{py}), 146.3 (C_{Ar}), 145.8 (C_{Ar}), 143.9 (C_{py}), 137.1 (C_{carbene-Au}), 135.4 (CH_{Ar}), 133.9 (CH_{Ar}), 131.3 (C_{Ar}), 129.9 (CH_{py}), 128.3 (C_{Ar}), 126.9 (CH_{Ar}), 125.4 (CH_{Ar}), 123.6 (CH_{py}), 30.3 (CH(CH₃)₂), 30.0 (CH(CH₃)₂), 26.2 (CH(CH₃)₂), 25.5 (CH(CH₃)₂), 23.7 (CH(CH₃)₂), 23.2 (COOCH₃ *cis* to py), 22.6 (CH(CH₃)₂), 19.0 (COOCH₃ *trans* to py). HRMS (ESI⁺): calcd for C₃₅H₄₄AuF₆N₄O₄Sb [M-SbF₆]⁺: *m/z* 781.3023; found: *m/z* 781.3022.

3.4 Synthesis of gold(III) complexes **5b** and **6b** via oxidative addition



Scheme S5. Synthesis of gold(III)-MIC complexes **5b** and **6b**.

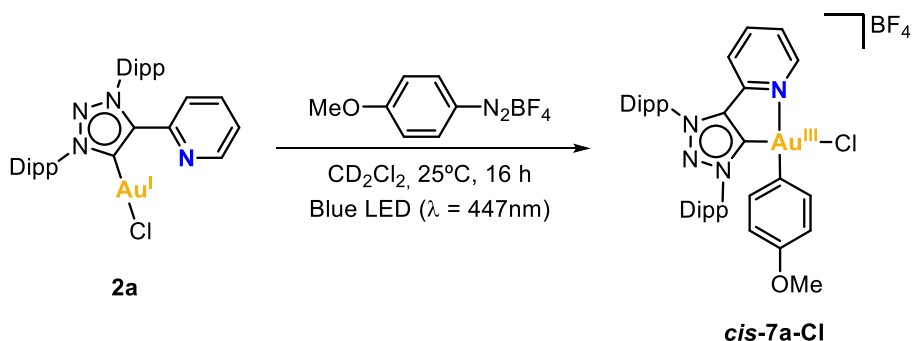
Under nitrogen atmosphere, a solution of **2b** (10.6 mg, 0.02 mmol, 1 eq) and biphenylene (10.4 mg, 0.07 mmol, 4.5 eq) in 1,2-dichloroethane (0.4 mL) was added to a solution of [AgSbF₆] (7.0 mg, 0.02 mmol, 1.3 eq) in 1,2-dichloroethane (0.35 mL). The reaction mixture was then stirred and heated at 90°C for 2h. After this time, it was filtered through a micro filter, obtaining a green solution that contains **5b**. Then, powdered KCl (12.1 mg, 0.16 mmol, 10.7 eq) was added and the mixture was stirred for 12h at 40°C. After the solution was cooled down to room temperature, it was filtered through a micro-filter to obtain a clear yellow solution. All the volatiles were removed under vacuum, and the solid residue was dissolved in the minimal amount of dichloromethane. By slow diffusion of diethyl ether into this latter solution, crystals of the desired complex **6b** were obtained.

For the synthesis of **5b**, [AgSbF₆] (6.2 mg, 0.02 mmol, 1.5 eq) was added to a solution of **6b** (10.4 mg, 0.01 mmol, 1 eq) in dichloromethane (0.5 mL) and the mixture was stirred at room temperature for 10 minutes. Then, it was filtered through a micro filter to obtain a clear yellow solution. The volatiles were removed under vacuum, yielding the desired complex **5b** as a pale yellow solid.

Synthesis of 6b. Yield: 7.7 mg (60%). ¹H NMR (400 MHz, CD₂Cl₂) δ 8.56 (d, *J* = 4.9 Hz, 2H, CH_{pym}), 8.02 (dd, *J* = 7.5, 1.4 Hz, 1H, CH_{BPL}), 7.62 (t, *J* = 7.8 Hz, 1H, CH_{Ar}), 7.55 (t, *J* = 7.8 Hz, 1H, CH_{Ar}), 7.43 (dd, *J* = 7.8, 1.4 Hz, 1H, CH_{Ar}), 7.39 (dd, *J* = 7.8, 1.4 Hz, 1H, CH_{Ar}), 7.32 (dd, *J* = 7.8, 1.4 Hz, 1H, CH_{Ar}), 7.29 (dd, *J* = 7.7, 1.5 Hz, 2H, CH_{BPL}), 7.24 (dd, *J* = 7.8, 1.4 Hz, 1H, CH_{Ar}), 7.12 (t, *J* = 4.9 Hz, 1H, CH_{pym}), 7.08 (td, *J* = 7.4, 1.4 Hz, 1H, CH_{BPL}), 7.00 (tdd, *J* = 7.4, 5.9, 1.4 Hz, 2H, CH_{BPL}), 6.81 (dd, *J* = 7.7, 1.2 Hz, 1H, CH_{BPL}), 6.58 (td, *J* = 7.6, 1.5 Hz, 1H, CH_{BPL}), 2.83 – 2.69 (m, 2H, CH(CH₃)₂), 2.53 – 2.42 (m, 2H, CH(CH₃)₂), 1.50 (d, *J* = 6.6 Hz, 3H, CH(CH₃)₂), 1.34 (d, *J* = 6.8 Hz, 3H, CH(CH₃)₂), 1.27 (d, *J* = 6.8 Hz, 3H, CH(CH₃)₂), 1.21 (d, *J* = 6.8 Hz, 3H, CH(CH₃)₂), 1.16 (d, *J* = 6.9 Hz, 3H, CH(CH₃)₂), 1.01 (d, *J* = 6.9 Hz, 3H, CH(CH₃)₂), 0.79 (d, *J* = 6.8 Hz, 3H, CH(CH₃)₂), 0.71 (d, *J* = 6.7 Hz, 3H, CH(CH₃)₂). ¹³C NMR (101 MHz, CD₂Cl₂) δ 180.1 (C_{carbene-Au}), 160.3 (C_{BPL-Au trans to carbene}), 157.7 (CH_{pym}, 2C), 156.6 (C_{pym}), 154.9 (C_{BPL}), 153.7 (C_{BPL}), 152.3 (C_{BPL-Au cis to carbene}), 147.4 (C_{Ar}), 146.4 (C_{Ar}), 146.2 (C_{tz}), 145.4 (C_{Ar}), 145.1 (C_{Ar}), 134.9 (C_{Ar}), 133.5 (CH_{BPL}), 132.6 (C_{Ar}), 132.2 (CH_{Ar}), 132.1 (CH_{Ar}), 131.8 (CH_{BPL}), 127.3 (CH_{BPL}), 127.1 (CH_{BPL}), 126.9 (CH_{BPL}), 126.6 (CH_{BPL}), 124.8 (CH_{Ar}, 3C), 124.6 (CH_{Ar}), 121.8 (CH_{BPL}), 121.3 (CH_{pym}), 120.8 (CH_{BPL}), 30.4 (CH(CH₃)₂), 30.3 (CH(CH₃)₂), 29.6 (CH(CH₃)₂), 29.5 (CH(CH₃)₂), 27.4 (CH(CH₃)₂), 26.0 (CH(CH₃)₂), 25.0 (CH(CH₃)₂), 24.8 (CH(CH₃)₂), 23.7 (CH(CH₃)₂), 23.5 (CH(CH₃)₂), 23.0 (CH(CH₃)₂), 22.2 (CH(CH₃)₂). HRMS (ESI⁺): calcd for C₄₂H₄₅AuClN₅ [M-Cl]⁺: *m/z* 816.3335; found: *m/z* 816.3342.

Synthesis of 5b. Yield: 12.2 mg (78%). ¹H NMR (400 MHz, 248K, CD₂Cl₂) δ 9.48 (br s, 1H, CH_{pym}), 8.98 (br s, 1H, CH_{pym}), 7.94 (t, *J* = 5.3 Hz, 1H, CH_{pym}), 7.75 (dt, *J* = 12.7 Hz, 7.9 Hz, 2H, CH_{Ar}), 7.48 (d, *J* = 7.9 Hz, 4H, CH_{Ar}), 7.41 (dd, *J* = 7.6, 1.5 Hz, 1H, CH_{BPL}), 7.35 (d, *J* = 7.6 Hz, 1H, CH_{BPL}), 7.32 – 7.25 (m, 2H, CH_{BPL}), 7.20 (td, *J* = 7.5, 1.5 Hz, 1H, CH_{BPL}), 7.04 (t, *J* = 7.3 Hz, 1H, CH_{BPL}), 6.16 (td, *J* = 7.6, 1.6 Hz, 1H, CH_{BPL}), 6.11 (d, *J* = 7.9 Hz, 1H, CH_{BPL}), 2.42 (hept, *J* = 6.8 Hz, 2H, CH(CH₃)₂), 2.21 (hept, *J* = 6.8 Hz, 2H, CH(CH₃)₂), 1.16 (d, *J* = 6.9 Hz, 12H, CH(CH₃)₂), 1.12 (d, *J* = 6.7 Hz, 12H, CH(CH₃)₂). ¹³C NMR (101 MHz, 248K, CD₂Cl₂) δ 182.8 (C_{carbene-Au}), 161.6 (CH_{pym}), 160.1 (C_{BPL-Au trans to carbene}), 157.7 (CH_{pym}), 156.4 (C_{pym}), 153.2 (C_{BPL}), 153.2 (C_{BPL}), 149.8 (C_{tz}), 149.4 (C_{BPL-Au cis to carbene}), 145.4 (C_{Ar}, 2C), 144.9 (C_{Ar}, 2C), 134.7 (CH_{BPL}), 133.4 (CH_{Ar}), 133.1 (CH_{Ar}), 132.9 (C_{Ar}), 131.5 (CH_{BPL}), 130.1 (C_{Ar}), 129.3 (CH_{BPL}), 128.8 (CH_{BPL}), 128.2 (CH_{BPL}), 127.1 (CH_{BPL}), 125.6 (CH_{Ar}, 2C), 125.1 (CH_{Ar}, 2C), 124.1 (CH_{pym}), 122.6 (CH_{BPL}), 122.5 (CH_{BPL}), 29.8 (CH(CH₃)₂, 2C), 29.5 (CH(CH₃)₂, 2C), 25.0 (CH(CH₃)₂, 2C), 24.9 (CH(CH₃)₂, 2C), 23.2 (CH(CH₃)₂, 4C). HRMS (ESI⁺): calcd for C₄₂H₄₅AuF₆N₅Sb [M-SbF₆]⁺: *m/z* 816.3335; found: *m/z* 816.3354.

3.5 Synthesis of gold(III) complex *cis-7a-Cl* via oxidative addition

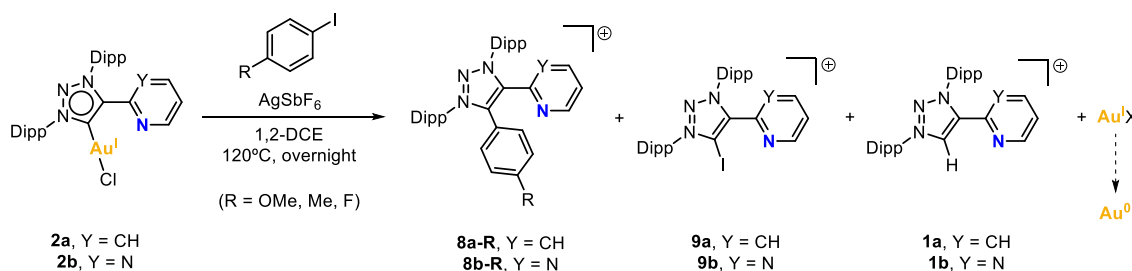


Scheme S6. Synthesis of gold(III)-MIC complex *cis-7a-Cl*.

The synthesis of complex *cis-7a-Cl* was carried out following a previous report that described the synthesis of Au(III) complexes by oxidative addition of diazonium salts.⁶ Under nitrogen atmosphere, a vial was charged with **2a** (41.2 mg, 0.06 mmol, 1 eq), 4-methoxybenzenediazonium tetrafluoroborate (13.3 mg, 0.06 mmol, 1 eq) and six small glass balls. Then, CD₂Cl₂ was added (1.8 mL) and the vial was sealed. The reaction mixture was irradiated with blue LED (λ = 447 nm) and stirred at 25°C for 16h. The ¹H NMR of the reaction crude showed the formation of the desired Au(III) complex in 51% yield. The desired product precipitated after the addition of cold Et₂O to the reaction crude. A further recrystallization of the product was performed by slow diffusion of diethyl ether into a concentrated solution in dichloromethane. Suitable crystals for X-ray diffraction analysis were obtained from a concentrated DMF solution. Complex *cis-7a-Cl* was isolated as pale-yellow crystals. Yield: 11.7 mg (22%).

¹H NMR (400 MHz, CD₂Cl₂) δ 9.52 (ddd, *J* = 5.5, 1.6, 0.8 Hz, 1H, CH_{py}), 8.19 (td, *J* = 7.9, 1.6 Hz, 1H, CH_{py}), 7.97 (ddd, *J* = 7.9, 5.5, 1.3 Hz, 1H, CH_{py}), 7.89 (t, *J* = 7.9 Hz, 1H, CH_{Ar}), 7.62 (d, *J* = 7.9 Hz, 2H, CH_{Ar}), 7.39 (t, *J* = 7.9 Hz, 1H, CH_{Ar}), 7.10 (d, *J* = 7.9 Hz, 2H, CH_{Ar}), 6.89 – 6.85 (m, 2H, CH_{Ar}), 6.73 (dt, *J* = 8.0, 1.1 Hz, 1H, CH_{py}), 6.41 – 6.36 (m, 2H, CH_{Ar}), 3.70 (s, 3H, OCH₃), 2.44 (hept, *J* = 6.8 Hz, 2H, CH(CH₃)₂), 2.30 (hept, *J* = 6.8 Hz, 2H, CH(CH₃)₂), 1.35 (d, *J* = 6.7 Hz, 6H, CH(CH₃)₂), 1.22 (d, *J* = 6.8 Hz, 6H, CH(CH₃)₂), 1.12 (d, *J* = 6.8 Hz, 6H, CH(CH₃)₂), 1.04 (d, *J* = 6.8 Hz, 6H, CH(CH₃)₂). ¹³C NMR (101 MHz, CD₂Cl₂) δ 159.0 (COCH₃), 151.5 (C_{carbene-Au}), 151.3 (C_{trz}), 150.4 (CH_{py}), 145.8 (C_{Ar}, 2C), 144.7 (C_{Ar}, 2C), 144.1 (CH_{py}), 144.0 (C_{py}), 135.1 (CH_{Ar}), 133.2 (CH_{Ar}), 132.9 (C_{Ar}), 132.5 (CH_{Ar}, 2C), 129.7 (CH_{py}), 128.9 (C_{Ar}), 126.9 (CH_{Ar}, 2C), 124.9 (CH_{Ar}, 2C), 122.5 (CH_{py}), 117.6 (C_{Ar-Au}), 115.6 (CH_{Ar}, 2C), 55.9 (OCH₃), 29.8 (CH(CH₃)₂, 4C), 26.7 (CH(CH₃)₂, 2C), 25.2 (CH(CH₃)₂, 2C), 24.1 (CH(CH₃)₂, 2C), 22.0 (CH(CH₃)₂, 2C). HRMS (ESI⁺): calcd for C₃₈H₄₅AuBClF₄N₄O [M-BF₄]⁺: *m/z* 805.2942; found: *m/z* 805.2956.

3.6 General procedure for the reactivity of gold(I) complexes **2a** and **2b** towards aryl halides



Scheme S7. Reactivity of complexes **2a** and **2b** towards aryl iodides.

A vial was charged with **2a** or **2b** (0.015 mmol), the aryl iodide (0.06 – 0.08 mmol), a magnetic stirring bar and 1,2-dichloroethane (0.5 mL). Then, $[\text{AgSbF}_6]$ (0.018 mmol) was added to the reaction mixture. The vial was sealed, stirred, and heated at 120°C overnight in the absence of light. After this time, the brown suspension was filtered, and all the volatiles were removed under vacuum. Then, CD_2Cl_2 was added to analyze the reaction outcome by ^1H NMR. By adding 1,3,5-trimethoxybenzene as internal standard, the yields of the products could be determined.

Reactivity of 2a with 4-iodoanisole. Complex **2a** (11.6 mg, 0.017 mmol, 1 eq), $[\text{AgSbF}_6]$ (7.1 mg, 0.021 mmol, 1.25 eq) and 4-iodoanisole (21.0 mg, 0.090 mmol, 5.4 eq) were employed. NMR yield: 41% (**8a-OMe**), 3% (**9a**), 24% (**1a**). Suitable crystals for X-ray diffraction analysis were obtained by slow diffusion of diethyl ether into a concentrated solution of the filtered crude in dichloromethane, showing the co-crystallization of **8a-OMe** and **9a** in a 0.89:0.11 ratio, respectively (see Figure S98).

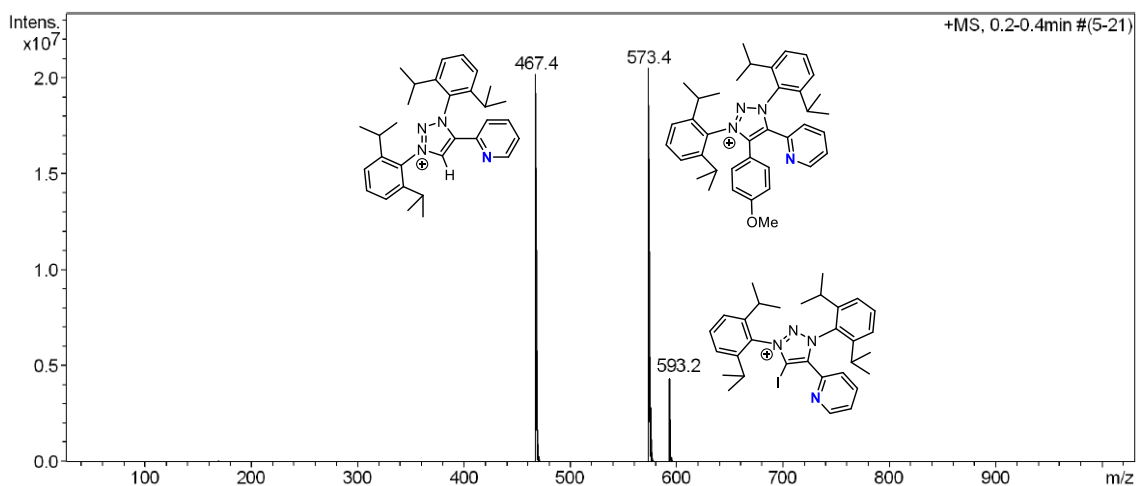


Figure S1. MS-ESI(+) of the reaction crude showing the peaks of **1a**, **8a-OMe** and **9a**.

Reactivity of 2b with 4-iodoanisole. Complex **2b** (10.0 mg, 0.014 mmol, 1 eq), [AgSbF₆] (5.3 mg, 0.015 mmol, 1.08 eq) and 4-iodoanisole (15.6 mg, 0.067 mmol, 4.7 eq) were employed. NMR yield: 65% (**8b-OMe**), 16% (**9b**) and 16% (**1b**). Product **8b-OMe** was isolated by chromatographic column on Al₂O₃ using CH₂Cl₂:MeOH (95:5). Suitable crystals for X-ray diffraction analysis were obtained by slow diffusion of diethyl ether into a concentrated solution of **8b-OMe** in dichloromethane. Characterization data of compound **8b-OMe**: ¹H NMR (400 MHz, CD₂Cl₂) δ 8.77 (d, *J* = 5.0 Hz, 2H, CH_{pym}), 7.71 (t, *J* = 7.8 Hz, 1H, CH_{Ar}), 7.65 (t, *J* = 7.9 Hz, 1H, CH_{Ar}), 7.57 (t, *J* = 5.0 Hz, 1H, CH_{pym}), 7.43 (d, *J* = 7.9 Hz, 2H, CH_{Ar}), 7.37 (d, *J* = 7.9 Hz, 2H, CH_{Ar}), 7.19 – 7.15 (m, 2H, CH_{Ar}), 6.90 – 6.86 (m, 2H, CH_{Ar}), 3.80 (s, 3H, OCH₃), 2.46 – 2.31 (m, 4H, CH(CH₃)₂), 1.21 (dd, *J* = 6.8, 1.3 Hz, 12H, CH(CH₃)₂), 1.10 (dd, *J* = 6.7, 1.4 Hz, 12H, CH(CH₃)₂). **HRMS (ESI+)**: calcd for C₃₇H₄₄ClN₅O [M-Cl]⁺: *m/z* 574.3540; found: *m/z* 574.3547.

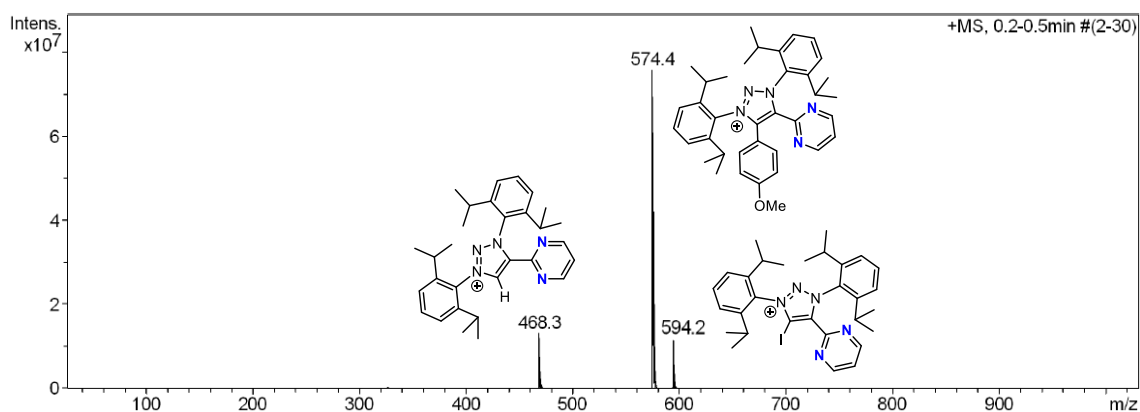


Figure S2. MS-ESI(+) of the reaction crude showing the peaks of **1b**, **8b-OMe** and **9b**.

Reactivity of 2a with 4-iodotoluene. Complex **2a** (10.4 mg, 0.015 mmol, 1 eq), [AgSbF₆] (7.2 mg, 0.021 mmol, 1.4 eq) and 4-iodotoluene (17.0 mg, 0.078 mmol, 5.2 eq) were employed. NMR yield: 34% (**8a-Me**), 3% (**9a**), 31% (**1a**). Product **8a-Me** was isolated by chromatographic column on Al₂O₃ using CH₂Cl₂:MeOH (95:5). Characterization data of compound **8a-Me**: ¹H NMR (400 MHz, CD₂Cl₂) δ 8.52 (d, *J* = 5.0 Hz, 1H), 7.77 (td, *J* = 7.9, 1.7 Hz, 1H), 7.70 (t, *J* = 7.9 Hz, 1H), 7.64 (t, *J* = 7.8 Hz, 1H), 7.45 – 7.40 (m, 3H), 7.38 – 7.34 (m, 3H), 7.20 (d, *J* = 8.1 Hz, 2H), 7.06 (d, *J* = 8.2 Hz, 2H), 2.43 – 2.33 (m, 7H), 1.21 (d, *J* = 6.8 Hz, 12H), 1.08 (d, *J* = 6.8 Hz, 12H). **HRMS (ESI+)**: calcd for C₃₈H₄₅F₆N₄Sb [M-SbF₆]⁺: *m/z* 557.3639; found: *m/z* 557.3638.

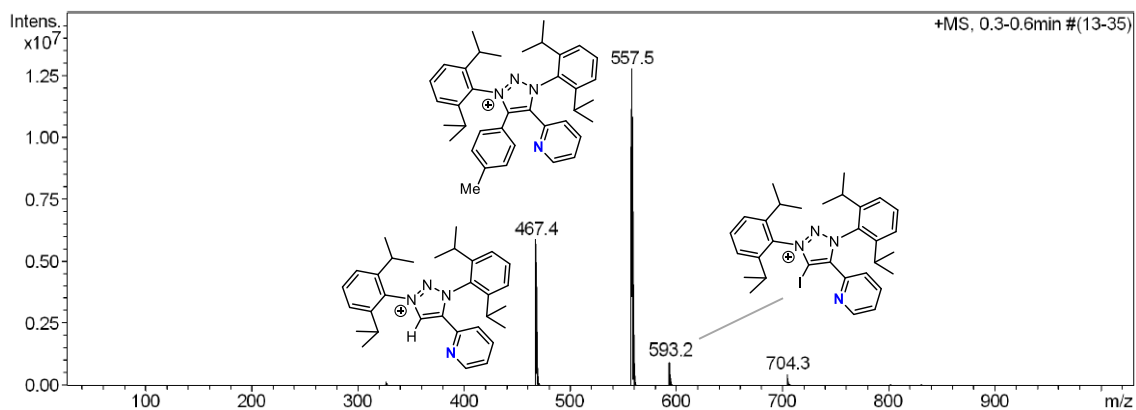


Figure S3. MS-ESI(+) of the reaction crude showing the peaks of **1a**, **8a-Me** and **9a**.

Reactivity of 2a with 4-fluoriodobenzene. Complex **2a** (9.9 mg, 0.014 mmol, 1 eq), [AgSbF₆] (5.8 mg, 0.017 mmol, 1.2 eq) and 4-fluoriodobenzene (14.1 mg, 0.064 mmol, 4.5 eq) were employed. NMR yield: 12% (**8a-F**), traces (**9a**), 66% (**1a**).

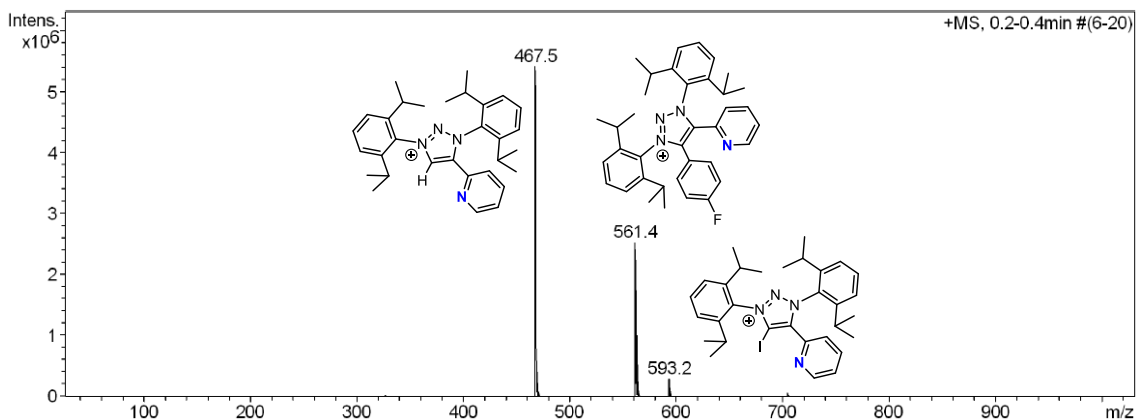
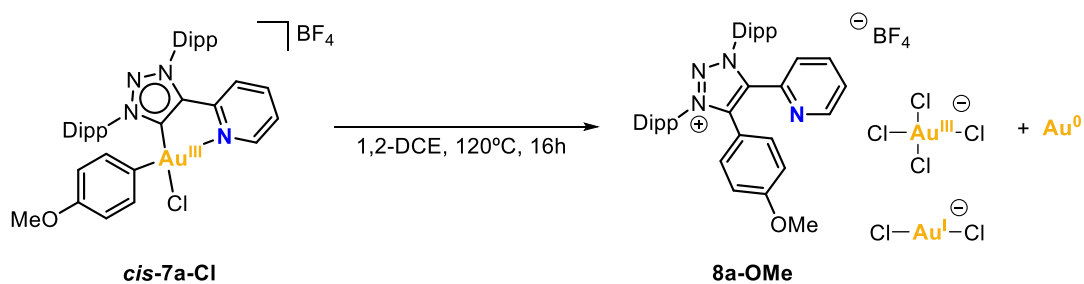


Figure S4. MS-ESI(+) of the reaction crude showing the peaks of **1a**, **8a-F** and **9a**.

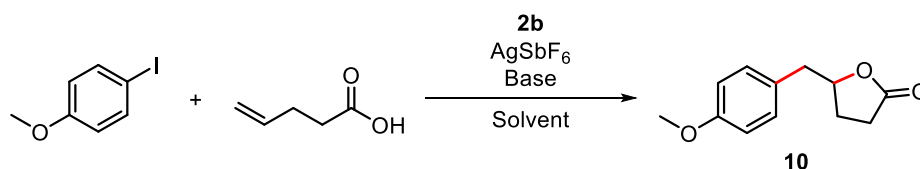
3.7 Reductive elimination from *cis*-7a-Cl to 8a-OMe



Scheme S8. Reductive elimination from *cis*-7a-Cl to **8a-OMe**.

A vial was charged with *cis*-**7a-Cl** (11.7 mg, 0.013 mmol), 1,2-dichloroethane (0.5 mL) and a magnetic stirring bar, then was sealed under nitrogen atmosphere. The solution was heated at 120°C and stirred for 16h. After this time, a clear yellow solution with Au(0) precipitate was obtained. The volatiles were removed under vacuum, and the solid residue was analyzed by ¹H NMR. Product **8a-OMe** was obtained in 96% yield. ¹H NMR (400 MHz, CD₂Cl₂) δ 8.51 (ddd, *J* = 4.8, 1.8, 1.0 Hz, 1H, CH_{py}), 7.78 (td, *J* = 7.8, 1.7 Hz, 1H, CH_{py}), 7.70 (t, *J* = 7.9 Hz, 1H, CH_{Ar}), 7.63 (t, *J* = 7.9 Hz, 1H, CH_{Ar}), 7.44-7.39 (m, 4H: 2CH_{Ar} and 2CH_{py}), 7.36 (d, *J* = 7.9 Hz, 2H, CH_{Ar}), 7.13-7.07 (m, 2H, CH_{Ar}), 6.91-6.85 (m, 2H, CH_{Ar}), 3.79 (s, 3H, OCH₃), 2.40 (m, 4H, CH(CH₃)₂), 1.21 (d, *J* = 6.9 Hz, 12H, CH(CH₃)₂), 1.09 (dd, *J* = 6.7, 5.9 Hz, 12H, CH(CH₃)₂). ¹³C NMR (101 MHz, CD₂Cl₂) δ 163.3 (COCH₃), 151.4 (CH_{py}), 145.9 (C_{Ar}, 4C), 143.4 (C_{trz}), 142.4 (C_{py}), 140.5 (C_{trz}), 138.3 (CH_{py}), 134.1 (CH_{Ar}), 133.5 (CH_{Ar}), 131.9 (CH_{Ar}, 2C), 130.3 (C_{Ar}), 129.5 (C_{Ar}), 126.8 (CH_{py}), 126.6 (CH_{py}), 125.9 (CH_{Ar}, 2C), 125.3 (CH_{Ar}, 2C), 115.8 (CH_{Ar}, 2C), 113.0 (C_{Ar}), 56.2 (OCH₃), 30.4 (CH(CH₃)₂, 2C), 30.3 (CH(CH₃)₂, 2C), 25.9 (CH(CH₃)₂, 2C), 25.5 (CH(CH₃)₂, 2C), 23.1 (CH(CH₃)₂, 2C), 22.9 (CH(CH₃)₂, 2C). HRMS (ESI⁺): calcd for C₃₈H₄₅N₄O⁺ [M]⁺: *m/z* 573.3588; found: *m/z* 573.3586. HRMS (ESI⁻): calcd for AuCl₄⁻ [M]⁻: *m/z* 338.8390; found: *m/z* 338.8425; calcd for AuCl₂⁻ [M]⁻: *m/z* 266.9043; found: *m/z* 266.9040.

4. Optimization of the arylation-lactonization reaction of γ -alkenoic acids



Scheme S9. Selected reaction to optimize the conditions for the arylation-lactonization of γ -alkenoic acids.

The reaction was carried under nitrogen atmosphere. A vial was charged with gold(I) complex **2b**, 4-iodoanisole, 4-pentenoic acid, a magnetic stirring bar, and the solvent of choice (0.4 mL), followed by the addition of a suspension of base and [AgSbF₆] in the solvent of choice. The vial was sealed and heated at the desired temperature overnight. The yields were calculated by ¹H NMR using 1,3,5-trimethoxybenzene as internal standard.

Table S1. Optimization of the temperature

Entry	2b (mol%)	Temperature	P/(P+SM) (%) [*]
1	10	rt.	0
2	10	50	0
3 ^a	20	80	15

Reaction conditions: 4-iodoanisole (1 eq), 4-pentenoic acid (1 eq), K₃PO₄ (1 eq), AgSbF₆ (1.5 eq), 1,2-dichloroethane, overnight. [4-iodoanisole] = 0.07M, V = 2 mL. ^a1.4 mL. *P stands for the integral of one proton of the expected product **10** and SM stands for the integral of one proton of the remaining starting material (4-iodoanisole).

Table S2. Optimization of the base

Entry	AgSbF ₆ (eq)	Base (eq.)	P/(P+SM) (%)
1	1.7	Li ₂ CO ₃ (1.2)	0
2	1.7	Na ₂ CO ₃ (1.2)	0
3	1.5	K ₂ CO ₃ (1.0)	0
4	1.6	Cs ₂ CO ₃ (1.2)	2
5	1.6	2,6-DTBP (1.0)	2
6	1.6	-	0

Reaction conditions: 4-iodoanisole (1 eq), 4-pentenoic acid (1 eq), **2b** (10 mol%), 1,2-dichloroethane, 80 °C, overnight. [4-iodoanisole] = 0.07M, V = 1.7 mL.

Table S3. Screening of conditions using stoichiometric amounts of gold complex **2b**

Entry	Iodoaryl (eq)	Acid (eq)	AgSbF ₆ (eq)	K ₃ PO ₄ (eq)	Solvent	P/(P+SM) (%)	Conv. (%)	Yield (%)
1 ^{a*}	1	1	1	1	1,2-DCE	0	nc	0
2 ^a	1	1	1	1.1	1,2-DCE	15	nc	nc
3 ^b	1	1	2.3	1.6	1,2-DCE	25	nc	nc
4	1	1	3.6	1	1,2-DCE	15	nc	nc
5	1	1	2.4	1.5	DCM	29	nc	nc
6	1	1	4.4	1.4	DCM	0	nc	0
7	5	1	6.6	1.4	1,2-DCE	0	nc	0
8	1	5	2.7	1.2	1,2-DCE	49	nc	nc
9 ^{**}	1	5	2.8	1.8	1,2-DCE	17	nc	nc
10 ^c	1	5	2.5	7.2	1,2-DCE	0	nc	0
11 ^d	1	10	2.7	1.2	1,2-DCE	38	nc	nc
12	1	5	2.8	1	TFE	88	92	63
13 ^{***}	1	5	2.6	1.2	TFE	>99	>99	67

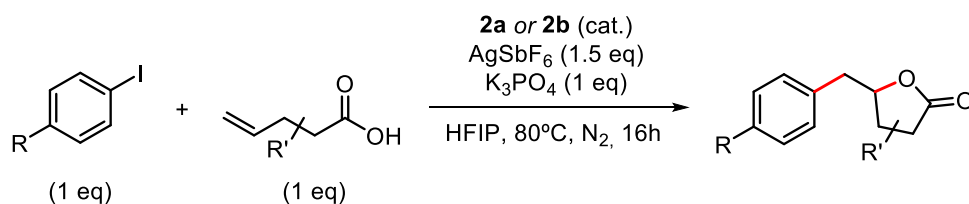
Reaction conditions: Complex **2b** (1 eq), 80 °C, overnight. [4-iodoanisole] = 0.02M, V = 1 mL. ^a1.4 mL, ^b2 mL, ^c0.85 mL, ^d0.6 mL. *Blank experiment without **2b**, **70 °C, ***100 °C. The notation “nc” stands for “not calculated”.

Table S4. Optimization of the solvent using substoichiometric amounts of complex **2b**

Entry	2b (mol%)	<i>AgSbF₆</i> (eq)	<i>K₃PO₄</i> (eq)	Solvent	<i>P/(P+SM)</i> (%)	Conv. (%)	Yield (%)
1	10	1.5	1.0	DMF	0	nc	0
2	10	1.5	1.2	toluene	0	nc	0
3	10	1.6	1.2	THF	0	nc	0
4	10	1.6	1.2	DCM	9	nc	nc
5	10	1.5	1.0	DMSO	0	nc	0
6	10	1.6	1.1	MeCN	0	nc	0
7	10	1.5	1.0	TFE	18	nc	nc
8	10	1.5	0.5	TFE	32	51	24
9*	10	1.5	1.0	TFE	37	51	28
10**	10	1.5	1.1	TFE	25	54	15
11 ^{a**}	40	2.0	1.1	TFE	80	79	44
12 ^{b**}	70	2.2	1.2	TFE	87	81	65
13 ^{a**}	1	1.1	0.5	TFE	2	38	1.6
14 ^c	10	1.5	1.0	HFIP	40	56	29

Reaction conditions: 4-iodoanisole (1 eq), 4-pentenoic acid (1 eq), 80 °C, overnight, solvent ([4-iodoanisole] = 0.08M), V = 1.4 mL. ^a0.65 mL, ^b0.55 mL, ^c1 mL. *100 °C. **24 h. The notation “nc” stands for “not calculated”.

5. Scope of the arylation-lactonization reaction of γ -alkenoic acids



Scheme S10. Selected reaction conditions for the gold-catalyzed arylation-lactonization of γ -alkenoic acids.

Table S5. Scope of the gold-catalyzed arylation-lactonization of γ -alkenoic acids towards the formation of products **10** – **16**.

Entry	R	Acid	Catalyst (mol%)	Product	Conv. (%)	Yield (%)
1	OMe		2a (10)	10	78	35
2	OMe		2b (10)	10	56	29
3	OMe		2a (20)	10	-	33*
4	H		2a (10)	11	nc	31
5	H		2b (10)	11	nc	50
6	H		2b (20)	11	nc	87
7	H		-	11	nc	0
8	Me		2a (10)	12	95	60
9	Me		2b (10)	12	98	81
10	CF ₃		2a (10)	13	nc	13
11	CF ₃		2b (10)	13	nc	11
12	NO ₂		2a (10)	14	12	1
13	NO ₂		2b (10)	14	5	1
14	OMe		2a (10)	15	49	37
15	OMe		2b (10)	15	67	41
16	OMe		2a (20)	15	-	25*
17	OMe		2a (10)	16	60	32
18	OMe		2b (10)	16	45	18
19	OMe		2a (20)	16	-	29*

Conversions and yields were calculated by ¹H NMR using 1,3,5-trimethoxybenzene as internal standard. *Isolated yield. Conversions are labeled as “nc” (not calculated) in those cases where volatile iodoaryl substrates were employed.

Synthesis of 10. For the synthesis of **10** was employed 4-iodoanisole (99.7 mg, 0.43 mmol, 1.0 eq), 4-pentenoic acid (45 μ L, 0.44 mmol, 1.0 eq), **2a** (60.0 mg, 0.09 mmol, 0.2 eq), [AgSbF₆] (226.6 mg, 0.66 mmol, 1.5 eq), K₃PO₄ (57.2 mg, 0.42 mmol, 1.0 eq), and HFIP (5 mL). The reaction mixture was heated in a sealed vial at 80°C for 16h. The reaction crude was filtered, and all volatiles were removed under high vacuum. The residue was purified by column chromatography using hexane:EtOAc (9:1). Compound **10** was obtained as a yellow oil. Yield: 28.6 mg (33%). The ¹H NMR and ¹³C NMR spectra matched with those reported in the literature.⁷

Synthesis of 11. For the synthesis of **11** was employed iodobenzene (9.3 μ L, 0.08 mmol, 1.0 eq), 4-pentenoic acid (8.5 μ L, 0.08 mmol, 1.0 eq), catalyst **2a** or **2b** (10 mol% or 20 mol%), [AgSbF₆] (0.13 mmol, 1.5 eq), K₃PO₄ (0.08 mmol, 1.0 eq), and HFIP (1 mL). The reaction mixture was heated in a sealed vial at 80°C for 16h. The reaction crude was filtered, and all volatiles were removed under high vacuum. The yield of product **11** was determined by ¹H NMR using 1,3,5-trimethoxybenzene as internal standard. Yield: 31% (employing **2a** 10 mol%), 50% (employing **2b** 10 mol%), 87% (employing **2b** 20 mol%). Out of the ¹H NMR of the crude, the signals of product **11** could be identified as they matched with the characterization reported in the literature.⁸

Synthesis of 12. For the synthesis of **12** was employed 4-iodotoluene (18.8 mg, 0.09 mmol, 1.0 eq), 4-pentenoic acid (9.0 μ L, 0.09 mmol, 1.0 eq), catalyst **2a** or **2b** (10 mol%), [AgSbF₆] (0.13 mmol, 1.5 eq), K₃PO₄ (0.08 mmol, 1.0 eq), and HFIP (1 mL). The reaction mixture was heated in a sealed vial at 80°C for 16h. The reaction crude was filtered, and all volatiles were removed under high vacuum. The yield of product **12** was determined by ¹H NMR using 1,3,5-trimethoxybenzene as internal standard. Yield: 60% (employing **2a**), 81% (employing **2b**). Out of the ¹H NMR of the crude, the signals of product **12** could be identified as they matched with the characterization reported in the literature.⁹

Synthesis of 13. For the synthesis of **13** was employed 4-iodobenzotrifluoride (12.3 μ L, 0.08 mmol, 1.0 eq), 4-pentenoic acid (8.5 μ L, 0.08 mmol, 1.0 eq), catalyst **2a** or **2b** (10 mol%), [AgSbF₆] (0.13 mmol, 1.5 eq), K₃PO₄ (0.08 mmol, 1.0 eq), and HFIP (1 mL). The reaction mixture was heated in a sealed vial at 80°C for 16h. The reaction crude was filtered, and all volatiles were removed under high vacuum. The yield of product **13** was determined by ¹H NMR using 1,3,5-trimethoxybenzene as internal standard. Yield: 13% (employing **2a**), 11% (employing **2b**). Out of the ¹H NMR of the crude, the signals of product **13** could be identified as they matched with the characterization reported in the literature.⁹

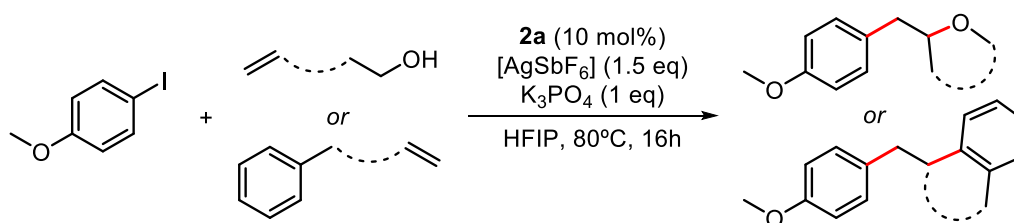
Synthesis of 14. For the synthesis of **14** was employed 1-iodo-4-nitrobenzene (21.7 mg, 0.09 mmol, 1.0 eq), 4-pentenoic acid (8.9 μ L, 0.09 mmol, 1.0 eq), catalyst **2a** or **2b** (10 mol%), [AgSbF₆] (0.13 mmol, 1.5 eq), K₃PO₄ (0.09 mmol, 1.0 eq), and HFIP (1 mL). The reaction mixture was heated in a sealed vial at 80°C for 16h. The reaction crude was filtered, and all volatiles were removed under high vacuum. The yield of product **14** was determined by ¹H NMR using 1,3,5-trimethoxybenzene as internal standard. Yield: 1% (employing **2a**), 1% (employing **2b**).

Synthesis of 15. For the synthesis of **15** was employed 4-iodoanisole (56.5 mg, 0.24 mmol, 1.0 eq), 2,2-dimethylpent-4-enoic acid (33 μ L, 0.24 mmol, 1.0 eq), **2a** (34.2 mg,

0.05 mmol, 0.2 eq), [AgSbF₆] (124.0 mg, 0.36 mmol, 1.5 eq), K₃PO₄ (32.5 mg, 0.24 mmol, 1.0 eq), and HFIP (2.6 mL). The reaction mixture was heated in a sealed vial at 80°C for 16h. The reaction crude was filtered, and all volatiles were removed under high vacuum. Then, ethyl acetate was added to the oily residue and the solution was filtered through a basic alumina plug. The product was isolated from preparative TLC using pentane:EtOAc (8:2). Compound **15** was obtained as a pale yellow oil. Yield: 14.4 mg (25%). ¹H NMR (400 MHz, CDCl₃): δ 7.16 – 7.13 (m, 2H, CH_{Ar}), 6.87 – 6.83 (m, 2H, CH_{Ar}), 4.59 (dq, *J* = 9.9, 6.2 Hz, 1H, CH_{Alk}), 3.79 (s, 3H, OCH₃), 3.04 (dd, *J* = 14.0, 6.4 Hz, 1H, CH₂), 2.82 (dd, *J* = 14.0, 6.3 Hz, 1H, CH₂), 2.06 (dd, *J* = 12.7, 5.9 Hz, 1H, CH₂), 1.80 (dd, *J* = 12.8, 9.9 Hz, 1H, CH₂), 1.23 (s, 3H, CH₃), 1.22 (s, 3H, CH₃). ¹³C NMR (101 MHz, CDCl₃): δ 181.9 (C=O), 158.7 (C_{Ar}), 130.5 (CH_{Ar}, 2C), 128.3 (C_{Ar}), 114.1 (CH_{Ar}, 2C), 77.6 (CH_{Alk}), 55.4 (OCH₃), 43.0 (CH₂), 40.8 (C_{Alk}), 40.6 (CH₂), 25.1 (CH₃), 24.6 (CH₃). HRMS (ESI⁺): calcd for C₁₄H₁₈O₃ [M+Na]⁺: *m/z* 257.1148; found: *m/z* 257.1143.

Synthesis of 16. For the synthesis of **16** was employed 4-iodoanisole (99.6 mg, 0.43 mmol, 1.0 eq), freshly prepared 3,3-dimethylpent-4-enoic acid¹⁰ (63 μL, 0.43 mmol, 1.0 eq), **2a** (60.8 mg, 0.09 mmol, 0.2 eq), [AgSbF₆] (222.3 mg, 0.65 mmol, 1.5 eq), K₃PO₄ (59.5 mg, 0.44 mmol, 1.0 eq), and HFIP (5 mL). The reaction mixture was heated in a sealed vial at 80°C for 16h. The reaction crude was filtered, and all volatiles were removed under high vacuum. Then, ethyl acetate was added to the oily residue and the solution was filtered through a basic alumina plug. The product was isolated from column chromatography using hexane:EtOAc (9:1). Compound **16** was obtained as a white solid. Colorless crystals suitable for X-ray diffraction were obtained by evaporation of a concentrated solution of **16** in methanol. Yield: 29.3 mg (29%). ¹H NMR (400 MHz, CDCl₃): δ 7.20 – 7.16 (m, 2H, CH_{Ar}), 6.86 – 6.83 (m, 2H, CH_{Ar}), 4.25 (dd, *J* = 9.3, 3.7 Hz, 1H, CH_{Alk}), 3.78 (s, 3H, OCH₃), 2.84 (dd, *J* = 14.6, 9.3 Hz, 1H, CH₂), 2.76 (dd, *J* = 14.6, 3.8 Hz, 1H, CH₂), 2.41 (d, *J* = 16.9 Hz, 1H, CH₂), 2.32 (d, *J* = 16.8 Hz, 1H, CH₂), 1.13 (s, 3H, CH₃), 1.12 (s, 3H, CH₃). ¹³C NMR (101 MHz, CDCl₃): δ 176.0 (C=O), 158.5 (C_{Ar}), 130.2 (CH_{Ar}, 2C), 129.7 (C_{Ar}), 114.1 (CH_{Ar}, 2C), 89.7 (CH_{Alk}), 55.4 (OCH₃), 45.0 (CH₂), 39.6 (C_{Alk}), 34.7 (CH₂), 25.2 (CH₃), 21.5 (CH₃). HRMS (ESI⁺): calcd for C₁₄H₁₈O₃ [M+Na]⁺: *m/z* 257.1148; found: *m/z* 257.1139. Calcd for C₁₄H₁₈O₃ [2M+Na]⁺: *m/z* 491.2404; found: *m/z* 491.2385.

6. Au(I)-catalyzed oxyarylation and 1,2-diarylation reactions of alkenes



Scheme S11. Oxyarylation and 1,2-diarylation reactions of alkenes catalyzed by complex **2a**.

The catalytic performance of Au(I) complex **2a** was tested in the oxyarylation and 1,2-diarylation reactions of olefins, under the previously optimized reaction conditions, using 4-iodoanisole as the aryl iodide counterpart (Scheme S11).

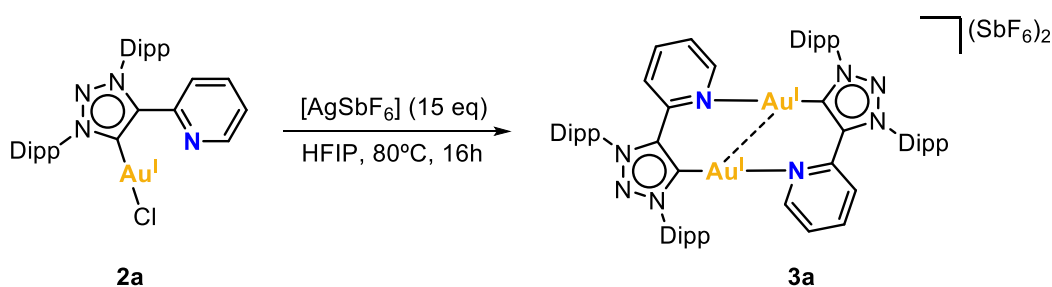
Under nitrogen atmosphere, a vial was charged with 4-iodoanisole (0.09 mmol, 1.0 eq), the alkene (0.09 mmol, 1.0 eq), catalyst **2a** (10 mol%), [AgSbF₆] (0.13 mmol, 1.5 eq), K₃PO₄ (0.09 mmol, 1.0 eq), and HFIP (1 mL). The vial was sealed and heated at 80°C for 16h. The reaction crude was filtered, and all volatiles were removed under high vacuum. The yield of the desired product was determined by ¹H NMR using 1,3,5-trimethoxybenzene as internal standard and according to the NMR characterization found in the literature.¹¹ The reactions tested are displayed in Table S6.

Table S6. Summary of the **2a**-catalyzed oxyarylation and 1,2-diarylation reactions of alkenes.

Entry	Alkene	Product	Yield (%)
1			18
2			25
3			5
4			0

7. Mechanistic studies

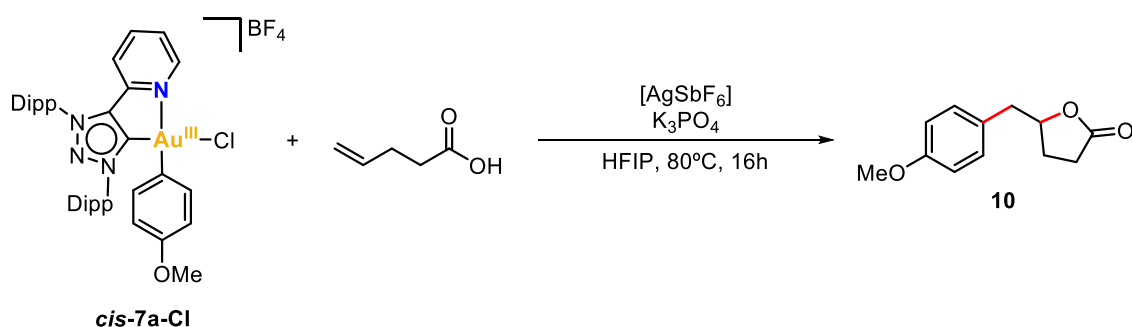
7.1 Role of the silver salt



Scheme S12. Reactivity of **2a** with AgSbF₆ under the reaction conditions optimized for the arylation-lactonization catalysis.

Under nitrogen, a vial was charged with **2a** (8.0 mg, 0.011 mmol, 1.0 eq), [AgSbF₆] (60.5 mg, 0.176 mmol, 15.4 eq), and a stirring bar. Then, HFIP (1 mL) was added, and the vial was sealed. The mixture was stirred and heated at 80°C for 16h. The reaction conditions simulated the conditions used in the arylation-lactonization catalysis in terms of solvent, time, temperature, and ratio [Au]:Ag⁺ (1:15). The reaction crude was filtered, and the volatiles were removed under vacuum. NMR analysis revealed that dimer **3a** was quantitatively formed. MS (ESI+) analysis showed a unique peak at *m/z* 704.3 corresponding to [(MIC^{^N^{py}})Au^I + MeCN]⁺.

7.2 Stoichiometric reaction from complex *cis-7a-Cl* to product **10**

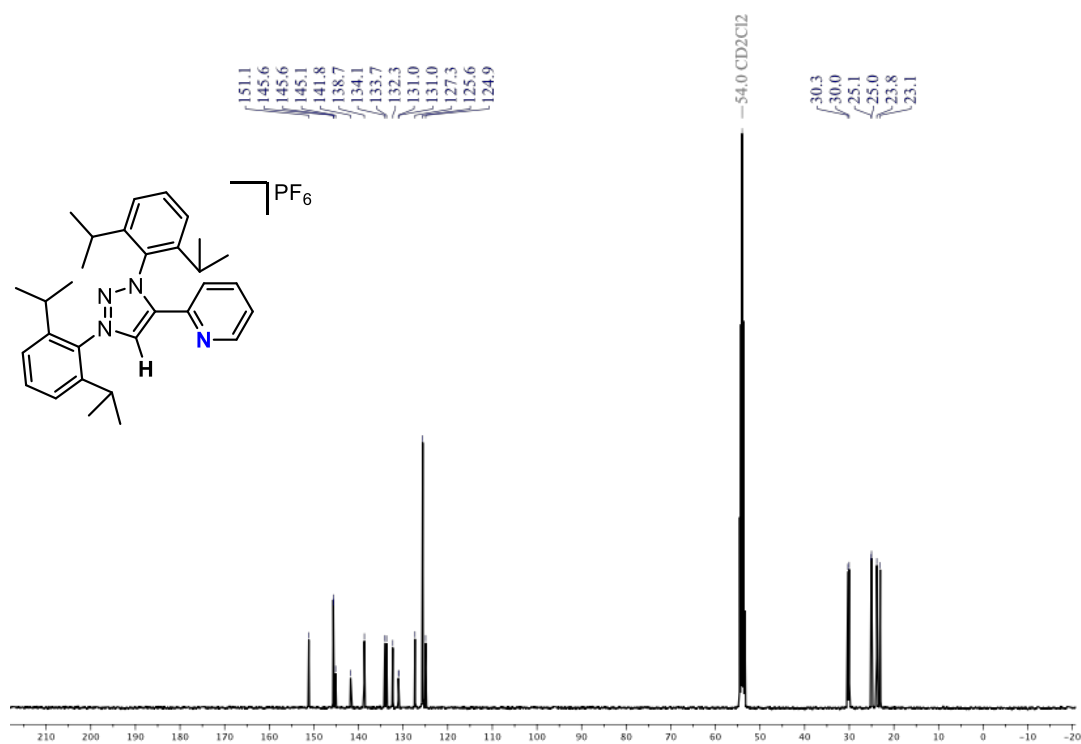
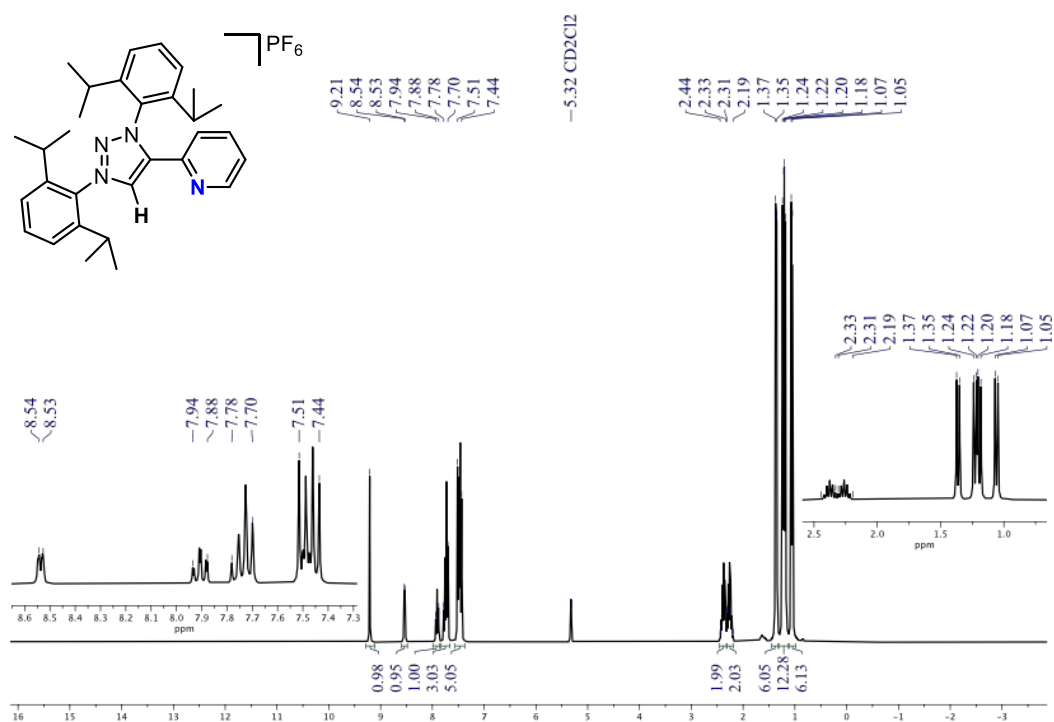


Scheme S13. Stoichiometric reaction of *cis-7a-Cl* towards the formation of product **10**.

In a glovebox, a vial was charged with complex *cis-7a-Cl* (7.0 mg, 0.008 mmol, 1.0 eq), [AgSbF₆] (3.2 mg, 0.009 mmol, 1.2 eq), K₃PO₄ (1.1 mg, 0.008 mmol, 1.0 eq) and a stirring bar. Outside the glovebox and under nitrogen atmosphere, a freshly solution of 4-pentenoic acid (1.0 μL, 0.010 mmol, 1.3 eq) in HFIP (0.8 mL) was added to the reaction mixture. The vial was sealed, stirred, and heated at 80°C for 16h. After this time, the white suspension was filtered, and the volatiles were removed under vacuum. NMR analysis of the solid residue revealed the formation of product **10** in 73% yield (NMR yield using mesitylene as internal standard). MS (ESI+) analysis showed a peak at *m/z* 207.0 corresponding to the [M+H]⁺ species of product **10**, and a peak at *m/z* 704.4 corresponding to [(MIC^{^N^{py}})Au^I + MeCN]⁺.

8. NMR and HRMS-ESI spectra

8.1 NMR and HRMS-ESI Spectra of triazolium salt 1a



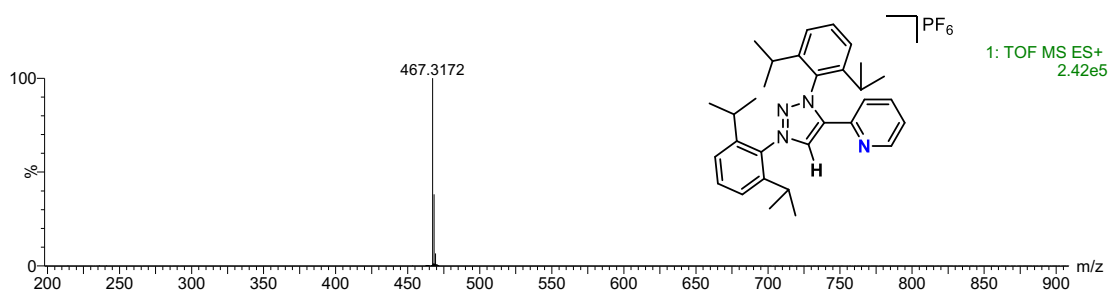


Figure S7. HRMS-ESI(+) of **1a**.

8.2 NMR and HRMS-ESI Spectra of triazolium salt **1b**

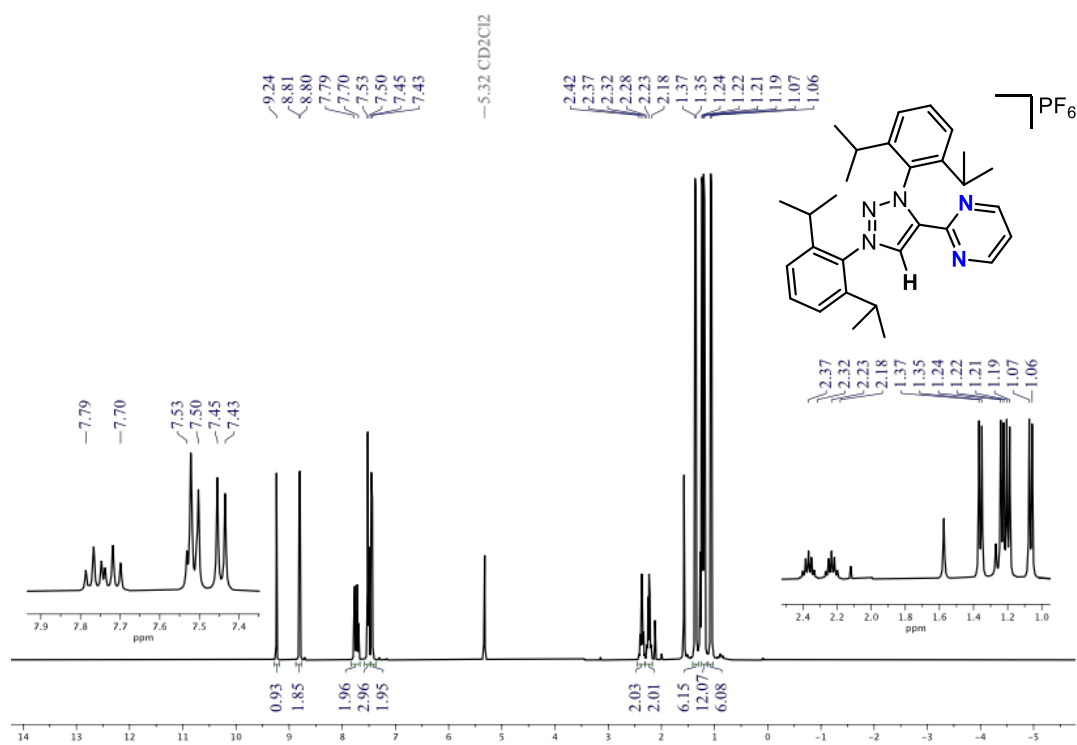


Figure S8. ¹H NMR (400MHz, 298K) of **1b** in CD₂Cl₂.

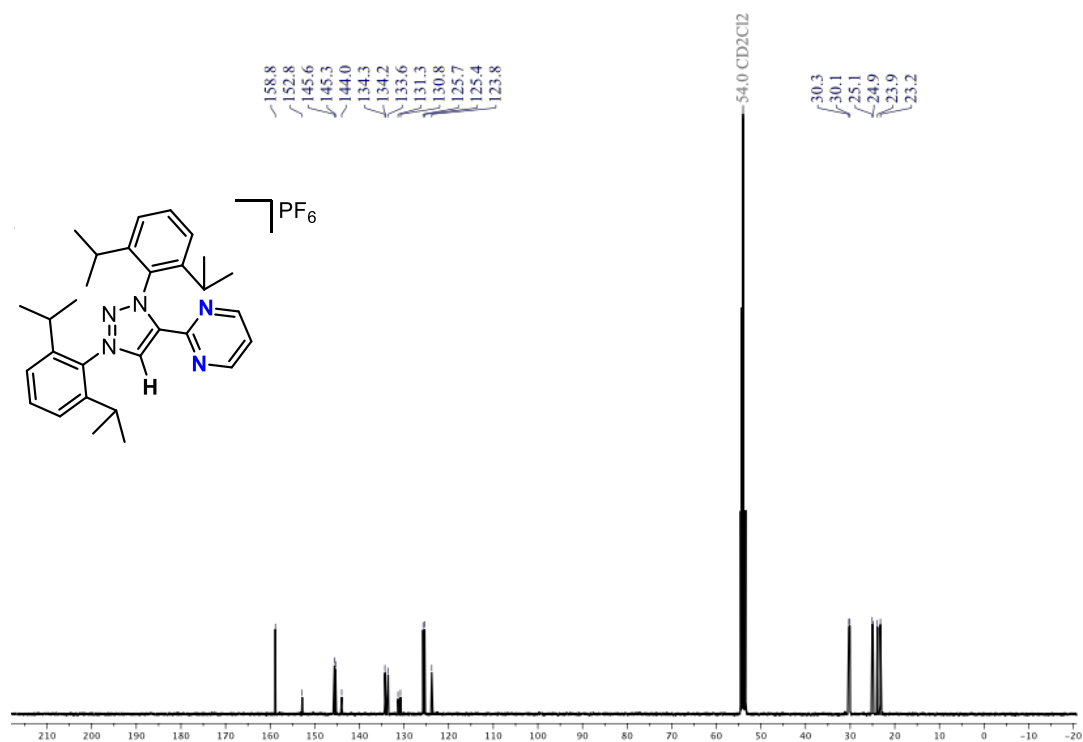


Figure S9. ^{13}C NMR (100MHz, 298K) of **1b** in CD_2Cl_2 .

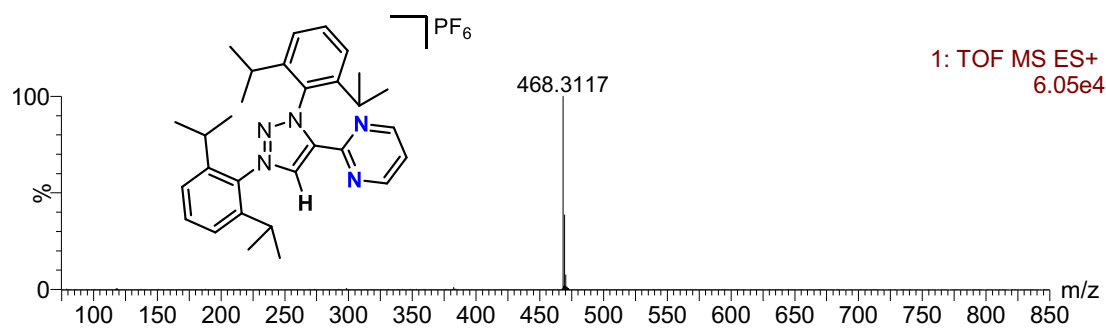


Figure S10. HRMS-ESI(+) of **1b**.

8.3 NMR Spectra of complex 2a

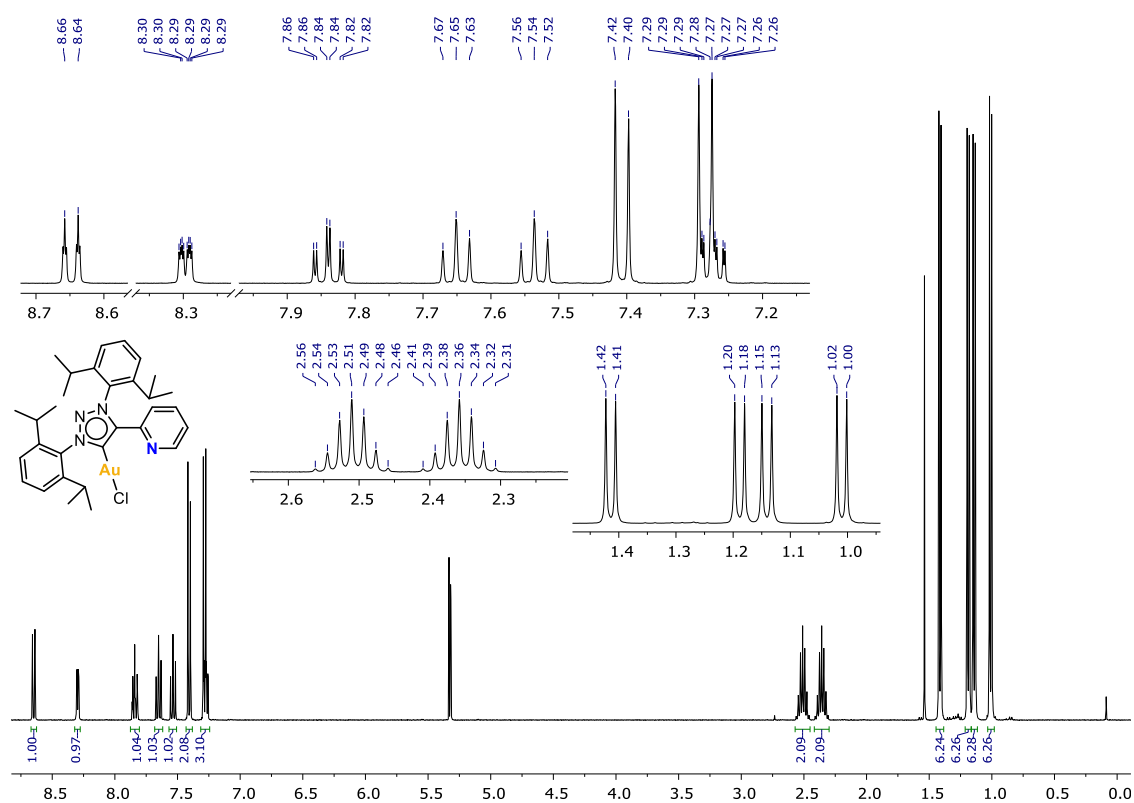


Figure S11. ¹H NMR (400MHz, 298K) of 2a in CD₂Cl₂.

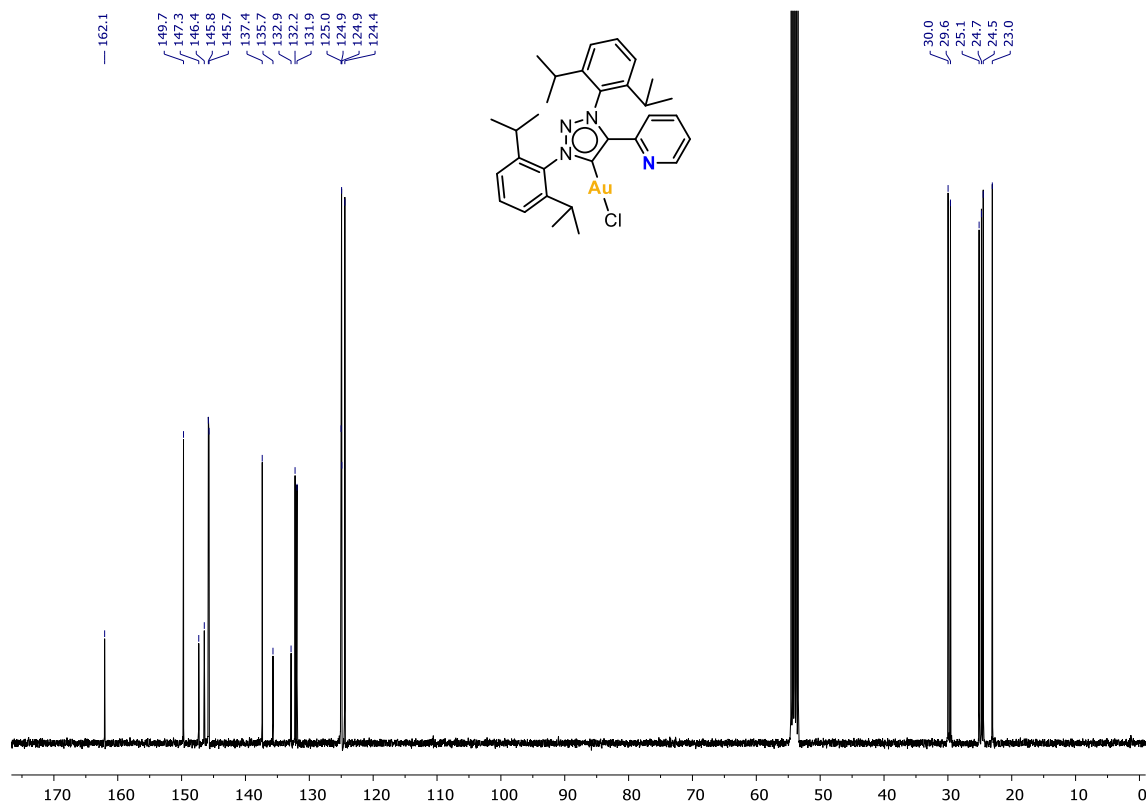


Figure S12. ¹³C NMR (101MHz, 298K) of 2a in CD₂Cl₂.

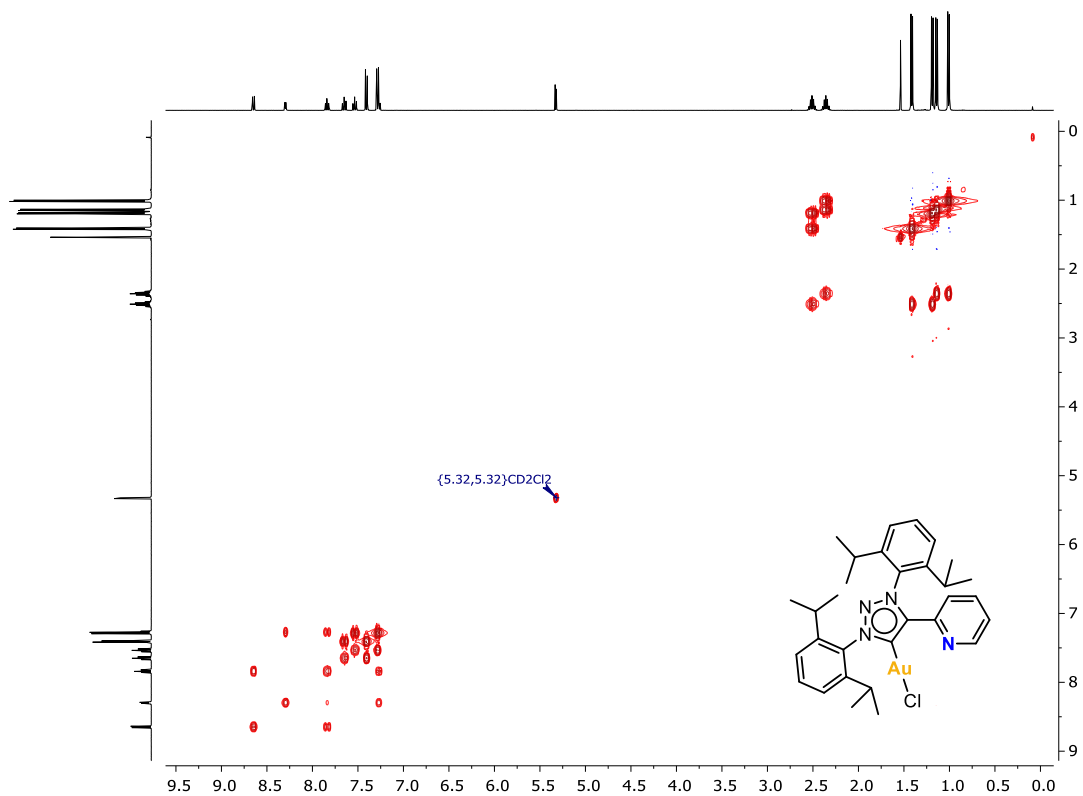


Figure S13. ^1H , ^1H -COSY NMR (400MHz, 298K) of **2a** in CD_2Cl_2 .

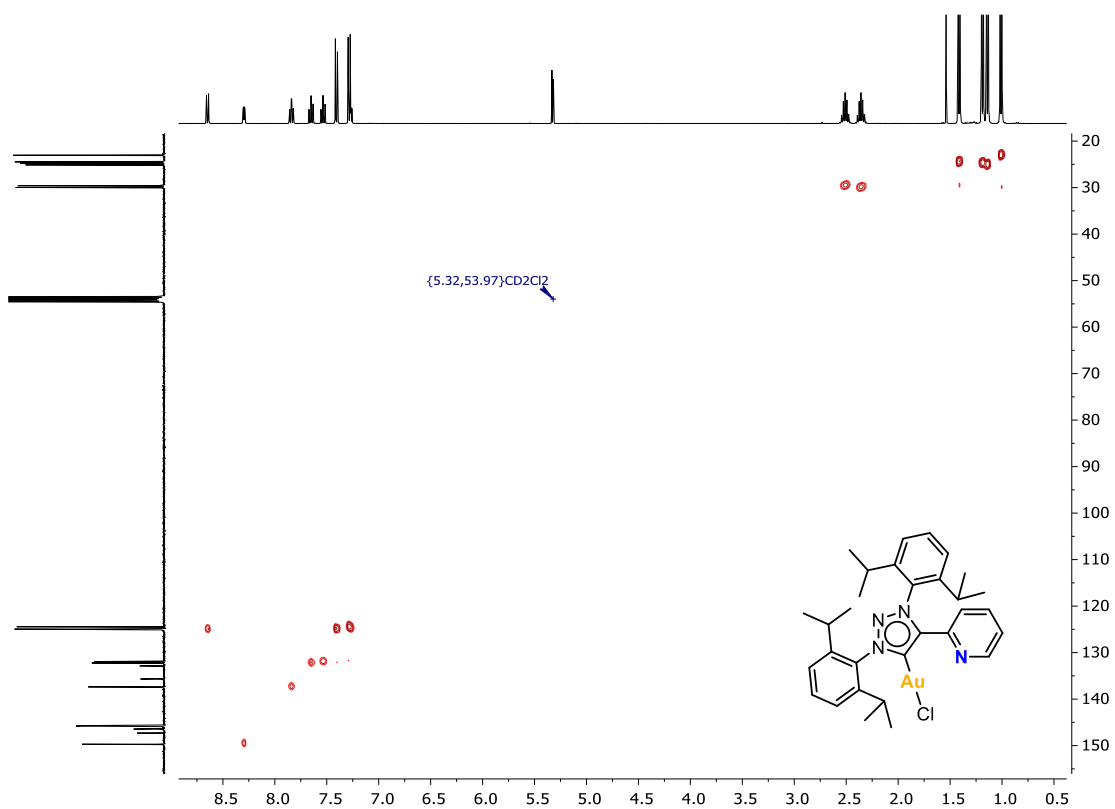


Figure S14. ^1H , ^{13}C -HSQC NMR (400MHz, 298K) of **2a** in CD_2Cl_2 .

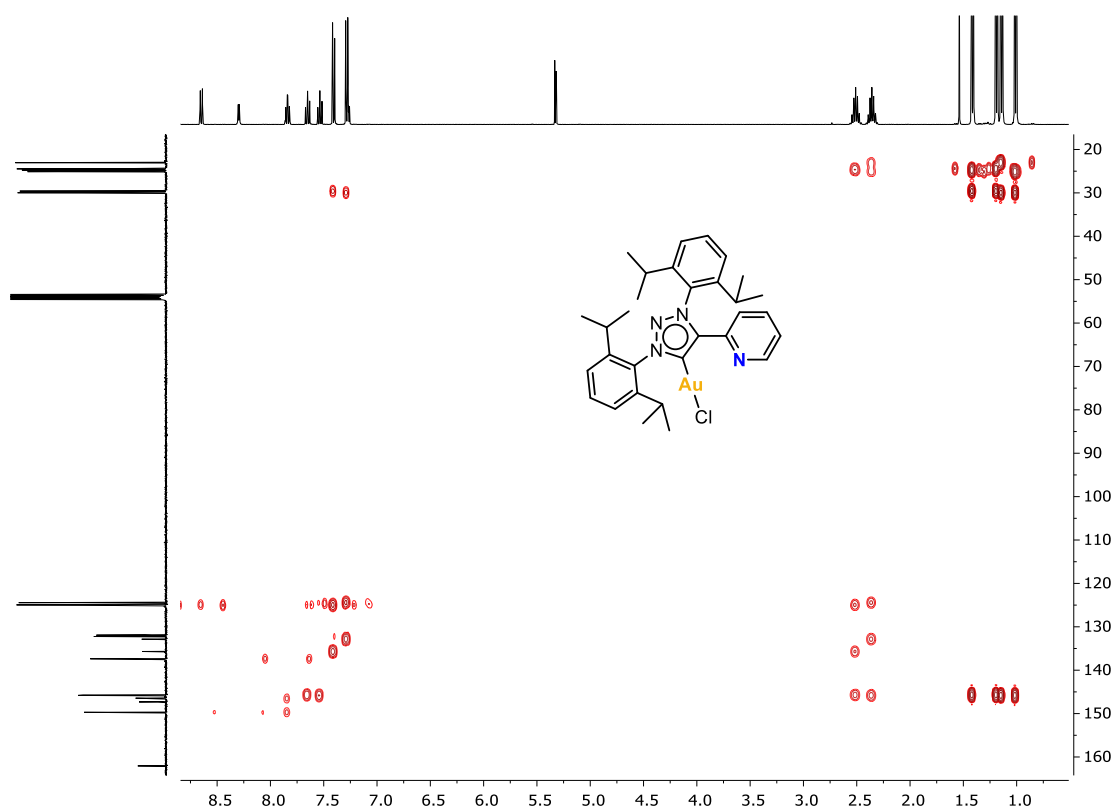
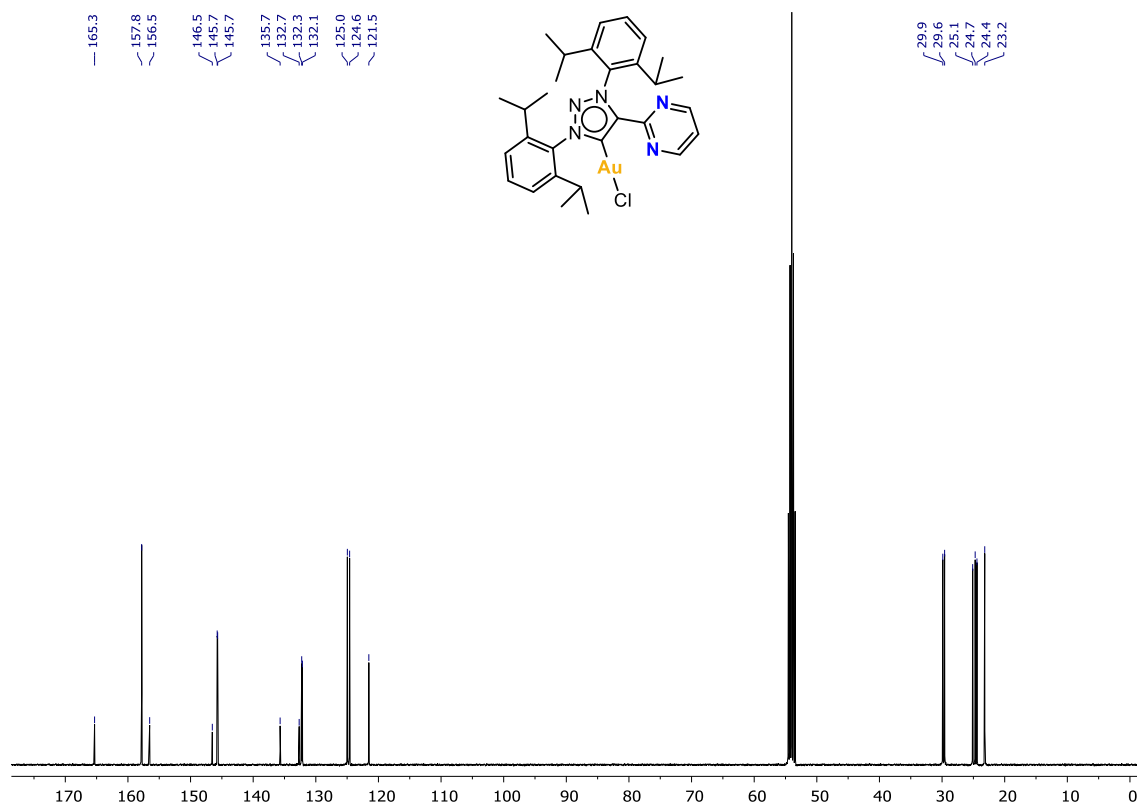
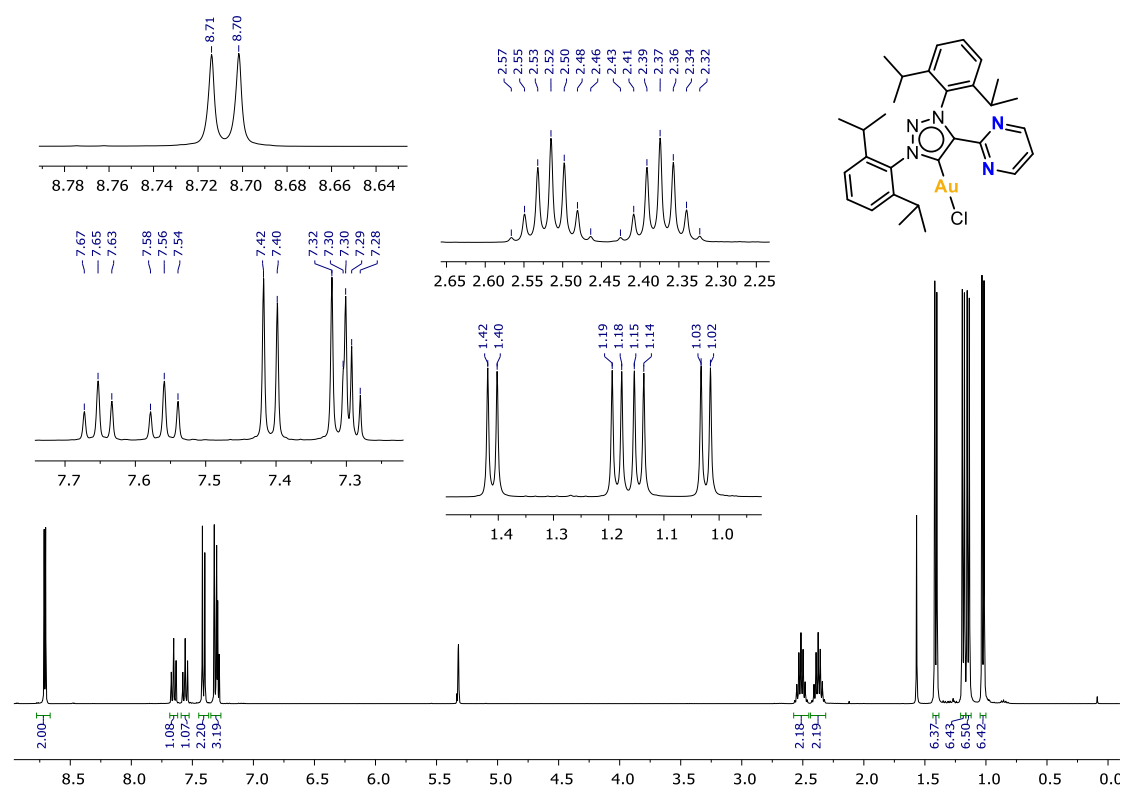


Figure S15. ^1H , ^{13}C -HMBC NMR (400MHz, 298K) of **2a** in CD_2Cl_2 .

8.4 NMR Spectra of complex 2b



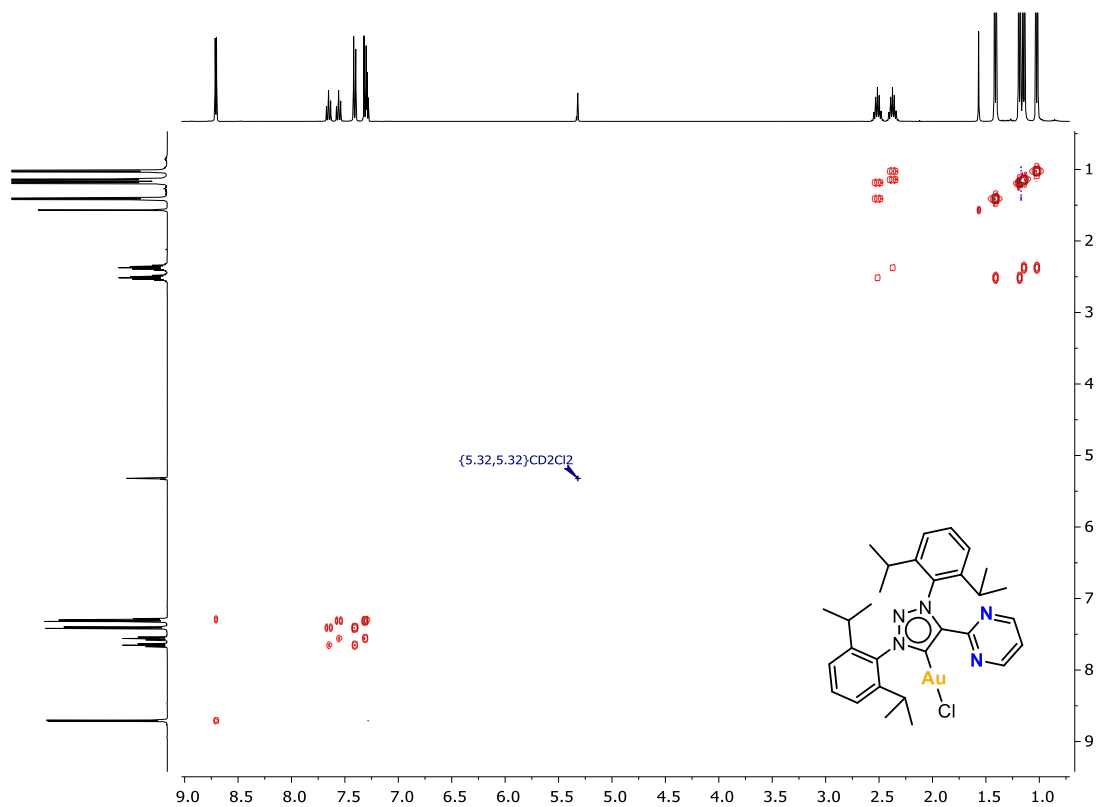


Figure S18. ^1H , ^1H -COSY NMR (400MHz, 298K) of **2b** in CD_2Cl_2 .

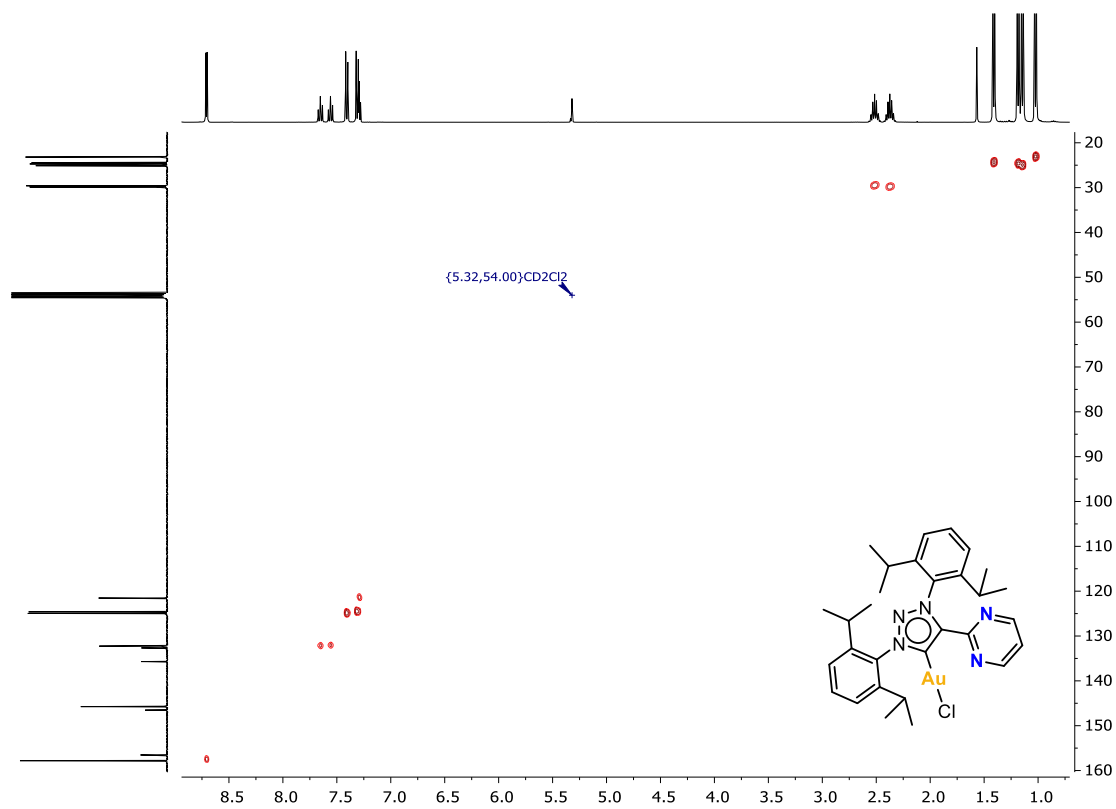


Figure S19. ^1H , ^{13}C -HSQC NMR (400MHz, 298K) of **2b** in CD_2Cl_2 .

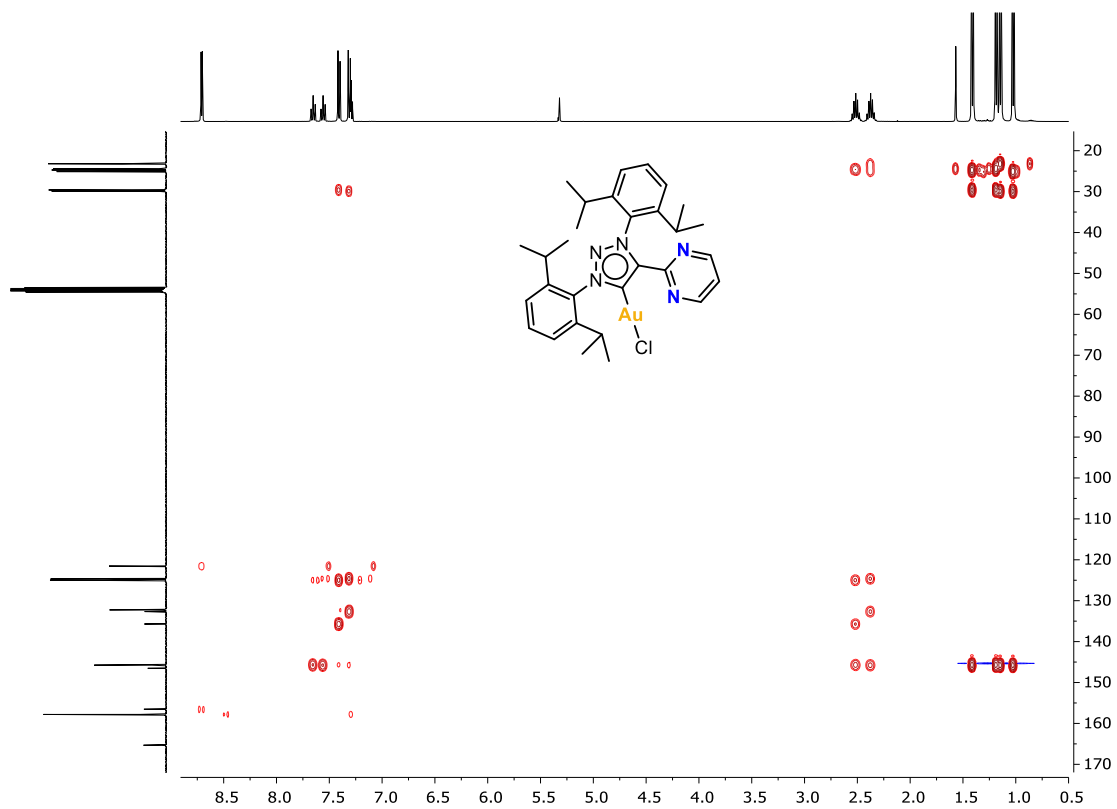


Figure S20. ^1H , ^{13}C -HMBC NMR (400MHz, 298K) of **2b** in CD_2Cl_2 .

8.5 NMR Spectra of complex 3a

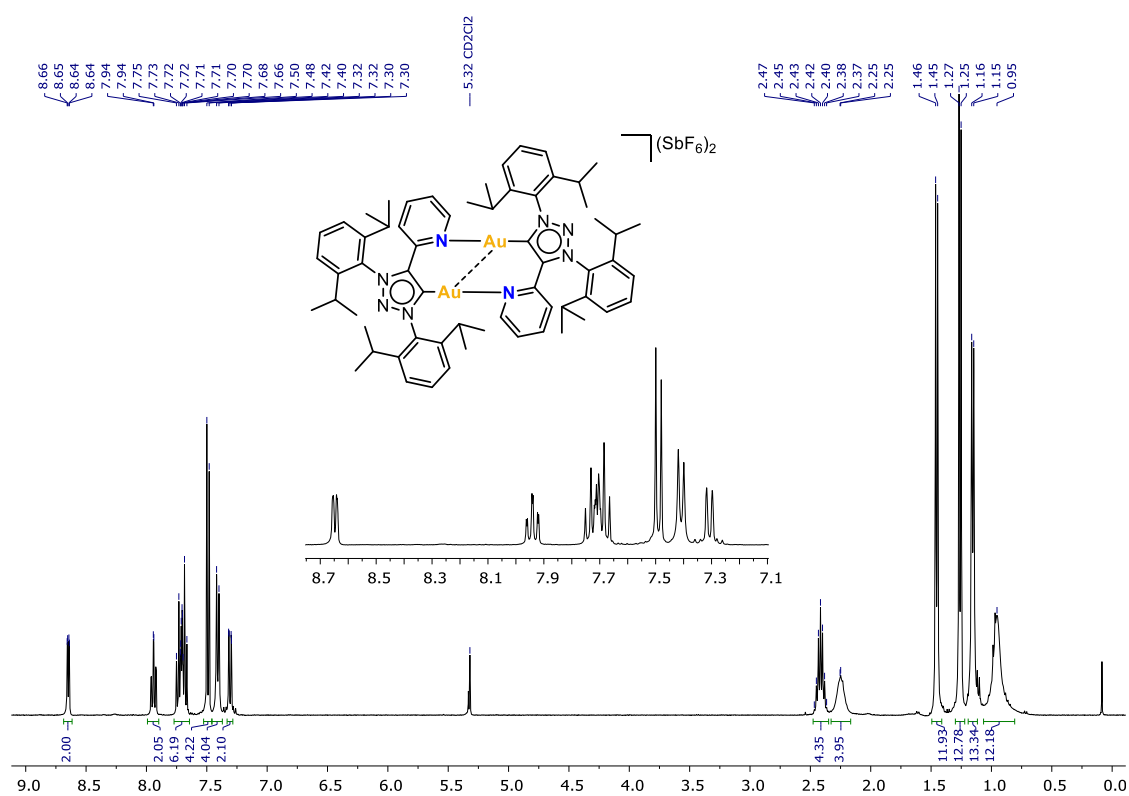


Figure S21. ¹H NMR (400MHz, 298K) of **3a** in CD₂Cl₂.

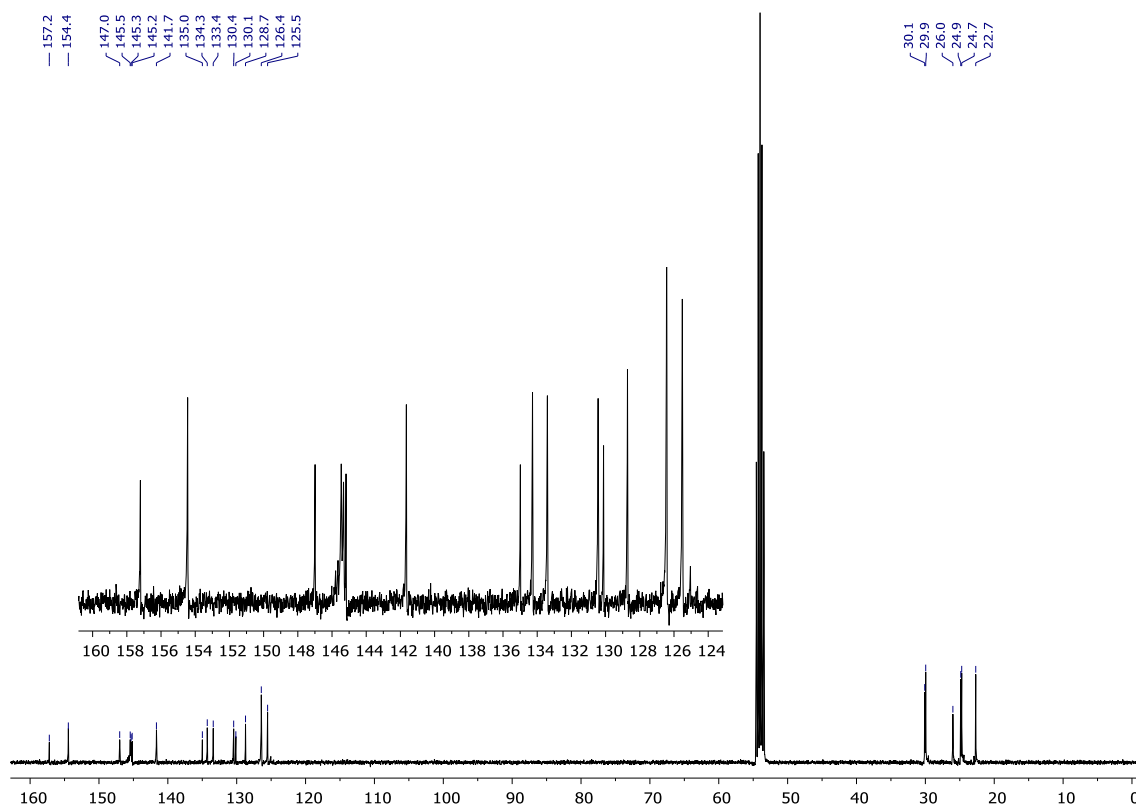


Figure S22. ¹³C NMR (101MHz, 298K) of **3a** in CD₂Cl₂.

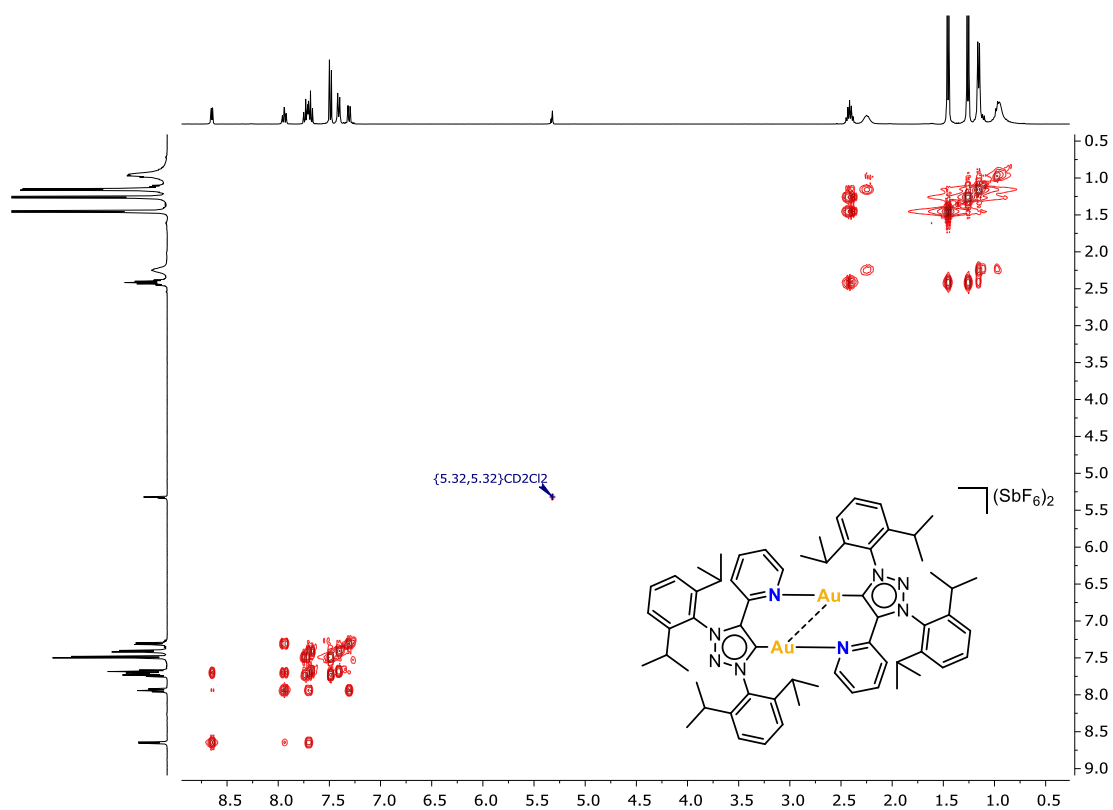


Figure S23. ^1H , ^1H -COSY NMR (400MHz, 298K) of **3a** in CD_2Cl_2 .

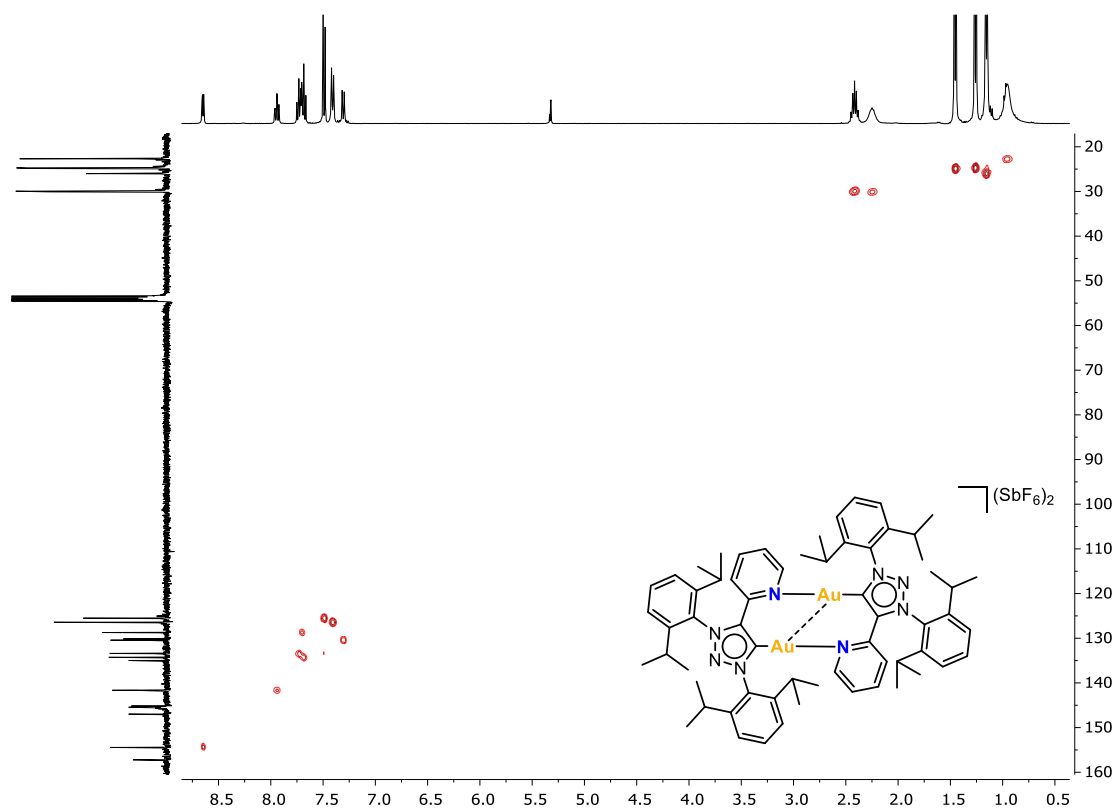


Figure S24. ^1H , ^{13}C -HSQC NMR (400MHz, 298K) of **3a** in CD_2Cl_2 .

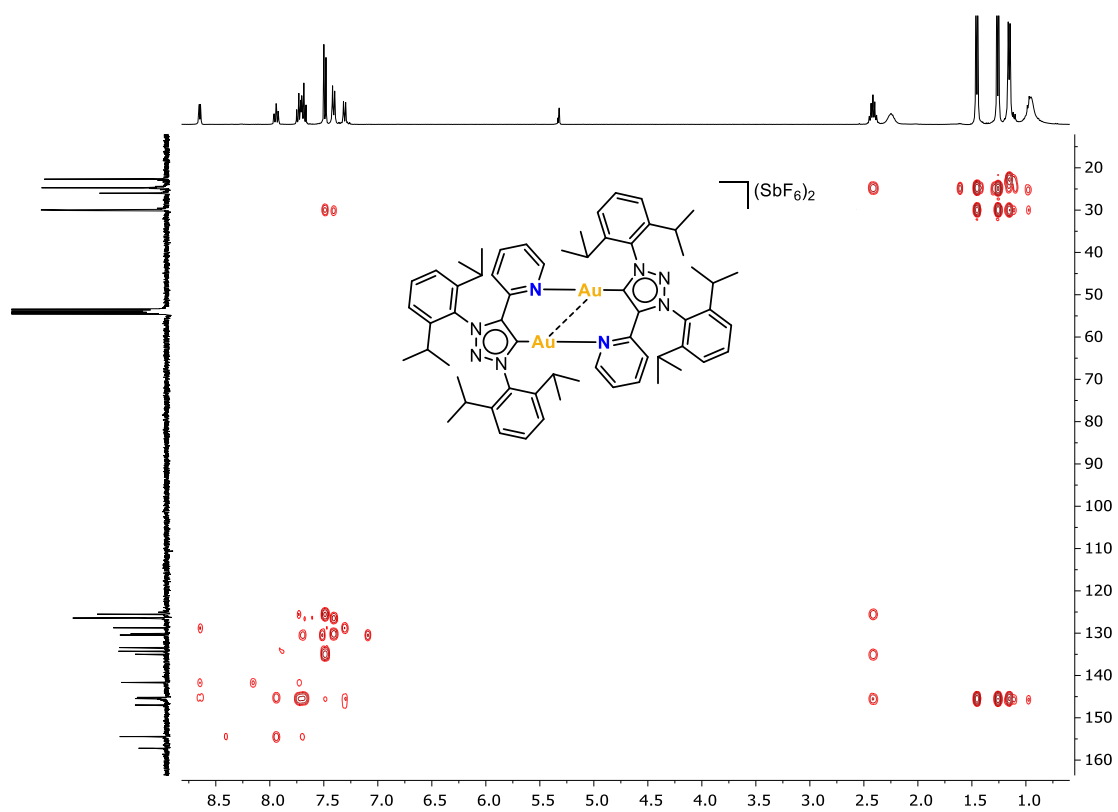


Figure S25. ^1H , ^{13}C -HMBC NMR (400MHz, 298K) of **3a** in CD_2Cl_2 .

8.6 NMR Spectra of complex 3b

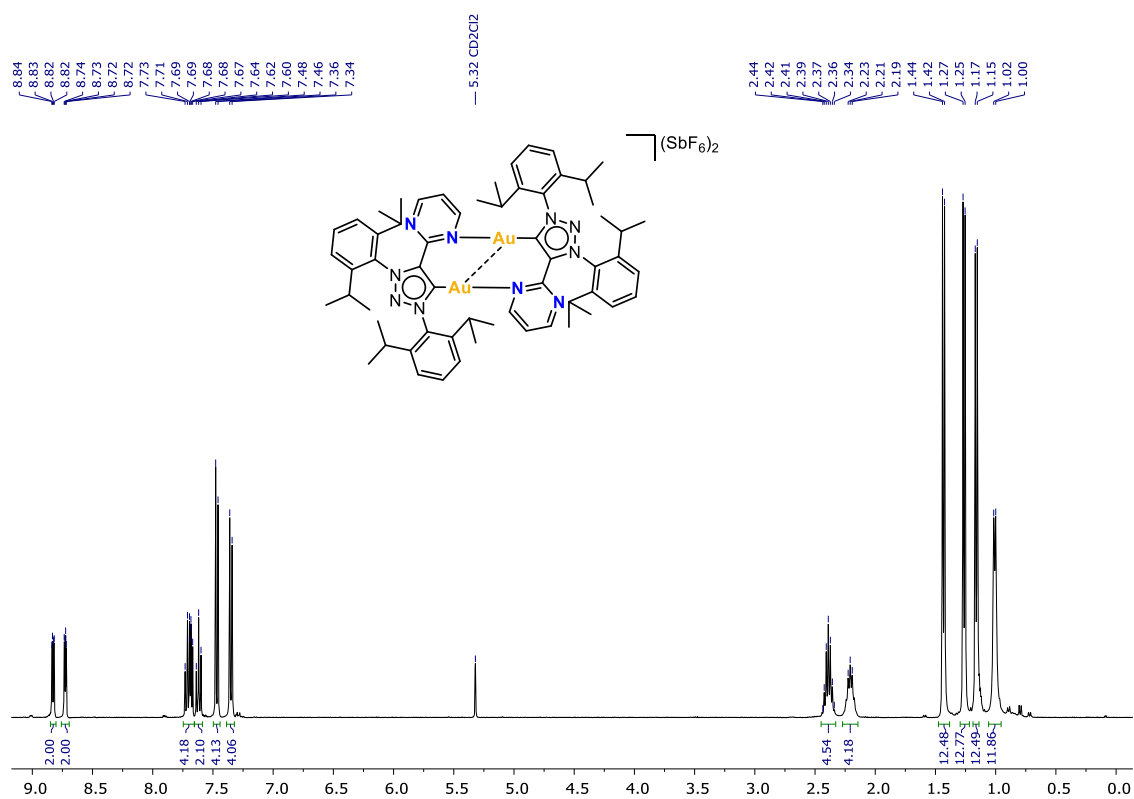


Figure S26. ¹H NMR (400MHz, 298K) of **3b** in CD₂Cl₂.

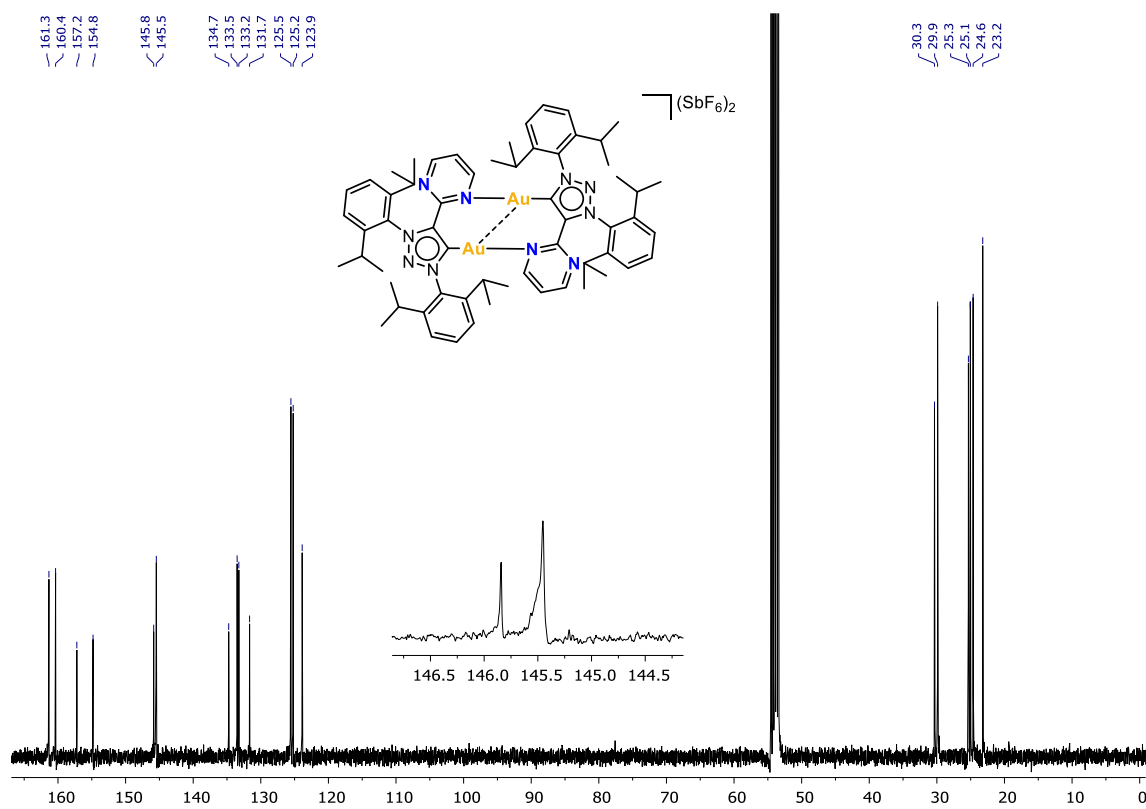


Figure S27. ¹³C NMR (101MHz, 298K) of **3b** in CD₂Cl₂.

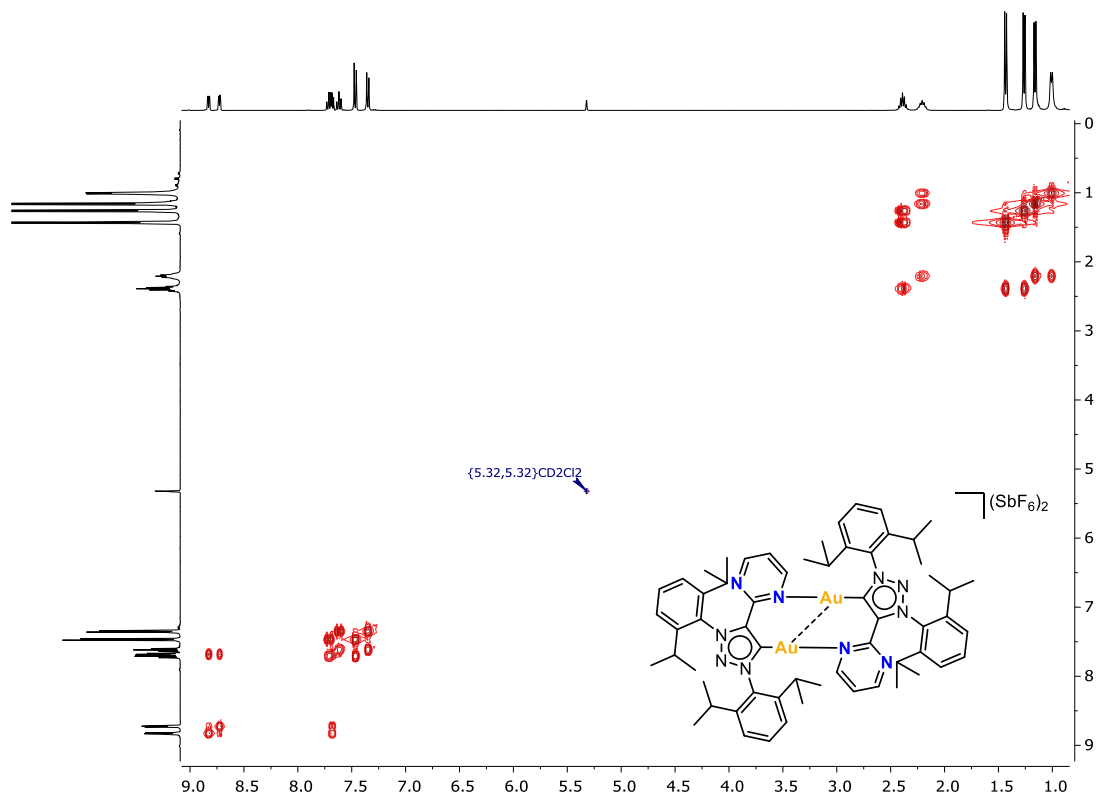


Figure S28. $^1\text{H}, ^1\text{H}$ -COSY NMR (400MHz, 298K) of **3b** in CD_2Cl_2 .

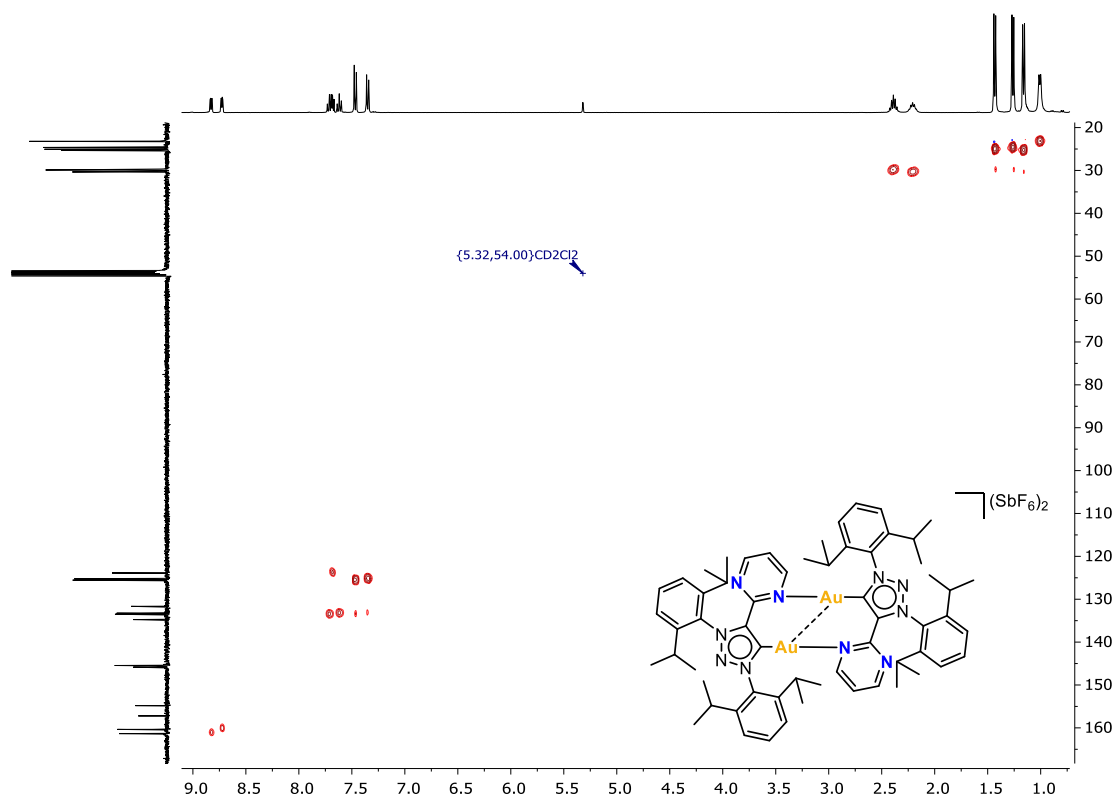


Figure S29. $^1\text{H}, ^{13}\text{C}$ -HSQC NMR (400MHz, 298K) of **3b** in CD_2Cl_2 .

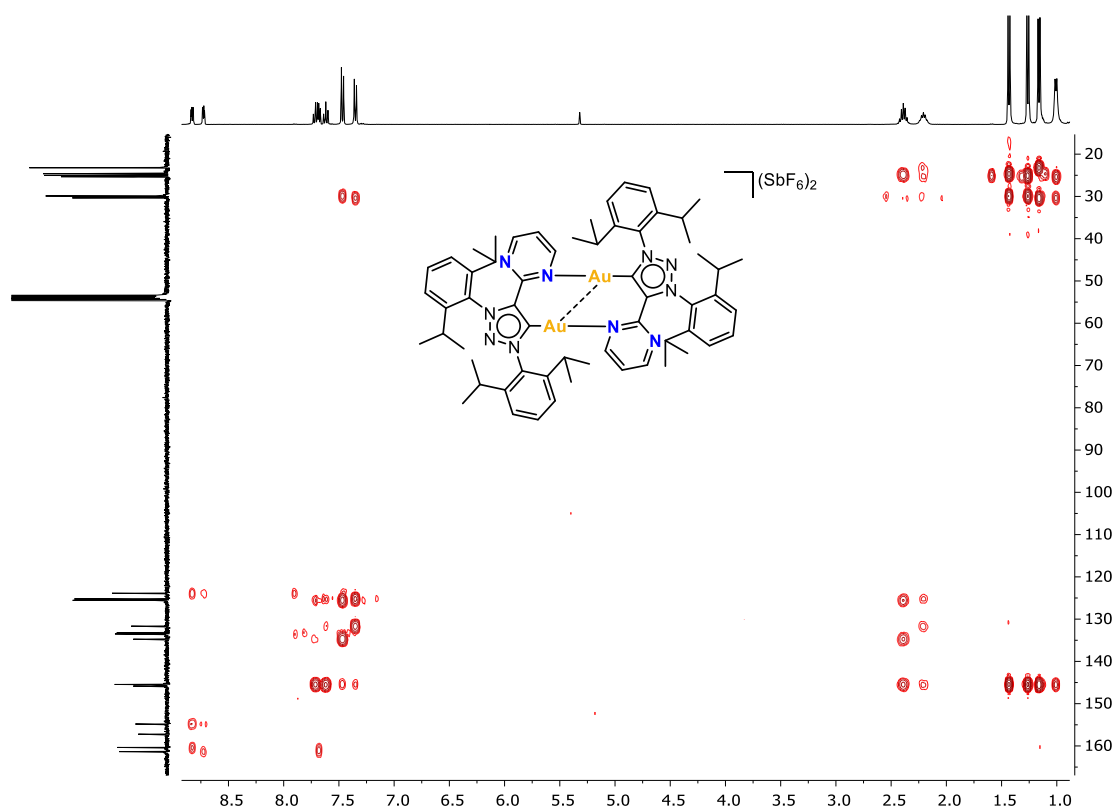


Figure S30. ^1H , ^{13}C -HMBC NMR (400MHz, 298K) of **3b** in CD_2Cl_2 .

8.7 NMR and HRMS-ESI Spectra of complex 4a-Cl

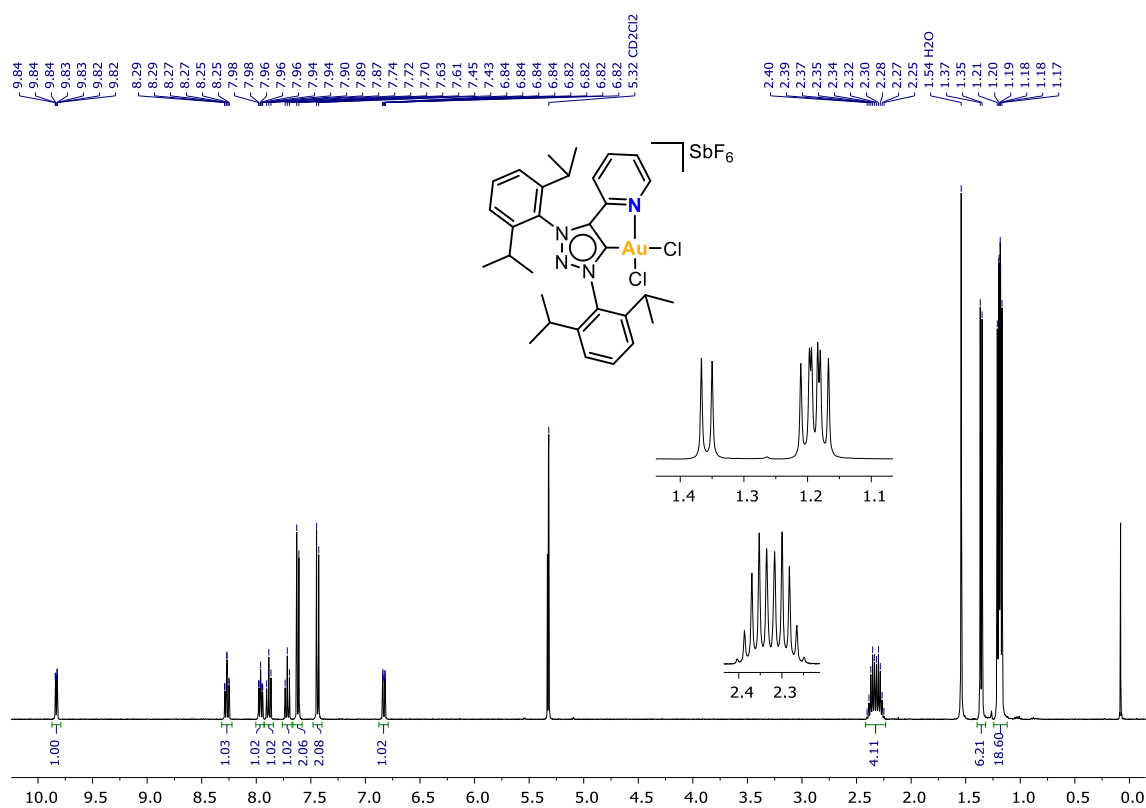


Figure S31. ^1H NMR (400MHz, 298K) of 4a-Cl in CD_2Cl_2 .

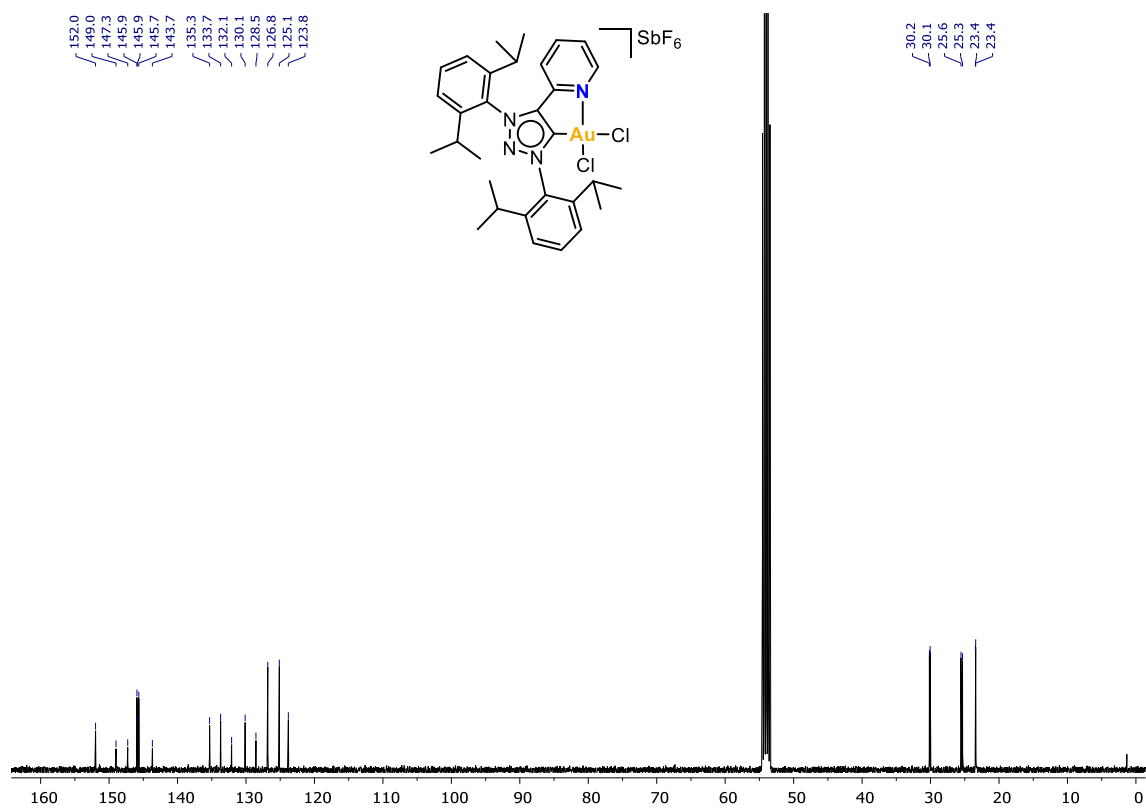


Figure S32. ^{13}C NMR (101MHz, 298K) of 4a-Cl in CD_2Cl_2 .

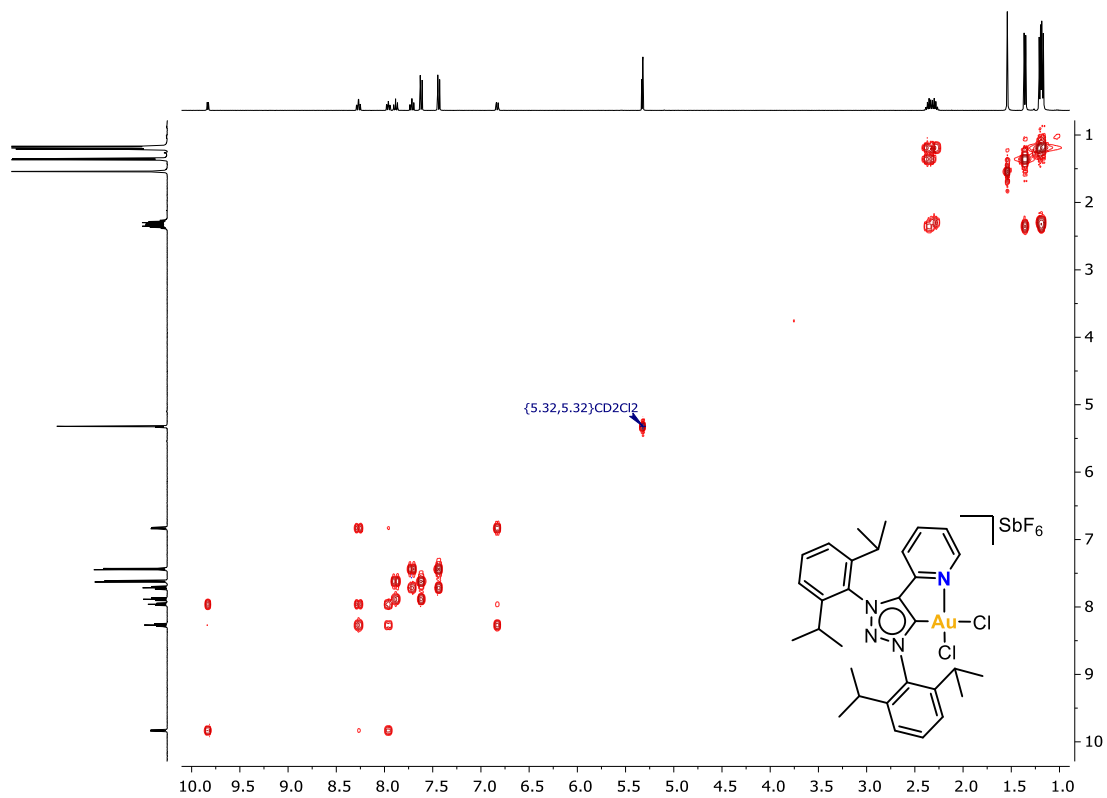


Figure S33. ^1H , ^1H -COSY NMR (400MHz, 298K) of **4a-Cl** in CD_2Cl_2 .

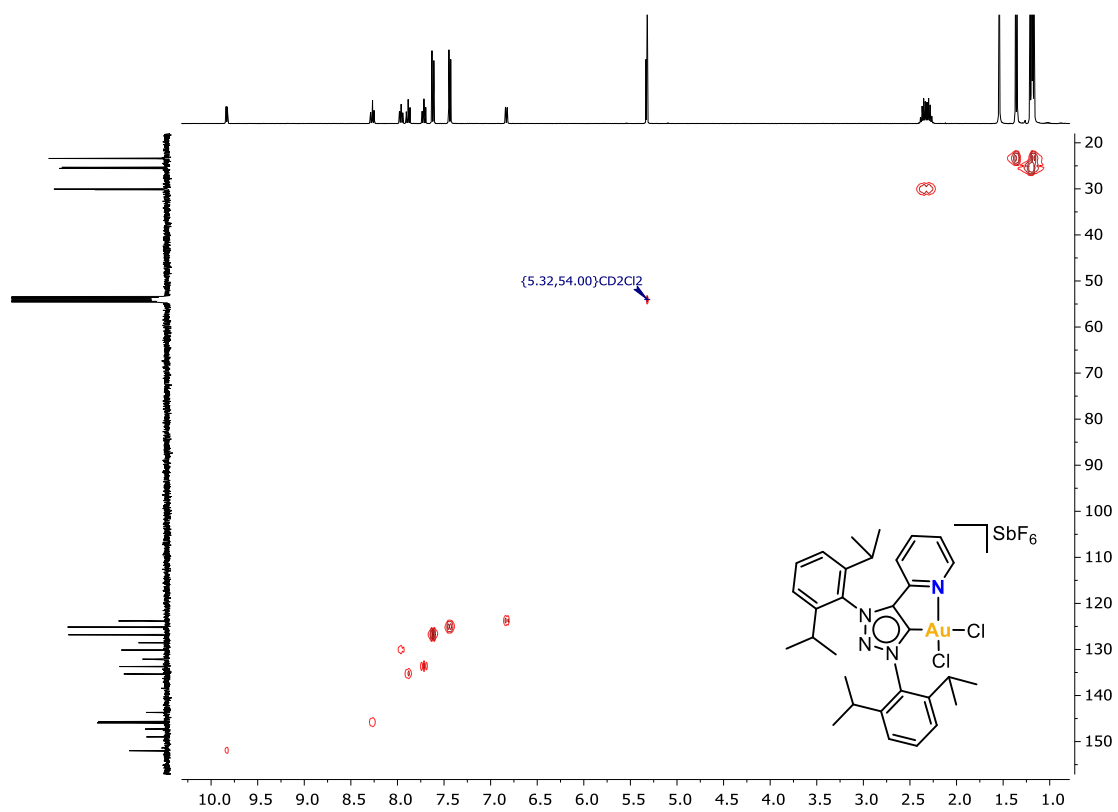


Figure S34. ^1H , ^{13}C -HSQC NMR (400MHz, 298K) of **4a-Cl** in CD_2Cl_2 .

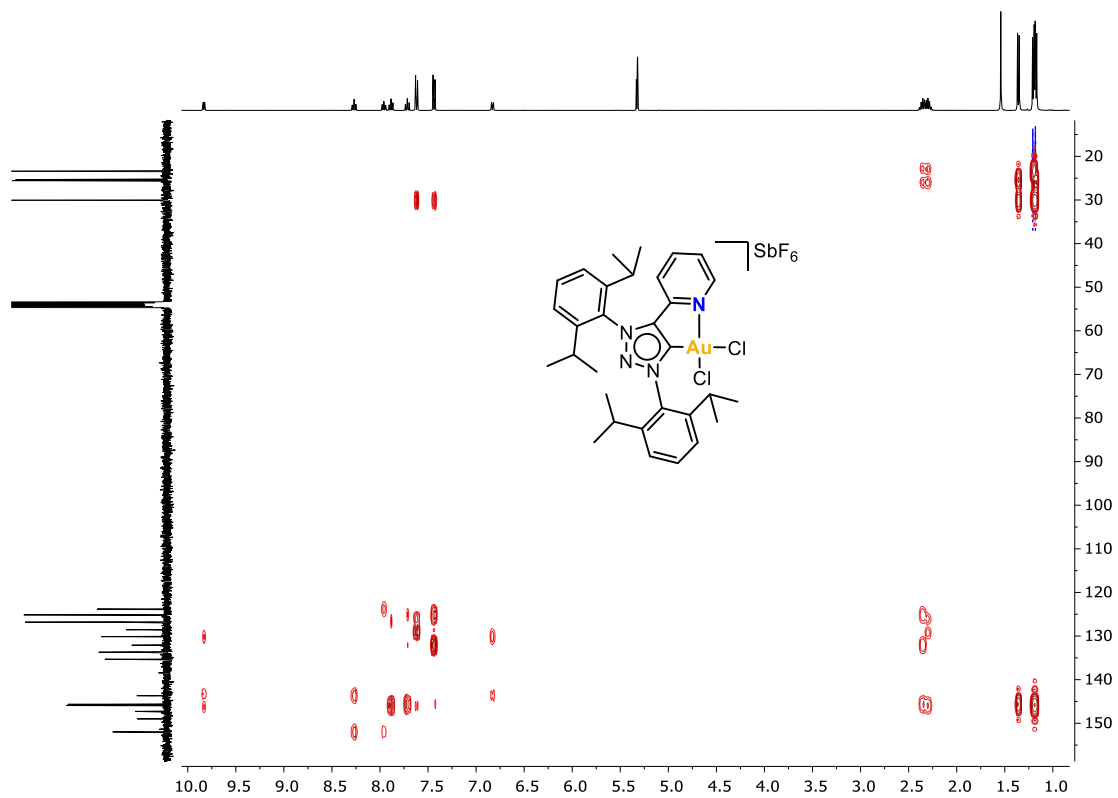


Figure S35. ^1H , ^{13}C -HMBC NMR (400 MHz, 298 K) of **4a-Cl** in CD_2Cl_2 .

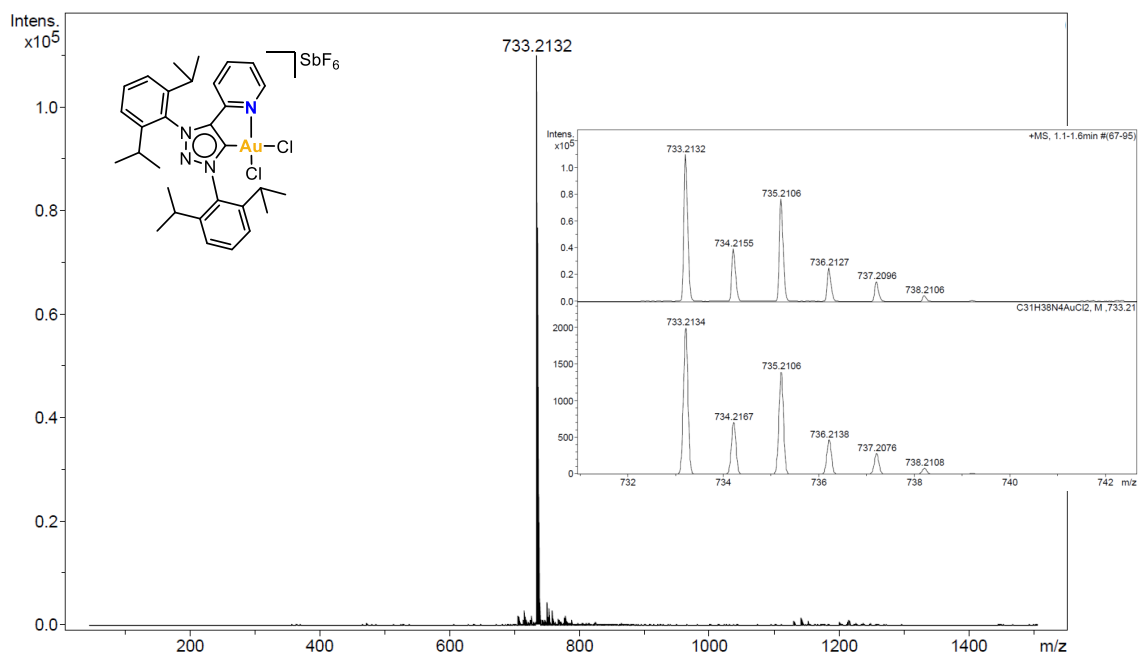


Figure S36. HRMS-ESI(+) of **4a-Cl**.

8.8 NMR and HRMS-ESI Spectra of complex 4a-OAc

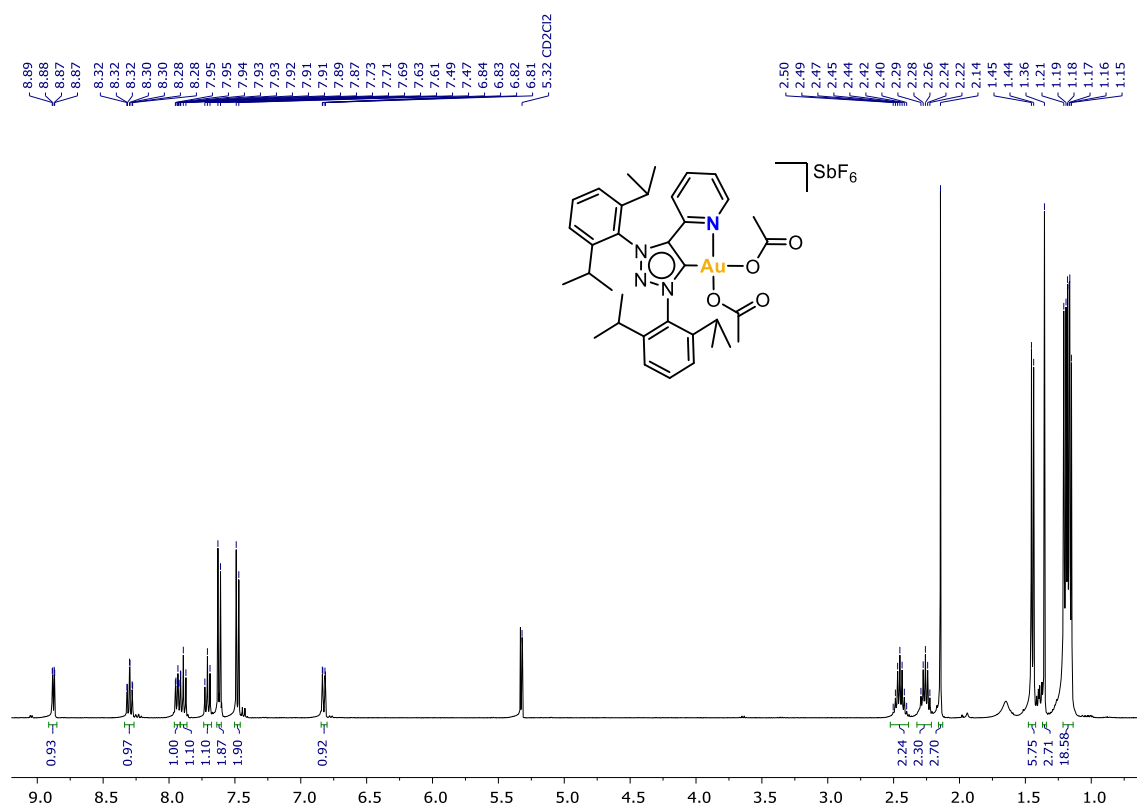


Figure S37. ¹H NMR (400MHz, 298K) of 4a-OAc in CD₂Cl₂.

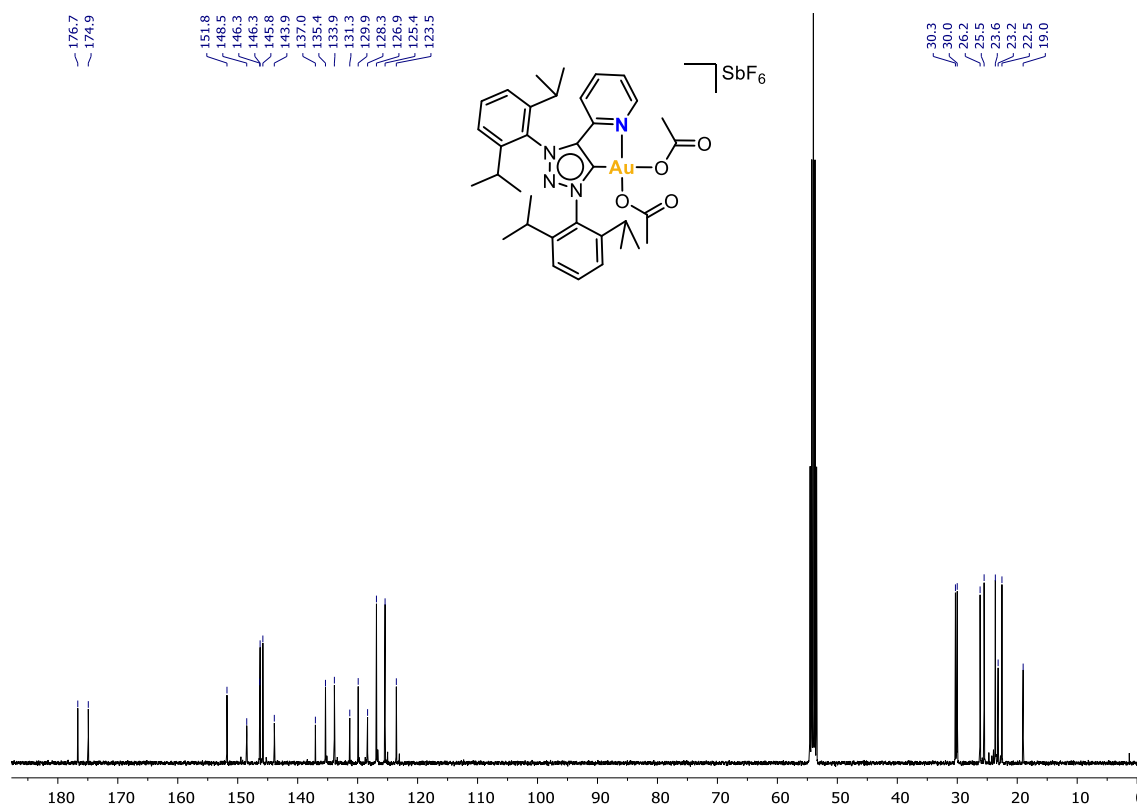


Figure S38. ¹³C NMR (101MHz, 298K) of 4a-OAc in CD₂Cl₂.

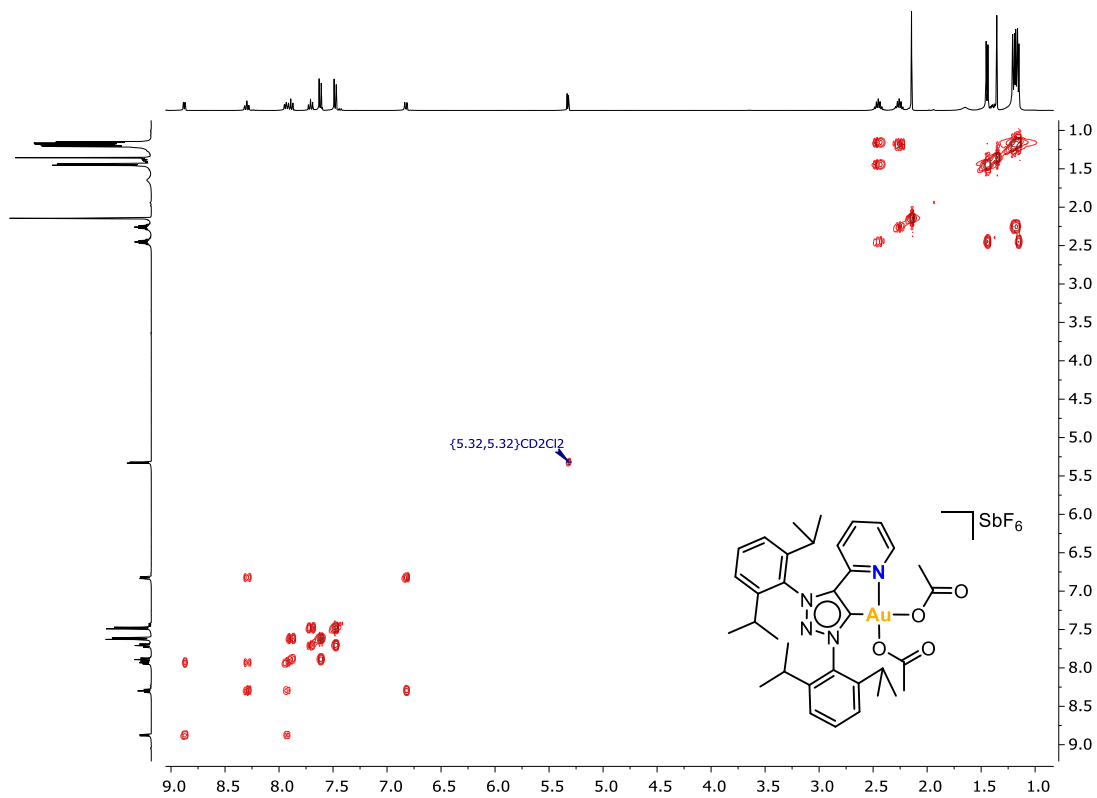


Figure S39. ^1H , ^1H -COSY NMR (400MHz, 298K) of **4a-OAc** in CD_2Cl_2 .

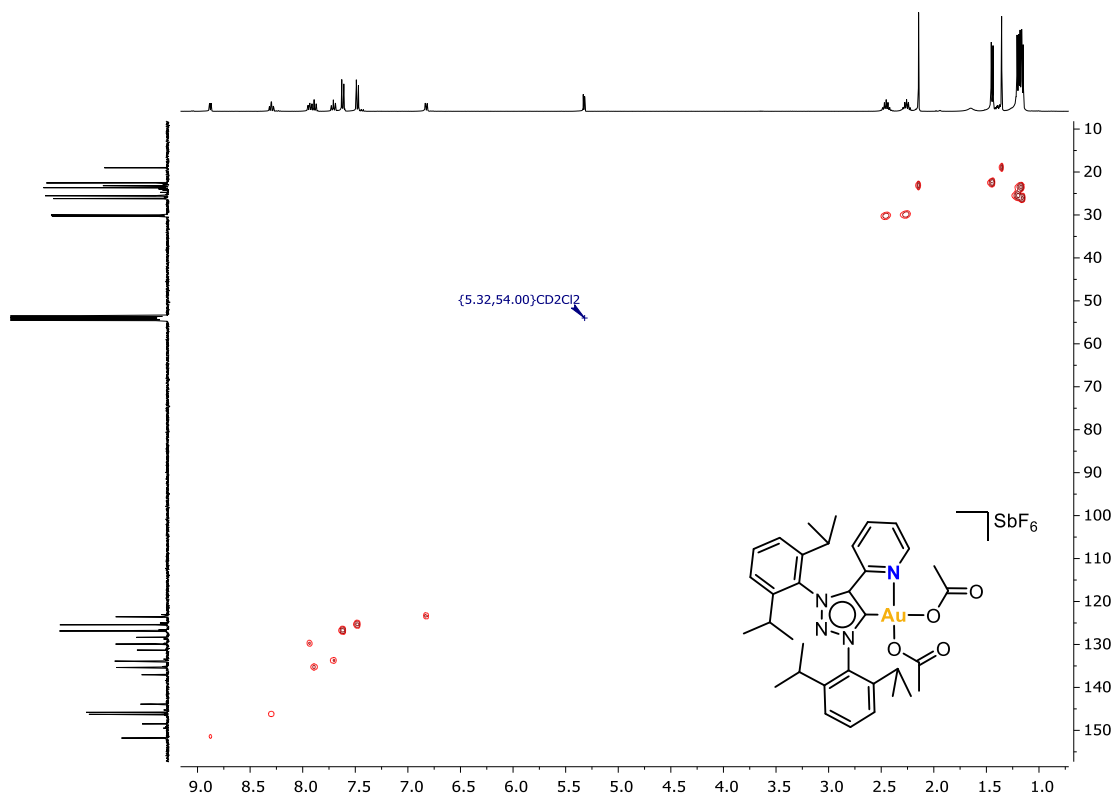


Figure S40. ^1H , ^{13}C -HSQC NMR (400MHz, 298K) of **4a-OAc** in CD_2Cl_2 .

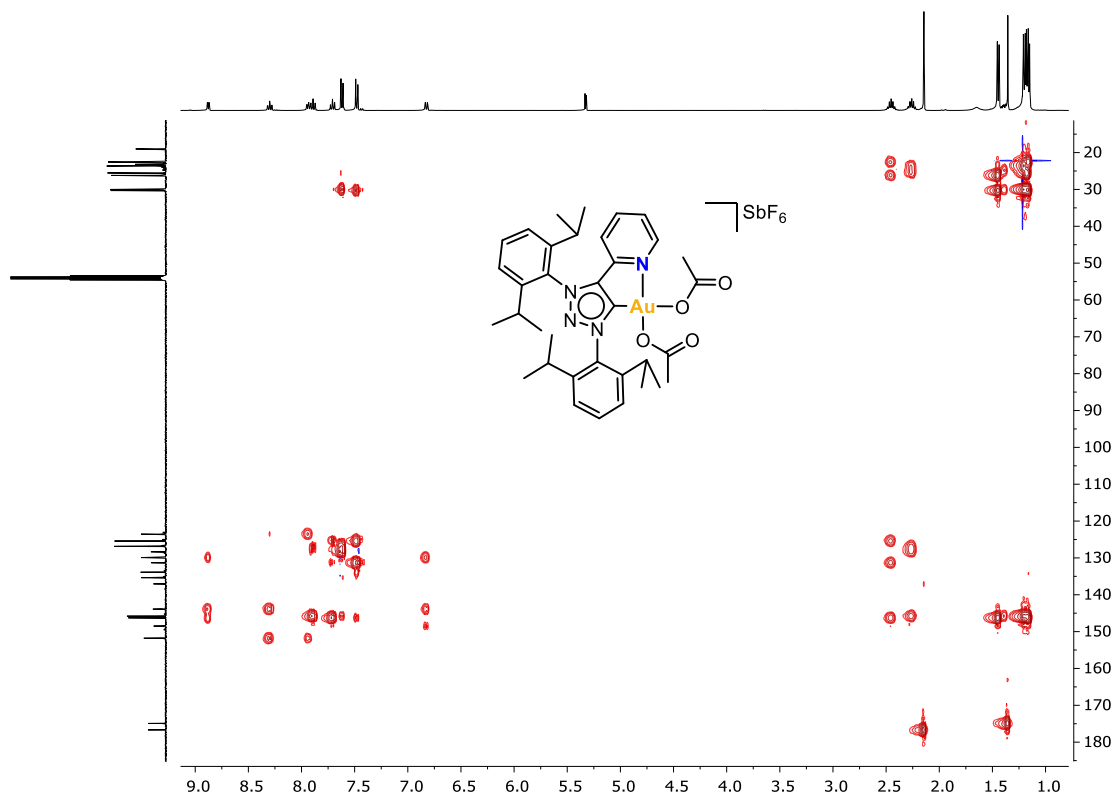


Figure S41. ^1H , ^{13}C -HMBC NMR (400MHz, 298K) of **4a-OAc** in CD_2Cl_2 .

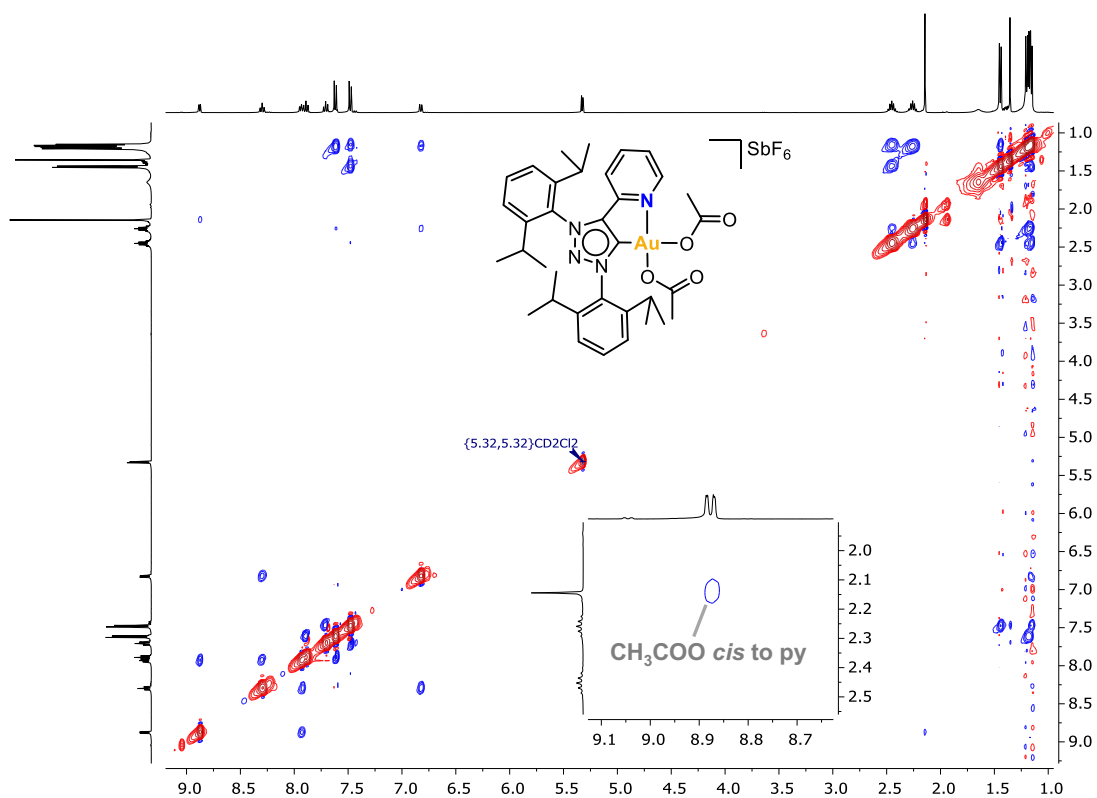


Figure S42. ^1H , ^1H -NOESY NMR (400MHz, 298K) of **4a-OAc** in CD_2Cl_2 .

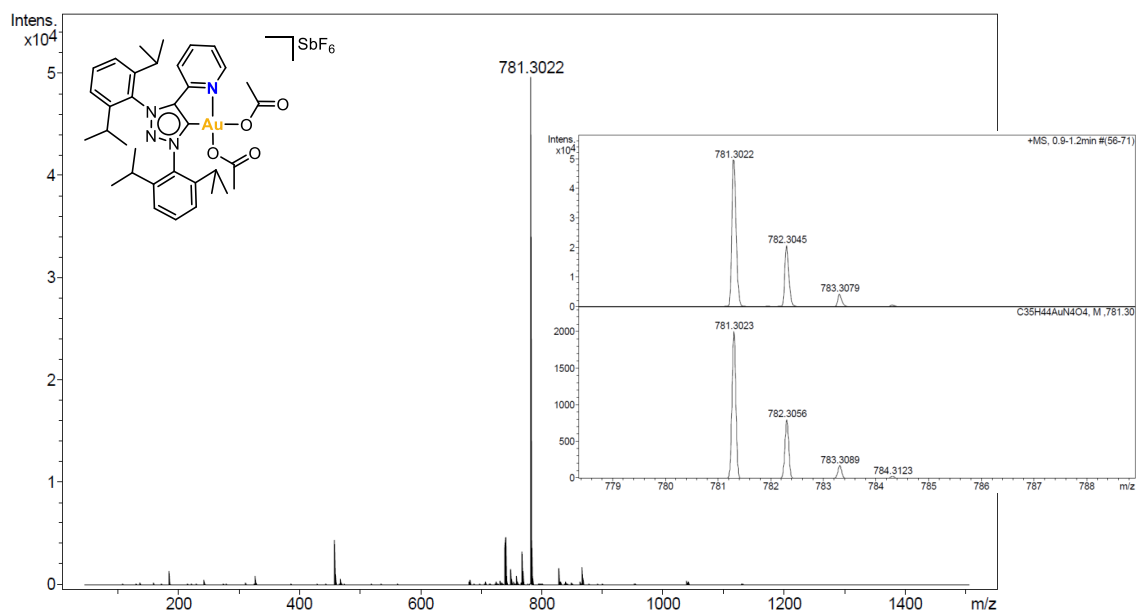


Figure S43. HRMS-ESI(+) of **4a-OAc**.

8.9 NMR and HRMS-ESI Spectra of complex **5b**

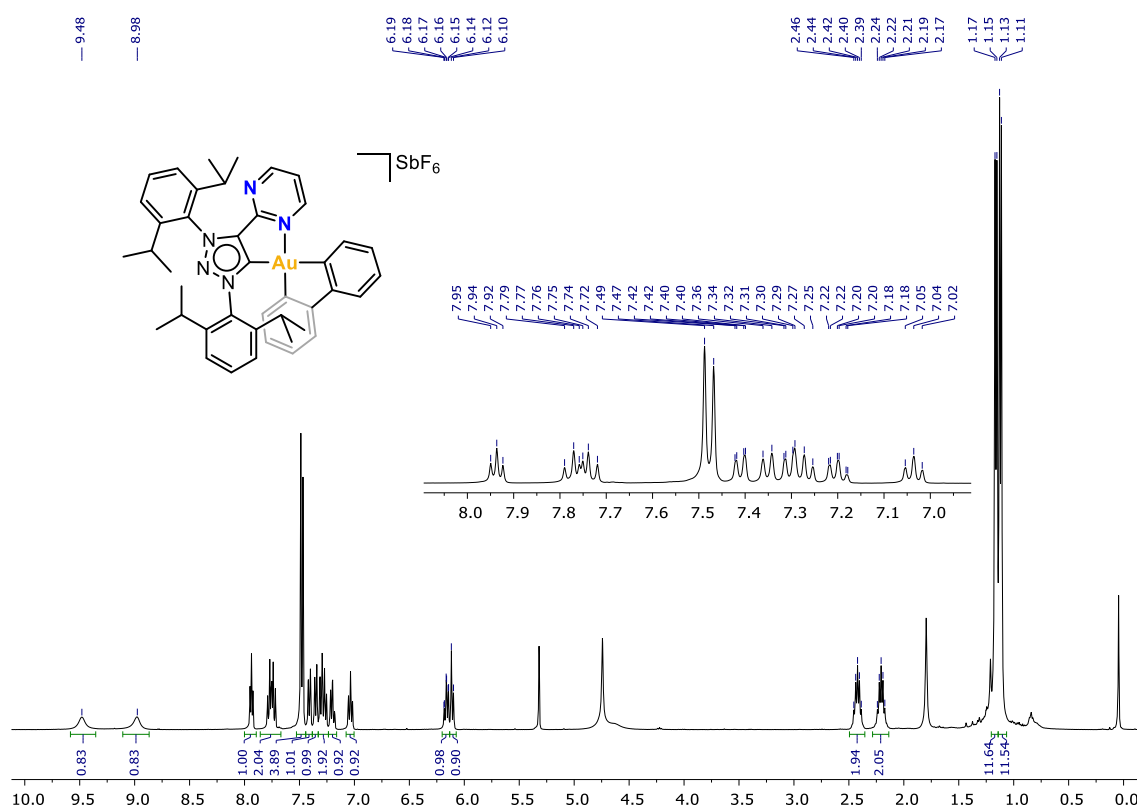


Figure S44. ^1H NMR (400MHz, 248K) of **5b** in CD_2Cl_2 .

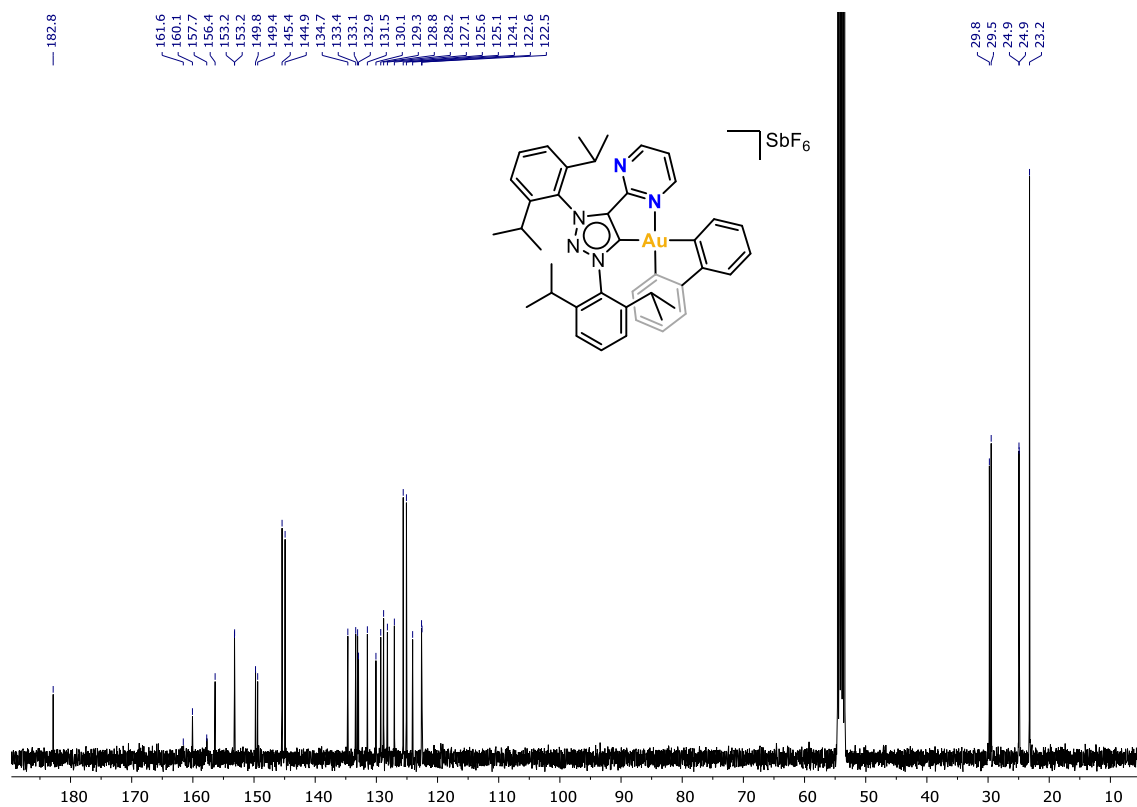


Figure S45. ^{13}C NMR (101MHz, 248K) of **5b** in CD_2Cl_2 .

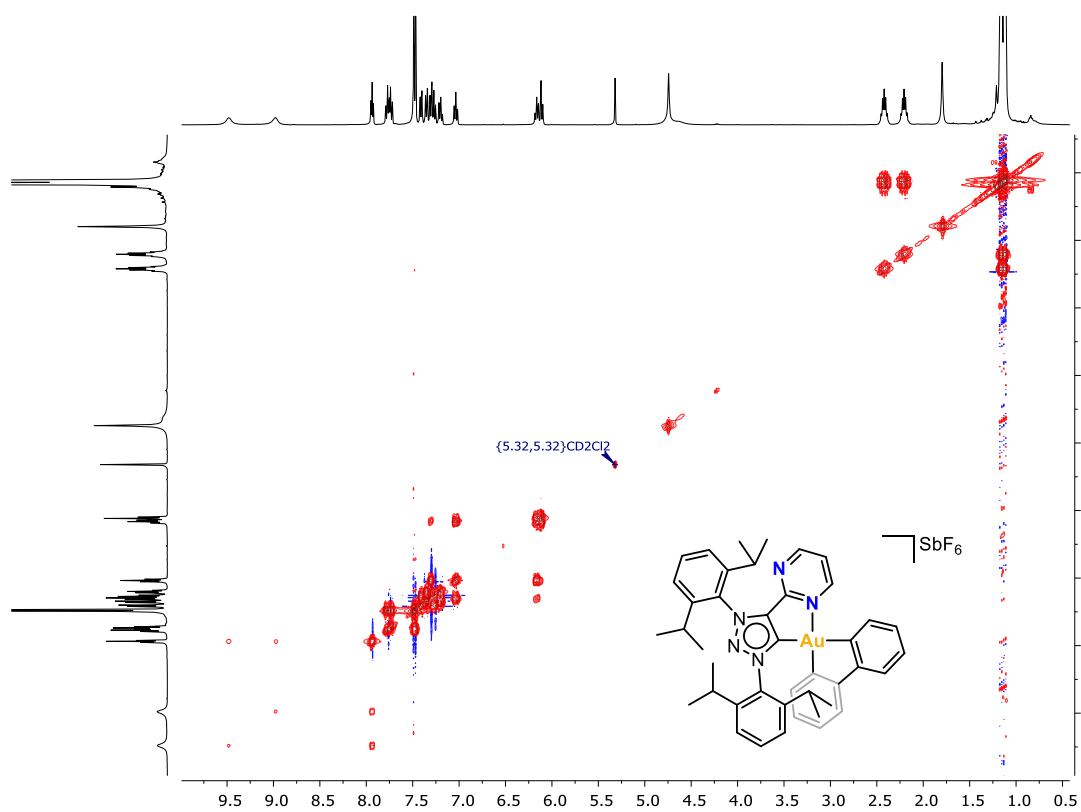


Figure S46. $^1\text{H}, ^1\text{H}$ -COSY NMR (400MHz, 248K) of **5b** in CD_2Cl_2 .

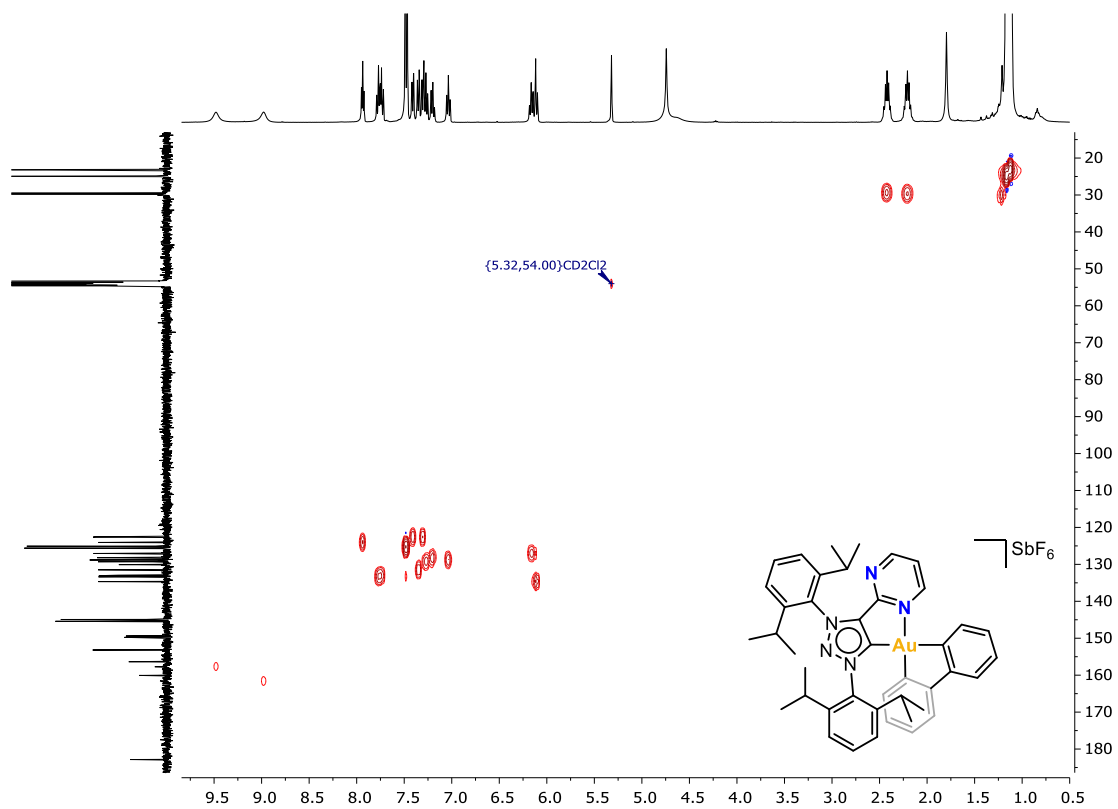


Figure S47. $^1\text{H}, ^{13}\text{C}$ -HSQC NMR (400MHz, 248K) of **5b** in CD_2Cl_2 .

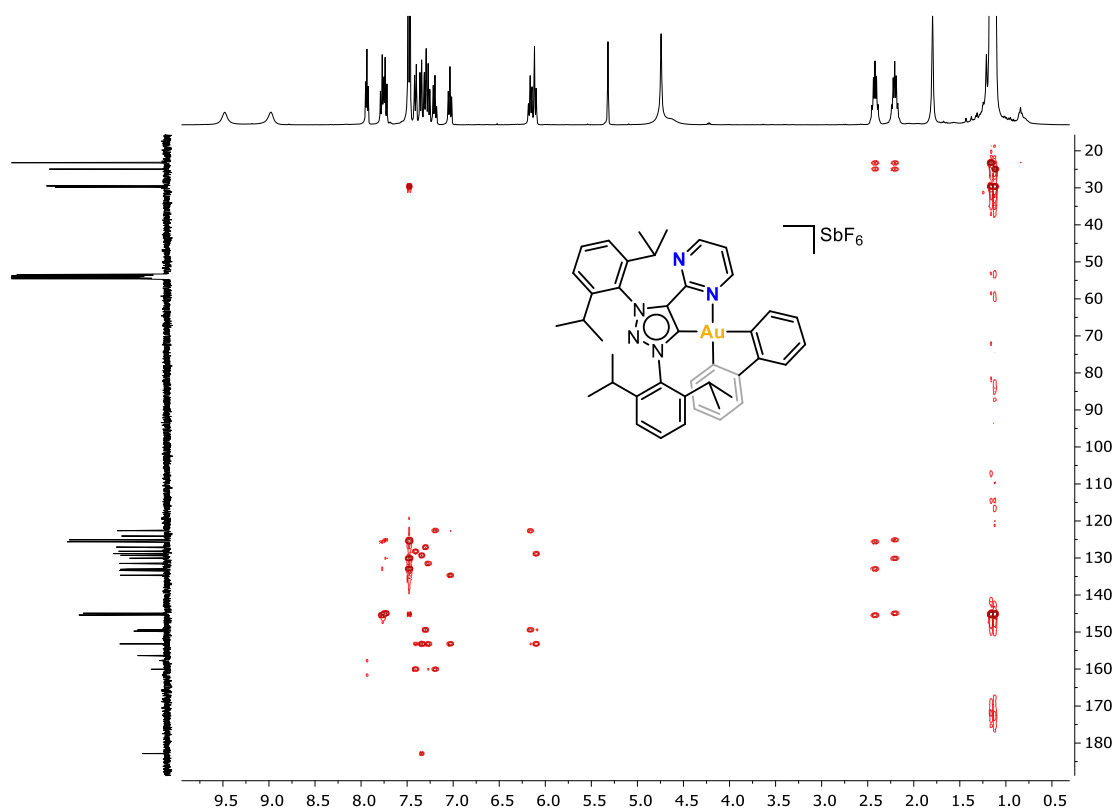


Figure S48. ^1H , ^{13}C -HMBC NMR (400MHz, 248K) of **5b** in CD_2Cl_2 .

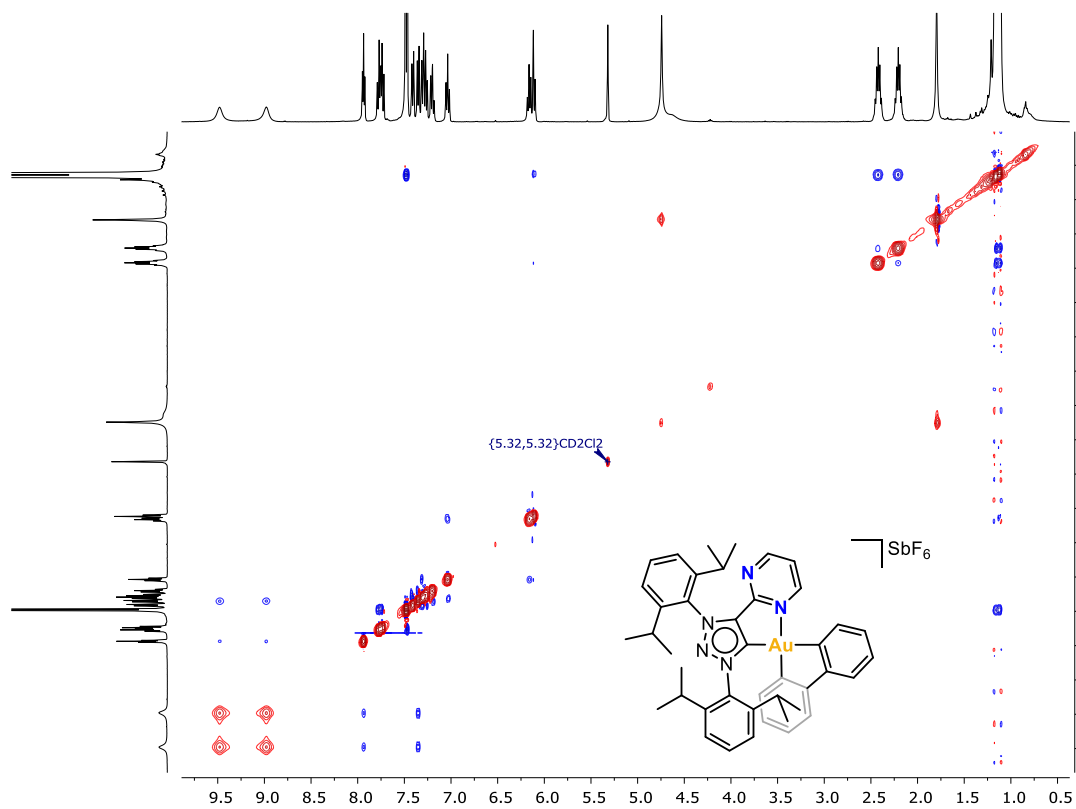


Figure S49. ^1H , ^1H -NOESY NMR (400MHz, 248K) of **5b** in CD_2Cl_2 .

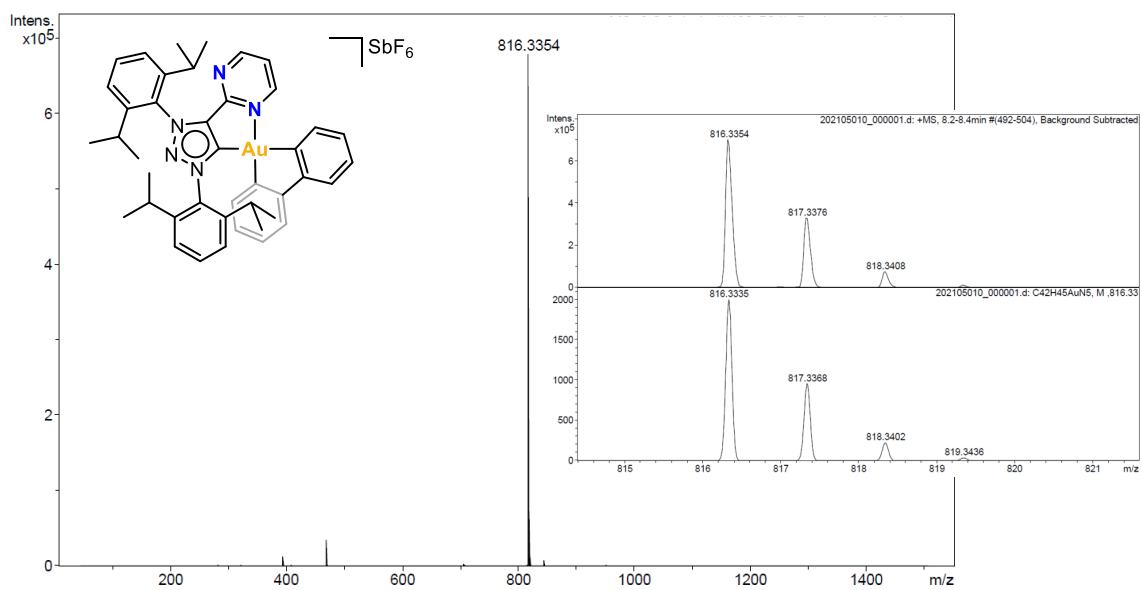


Figure S50. HRMS-ESI(+) of **5b**.

8.10 NMR and HRMS-ESI Spectra of complex 6b

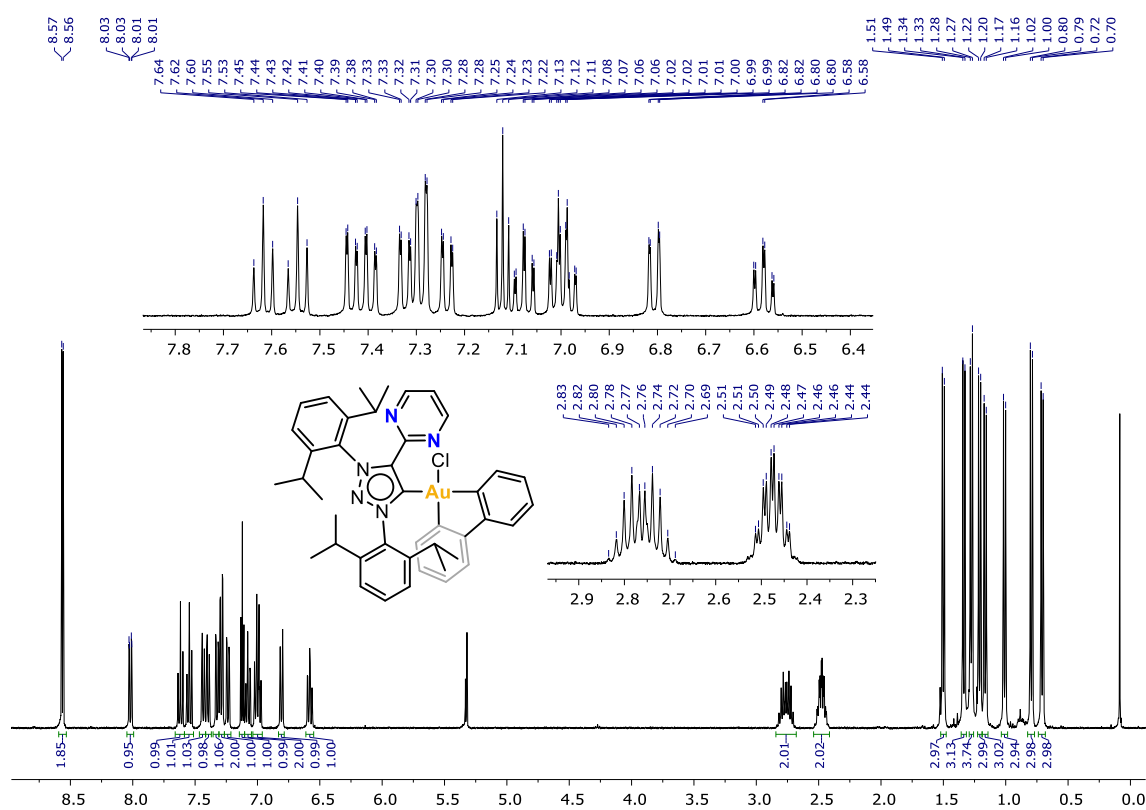


Figure S51. ¹H NMR (400MHz, 298K) of 6b in CD₂Cl₂.

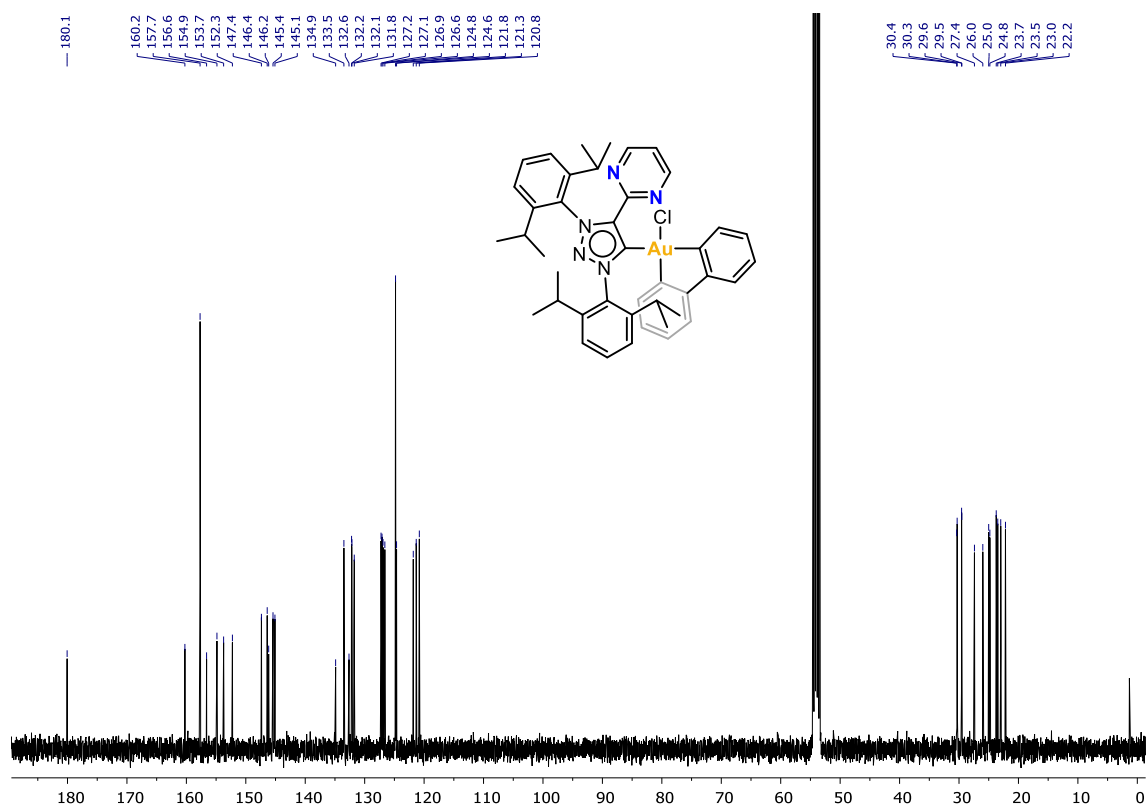


Figure S52. ¹³C NMR (101MHz, 298K) of 6b in CD₂Cl₂.

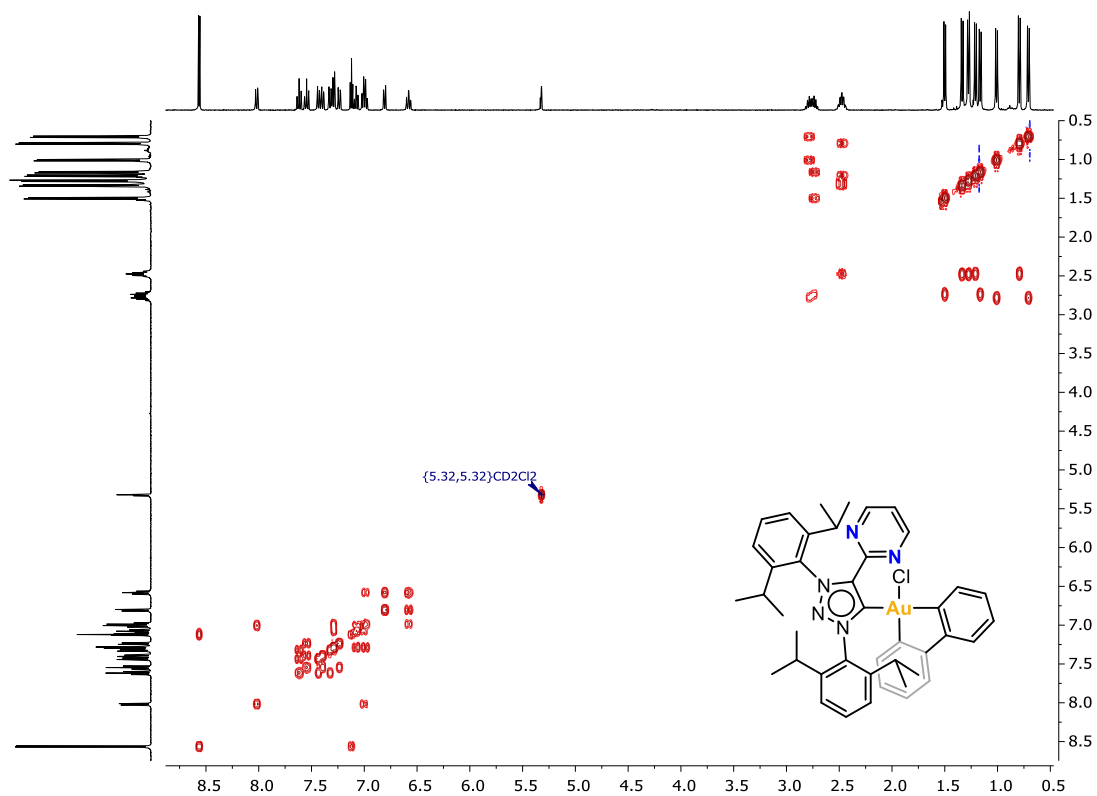


Figure S53. ^1H , ^1H -COSY NMR (400MHz, 298K) of **6b** in CD_2Cl_2 .

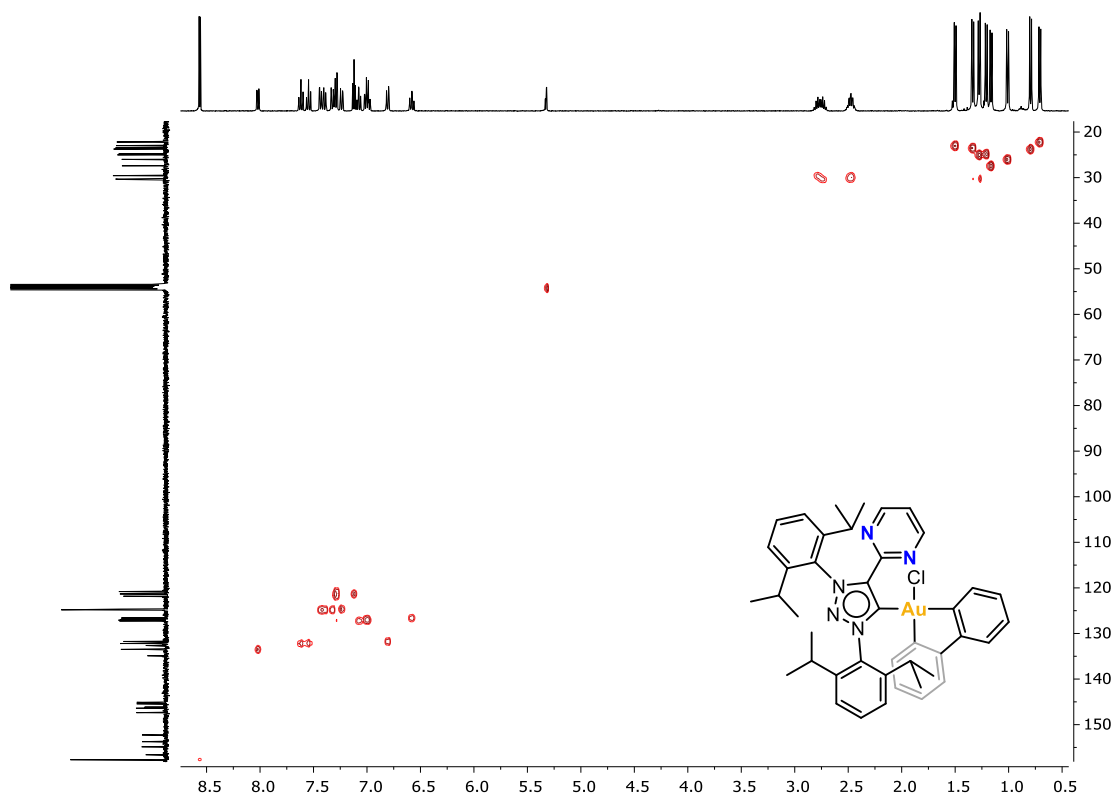


Figure S54. ^1H , ^{13}C -HSQC NMR (400MHz, 298K) of **6b** in CD_2Cl_2 .

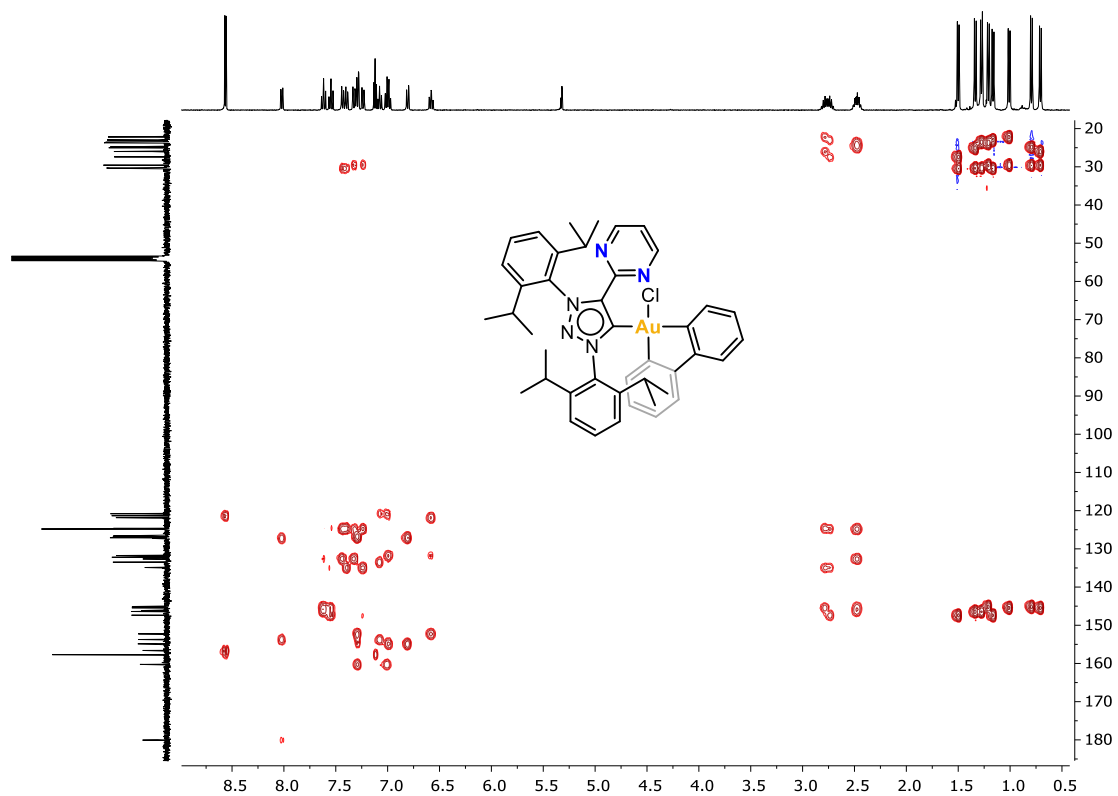


Figure S55. ^1H , ^{13}C -HMBC NMR (400MHz, 298K) of **6b** in CD_2Cl_2 .

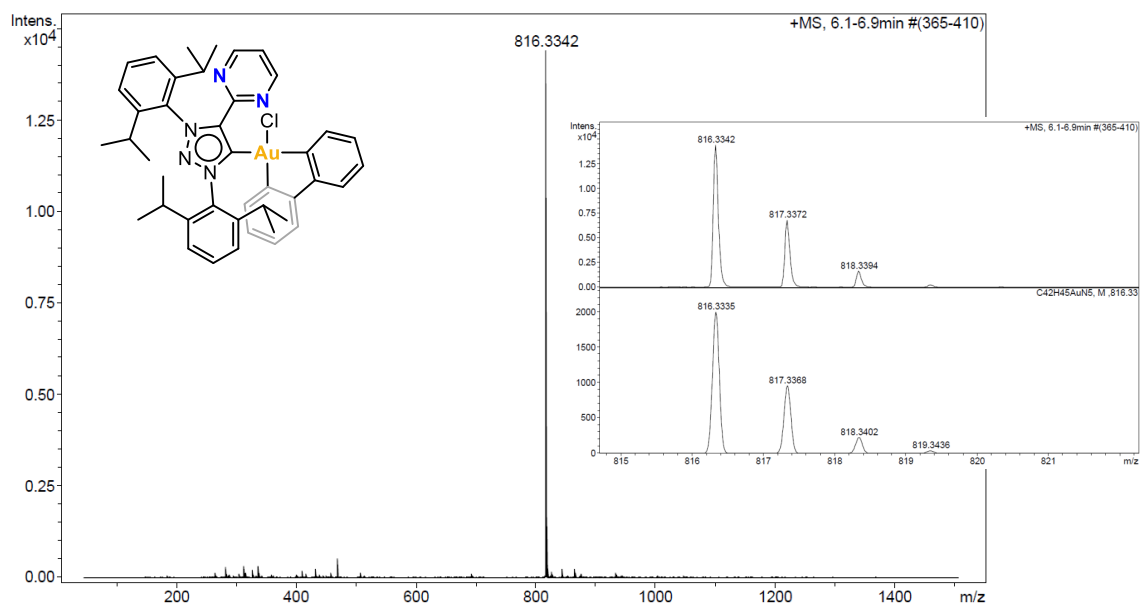


Figure S56. HRMS-ESI(+) of **6b**.

8.11 NMR and HRMS-ESI Spectra of complex *cis-7a-Cl*

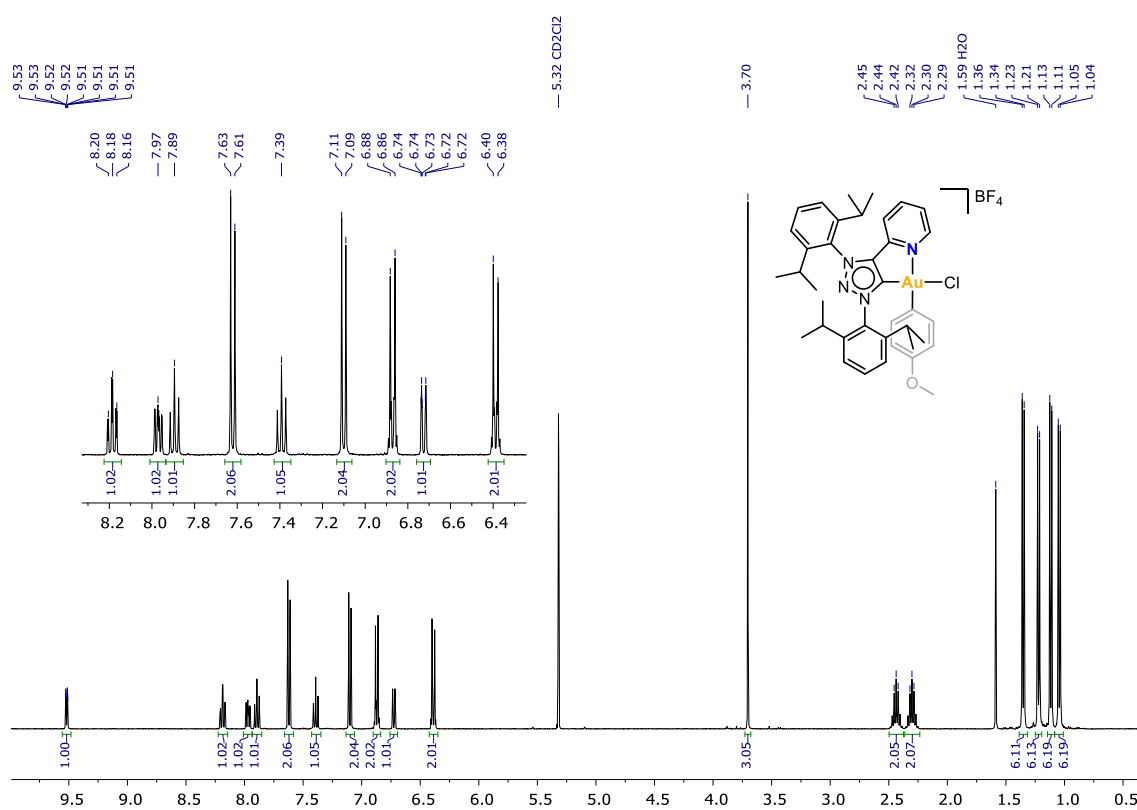


Figure S57. ^1H NMR (400MHz, 298K) of *cis-7a-Cl* in CD_2Cl_2 .

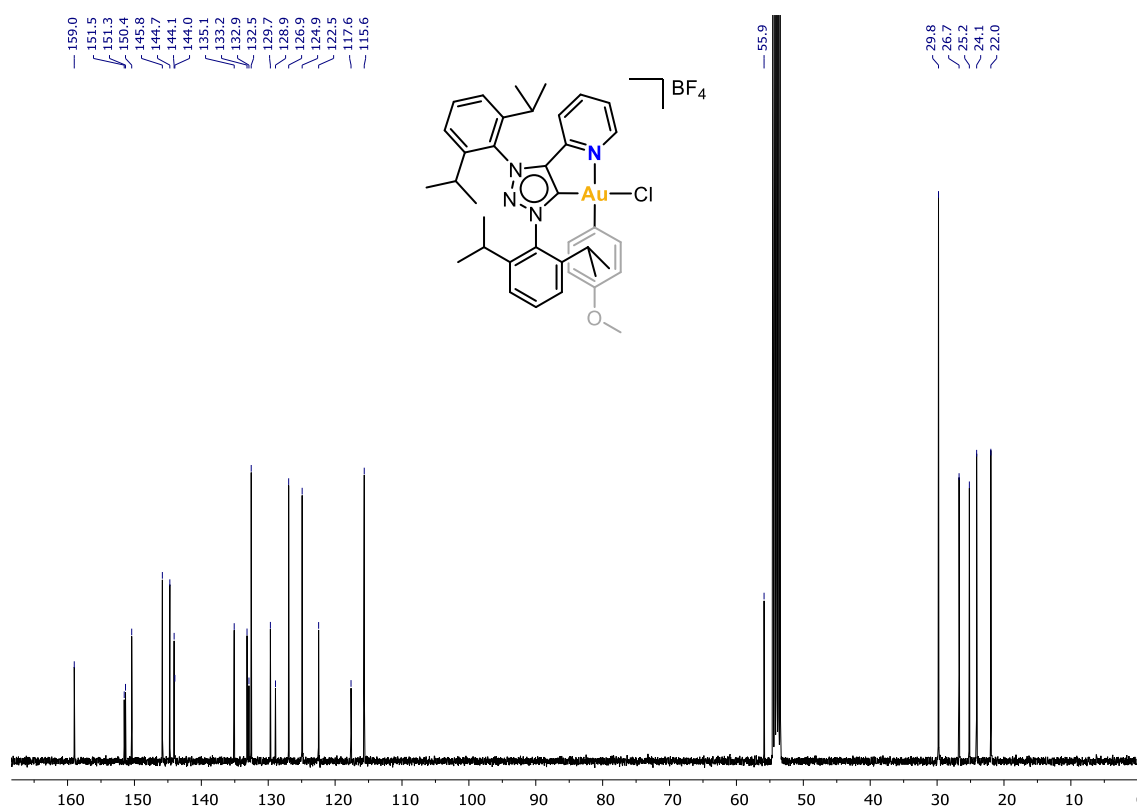


Figure S58. ^{13}C NMR (101MHz, 298K) of *cis-7a-Cl* in CD_2Cl_2 .

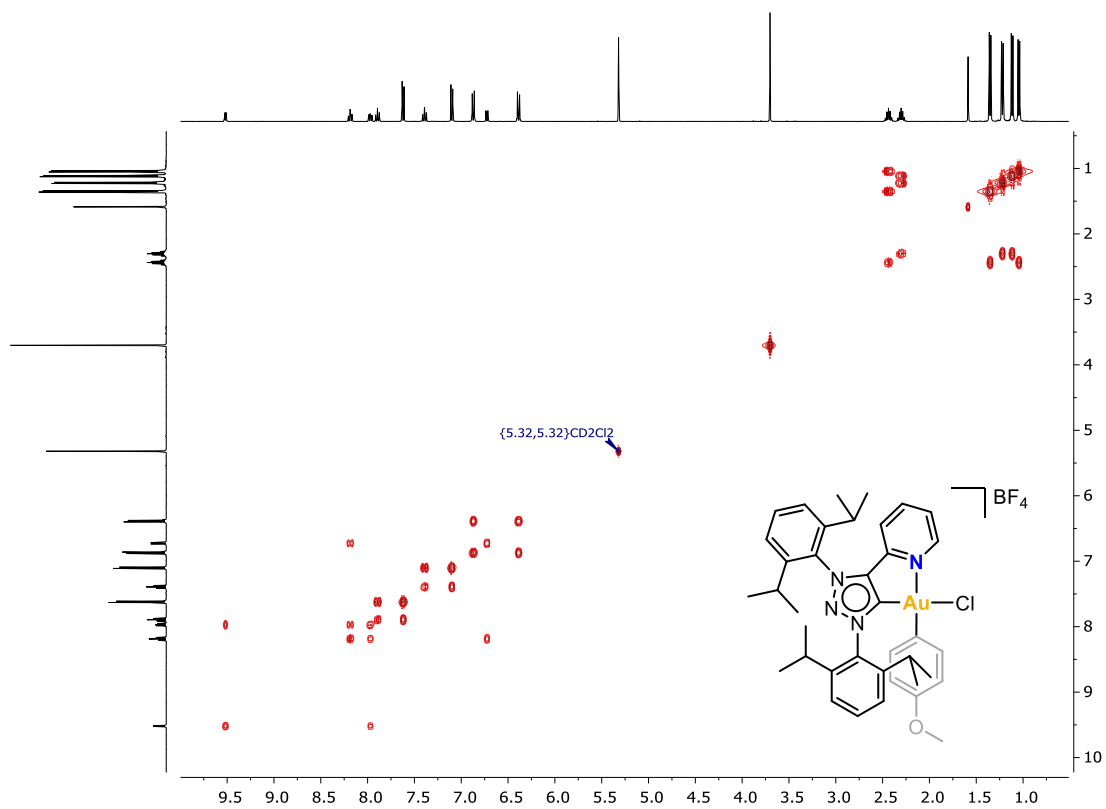


Figure S59. ^1H , ^1H -COSY NMR (400MHz, 298K) of *cis*-7a-Cl in CD_2Cl_2 .

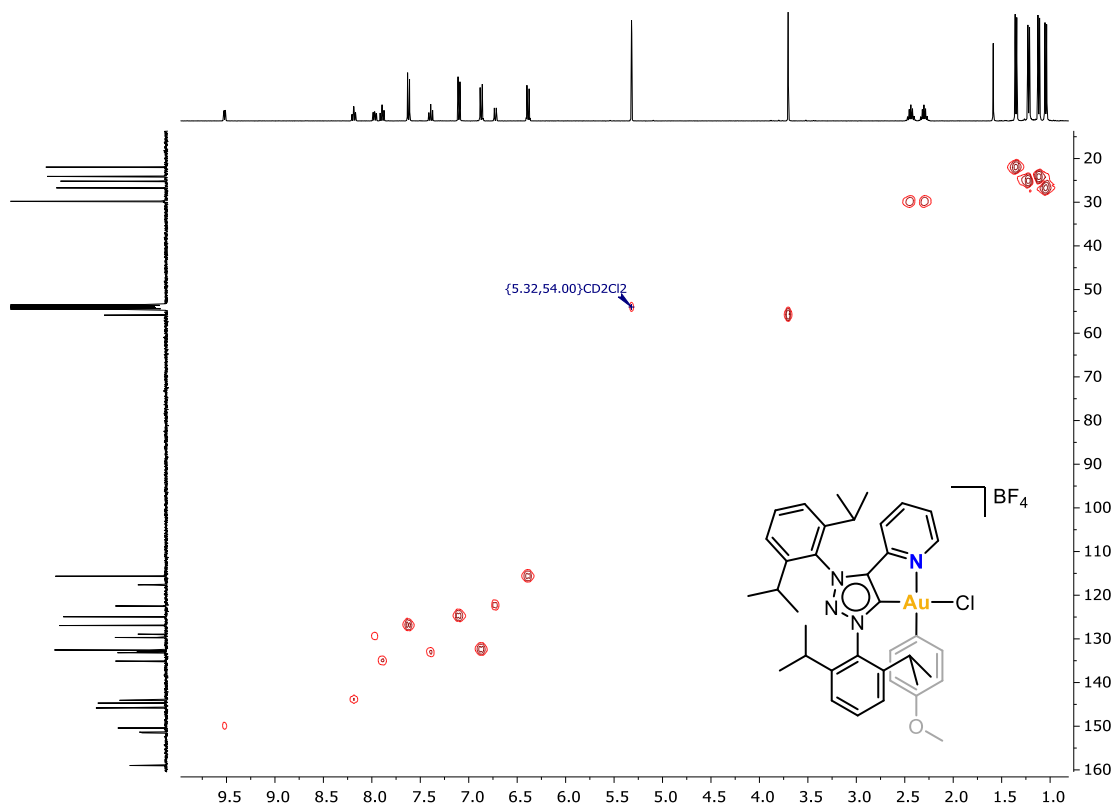


Figure S60. ^1H , ^{13}C -HSQC NMR (400MHz, 298K) of *cis*-7a-Cl in CD_2Cl_2 .

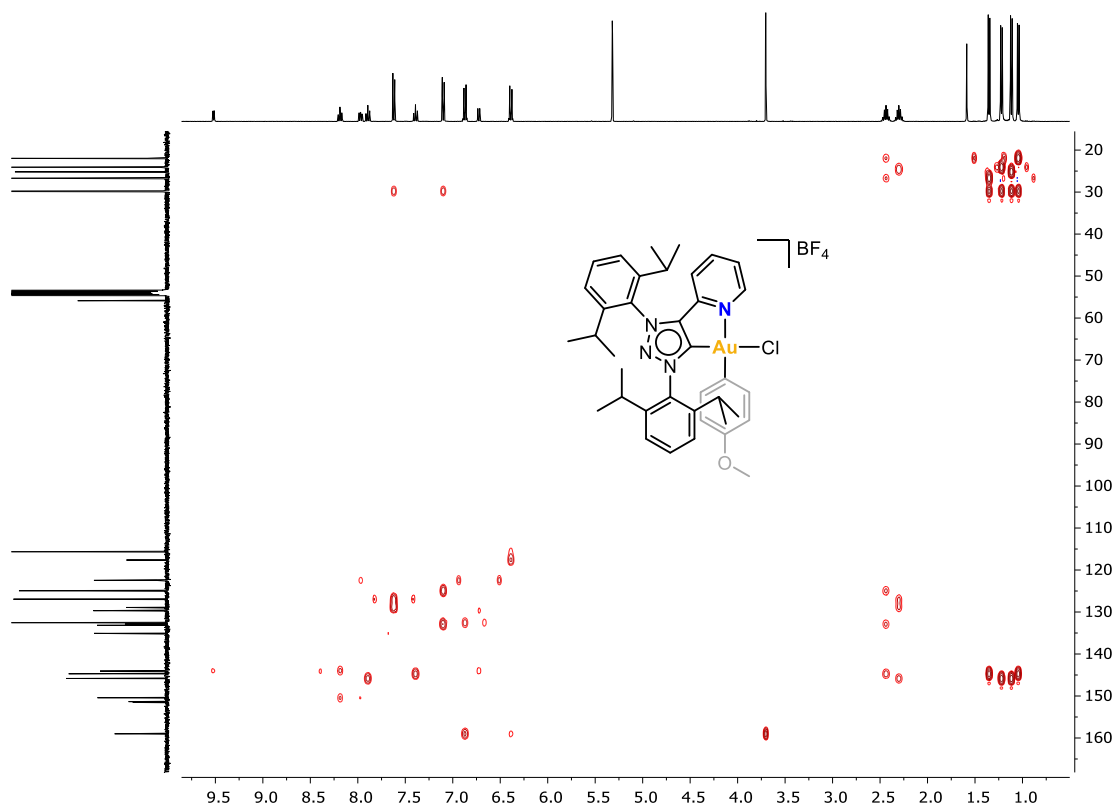


Figure S61. ^1H , ^{13}C -HMBC NMR (400MHz, 298K) of *cis*-7a-Cl in CD_2Cl_2 .

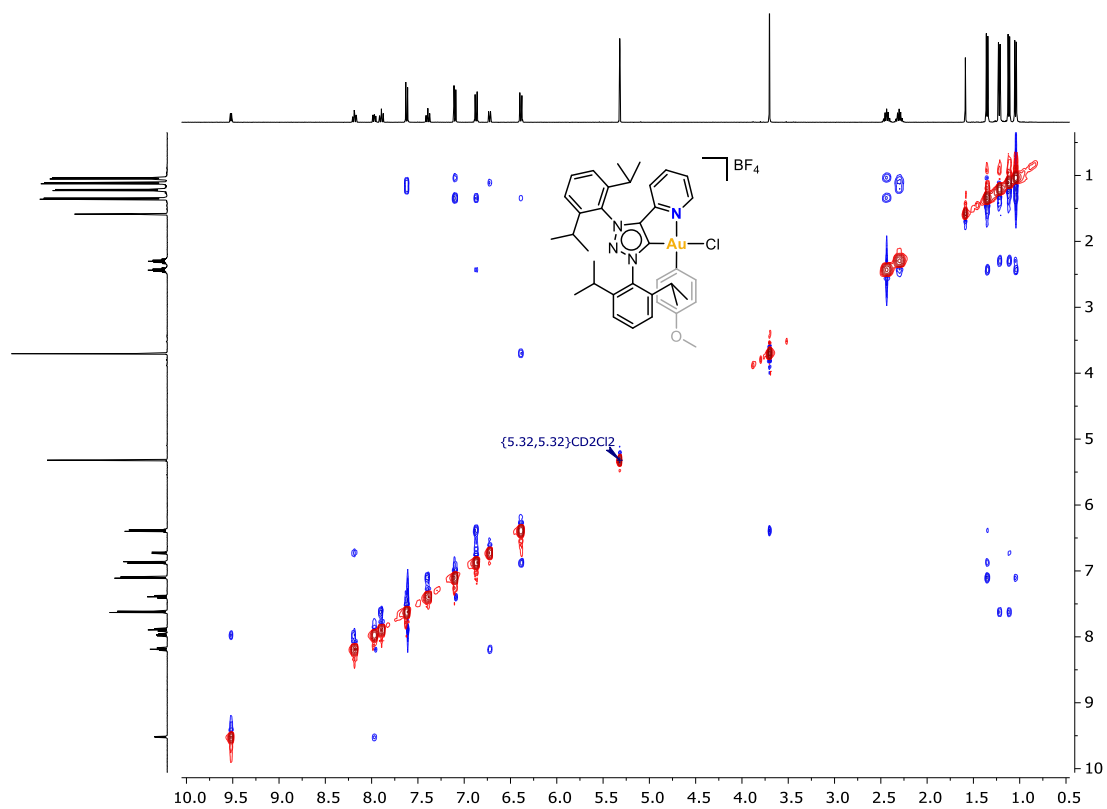


Figure S62. ^1H , ^1H -NOESY NMR (400MHz, 248K) of *cis*-7a-Cl in CD_2Cl_2 .

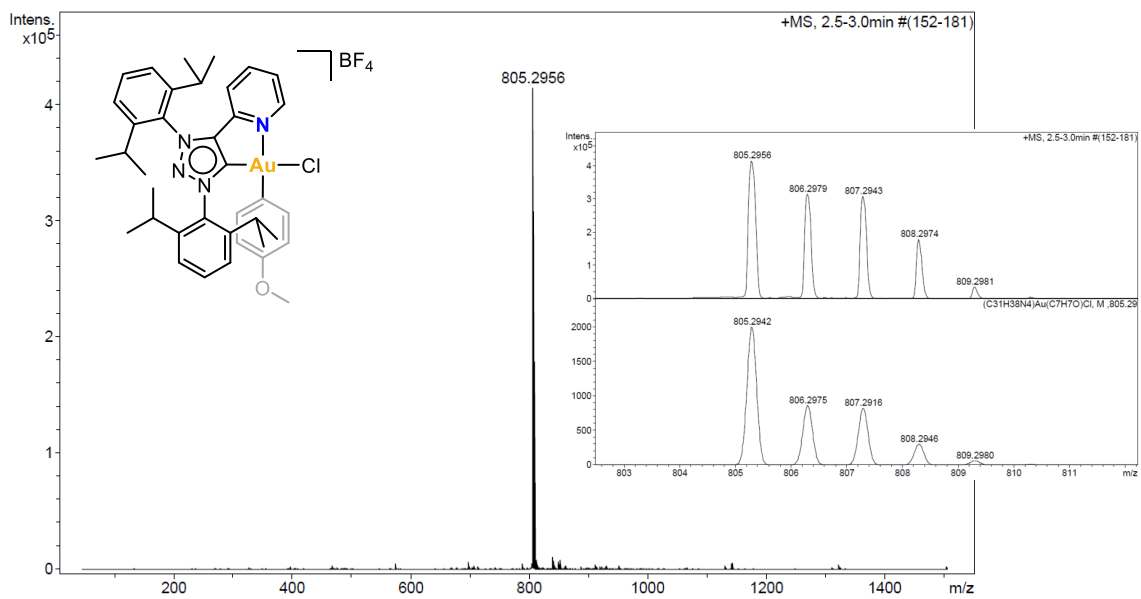
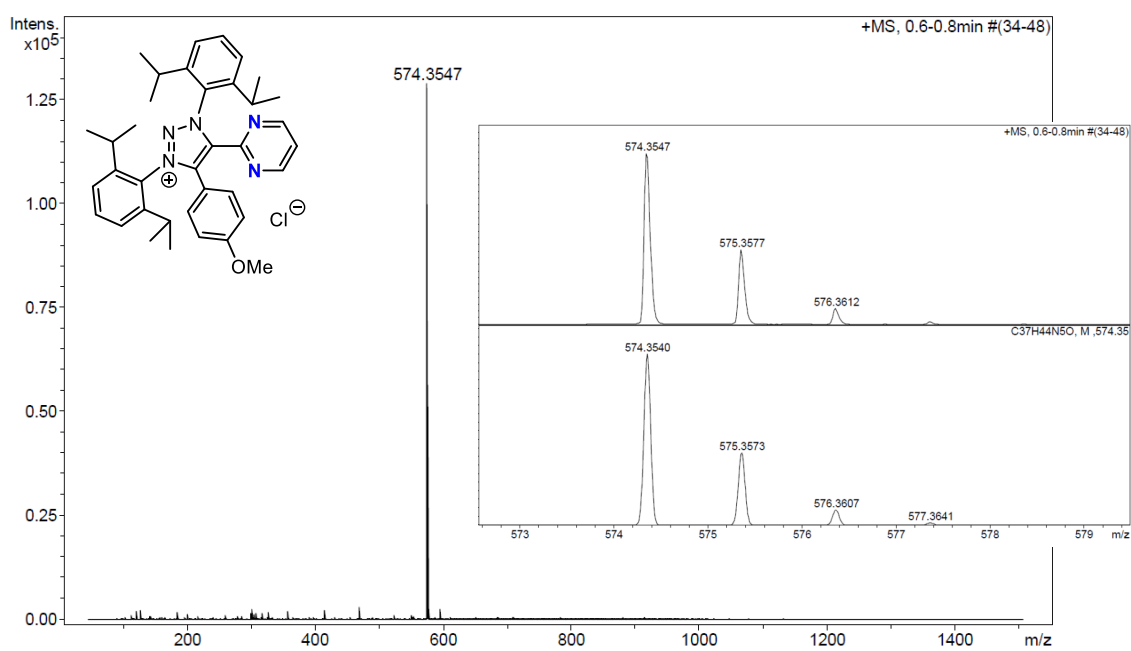
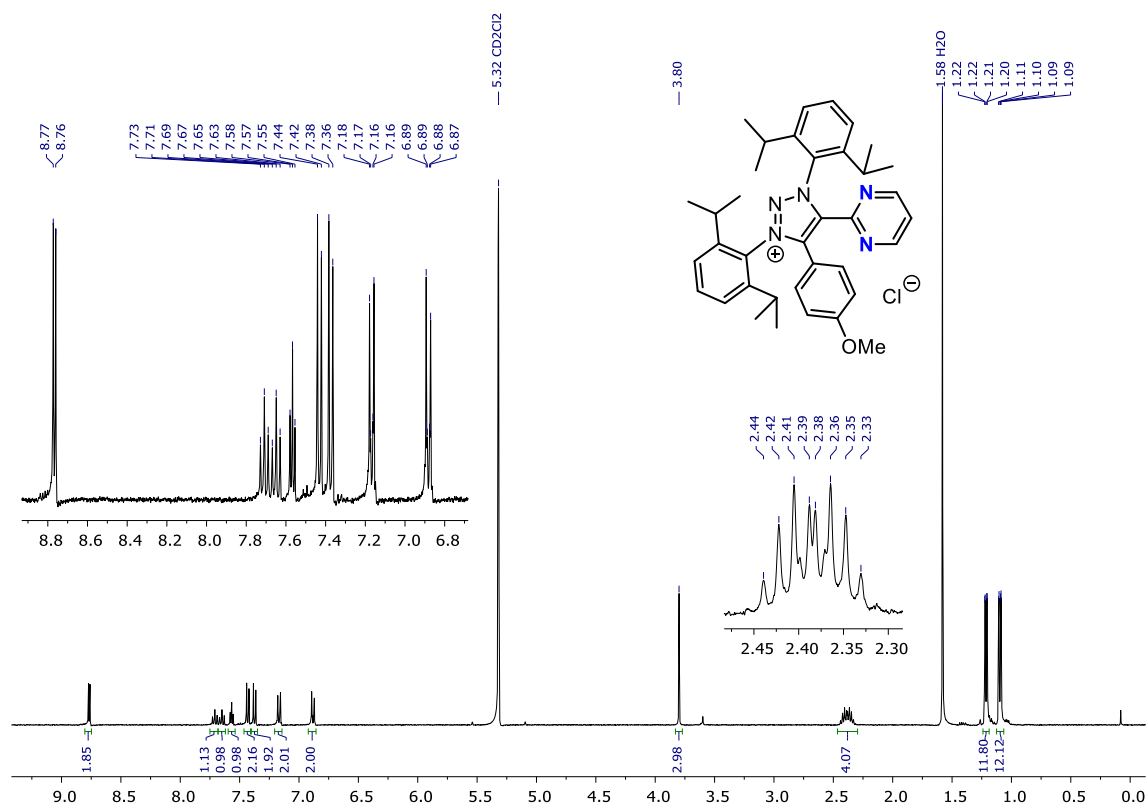


Figure S63. HRMS-ESI(+) of *cis*-7a-Cl.

8.12 NMR and HRMS-ESI Spectra of compound 8b-OMe



8.13 NMR and HRMS-ESI Spectra of compound 8a-Me

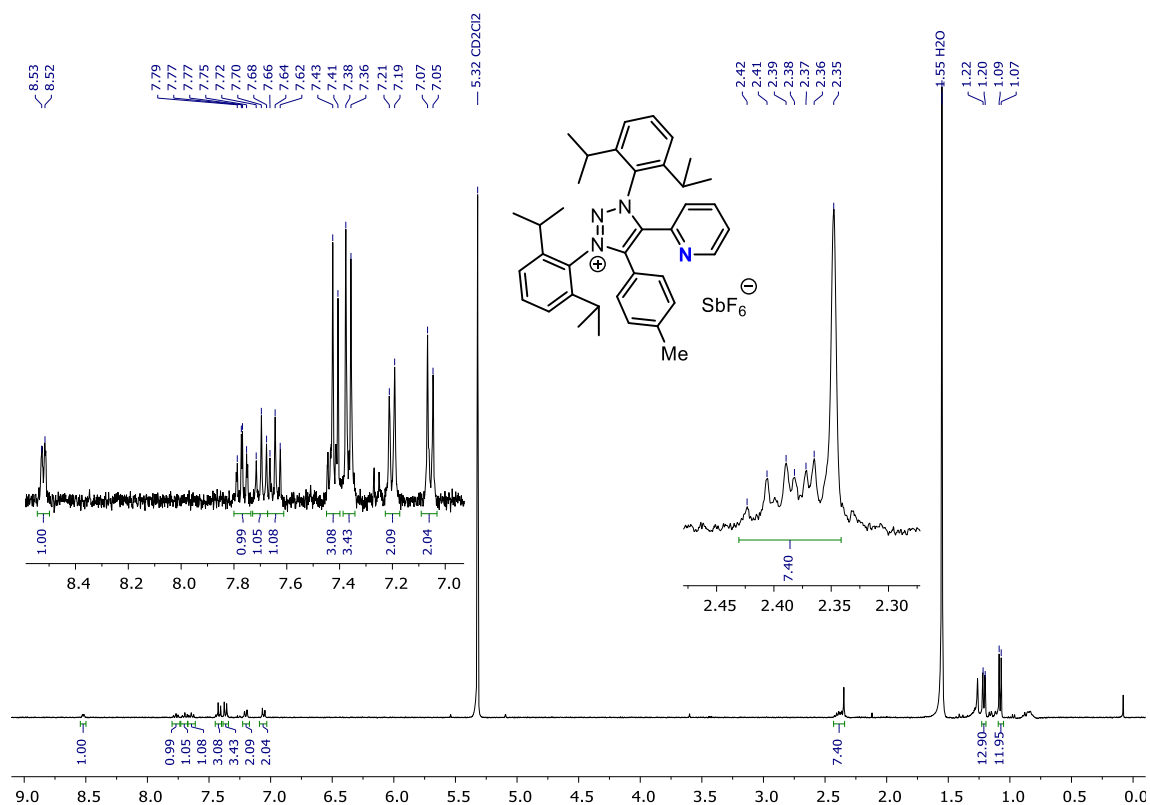


Figure S66. ¹H NMR (400MHz, 298K) of 8a-Me in CD₂Cl₂.

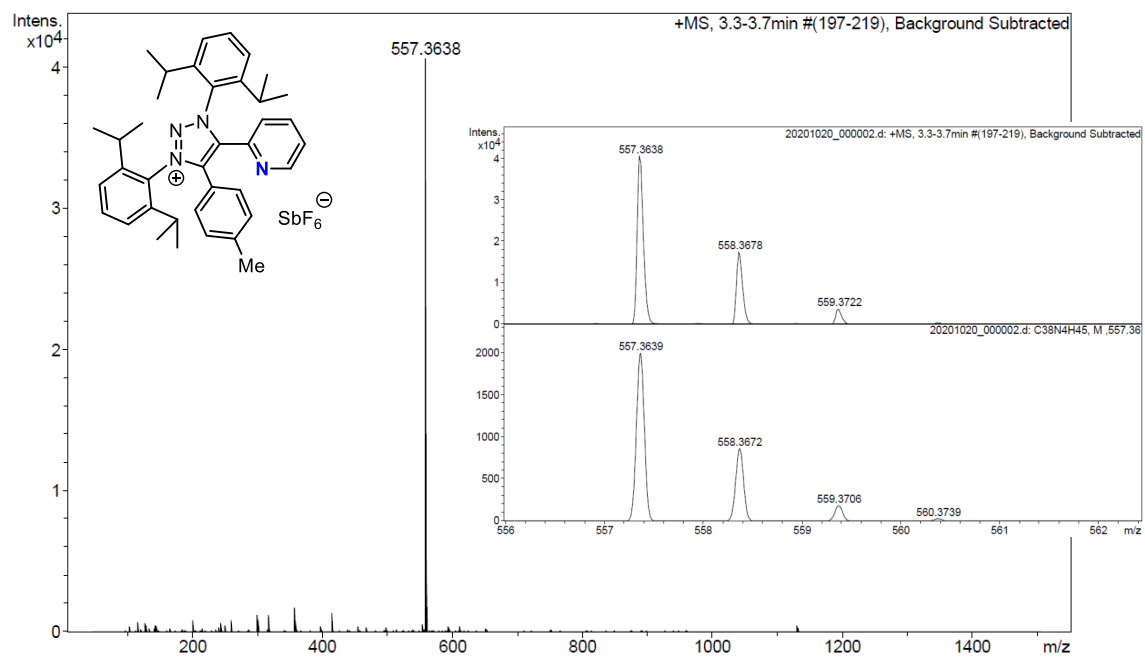
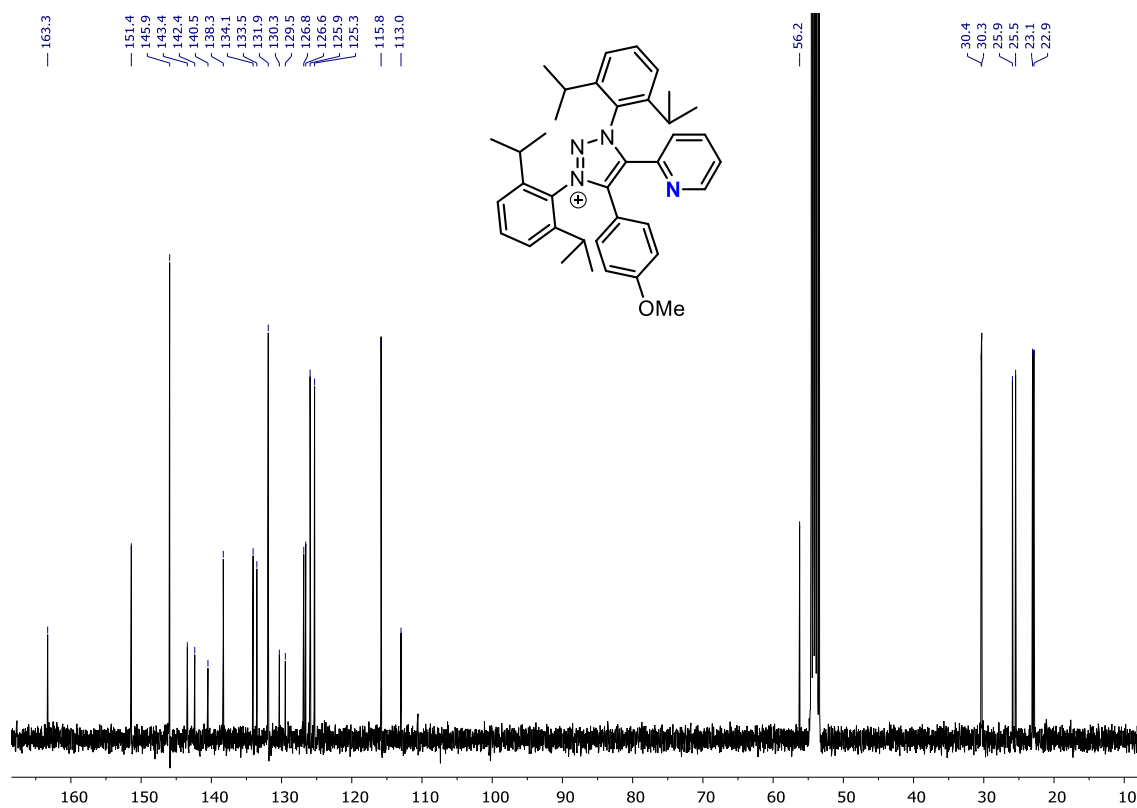
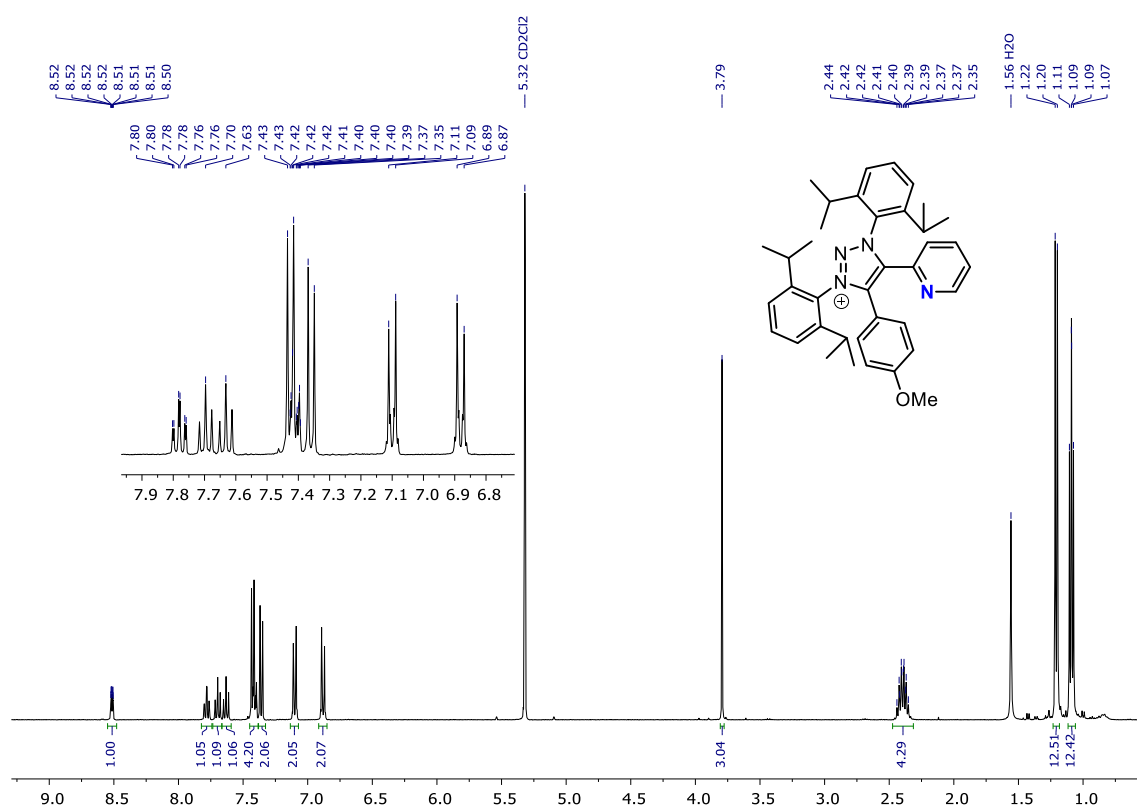


Figure S67. HRMS-ESI(+) of 8a-Me.

8.14 NMR and HRMS-ESI Spectra of compound 8a-OMe



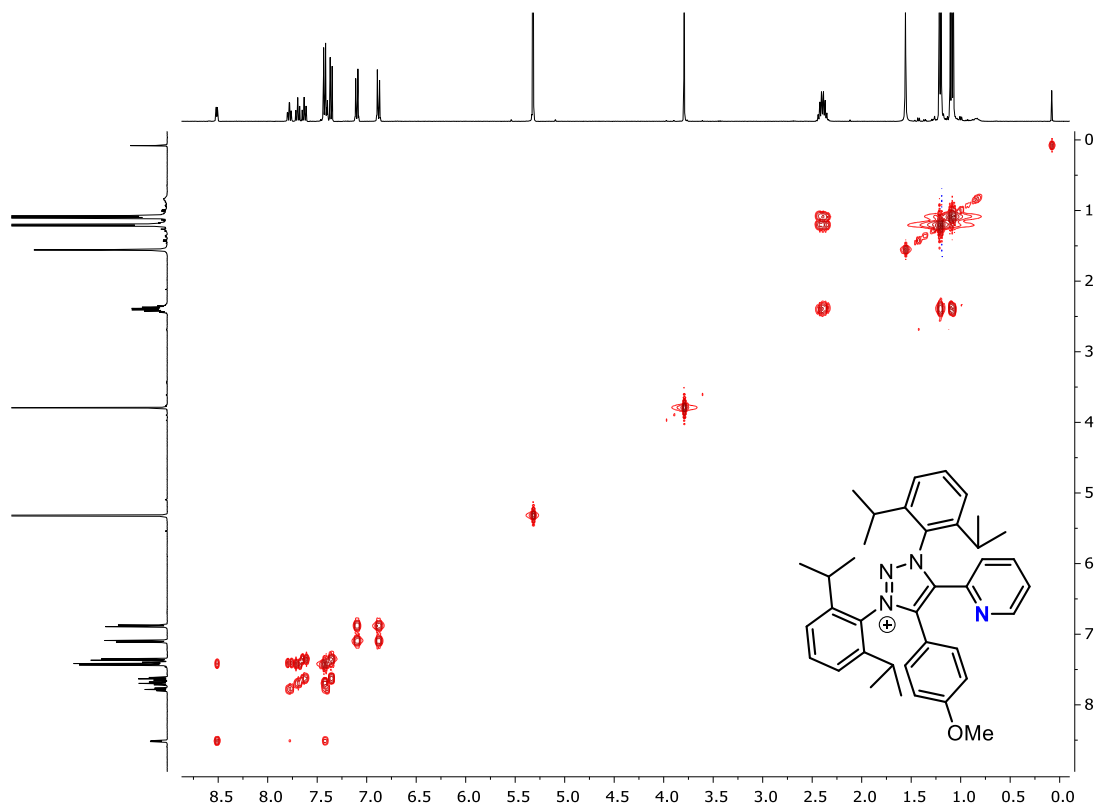


Figure S70. ^1H , ^1H -COSY NMR (400MHz, 298K) of **8a-OMe** in CD_2Cl_2 .

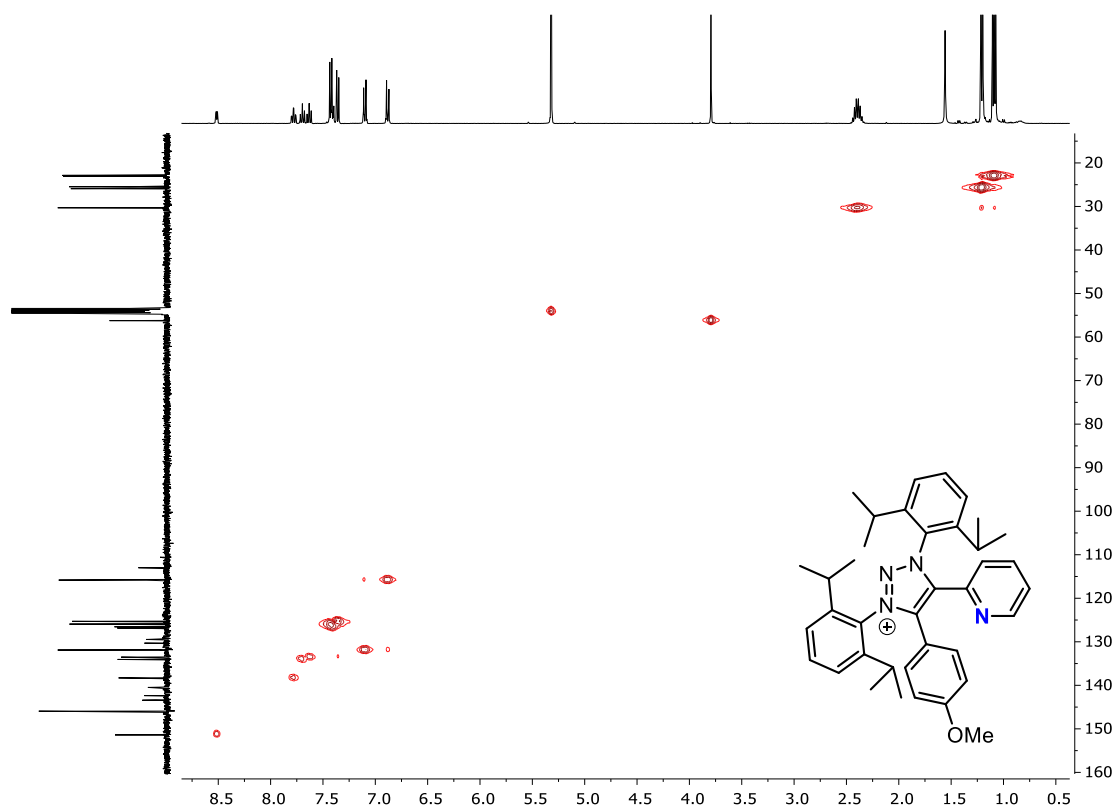


Figure S71. ^1H , ^{13}C -HSQC NMR (400MHz, 298K) of **8a-OMe** in CD_2Cl_2 .

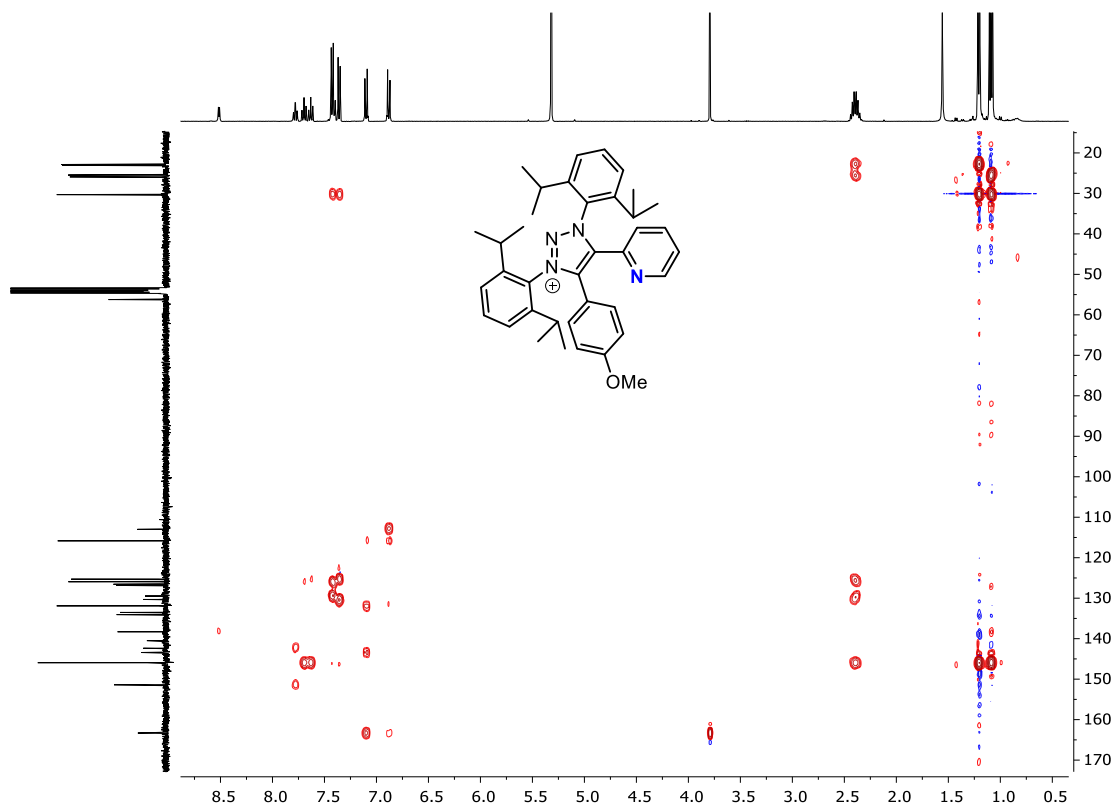


Figure S72. ^1H , ^{13}C -HMBC NMR (400MHz, 298K) of **8a-OMe** in CD_2Cl_2 .

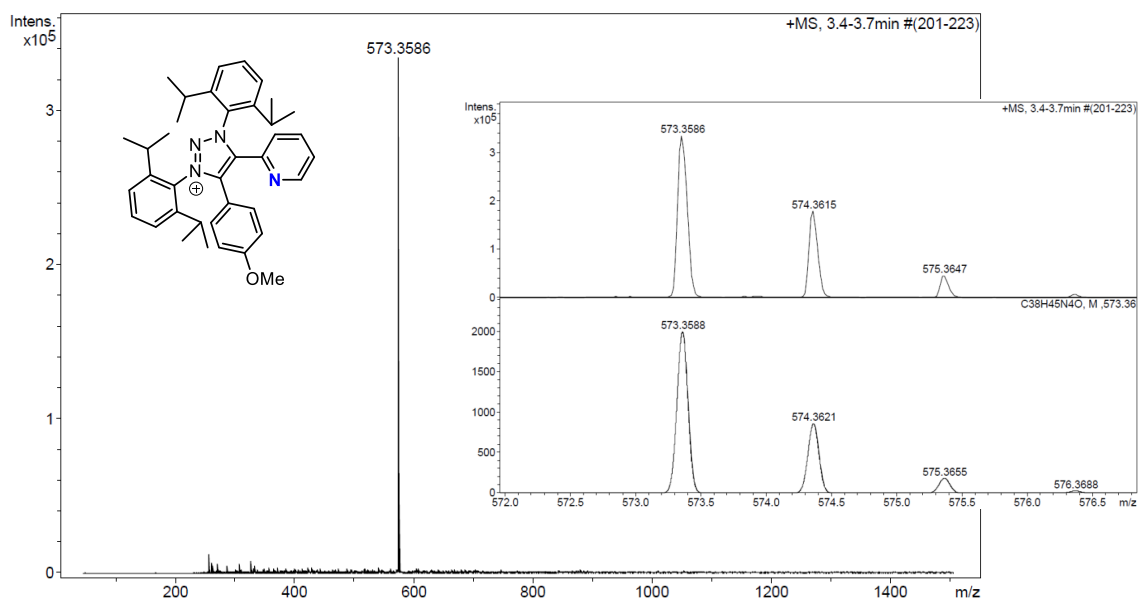


Figure S73. HRMS-ESI(+) of **8a-OMe**.

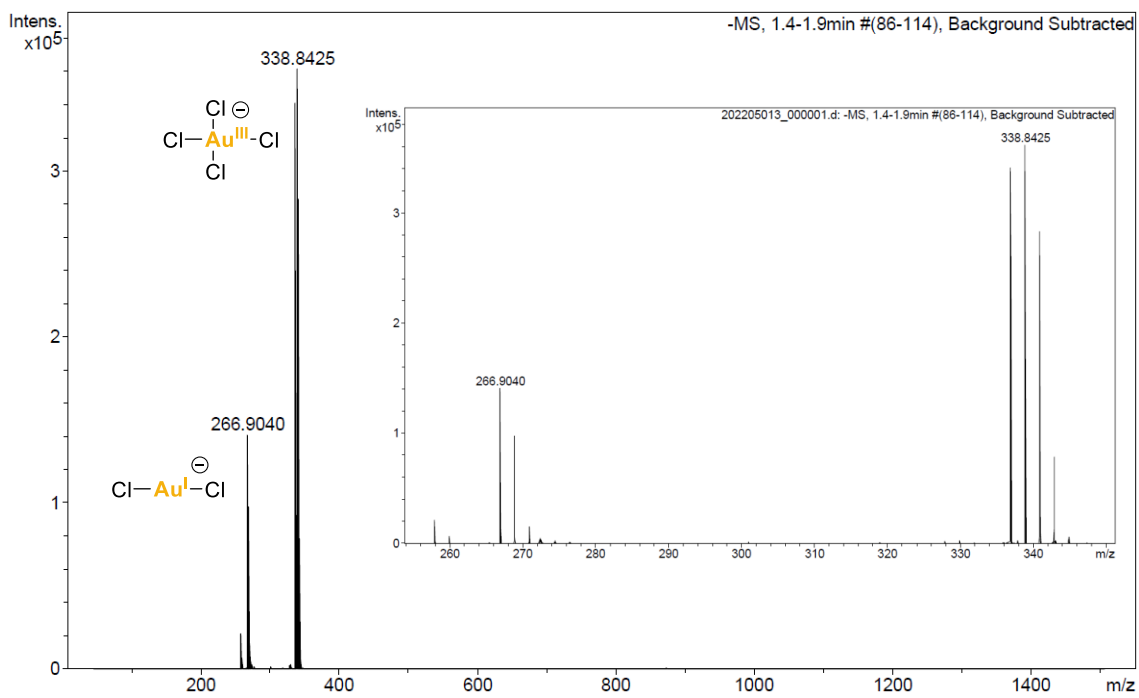


Figure S74. HRMS-ESI(-) of **8a-OMe**.

8.15 NMR Spectra of compound 10

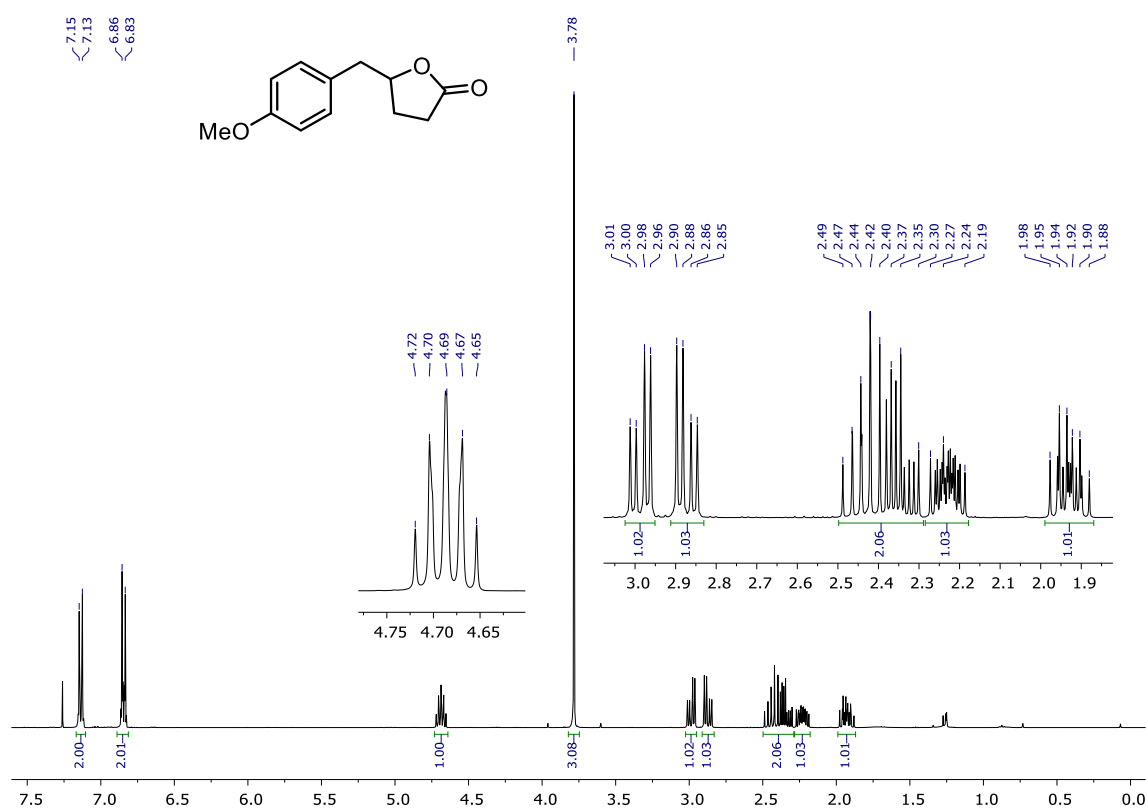


Figure S75. ¹H NMR (400MHz, 298K) of 10 in CDCl₃.

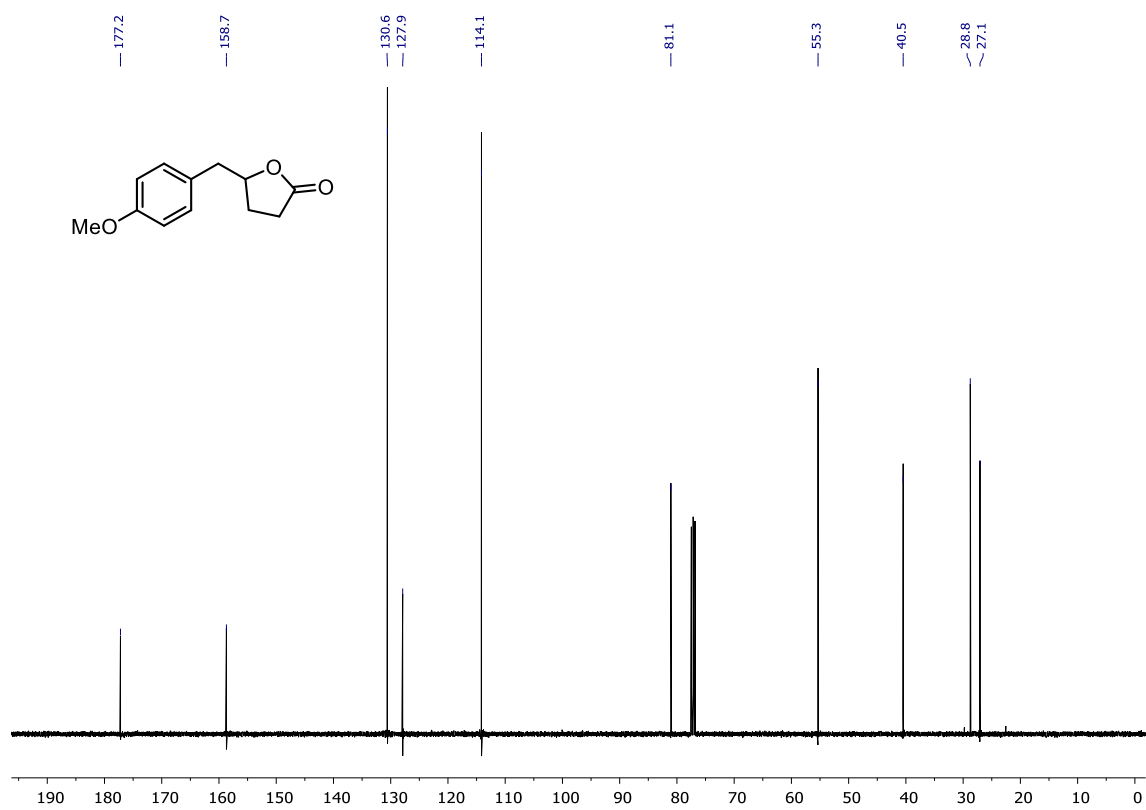


Figure S76. ¹³C NMR (101MHz, 298K) of 10 in CDCl₃.

8.16 NMR and HRMS-ESI Spectra of compound 15

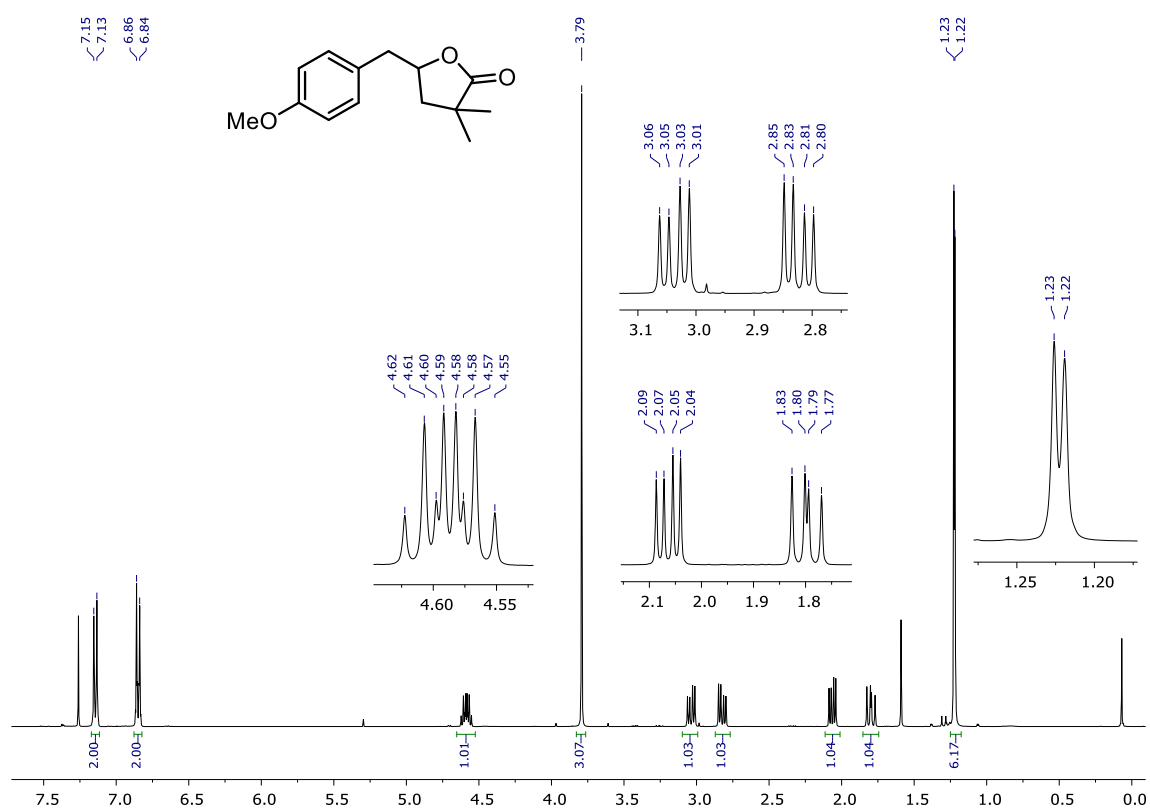


Figure S77. $^1\text{H NMR}$ (400MHz, 298K) of 15 in CDCl_3 .

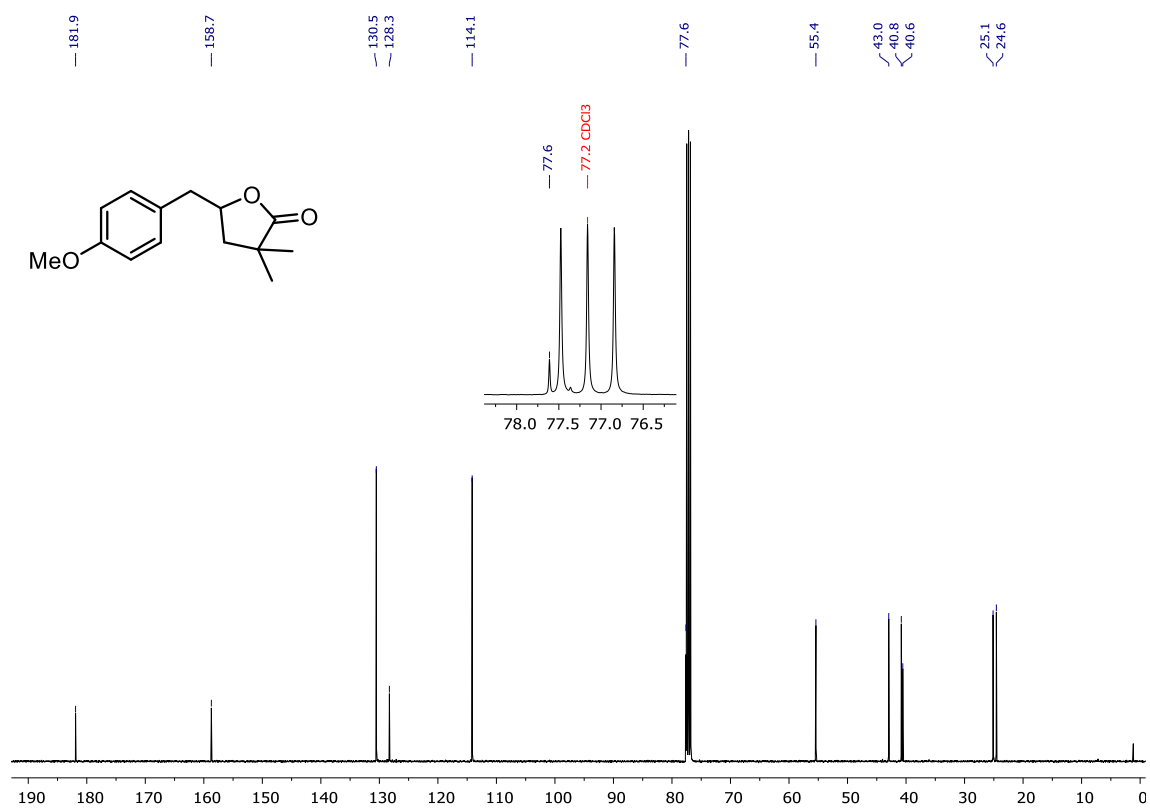


Figure S78. $^{13}\text{C NMR}$ (101MHz, 298K) of 15 in CDCl_3 .

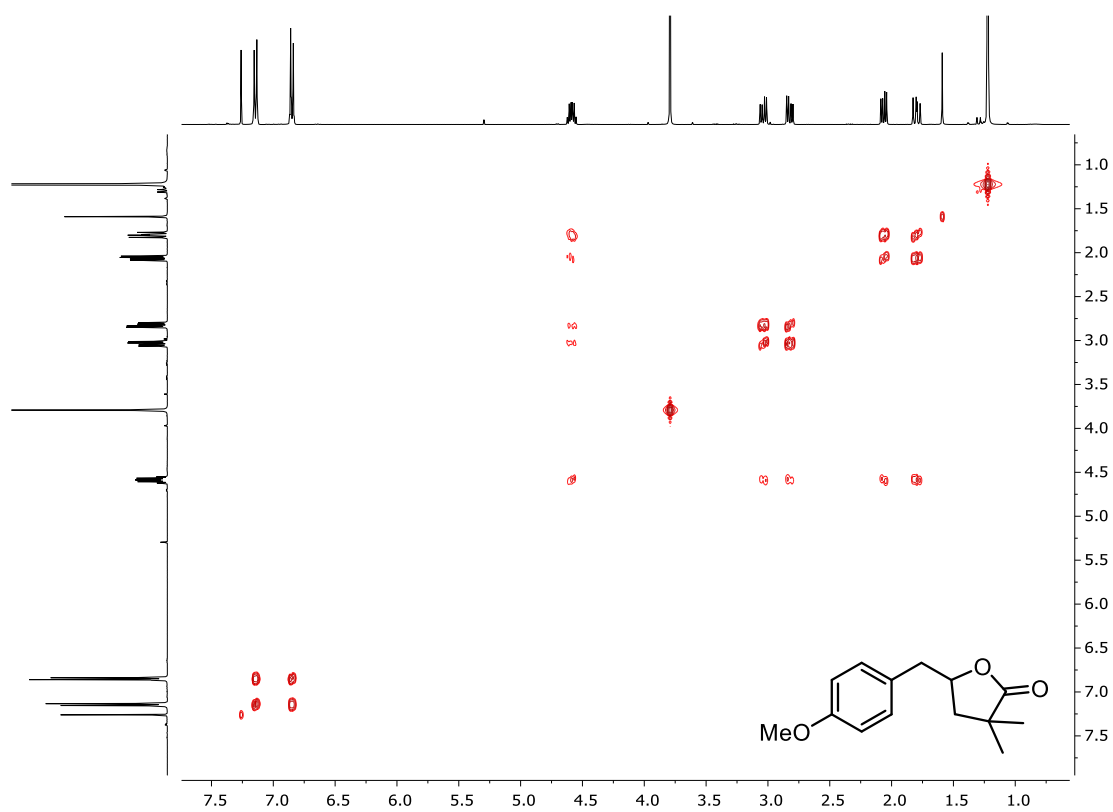


Figure S79. ^1H , ^1H -COSY NMR (400MHz, 298K) of **15** in CDCl_3 .

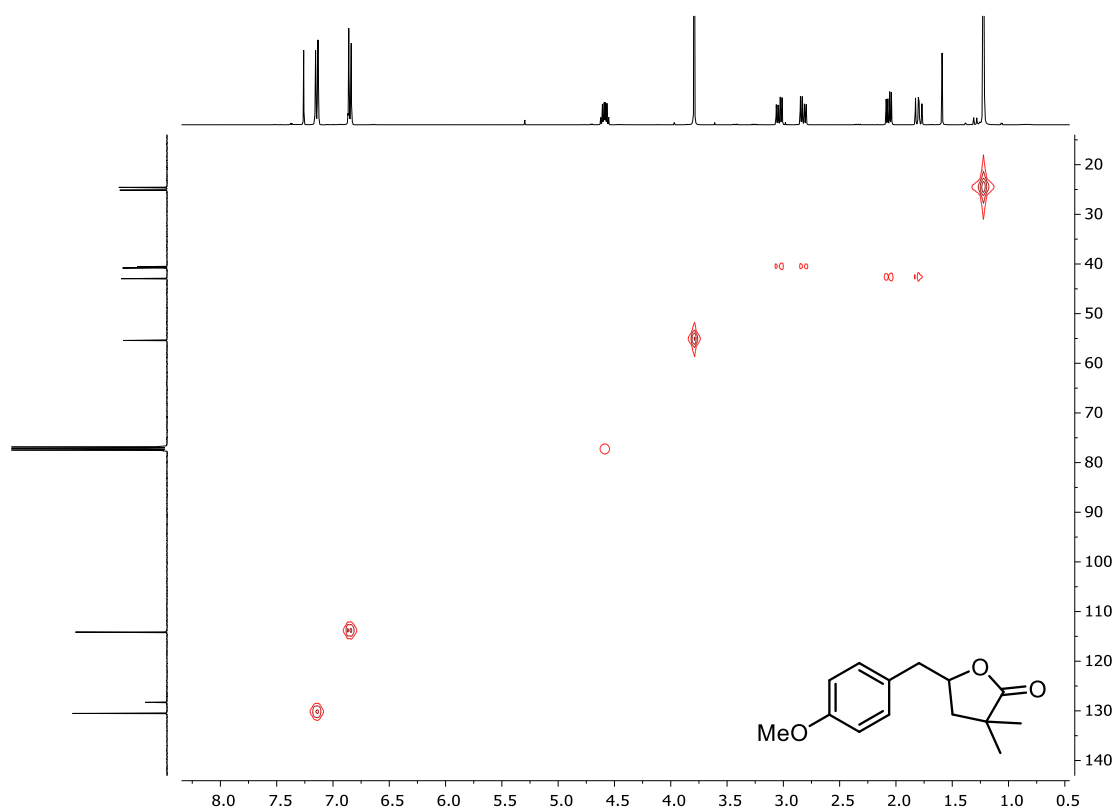


Figure S80. ^1H , ^{13}C -HSQC NMR (400MHz, 298K) of **15** in CDCl_3 .

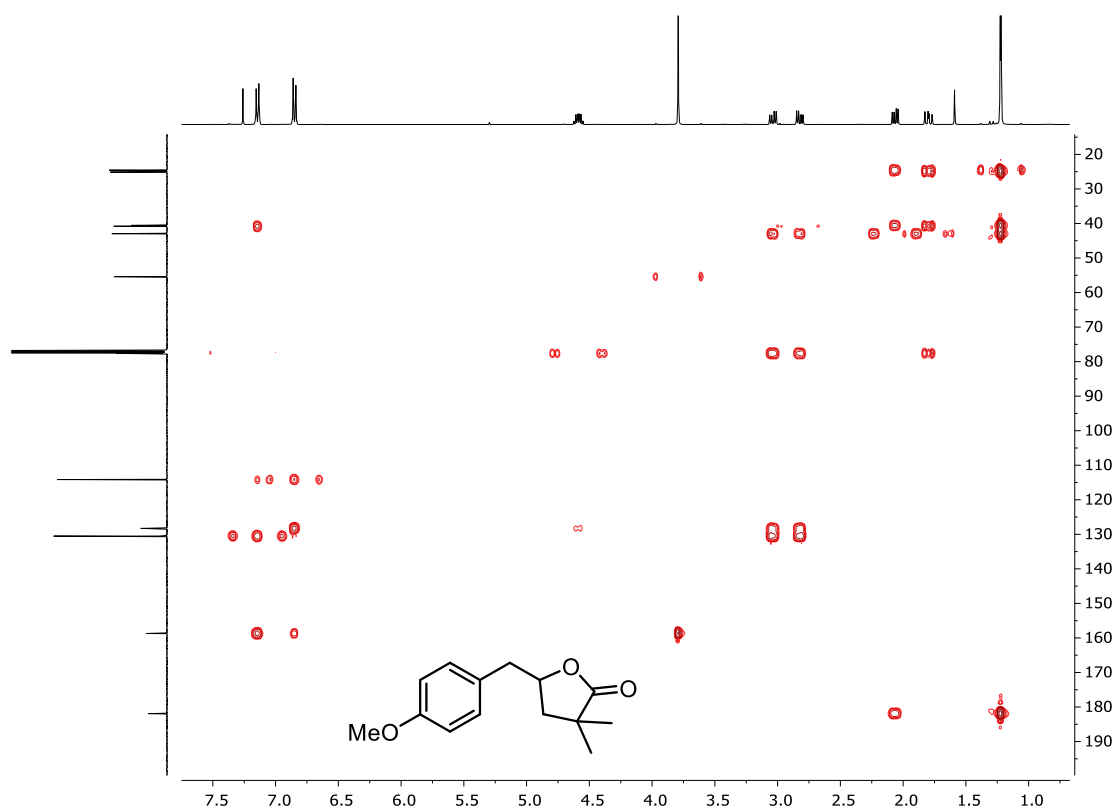


Figure S81. ^1H , ^{13}C -HMBC NMR (400MHz, 298K) of **15** in CDCl_3 .

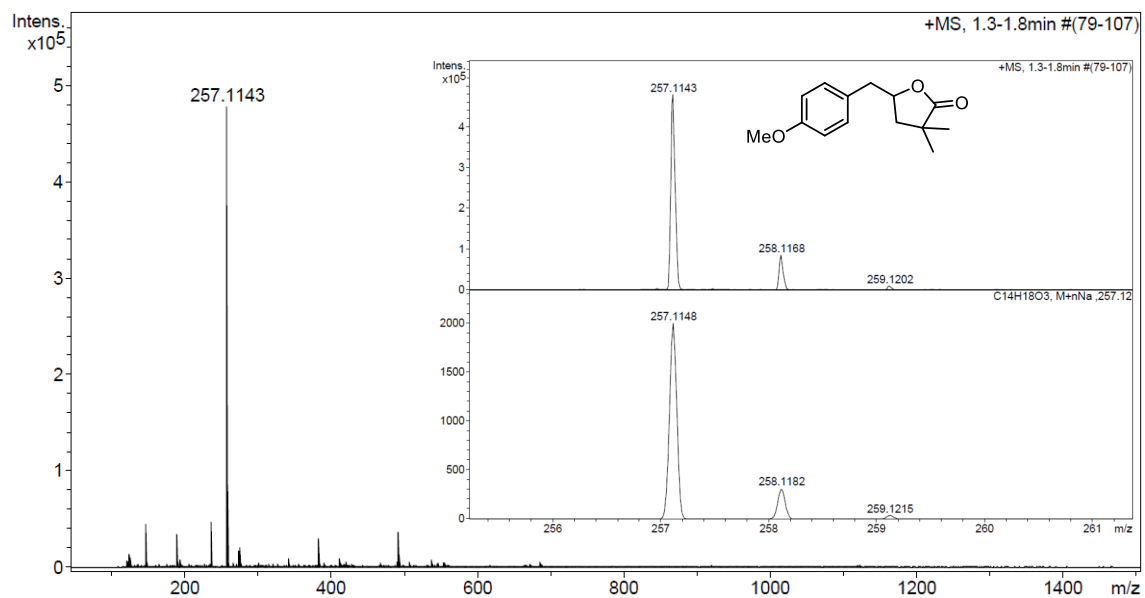


Figure S82. HRMS-ESI(+) of **15**.

8.17 NMR and HRMS-ESI Spectra of compound 16

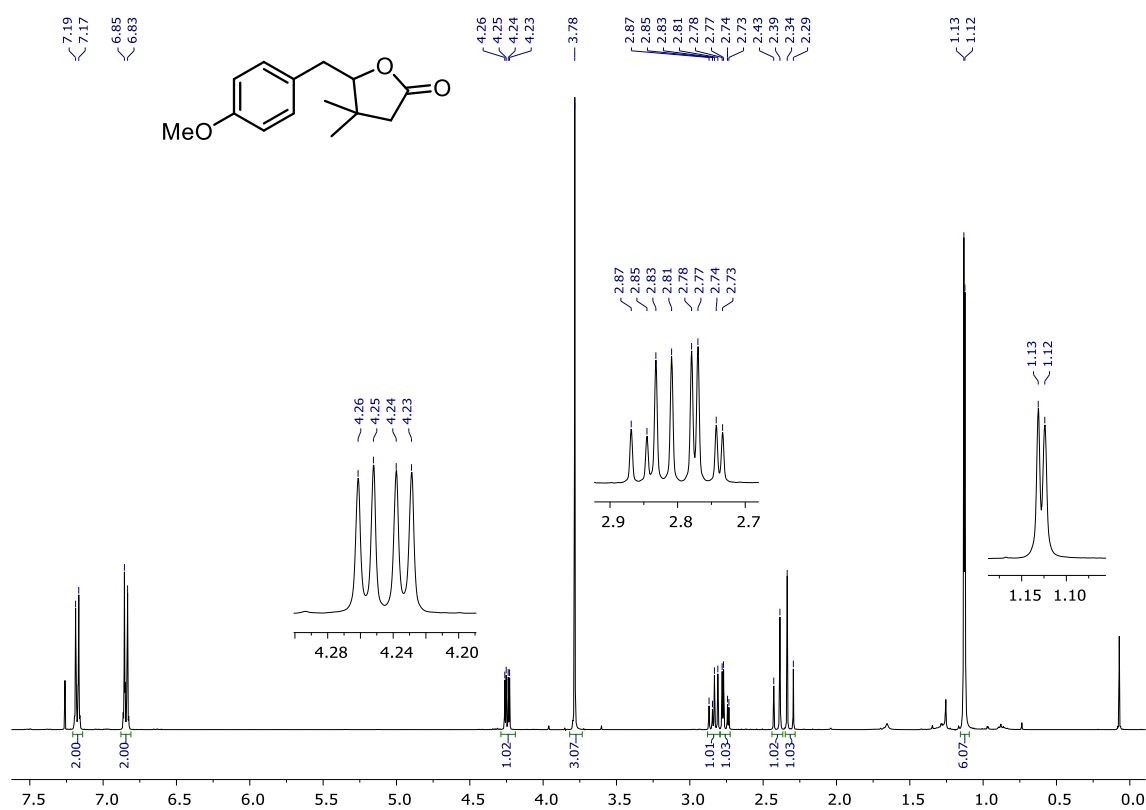


Figure S83. ¹H NMR (400MHz, 298K) of 16 in CDCl₃.

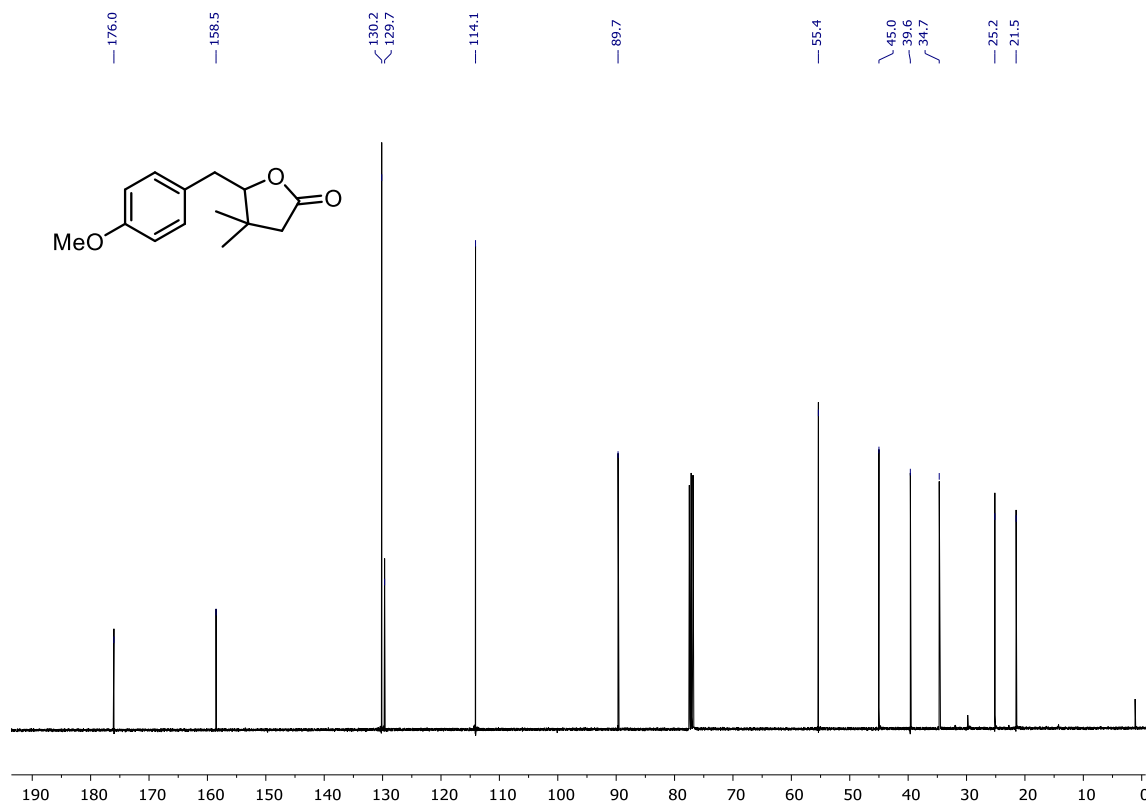


Figure S84. ¹³C NMR (101MHz, 298K) of 16 in CDCl₃.

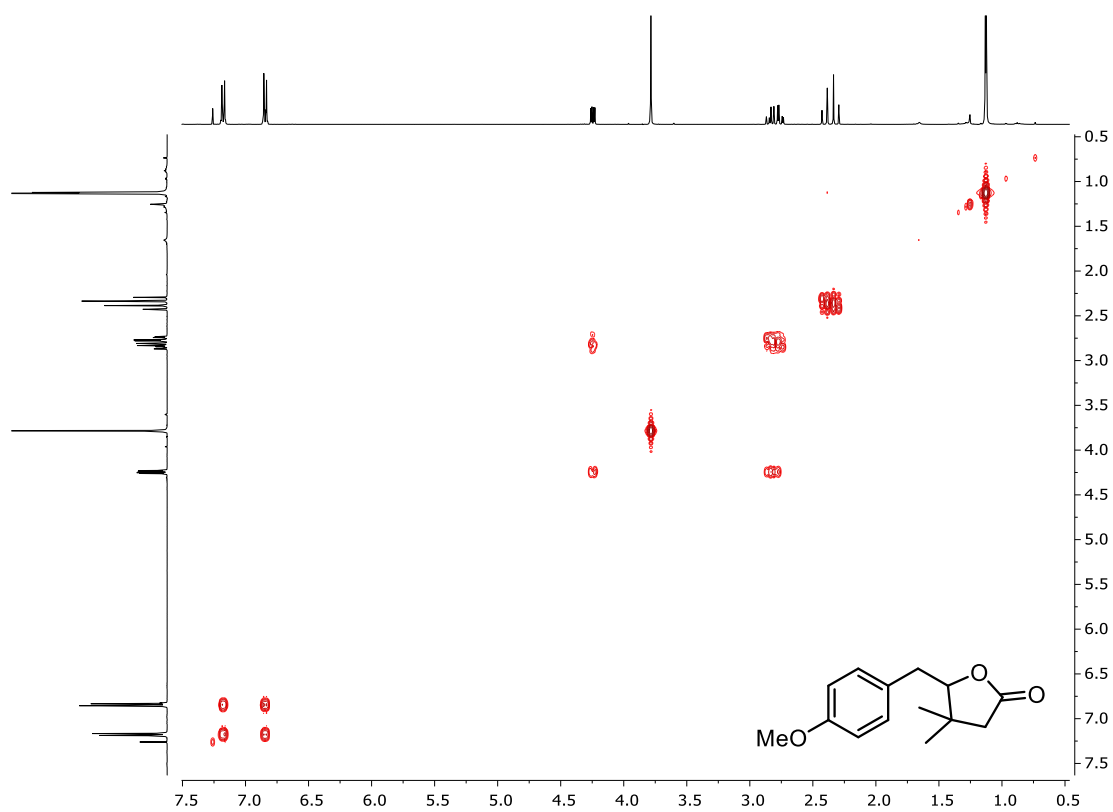


Figure S85. ^1H , ^1H -COSY NMR (400MHz, 298K) of **16** in CDCl_3 .

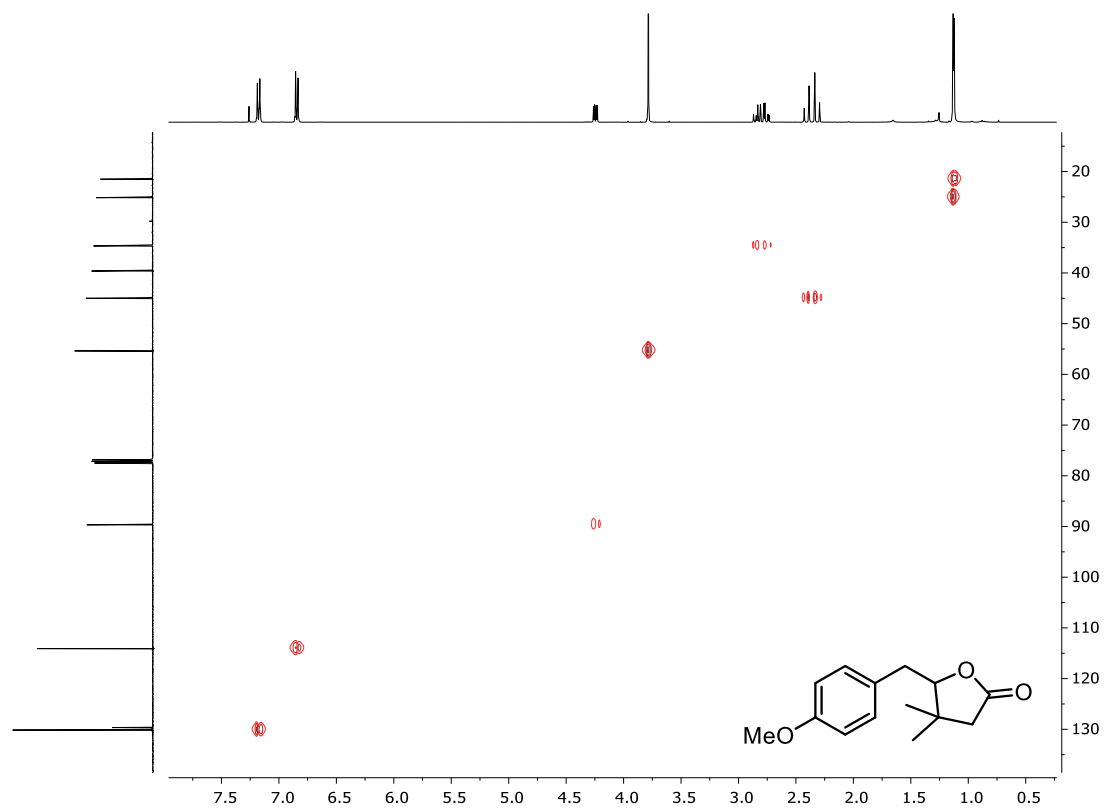


Figure S86. ^1H , ^{13}C -HSQC NMR (400MHz, 298K) of **16** in CDCl_3 .

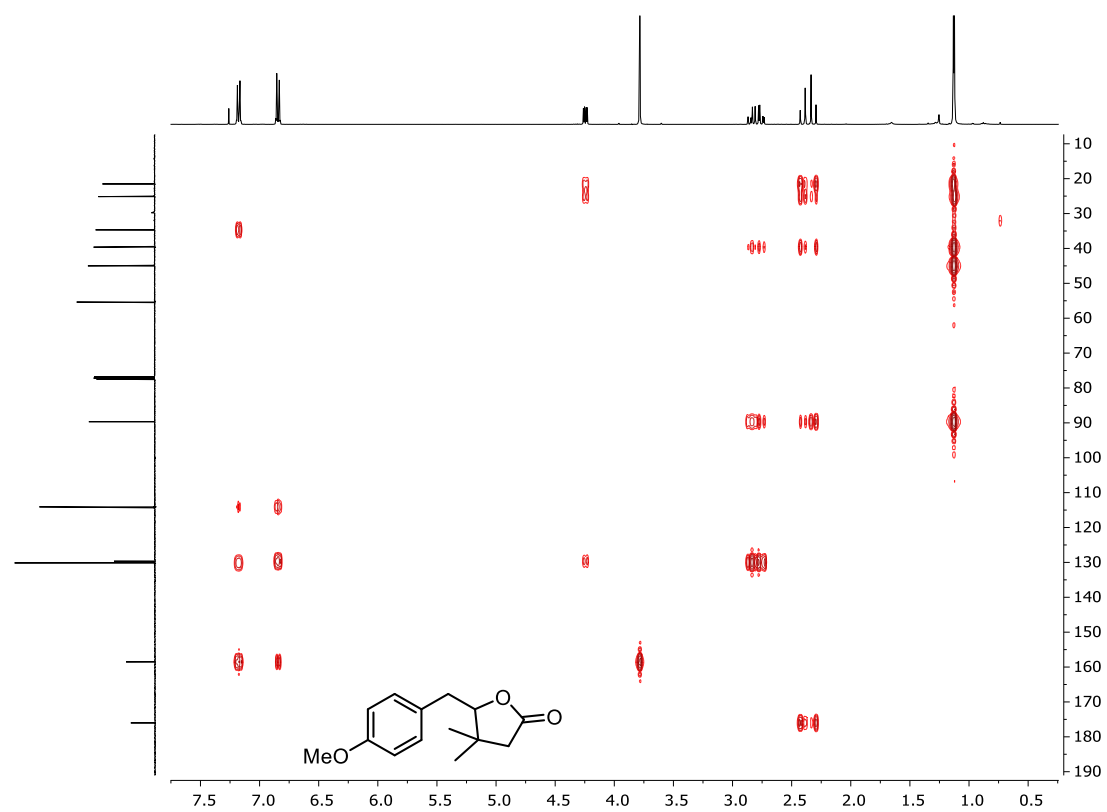


Figure S87. ^1H , ^{13}C -HMBC NMR (400MHz, 298K) of **16** in CDCl_3 .

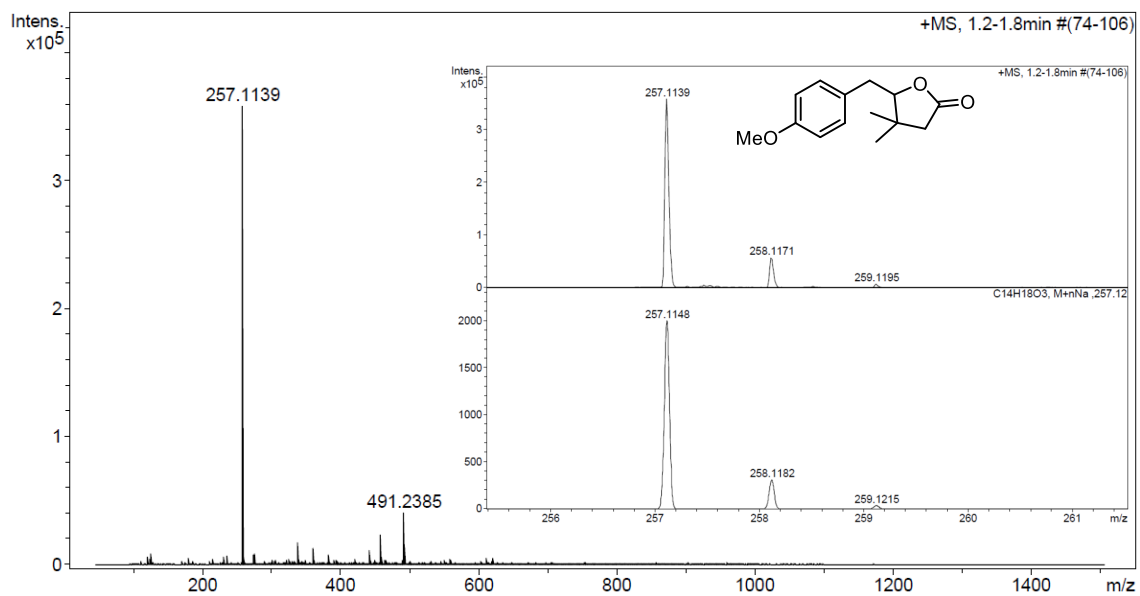


Figure S88. HRMS-ESI(+) of **16**.

9. X-Ray structures and crystallographic data

9.1 Complex 2a

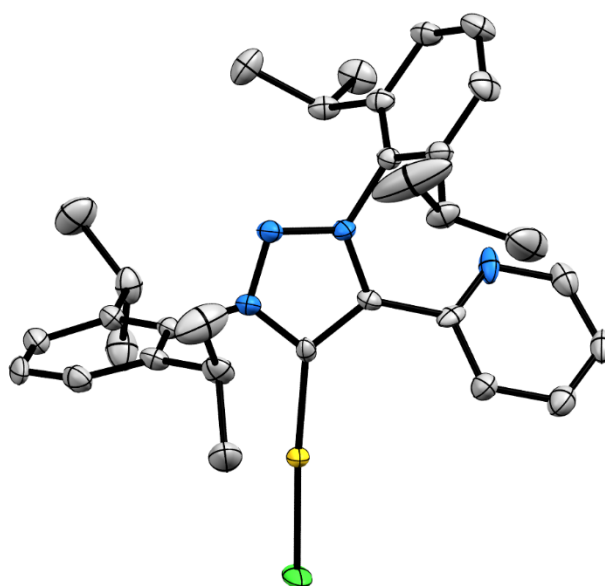


Figure S89. Crystal structure of **2a** (CCDC 2163609). Ellipsoids set at 50% probability; H atoms removed for clarity.

Table S7. Crystallographic parameters for **2a**.

Chemical formula	C ₃₁ H ₃₈ AuClN ₄	
Formula weight	699.07 g/mol	
Temperature	100(2) K	
Wavelength	0.71073 Å	
Crystal size	0.050 x 0.100 x 0.150 mm	
Crystal system	Monoclinic	
Space group	P 1 21/n 1	
Unit cell dimensions	a = 9.9684(5) Å	α = 90°
	b = 23.6287(10) Å	β = 101.309(2)°
	c = 12.9108(6) Å	γ = 90°
Volume	2982.0(2) Å ³	
Density (calculated)	1.557 g/cm ³	
Absorption coefficient	5.049 mm ⁻¹	
Final R indices	5846 data; I > 2σ(I)	R1 = 0.0473, wR2 = 0.1253
	All data	R1 = 0.0594, wR2 = 0.1360

A colorless prism-like specimen of C₃₁H₃₈AuClN₄, approximate dimensions 0.050 mm x 0.100 mm x 0.150 mm, was used for the X-ray crystallographic analysis. The X-ray

intensity data were measured on a D8 QUEST ECO three-circle diffractometer system equipped with a Ceramic x-ray tube (Mo K α , $\lambda = 0.71073 \text{ \AA}$) and a doubly curved silicon crystal Bruker Triumph monochromator. A total of 907 frames were collected. The total exposure time was 2.52 hours. The frames were integrated with the Bruker SAINT software package using a narrow-frame algorithm. The integration of the data using a monoclinic unit cell yielded a total of 116918 reflections to a maximum θ angle of 27.62° (0.77 \AA resolution), of which 6893 were independent (average redundancy 16.962, completeness = 99.5%, $R_{\text{int}} = 6.18\%$, $R_{\text{sig}} = 2.32\%$) and 5846 (84.81%) were greater than $2\sigma(F^2)$. The final cell constants of $a = 9.9684(5) \text{ \AA}$, $b = 23.6287(10) \text{ \AA}$, $c = 12.9108(6) \text{ \AA}$, $\beta = 101.309(2)^\circ$, volume = $2982.0(2) \text{ \AA}^3$, are based upon the refinement of the XYZ-centroids of 9612 reflections above $20 \sigma(I)$ with $5.743^\circ < 2\theta < 54.88^\circ$. Data were corrected for absorption effects using the Multi-Scan method (SADABS). The ratio of minimum to maximum apparent transmission was 0.779. The calculated minimum and maximum transmission coefficients (based on crystal size) are 0.5180 and 0.7860. The structure was solved and refined using the Bruker SHELXTL Software Package, using the space group $P 1 21/n 1$, with $Z = 4$ for the formula unit, $C_{31}H_{38}AuClN_4$. The final anisotropic full-matrix least-squares refinement on F^2 with 342 variables converged at $R1 = 4.73\%$, for the observed data and $wR2 = 13.60\%$ for all data. The goodness-of-fit was 1.088. The largest peak in the final difference electron density synthesis was $7.653 \text{ e}^-/\text{\AA}^3$ and the largest hole was $-1.434 \text{ e}^-/\text{\AA}^3$ with an RMS deviation of $0.206 \text{ e}^-/\text{\AA}^3$. On the basis of the final model, the calculated density was 1.557 g/cm^3 and $F(000)$, 1392 e^- .

9.2 Complex 2b

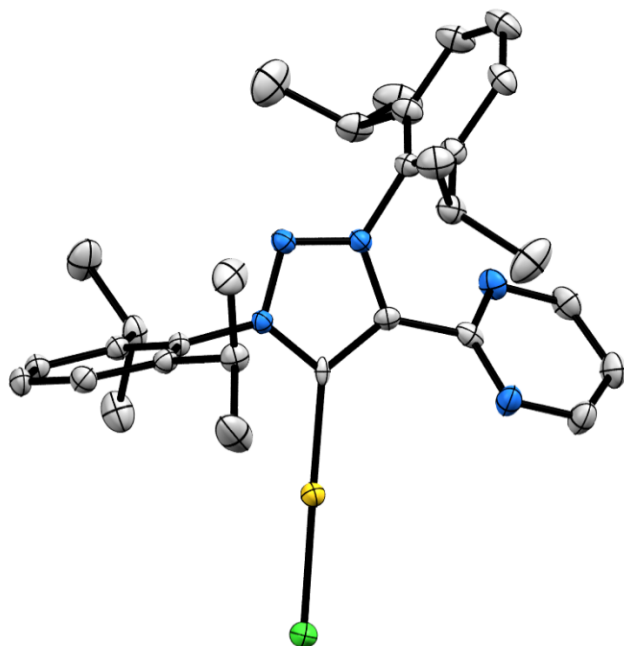


Figure S90. Crystal structure of **2b** (CCDC 2163610). Ellipsoids set at 50% probability; H atoms and solvent molecules omitted for clarity.

Table S8. Crystallographic parameters for **2b**.

Chemical formula	C ₃₂ H ₄₂ AuClN ₅ O _{0.46}	
Formula weight	736.44 g/mol	
Temperature	100(2) K	
Wavelength	0.71076 Å	
Crystal size	0.080 x 0.130 x 0.140 mm	
Crystal system	Triclinic	
Space group	P -1	
Unit cell dimensions	a = 9.426(7) Å	α = 108.17(2)°
	b = 12.481(9) Å	β = 91.20(3)°
	c = 15.289(12) Å	γ = 110.83(2)°
Volume	1580.(2) Å ³	
Density (calculated)	1.548 g/cm ³	
Absorption coefficient	4.771 mm ⁻¹	
Final R indices	8553 data; I > 2σ(I)	R1 = 0.0340, wR2 = 0.0740
	All data	R1 = 0.0482, wR2 = 0.0854

A colorless prism-like specimen of C₃₂H₄₂AuClN₅O_{0.46}, approximate dimensions 0.080 mm x 0.130 mm x 0.140 mm, was used for the X-ray crystallographic analysis. The X-ray intensity data were measured on a D8 QUEST ECO three-circle diffractometer system equipped with a Ceramic x-ray tube (Mo Kα, λ = 0.71076 Å) and a doubly curved silicon crystal Bruker Triumph monochromator. A total of 1634 frames were collected. The total exposure time was 2.27 hours. The frames were integrated with the Bruker SAINT software package using a narrow-frame algorithm. The integration of the data using a triclinic unit cell yielded a total of 172440 reflections to a maximum θ angle of 30.74° (0.70 Å resolution), of which 9738 were independent (average redundancy 17.708, completeness = 98.9%, R_{int} = 7.14%, R_{sig} = 2.66%) and 8553 (87.83%) were greater than 2σ(F²). The final cell constants of \underline{a} = 9.426(7) Å, \underline{b} = 12.481(9) Å, \underline{c} = 15.289(12) Å, α = 108.17(2)°, β = 91.20(3)°, γ = 110.83(2)°, volume = 1580.(2) Å³, are based upon the refinement of the XYZ-centroids of 9895 reflections above 20 σ(I) with 5.389° < 2θ < 59.94°. Data were corrected for absorption effects using the Multi-Scan method (SADABS). The ratio of minimum to maximum apparent transmission was 0.795. The calculated minimum and maximum transmission coefficients (based on crystal size) are 0.5929 and 0.7461. The structure was solved and refined using the Bruker SHELXTL Software Package, using the space group P -1, with Z = 2 for the formula unit, C₃₂H₄₂AuClN₅O_{0.46}. The final anisotropic full-matrix least-squares refinement on F² with 366 variables converged at R1 = 3.40%, for the observed data and wR2 = 8.54% for all data. The goodness-of-fit was 1.185. The largest peak in the final difference electron density synthesis was 4.477 e⁻/Å³ and the largest hole was -2.675 e⁻/Å³ with an RMS deviation of 0.167 e⁻/Å³. On the basis of the final model, the calculated density was 1.548 g/cm³ and F(000), 737 e⁻.

9.3 Complex 3a

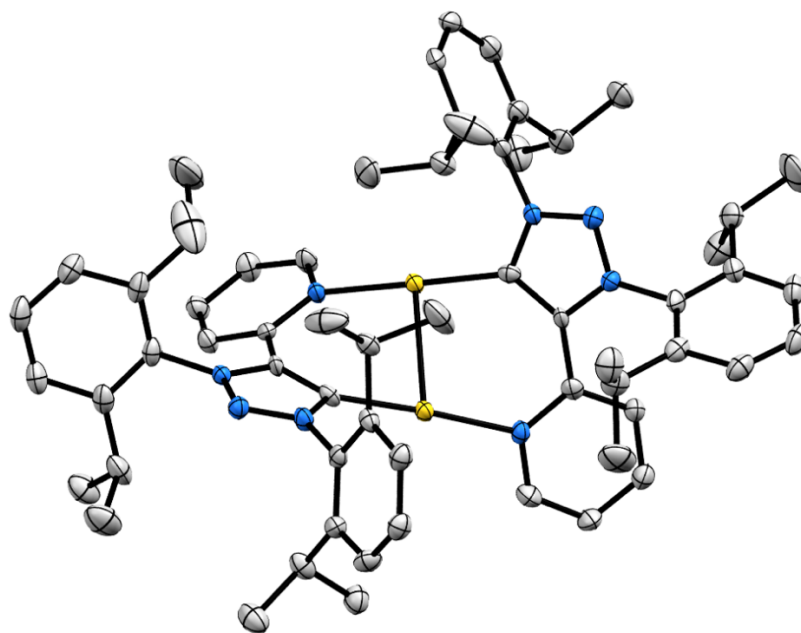


Figure S91. Crystal structure of **3a** (CCDC 2163617). Ellipsoids set at 50% probability; H atoms, SbF_6^- anions and solvent molecules are omitted for clarity.

Table S9. Crystallographic parameters for **3a**.

Chemical formula	$\text{C}_{67}\text{H}_{88}\text{Au}_2\text{Cl}_2\text{F}_{12}\text{N}_8\text{OSb}_2$	
Formula weight	1957.78 g/mol	
Temperature	100(2) K	
Wavelength	0.71073 Å	
Crystal size	0.040 x 0.250 x 0.280 mm	
Crystal system	Monoclinic	
Space group	P 1 21/c 1	
Unit cell dimensions	$a = 16.5318(8)$ Å	$\alpha = 90^\circ$
	$b = 17.9336(8)$ Å	$\beta = 107.017(2)^\circ$
	$c = 25.9388(12)$ Å	$\gamma = 90^\circ$
Volume	$7353.5(6)$ Å ³	
Density (calculated)	1.768 g/cm ³	
Absorption coefficient	4.854 mm ⁻¹	
Final R indices	13720 data; $I > 2\sigma(I)$	R1 = 0.0513, wR2 = 0.1039
	All data	R1 = 0.0745, wR2 = 0.1178

A colorless plate-like specimen of $\text{C}_{67}\text{H}_{88}\text{Au}_2\text{Cl}_2\text{F}_{12}\text{N}_8\text{OSb}_2$, approximate dimensions 0.040 mm x 0.250 mm x 0.280 mm, was used for the X-ray crystallographic analysis. The X-ray intensity data were measured on a D8 QUEST ECO three-circle diffractometer

system equipped with a Ceramic x-ray tube (Mo K α , $\lambda = 0.71073 \text{ \AA}$) and a doubly curved silicon crystal Bruker Triumph monochromator. A total of 1837 frames were collected. The total exposure time was 1.89 hours. The frames were integrated with the Bruker SAINT software package using a wide-frame algorithm. The integration of the data using a monoclinic unit cell yielded a total of 387971 reflections to a maximum θ angle of 27.54° (0.77 \AA resolution), of which 16936 were independent (average redundancy 22.908, completeness = 99.8%, $R_{\text{int}} = 9.55\%$, $R_{\text{sig}} = 3.26\%$) and 13720 (81.01%) were greater than $2\sigma(F^2)$. The final cell constants of $a = 16.5318(8) \text{ \AA}$, $b = 17.9336(8) \text{ \AA}$, $c = 25.9388(12) \text{ \AA}$, $\beta = 107.017(2)^\circ$, volume = $7353.5(6) \text{ \AA}^3$, are based upon the refinement of the XYZ-centroids of 9283 reflections above $20 \sigma(I)$ with $5.632^\circ < 2\theta < 54.95^\circ$. Data were corrected for absorption effects using the Multi-Scan method (SADABS). The ratio of minimum to maximum apparent transmission was 0.564. The calculated minimum and maximum transmission coefficients (based on crystal size) are 0.3430 and 0.8300. The structure was solved and refined using the Bruker SHELXTL Software Package, using the space group P 1 21/c 1, with $Z = 4$ for the formula unit, $C_{67}H_{88}Au_2Cl_2F_{12}N_8OSb_2$. The final anisotropic full-matrix least-squares refinement on F^2 with 859 variables converged at $R1 = 5.13\%$, for the observed data and $wR2 = 11.78\%$ for all data. The goodness-of-fit was 1.242. The largest peak in the final difference electron density synthesis was $3.857 \text{ e}^-/\text{\AA}^3$ and the largest hole was $-2.415 \text{ e}^-/\text{\AA}^3$ with an RMS deviation of $0.214 \text{ e}^-/\text{\AA}^3$. On the basis of the final model, the calculated density was 1.768 g/cm^3 and $F(000)$, 3824 e^- .

9.4 Complex **3b**·biphenylene

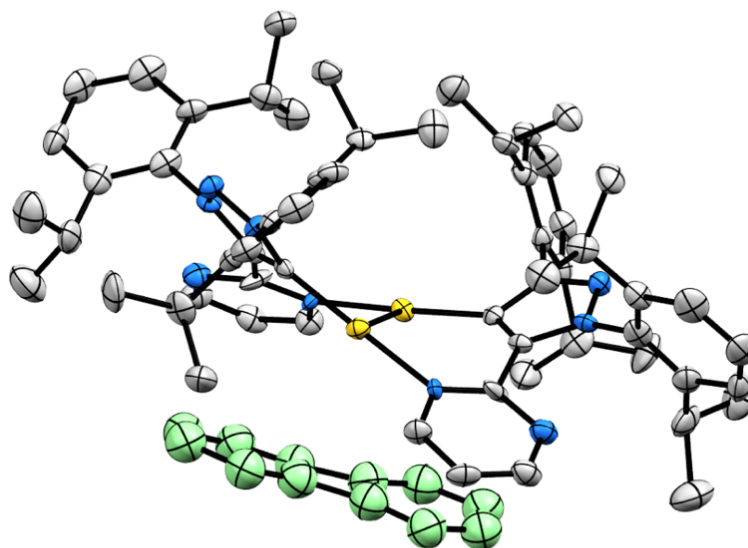


Figure S92. Crystal structure of **3b**·biphenylene (CCDC 2163613). Ellipsoids set at 50% probability; H atoms and SbF_6^- anions omitted for clarity. One molecule of biphenylene (in green) co-crystallized with one molecule of the dimeric Au(I) complex.

Table S10. Crystallographic parameters for **3b·biphenylene**.

Chemical formula	C ₇₂ H ₈₂ Au ₂ F ₁₂ N ₁₀ Sb ₂	
Formula weight	1952.90 g/mol	
Temperature	100(2) K	
Wavelength	0.71073 Å	
Crystal size	0.060 x 0.180 x 0.230 mm	
Crystal system	Orthorhombic	
Space group	P b c n	
Unit cell dimensions	a = 25.668(9) Å	α = 90°
	b = 11.721(4) Å	β = 90°
	c = 25.249(9) Å	γ = 90°
Volume	7596.(5) Å ³	
Density (calculated)	1.708 g/cm ³	
Absorption coefficient	4.630 mm ⁻¹	
Final R indices	6113 data; I>2σ(I)	R1 = 0.0652, wR2 = 0.1282
	All data	R1 = 0.1075, wR2 = 0.1510

A yellow plate-like specimen of C₇₂H₈₂Au₂F₁₂N₁₀Sb₂, approximate dimensions 0.060 mm x 0.180 mm x 0.230 mm, was used for the X-ray crystallographic analysis. The X-ray intensity data were measured on a D8 QUEST ECO three-circle diffractometer system equipped with a Ceramic x-ray tube (Mo Kα, λ = 0.71073 Å) and a doubly curved silicon crystal Bruker Triumph monochromator. A total of 1107 frames were collected. The total exposure time was 1.54 hours. The frames were integrated with the Bruker SAINT software package using a wide-frame algorithm. The integration of the data using an orthorhombic unit cell yielded a total of 330522 reflections to a maximum θ angle of 27.36° (0.77 Å resolution), of which 8574 were independent (average redundancy 38.549, completeness = 99.7%, R_{int} = 13.94%, R_{sig} = 3.73%) and 6113 (71.30%) were greater than 2σ(F²). The final cell constants of a = 25.668(9) Å, b = 11.721(4) Å, c = 25.249(9) Å, volume = 7596.(5) Å³, are based upon the refinement of the XYZ-centroids of 274 reflections above 20 σ(I) with 5.129° < 2θ < 34.22°. Data were corrected for absorption effects using the Multi-Scan method (SADABS). The ratio of minimum to maximum apparent transmission was 0.706. The calculated minimum and maximum transmission coefficients (based on crystal size) are 0.4160 and 0.7690. The structure was solved and refined using the Bruker SHELXTL Software Package, using the space group P b c n, with Z = 4 for the formula unit, C₇₂H₈₂Au₂F₁₂N₁₀Sb₂. The final anisotropic full-matrix least-squares refinement on F² with 496 variables converged at R1 = 6.52%, for the observed data and wR2 = 15.10% for all data. The goodness-of-fit was 1.243. The largest peak in the final difference electron density synthesis was 2.851 e⁻/Å³ and the largest hole was -2.625 e⁻/Å³ with an RMS deviation of 0.229 e⁻/Å³. On the basis of the final model, the calculated density was 1.708 g/cm³ and F(000), 3808 e⁻.

9.5 Complex 4a-Cl

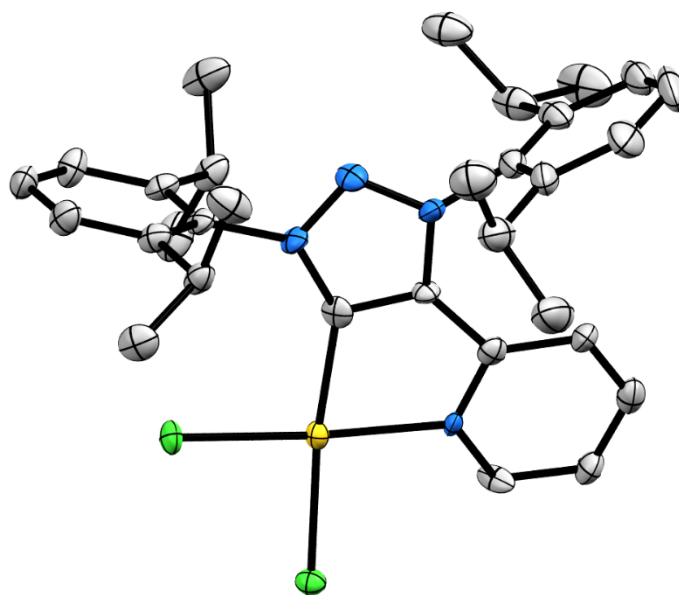


Figure S93. Crystal structure of **4a-Cl** (CCDC 2613611). Ellipsoids set at 50% probability; H atoms, SbF_6^- anion and solvent molecules are omitted for clarity.

Table S11. Crystallographic parameters for **4a-Cl**.

Chemical formula	$\text{C}_{35}\text{H}_{50}\text{AuCl}_2\text{F}_6\text{N}_4\text{O}_2\text{Sb}$	
Formula weight	1062.40 g/mol	
Temperature	100(2) K	
Wavelength	0.71076 Å	
Crystal size	0.180 x 0.180 x 0.500 mm	
Crystal system	Triclinic	
Space group	P -1	
Unit cell dimensions	$a = 12.5020(6)$ Å	$\alpha = 83.846(2)^\circ$
	$b = 15.3475(8)$ Å	$\beta = 81.645(2)^\circ$
	$c = 22.3529(11)$ Å	$\gamma = 79.159(2)^\circ$
Volume	$4153.6(4)$ Å ³	
Density (calculated)	1.699 g/cm ³	
Absorption coefficient	4.368 mm ⁻¹	
Final R indices	17621 data; $I > 2\sigma(I)$	R1 = 0.0586, wR2 = 0.1292
	All data	R1 = 0.0762, wR2 = 0.1402

A yellow plate-like specimen of $\text{C}_{35}\text{H}_{50}\text{AuCl}_2\text{F}_6\text{N}_4\text{O}_2\text{Sb}$, approximate dimensions 0.180 mm x 0.180 mm x 0.500 mm, was used for the X-ray crystallographic analysis. The X-

ray intensity data were measured on a D8 QUEST ECO three-circle diffractometer system equipped with a Ceramic x-ray tube (Mo K α , $\lambda = 0.71076 \text{ \AA}$) and a doubly curved silicon crystal Bruker Triumph monochromator. A total of 2489 frames were collected. The total exposure time was 2.77 hours. The frames were integrated with the Bruker SAINT software package using a narrow-frame algorithm. The integration of the data using a triclinic unit cell yielded a total of 253080 reflections to a maximum θ angle of 28.38° (0.75 \AA resolution), of which 20753 were independent (average redundancy 12.195, completeness = 99.7%, $R_{\text{int}} = 6.64\%$, $R_{\text{sig}} = 3.14\%$) and 17621 (84.91%) were greater than $2\sigma(F^2)$. The final cell constants of $a = 12.5020(6) \text{ \AA}$, $b = 15.3475(8) \text{ \AA}$, $c = 22.3529(11) \text{ \AA}$, $\alpha = 83.846(2)^\circ$, $\beta = 81.645(2)^\circ$, $\gamma = 79.159(2)^\circ$, volume = $4153.6(4) \text{ \AA}^3$, are based upon the refinement of the XYZ-centroids of 9298 reflections above $20 \sigma(I)$ with $6.073^\circ < 2\theta < 56.49^\circ$. Data were corrected for absorption effects using the Multi-Scan method (SADABS). The ratio of minimum to maximum apparent transmission was 0.794. The calculated minimum and maximum transmission coefficients (based on crystal size) are 0.4789 and 0.6035. The structure was solved and refined using the Bruker SHELXTL Software Package, using the space group $P -1$, with $Z = 4$ for the formula unit, $C_{35}H_{50}AuCl_2F_6N_4O_2Sb$. The final anisotropic full-matrix least-squares refinement on F^2 with 933 variables converged at $R1 = 5.86\%$, for the observed data and $wR2 = 14.02\%$ for all data. The goodness-of-fit was 1.236. The largest peak in the final difference electron density synthesis was $4.225 \text{ e}^-/\text{\AA}^3$ and the largest hole was $-3.184 \text{ e}^-/\text{\AA}^3$ with an RMS deviation of $0.224 \text{ e}^-/\text{\AA}^3$. On the basis of the final model, the calculated density was 1.699 g/cm^3 and $F(000)$, 2088 e^- .

9.6 Complex 4a-OAc

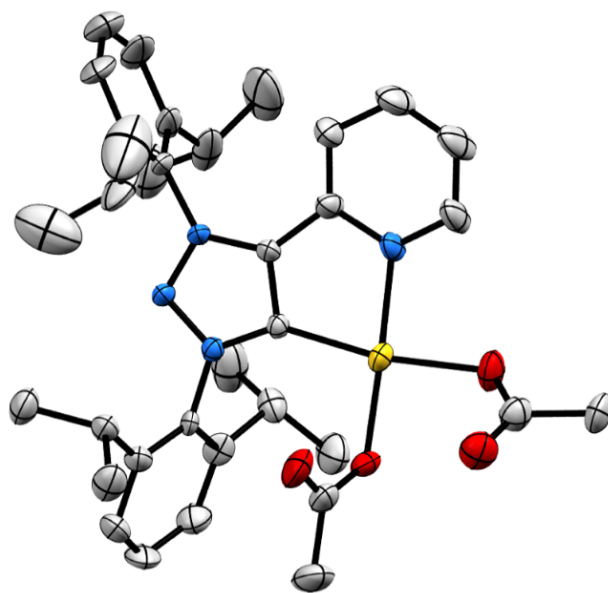


Figure S94. Crystal structure of **4a-OAc** (CCDC 2163608). Ellipsoids set at 50% probability; H atoms, SbF_6^- anion and solvent molecules are omitted for clarity.

Table S12. Crystallographic parameters for **4a-OAc**.

Chemical formula	C ₃₅ H ₄₈ AuF ₆ N ₄ O ₆ Sb	
Formula weight	1053.49 g/mol	
Temperature	100(2) K	
Wavelength	0.71076 Å	
Crystal size	0.250 x 0.400 x 0.550 mm	
Crystal system	Triclinic	
Space group	P -1	
Unit cell dimensions	a = 11.63(4) Å	α = 76.35(10)°
	b = 12.52(5) Å	β = 72.58(7)°
	c = 15.71(6) Å	γ = 65.54(8)°
Volume	1970.(13) Å ³	
Density (calculated)	1.776 g/cm ³	
Absorption coefficient	4.480 mm ⁻¹	
Final R indices	8205 data; I > 2σ(I)	R1 = 0.0894, wR2 = 0.2113
	All data	R1 = 0.1121, wR2 = 0.2361

A yellow block-like specimen of C₃₅H₄₈AuF₆N₄O₆Sb, approximate dimensions 0.250 mm x 0.400 mm x 0.550 mm, was used for the X-ray crystallographic analysis. The X-ray intensity data were measured on a D8 QUEST ECO three-circle diffractometer system equipped with a Ceramic x-ray tube (Mo Kα, λ = 0.71076 Å) and a doubly curved silicon crystal Bruker Triumph monochromator. A total of 1206 frames were collected. The total exposure time was 2.68 hours. The frames were integrated with the Bruker SAINT software package using a narrow-frame algorithm. The integration of the data using a triclinic unit cell yielded a total of 86475 reflections to a maximum θ angle of 28.35° (0.75 Å resolution), of which 9804 were independent (average redundancy 8.820, completeness = 99.6%, R_{int} = 4.12%, R_{sig} = 2.38%) and 8205 (83.69%) were greater than 2σ(F²). The final cell constants of \underline{a} = 11.63(4) Å, \underline{b} = 12.52(5) Å, \underline{c} = 15.71(6) Å, α = 76.35(10)°, β = 72.58(7)°, γ = 65.54(8)°, volume = 1970.(13) Å³, are based upon the refinement of the XYZ-centroids of 9316 reflections above 20 σ(I) with 5.744° < 2θ < 56.54°. Data were corrected for absorption effects using the Multi-Scan method (SADABS). The ratio of minimum to maximum apparent transmission was 0.592. The calculated minimum and maximum transmission coefficients (based on crystal size) are 0.4415 and 0.7457. The structure was solved and refined using the Bruker SHELXTL Software Package, using the space group P -1, with Z = 2 for the formula unit, C₃₅H₄₈AuF₆N₄O₆Sb. The final anisotropic full-matrix least-squares refinement on F² with 478 variables converged at R1 = 8.94%, for the observed data and wR2 = 23.61% for all data. The goodness-of-fit was 1.062. The largest peak in the final difference electron density synthesis was 10.949 e⁻/Å³ and the largest hole was -6.868 e⁻/Å³ with an RMS deviation of 0.335 e⁻/Å³. On the basis of the final model, the calculated density was 1.776 g/cm³ and F(000), 1036 e⁻.

9.7 Complex 5b

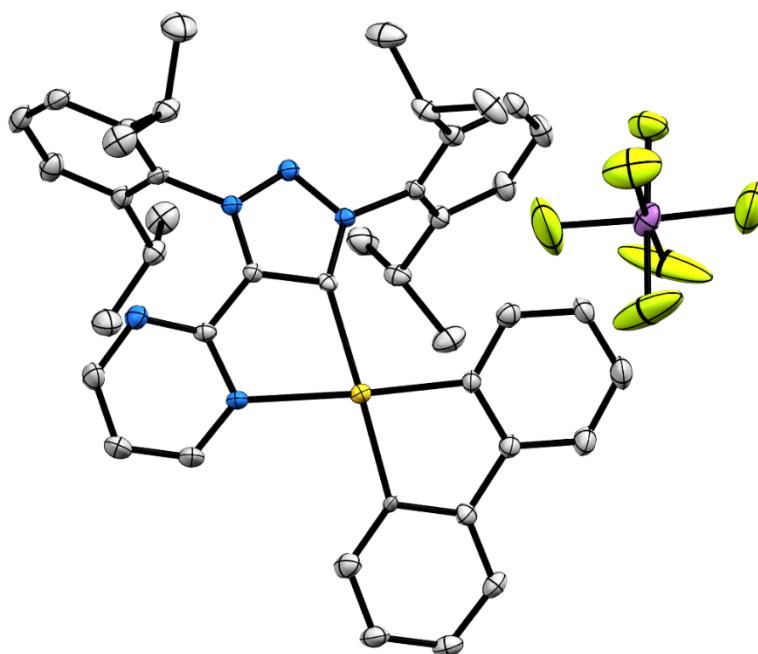


Figure S95. Crystal structure of **5b** (CCDC 2163614). Ellipsoids set at 50% probability; H atoms removed for clarity.

Table S13. Crystallographic parameters for **5b**.

Chemical formula	C ₄₂ H ₄₅ AuF ₆ N ₅ Sb	
Formula weight	1052.54 g/mol	
Temperature	100(2) K	
Wavelength	0.71073 Å	
Crystal size	0.060 x 0.070 x 0.400 mm	
Crystal system	Monoclinic	
Space group	P 1 21/n 1	
Unit cell dimensions	a = 17.0009(7) Å	α = 90°
	b = 11.7830(5) Å	β = 98.260(2)°
	c = 19.9923(8) Å	γ = 90°
Volume	3963.3(3) Å ³	
Density (calculated)	1.764 g/cm ³	
Absorption coefficient	4.445 mm ⁻¹	
Final R indices	9697 data; I > 2σ(I)	R1 = 0.0478, wR2 = 0.1097
	All data	R1 = 0.0642, wR2 = 0.1221

A yellow-green needle-like specimen of $C_{42}H_{45}AuF_6N_5Sb$, approximate dimensions 0.060 mm x 0.070 mm x 0.400 mm, was used for the X-ray crystallographic analysis. The X-ray intensity data were measured on a D8 QUEST ECO three-circle diffractometer system equipped with a Ceramic x-ray tube (Mo $K\alpha$, $\lambda = 0.71073 \text{ \AA}$) and a doubly curved silicon crystal Bruker Triumph monochromator. A total of 1507 frames were collected. The total exposure time was 3.74 hours. The frames were integrated with the Bruker SAINT software package using a narrow-frame algorithm. The integration of the data using a monoclinic unit cell yielded a total of 261601 reflections to a maximum θ angle of 30.11° (0.71 \AA resolution), of which 11643 were independent (average redundancy 22.469, completeness = 99.7%, $R_{\text{int}} = 7.53\%$, $R_{\text{sig}} = 2.75\%$) and 9697 (83.29%) were greater than $2\sigma(F^2)$. The final cell constants of $a = 17.0009(7) \text{ \AA}$, $b = 11.7830(5) \text{ \AA}$, $c = 19.9923(8) \text{ \AA}$, $\beta = 98.260(2)^\circ$, volume = $3963.3(3) \text{ \AA}^3$, are based upon the refinement of the XYZ-centroids of 9273 reflections above $20 \sigma(I)$ with $5.950^\circ < 2\theta < 60.08^\circ$. Data were corrected for absorption effects using the Multi-Scan method (SADABS). The ratio of minimum to maximum apparent transmission was 0.629. The calculated minimum and maximum transmission coefficients (based on crystal size) are 0.2690 and 0.7760. The structure was solved and refined using the Bruker SHELXTL Software Package, using the space group $P 1 21/n 1$, with $Z = 4$ for the formula unit, $C_{42}H_{45}AuF_6N_5Sb$. The final anisotropic full-matrix least-squares refinement on F^2 with 504 variables converged at $R1 = 4.78\%$, for the observed data and $wR2 = 12.21\%$ for all data. The goodness-of-fit was 1.063. The largest peak in the final difference electron density synthesis was $9.167 \text{ e}^-/\text{\AA}^3$ and the largest hole was $-4.458 \text{ e}^-/\text{\AA}^3$ with an RMS deviation of $0.221 \text{ e}^-/\text{\AA}^3$. On the basis of the final model, the calculated density was 1.764 g/cm^3 and $F(000)$, 2064 e^- .

9.8 Complex 6b

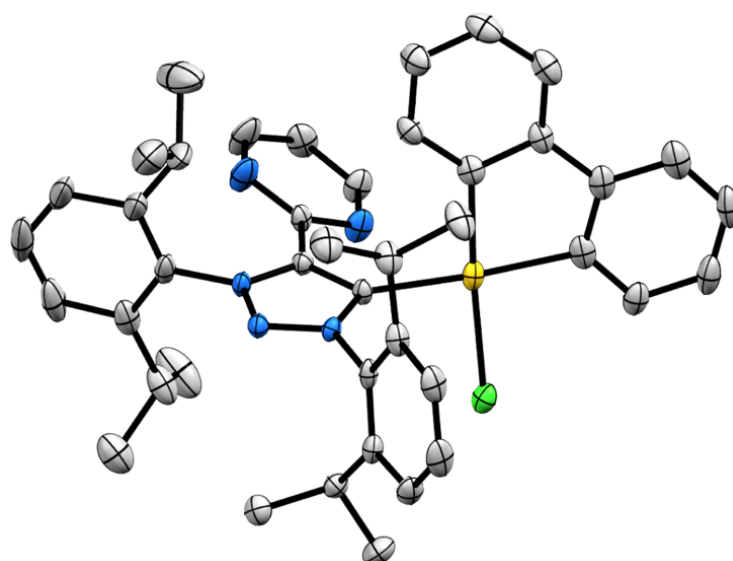


Figure S96. Crystal structure of **6b** (CCDC 2163615). Ellipsoids set at 50% probability; H atoms removed for clarity.

Table S14. Crystallographic parameters for **6b**.

Chemical formula	C ₄₆ H ₅₅ AuClN ₅ O	
Formula weight	926.36 g/mol	
Temperature	100(2) K	
Wavelength	0.71076 Å	
Crystal size	0.110 x 0.110 x 0.150 mm	
Crystal system	Triclinic	
Space group	P -1	
Unit cell dimensions	a = 12.25(2) Å	α = 89.58(3)°
	b = 15.50(2) Å	β = 84.70(4)°
	c = 23.22(4) Å	γ = 85.16(4)°
Volume	4374.(12) Å ³	
Density (calculated)	1.406 g/cm ³	
Absorption coefficient	3.462 mm ⁻¹	
Final R indices	16770 data; I>2σ(I)	R1 = 0.0509, wR2 = 0.1007
	All data	R1 = 0.0801, wR2 = 0.1158

A colorless prism-like specimen of C₄₆H₅₅AuClN₅O, approximate dimensions 0.110 mm x 0.110 mm x 0.150 mm, was used for the X-ray crystallographic analysis. The X-ray intensity data were measured on a D8 QUEST ECO three-circle diffractometer system equipped with a Ceramic x-ray tube (Mo Kα, λ = 0.71076 Å) and a doubly curved silicon crystal Bruker Triumph monochromator. A total of 1467 frames were collected. The total exposure time was 3.26 hours. The frames were integrated with the Bruker SAINT software package using a narrow-frame algorithm. The integration of the data using a triclinic unit cell yielded a total of 285667 reflections to a maximum θ angle of 28.32° (0.75 Å resolution), of which 21662 were independent (average redundancy 13.187, completeness = 99.2%, R_{int} = 8.17%, R_{sig} = 3.95%) and 16770 (77.42%) were greater than 2σ(F²). The final cell constants of $\underline{a} = 12.25(2)$ Å, $\underline{b} = 15.50(2)$ Å, $\underline{c} = 23.22(4)$ Å, α = 89.58(3)°, β = 84.70(4)°, γ = 85.16(4)°, volume = 4374.(12) Å³, are based upon the refinement of the XYZ-centroids of 9795 reflections above 20 σ(I) with 5.578° < 2θ < 56.18°. Data were corrected for absorption effects using the Multi-Scan method (SADABS). The ratio of minimum to maximum apparent transmission was 0.717. The calculated minimum and maximum transmission coefficients (based on crystal size) are 0.5345 and 0.7457. The structure was solved and refined using the Bruker SHELXTL Software Package, using the space group P -1, with Z = 4 for the formula unit, C₄₆H₅₅AuClN₅O. The final anisotropic full-matrix least-squares refinement on F² with 993 variables converged at R1 = 5.09%, for the observed data and wR2 = 11.58% for all data. The goodness-of-fit was 1.271. The largest peak in the final difference electron density synthesis was 4.528 e⁻/Å³ and the largest hole was -3.736 e⁻/Å³ with an RMS deviation of 0.170 e⁻/Å³. On the basis of the final model, the calculated density was 1.406 g/cm³ and F(000), 1880 e⁻.

9.9 Complex *cis-7a-Cl*

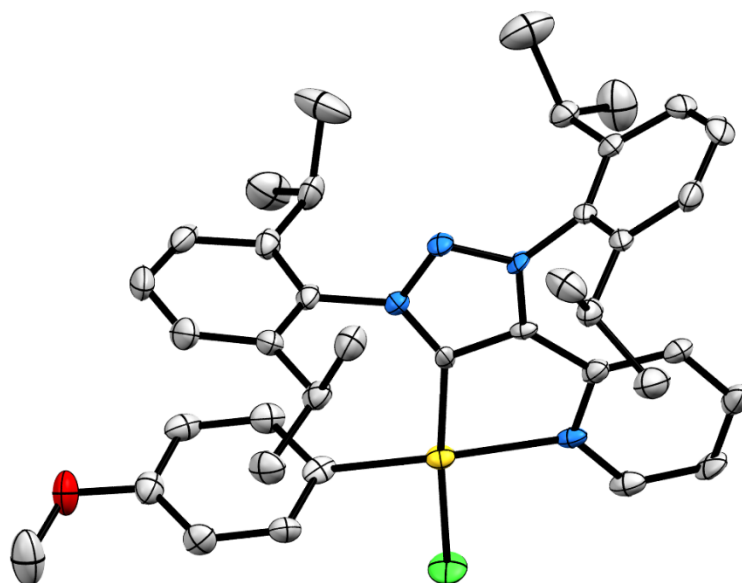


Figure S97. Crystal structure of *cis-7a-Cl* (CCDC 2176932). Ellipsoids set at 50% probability; H atoms, BF_4^- anion and solvent molecules are omitted for clarity.

Table S15. Crystallographic parameters for *cis-7a-Cl*. The chemical formula is given for 4 molecules of complex *cis-7a-Cl* and 5 molecules of N,N-dimethylformamide.

Chemical formula	$\text{C}_{167}\text{H}_{215}\text{Au}_4\text{B}_4\text{Cl}_4\text{F}_{16}\text{N}_{21}\text{O}_9$	
Formula weight	3937.49 g/mol	
Temperature	100(2) K	
Wavelength	0.71073 Å	
Crystal size	0.040 x 0.040 x 0.200 mm	
Crystal system	Triclinic	
Space group	P -1	
Unit cell dimensions	$a = 16.4149(8) \text{ \AA}$	$\alpha = 64.1050(10)^\circ$
	$b = 23.5323(12) \text{ \AA}$	$\beta = 80.992(2)^\circ$
	$c = 24.8306(13) \text{ \AA}$	$\gamma = 81.2460(10)^\circ$
Volume	$8484.1(7) \text{ \AA}^3$	
Density (calculated)	1.541 g/cm ³	
Absorption coefficient	3.591 mm ⁻¹	
Final R indices	27208 data; $I > 2\sigma(I)$	R1 = 0.0658, wR2 = 0.1318
	All data	R1 = 0.1132, wR2 = 0.1554

A colorless plate-like specimen of $\text{C}_{167}\text{H}_{215}\text{Au}_4\text{B}_4\text{Cl}_4\text{F}_{16}\text{N}_{21}\text{O}_9$, approximate dimensions 0.040 mm x 0.040 mm x 0.200 mm, was used for the X-ray crystallographic analysis. The X-ray intensity data were measured on a D8 QUEST ECO three-circle diffractometer

system equipped with a Ceramic x-ray tube (Mo K α , $\lambda = 0.71073 \text{ \AA}$) and a doubly curved silicon crystal Bruker Triumph monochromator. A total of 1043 frames were collected. The total exposure time was 8.69 hours. The frames were integrated with the Bruker SAINT software package using a narrow-frame algorithm. The integration of the data using a triclinic unit cell yielded a total of 512292 reflections to a maximum θ angle of 27.61° (0.77 \AA resolution), of which 39296 were independent (average redundancy 13.037, completeness = 99.7%, $R_{\text{int}} = 14.35\%$, $R_{\text{sig}} = 7.00\%$) and 27208 (69.24%) were greater than $2\sigma(F^2)$. The final cell constants of $a = 16.4149(8) \text{ \AA}$, $b = 23.5323(12) \text{ \AA}$, $c = 24.8306(13) \text{ \AA}$, $\alpha = 64.1050(10)^\circ$, $\beta = 80.992(2)^\circ$, $\gamma = 81.2460(10)^\circ$, volume = $8484.1(7) \text{ \AA}^3$, are based upon the refinement of the XYZ-centroids of 9838 reflections above $20 \sigma(I)$ with $5.770^\circ < 2\theta < 53.65^\circ$. Data were corrected for absorption effects using the Multi-Scan method (SADABS). The ratio of minimum to maximum apparent transmission was 0.802. The calculated minimum and maximum transmission coefficients (based on crystal size) are 0.5340 and 0.8700. The structure was solved and refined using the Bruker SHELXTL Software Package, using the space group P -1, with $Z = 2$ for the formula unit, $\text{C}_{167}\text{H}_{215}\text{Au}_4\text{B}_4\text{Cl}_4\text{F}_{16}\text{N}_{21}\text{O}_9$. The final anisotropic full-matrix least-squares refinement on F^2 with 2037 variables converged at $R1 = 6.58\%$, for the observed data and $wR2 = 15.54\%$ for all data. The goodness-of-fit was 1.098. The largest peak in the final difference electron density synthesis was $2.818 \text{ e}^-/\text{\AA}^3$ and the largest hole was $-4.916 \text{ e}^-/\text{\AA}^3$ with an RMS deviation of $0.200 \text{ e}^-/\text{\AA}^3$. On the basis of the final model, the calculated density was 1.541 g/cm^3 and $F(000)$, 3968 e^- .

9.10 Compounds 8a-OMe and 9a

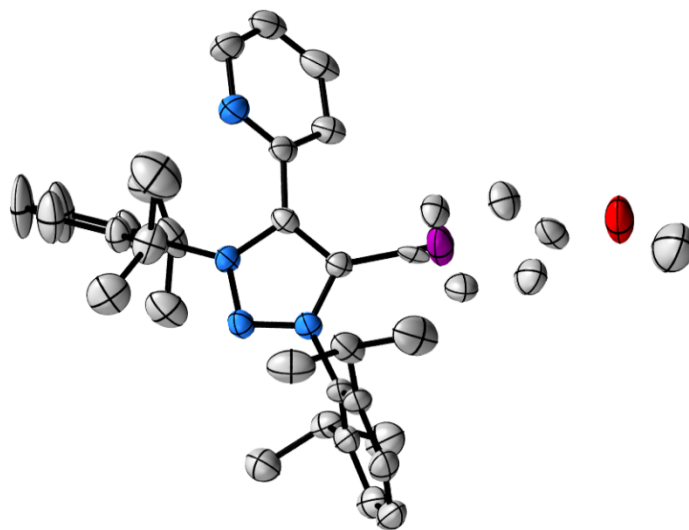


Figure S98. Crystal structure of **8a-OMe** co-crystallized with a minor amount of compound **9a** in a 0.89:0.11 ratio (CCDC 2163612). Ellipsoids set at 50% probability; H atoms and SbF_6^- anion removed for clarity.

Table S16. Crystallographic parameters for the co-crystallization of **8a-OMe** and **9a** in a 0.89:0.11 ratio.

Chemical formula	C _{37.26} H _{44.26} F ₆ I _{0.11} N ₄ O _{0.89} Sb	
Formula weight	811.62 g/mol	
Temperature	100(2) K	
Wavelength	0.71076 Å	
Crystal size	0.210 x 0.220 x 0.240 mm	
Crystal system	Monoclinic	
Space group	P 1 21/n 1	
Unit cell dimensions	a = 12.29(4) Å	α = 90°
	b = 16.44(5) Å	β = 101.35(6)°
	c = 19.22(6) Å	γ = 90°
Volume	3807.(19) Å ³	
Density (calculated)	1.416 g/cm ³	
Absorption coefficient	0.873 mm ⁻¹	
Final R indices	4525 data; I>2σ(I)	R1 = 0.0680, wR2 = 0.1365
	All data	R1 = 0.0892, wR2 = 0.1468

A colorless prism-like specimen of C_{37.26}H_{44.26}F₆I_{0.11}N₄O_{0.89}Sb, approximate dimensions 0.210 mm x 0.220 mm x 0.240 mm, was used for the X-ray crystallographic analysis. The X-ray intensity data were measured on a D8 QUEST ECO three-circle diffractometer system equipped with a Ceramic x-ray tube (Mo Kα, λ = 0.71076 Å) and a doubly curved silicon crystal Bruker Triumph monochromator. A total of 1006 frames were collected. The total exposure time was 8.38 hours. The frames were integrated with the Bruker SAINT software package using a narrow-frame algorithm. The integration of the data using a monoclinic unit cell yielded a total of 69569 reflections to a maximum θ angle of 23.61° (0.89 Å resolution), of which 5671 were independent (average redundancy 12.268, completeness = 99.1%, R_{int} = 7.44%, R_{sig} = 3.54%) and 4525 (79.79%) were greater than 2σ(F²). The final cell constants of a = 12.29(4) Å, b = 16.44(5) Å, c = 19.22(6) Å, β = 101.35(6)°, volume = 3807.(19) Å³, are based upon the refinement of the XYZ-centroids of 9982 reflections above 20 σ(I) with 6.003° < 2θ < 45.68°. Data were corrected for absorption effects using the Multi-Scan method (SADABS). The ratio of minimum to maximum apparent transmission was 0.866. The calculated minimum and maximum transmission coefficients (based on crystal size) are 0.6449 and 0.7449. The structure was solved and refined using the Bruker SHELXTL Software Package, using the space group P 1 21/n 1, with Z = 4 for the formula unit, C_{37.26}H_{44.26}F₆I_{0.11}N₄O_{0.89}Sb. The final anisotropic full-matrix least-squares refinement on F² with 458 variables converged at R1 = 6.80%, for the observed data and wR2 = 14.68% for all data. The goodness-of-fit was 1.185. The largest peak in the final difference electron density synthesis was 1.114 e⁻/Å³ and the largest hole was -1.089 e⁻/Å³ with an RMS deviation of 0.090 e⁻/Å³. On the basis of the final model, the calculated density was 1.416 g/cm³ and F(000), 1654 e⁻.

9.11 Compound 8b-OMe

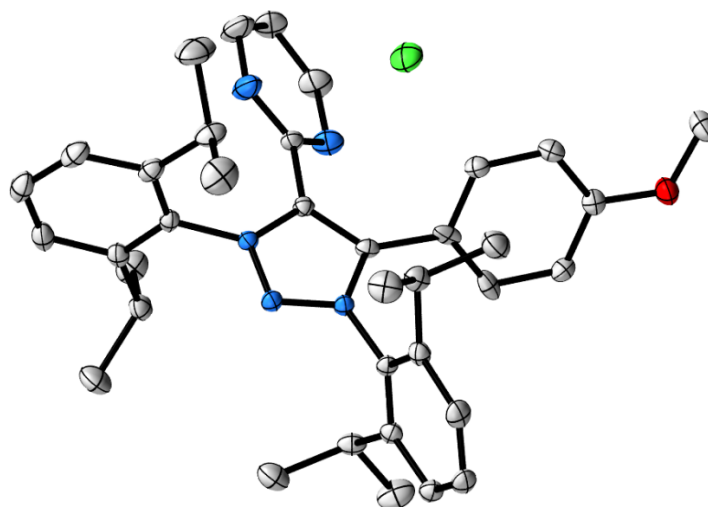


Figure S99. Crystal structure of **8b-OMe** (CCDC 2163616). Ellipsoids set at 50% probability; H atoms removed for clarity.

Table S17. Crystallographic parameters for **8b-OMe**.

Chemical formula	C ₃₇ H ₄₆ ClN ₅ O ₂	
Formula weight	628.24 g/mol	
Temperature	100(2) K	
Wavelength	0.71076 Å	
Crystal size	0.080 x 0.090 x 0.190 mm	
Crystal system	Monoclinic	
Space group	P 1 21/c 1	
Unit cell dimensions	a = 11.589(10) Å	α = 90°
	b = 11.486(9) Å	β = 97.78(2)°
	c = 26.60(3) Å	γ = 90°
Volume	3508.(5) Å ³	
Density (calculated)	1.190 g/cm ³	
Absorption coefficient	0.148 mm ⁻¹	
Final R indices	6967 data; I > 2σ(I)	R1 = 0.0602, wR2 = 0.1425
	All data	R1 = 0.0697, wR2 = 0.1481

A colorless prism-like specimen of C₃₇H₄₆ClN₅O₂, approximate dimensions 0.080 mm x 0.090 mm x 0.190 mm, was used for the X-ray crystallographic analysis. The X-ray intensity data were measured on a D8 QUEST ECO three-circle diffractometer system equipped with a Ceramic x-ray tube (Mo Kα, λ = 0.71076 Å) and a doubly curved silicon crystal Bruker Triumph monochromator. A total of 774 frames were collected. The total

exposure time was 17.20 hours. The frames were integrated with the Bruker SAINT software package using a narrow-frame algorithm. The integration of the data using a monoclinic unit cell yielded a total of 107985 reflections to a maximum θ angle of 27.50° (0.77 \AA resolution), of which 8030 were independent (average redundancy 13.448, completeness = 99.8%, $R_{\text{int}} = 4.51\%$, $R_{\text{sig}} = 2.04\%$) and 6967 (86.76%) were greater than $2\sigma(F^2)$. The final cell constants of $a = 11.589(10) \text{ \AA}$, $b = 11.486(9) \text{ \AA}$, $c = 26.60(3) \text{ \AA}$, $\beta = 97.78(2)^\circ$, volume = 3508.5 \AA^3 , are based upon the refinement of the XYZ-centroids of 9889 reflections above $20 \sigma(I)$ with $5.648^\circ < 2\theta < 56.59^\circ$. Data were corrected for absorption effects using the Multi-Scan method (SADABS). The ratio of minimum to maximum apparent transmission was 0.950. The calculated minimum and maximum transmission coefficients (based on crystal size) are 0.9720 and 0.9880. The structure was solved and refined using the Bruker SHELXTL Software Package, using the space group $P 1 21/c 1$, with $Z = 4$ for the formula unit, $C_{37}H_{46}ClN_5O_2$. The final anisotropic full-matrix least-squares refinement on F^2 with 423 variables converged at $R1 = 6.02\%$, for the observed data and $wR2 = 14.81\%$ for all data. The goodness-of-fit was 1.123. The largest peak in the final difference electron density synthesis was $1.307 \text{ e}^-/\text{\AA}^3$ and the largest hole was $-0.508 \text{ e}^-/\text{\AA}^3$ with an RMS deviation of $0.058 \text{ e}^-/\text{\AA}^3$. On the basis of the final model, the calculated density was 1.190 g/cm^3 and $F(000)$, 1344 e^- .

9.12 Compound 16

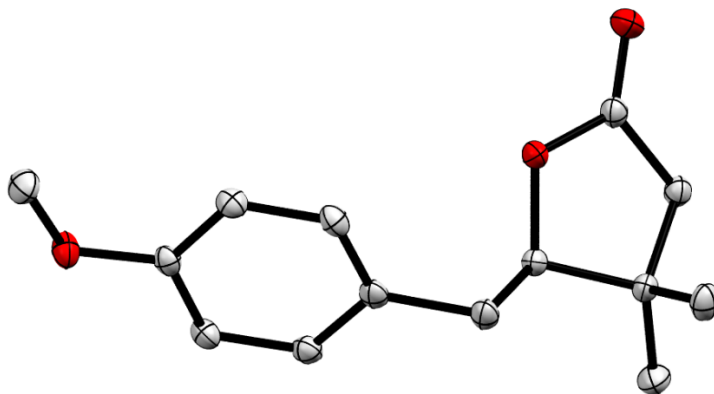


Figure S100. Crystal structure of **16** (CCDC 2163877). Ellipsoids set at 50% probability; H atoms removed for clarity.

Table S18. Crystallographic parameters for **16**.

Chemical formula	C ₁₄ H ₁₈ O ₃	
Formula weight	234.28 g/mol	
Temperature	100(2) K	
Wavelength	0.71073 Å	
Crystal size	0.370 x 0.370 x 0.450 mm	
Crystal system	Orthorhombic	
Space group	P 21 21 21	
Unit cell dimensions	a = 6.3989(2) Å	α = 90°
	b = 7.1432(2) Å	β = 90°
	c = 27.0217(7) Å	γ = 90°
Volume	1235.12(6) Å ³	
Density (calculated)	1.260 g/cm ³	
Absorption coefficient	0.087 mm ⁻¹	
Final R indices	3051 data; I>2σ(I)	R1 = 0.0282, wR2 = 0.0731
	All data	R1 = 0.0287, wR2 = 0.0736

A colorless prism-like specimen of C₁₄H₁₈O₃, approximate dimensions 0.370 mm x 0.370 mm x 0.450 mm, was used for the X-ray crystallographic analysis. The X-ray intensity data were measured on a D8 QUEST ECO three-circle diffractometer system equipped with a Ceramic x-ray tube (Mo Kα, λ = 0.71073 Å) and a doubly curved silicon crystal Bruker Triumph monochromator. A total of 364 frames were collected. The total exposure time was 0.51 hours. The frames were integrated with the Bruker SAINT software package using a narrow-frame algorithm. The integration of the data using an orthorhombic unit cell yielded a total of 6921 reflections to a maximum θ angle of 28.50° (0.74 Å resolution), of which 3097 were independent (average redundancy 2.235, completeness = 98.8%, R_{int} = 1.23%, R_{sig} = 1.68%) and 3051 (98.51%) were greater than 2σ(F²). The final cell constants of \underline{a} = 6.3989(2) Å, \underline{b} = 7.1432(2) Å, \underline{c} = 27.0217(7) Å, volume = 1235.12(6) Å³, are based upon the refinement of the XYZ-centroids of 7019 reflections above 20 σ(I) with 5.899° < 2θ < 68.62°. Data were corrected for absorption effects using the Multi-Scan method (SADABS). The ratio of minimum to maximum apparent transmission was 0.873. The calculated minimum and maximum transmission coefficients (based on crystal size) are 0.9620 and 0.9680. The structure was solved and refined using the Bruker SHELXTL Software Package, using the space group P 21 21 21, with Z = 4 for the formula unit, C₁₄H₁₈O₃. The final anisotropic full-matrix least-squares refinement on F² with 157 variables converged at R1 = 2.82%, for the observed data and wR2 = 7.36% for all data. The goodness-of-fit was 1.063. The largest peak in the final difference electron density synthesis was 0.278 e⁻/Å³ and the largest hole was -0.163 e⁻/Å³ with an RMS deviation of 0.033 e⁻/Å³. On the basis of the final model, the calculated density was 1.260 g/cm³ and F(000), 504 e⁻.

10. References

1. Mintz, M. J.; Walling, C., *Org. Synth.* **1973**, *5*, 184-187.
2. (a) Wirschun, W.; Winkler, M.; Lutz, K.; Jochims, J. C., *J. Chem. Soc., Perkin Trans.* **1998**, 1755-1762; (b) Wirschun, W., *J. Prakt. Chem.* **1998**, *340*, 300-308; (c) Al-Masoudi, N.; Hassan, N. A.; Al-Soud, Y. A.; Schmidt, P.; Gaafar, A. E.-D. M.; Weng, M.; Marino, S.; Schoch, A.; Amer, A.; Jochims, J. C., *J. Chem. Soc., Perkin Trans.* **1998**, *1998*, 947-954.
3. Bouffard, J.; Keitz, B. K.; Tonner, R.; Lavallo, V.; Guisado-Barrios, G.; Frenking, G.; Grubbs, R. H.; Bertrand, G., *Organometallics* **2011**, *30*, 2617-2627.
4. Hettmanczyk, L.; Manck, S.; Hoyer, C.; Hohloch, S.; Sarkar, B., *Chem. Commun.* **2015**, *51*, 10949-10952.
5. Zhao, X.-F.; Zhang, C., *Synthesis* **2007**, *2007*, 551-557.
6. Huang, L.; Rominger, F.; Rudolph, M.; Hashmi, A. S. K., *Chem. Commun.* **2016**, *52*, 6435-6438.
7. Nagumo, S.; Ono, M.; Kakimoto, Y.-i.; Furukawa, T.; Hisano, T.; Mizukami, M.; Kawahara, N.; Akita, H., *J. Org. Chem.* **2002**, *67*, 6618-6622.
8. Zhang, G.; Cui, L.; Wang, Y.; Zhang, L., *J. Am. Chem. Soc.* **2010**, *132*, 1474-1475.
9. Ariyaratna, J. P.; Wu, F.; Colombo, S. K.; Hillary, C. M.; Li, W., *Org. Lett.* **2018**, *20*, 6462-6466.
10. Berg, N.; Bergwinkl, S.; Nuernberger, P.; Horinek, D.; Gschwind, R. M., *J. Am. Chem. Soc.* **2021**, *143*, 724-735.
11. (a) Rigoulet, M.; Thillaye du Boullay, O.; Amgoune, A.; Bourissou, D., *Angew. Chem. Int. Ed.* **2020**, *59*, 16625-16630; (b) Chintawar, C. C.; Yadav, A. K.; Patil, N. T., *Angew. Chem. Int. Ed.* **2020**, *59*, 11808-11813.

ANNEX 3. Supporting information Chapter IV

SUPPORTING INFORMATION

Novel NHC-based Au(I) complexes as precursors of highly pure Au(0) nuggets under oxidative conditions

Pau Font,[†] Nikolaos V. Tzouras,[‡] Argyro T. Papastavrou,[‡] Georgios C. Vougioukalakis,^{‡,*} Xavi Ribas^{†,*}

Table of Contents

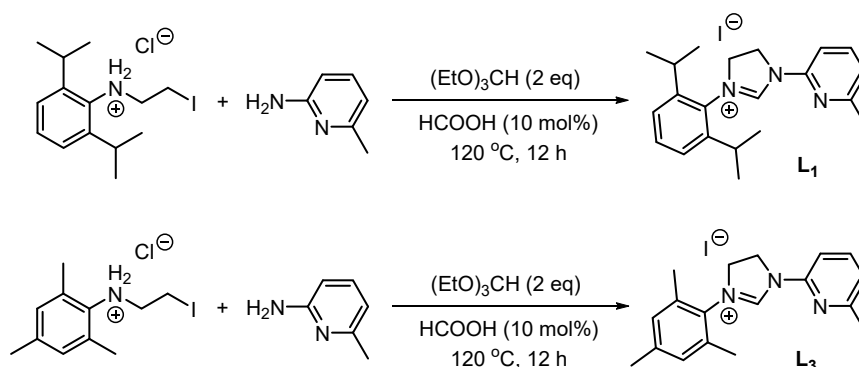
S1. General considerations	3
S2. Synthesis of imidazolinium salts	3
S3. Synthesis of gold(I) complexes	5
<i>S3.1. General procedure for the synthesis of complexes 1, 2 and 3</i>	5
<i>S3.2. Synthesis of complex 4</i>	7
S4. Reactivity and products	8
S5. NMR, HRMS-ESI and IR spectra	10
<i>S5.1. Compound L1</i>	10
<i>S5.2. Compound L3</i>	11
<i>S5.3. Complex 1</i>	13
<i>S5.4. Complex 2</i>	17
<i>S5.5. Complex 3</i>	20
<i>S5.6. Complex 4</i>	23
<i>S5.7. Compound L1^{ox}-I</i>	27
<i>S5.8. Compound L2^{ox}</i>	32
<i>S5.9. Compound L2^{ox}-I</i>	35
<i>S5.10. Compound L3^{ox}</i>	38
S6. Experiments using water and ¹⁸O-labeled water as additive	42
S7. X-Ray structures and crystallographic data	44
<i>S7.1. Complex 1</i>	44
<i>S7.2. Complex 2</i>	45
<i>S7.3. Complex 3</i>	47
<i>S7.4. Complex 4</i>	48
S8. SEM-EDX characterization of Au(0) macroaggregates	50
<i>S8.1. SEM images</i>	50
<i>S8.2. SEM-EDX analysis</i>	53
S9. Heterogeneous Au(0) catalysis attempts	57
S10. References	58

S1. General considerations

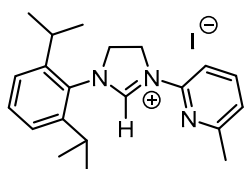
All reagents and solvents were purchased from Sigma Aldrich, Fischer Scientific, TCI or Fluorochem and were used without further purification. NMR spectra were recorded at 298K, unless otherwise specified, on Bruker spectrometers operating at 400 MHz (^1H NMR) and 101 MHz ($^{13}\text{C}\{^1\text{H}\}$ NMR), or on a Varian Mercury 200 MHz spectrometer, and referenced to residual solvents (δ in ppm and J in hertz). High resolution mass spectra (HRMS) were recorded on a Bruker MicroTOF-Q IITM or a QTOF maxis Impact (Bruker) spectrometer using ESI source at Serveis Tècnics de Recerca, University of Girona, or at the National and Kapodistrian University of Athens. For reactions carried out under an inert atmosphere, a N_2 drybox with O_2 and H_2O concentrations <1 ppm was employed, or standard Schleck techniques were followed. SEM images of the Au(0) nuggets were carried out with a scanning electron microscope (FE-SEM Hitachi, Japan, S-4100). Digital images were collected and processed by the Quarz PCI program. SEM-EDX analysis was performed with a scanning electron microscope (Zeiss DSM 960 Germany, EDX Bruker, Quantax Esprit Spectrometer SVE III).

S2. Synthesis of imidazolinium salts

Imidazolinium salts **L2** and **L4** were prepared according to the procedures outlined in the literature.^{1,2} Imidazolinium salts **L1** and **L3** were prepared according to the procedures³ outlined in the literature with the modifications illustrated in Scheme S1.

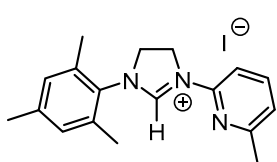


Scheme S1. General reaction conditions for the synthesis of imidazolinium salts **L1** and **L3**.



L1. To a mixture of N-(2-iodoethyl)-2,6-diisopropylbenzenaminium chloride (1.4 g, 3.81 mmol, prepared as described in the literature³), 6-methylpyridin-2-amine (0.41 g, 3.81 mmol) and triethylorthoformate (1.27 mL, 7.62 mmol) in a flame-dried pressure tube with a screw-top cap and a magnetic stirring bar, a catalytic amount of formic acid (14 μL , 10 mol%) was added via micropipette under argon, and the mixture was heated to $120\text{ }^\circ\text{C}$ in a pre-heated oil bath for 12 h. Toluene was added to the resulting dark mixture, and since no precipitation was observed, the mixture was transferred to a larger vessel and the solvent was removed. The mixture was dried for a prolonged period of time under vacuum on a rotary evaporator, as well as under high vacuum to remove the excess of triethylorthoformate and other volatile impurities

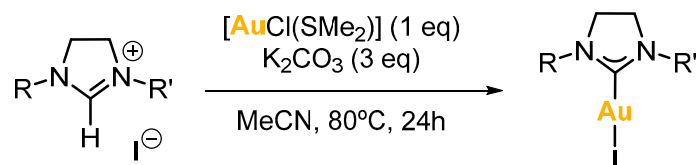
inhibiting precipitation. The resulting viscous red/brown residue was dissolved in a minimal amount of pure acetone and trituration with diethyl ether, leading to the precipitation of a solid. The solid was collected on a frit, washed with toluene (2x5 mL) and diethyl ether (2x5 mL), and then dried under vacuum. This process was repeated once on the supernatant, affording the product as a light brown powder in 22% yield (375 mg, 0.83 mmol). **¹H NMR** (200 MHz, CDCl₃) δ 9.23 (s, 1H, N(CH)N), 7.81 (t, *J* = 7.8 Hz, 1H, CH_{py}), 7.56 – 7.44 (m, 1H, CH_{Ar}), 7.38 (d, *J* = 8.3 Hz, 1H, CH_{py}), 7.32 (d, *J* = 7.5 Hz, 2H, CH_{Ar}), 7.15 (d, *J* = 7.7 Hz, 1H, CH_{py}), 5.20 (t, *J* = 11.1 Hz, 2H, NCH₂), 4.91 – 4.62 (m, 2H, NCH₂), 3.12 – 2.96 (m, 2H, CH(CH₃)₂), 2.48 (s, 3H, CH₃), 1.36 (d, *J* = 6.8 Hz, 6H, CH(CH₃)₂), 1.30 (d, *J* = 6.8 Hz, 6H, CH(CH₃)₂). **¹³C{¹H} NMR** (50 MHz, CDCl₃) δ 158.7, 153.6, 146.7, 146.2, 140.2, 131.7, 129.7, 125.2, 122.7, 109.3, 55.7 (NCH₂), 48.7 (NCH₂), 28.9 (CH(CH₃)₂), 25.2 (CH(CH₃)₂), 24.4 (CH(CH₃)₂), 24.2 (CH₃). **HRMS (ESI+)**: calcd for C₂₁H₂₈N₃⁺ [M]⁺: *m/z* 322.2278; found: *m/z* 322.2299.



L3. To a mixture of N-(2-iodoethyl)-2,4,6-trimethylbenzenaminium chloride (977 mg, 3.0 mmol, prepared as described in the literature³), 6-methylpyridin-2-amine (324 mg, 3.0 mmol) and triethylorthoformate (1.0 mL, 6.0 mmol) in a flame-dried pressure tube with a screw-top cap and a magnetic stirring bar, a catalytic amount of formic acid (10 mol%) was added via micropipette under argon, and the mixture was heated to 120 °C in a pre-heated oil bath for 12 h. Toluene was added to the resulting mixture and a precipitate formed. The solid was collected on a frit, washed with toluene (2x5 mL) and diethyl ether (2x5 mL) and then dried under vacuum. Gradient column chromatography on silica gel using DCM/MeOH 95/5-90/10 afforded the product as a white powder in an 8% yield (102 mg, 0.25 mmol). **¹H NMR** (200 MHz, CDCl₃) δ 9.68 (s, 1H, N(CH)N), 7.89 – 7.72 (m, 1H, CH_{py}), 7.54 (d, *J* = 8.2 Hz, 1H, CH_{py}), 7.13 (d, *J* = 7.4 Hz, 1H, CH_{py}), 7.01 (s, 2H, CH_{Ar}), 5.34 – 4.87 (m, 2H, NCH₂), 4.75 – 4.55 (m, 2H, NCH₂), 2.50 (s, 3H, CH₃), 2.41 (s, 6H, 2xCH₃), 2.33 (s, 3H, CH₃). **¹³C{¹H} NMR** (50 MHz, CDCl₃) δ 158.4, 153.9, 146.5, 140.7, 139.7, 134.7, 130.1, 129.9, 122.2, 108.8, 53.1 (NCH₂), 48.1 (NCH₂), 24.0 (CH₃), 20.9 (CH₃), 18.5 (CH₃, 2C). **HRMS (ESI+)**: calcd for C₂₁H₂₈N₃⁺ [M]⁺: *m/z* 280.1808; found: *m/z* 280.1841.

S3. Synthesis of gold(I) complexes

S3.1. General procedure for the synthesis of complexes 1, 2 and 3



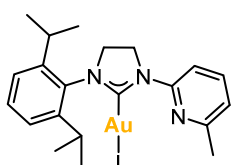
L1 R = Dipp, R' = 2-(6-methylpyridinyl)

L2 R = Dipp, R' = 8-quinolinyl

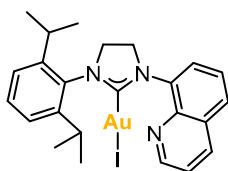
L3 R = Mes, R' = 2-(6-methylpyridinyl)

Scheme S2. General reaction conditions for the synthesis of complexes **1**, **2** and **3**.

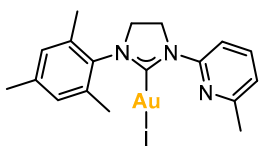
For the synthesis of NHC-Au(I) complexes **1**, **2** and **3**, the corresponding imidazolium salt **L1**, **L2** or **L3** (1 eq), chloro(dimethylsulfide)gold(I) (1 eq), and potassium carbonate (3 eq), were reacted in acetonitrile for 24 hours at 80°C. After this time, the reaction mixture was filtered over Celite® and all volatiles were removed under vacuum. The product was purified by column chromatography. The fractions that contained the product were combined, and the solvent was removed under vacuum to afford the gold(I) complexes as solids.



Complex 1. The imidazolium iodide salt **L1** (102.4 mg, 0.23 mmol, 1.0 eq.), K_2CO_3 (126.7 mg, 0.92 mmol, 4.0 eq.) and $[AuCl(SMe_2)]$ (87.2 mg, 0.30 mmol, 1.3 eq.) were reacted in acetonitrile (1 mL). The product was purified by column chromatography using DCM:hexane (4:1). By slow diffusion of pentane into a concentrated solution of complex **1** in chloroform, pale yellow crystals suitable for X-ray diffraction analysis were obtained (59.3 mg, 40% yield). 1H NMR (400 MHz, $CDCl_3$) δ 8.58 (d, $J = 8.3$ Hz, 1H, CH_{py}), 7.63 (t, $J = 7.8$ Hz, 1H, CH_{py}), 7.43 (t, $J = 7.8$ Hz, 1H, CH_{Ar}), 7.24 (d, $J = 7.8$ Hz, 2H, CH_{Ar}), 7.02 (d, $J = 7.5$ Hz, 1H, CH_{py}), 4.59 – 4.52 (m, 2H, NCH_2), 3.95 – 3.87 (m, 2H, NCH_2), 2.97 (hept, $J = 6.8$ Hz, 2H, $CH(CH_3)_2$), 2.53 (s, 3H, CH_3), 1.39 (d, $J = 6.8$ Hz, 6H, $CH(CH_3)_2$), 1.26 (d, $J = 6.9$ Hz, 6H, $CH(CH_3)_2$). $^{13}C\{^1H\}$ NMR (101 MHz, $CDCl_3$) δ 201.0 ($C_{carbene-Au}$), 157.3 (C_{py}), 151.9 (C_{py}), 146.2 (C_{Ar} , 2C), 138.3 (CH_{py}), 134.7 (C_{Ar}), 130.3 (CH_{Ar}), 124.8 (CH_{Ar} , 2C), 120.5 (CH_{py}), 111.4 (CH_{py}), 53.1 (NCH_2), 48.7 (NCH_2), 28.7 ($CH(CH_3)_2$, 2C), 25.0 ($CH(CH_3)_2$, 2C), 24.6 ($CH(CH_3)_2$, 2C), 24.4 (CH_3). **HRMS (ESI+):** calcd for $C_{21}H_{27}AuIN_3$ $[M+H]^+$: m/z 646.0988; found: m/z 646.0984; $[M+Na]^+$: m/z 668.0807; found: 668.0840; $[2M-I]^+$: m/z 1163.2780; found: 1163.2804. **IR-FT (ATR)** $\tilde{\nu}$ (cm^{-1}): 2961, 2923, 2862, 1710, 1676, 1595, 1576, 1493, 1431, 1320, 1274, 1054, 810, 787, 766, 735, 663, 457.

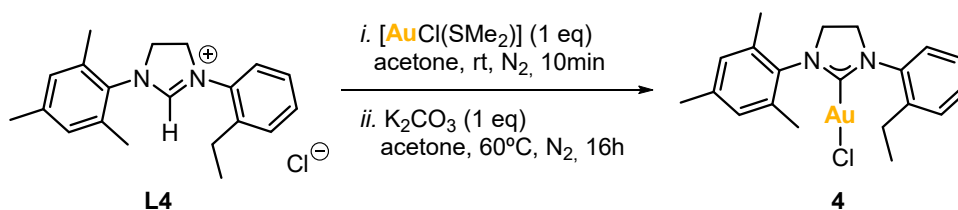


Complex 2. The imidazolium iodide salt **L2** (180.0 mg, 0.37 mmol, 1.0 eq.), K_2CO_3 (261.2 mg, 1.89 mmol, 5.1 eq.) and $[AuCl(SMe_2)]$ (139.1 mg, 0.47 mmol, 1.3 eq.) were reacted in acetonitrile (2 mL). After the filtration over Celite®, the product was purified by filtering the residue over a pad of silica using DCM. The solvent was removed to obtain a yellow solid. It was washed with hexane and diethyl ether to afford complex **2** as a white solid (105.8 mg, 42% yield). 1H NMR (400 MHz, $CDCl_3$) δ 8.96 (dd, $J = 4.2, 1.7$ Hz, 1H, CH_{Quin}), 8.23 (dd, $J = 8.3, 1.7$ Hz, 1H, CH_{Quin}), 8.10 (dd, $J = 7.3, 1.4$ Hz, 1H, CH_{Quin}), 7.87 (dd, $J = 8.2, 1.4$ Hz, 1H, CH_{Quin}), 7.60 (dd, $J = 8.3, 7.4$ Hz, 1H, CH_{Quin}), 7.50 (dd, $J = 8.3, 4.2$ Hz, 1H, CH_{Quin}), 7.42 (t, $J = 7.8$ Hz, 1H, CH_{Ar}), 7.25 (d, $J = 7.8$ Hz, 2H, CH_{Ar}), 4.72 – 4.64 (m, 2H, NCH_2), 4.12 – 4.04 (m, 2H, NCH_2), 3.23 (hept, $J = 6.9$ Hz, 2H, $CH(CH_3)_2$), 1.43 (d, $J = 6.8$ Hz, 6H, $CH(CH_3)_2$), 1.39 (d, $J = 6.8$ Hz, 6H, $CH(CH_3)_2$). $^{13}C\{^1H\}$ NMR (101 MHz, $CDCl_3$) δ 203.7 ($C_{carbene-Au}$), 150.4 (CH_{Quin}), 146.8 ($C_{Ar}, 2C$), 144.1 (C_{Quin}), 137.6 (C_{Quin}), 136.6 (CH_{Quin}), 134.6 (C_{Ar}), 130.0 (CH_{Ar}), 129.6 (C_{Quin}), 128.8 (CH_{Quin}), 128.3 (CH_{Quin}), 126.4 (CH_{Quin}), 124.7 ($CH_{Ar}, 2C$), 122.0 (CH_{Quin}), 54.4 (NCH_2), 53.0 (NCH_2), 28.7 ($CH(CH_3)_2, 2C$), 25.3 ($CH(CH_3)_2, 2C$), 24.6 ($CH(CH_3)_2, 2C$). HRMS (ESI+): calcd for $C_{24}H_{27}AuIN_3$ $[M+H]^+$: m/z 682.0988; found: m/z 682.0974; $[2M-I]^+$: m/z 1235.2780; found: 1235.2746.



Complex 3. The imidazolium iodide salt **L3** (67.5 mg, 0.17 mmol, 1.0 eq.), K_2CO_3 (91.1 mg, 0.66 mmol, 4.0 eq.) and $[AuCl(SMe_2)]$ (63.8 mg, 0.22 mmol, 1.3 eq.) were reacted in acetonitrile (1 mL). The product was purified by column chromatography using DCM. By slow diffusion of pentane into a concentrated solution of complex **3** in chloroform, crystals suitable for X-ray diffraction analysis were obtained (32.9 mg, 33% yield). 1H NMR (400 MHz, $CDCl_3$) δ 8.54 (d, $J = 8.2$ Hz, 1H, CH_{py}), 7.62 (t, $J = 7.9$ Hz, 1H, CH_{py}), 7.02 (d, $J = 7.5$ Hz, 1H, CH_{py}), 6.94 (s, 2H, CH_{Ar}), 4.57 – 4.48 (m, 2H, NCH_2), 3.94 – 3.85 (m, 2H, NCH_2), 2.52 (s, 3H, CH_{3py}), 2.30 (s, 3H, CH_{3Ar}), 2.27 (s, 6H, CH_{3Ar}). $^{13}C\{^1H\}$ NMR (101 MHz, $CDCl_3$) δ 192.2 ($C_{carbene-Au}$), 157.3 (C_{py}), 151.9 (C_{py}), 139.3 (C_{Ar}), 138.3 (CH_{py}), 135.5 (C_{Ar}), 135.1 ($C_{Ar}, 2C$), 130.0 ($CH_{Ar}, 2C$), 120.6 (CH_{py}), 112.0 (CH_{py}), 50.3 (NCH_2), 48.8 (NCH_2), 24.3 (CH_{3py}), 21.2 (CH_{3Ar}), 18.2 ($CH_{3Ar}, 2C$). HRMS (ESI+): calcd for $C_{18}H_{21}AuIN_3$ $[M+Na]^+$: m/z 626.0338; found: m/z 626.0336; $[(C_{18}H_{21}N_3)_2Au]^+$: m/z 755.3131; found: 755.3150; $[2M-I]^+$: m/z 1079.1841; found: 1079.1830.

S3.2. Synthesis of complex 4



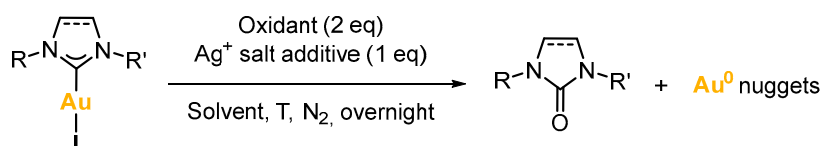
Scheme S3. Synthesis of complex 4.

For the synthesis of NHC-Au(I) complex **4**, imidazolium salt **L4** (60.1 mg, 0.18 mmol, 1.0 eq) and chloro(dimethylsulfide)gold(I) (54.8 mg, 0.19 mmol, 1.0 eq) were mixed in acetone (0.6 mL) under nitrogen atmosphere and stirred at room temperature for 10 minutes. Then, potassium carbonate (27.6 mg, 0.20 mmol, 1.1 eq) was added, and the mixture was stirred and heated at 60°C for 16 hours. After this time, the reaction mixture was cooled down to room temperature; then, the solvent was removed under reduced pressure, and DCM was added. The mixture was filtered over a pad of silica, which was washed with more DCM, and the resulting solution was concentrated to the minimal volume. Next, pentane was added to precipitate the desired product. It was washed with more pentane, and it was dried under vacuum. Complex **4** was obtained as a white solid (75.5 mg, 67% yield). **¹H NMR** (400 MHz, CDCl₃) δ 7.40 – 7.24 (m, 4H, CH_{Ar}), 6.94 (d, *J* = 0.7 Hz, 2H, CH_{Ar}), 4.11 (t, *J* = 9.6 Hz, 2H, NCH₂), 3.96 (td, *J* = 10.4, 1.7 Hz, 2H, NCH₂), 2.76 (q, *J* = 7.6 Hz, 2H, CH₂CH₃), 2.31 (s, 6H, CH₃), 2.30 (s, 3H, CH₃), 1.35 (t, *J* = 7.6 Hz, 3H, CH₂CH₃). **¹³C{¹H} NMR** (101 MHz, CDCl₃) δ 195.0 (C_{carbene}-Au), 141.2 (C_{Ar}), 139.1 (C_{Ar}), 138.4 (C_{Ar}), 135.6 (C_{Ar}, 2C), 134.8 (C_{Ar}), 129.9 (CH_{Ar}, 2C), 129.9 (CH_{Ar}), 129.5 (CH_{Ar}), 128.4 (CH_{Ar}), 127.5 (CH_{Ar}), 53.3 (NCH₂), 51.0 (NCH₂), 24.4 (CH₂CH₃), 21.2 (CH₃), 18.1 (CH₃, 2C), 15.0 (CH₂CH₃). **HRMS (ESI⁺)**: calcd for C₂₀H₂₄AuClN₂ [M+Na]⁺: *m/z* 547.1186; found: *m/z* 547.1181; [2M+Na]⁺: *m/z* 1071.2479; found: 1071.2438; [2M-Cl]⁺: *m/z* 1013.2899; found: 1013.2865. **IR-FT (ATR)** $\tilde{\nu}$ (cm⁻¹): 2951, 2919, 2863, 1500, 1453, 1437, 1321, 1276, 1194, 1120, 1034, 1018, 852, 844, 769, 739, 658, 606, 580, 572, 549, 517, 442.

S4. Reactivity and products

The gold(I) complexes were reacted with two equivalents of an oxidant and, in some cases, one equivalent of a silver salt was used as additive. The reactivity towards the formation of Au(0) nuggets and azolones is displayed in Table S1. All reactions were run in a sealed vial under nitrogen atmosphere, and were heated and stirred overnight in the absence of light.

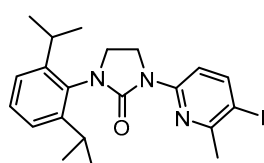
Table S1. Reactivity of gold(I) complexes towards the formation of Au(0) nuggets and azolones.



Entry	Complex	Oxidant	Additive	Solvent	T (°C)	Yield to Au(0)	NHC=O (yield %)*
1	1	PhI(OAc) ₂	AgOAc	1,2-DCE	90	75	Detected MS
2	1	PhI(OAc) ₂	-	1,2-DCE	90	46	Detected MS
3	1	PhI(OAc) ₂	-	MeCN	90	60	L1^{ox}-I (53)
4	1	H ₂ O ₂	AgOAc	1,2-DCE	90	0	0
5	1	H ₂ O ₂	-	1,2-DCE	90	0	Detected MS
6	1	PhICl ₂	-	DCM	rt	0	Detected MS
7	2	-	-	1,2-DCE	100	0	0
8	2	PhI(OAc) ₂	AgOAc	1,2-DCE	90	85	Detected MS
9	2	PhI(OAc) ₂	-	1,2-DCE	90	90	L2^{ox} (22) L2^{ox}-I (17)
10	2	PhI(OAc) ₂	AgOAc	DCM	70	91	Detected MS
11	2	PhI(OAc) ₂	-	MeCN	90	56	L2^{ox} (34)
12	2	CH ₃ CO ₃ H	-	1,2-DCE	90	34	Detected NMR
13	3	PhI(OAc) ₂	AgOAc	1,2-DCE	90	>99	L3^{ox} (60)
14	3	XeF ₂	-	CDCl ₃	rt	0	Detected MS
15	4	PhI(OAc) ₂	-	DCM	rt	0	0
16	4^a	PhI(OAc) ₂	-	DCM	100	97	Detected MS
17	4	PhI(OAc) ₂	-	1,2-DCE	90	32	Detected MS
18	(IPr)AuCl	PhI(OAc) ₂	AgOAc	1,2-DCE	90	0	0
19	(IPr)AuCl	PhI(OAc) ₂	-	1,2-DCE	90	0	0
20	(SIPr)AuCl	PhI(OAc) ₂	AgOAc	1,2-DCE	90	0	0
21	(SIPr)AuCl	PhI(OAc) ₂	-	1,2-DCE	90	11	6

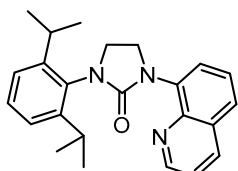
*Isolated yield. ^a5h of reaction.

The azolones that were isolated from the reaction crudes were characterized by NMR and HRMS as described below.

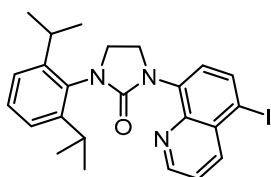


Compound L1^{ox}-I. ¹H NMR (400 MHz, 228K, CDCl₃) δ 7.91 – 7.83 (m, 2H, CH_{py}), 7.38 (t, *J* = 7.7 Hz, 1H, CH_{Ar}), 7.23 (d, *J* = 7.6 Hz, 2H, CH_{Ar}), 4.23 (t, *J* = 8.2 Hz, 2H, NCH₂), 3.71 (t, *J* = 8.2 Hz, 2H, NCH₂), 2.98 (hept, *J* = 6.8 Hz, 2H, CH(CH₃)₂), 2.63 (s, 3H, CH₃), 1.23 (d, *J* = 6.9 Hz, 6H, CH(CH₃)₂), 1.20 (d, *J* = 6.6 Hz, 6H, CH(CH₃)₂). ¹³C{¹H} NMR (101 MHz, CDCl₃) δ 157.7 (C_{py}), 156.2 (C=O), 152.1 (C_{py}), 148.0 (C_{Ar}, 2C), 147.3 (CH_{py}), 132.8 (C_{Ar}), 129.2 (CH_{Ar}), 124.3 (CH_{Ar}, 2C), 112.2

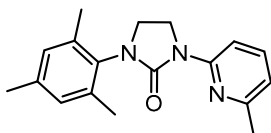
(CH_{py}), 86.2 (C_{py}-I), 45.7 (NCH₂), 41.7 (NCH₂), 28.9 (CH(CH₃)₂, 2C), 28.8 (CH₃), 24.6 (CH(CH₃)₂, 2C), 24.4 (CH(CH₃)₂, 2C). **HRMS (ESI+)**: calcd for C₂₁H₂₆IN₃O [M+H]⁺: *m/z* 464.1193; found: *m/z* 464.1193; [M+Na]⁺: *m/z* 486.1013; found: *m/z* 486.1012; [2M+Na]⁺: *m/z* 949.2133; found: *m/z* 949.2141.



Compound L2^{ox}. **¹H NMR** (400 MHz, CDCl₃) δ 8.93 (dd, *J* = 4.2, 1.8 Hz, 1H, CH_{Ar}), 8.17 (dd, *J* = 8.3, 1.8 Hz, 1H, CH_{Ar}), 7.93 (dd, *J* = 7.5, 1.4 Hz, 1H, CH_{Ar}), 7.71 (dd, *J* = 8.2, 1.4 Hz, 1H, CH_{Ar}), 7.56 (dd, *J* = 8.2, 7.5 Hz, 1H, CH_{Ar}), 7.42 (dd, *J* = 8.3, 4.1 Hz, 1H, CH_{Ar}), 7.35 (dd, *J* = 8.3, 7.1 Hz, 1H, CH_{Ar}), 7.23 (d, *J* = 7.7 Hz, 2H, CH_{Ar}), 4.45 – 4.40 (m, 2H, NCH₂), 3.90 – 3.84 (m, 2H, NCH₂), 3.32 (hept, *J* = 6.9 Hz, 2H, CH(CH₃)₂), 1.32 (d, *J* = 6.9 Hz, 6H, CH(CH₃)₂), 1.30 (d, *J* = 6.8 Hz, 6H, CH(CH₃)₂). **¹³C{¹H} NMR** (101 MHz, CDCl₃) δ 159.5 (C=O), 149.3 (CH_{Quin}), 148.5 (C_{Ar}, 2C), 144.3 (C_{Quin}), 138.3 (C_{Quin}), 136.5 (CH_{Quin}), 133.8 (C_{Ar}), 129.7 (C_{Quin}), 128.8 (CH_{Ar}), 127.5 (CH_{Quin}), 126.7 (CH_{Quin}), 126.1 (CH_{Quin}), 124.2 (CH_{Ar}, 2C), 121.3 (CH_{Quin}), 47.4 (NCH₂), 47.0 (NCH₂), 28.8 (CH(CH₃)₂, 2C), 24.8 (CH(CH₃)₂, 2C), 24.5 (CH(CH₃)₂, 2C). **HRMS (ESI+)**: calcd for C₂₄H₂₇N₃O [M+H]⁺: *m/z* 374.2227; found: *m/z* 374.2211; [M+Na]⁺: *m/z* 396.2046; found: 396.2036; [2M+Na]⁺: *m/z* 769.4200; found: *m/z* 769.4164.



Compound L2^{ox}-I. **¹H NMR** (400 MHz, CDCl₃) δ 8.88 (dd, *J* = 4.1, 1.6 Hz, 1H, CH_{Quin}), 8.39 (dd, *J* = 8.5, 1.6 Hz, 1H, CH_{Quin}), 8.13 (d, *J* = 8.1 Hz, 1H, CH_{Quin}), 7.69 (d, *J* = 8.0 Hz, 1H, CH_{Quin}), 7.49 (dd, *J* = 8.6, 4.1 Hz, 1H, CH_{Quin}), 7.35 (dd, *J* = 8.3, 7.1 Hz, 1H, CH_{Ar}), 7.23 (d, *J* = 7.4 Hz, 2H, CH_{Ar}), 4.46 – 4.39 (m, 2H, NCH₂), 3.89 – 3.83 (m, 2H, NCH₂), 3.28 (hept, *J* = 6.9 Hz, 2H, CH(CH₃)₂), 1.32 (d, *J* = 6.9 Hz, 6H, CH(CH₃)₂), 1.29 (d, *J* = 6.8 Hz, 6H, CH(CH₃)₂). **¹³C{¹H} NMR** (101 MHz, CDCl₃) δ 159.2 (C=O), 149.9 (CH_{Quin}), 148.4 (C_{Ar}, 2C), 144.8 (C_{Quin}), 140.9 (CH_{Quin}), 139.4 (C_{Quin}), 137.7 (CH_{Quin}), 133.5 (C_{Ar}), 131.2 (C_{Quin}), 129.0 (CH_{Ar}), 128.5 (CH_{Quin}), 124.2 (CH_{Ar}, 2C), 122.9 (CH_{Quin}), 95.3 (C_{Quin}-I), 47.4 (NCH₂), 47.0 (NCH₂), 28.8 (CH(CH₃)₂, 2C), 24.8 (CH(CH₃)₂, 2C), 24.5 (CH(CH₃)₂, 2C). **HRMS (ESI+)**: calcd for C₂₄H₂₆IN₃O [M+H]⁺: *m/z* 500.1193; found: *m/z* 500.1184; [M+Na]⁺: *m/z* 522.1013; found: 522.0999.



Compound L3^{ox}. **¹H NMR** (400 MHz, CDCl₃) δ 8.11 (d, *J* = 8.4 Hz, 1H, CH_{py}), 7.51 (t, *J* = 7.9 Hz, 1H, CH_{py}), 6.93 (s, 2H, CH_{Ar}), 6.78 (d, *J* = 7.3 Hz, 1H, CH_{py}), 4.31 – 4.23 (m, 2H, NCH₂), 3.74 – 3.67 (m, 2H, NCH₂), 2.47 (s, 3H, CH_{3py}), 2.29 (s, 3H, CH_{3Ar}), 2.25 (s, 6H, CH_{3Ar}). **¹³C{¹H} NMR** (101 MHz, CDCl₃) δ 156.3 (C_{py}), 155.9 (C=O), 152.4 (C_{py}), 138.0 (C_{Ar}), 137.7 (CH_{py}), 137.0 (C_{Ar}, 2C), 133.1 (C_{Ar}), 129.5 (CH_{Ar}, 2C), 116.8 (CH_{py}), 109.9 (CH_{py}), 43.2 (NCH₂), 42.0 (NCH₂), 24.5 (CH_{3py}), 21.1 (CH_{3Ar}), 18.0 (CH_{3Ar}, 2C). **HRMS (ESI+)**: calcd for C₁₈H₂₁N₃O [M+H]⁺: *m/z* 296.1757; found: *m/z* 296.1774; [M+Na]⁺: *m/z* 318.1577; found: 318.1595; [2M+Na]⁺: *m/z* 613.3261; found: *m/z* 613.3278.

S5. NMR, HRMS-ESI and IR spectra

S5.1. Compound L1

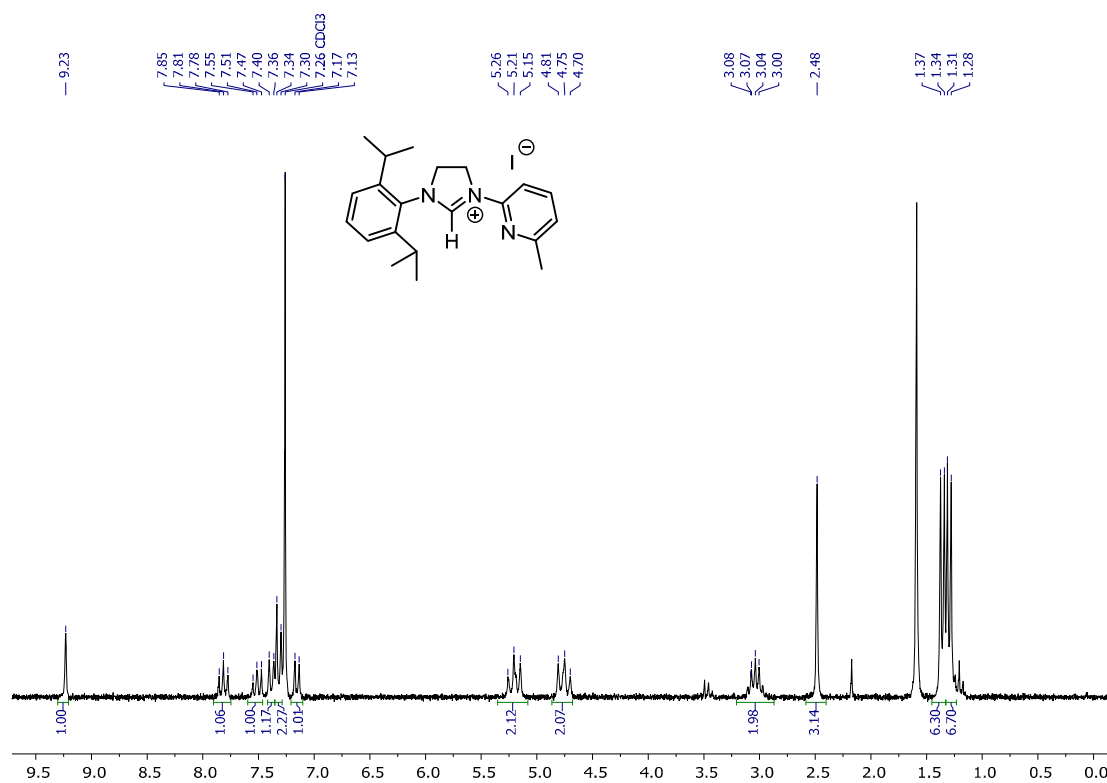


Figure S1. ^1H NMR (200MHz, 298K) of L1 in CDCl_3 .

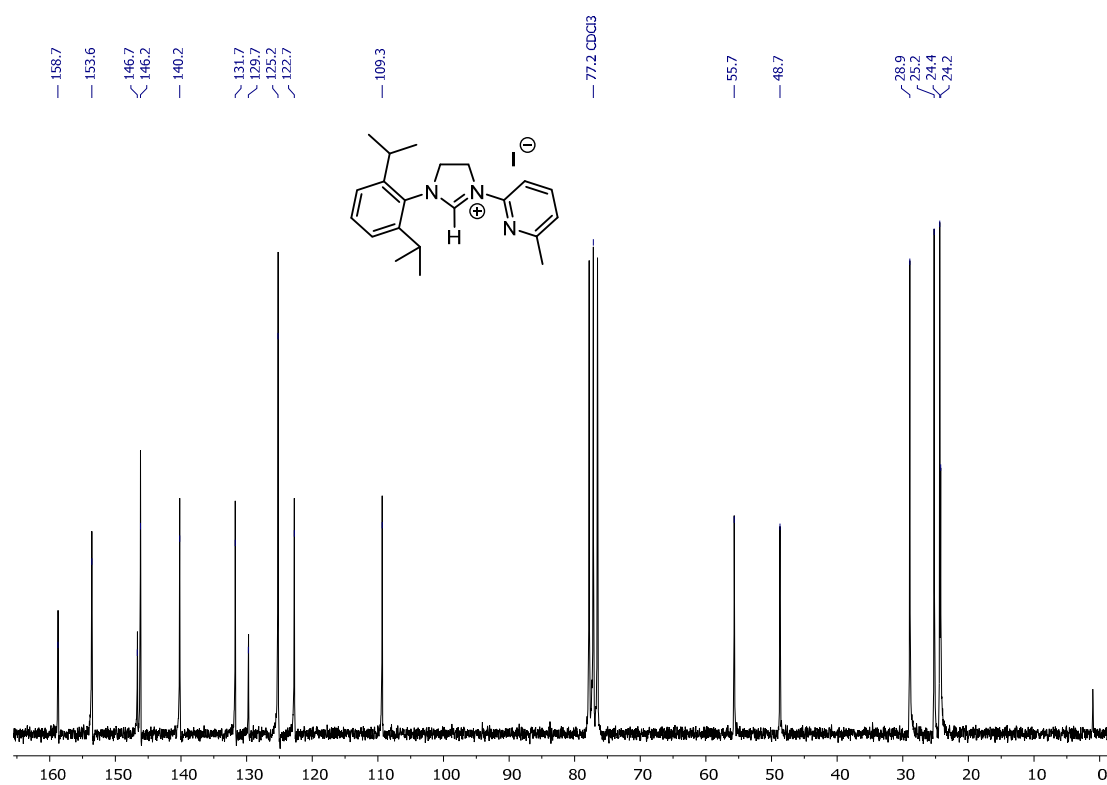


Figure S2. $^{13}\text{C}\{^1\text{H}\}$ NMR (50MHz, 298K) of L1 in CDCl_3 .

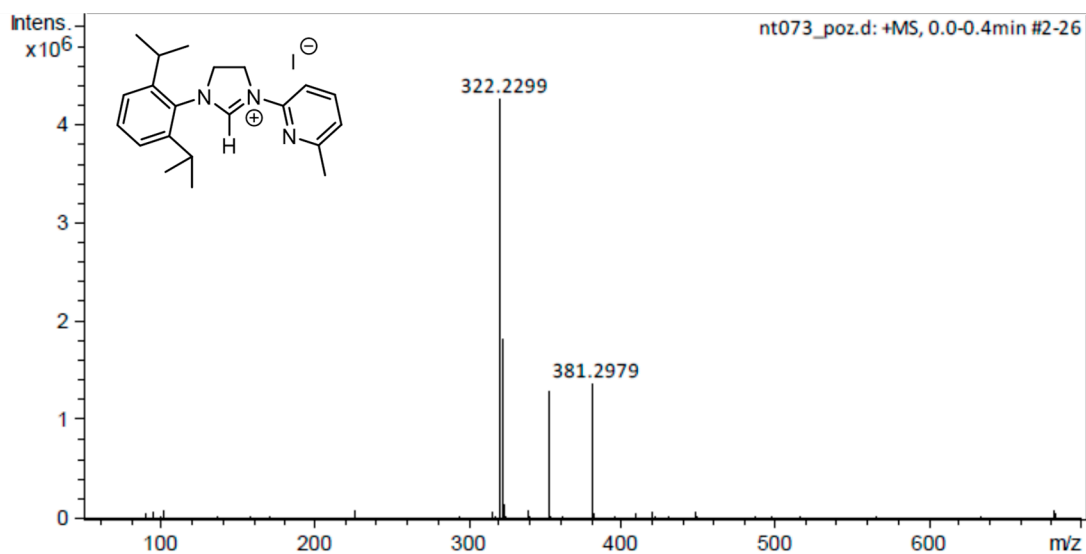


Figure S3. HRMS-ESI(+) of L1.

S5.2. Compound L3

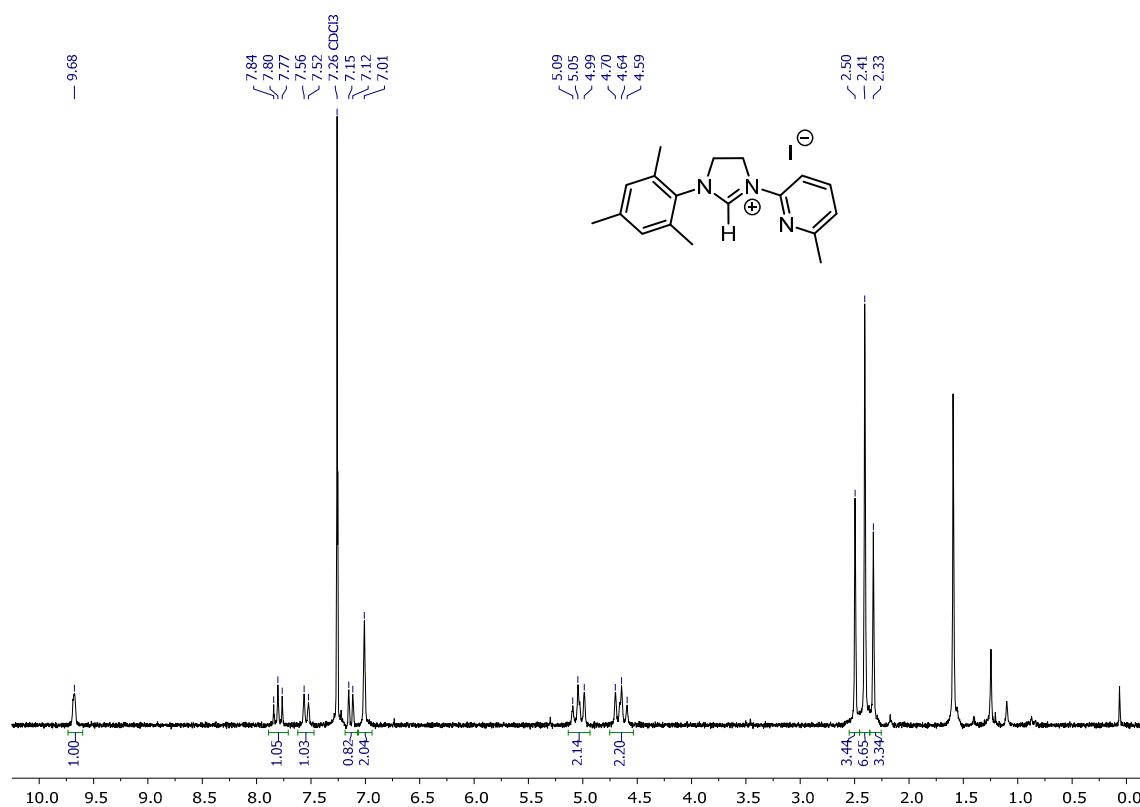


Figure S4. ¹H NMR (200MHz, 298K) of L3 in CDCl₃.

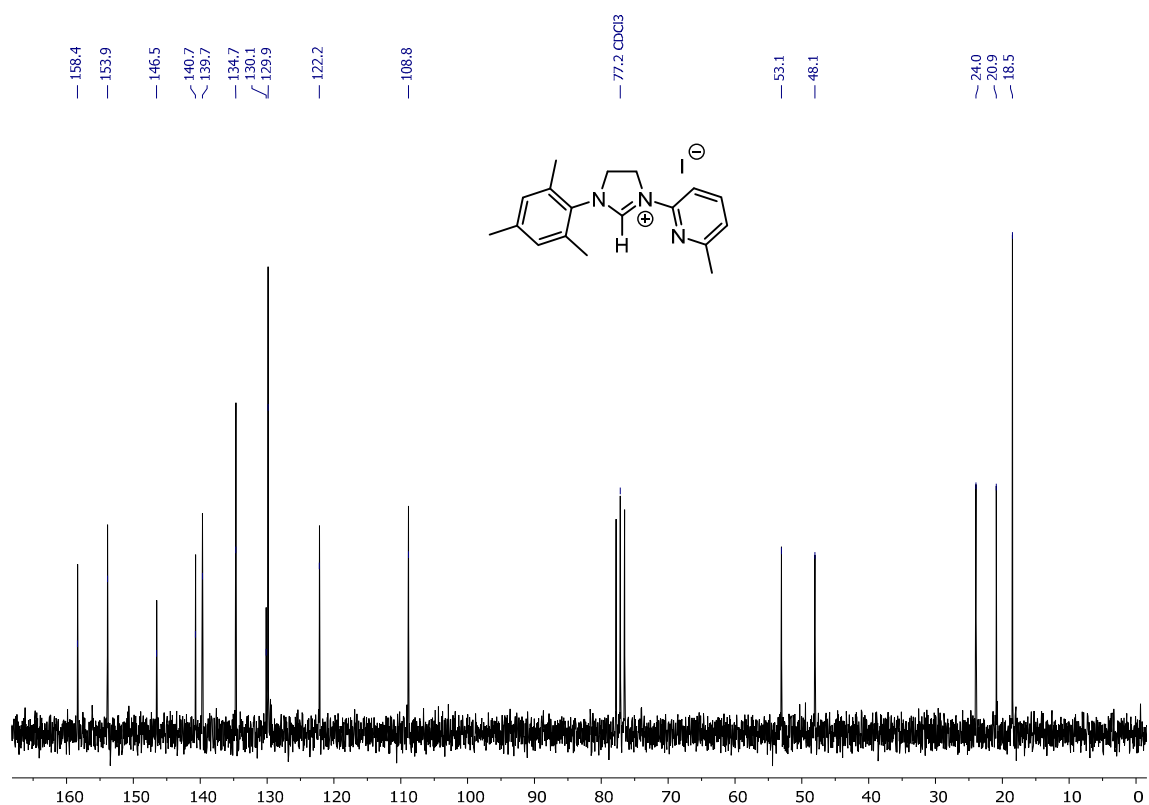


Figure S5. ¹³C{¹H} NMR (50MHz, 298K) of L3 in CDCl₃.

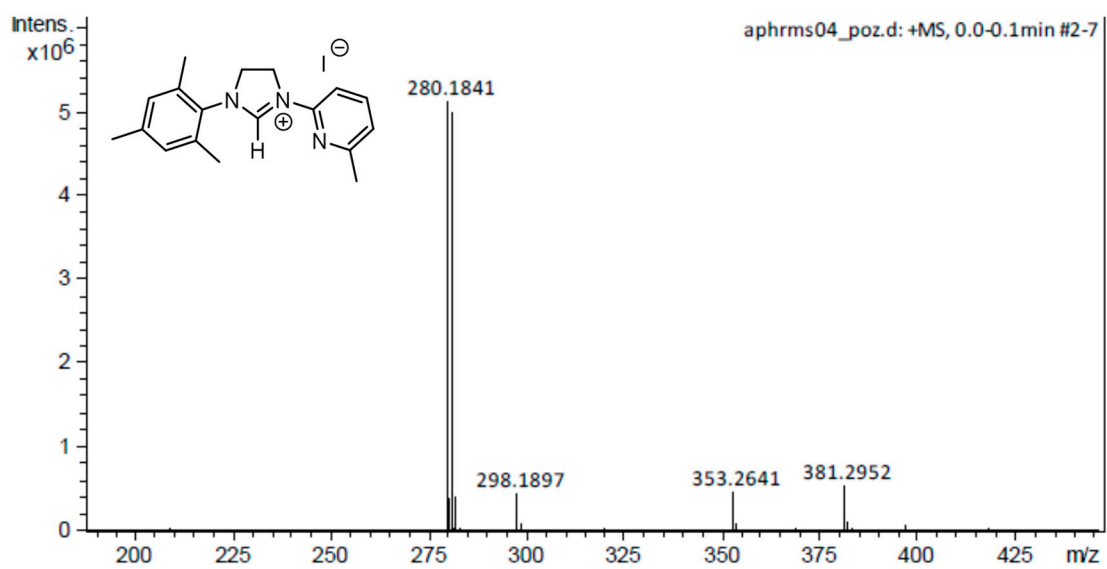
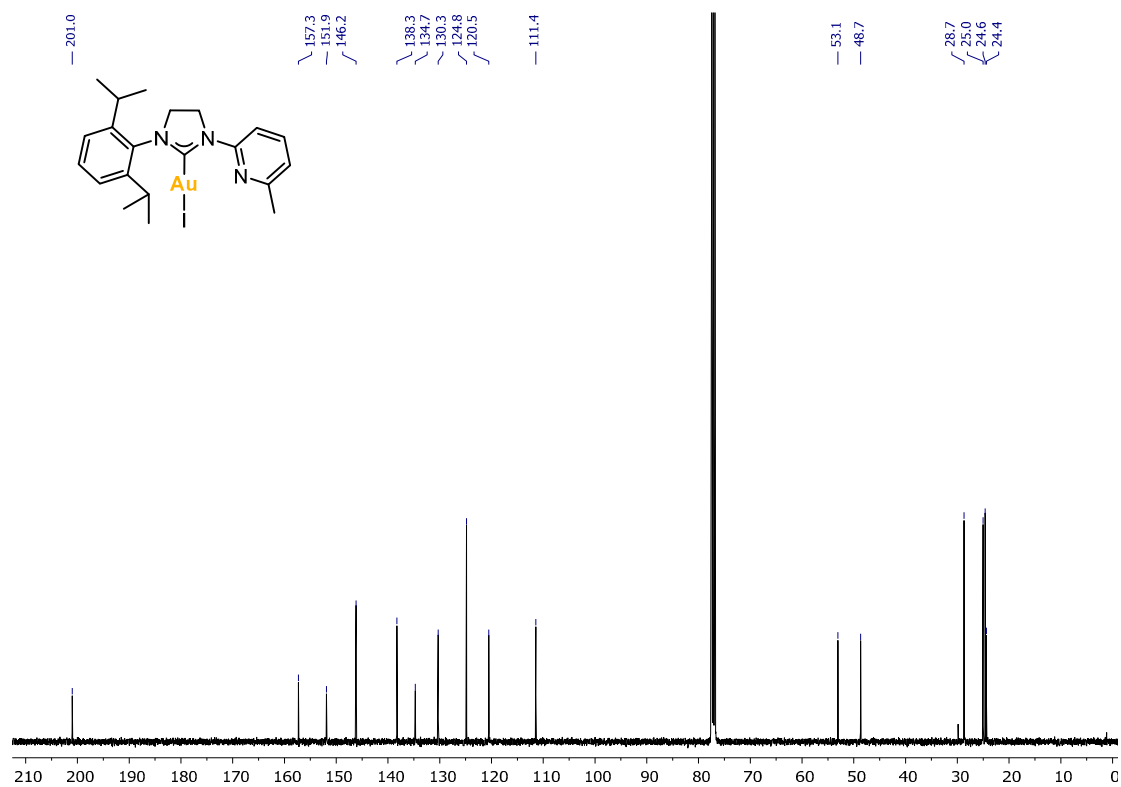
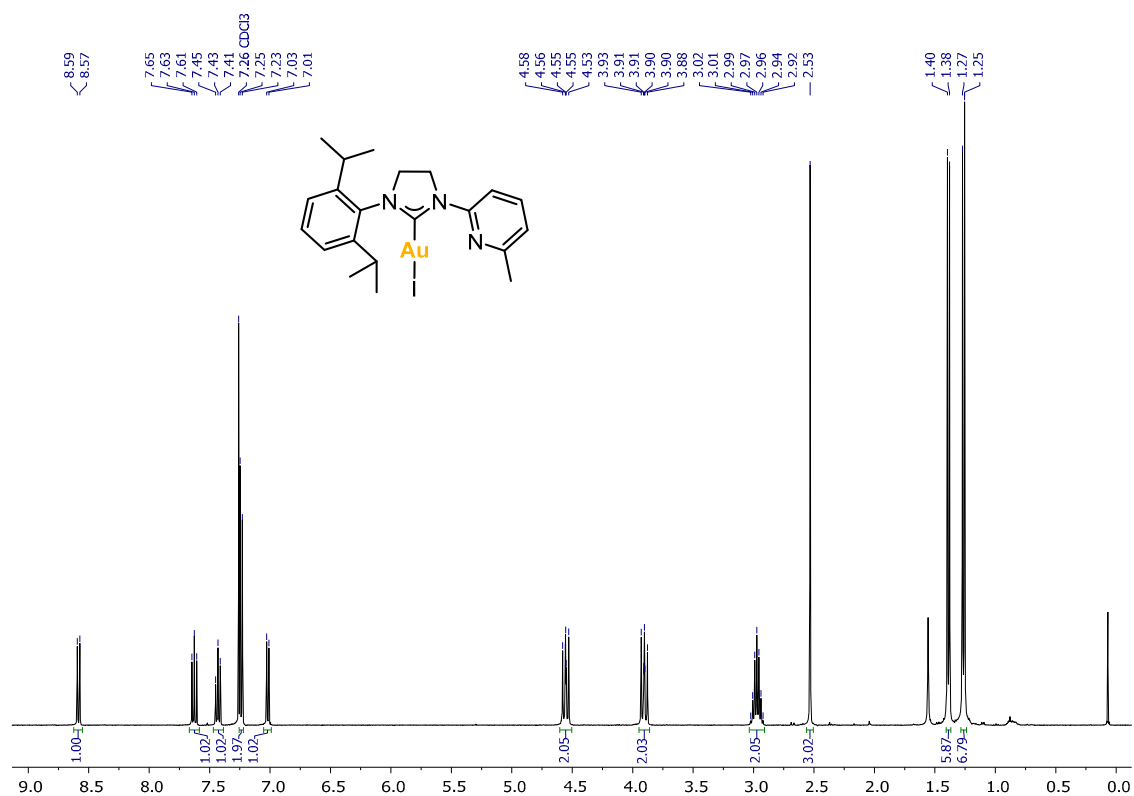


Figure S6. HRMS-ESI(+) of L3.

S5.3. Complex 1



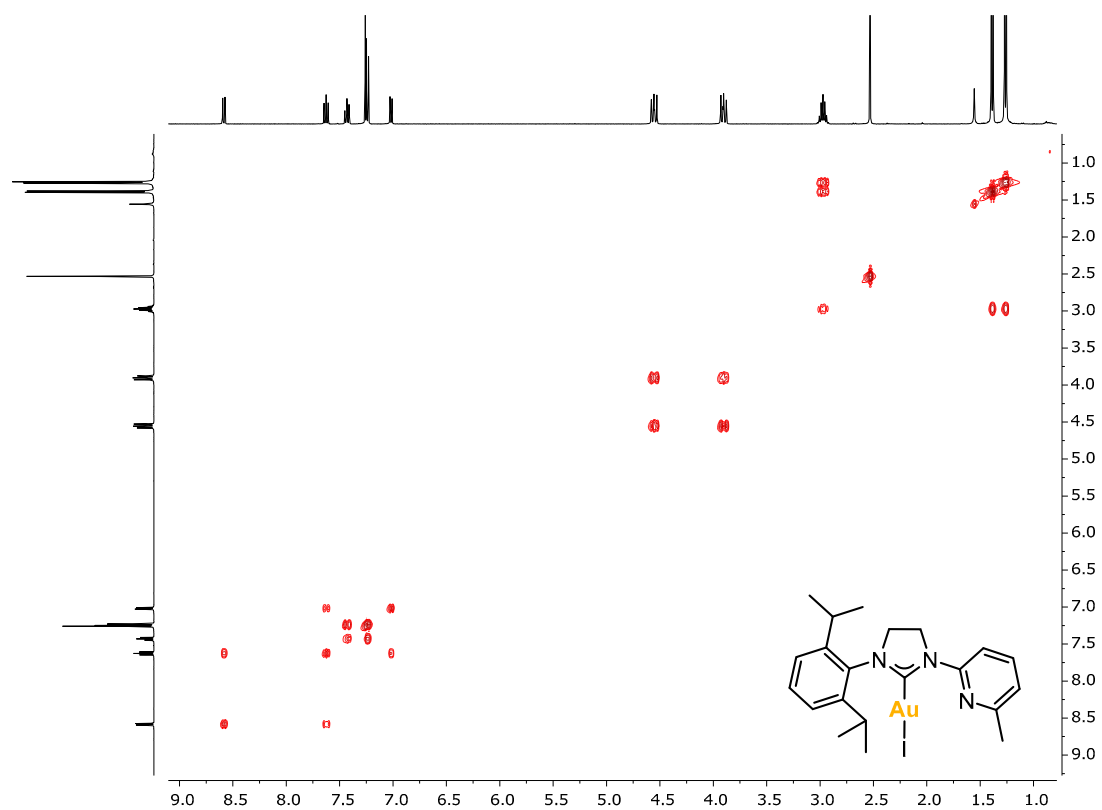


Figure S9. $^1\text{H}, ^1\text{H}$ -COSY NMR (400MHz, 298K) of **1** in CDCl_3 .

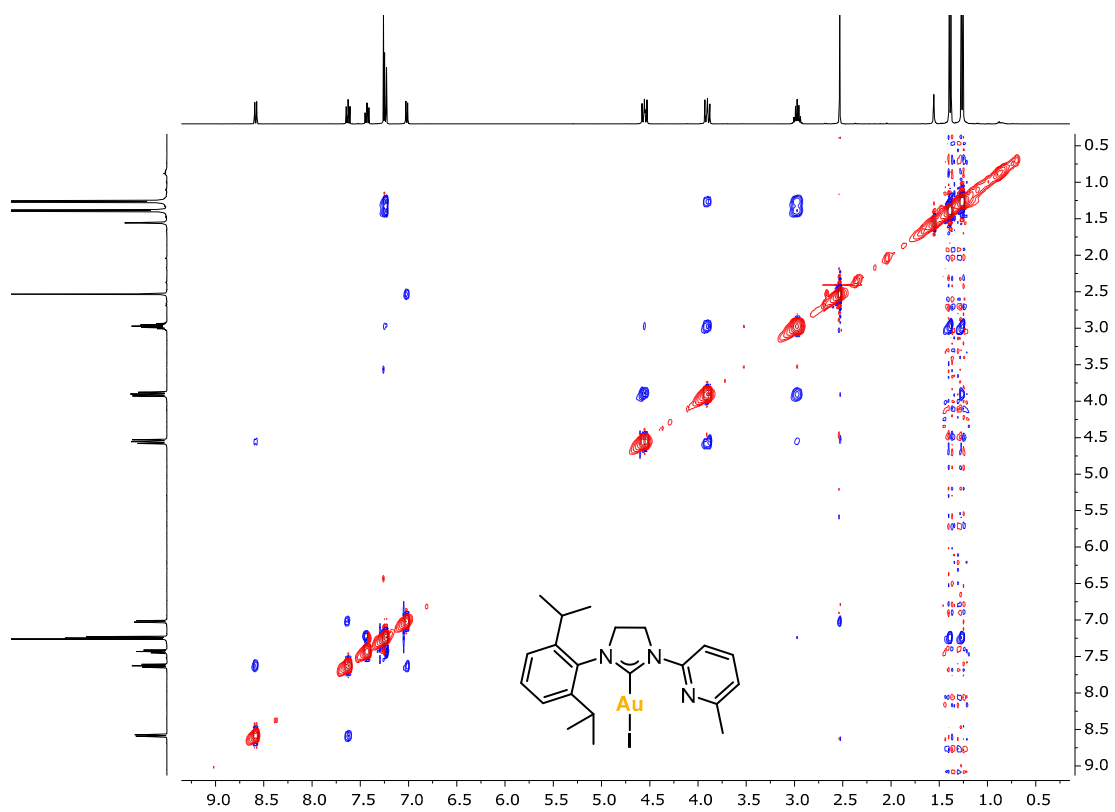


Figure S10. $^1\text{H}, ^1\text{H}$ -NOESY NMR (400MHz, 298K) of **1** in CDCl_3 .

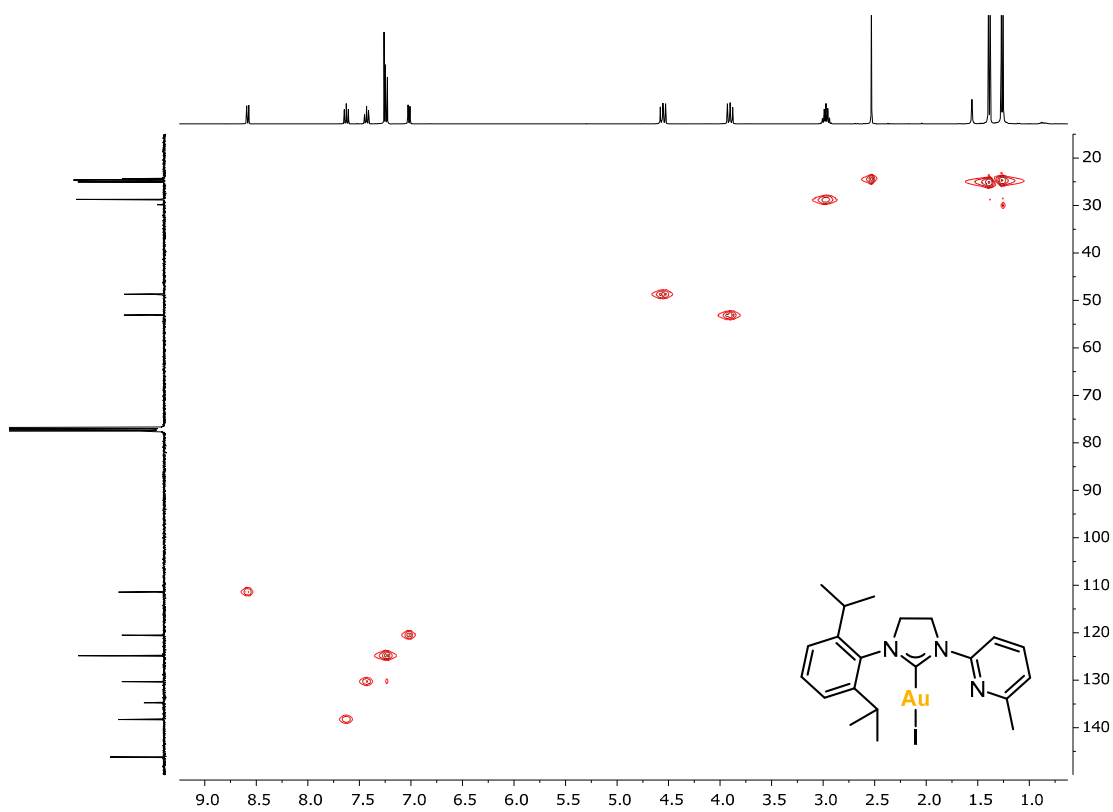


Figure S11. ^1H , ^{13}C -HSQC NMR (400MHz, 298K) of **1** in CDCl_3 .

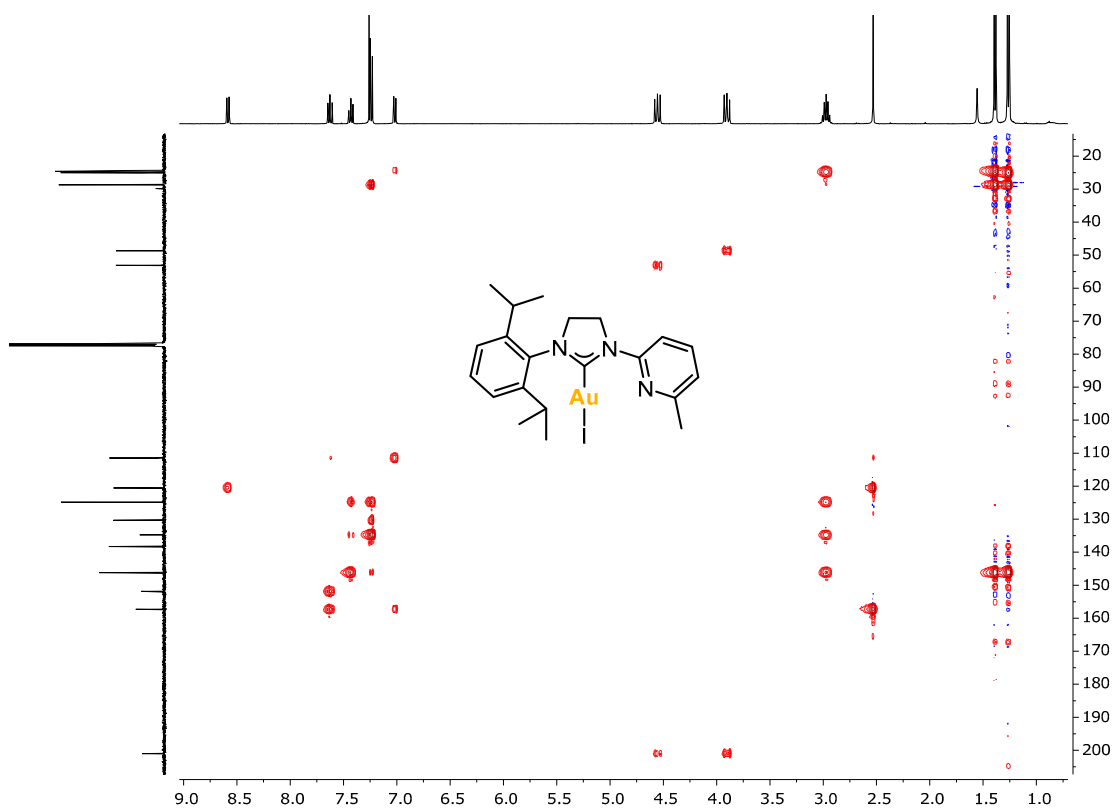


Figure S12. ^1H , ^{13}C -HMBC NMR (400MHz, 298K) of **1** in CDCl_3 .

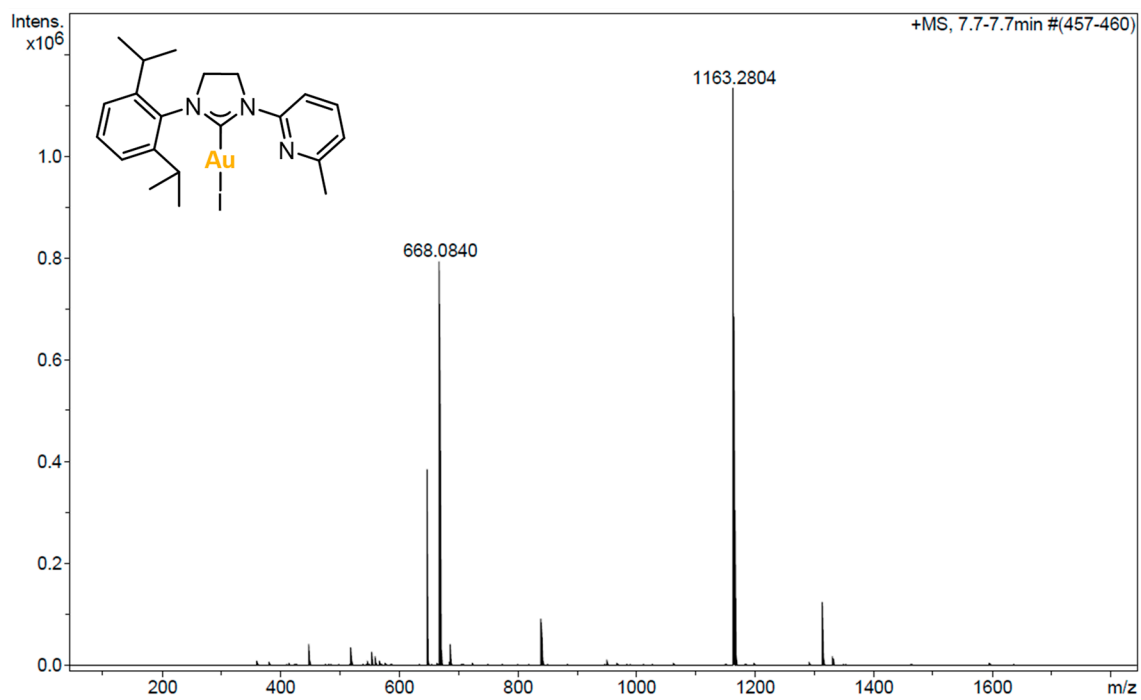


Figure S13. HRMS-ESI(+) of 1.

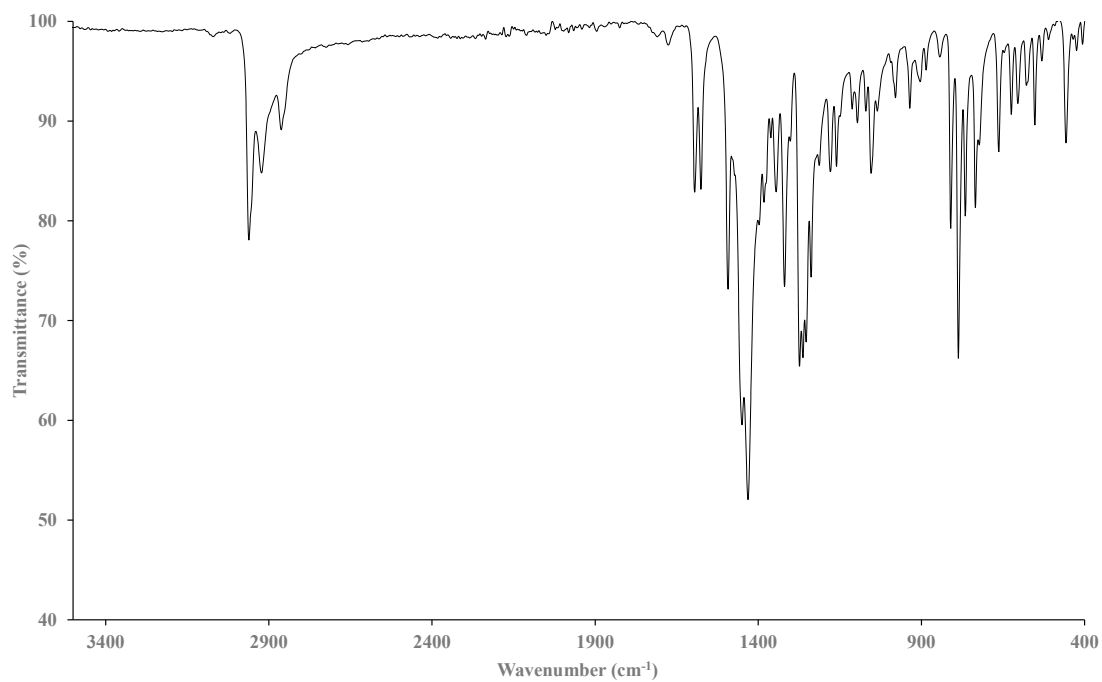


Figure S14. IR spectrum of 1.

S5.4. Complex 2

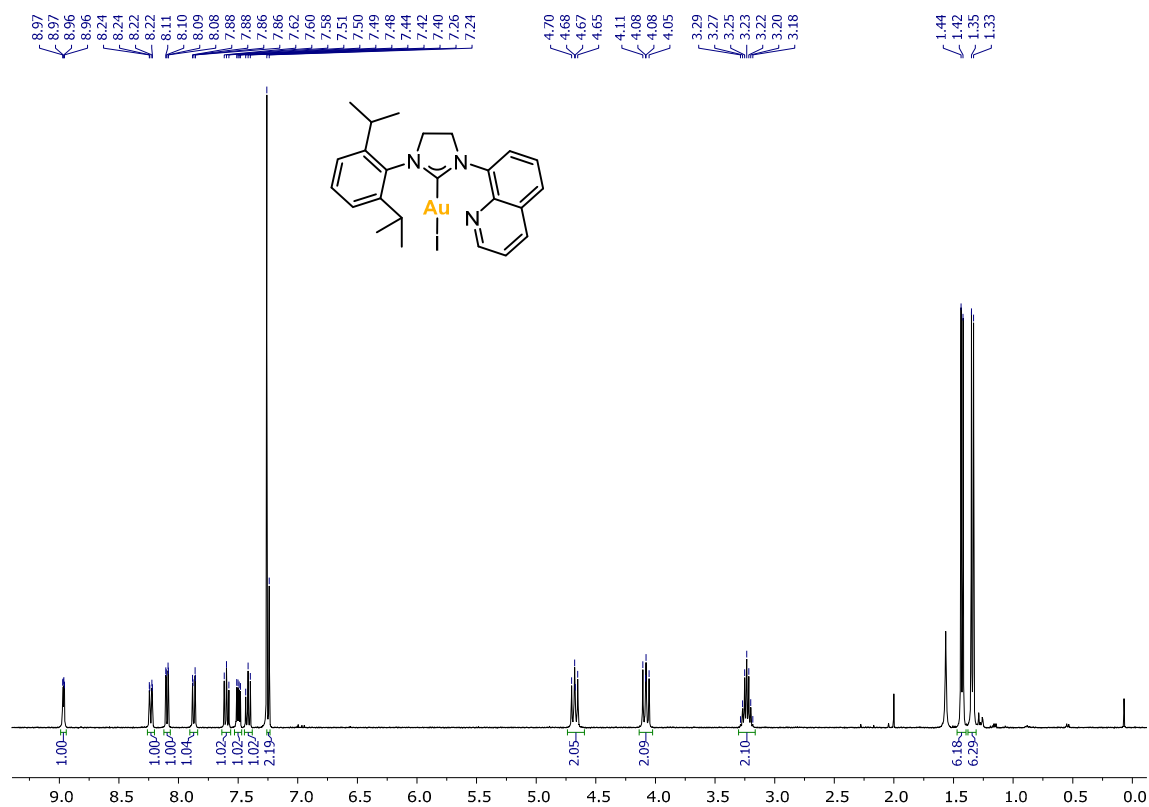


Figure S15. $^1\text{H NMR}$ (400MHz, 298K) of **2** in CDCl_3 .

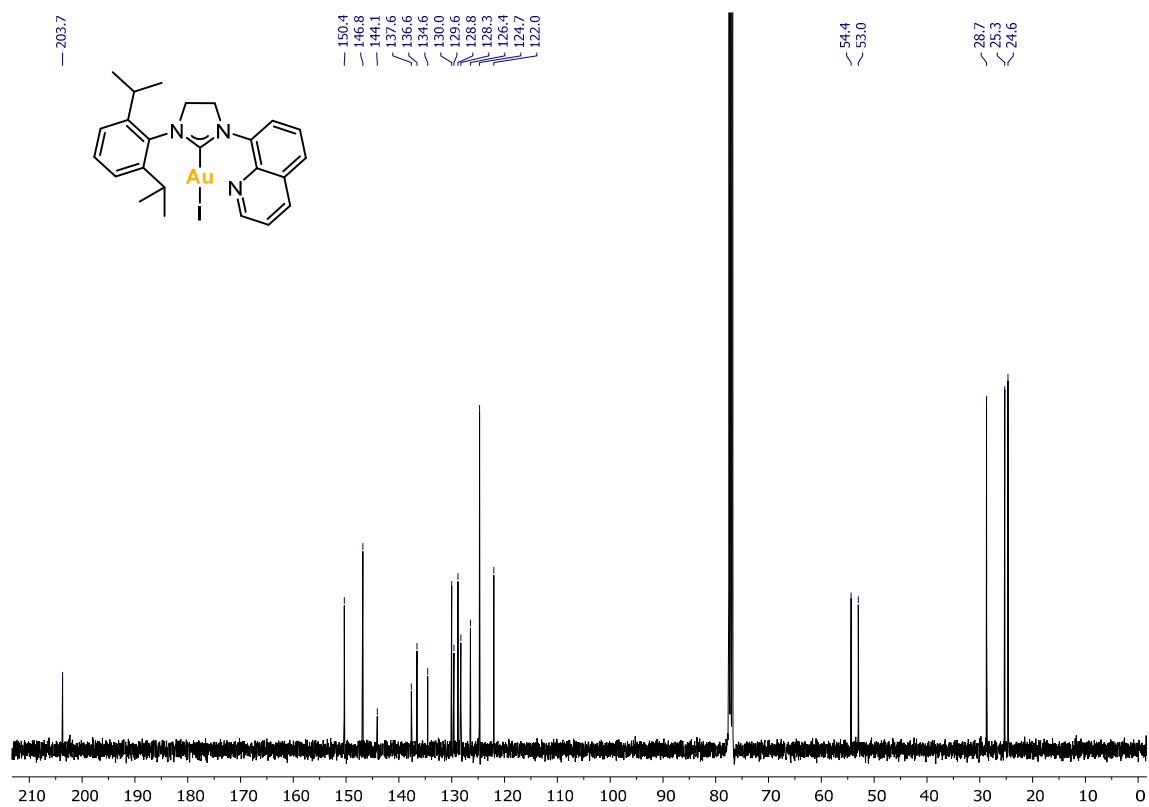


Figure S16. $^{13}\text{C}\{^1\text{H}\}$ NMR (101MHz, 298K) of **2** in CDCl_3 .

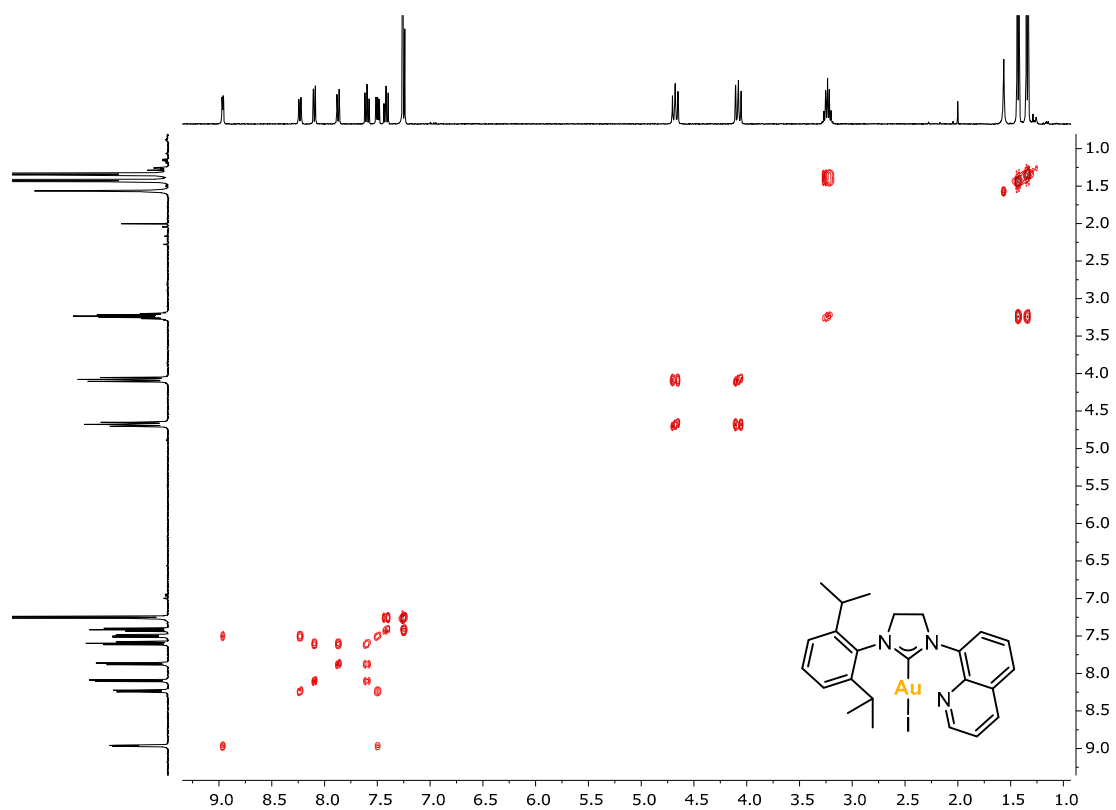


Figure S17. $^1\text{H}, ^1\text{H}$ -COSY NMR (400MHz, 298K) of **2** in CDCl_3 .

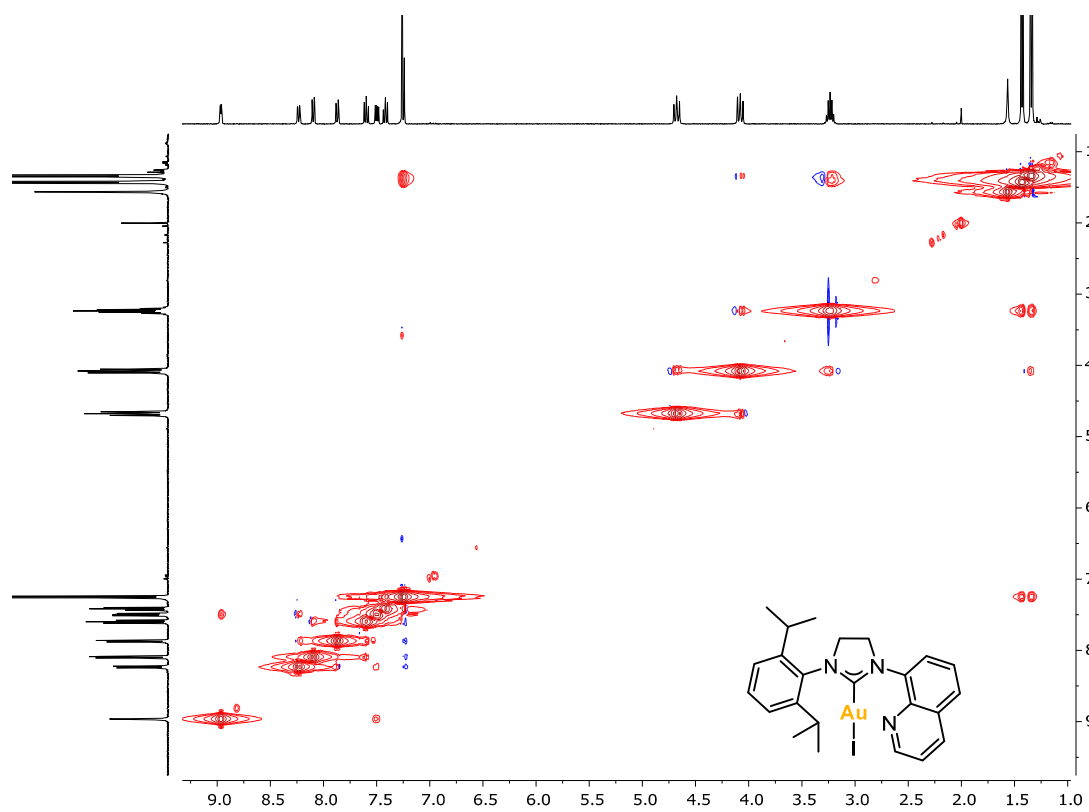


Figure S18. $^1\text{H}, ^1\text{H}$ -NOESY NMR (400MHz, 298K) of **2** in CDCl_3 .

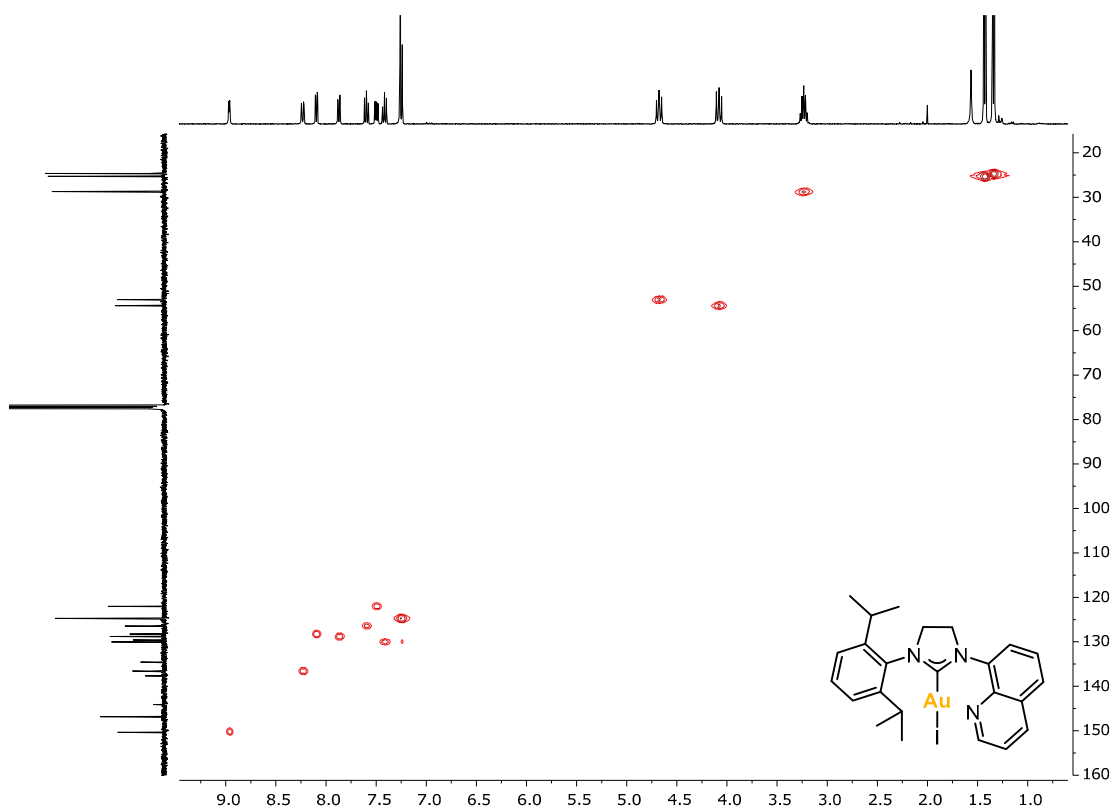


Figure S19. ^1H , ^{13}C -HSQC NMR (400MHz, 298K) of **2** in CDCl_3 .

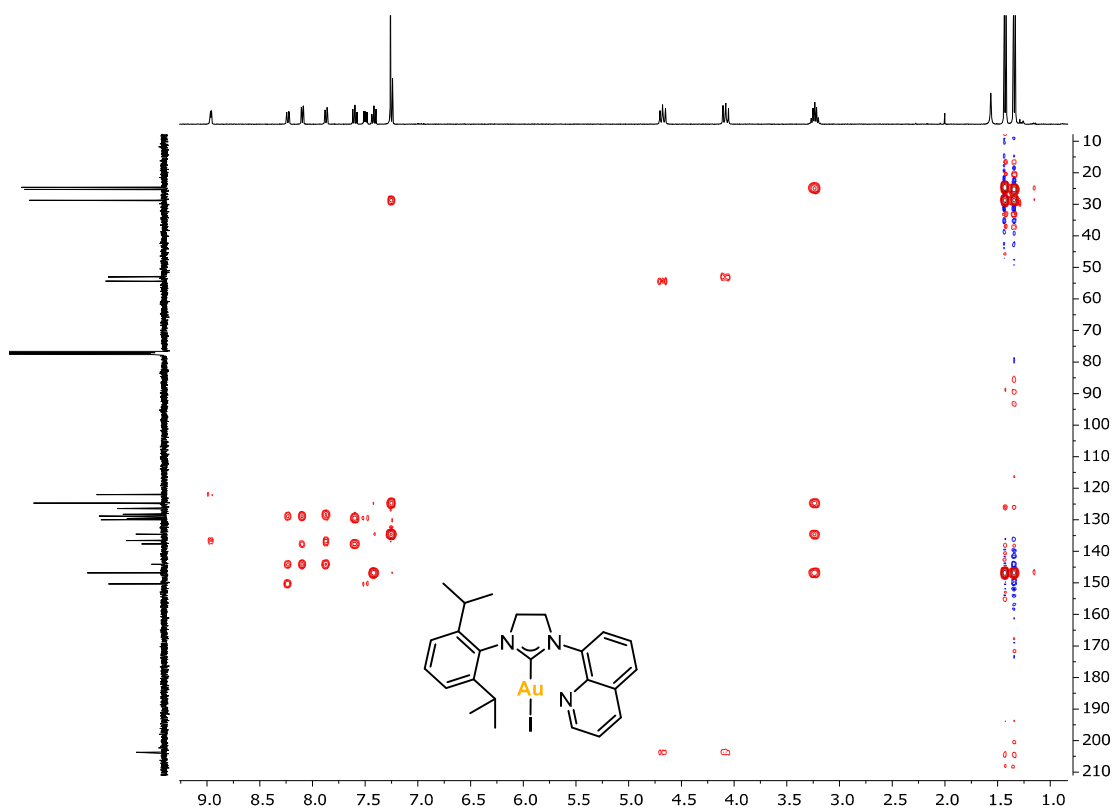


Figure S20. ^1H , ^{13}C -HMBC NMR (400MHz, 298K) of **2** in CDCl_3 .

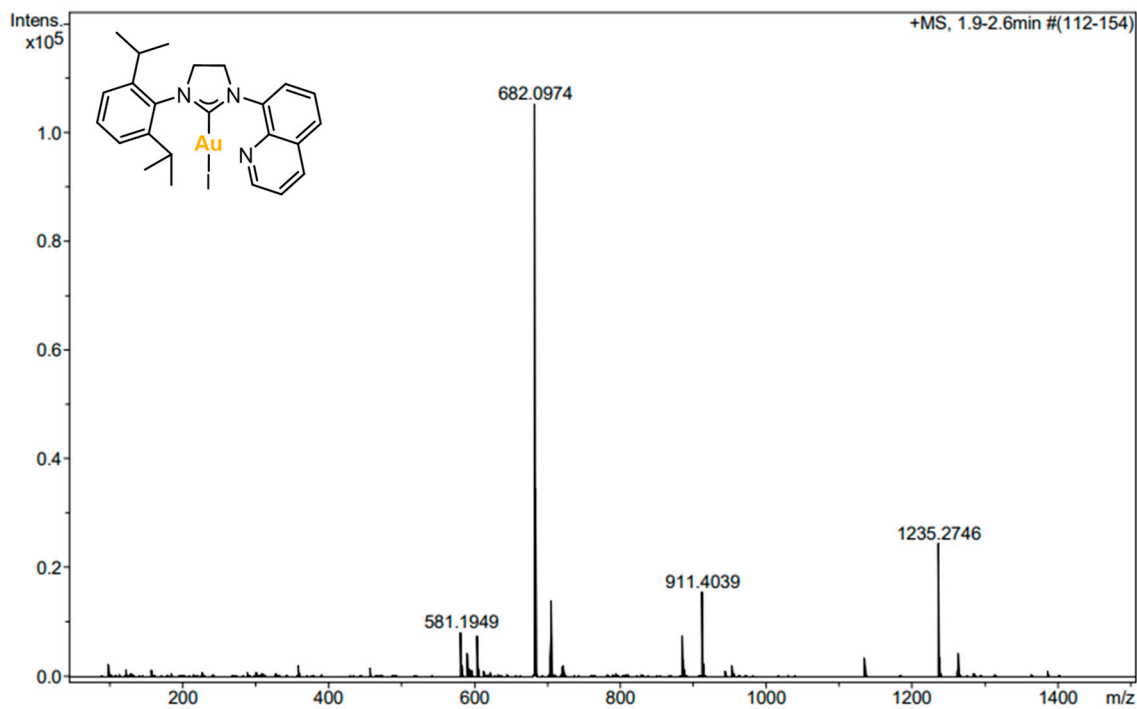


Figure S21. HRMS-ESI(+) of 2.

S5.5. Complex 3

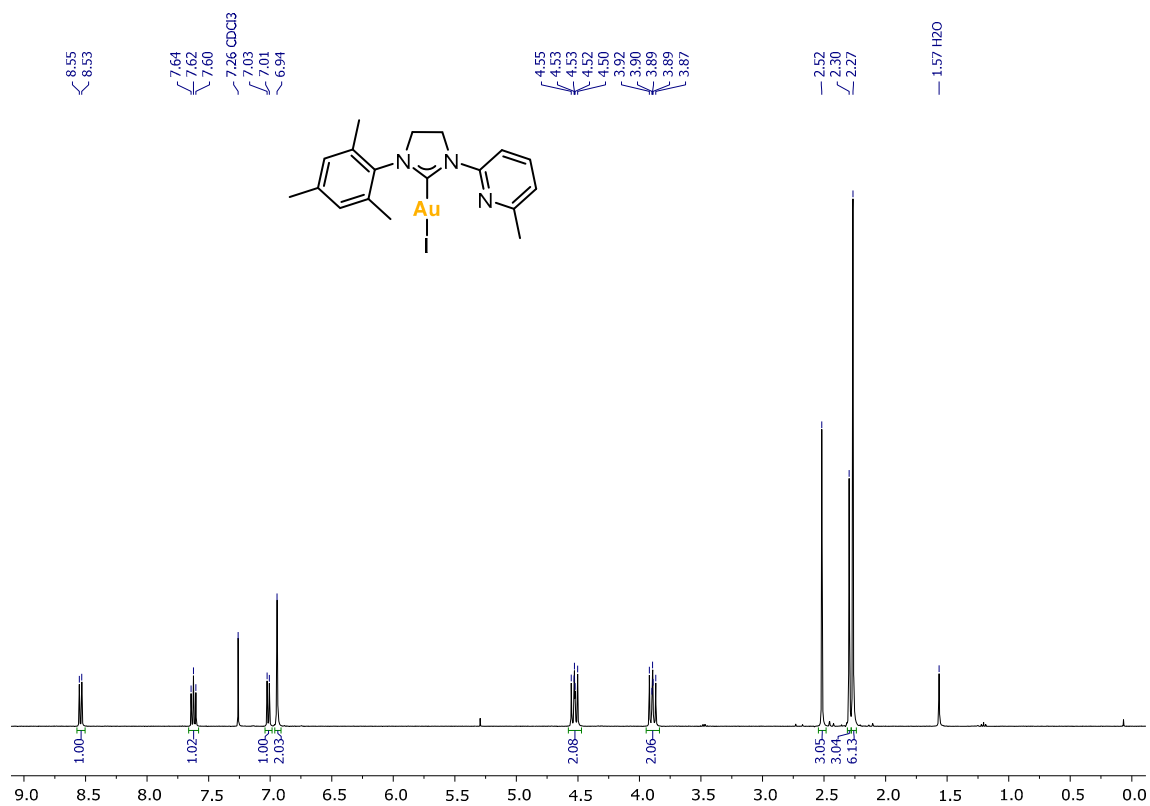


Figure S22. ^1H NMR (400MHz, 298K) of 3 in CDCl_3 .

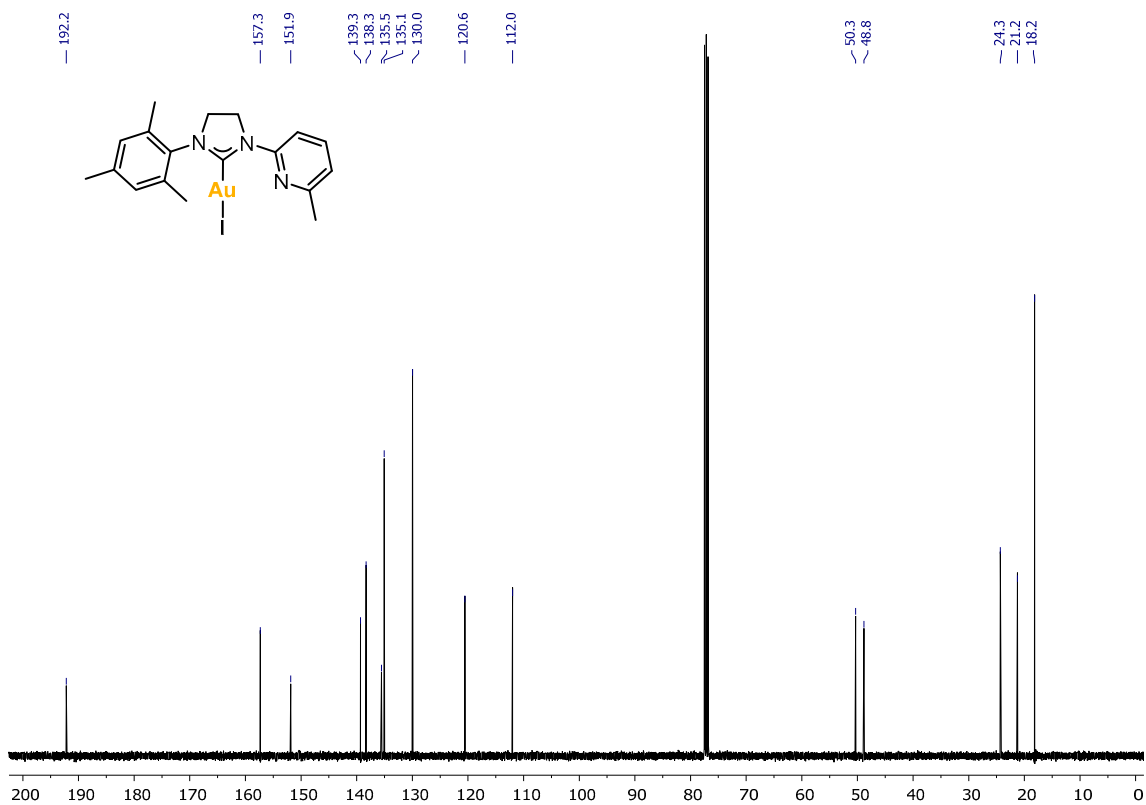


Figure S23. $^{13}\text{C}\{^1\text{H}\}$ NMR (101MHz, 298K) of **3** in CDCl_3 .

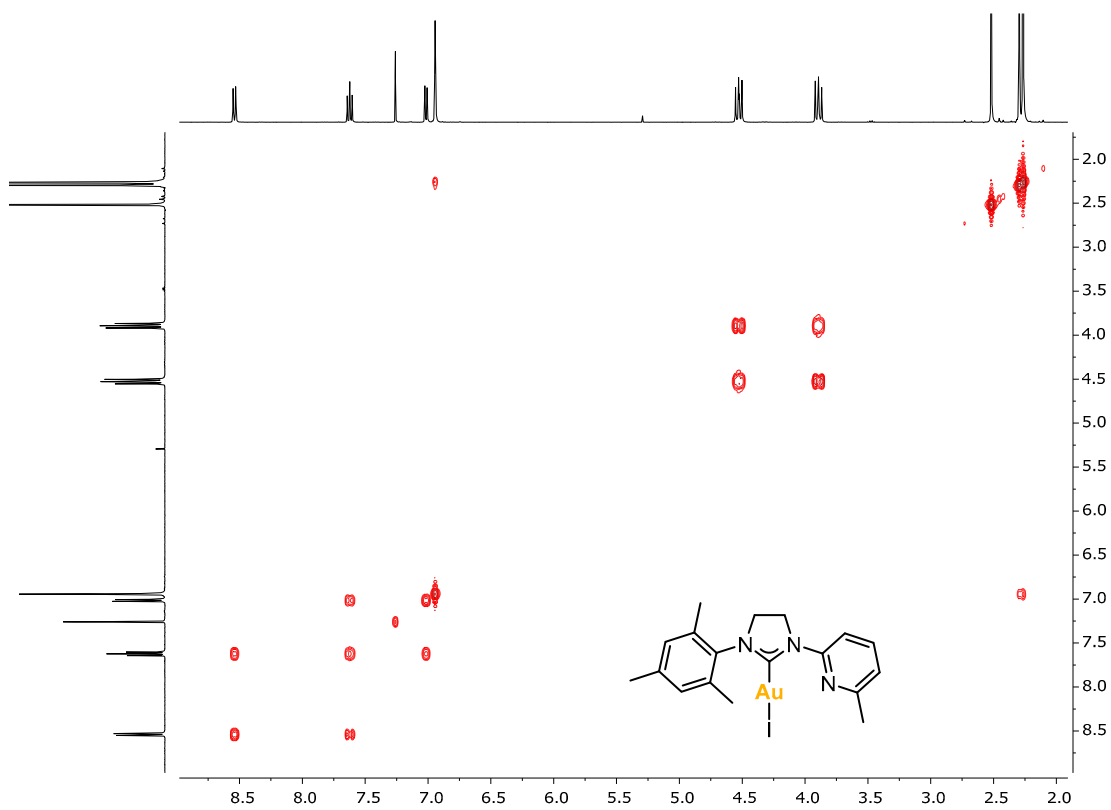


Figure S24. $^1\text{H},^1\text{H}$ -COSY NMR (400MHz, 298K) of **3** in CDCl_3 .

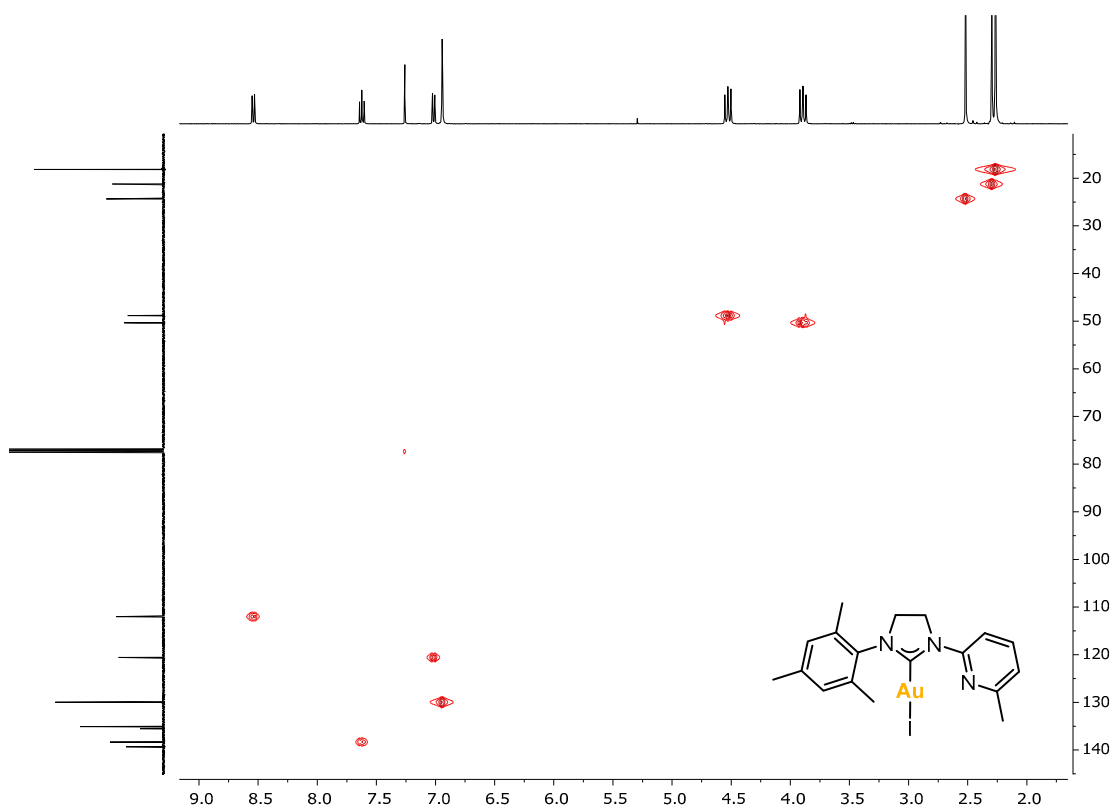


Figure S25. ^1H , ^{13}C -HSQC NMR (400MHz, 298K) of **3** in CDCl_3 .

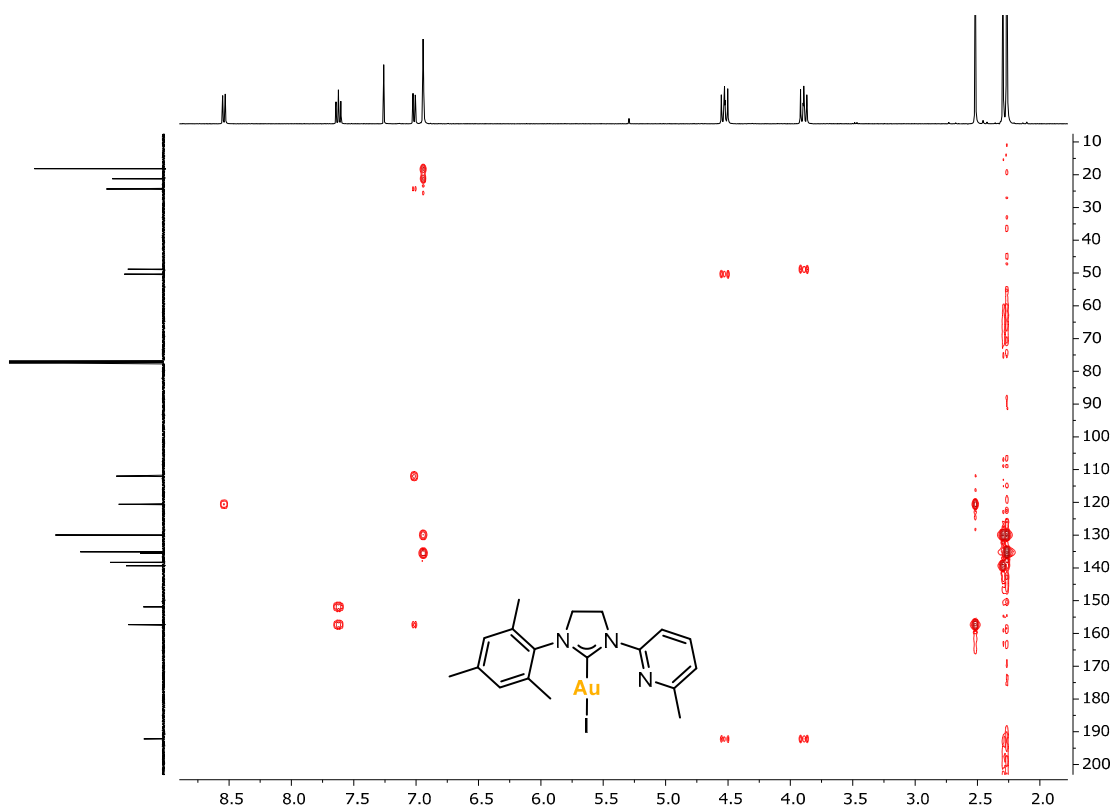
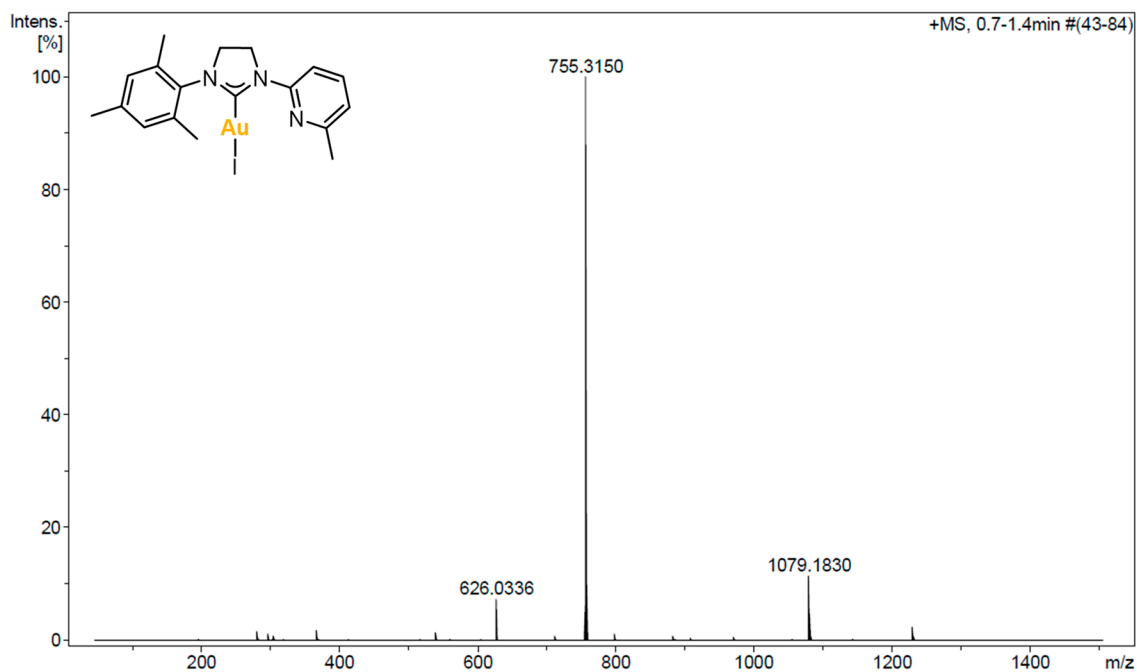
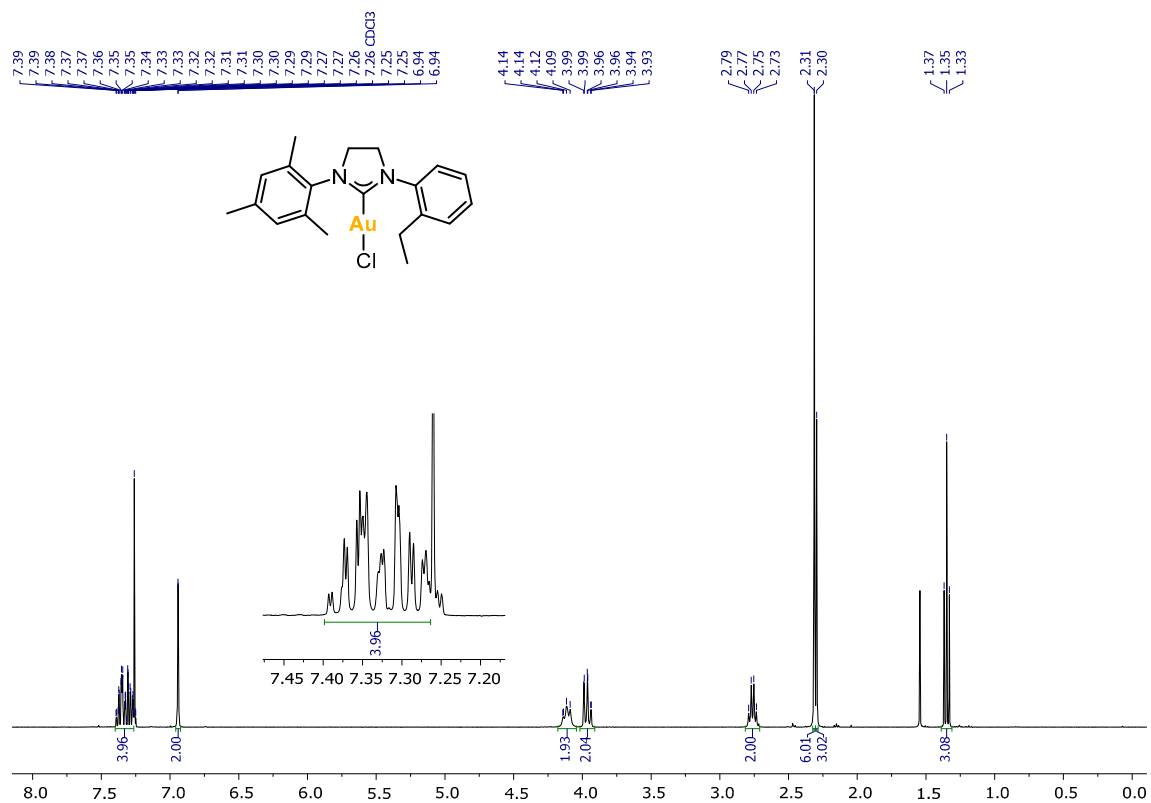


Figure S26. ^1H , ^{13}C -HMBC NMR (400MHz, 298K) of **3** in CDCl_3 .



S5.6. Complex 4



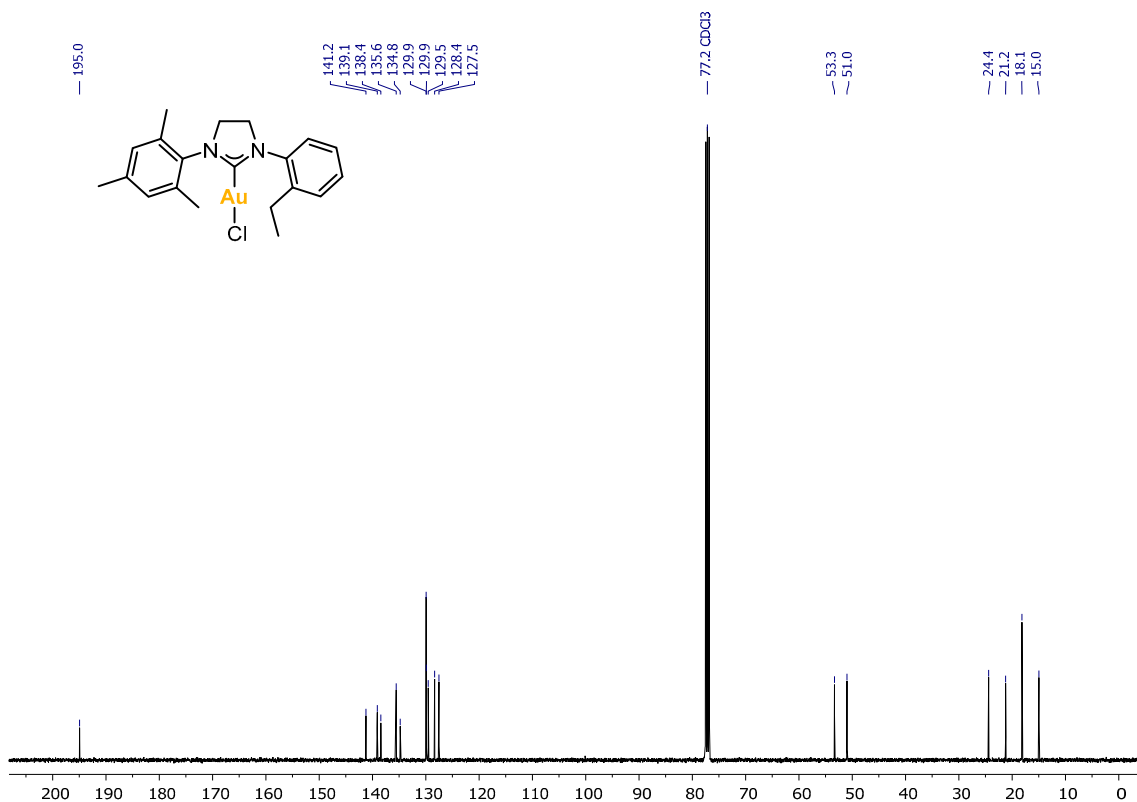


Figure S29. $^{13}\text{C}\{^1\text{H}\}$ NMR (101MHz, 298K) of **4** in CDCl_3 .

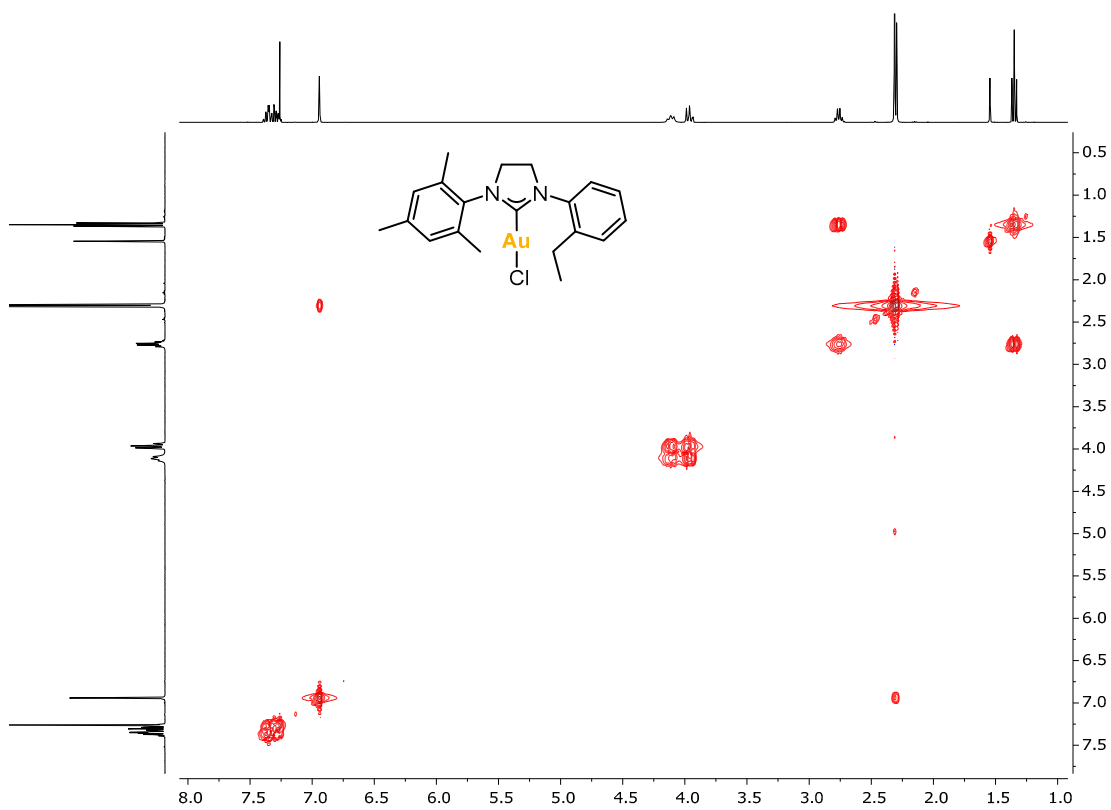


Figure S30. $^1\text{H},^1\text{H}$ -COSY NMR (400MHz, 298K) of **4** in CDCl_3 .

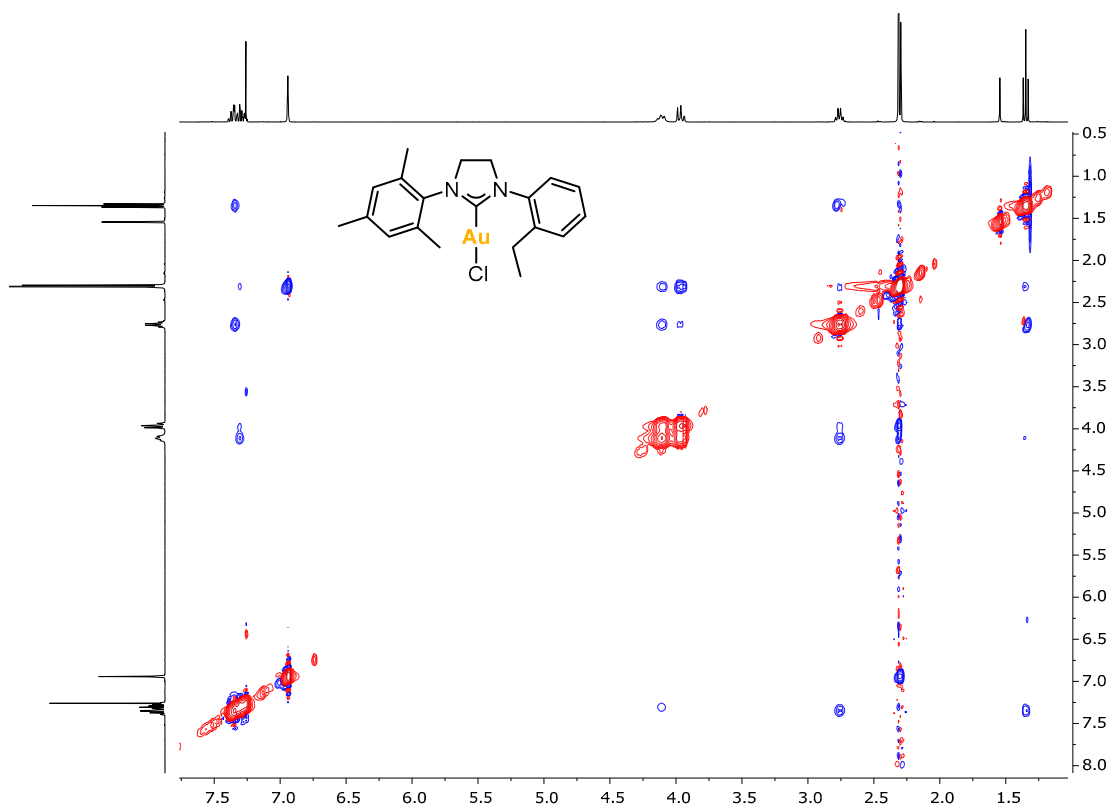


Figure S31. ^1H , ^1H -NOESY NMR (400MHz, 298K) of **4** in CDCl_3 .

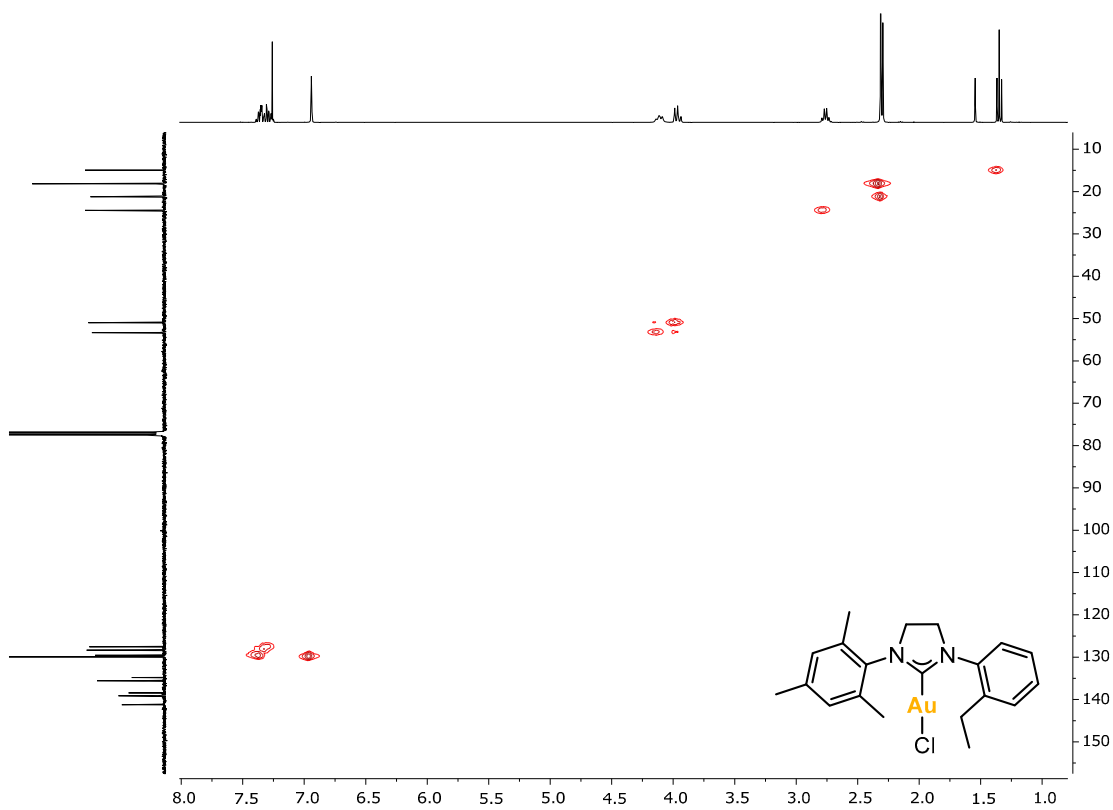


Figure S32. ^1H , ^{13}C -HSQC NMR (400MHz, 298K) of **4** in CDCl_3 .

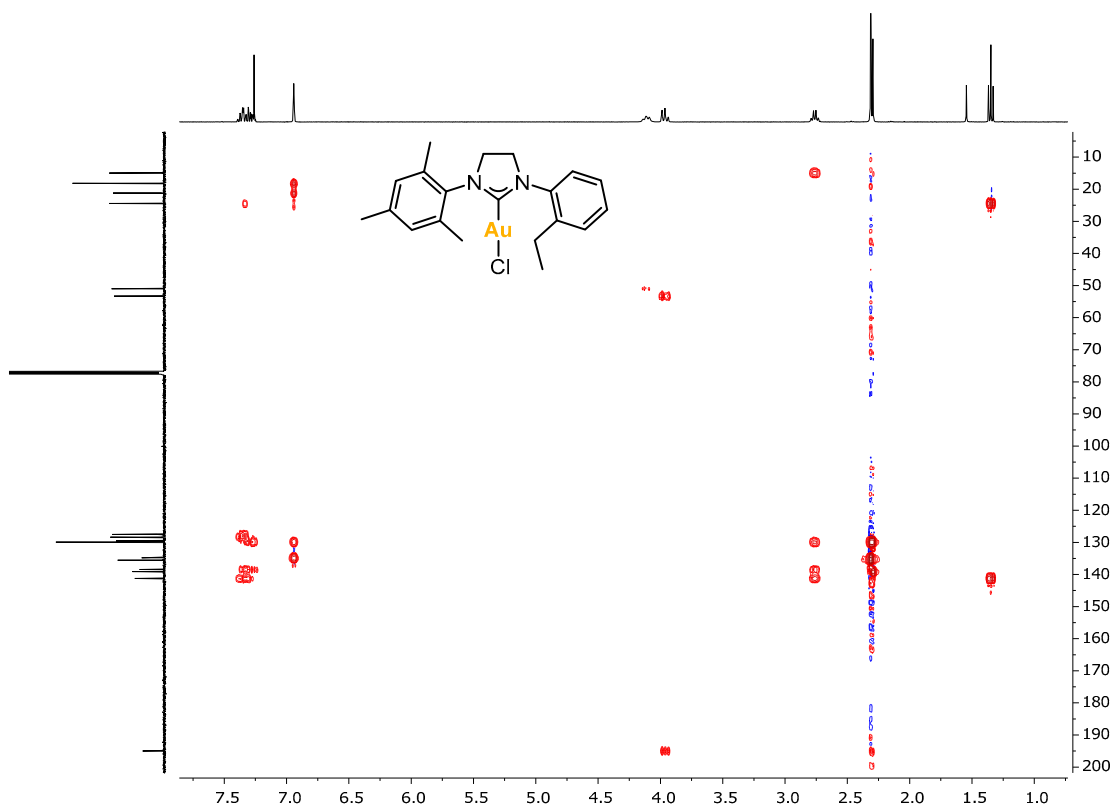


Figure S33. ^1H , ^{13}C -HMBC NMR (400MHz, 298K) of **4** in CDCl_3 .

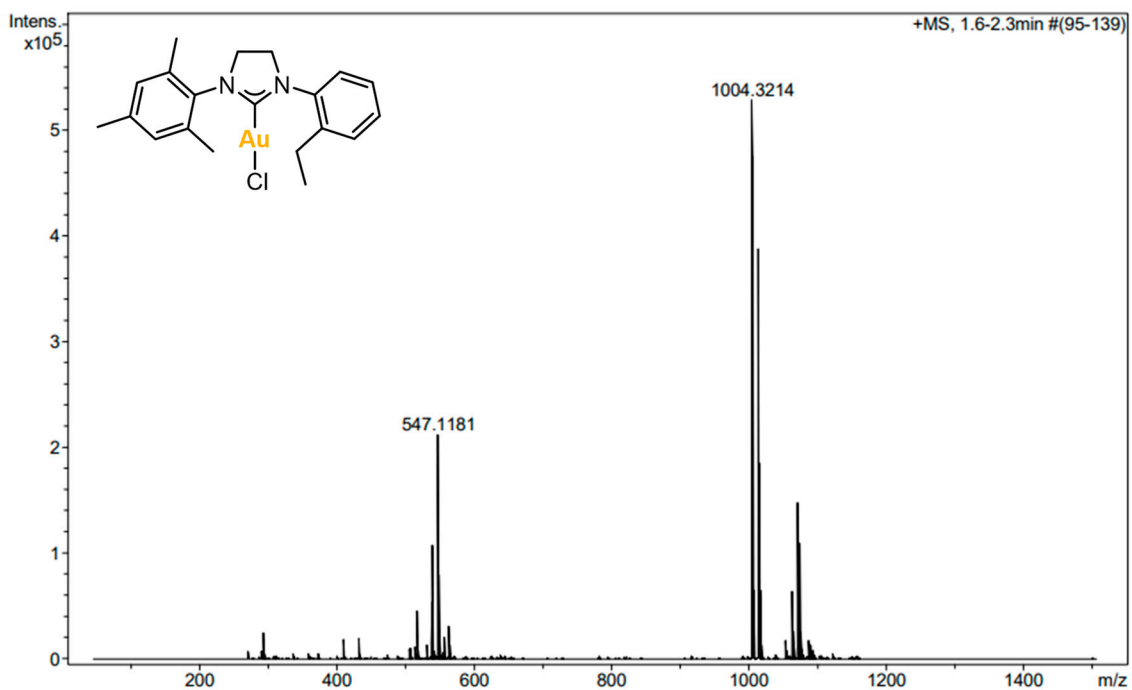


Figure S34. HRMS-ESI(+) of **4**.

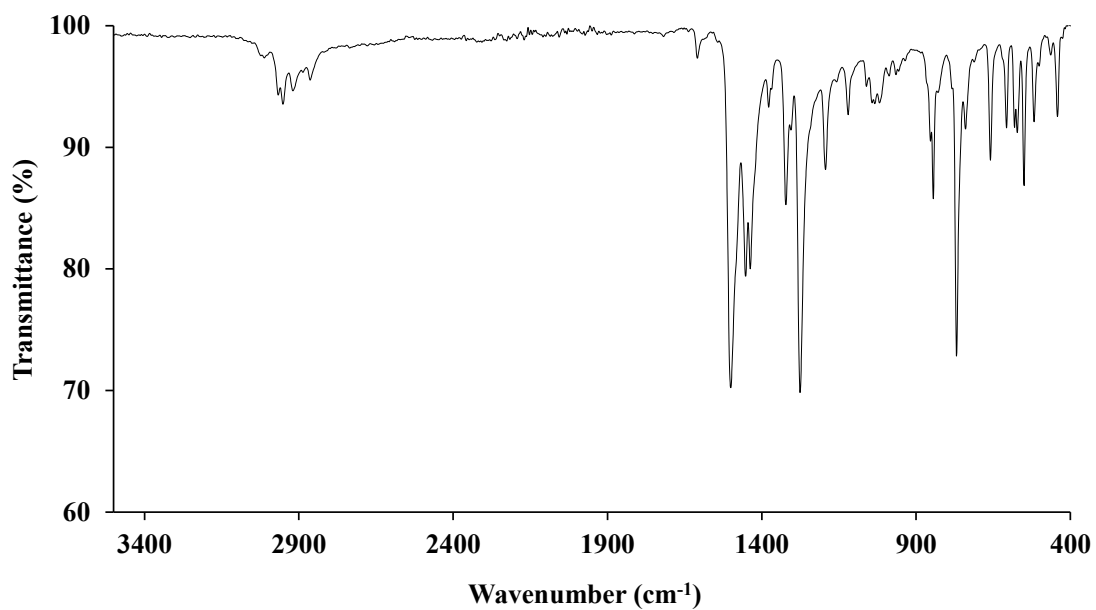


Figure S35. IR spectrum of 4.

S5.7. Compound L1^{ox}-I

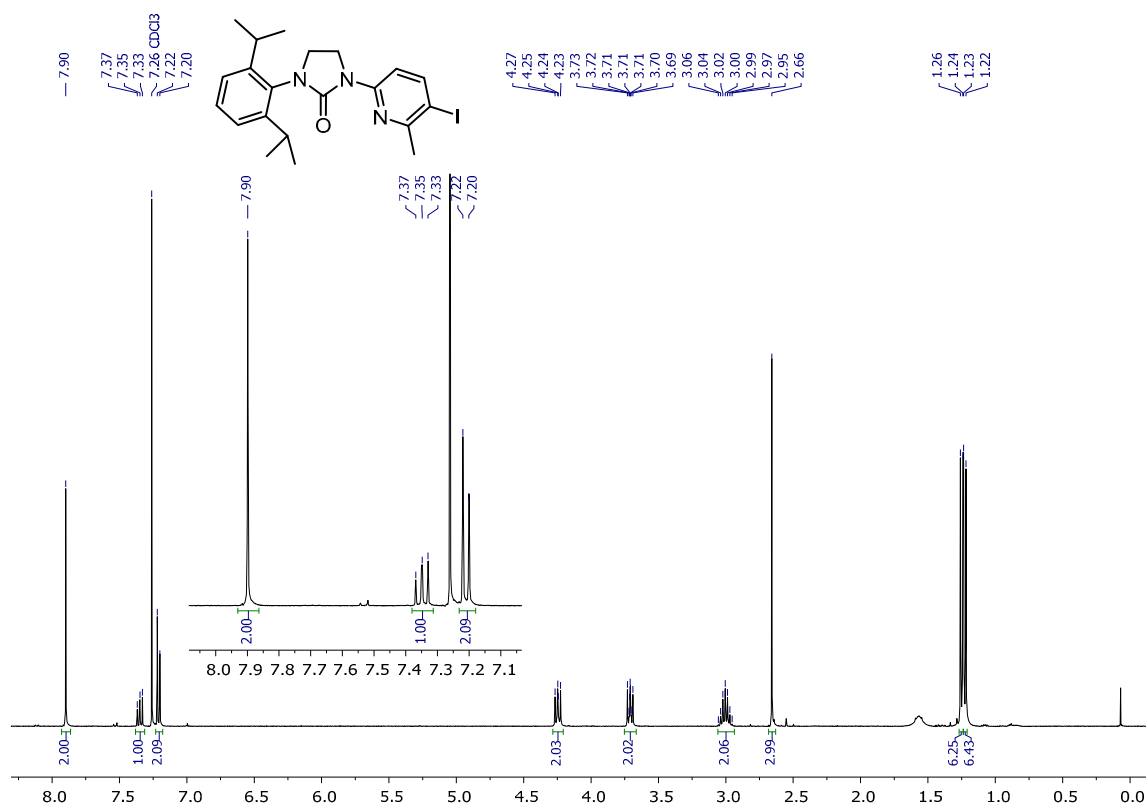


Figure S36. ¹H NMR (400MHz, 298K) of L1^{ox}-I in CDCl₃.

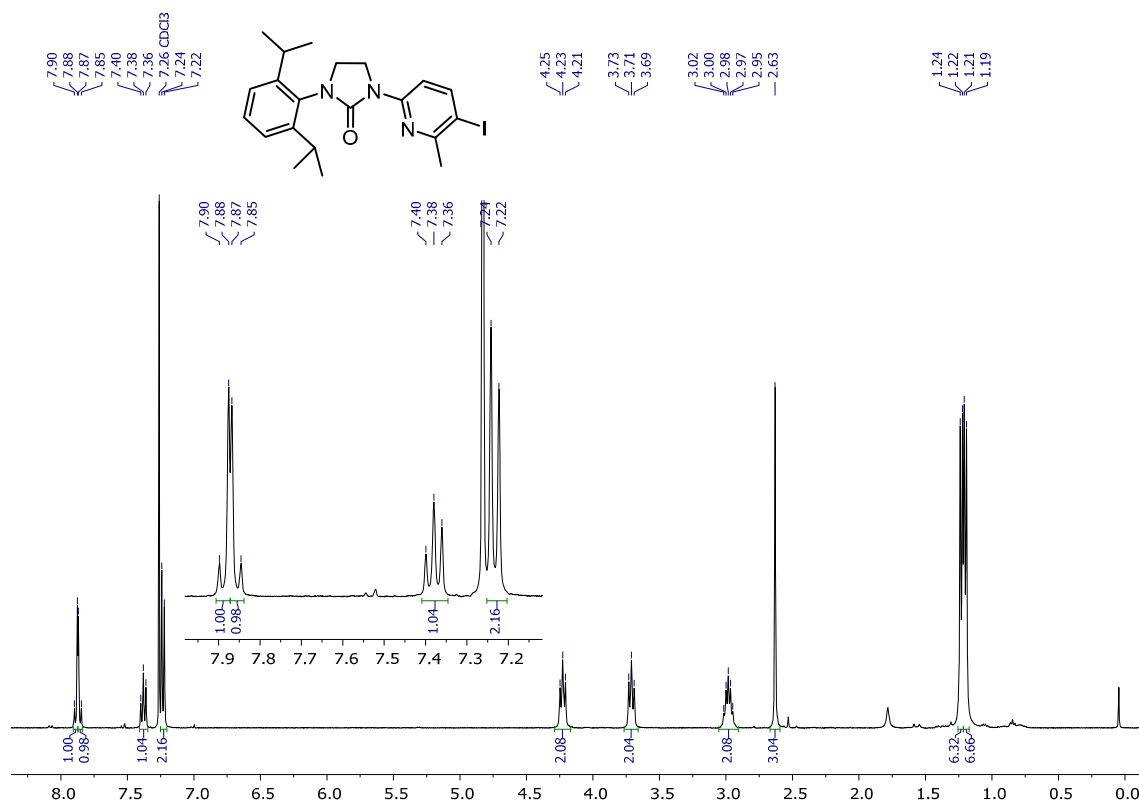


Figure S37. ¹H NMR (400MHz, 228K) of L1^{ox}-I in CDCl₃.

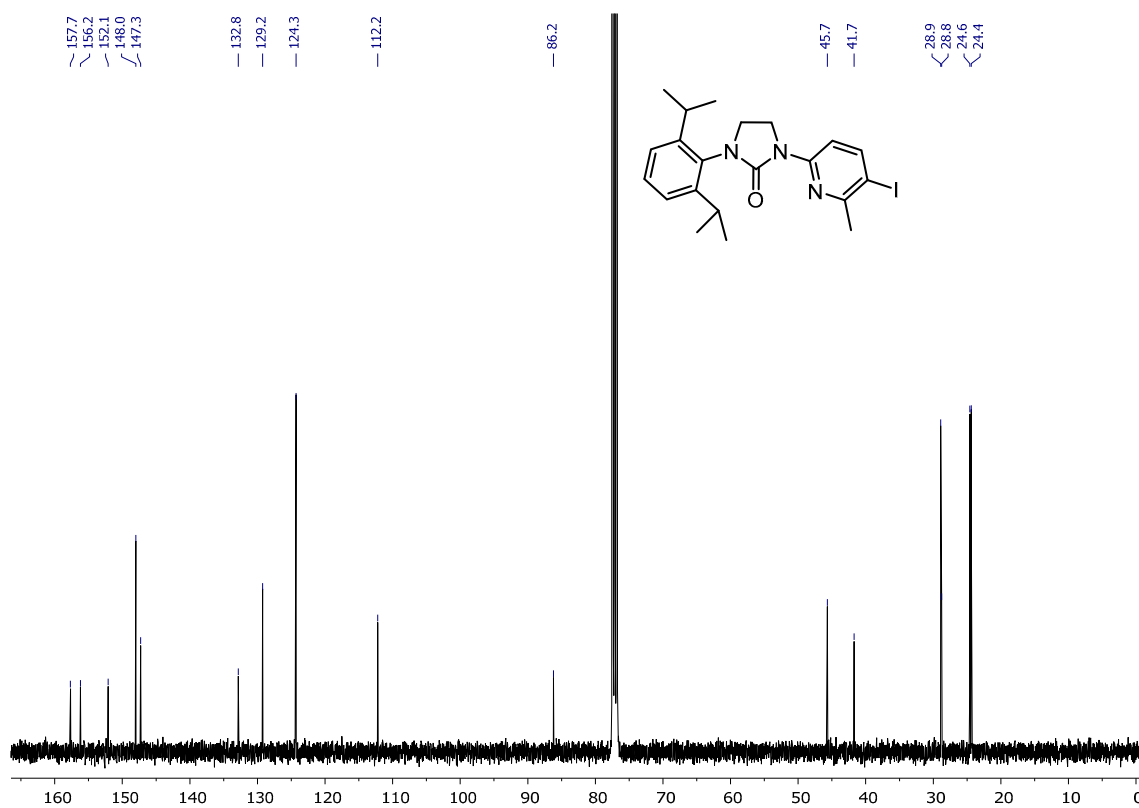


Figure S38. ¹³C{¹H} NMR (101MHz, 298K) of L1^{ox}-I in CDCl₃.

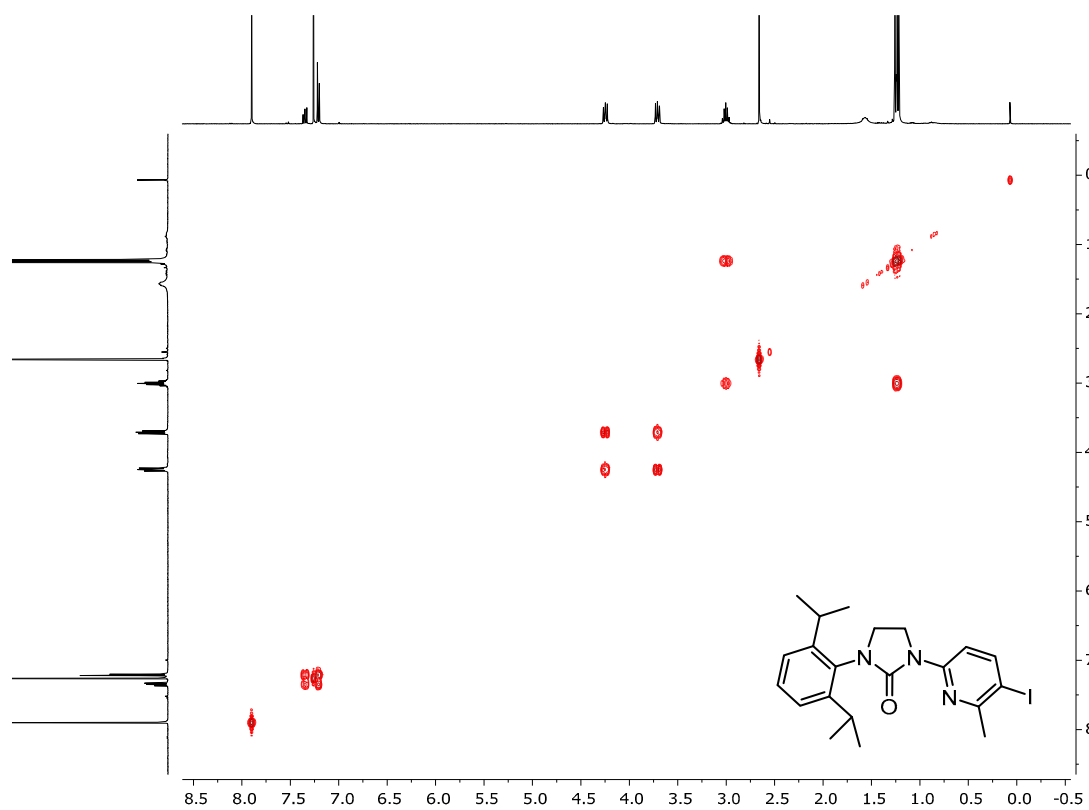


Figure S39. ^1H , ^1H -COSY NMR (400MHz, 298K) of $\text{L1}^{\text{ox-I}}$ in CDCl_3 .

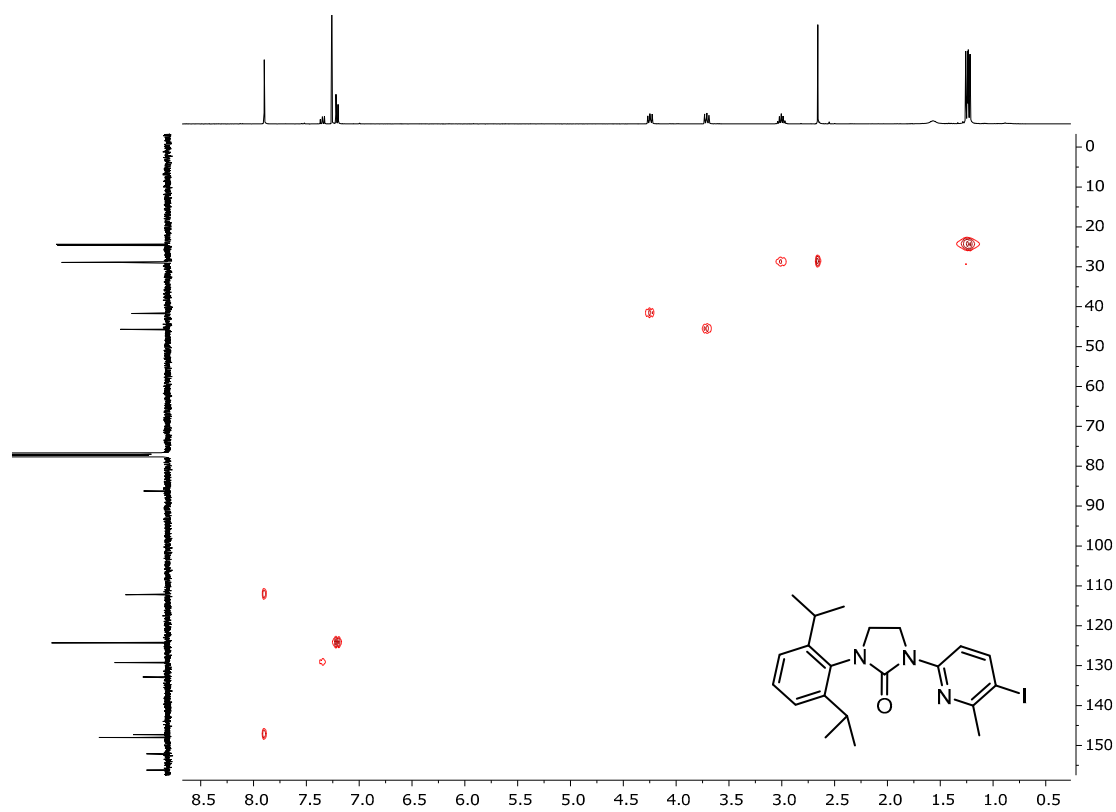


Figure S40. ^1H , ^{13}C -HSQC NMR (400MHz, 298K) of $\text{L1}^{\text{ox-I}}$ in CDCl_3 .

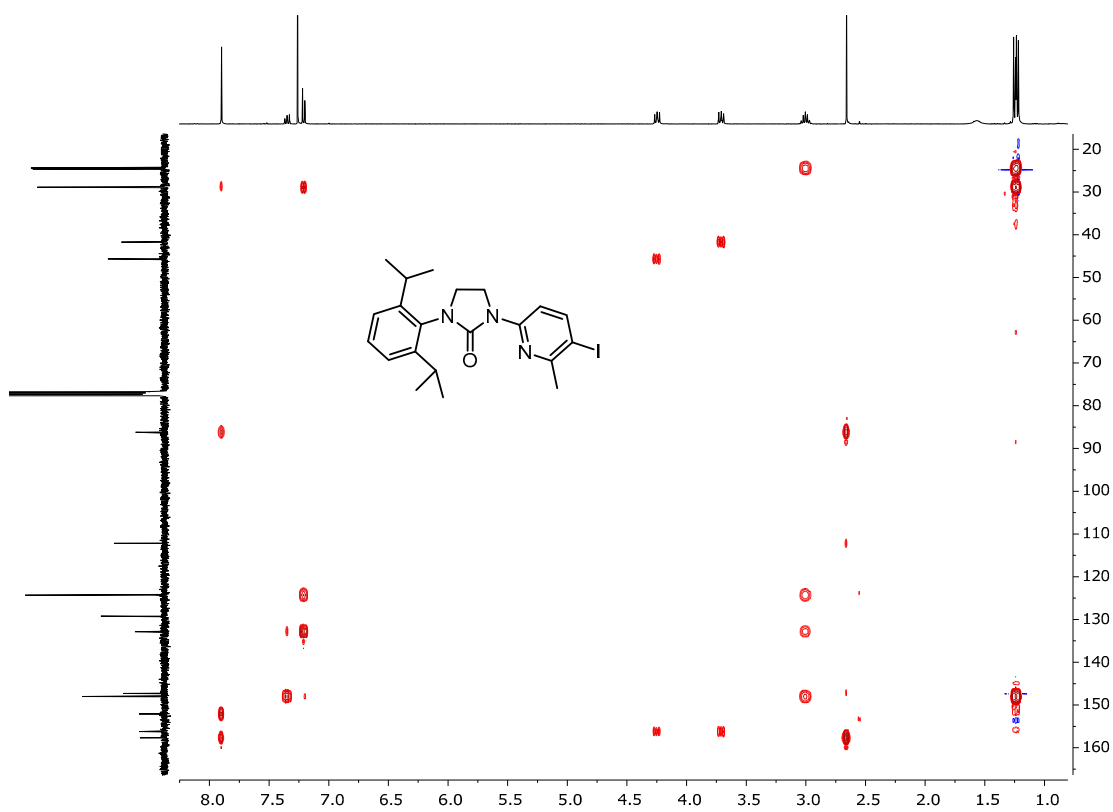


Figure S41. ^1H , ^{13}C -HMBC NMR (400MHz, 298K) of $\text{L1}^{\text{ox-I}}$ in CDCl_3 .

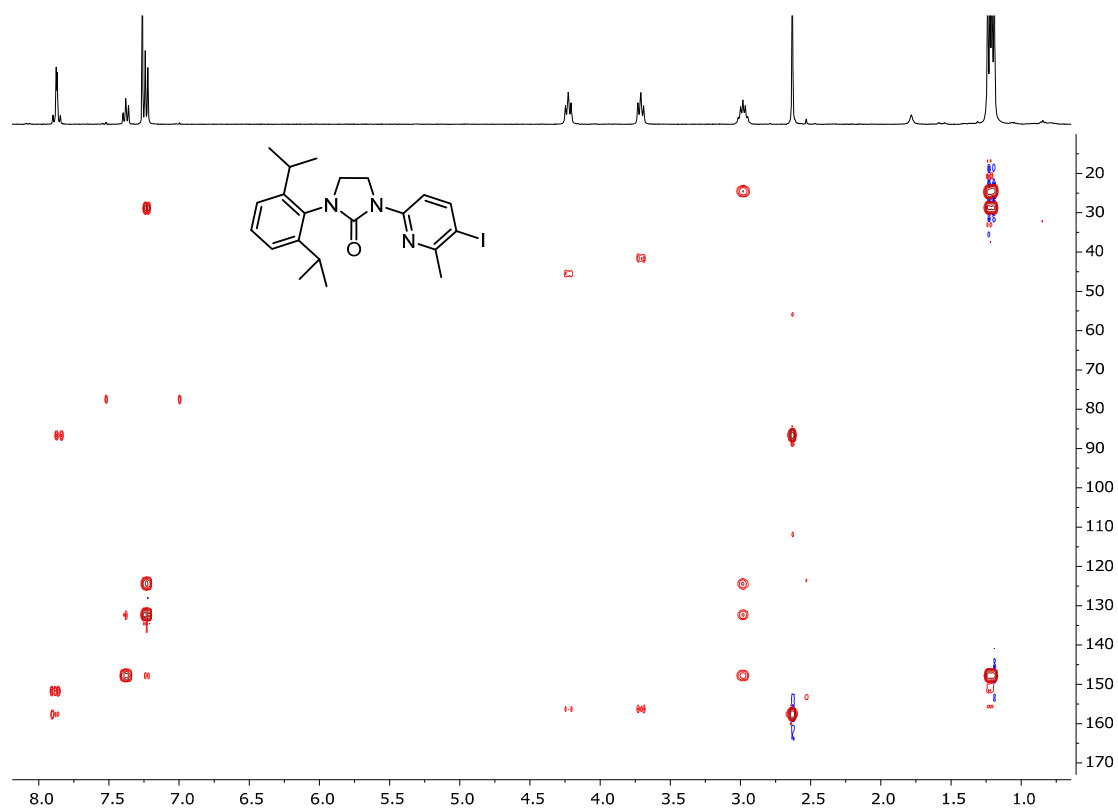


Figure S42. ^1H , ^{13}C -HMBC NMR (400MHz, 228K) of $\text{L1}^{\text{ox-I}}$ in CDCl_3 .

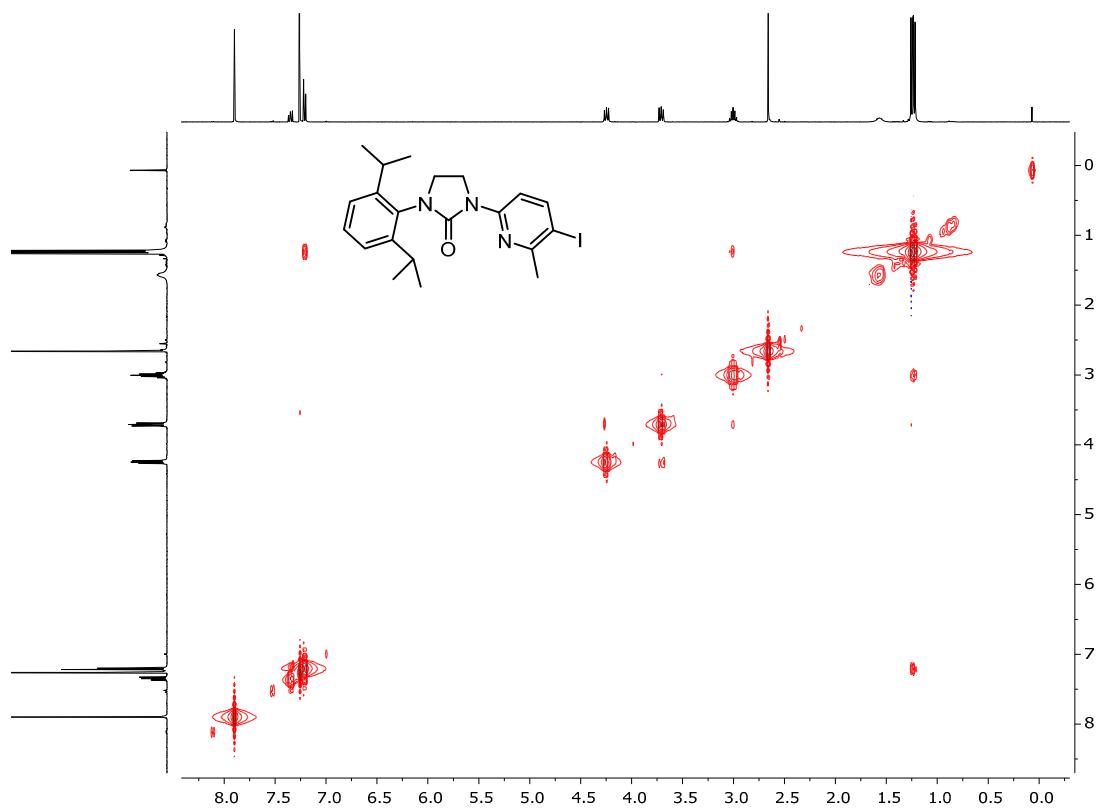


Figure S43. ^1H , ^1H -NOESY NMR (400MHz, 298K) of $\text{L1}^{\text{ox-I}}$ in CDCl_3 .

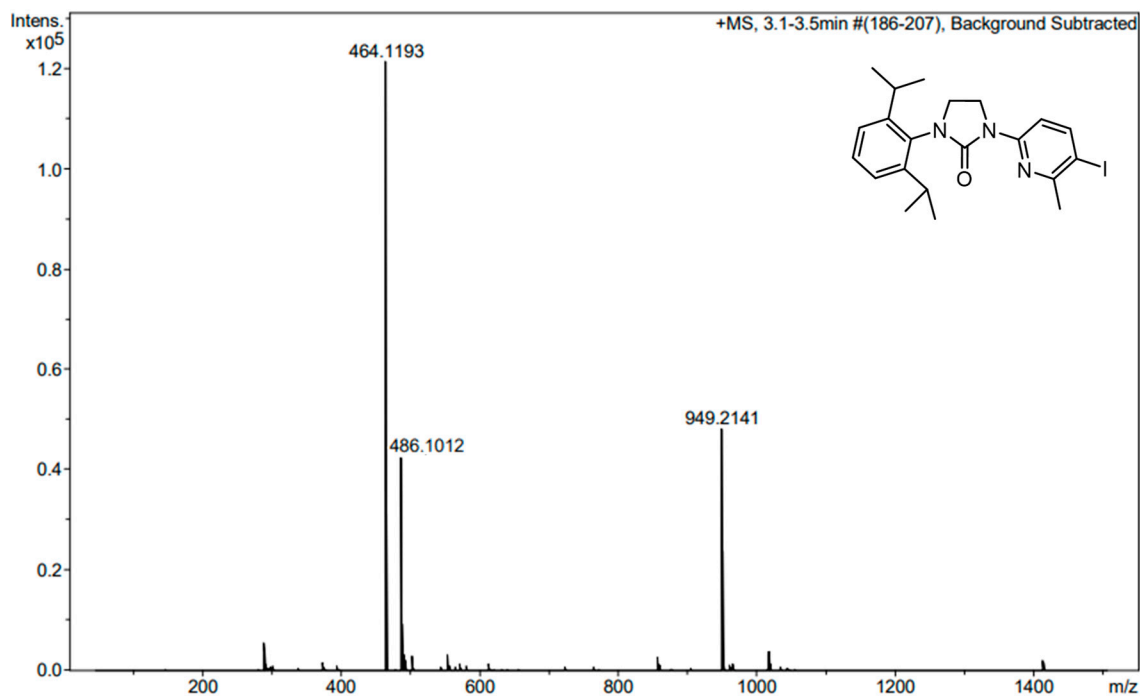


Figure S44. HRMS-ESI(+) of $\text{L1}^{\text{ox-I}}$.

S5.8. Compound L2^{ox}

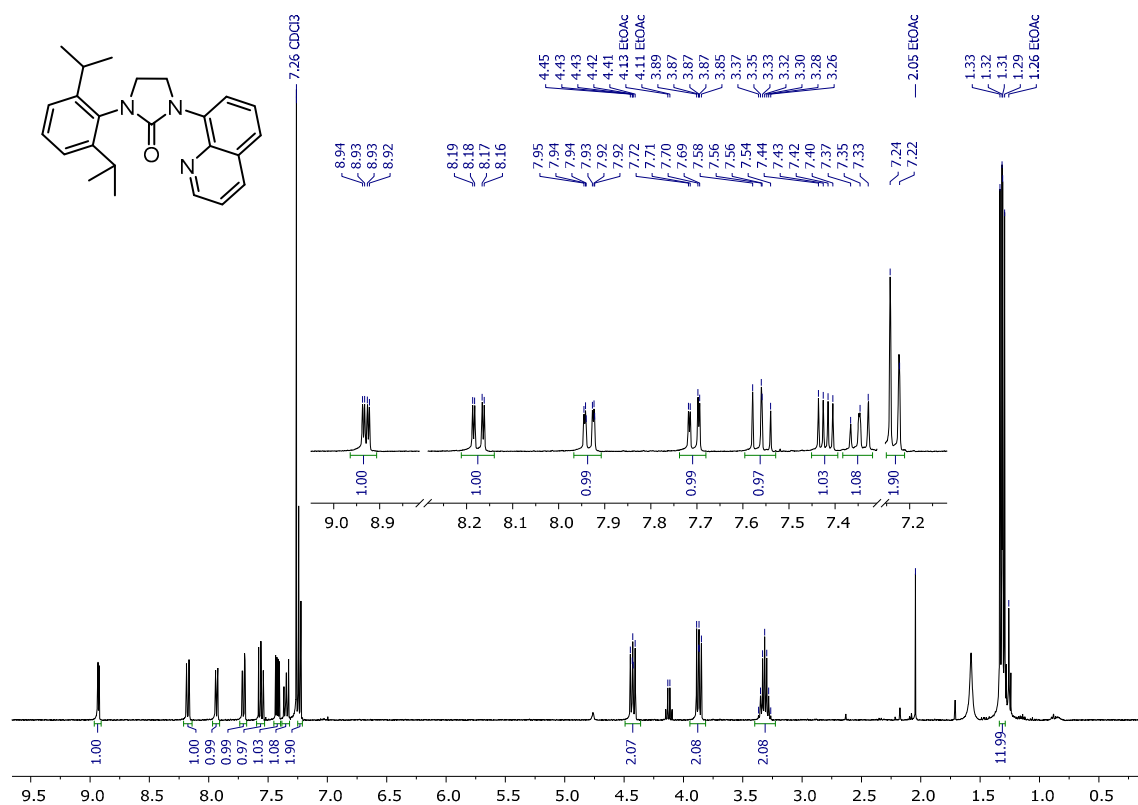


Figure S45. ¹H NMR (400MHz, 298K) of L2^{ox} in CDCl₃.

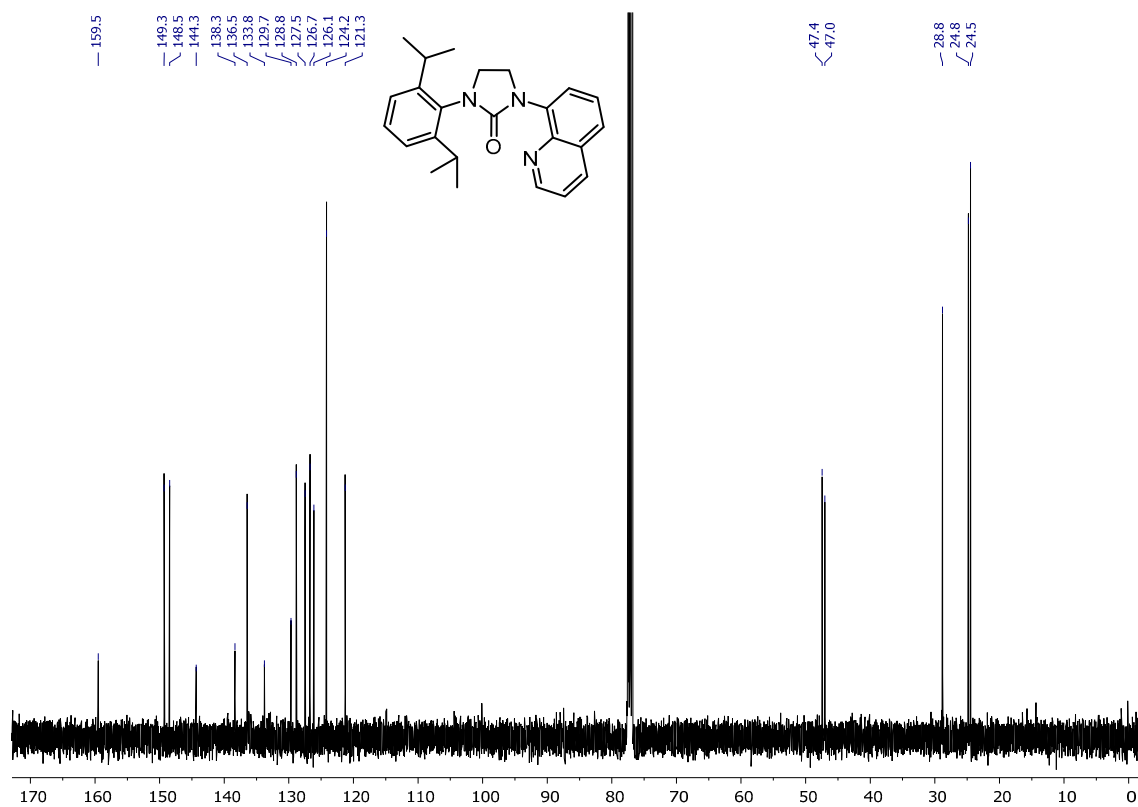


Figure S46. ¹³C{¹H} NMR (101MHz, 298K) of L2^{ox} in CDCl₃.

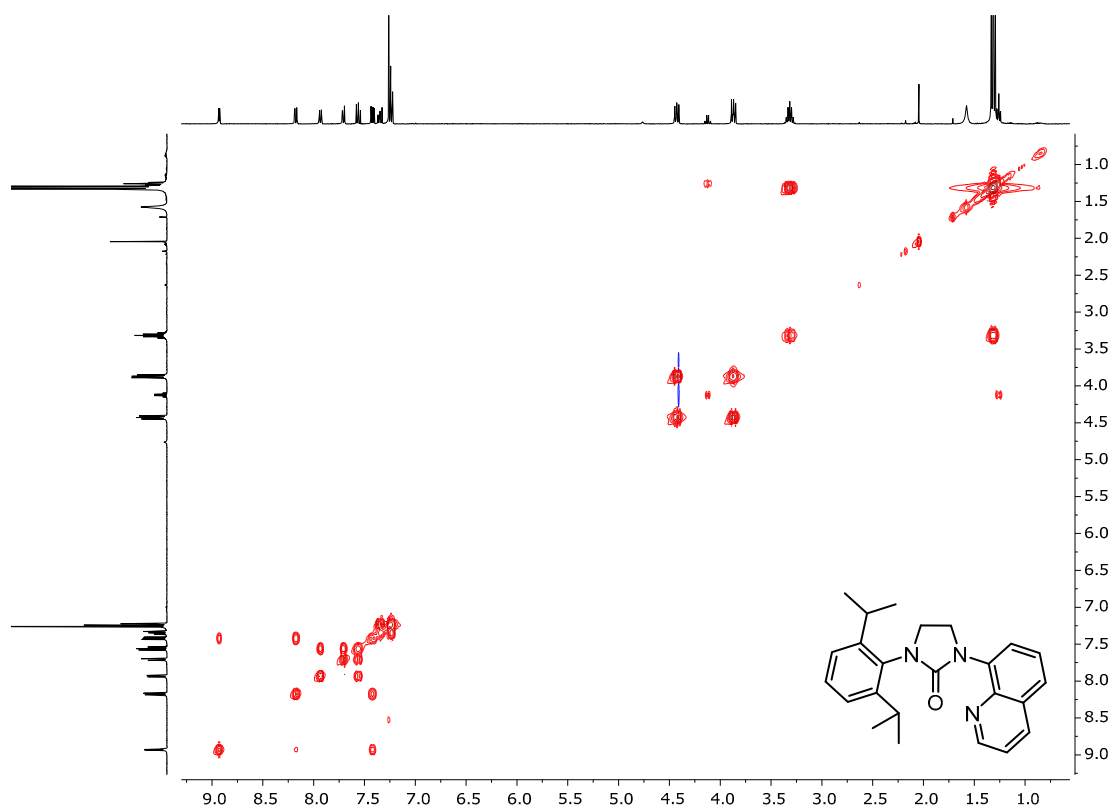


Figure S47. ^1H , ^1H -COSY NMR (400MHz, 298K) of L2^{ox} in CDCl_3 .

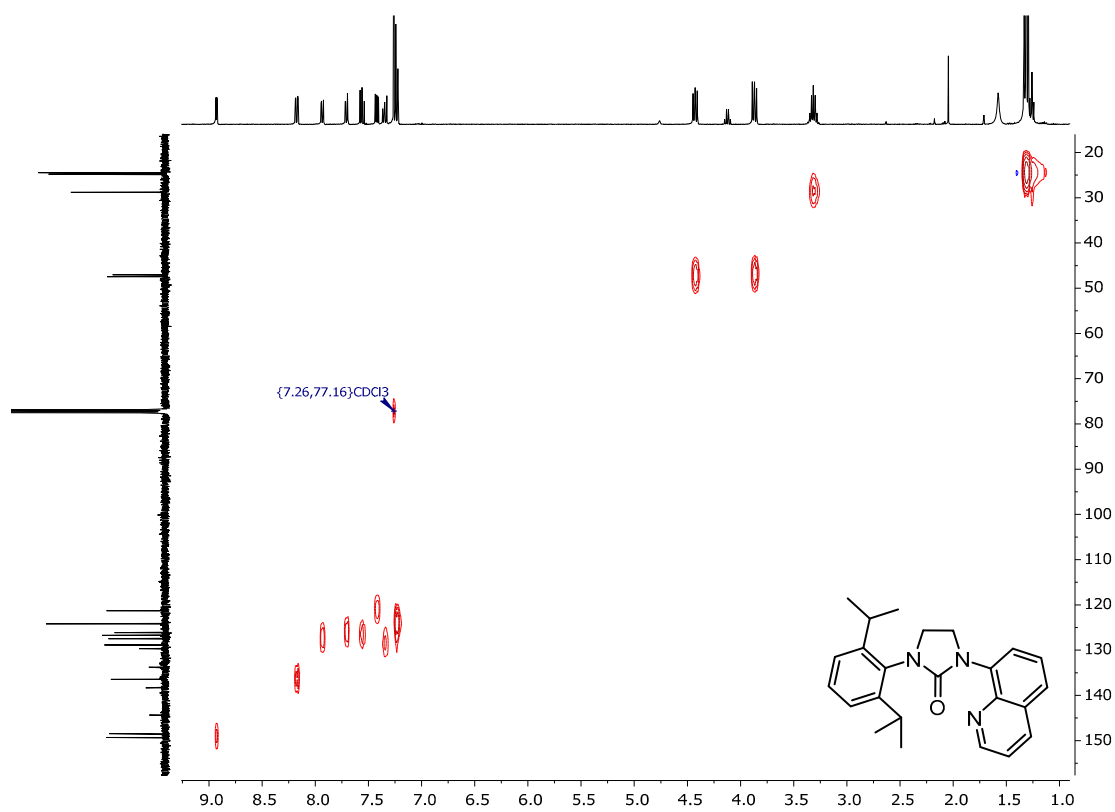


Figure S48. ^1H , ^{13}C -HSQC NMR (400MHz, 298K) of L2^{ox} in CDCl_3 .

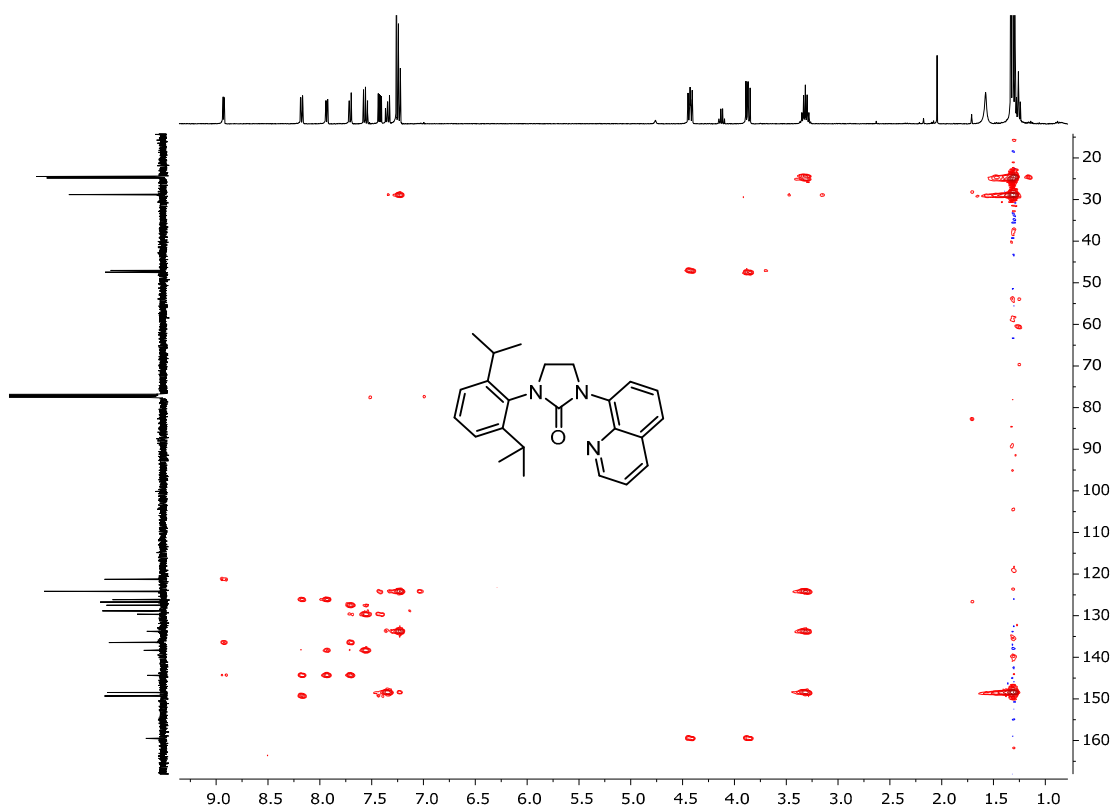


Figure S49. ^1H , ^{13}C -HMBC NMR (400MHz, 298K) of L2^{ox} in CDCl_3 .

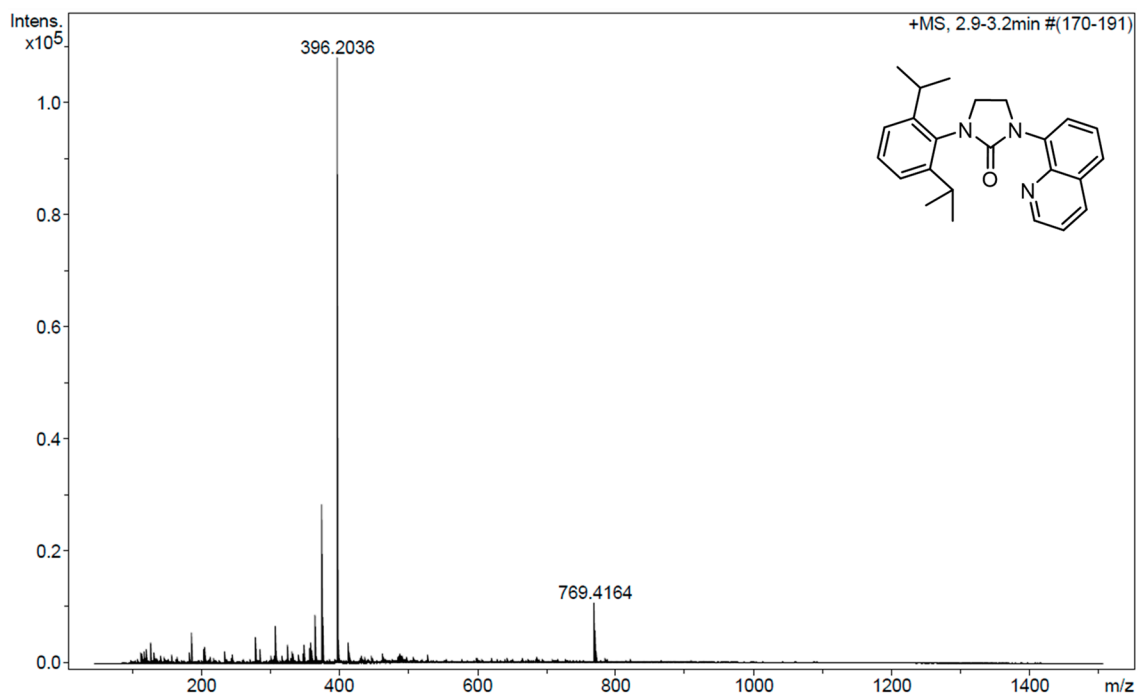


Figure S50. HRMS-ESI(+) of L2^{ox}.

S5.9. Compound L2^{ox}-I

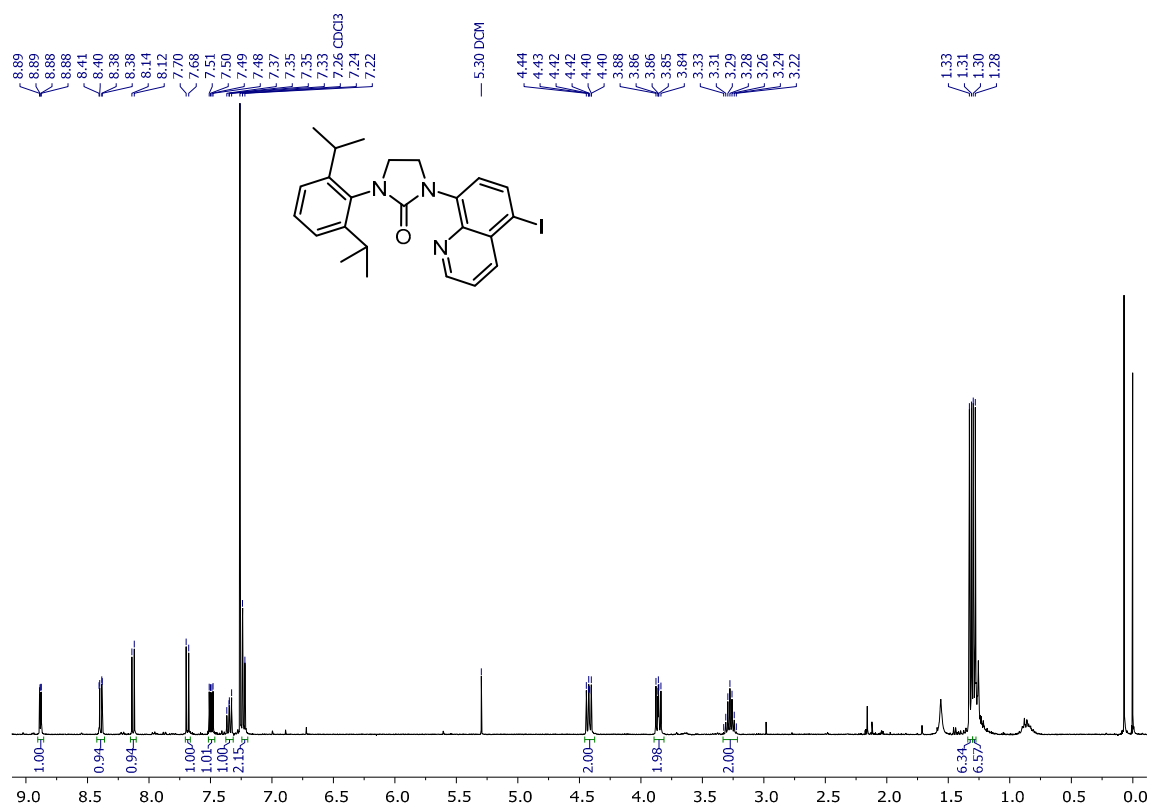


Figure S51. ¹H NMR (400MHz, 298K) of L2^{ox}-I in CDCl₃.

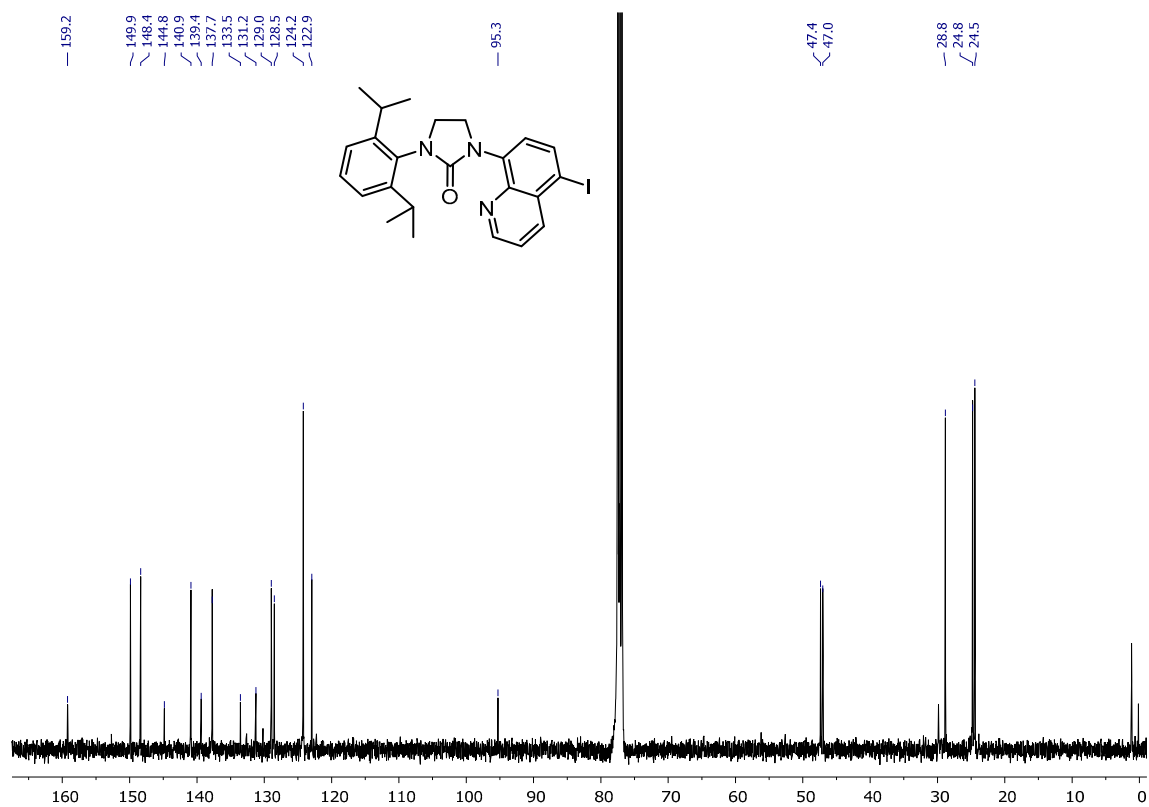


Figure S52. ¹³C {¹H} NMR (101MHz, 298K) of L2^{ox}-I in CDCl₃.

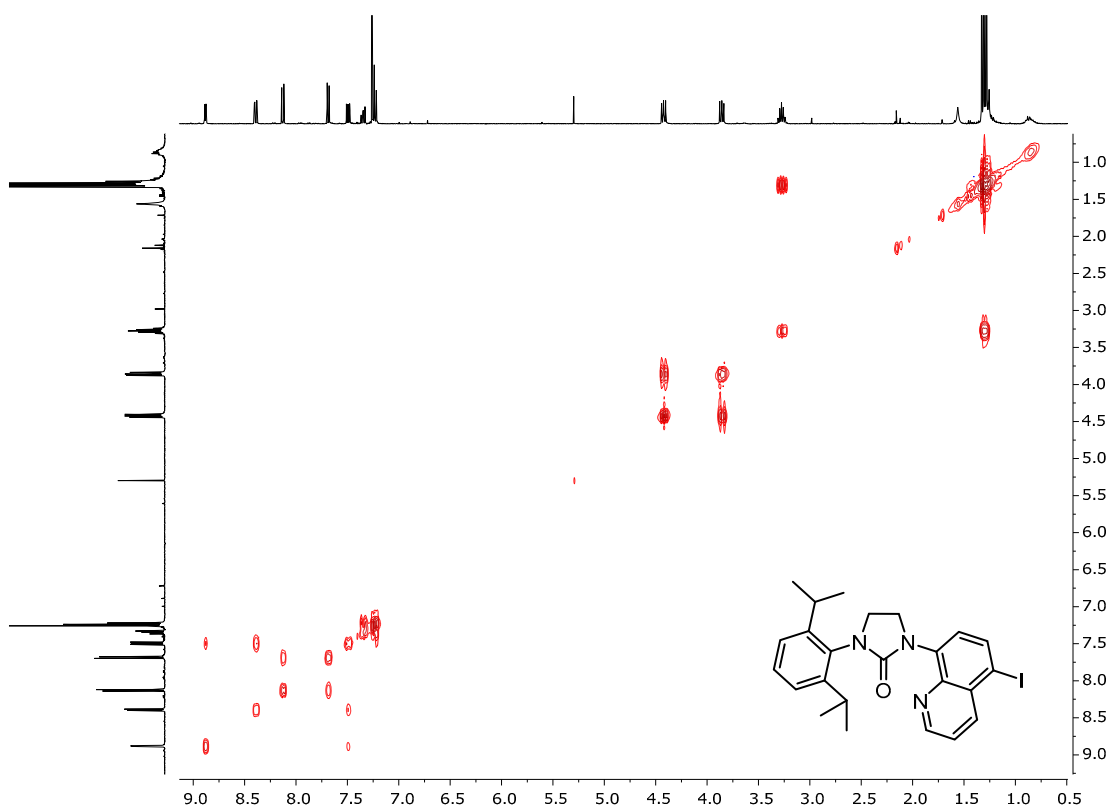


Figure S53. ^1H , ^1H -COSY NMR (400MHz, 298K) of $\text{L2}^{\text{ox-I}}$ in CDCl_3 .

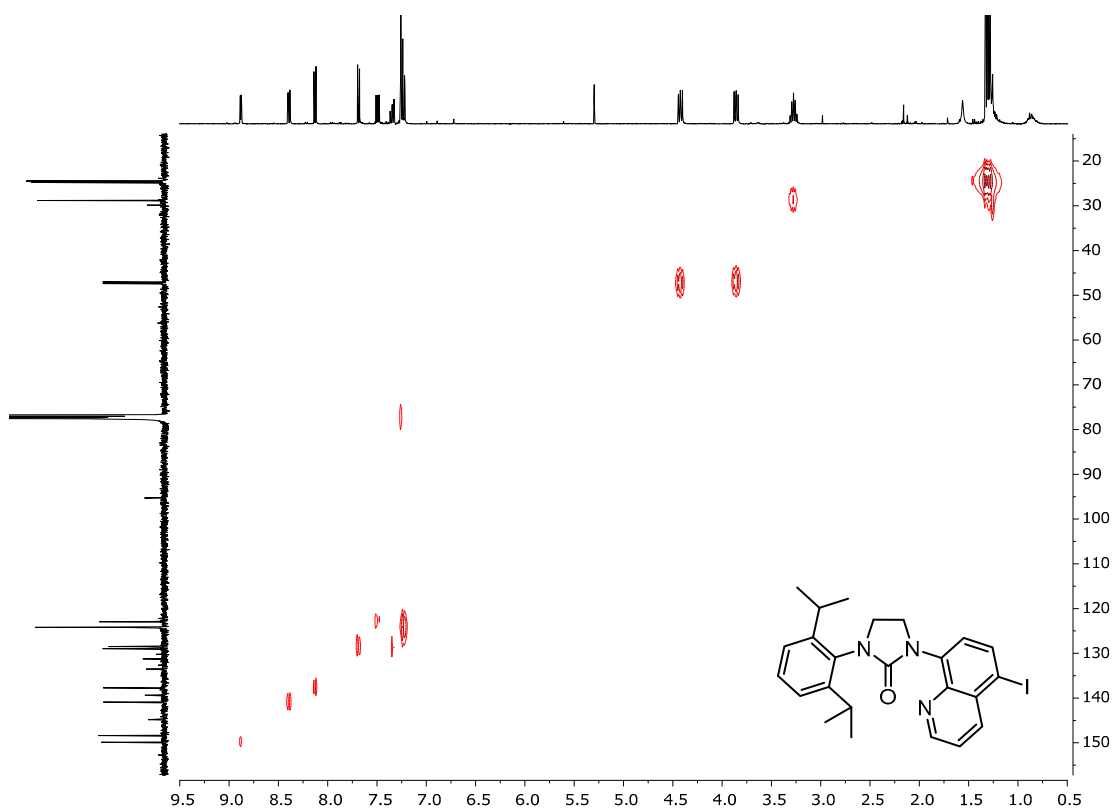


Figure S54. ^1H , ^{13}C -HSQC NMR (400MHz, 298K) of $\text{L2}^{\text{ox-I}}$ in CDCl_3 .

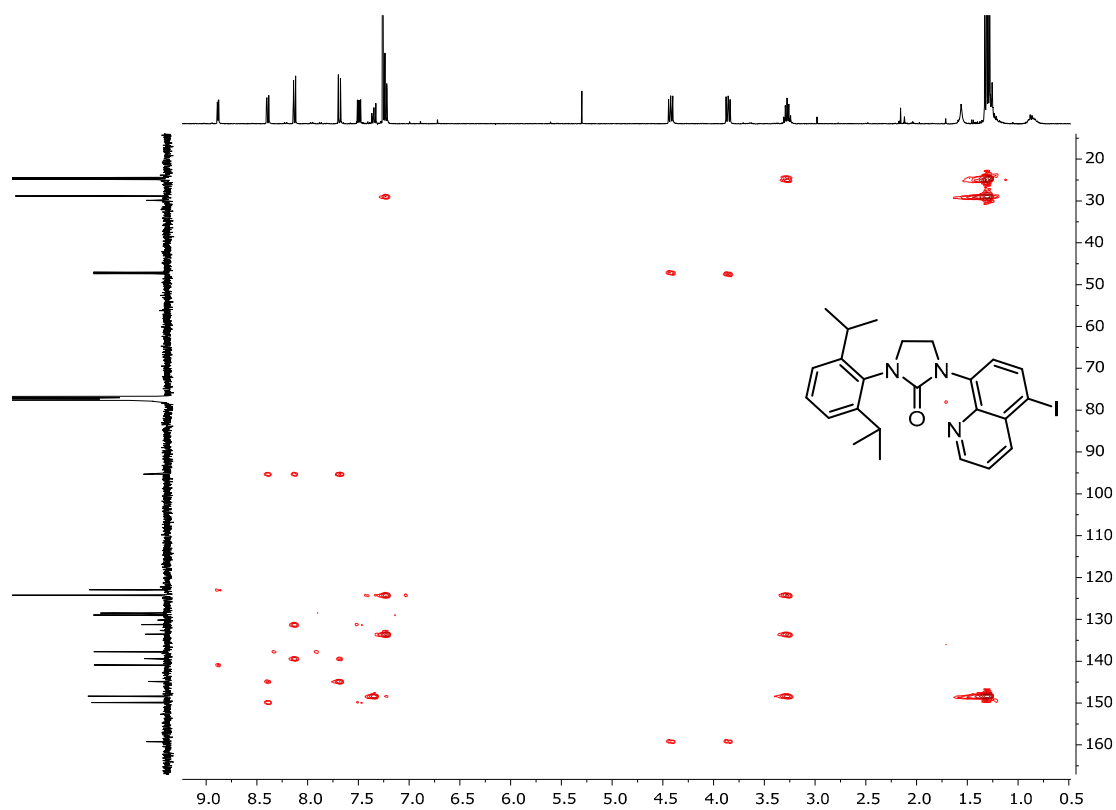


Figure S55. ^1H , ^{13}C -HMBC NMR (400MHz, 298K) of L2^{ox}-I in CDCl_3 .

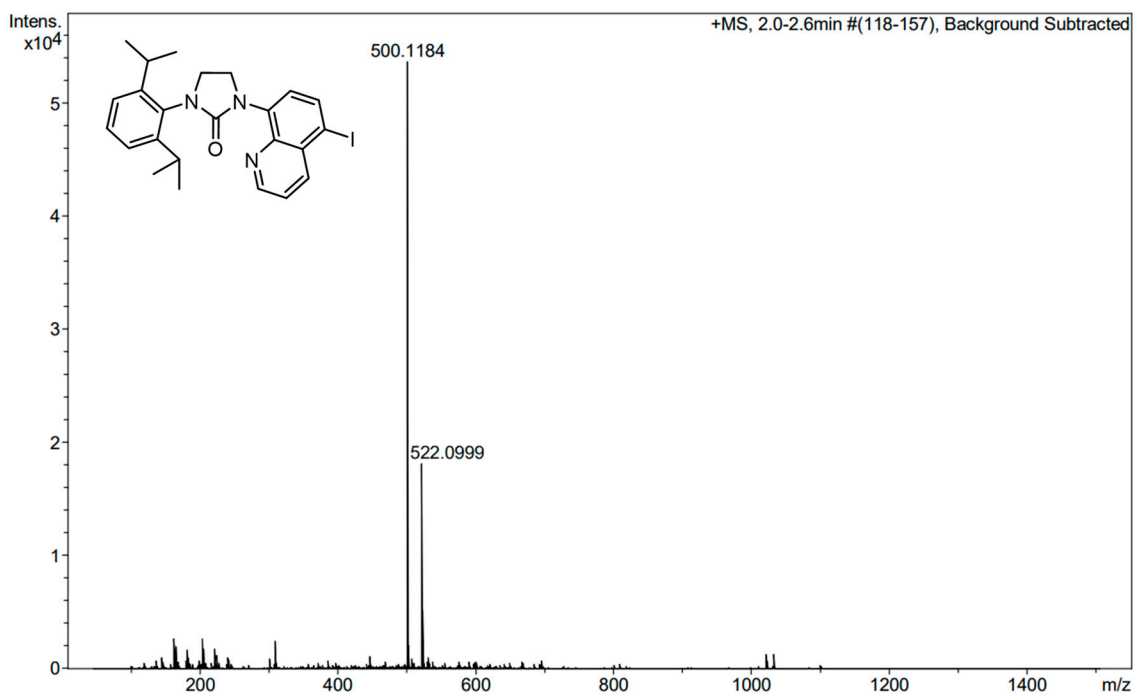


Figure S56. HRMS-ESI(+) of L2^{ox}-I.

S5.10. Compound L3^{ox}

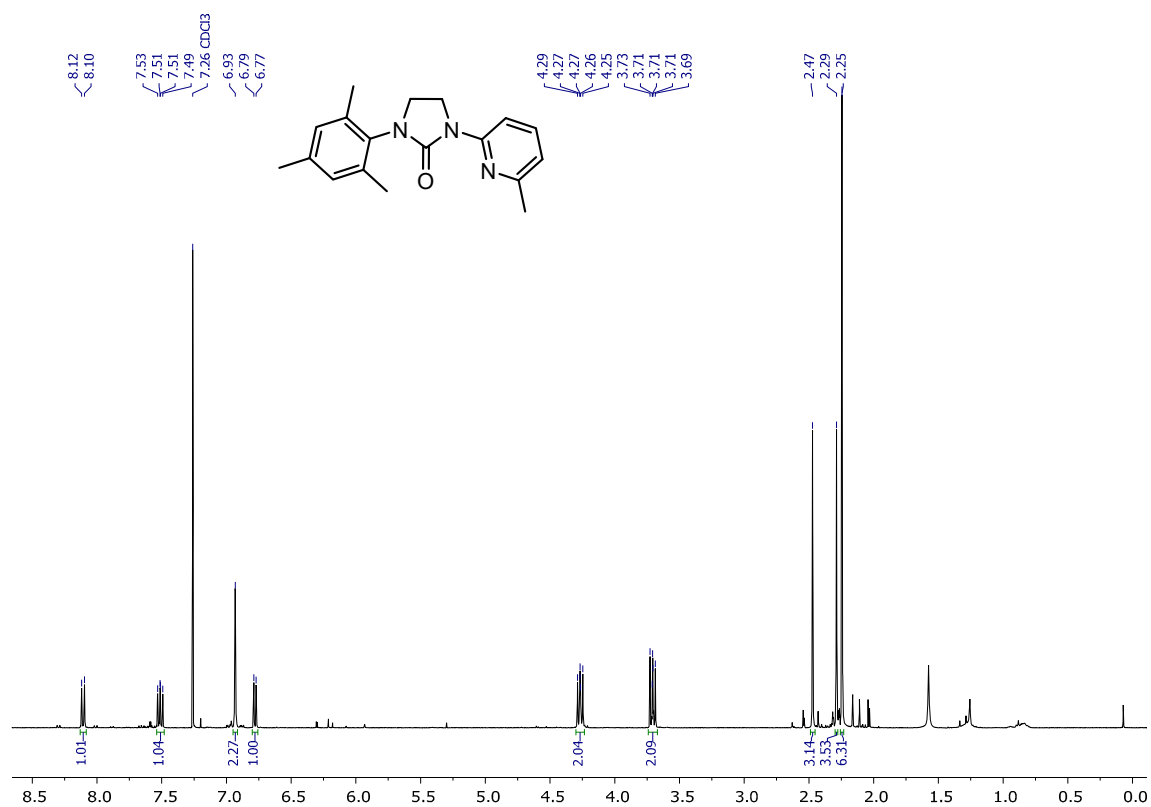


Figure S57. ¹H NMR (400MHz, 298K) of L3^{ox} in CDCl₃.

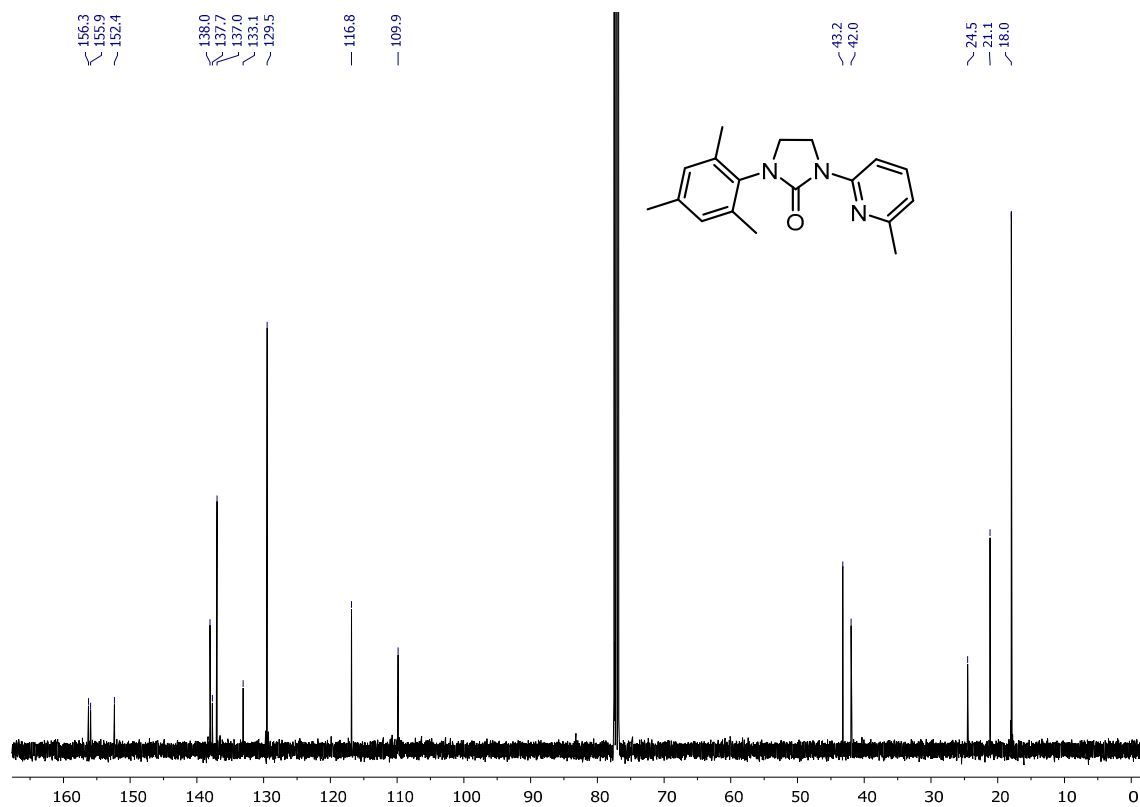
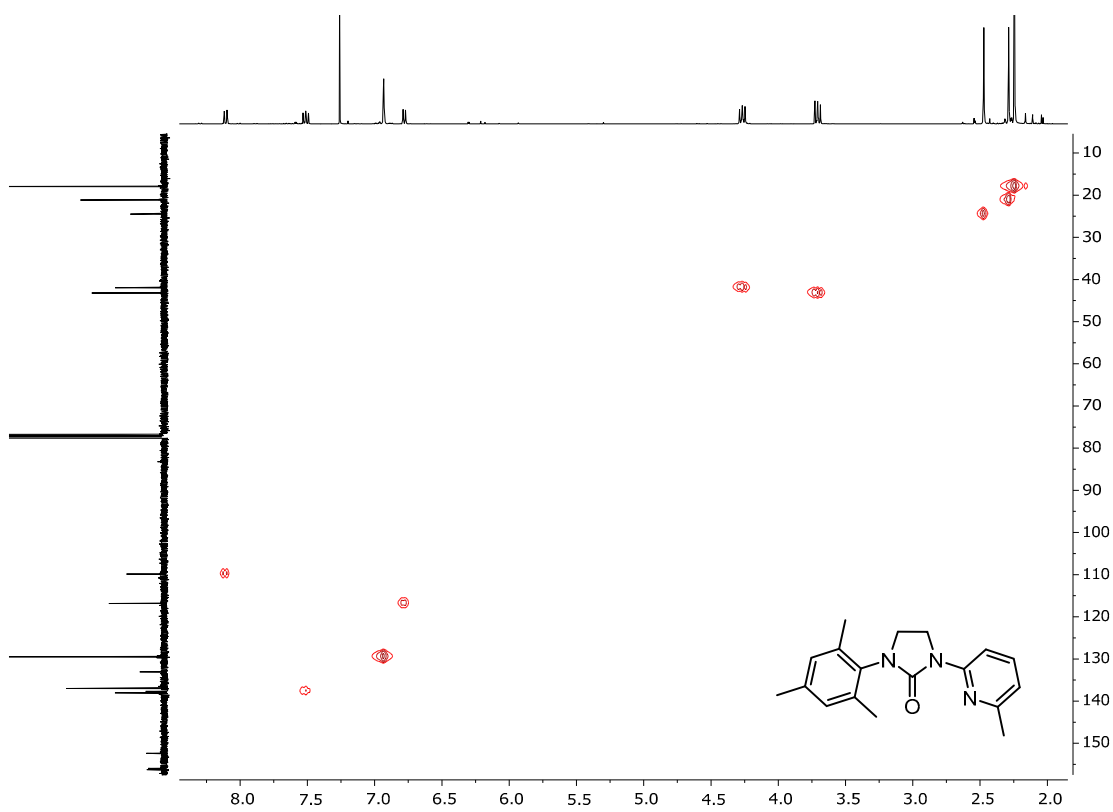
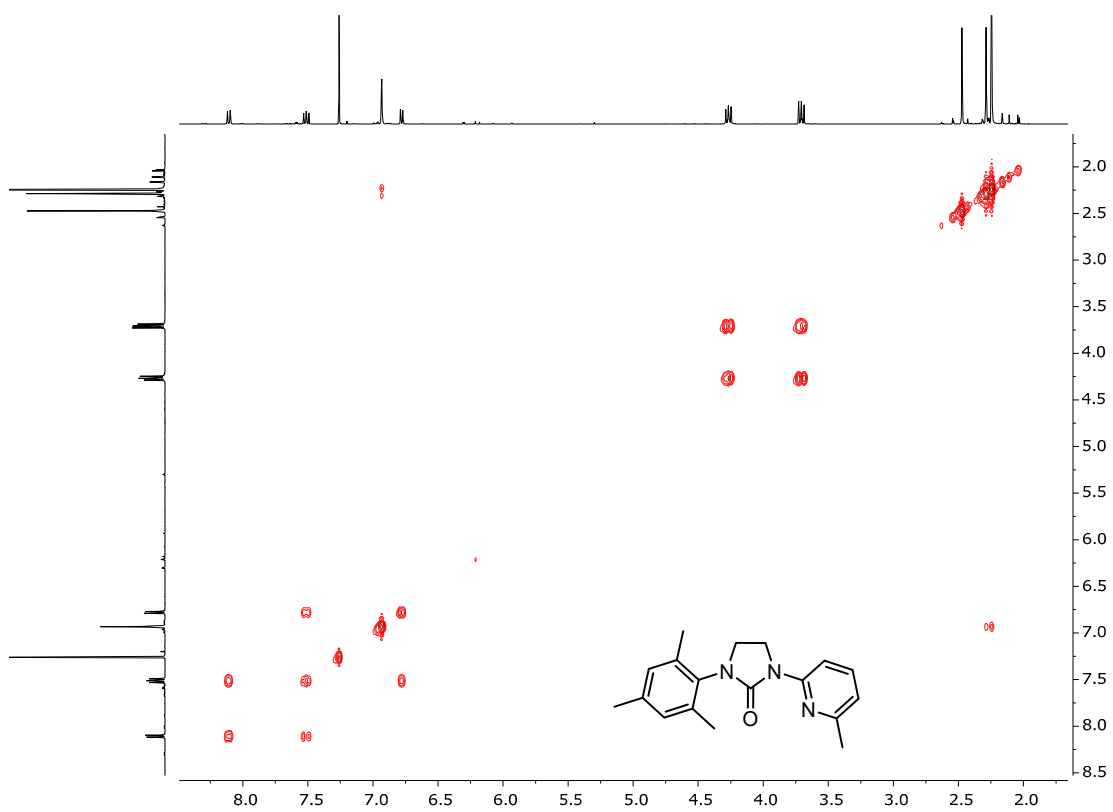


Figure S58. ¹³C{¹H} NMR (101MHz, 298K) of L3^{ox} in CDCl₃.



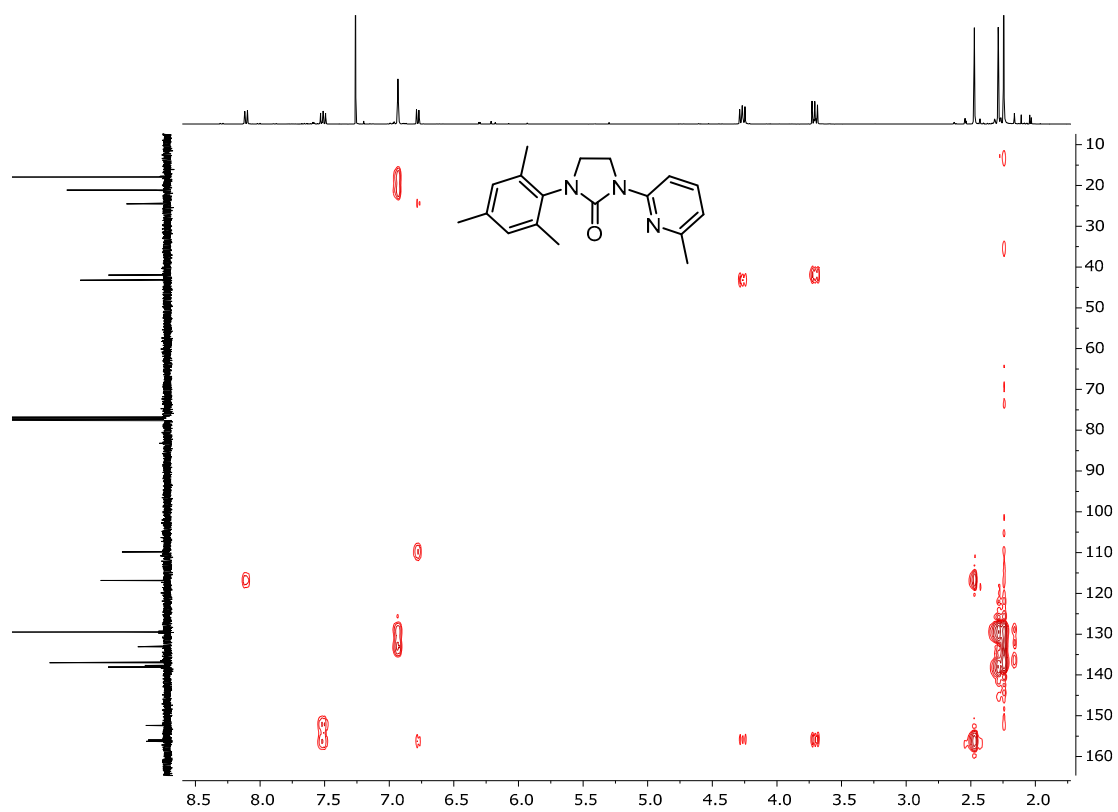


Figure S61. ^1H , ^{13}C -HMBC NMR (400 MHz, 298 K) of L3^{ox} in CDCl_3 .

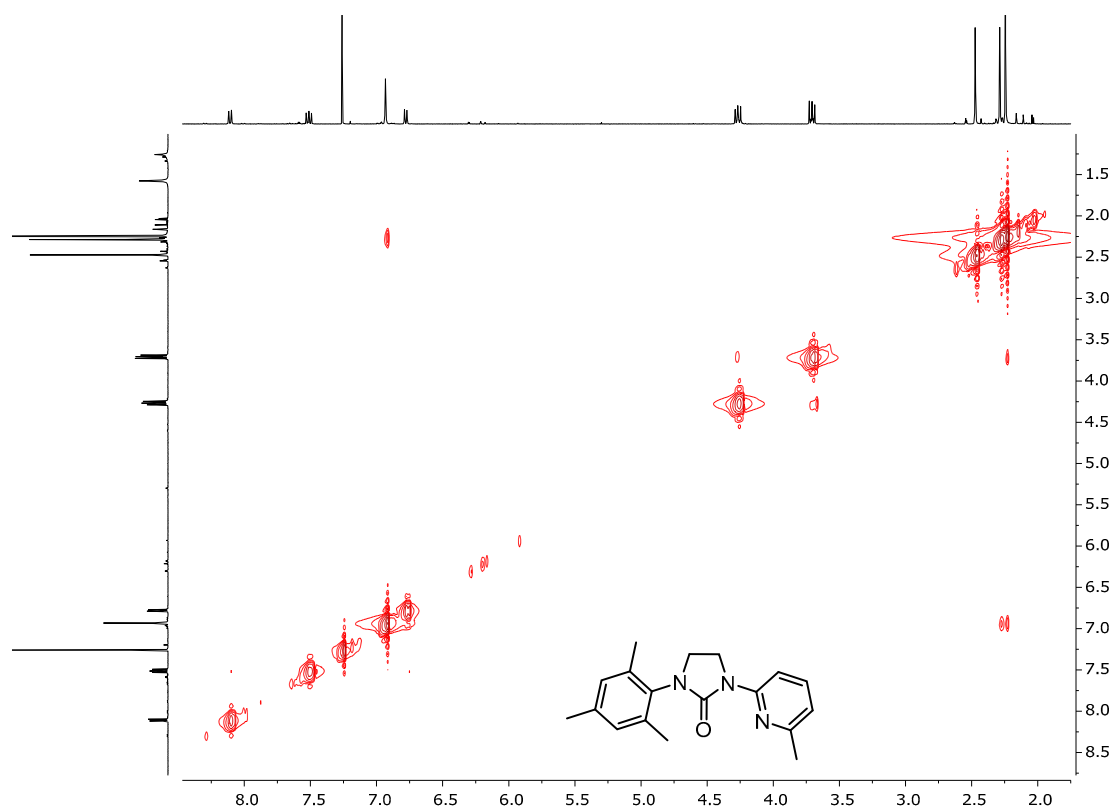


Figure S62. ^1H , ^1H -NOESY NMR (400 MHz, 298 K) of L3^{ox} in CDCl_3 .

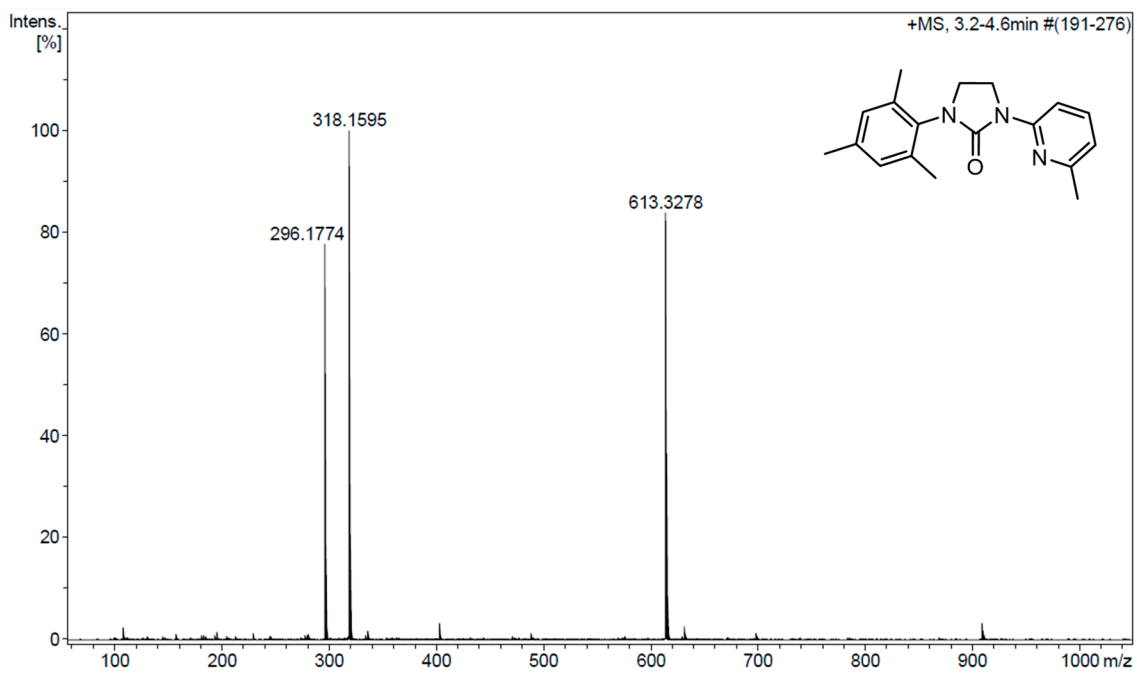
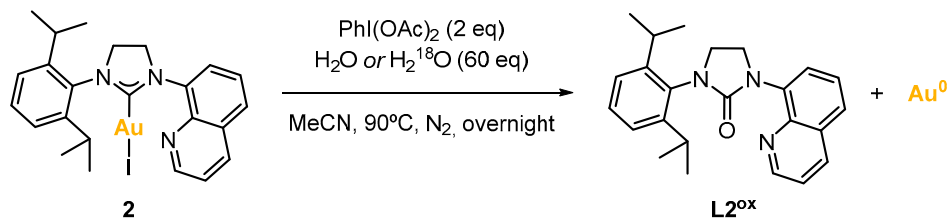


Figure S63. HRMS-ESI(+) of L3^{ox}.

S6. Experiments using water and ^{18}O -labeled water as additive

The origin of the oxygen atom in the formed imidazolinones was investigated by taking complex **2** as a case study and causing it to react with $\text{PhI}(\text{OAc})_2$, employing water or 97% ^{18}O -labeled water as additive (Scheme S4).



Scheme S4. Reaction of complex **2** with $\text{PhI}(\text{OAc})_2$ as oxidant and water as additive.

Complex **2** (12.3 mg, 0.018 mmol, 1.0 eq) and $\text{PhI}(\text{OAc})_2$ (12.1 mg, 0.038 mmol, 2.0 eq) were weighed in a vial. In the Schlenk line, the atmosphere of the vial was replaced with nitrogen. Then, anhydrous acetonitrile (0.8 mL) and water or ^{18}O -water (20 μL , 1.109 mmol, 61.6 eq) were added. The vial was sealed, and the mixture was allowed to react overnight at 90°C. The reaction crude was a clear brown solution with $\text{Au}(0)$ nuggets. The nuggets were separated by decantation, thoroughly washed with abundant acetonitrile several times, and dried. On the other hand, the solution was analyzed by HRMS-ESI to detect the formation of imidazolinone **L2^{ox}** and, when using H_2^{18}O , to detect and calculate the incorporation of ^{18}O (Figures S64 and S65). The imidazolinone **L2^{ox}** products were isolated by preparative TLC using a $\text{DCM}:\text{EtOAc}$ (9:1) mixture as eluent.

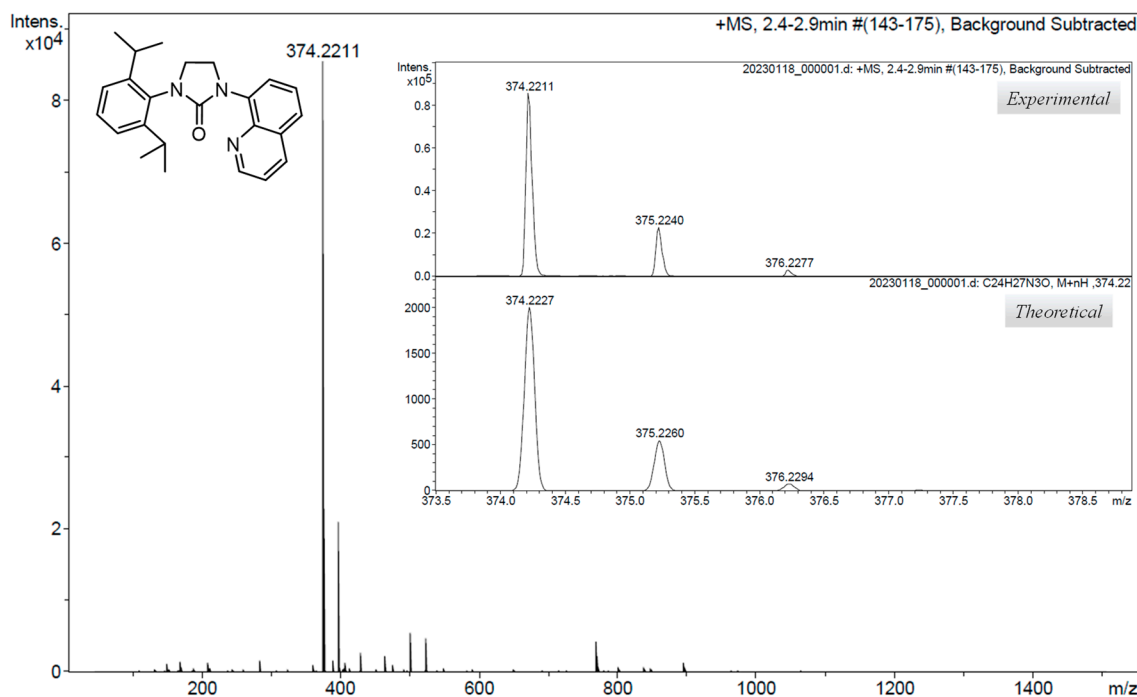


Figure S64. HRMS-ESI(+) of the reaction crude of complex **2**, $\text{PhI}(\text{OAc})_2$ and water (Table S2, entry 1); close-up of the peak at $m/z = 374.2$ corresponding to the $[\text{M}+\text{H}]^+$ species for $\text{NHC}=\text{}^{16}\text{O}$; and comparison to the theoretical isotopic pattern.

For the reaction using H₂¹⁸O, the percentage of ¹⁸O-labeled imidazolinone was calculated using the intensities of the isotopic patterns of the peaks at 374.2 and 376.2, corresponding to NHC=¹⁶O and NHC=¹⁸O, respectively.

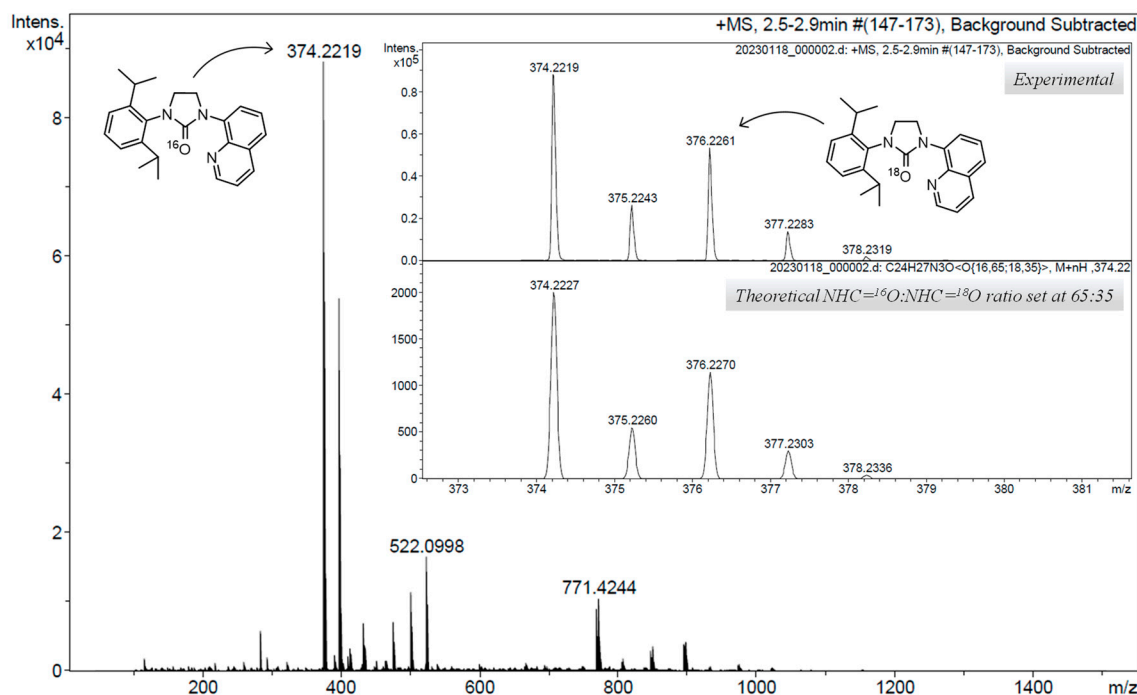


Figure S65. HRMS-ESI(+) of the reaction crude of complex **2**, PhI(OAc)₂ and ¹⁸O-labeled water (Table S2, entry 2); close-up of the peaks at *m/z* = 374.2 and 376.2 corresponding to the [M+H]⁺ species for NHC=¹⁶O and NHC=¹⁸O; and comparison to the theoretical isotopic pattern for an NHC=¹⁶O:NHC=¹⁸O ratio set at 65:35.

The results of the experiments using water are summarized in Table S2.

Table S2. Results of the reaction of complex **2** with PhI(OAc)₂ and water (Scheme S4).

Entry	Additive	Conv. Au(0)	^a Yield NHC=O	^b NHC= ¹⁶ O/ NHC= ¹⁸ O
1	H ₂ O	88%	48%	100/0
2	H ₂ ¹⁸ O	97%	41%	65/35

^a Isolated yield. ^b The ratio of non-labeled to labeled imidazolinone was calculated from the HRMS-ESI spectrum (Figure S65).

S7. X-Ray structures and crystallographic data

S7.1. Complex 1

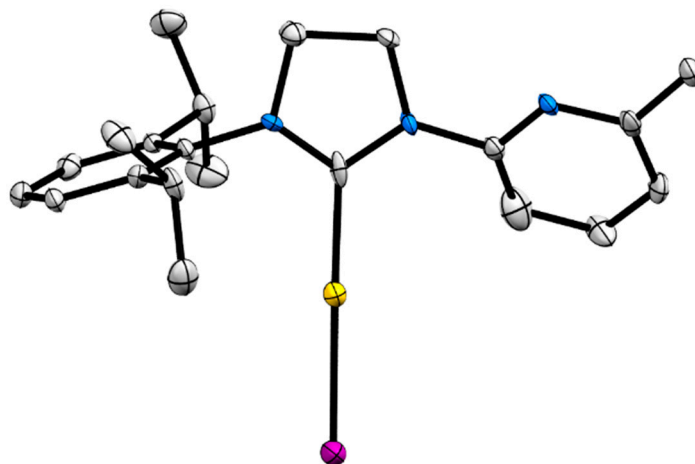


Figure S66. Crystal structure of **1** (CCDC 2238757). Ellipsoids set at 50% probability; H atoms are omitted for clarity.

Table S3. Crystallographic parameters for **1**.

Chemical formula	C ₂₁ H ₂₇ AuIN ₃	
Formula weight	645.32 g/mol	
Temperature	100(2) K	
Wavelength	0.71073 Å	
Crystal size	0.010 x 0.050 x 0.300 mm	
Crystal system	Monoclinic	
Space group	P 1 21/n 1	
Unit cell dimensions	a = 11.191(2) Å	α = 90°
	b = 17.029(3) Å	β = 103.500(6)°
	c = 11.632(2) Å	γ = 90°
Volume	2155.5(7) Å ³	
Density (calculated)	1.988 g/cm ³	
Absorption coefficient	8.266 mm ⁻¹	
Final R indices	3780 data; I > 2σ(I)	R1 = 0.0611, wR2 = 0.1278
	All data	R1 = 0.1120, wR2 = 0.1550

A colorless needle-like specimen of C₂₁H₂₇AuIN₃, with approximate dimensions 0.010 mm x 0.050 mm x 0.300 mm, was used for the X-ray crystallographic analysis. A total of 542 frames were collected. The total exposure time was 2.00 hours. The frames were integrated with the Bruker SAINT software package using a narrow-frame algorithm. The integration of the data using a monoclinic unit cell yielded a total of 49421 reflections to a maximum θ angle of 28.52° (0.74 Å resolution), of which 5442 were independent

(average redundancy 9.081, completeness = 99.3%, $R_{\text{int}} = 15.63\%$, $R_{\text{sig}} = 7.44\%$) and 3780 (69.46%) were greater than $2\sigma(F_2)$. The final cell constants of $a = 11.191(2)$ Å, $b = 17.029(3)$ Å, $c = 11.632(2)$ Å, $\beta = 103.500(6)^\circ$, volume = $2155.5(7)$ Å³, are based upon the refinement of the XYZ-centroids of 9886 reflections above $20 \sigma(I)$ with $5.139^\circ < 2\theta < 56.75^\circ$. Data were corrected for absorption effects using the Numerical Mu From Formula method (SADABS). The ratio of minimum to maximum apparent transmission was 0.232. The calculated minimum and maximum transmission coefficients (based on crystal size) were 0.1910 and 0.9220. The structure was solved and refined by means of the Bruker SHELXTL Software Package using the space group $P 1 21/n 1$, with $Z = 4$ for the formula unit, $C_{21}H_{27}AuIN_3$. The final anisotropic full-matrix least-squares refinement on F^2 , with 240 variables, converged at $R_1 = 6.11\%$ for the observed data and $wR_2 = 15.50\%$ for all data. The goodness-of-fit was 1.138. The largest peak in the final difference electron density synthesis was $4.529 \text{ e}^-/\text{Å}^3$, and the largest hole was $-4.080 \text{ e}^-/\text{Å}^3$ with an RMS deviation of $0.334 \text{ e}^-/\text{Å}^3$. On the basis of the final model, the calculated density was 1.988 g/cm^3 and $F(000)$, 1224 e^- .

S7.2. Complex 2

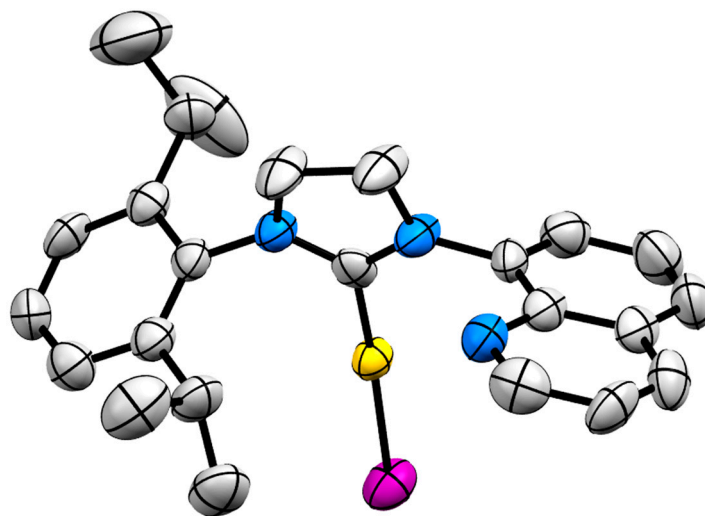


Figure S67. Crystal structure of **2** (CCDC2238754). Ellipsoids set at 50% probability; H atoms are omitted for clarity.

Table S4. Crystallographic parameters for **2**.

Chemical formula	C ₂₄ H ₂₇ AuIN ₃	
Formula weight	681.35 g/mol	
Temperature	100(2) K	
Wavelength	0.71073 Å	
Crystal size	0.250 x 0.250 x 0.200 mm	
Crystal system	Monoclinic	
Space group	P 21/c	
Unit cell dimensions	a = 10.353(2) Å	α = 90°
	b = 13.845(3) Å	β = 104.203(4)°
	c = 17.507(4) Å	γ = 90°
Volume	2432.6(9) Å ³	
Density (calculated)	1.860 g/cm ³	
Absorption coefficient	7.331 mm ⁻¹	
Final R indices	3439 data; I>2σ(I)	R1 = 0.0508, wR2 = 0.0925
	All data	R1 = 0.0873, wR2 = 0.1089

A yellow specimen of C₂₄H₂₇AuIN₃, with approximate dimensions 0.250 mm x 0.250 mm x 0.200 mm, was used for the X-ray crystallographic analysis. The measurement was carried out on a *BRUKER SMART APEX CCD* diffractometer using graphite-monochromated Mo Kα radiation ($\lambda = 0.71073$ Å) from an x-Ray tube. The measurements were made in the range from 1.90 to 28.30° for θ . Hemi-sphere data collection was carried out with ω and ϕ scans. A total of 9725 reflections were collected, of which 5087 ($R_{\text{int}} = 0.061$) were unique. The programs used were the following: data collection, Smart; data reduction, Saint+; and absorption correction, SADABS. Structure solution and refinement were performed using SHELXL. The structure was solved by direct methods and refined by the full-matrix least-squares methods on F^2 . The non-hydrogen atoms were refined anisotropically. The H-atoms were placed in geometrically optimized positions and forced to ride on the atoms to which they are attached.

S7.3. Complex 3

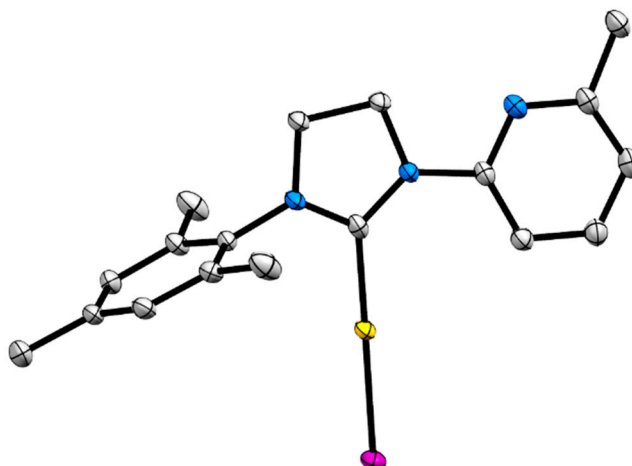


Figure S68. Crystal structure of **3** (CCDC 2238755). Ellipsoids set at 50% probability; H atoms are omitted for clarity.

Table S5. Crystallographic parameters for **3**.

Chemical formula	C ₁₈ H ₂₁ AuIN ₃	
Formula weight	603.24 g/mol	
Temperature	100(2) K	
Wavelength	0.71073 Å	
Crystal size	0.150 x 0.200 x 0.200 mm	
Crystal system	Monoclinic	
Space group	P 1 21/c 1	
Unit cell dimensions	a = 9.1638(5) Å	α = 90°
	b = 12.7701(7) Å	β = 102.7840(10)°
	c = 15.9946(8) Å	γ = 90°
Volume	1825.33(17) Å ³	
Density (calculated)	2.195 g/cm ³	
Absorption coefficient	9.754 mm ⁻¹	
Final R indices	5734 data; I > 2σ(I)	R1 = 0.0240, wR2 = 0.0500
	All data	R1 = 0.0307, wR2 = 0.0526

A colorless block-like specimen of C₁₈H₂₁AuIN₃, with approximate dimensions of 0.150 mm x 0.200 mm x 0.200 mm, was used for the X-ray crystallographic analysis. A total of 428 frames were collected. The total exposure time was 1.19 hours. The frames were integrated with the Bruker SAINT software package using a narrow-frame algorithm. The integration of the data, using a monoclinic unit cell, yielded a total of 37990 reflections to a maximum θ angle of 32.21° (0.67 Å resolution), of which 6435 were independent (average redundancy 5.904, completeness = 99.7%, R_{int} = 4.63%, R_{sig} = 2.97%) and 5734

(89.11%) were greater than $2\sigma(F_2)$. The final cell constants of $a = 9.1638(5) \text{ \AA}$, $b = 12.7701(7) \text{ \AA}$, $c = 15.9946(8) \text{ \AA}$, $\beta = 102.7840(10)^\circ$, volume = $1825.33(17) \text{ \AA}^3$, were based upon the refinement of the XYZ-centroids of 121 reflections above $20 \sigma(I)$ with $6.568^\circ < 2\theta < 49.17^\circ$. Data were corrected for absorption effects using the Numerical Mu From Formula method (SADABS). The ratio of minimum to maximum apparent transmission was 0.221. The calculated minimum and maximum transmission coefficients (based on crystal size) were 0.2460 and 0.3220. The structure was solved and refined by means of the Bruker SHELXTL Software Package, using the space group $P 1 21/c 1$, with $Z = 4$ for the formula unit, $C_{18}H_{21}AuIN_3$. The final anisotropic full-matrix least-squares refinement on F^2 with 212 variables converged at $R1 = 2.40\%$ for the observed data and $wR2 = 5.26\%$ for all data. The goodness-of-fit was 1.096. The largest peak in the final difference electron density synthesis was $1.621 \text{ e}^-/\text{\AA}^3$, and the largest hole was $-0.850 \text{ e}^-/\text{\AA}^3$ with an RMS deviation of $0.156 \text{ e}^-/\text{\AA}^3$. On the basis of the final model, the calculated density was 2.195 g/cm^3 and $F(000)$, 1128 e^- .

S7.4. Complex 4

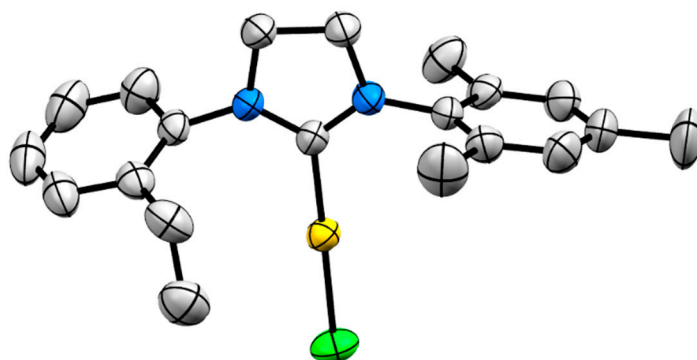


Figure S69. Crystal structure of **4** (CCDC 2238756). Ellipsoids set at 50% probability; H atoms are omitted for clarity.

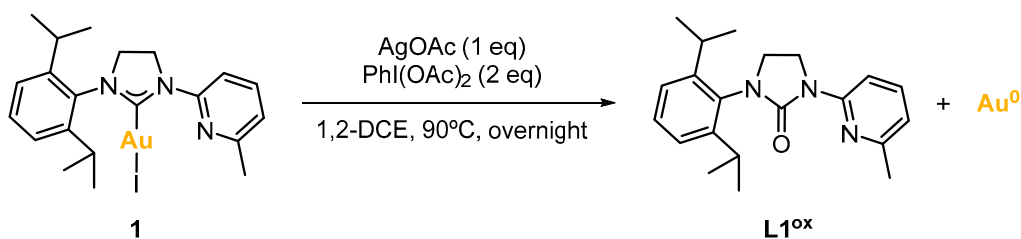
Table S6. Crystallographic parameters for **4**.

Chemical formula	C ₂₀ H ₂₄ AuCIN ₂	
Formula weight	524.83 g/mol	
Temperature	300(2) K	
Wavelength	0.71076 Å	
Crystal size	0.080 x 0.100 x 0.280 mm	
Crystal system	Monoclinic	
Space group	P 1 21/c 1	
Unit cell dimensions	a = 19.07(2) Å	α = 90°
	b = 8.236(11) Å	β = 92.08(4)°
	c = 12.435(15) Å	γ = 90°
Volume	1952.(4) Å ³	
Density (calculated)	1.786 g/cm ³	
Absorption coefficient	7.678 mm ⁻¹	
Final R indices	3779 data; I>2σ(I)	R1 = 0.0312, wR2 = 0.0630
	All data	R1 = 0.0705, wR2 = 0.0724

A colorless needle-like specimen of C₂₀H₂₄AuCIN₂, with approximate dimensions of 0.080 mm x 0.100 mm x 0.280 mm, was used for the X-ray crystallographic analysis. The X-ray intensity data were measured on a three-circle diffractometer system equipped with a ceramic x-ray tube (Mo Kα, λ = 0.71076 Å) and a doubly curved silicon crystal Bruker Triumph monochromator. A total of 1734 frames were collected. The total exposure time was 13.00 hours. The frames were integrated with the Bruker SAINT software package using a narrow-frame algorithm. The integration of the data using a monoclinic unit cell yielded a total of 112940 reflections to a maximum θ angle of 29.64° (0.72 Å resolution), of which 4883 were independent (average redundancy 23.129, completeness = 88.6%, R_{int} = 6.71%, R_{sig} = 3.82%) and 3779 (77.39%) were greater than 2σ(F₂). The final cell constants of \underline{a} = 19.07(2) Å, \underline{b} = 8.236(11) Å, \underline{c} = 12.435(15) Å, β = 92.08(4)°, volume = 1952.(4) Å³, were based upon the refinement of the XYZ-centroids of 9603 reflections above 20 σ(I), with 5.892° < 2θ < 53.88°. Data were corrected for absorption effects using the Multi-Scan method (SADABS). The ratio of minimum to maximum apparent transmission was 0.552. The calculated minimum and maximum transmission coefficients (based on crystal size) were 0.4117 and 0.7455. The structure was solved and refined by means of the Bruker SHELXTL Software Package, using the space group P 1 21/c 1, with Z = 4 for the formula unit, C₂₀H₂₄AuCIN₂. The final anisotropic full-matrix least-squares refinement on F² with 221 variables converged at R1 = 3.12% for the observed data and wR2 = 7.24% for all data. The goodness-of-fit was 1.176. The largest peak in the final difference electron density synthesis was 1.706 e⁻/Å³, and the largest hole was -2.804 e⁻/Å³ with an RMS deviation of 0.183 e⁻/Å³. On the basis of the final model, the calculated density was 1.786 g/cm³ and F(000), 1016 e⁻.

S8. SEM-EDX characterization of Au(0) macroaggregates

In order to analyze the obtained Au(0) macroaggregates on a general basis, from the reactions of Au(I) complexes with oxidants (Section 4), the reaction depicted in Scheme S4 was selected as the case study. The Au(0) nuggets were isolated from the reaction outcome by decantation, then washed with abundant 1,2-DCE and, finally, dried under vacuum. The dried Au(0) nuggets were morphologically characterized by scanning electron microscopy (SEM), and energy-dispersive x-ray spectroscopy (EDX) allowed for the analysis of the elemental composition.



Scheme S5. Formation of product **L1^{ox}** and Au(0) macroaggregates from complex **1**.

S8.1. SEM images

The images displayed herein show that the Au(0) macroaggregates have irregular shapes and sizes, reaching particle lengths of up to ~500 μ m. The surfaces of the particles are irregular and feature both granulated and flat domains.

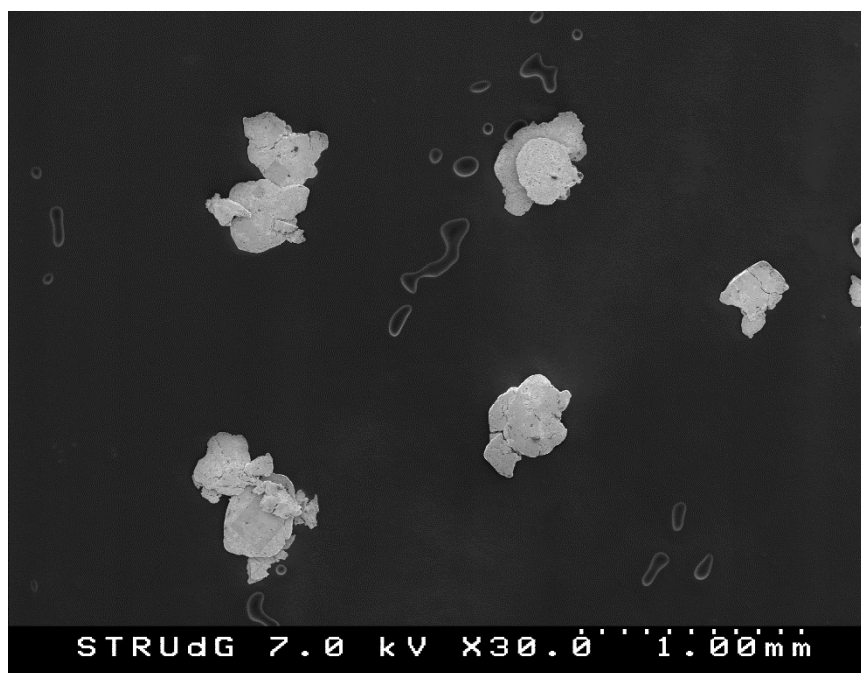


Figure S70. SEM image at x30.

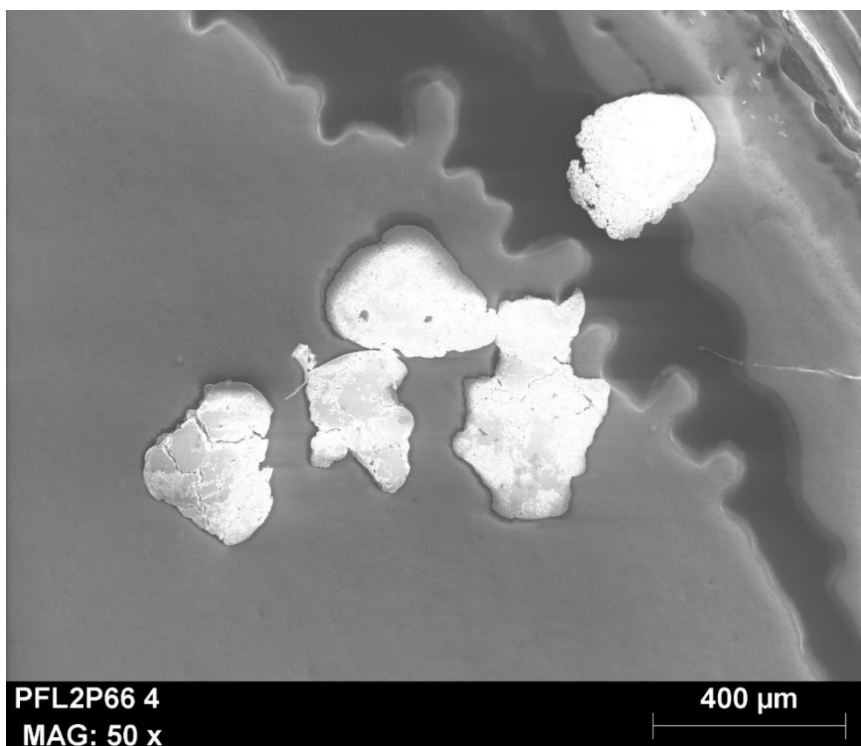


Figure S71. SEM image at x50.

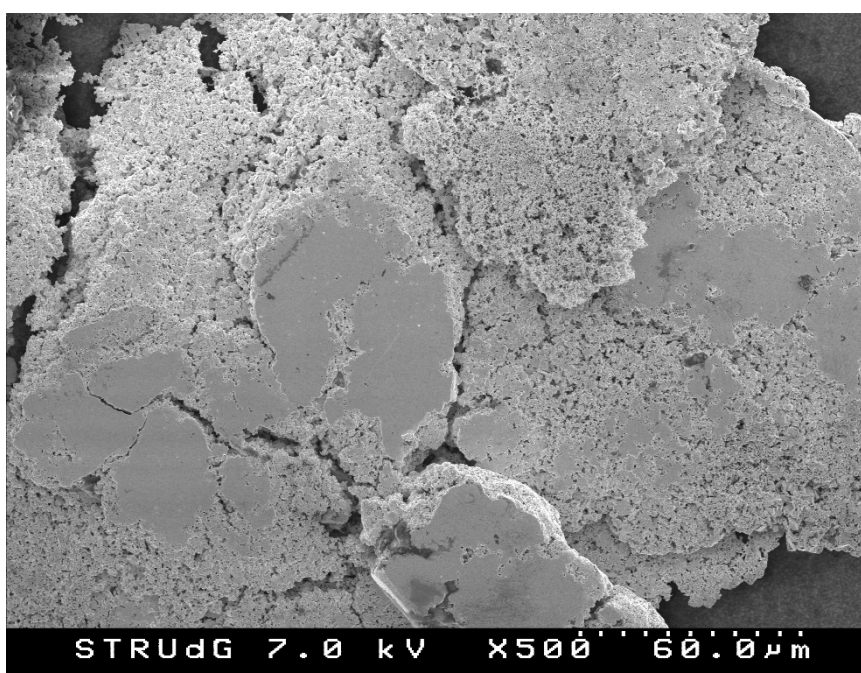


Figure S72. SEM image at x500.

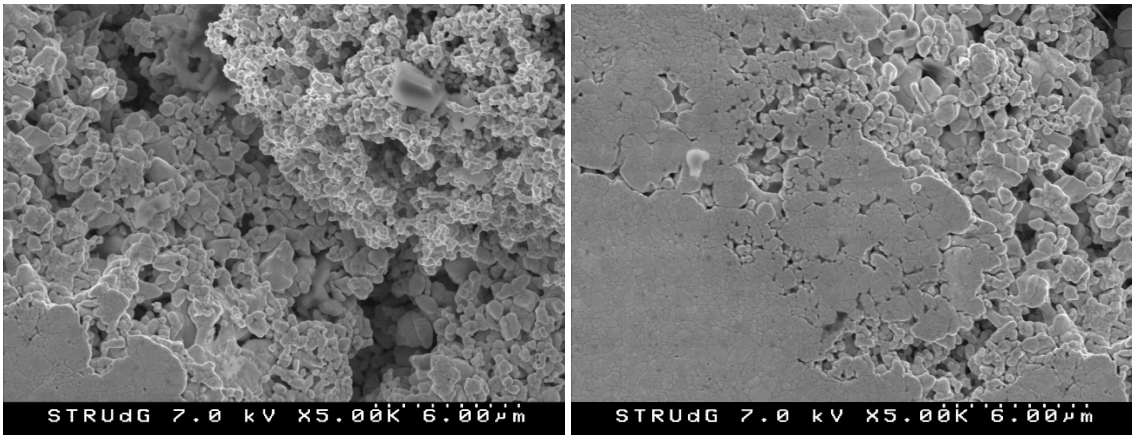


Figure S73. SEM images at x5K.

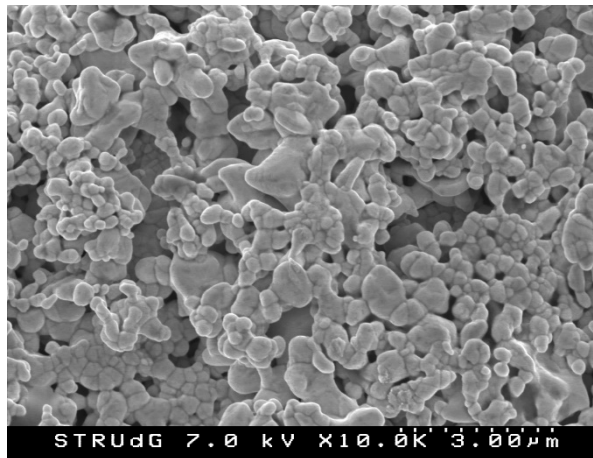
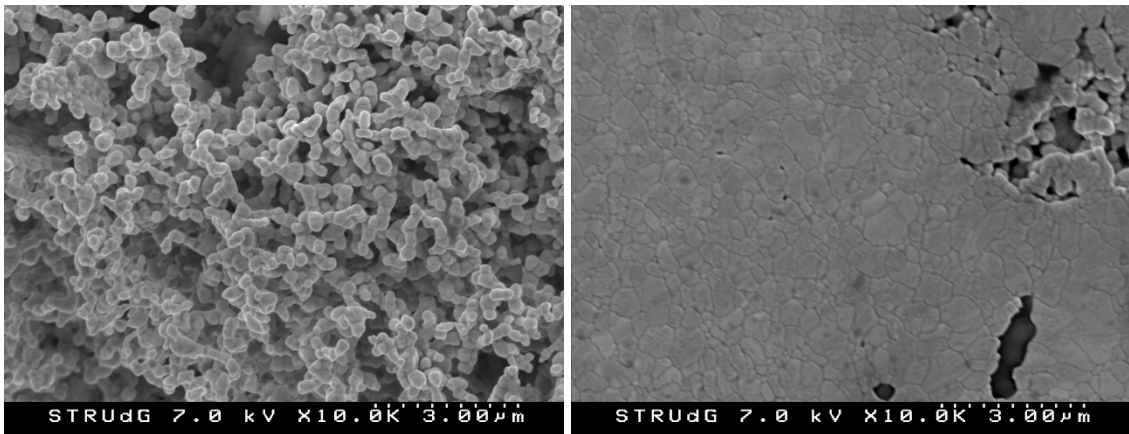


Figure S74. SEM images at x10K.

S8.2. SEM-EDX analysis

The determination of the elemental composition of the particles was carried out at morphologically different regions of the particles. All of them showed high purity on Au, and the observed C and N could be attributed to impurities from the carbon tape support.

SEM-EDX of a granulated region

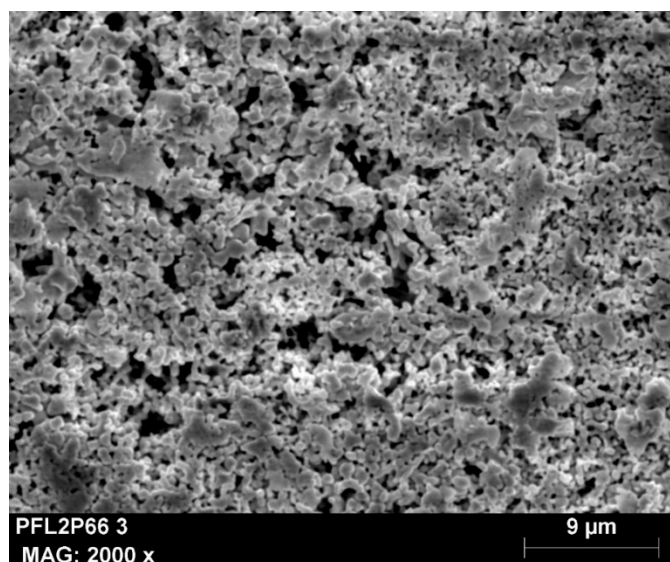


Figure S75. Granulated zone analyzed by SEM-EDX.

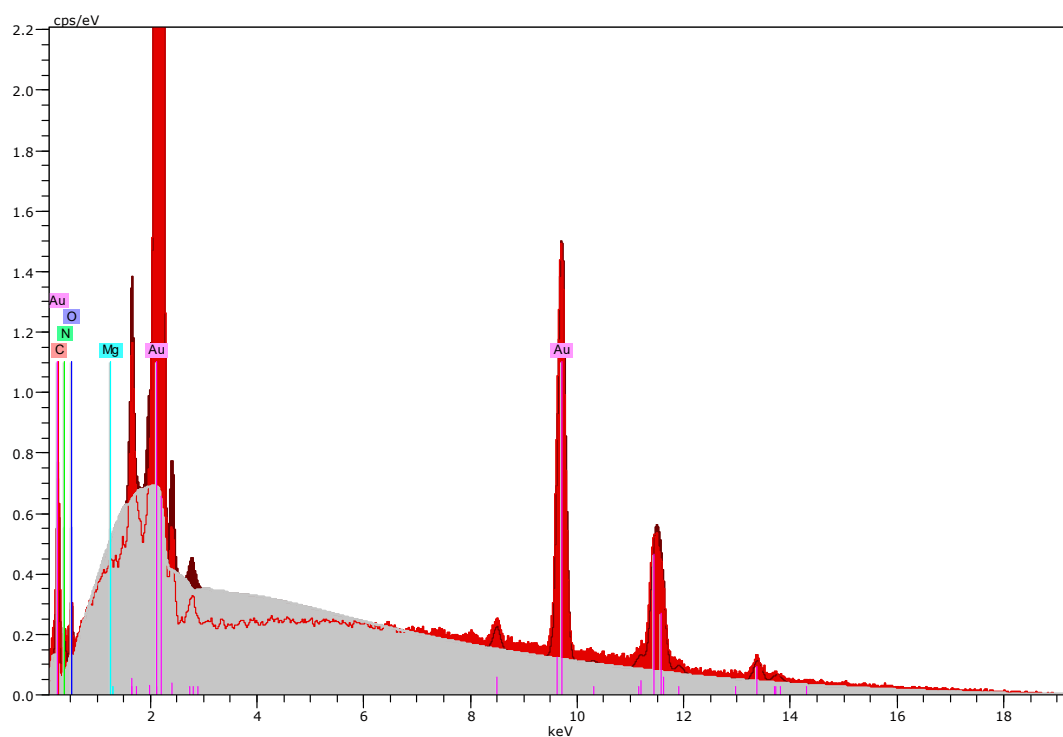


Figure S76. EDX spectrum of a granulated region.

Element	Series	unn. C [wt.%]	norm. C [wt.%]	Atom. C [at.%]
Carbon	K-series	9.22	7.21	45.01
Nitrogen	K-series	3.29	2.57	13.77
Oxygen	K-series	2.05	1.60	7.51
Magnesium	K-series	0.00	0.00	0.00
Gold	L-series	113.18	88.61	33.71
Total:		127.73	100.00	100.00

SEM-EDX of a flat region

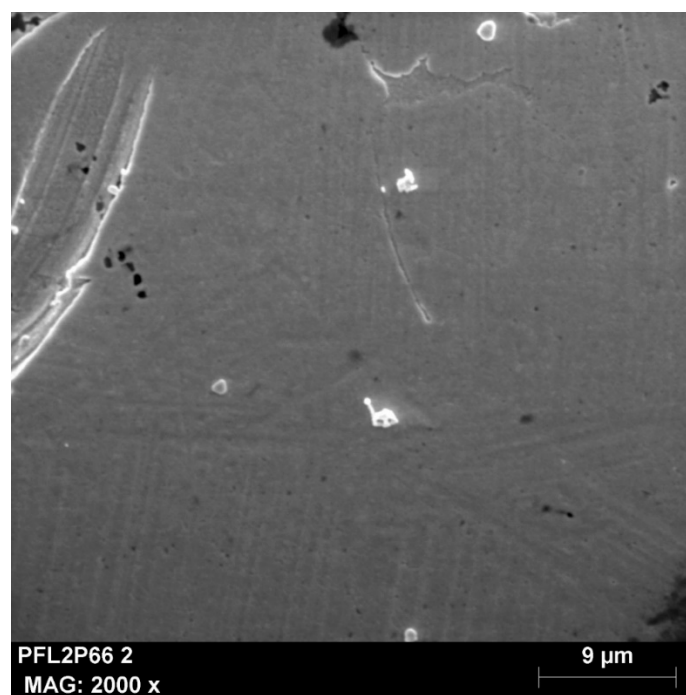


Figure S77. Flat zone analyzed by SEM-EDX.

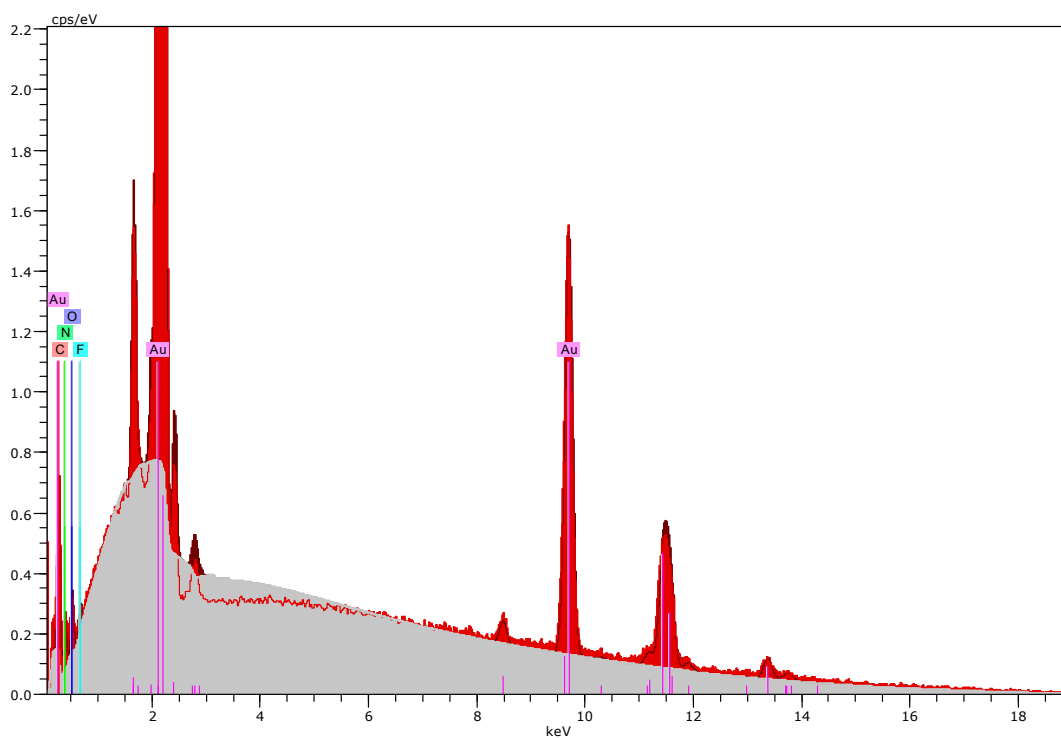


Figure S78. EDX spectrum of a flat region.

Element	Series	unn. C [wt.%]	norm. C [wt.%]	Atom. C [at.%]
Carbon	K-series	8.07	6.91	42.01
Nitrogen	K-series	3.50	2.99	15.61
Oxygen	K-series	1.97	1.69	7.71
Fluorine	K-series	0.64	0.55	2.11
Gold	L-series	102.62	87.85	32.56
Total:		116.81	100.00	100.00

SEM-EDX of a mixed zone, with granulated and flat regions.

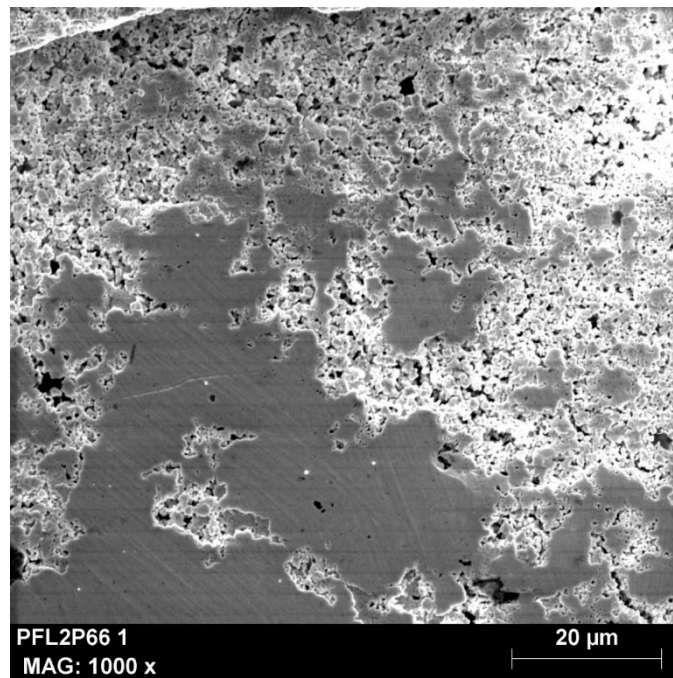


Figure S79. Mixed zone analyzed by SEM-EDX.

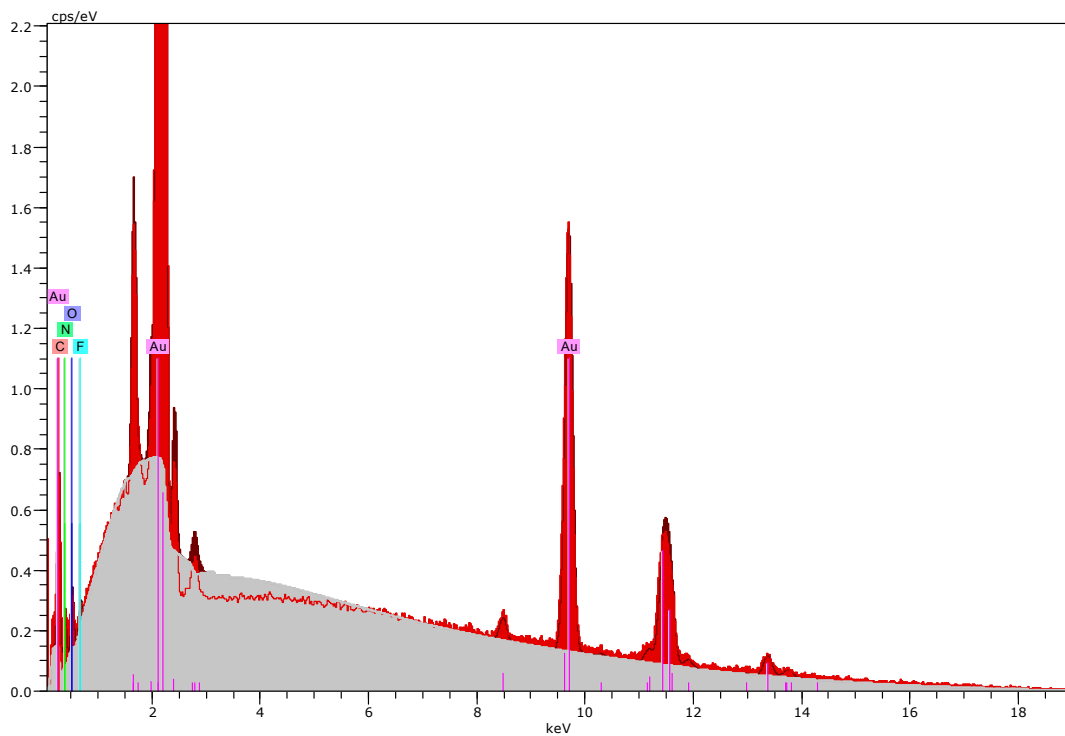


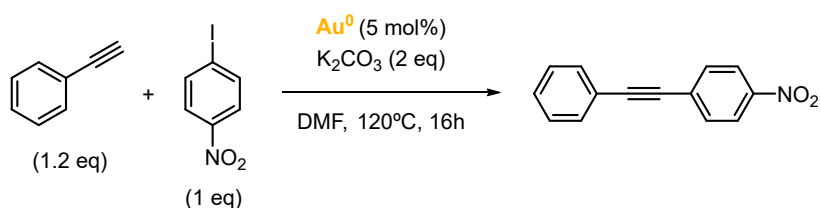
Figure S80. EDX spectrum of a mixed zone.

Element	Series	unn. C [wt.%]	norm. C [wt.%]	Atom. C [at.%]
Carbon	K-series	7.69	6.12	39.78
Nitrogen	K-series	3.35	2.67	14.87
Oxygen	K-series	1.85	1.47	7.18
Fluorine	K-series	0.87	0.69	2.85
Gold	L-series	111.97	89.05	35.32
Total:		125.73	100.00	100.00

S9. Heterogeneous Au(0) catalysis attempts

Isolated Au(0) nuggets were tested as heterogeneous catalysts in coupling reactions, such as in Sonogashira, A3 and Glaser couplings.

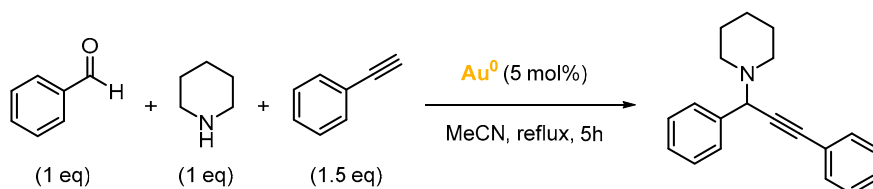
Sonogashira coupling



Scheme S6. Sonogashira coupling attempt using Au(0) nuggets as heterogeneous catalysts.

By analyzing the reaction crude by GC-MS, the desired coupling product was not detected.

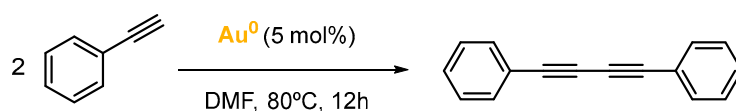
A3 coupling



Scheme S7. A3 coupling attempt using Au(0) nuggets as heterogeneous catalysts.

By analyzing the reaction crude by GC-MS, traces of the desired coupling product were detected, as well as in the blank experiment. Thus, no relevant catalytic activity was attributed to gold(0).

Glaser coupling



Scheme S8. Glaser coupling attempt using Au(0) nuggets as heterogeneous catalysts.

By analyzing the reaction crude by GC-MS, the desired homocoupling product was not detected.

S10. References

- Papastavrou, A. T.; Pauze, M.; Gómez-Bengoa, E.; Vougioukalakis, G. C., Unprecedented Multicomponent Organocatalytic Synthesis of Propargylic Esters via CO₂ Activation. *ChemCatChem* **2019**, *11*, 5379–5386.
- Liori, A. A.; Stamatopoulos, I. K.; Papastavrou, A. T.; Pinaka, A.; Vougioukalakis, G. C., A Sustainable, User-Friendly Protocol for the Pd-Free Sonogashira Coupling Reaction. *Eur. J. Org. Chem.* **2018**, *2018*, 6134–6139.
- Prasad, B.; Gilbertson, S., One-Pot Synthesis of N-Heterocyclic Carbene Ligands From a N-(2-iodoethyl)arylamine salts. *Org. Lett.* **2009**, *11*, 3710–3713.

ANNEX 4. Supporting information Chapter V.3

SUPPORTING INFORMATION

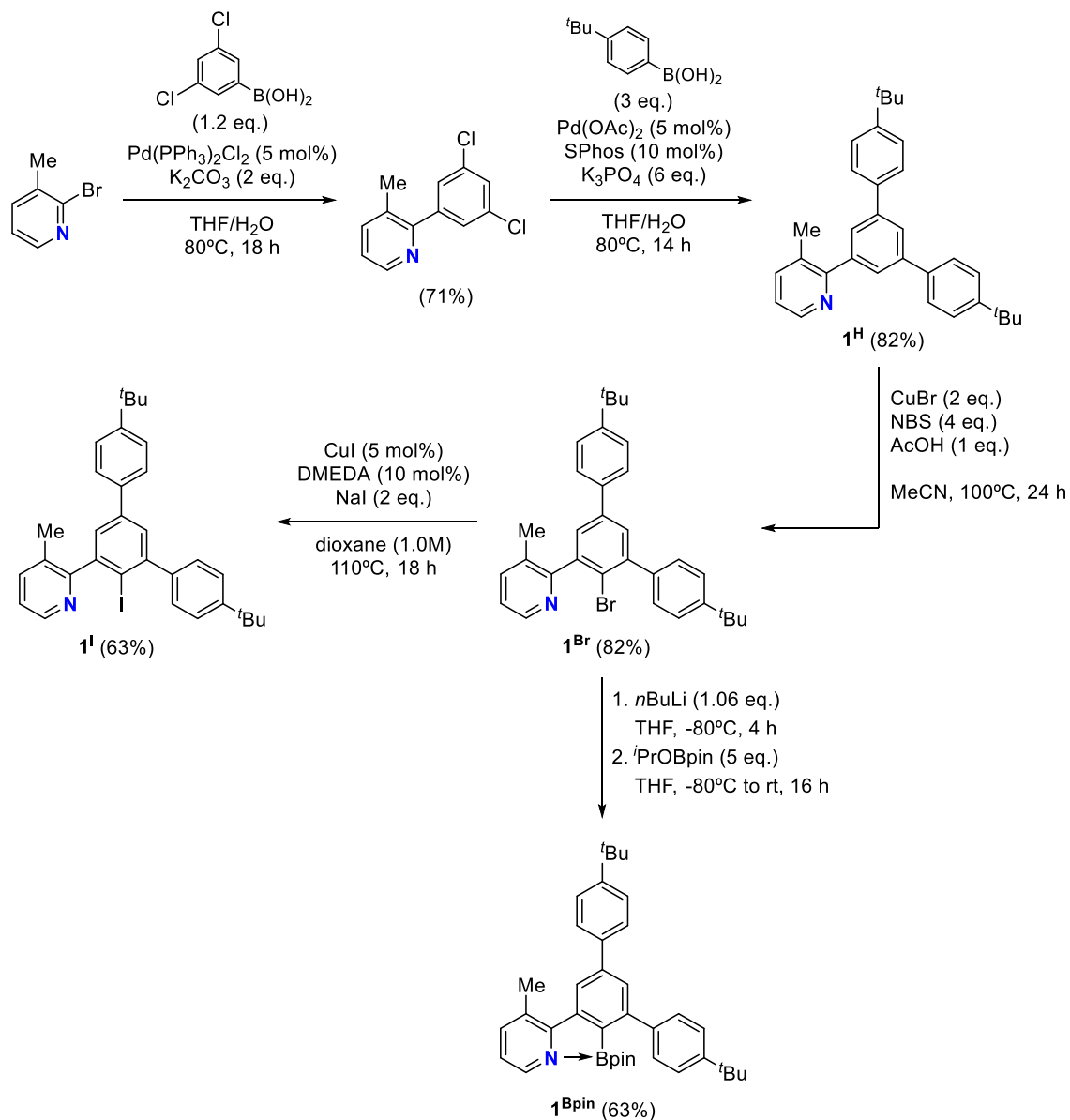
Boron-to-gold(III) Transmetalation as a Synthetic Strategy to access (N[^]C[^]C)-Biscyclometalated Gold(III) Complexes

Table of contents

1. Synthesis of ligand precursors and complexes 1AuCl and 2AuCl.....	360
2. Characterization of products.....	368
3. NMR and HRMS spectra	371
4. XRD analysis	389
5. References.....	392

1. Synthesis of ligand precursors and complexes 1^{I} and 2^{AuCl}

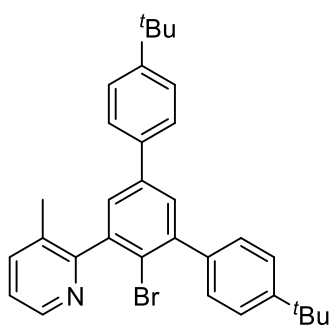
The synthesis of ligand precursors 1^{I} and 1^{Bpin} is depicted in Scheme 1.



Scheme 1. Synthetic route towards ligand precursors 1^{I} and 1^{Bpin} .

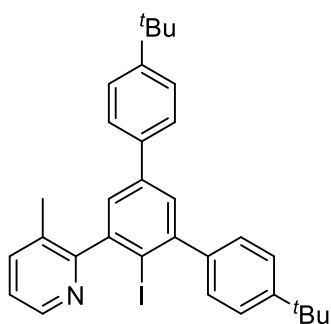
The synthesis of 1^{H} was done following the reported protocol.¹

Compound 1^{Br}. The bromination conditions were based on a previous reported protocol.²



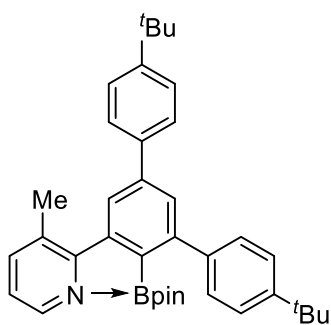
A solution of **1^H** (681.9 mg, 1.57 mmol, 1.0 eq.), NBS (1123.1 mg, 6.31 mmol, 4.0 eq.), CuBr (450.6 mg, 3.14 mmol, 2.0 eq.) and AcOH (91 μ L, 1.59 mmol, 1.0 eq.) in MeCN (27 mL) was stirred in a Schlenk flask under N₂ atmosphere at 100°C for 24 hours. After cooling the reaction mixture to room temperature, Na₂S (15 mL, 1 g/10 mL H₂O) and EtOAc (90 mL) were added, and the mixture was stirred for 10 minutes. Then, the organic phase was washed with brine, dried over MgSO₄, and concentrated under reduced pressure. The residue was subjected to column chromatography on silica gel using hexane:EtOAc (5:1) to afford product **1^{Br}** as a white solid (667.3 mg, 82% yield).

Compound 1^I. The bromination conditions were based on a previous reported protocol.³ A



solution of **1^{Br}** (257.8 mg, 0.50 mmol, 1.0 eq.), CuI (5.6 mg, 0.03 mmol, 0.06 eq.), NaI (153.1 mg, 1.02 mmol, 2.0 eq.) and DMEDA (6.3 μ L, 0.06 mmol, 0.12 eq.) in dioxane (0.5 mL) was stirred in a Schlenk flask under N₂ atmosphere at 110°C for 18 hours. After cooling the reaction mixture to room temperature, it was filtered over a pad of Celite®. The resulting solution was extracted with EtOAc and brine. The organic layer was dried over MgSO₄, and concentrated under reduced pressure. The residue was subjected to column chromatography on silica gel using a gradient from hexane:EtOAc (20:1) to hexane:EtOAc (12:1). Product **1^I** was obtained as a white solid (176.5 mg, 63% yield).

Compound 1^{Bpin}. Product **1^{Br}** (392.1 mg, 0.76 mmol, 1.0 eq.) was dissolved in dry THF (9

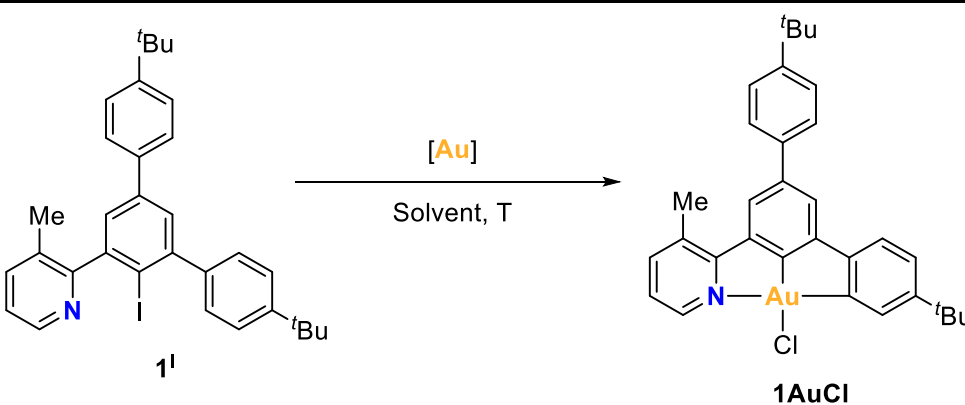


mL) in a Schlenk flask under inert atmosphere. The solution was cooled down to -80°C in a dry ice/*n*-PrOH bath. Then, 1.6M *n*BuLi in hexanes (510 μ L, 0.82 mmol, 1.07 eq.) was added dropwise. The mixture was stirred for 4 hours at -80°C. After this time, under inert atmosphere, 2-isopropoxy-4,4,5,5-tetramethyl-1,3,2-dioxaborolane (790 μ L, 3.86 mmol, 5.0 eq.) was added dropwise and the mixture was let to react under stirring while being warmed from -80°C to room temperature for 16 hours. After this time,

MeOH was added to quench the reaction. Then, the solvent was removed under vacuum. DCM was added, and the solution was washed with brine. The organic layer was dried over MgSO₄ and concentrated under reduced pressure. The expected product was purified by column chromatography on silica gel using heane:EtOAc:toluene (2:2:1), affording **1^{Bpin}** as a white solid (319.3 mg, 63% yield). Crystals of **1^{Bpin}** suitable for XRD were obtained by recrystallization in hot EtOAc.

Complex 1AuCl. In Table 1, the metalation attempts by oxidative addition from ligand precursor **1^I** are displayed. In Table 2, the transmetalation attempts from precursor **1^{Bpin}** are displayed.

Table 1. Reaction conditions for the oxidative addition of **1^I** towards **1AuCl**.



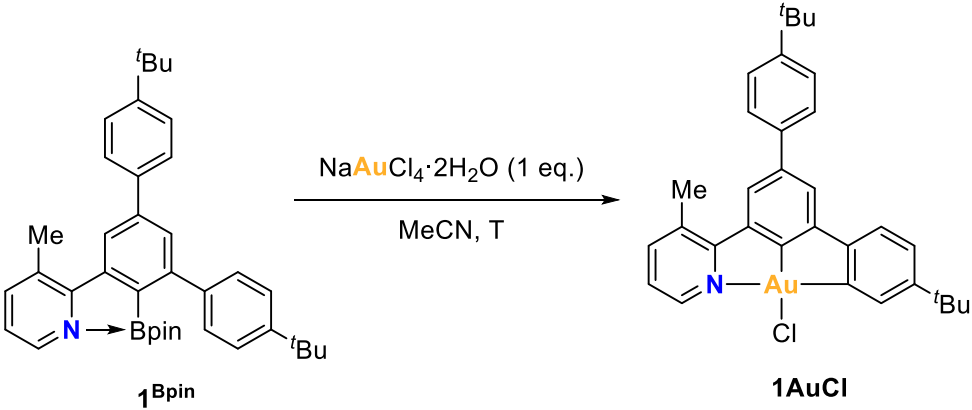
Entry	[Au]	Solvent	T (°C)	[1 ^I] (M)	Yield (%)
1	AuI	Toluene	60	0.03	0
2	AuI	DCM	40	0.03	0
3	AuI	THF	60	0.03	0
4 ^{a,c}	AuI	Toluene	140	0.03	0
5 ^{b,c}	AuI	Toluene	140	0.06	0
6 ^{b,c}	AuCl(DMS)	Toluene	140	0.18	24

General reaction conditions: **1^I** (1 eq.), Au complex (1 eq.), overnight, V = 1 mL. Reaction run in a sealed vial. ^a Reaction run in a 3-mL Schlenk. ^b 1.1 eq. of Au complex, t = 24 h, V = 0.5 mL. ^c Decomposition to Au(0) observed.

When AuI was employed, the ¹H NMR spectra of the reaction crudes did not show signals corresponding to the N-coordination between the gold center and the pyridine moiety.

However, the ^1H NMR spectrum of the reaction crude from the reaction displayed in entry 6 indicated the formation of **1AuCl**. The complex was isolated by column chromatography using hexane:EtOAc (8:2) on silica gel, obtaining a 24% isolated yield.

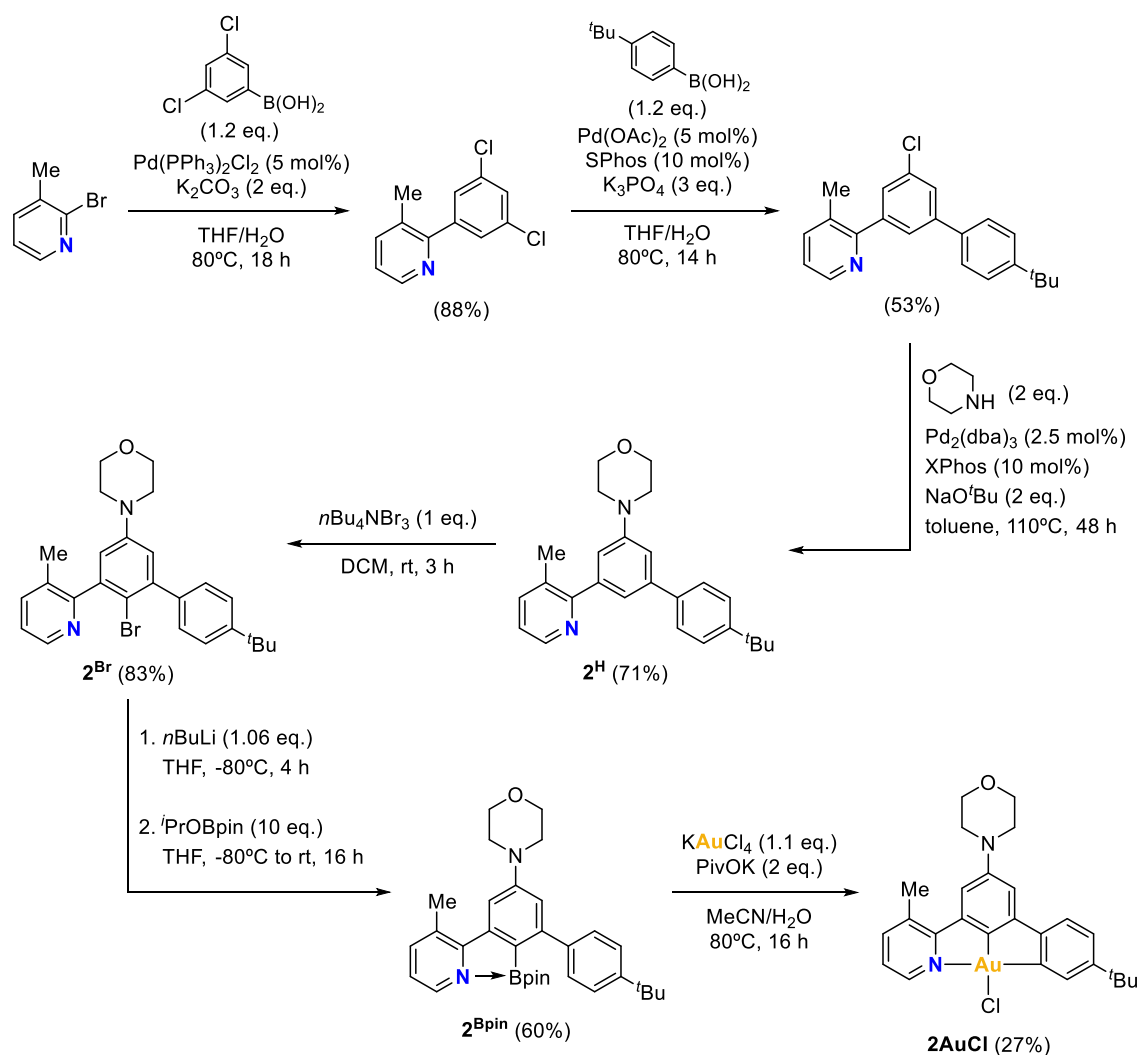
Table 2. Reaction conditions for the transmetalation of **1^{Bpin}** towards **1AuCl**.



Entry	T (°C)	[1^{Bpin}] (M)	NMR yield (%)
1^a	90	0.06	46
2^b	100	0.06	65
3	120	0.06	51
4^c	120	0.10	49
5^c	120	0.20	54
6^d	120	0.06	63

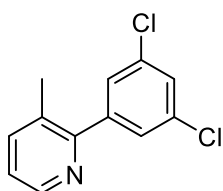
General reaction conditions: **1^{Bpin}** (1 eq.), NaAuCl₄·2H₂O (1 eq.), overnight, V = 0.35 mL. Reaction run in a 3-mL Schlenk. NMR yields of **1AuCl** obtained using mesitylene as internal standard. ^aReflux, V = 1 mL. ^bReaction run in a sealed vial. ^ct = 24h. ^dLutidine (2 eq.) added as a base.

The synthesis of complex **2AuCl** is depicted in Scheme 2.



Scheme 2. Synthetic route towards complex **2AuCl**.

2-(3,5-dichlorophenyl)-3-methylpyridine. In a Schlenk flask, 2-bromo-3-methylpyridine

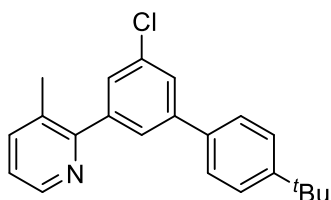


(0.8 mL, 7.18 mmol, 1 eq.), 3,5-dichlorophenylboronic acid (1682.5 mg, 8.82 mmol, 1.2 eq.), and K₂CO₃ (2080.6 mg, 15.05 mmol, 2.1 eq.) were dissolved in a 2:1 mixture of THF:H₂O (38 mL). The mixture was degassed by bubbling N₂ in the Schlenk line for 10 minutes. Then, under N₂ flow, Pd(PPh₃)₂Cl₂ (257.6 mg, 0.37 mmol, 0.05 eq.) was added. The

Schlenk flask was sealed, and the mixture was stirred and heated at 80°C for 18 hours. The reaction crude was transferred to a separation funnel, and it was washed with brine (x3). The organic layer was dried with MgSO₄ and concentrated under vacuum. The expected product

was purified by column chromatography using hexane:Et₂O (9:1) on silica gel. Product **1** was obtained as a white solid (1512.6 mg, 88% yield).

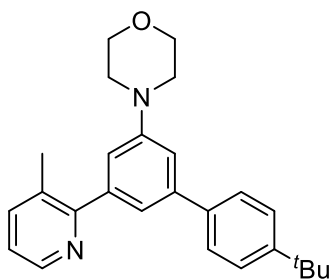
2-(4'-(*tert*-butyl)-5-chloro-[1,1'-biphenyl]-3-yl)-3-methylpyridine. In a Schlenk flask, 2-



(3,5-dichlorophenyl)-3-methylpyridine (572.1 mg, 2.40 mmol, 1 eq.), 4-*tert*-butylphenylboronic acid (515.9 mg, 2.90 mmol, 1.2 eq.), and K₃PO₄ (1592.7 mg, 7.50 mmol, 3.1 eq.) were dissolved in a 5:3 mixture of THF:H₂O (16 mL). The mixture was degassed by bubbling N₂ in the Schlenk line for 10 minutes.

Then, under N₂ flow, Pd(OAc)₂ (26.9 mg, 0.12 mmol, 0.05 eq.) and SPhos (101.0 mg, 0.25 mmol, 0.10 eq.) were added. The Schlenk flask was sealed, and the mixture was stirred and heated at 80°C for 14 hours. The reaction crude was extracted with EtOAc and washed with brine (x3). The organic layer was dried with MgSO₄ and concentrated under vacuum. The expected product was purified by column chromatography using a gradient from 100% hexane to hexane:EtOAc (9:1) on silica gel. The product was obtained as a colorless oil (429.4 mg, 53% yield).

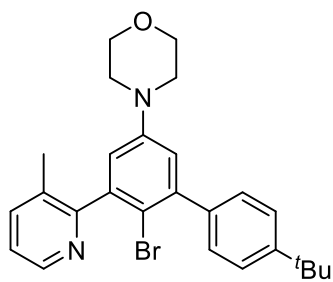
Compound 2^H. A vial with 2-(4'-(*tert*-butyl)-5-chloro-[1,1'-biphenyl]-3-yl)-3-methylpyridine



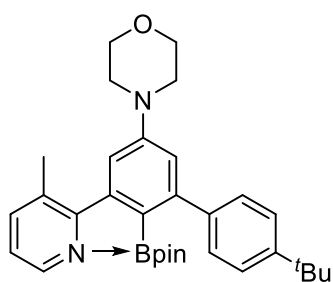
(252.9 mg, 0.75 mmol, 1 eq.) and an empty 20mL-sealable vial were entered inside the glovebox. To the empty sealable vial, XPhos (36.6 mg, 0.08 mmol, 0.10 eq.), NaO^tBu (145.2 mg, 1.51 mmol, 2.0 eq.) and Pd₂(dba)₃ (18.6 mg, 0.02 mmol, 0.027 eq.) were weighed. Anhydrous toluene (4.5 mL) was added to the other vial, and the starting material was transferred to the

sealable vial in solution. A magnetic stirring bar was added and the vial was sealed with a septum-containing sealable cap. Outside the glovebox, morpholine (140 μL, 1.62 mmol, 2.1 eq.) was added to the reaction vial, through the septum of the cap, with a syringe coupled to a stainless steel needle. The reaction mixture was stirred and heated at 110°C for 48 hours. The reaction crude was extracted with DCM and washed with brine (x3). The organic layer was dried with MgSO₄ and concentrated under vacuum. The expected product was purified by column chromatography using hexane:EtOAc (6:4) on silica gel. Product **3** was obtained as a pale yellow solid (206.3 mg, 71% yield). This reaction also works in 400 mg scale.

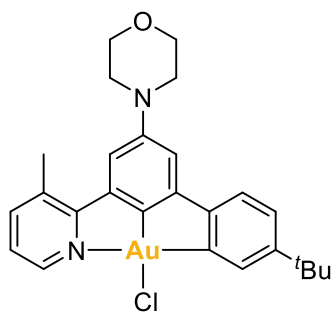
Compound 2^{Br}. The selective bromination of **2^H** to afford **2^{Br}** was based on a previously reported strategy.⁴ This reaction was run at open-air with no need for anhydrous or inert conditions. To a round-bottom flask charged with a magnetic stirring bar, product **2^H** (577.3 mg, 1.49 mmol, 1 eq.) and DCM (10.6 mL) were added. In a vial, *n*Bu₄NBr₃ (724.7 mg, 1.50 mmol, 1.0 eq.) was dissolved in DCM (10.6 mL). The solution of *n*Bu₄NBr₃ was added dropwise on the solution of **2^H** under stirring, for 3 minutes. The reaction mixture was let to react for 3 hours under stirring at room temperature. After the reaction time, 30 mL DCM were added to the crude. Then, extractions with NaOH 1M (2 x 30 mL) and H₂O (3 x 30 mL) were done. The organic layer was dried with MgSO₄ and concentrated under vacuum. Over this concentrated DCM solution, Et₂O was let to slowly diffuse overnight in the fridge. Product **2^{Br}** precipitated as a white solid, which was subsequently filtered and dried (573.4 mg, 83% yield).



Compound 2^{Bpin}. To a Schlenk flask were charged product **2^{Br}** (512.1 mg, 1.10 mmol, 1 eq.) and a magnetic stirring bar. Under N₂, anhydrous THF (22 mL) was added, and a colorless solution was obtained. The Schlenk flask was cooled down to -80°C using an EtOH/liq. N₂ cold bath. Then, 2.5M *n*BuLi in hexanes (1.2 mL, 3.0 mmol, 2.7 eq.) was added dropwise. The mixture was let to react at -80°C under stirring for 4 hours. The solution turned yellow. After the reaction time, 2-isopropoxy-4,4,5,5-tetramethyl-1,3,2-dioxaborolane (2.2 mL, 10.8 mmol, 9.8 eq.) was added dropwise, and the mixture was let to react under stirring while being warmed from -80°C to room temperature for 16 hours. After this time, MeOH was added to quench the reaction. Then, the solvent was removed under vacuum. DCM was added and a white solid precipitated, which was filtered off. The remaining yellow solution was subjected to extractions with brine (x3). The organic layer was dried with MgSO₄ and concentrated under vacuum. The expected product was purified by column chromatography using hexane:EtOAc (1:9) on silica gel. Product **2^{Bpin}** was obtained as a yellow solid (341.5 mg, 60% yield). Crystals of **2^{Bpin}** suitable for XRD were obtained by recrystallization in hot hexane.



Complex 2AuCl. Product **2^{Bpin}** (15.0 mg, 0.03 mmol, 1 eq.) and potassium pivalate (8.5 mg, 0.06 mmol, 2.1 eq.) were weighed in a sealable vial. Then,



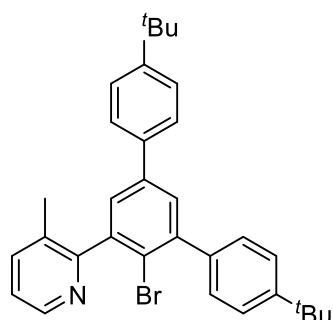
MeCN (0.4 mL) and H₂O (0.4 mL) were added, and the resulting solution was stirred. At this point, KAuCl₄ (12.0 mg, 0.03 mmol, 1.1 eq.) dissolved in MeCN (0.2 mL) was added. The vial was sealed and the reaction mixture was stirred and heated at 80°C for 16 hours. The precipitate in the reaction crude was filtered and dried. The expected product was purified

by subjecting the isolated solid to a preparative TLC using DCM:MeOH (48:2) on silica. Complex **2AuCl** was obtained as a yellow solid (4.9 mg, 27% yield).

2. Characterization of products

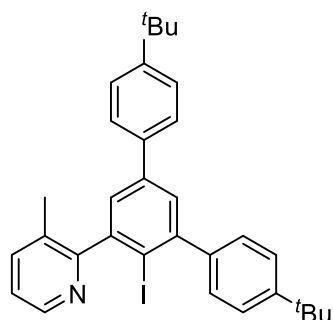
The characterization of products 2-(3,5-dichlorophenyl)-3-methylpyridine, **1^H**, and **1AuCl** matched with that that had previously been reported.¹

Compound 1^{Br}. ¹H NMR (400 MHz, CDCl₃, 298 K): δ (ppm) 8.61 (d, *J* = 4.7 Hz, 1H), 7.73



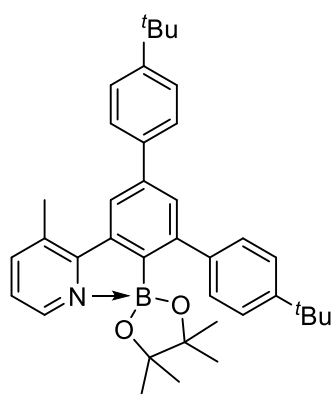
(d, *J* = 7.6 Hz, 1H), 7.62 (d, *J* = 1.9 Hz, 1H), 7.57 (d, *J* = 8.3 Hz, 2H), 7.52 – 7.41 (m, 7H), 7.40 – 7.32 (m, 1H), 2.27 (s, 3H), 1.38 (s, 9H), 1.34 (s, 9H). ¹³C{¹H} NMR (101 MHz, CD₂Cl₂, 298 K): δ (ppm) 151.1, 150.7, 144.0, 140.4, 138.5, 136.6, 130.0, 129.3, 127.5, 126.9, 126.0, 125.1, 123.4, 121.5 (C–Br), 34.8, 34.7, 31.5, 31.5, 19.2.

Compound 1^I. ¹H NMR (400 MHz, CDCl₃, 298 K): δ (ppm) 8.58 (d, *J* = 4.5 Hz, 1H), 7.66



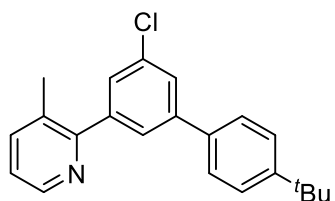
(d, *J* = 7.9 Hz, 1H), 7.57 (d, *J* = 8.2 Hz, 3H), 7.49 – 7.41 (m, 5H), 7.36 (d, *J* = 8.3 Hz, 2H), 7.34 – 7.28 (m, 1H), 2.22 (s, 3H), 1.38 (s, 9H), 1.34 (s, 9H). ¹³C{¹H} NMR (101 MHz, CD₂Cl₂, 298 K): δ (ppm) 151.1, 150.7, 148.4, 142.0, 141.1, 136.7, 129.3, 128.2, 126.8, 126.3, 126.0, 125.0, 123.3, 100.6 (C–I), 34.8, 34.7, 31.6, 31.4, 19.4. **HRMS (ESI+)**: calcd for C₃₂H₃₄IN [M+H]⁺: *m/z* = 560.18142; found: *m/z* = 560.18034.

Compound 1^{Bpin}. ¹H NMR (400 MHz, CD₂Cl₂, 298 K): δ (ppm) 8.56 – 8.52 (m, 1H), 7.79



(d, *J* = 1.7 Hz, 1H), 7.72 – 7.68 (m, 1H), 7.61 (d, *J* = 8.4 Hz, 2H), 7.55 (d, *J* = 1.5 Hz, 1H), 7.48 (d, *J* = 8.4 Hz, 2H), 7.44 (s, 4H), 7.26 (dd, *J* = 7.7, 5.1 Hz, 1H), 2.56 (s, 3H), 1.35 (s, 18H), 0.89 (s, 12H). **HRMS (ESI+)**: calcd for C₃₈H₄₆BNO₂ [M+H]⁺: *m/z* = 560.36999; found: *m/z* = 560.36911.

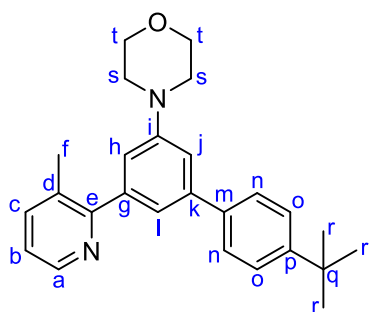
2-(4'-(*tert*-butyl)-5-chloro-[1,1'-biphenyl]-3-yl)-3-methylpyridine. $^1\text{H NMR}$ (400 MHz,



CD_2Cl_2 , 298 K): δ (ppm) 8.51 (ddd, $J = 4.8, 1.7, 0.7$ Hz, 1H), 7.65 – 7.61 (m, 3H), 7.59 – 7.55 (m, 2H), 7.52 – 7.47 (m, 3H), 7.23 (dd, $J = 7.7, 4.7$ Hz, 1H), 2.39 (s, 3H), 1.36 (s, 9H). $^{13}\text{C}\{^1\text{H}\}$

NMR (101 MHz, CD_2Cl_2 , 298 K): δ (ppm) 157.7, 151.8, 147.6, 143.5, 143.1, 139.1, 137.2, 134.8, 131.5, 128.1, 127.3 (2C), 126.8, 126.5, 126.5 (2C), 123.1, 35.1, 31.6 (3C), 20.4. **HRMS (ESI+)**: calcd for $\text{C}_{22}\text{H}_{22}\text{ClN}$ $[\text{M}+\text{H}]^+$: $m/z = 336.15135$; found: $m/z = 336.15080$.

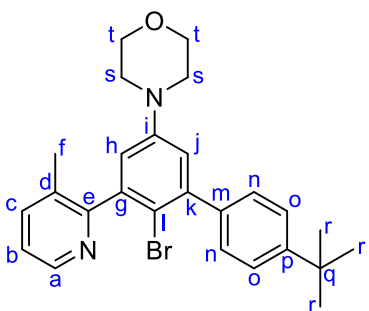
Compound 2^H. $^1\text{H NMR}$ (400 MHz, CDCl_3 , 298 K): δ (ppm) 8.55 – 8.52 (m, 1H, **Ha**), 7.61



– 7.57 (m, 1H, **Hc**), 7.57 – 7.54 (m, 2H, **Hn**), 7.47 – 7.43 (m, 2H, **Ho**), 7.21 (s, 1H, **Hi**), 7.19 (dd, $J = 7.7, 4.8$ Hz, 1H, **Hb**), 7.15 (dd, $J = 2.5, 1.5$ Hz, 1H, **Hj**), 7.03 (dd, $J = 2.4, 1.4$ Hz, 1H, **Hh**), 3.91 – 3.86 (m, 4H, **Ht**), 3.29 – 3.25 (m, 4H, **Hs**), 2.38 (s, 3H, **Hf**), 1.36 (s, 9H, **Hr**). $^{13}\text{C}\{^1\text{H}\}$ **NMR** (101

MHz, CDCl_3 , 298 K): δ (ppm) 159.3 (**Ce**), 151.8 (**Ci**), 150.5 (**Cp**), 147.0 (**Ca**), 142.0 (**Cg**), 142.0 (**Ck**), 138.8 (**Cm**), 138.6 (**Cc**), 131.1 (**Cd**), 127.1 (2C, **Cn**), 125.7 (2C, **Co**), 122.3 (**Cb**), 119.9 (**Cl**), 115.3 (**Ch**), 114.5 (**Cj**), 67.1 (2C, **Ct**), 49.6 (2C, **Cs**), 34.7 (**Cq**), 31.5 (3C, **Cr**), 20.3 (**Cf**). **HRMS (ESI+)**: calcd for $\text{C}_{26}\text{H}_{30}\text{N}_2\text{O}$ $[\text{M}+\text{H}]^+$: $m/z = 387.2431$; found: $m/z = 387.2437$.

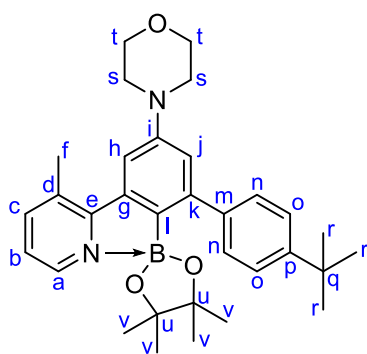
Compound 2^{Br}. $^1\text{H NMR}$ (400 MHz, CD_2Cl_2 , 298 K): δ (ppm) 8.47 (ddd, $J = 4.8, 1.6, 0.7$



Hz, 1H, **Ha**), 7.60 (ddd, $J = 7.6, 1.7, 0.8$ Hz, 1H, **Hc**), 7.48 – 7.44 (m, 2H, **Ho**), 7.41 – 7.37 (m, 2H, **Hn**), 7.24 (dd, $J = 7.7, 4.8$ Hz, 1H, **Hb**), 6.89 (d, $J = 3.1$ Hz, 1H, **Hj**), 6.76 (d, $J = 3.1$ Hz, 1H, **Hh**), 3.82 – 3.78 (m, 4H, **Ht**), 3.18 – 3.14 (m, 4H, **Hs**), 2.19 (s, 3H, **Hf**), 1.37 (s, 9H, **Hr**). $^{13}\text{C}\{^1\text{H}\}$ **NMR** (101 MHz, CD_2Cl_2 , 298 K): δ (ppm) 160.3 (**Ce**), 151.1

(**Cp**), 150.8 (**Ci**), 147.0 (**Ca**), 144.3 (**Ck**), 143.6 (**Cg**), 139.6 (**Cm**), 138.1 (**Cc**), 132.3 (**Cd**), 129.7 (2C, **Cn**), 125.4 (2C, **Co**), 123.3 (**Cb**), 118.3 (**Cj**), 116.2 (**Ch**), 112.4 (**Cl**), 67.2 (2C, **Ct**), 49.4 (2C, **Cs**), 35.1 (**Cq**), 31.7 (3C, **Cr**), 19.3 (**Cf**). **HRMS (ESI+)**: calcd for $\text{C}_{26}\text{H}_{29}\text{BrN}_2\text{O}$ $[\text{M}+\text{H}]^+$: $m/z = 465.1536$; found: $m/z = 465.1551$; $[\text{2M}+\text{H}]^+$: $m/z = 931.2986$; found: $m/z = 931.3010$.

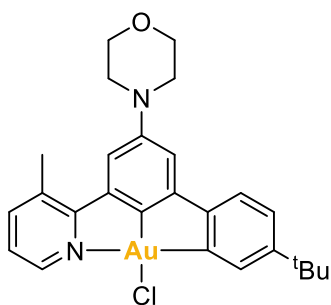
Compound 2^{Bpin}. ¹H NMR (400 MHz, CD₂Cl₂, 298 K): δ (ppm) 8.45 (ddd, *J* = 5.0, 1.6, 0.7



Hz, 1H, **Ha**), 7.60 (ddd, *J* = 7.7, 1.7, 0.8 Hz, 1H, **Hc**), 7.42 – 7.39 (m, 2H, **Ho**), 7.39 – 7.35 (m, 2H, **Kn**), 7.19 (dd, *J* = 7.6, 4.9 Hz, 1H, **Hb**), 6.91 (d, *J* = 2.4 Hz, 1H, **Hh**), 6.86 (d, *J* = 2.4 Hz, 1H, **Hj**), 3.85 – 3.80 (m, 4H, **Ht**), 3.24 – 3.18 (m, 4H, **Ho**), 2.38 (s, 3H, **Hf**), 1.34 (s, 9H, **Ho**), 0.84 (s, 12H, **Hv**). ¹³C{¹H} NMR (101 MHz, CD₂Cl₂, 298 K): δ (ppm)

159.7 (**Ce**), 151.7 (**Ca**), 150.5 (**Cp**), 148.6 (**Ck**), 145.8 (**Cg**), 145.2 (**Ca**), 141.8 (**Cm**), 139.6 (**Cc**), 132.0 (**Cd**), 129.4 (2C, **Cn**), 125.3 (2C, **Co**), 122.6 (**Cb**), 116.5 (**Cj**), 113.7 (**Ch**), 82.9 (2C, **Cu**), 67.3 (2C, **Ct**), 49.6 (2C, **Cs**), 34.9 (**Cq**), 31.7 (3C, **Cr**), 25.7 (4C, **Cv**), 20.6 (**Cf**). The carbon directly bonded to B atom is not seen, but HMBC reveals it should appear at 125.8 ppm. **HRMS (ESI+)**: calcd for C₃₂H₄₁BN₂O₃ [M+H]⁺: *m/z* = 513.3289; found: *m/z* = 513.3301; [2M+H]⁺: *m/z* = 1025.6513; found: *m/z* = 1025.6498.

Complex 2AuCl. ¹H NMR (400 MHz, CD₂Cl₂, 298 K): δ (ppm) 8.97 (dd, *J* = 5.4, 1.6 Hz,



1H), 7.86 (d, *J* = 2.0 Hz, 1H), 7.64 (dd, *J* = 8.2, 1.5 Hz, 1H), 7.30 (dd, *J* = 7.8, 5.3 Hz, 1H), 7.20 (dd, *J* = 8.0, 2.0 Hz, 1H), 7.16 – 7.11 (m, 2H), 6.80 (d, *J* = 2.2 Hz, 1H), 3.90 – 3.85 (m, 4H), 3.24 – 3.19 (m, 4H), 2.65 (s, 3H), 1.35 (s, 9H). **HRMS (ESI+)**: calcd for C₂₆H₂₈AuClN₂O [M]⁺: *m/z* = 616.1550; found: *m/z* = 616.1508.

3. NMR and HRMS spectra

3.1. Compound 1^{Br}

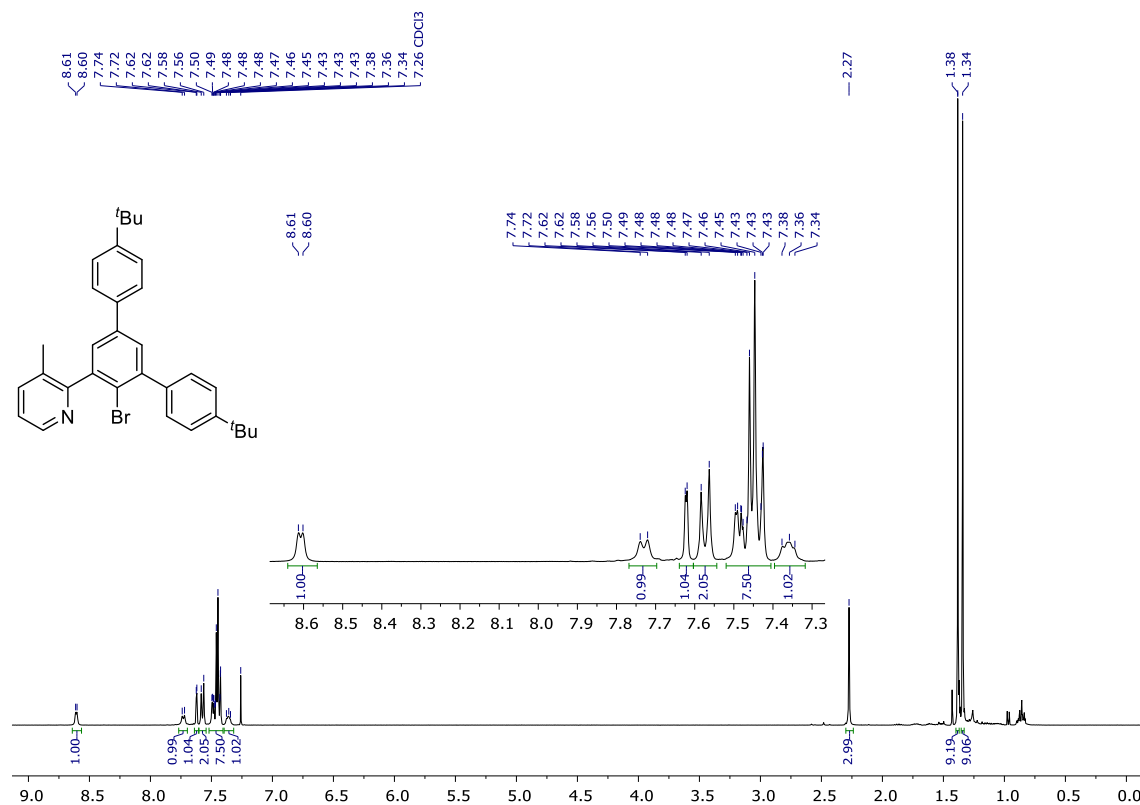


Figure 1. ¹H NMR (400MHz, 298K) of compound 1^{Br} in CDCl₃.

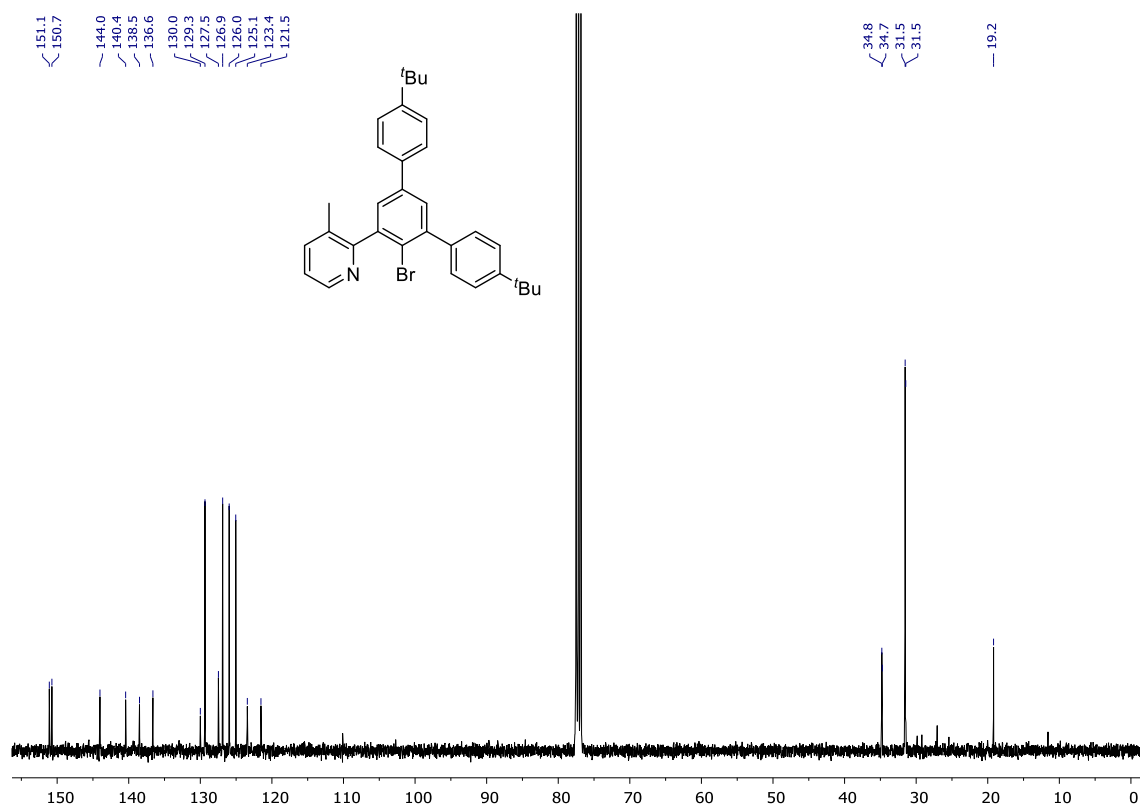


Figure 2. ¹³C{¹H} NMR (101MHz, 298K) of compound 1^{Br} in CDCl₃.

3.2. Compound 1^I

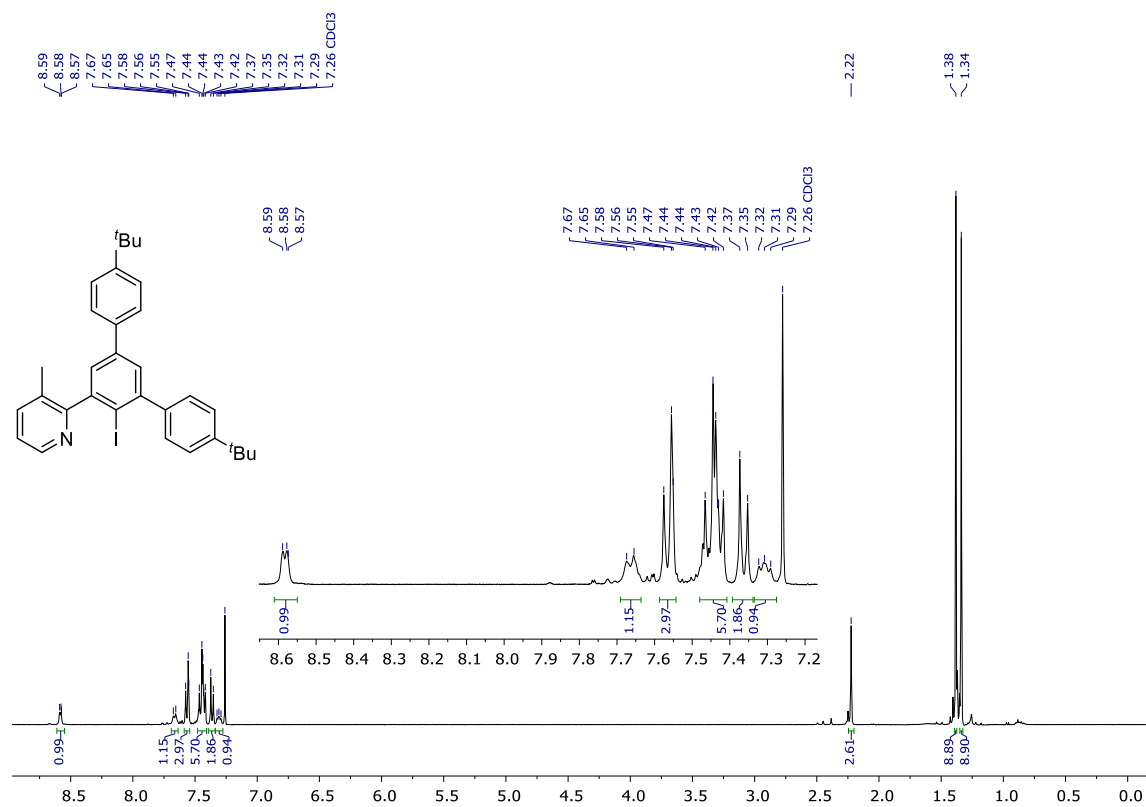


Figure 3. ¹H NMR (400MHz, 298K) of compound 1^I in CDCl₃.

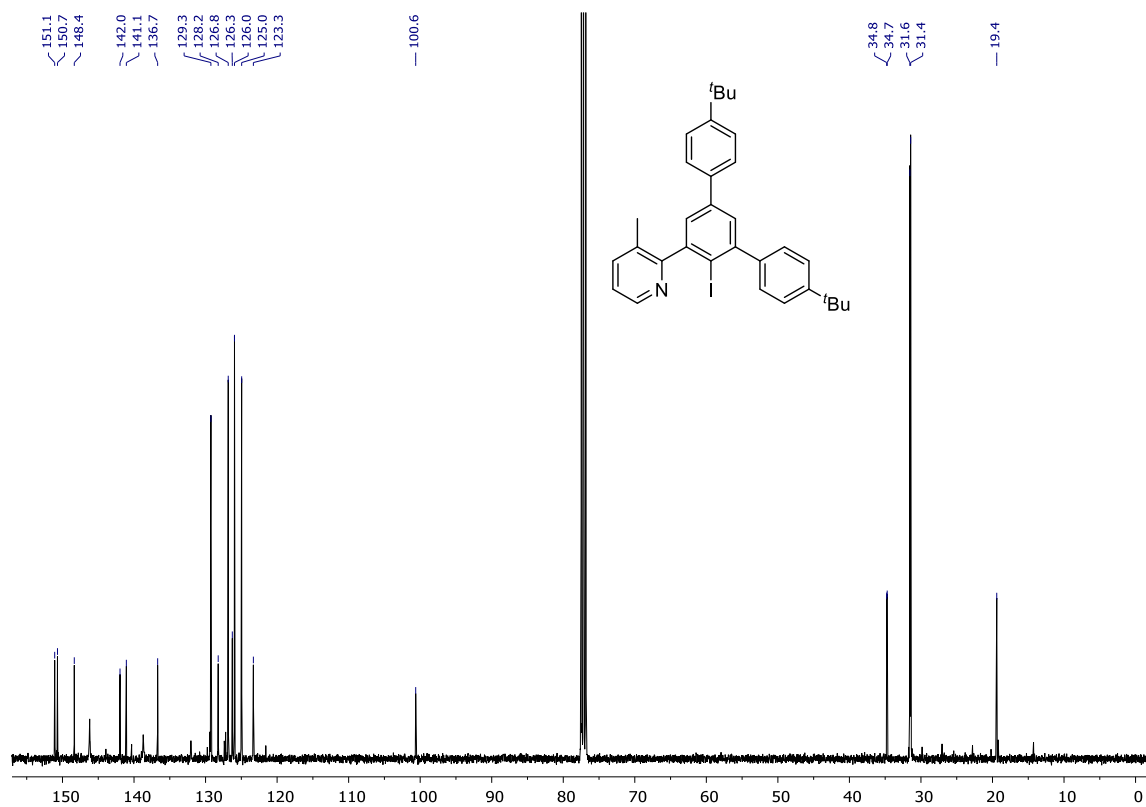
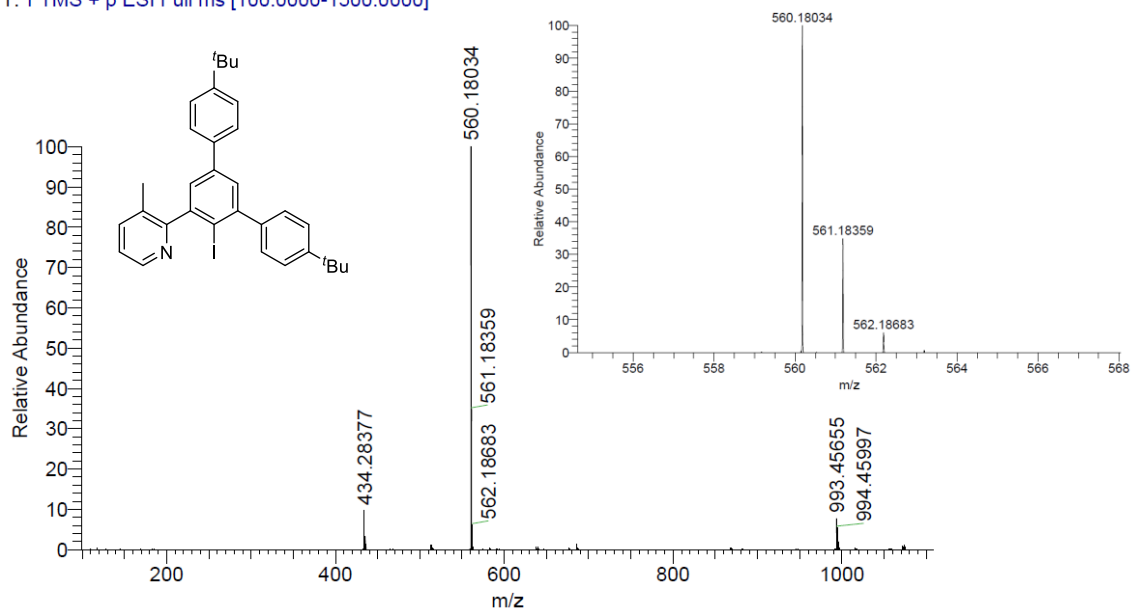
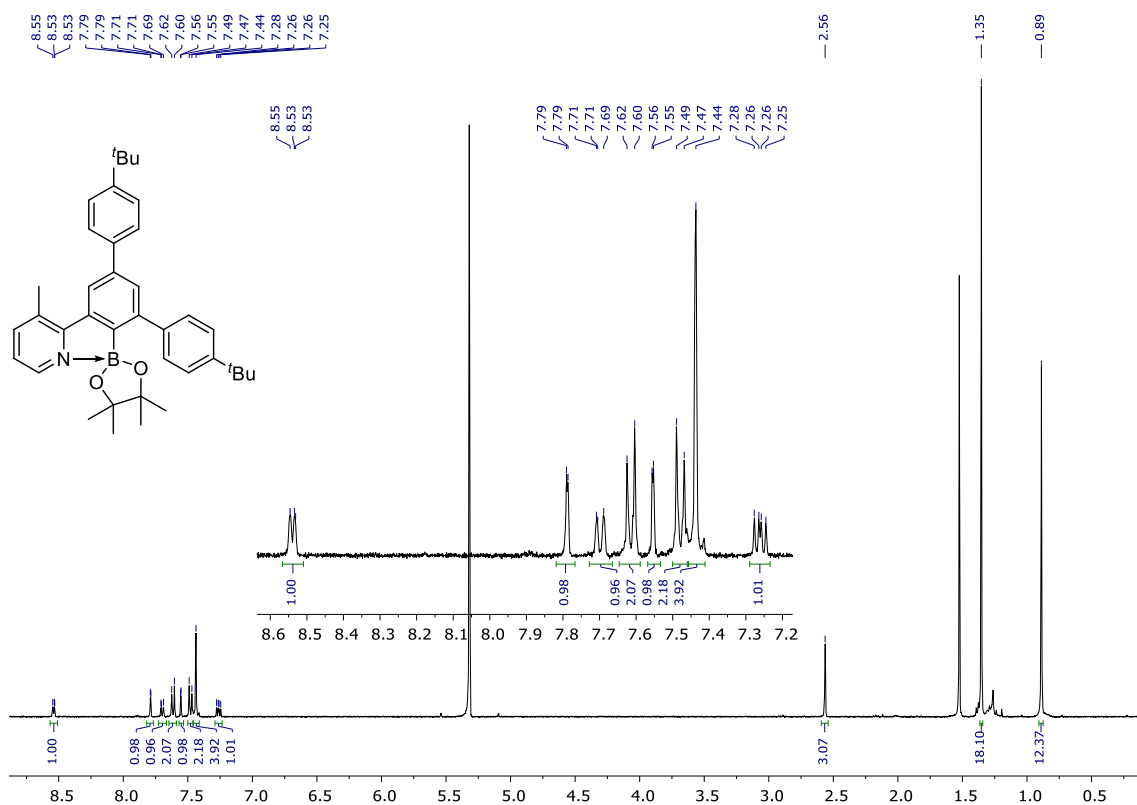


Figure 4. ¹³C{¹H} NMR (101MHz, 298K) of compound 1^I in CDCl₃.

21_neQEx_1577 #38-50 RT: 0.38-0.47 AV: 6 SB: 23 0.04-0.25 , 0.73-0.97 NL: 7.81E8
T: FTMS + p ESI Full ms [100.0000-1500.0000]



3.3. Compound **1**^{Bpin}



21_neQEx_1578 #38-50 RT: 0.38-0.47 AV: 6 SB: 23 0.04-0.25 , 0.73-0.97 NL: 1.02E9
T: FTMS + p ESI Full ms [100.0000-1500.0000]

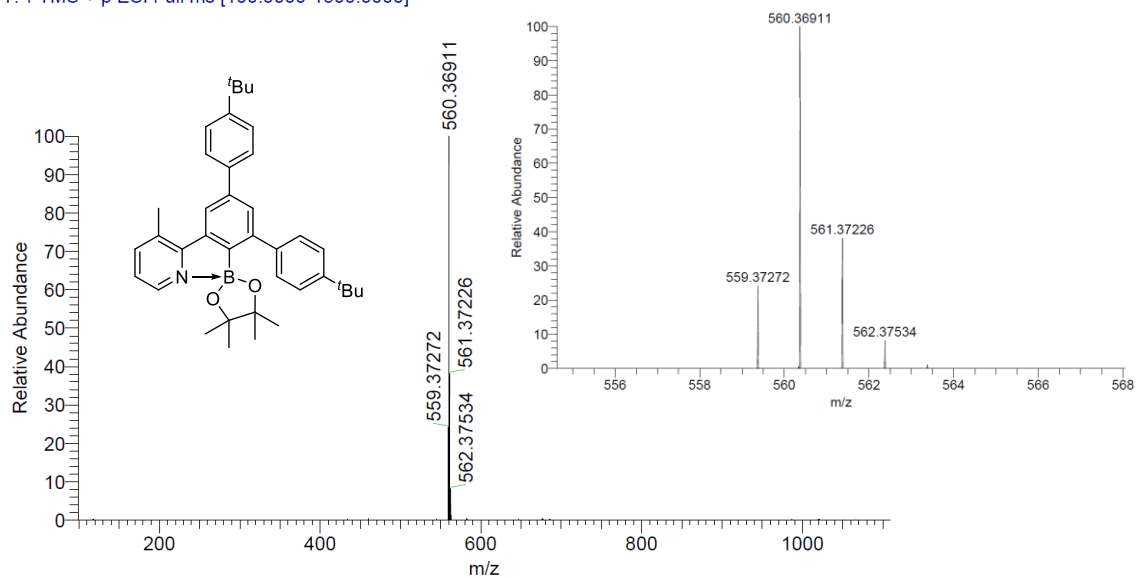


Figure 7. HRMS-ESI(+) of compound 1^{Bpin}.

3.4. 2-(4'-(*tert*-butyl)-5-chloro-[1,1'-biphenyl]-3-yl)-3-methylpyridine

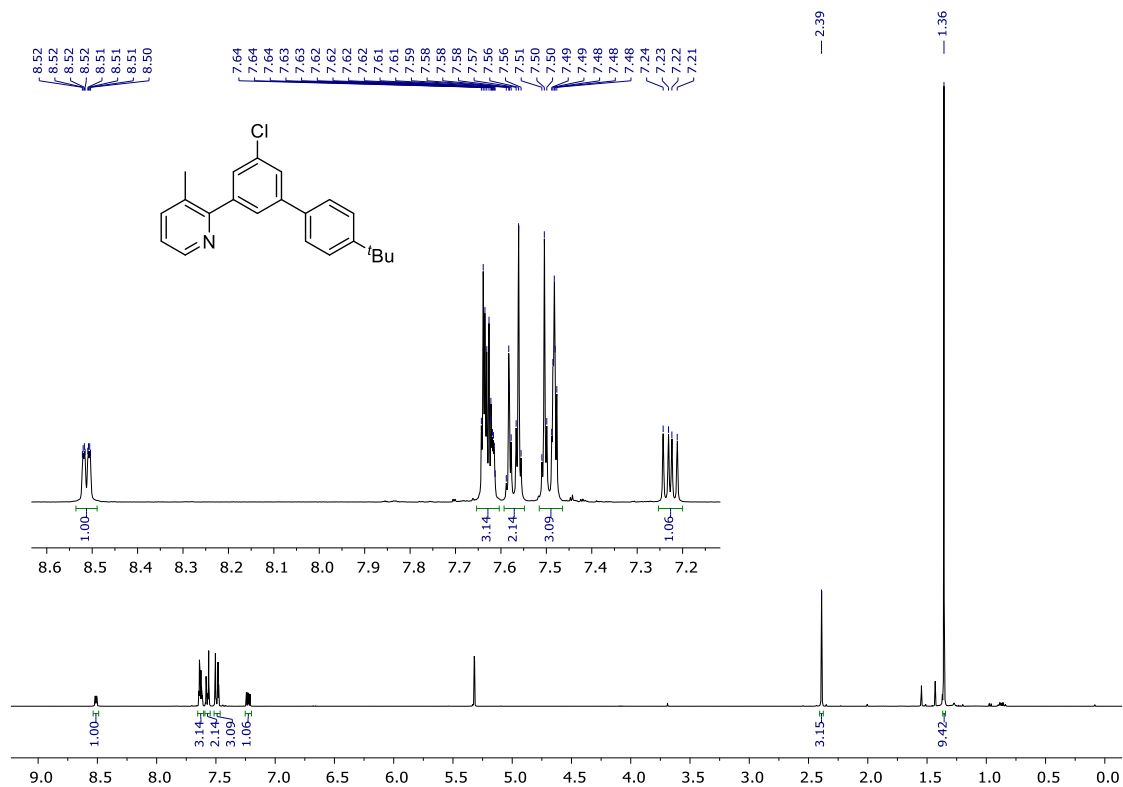


Figure 8. ¹H NMR (400MHz, 298K) of 2-(4'-(*tert*-butyl)-5-chloro-[1,1'-biphenyl]-3-yl)-3-methylpyridine in CD₂Cl₂.

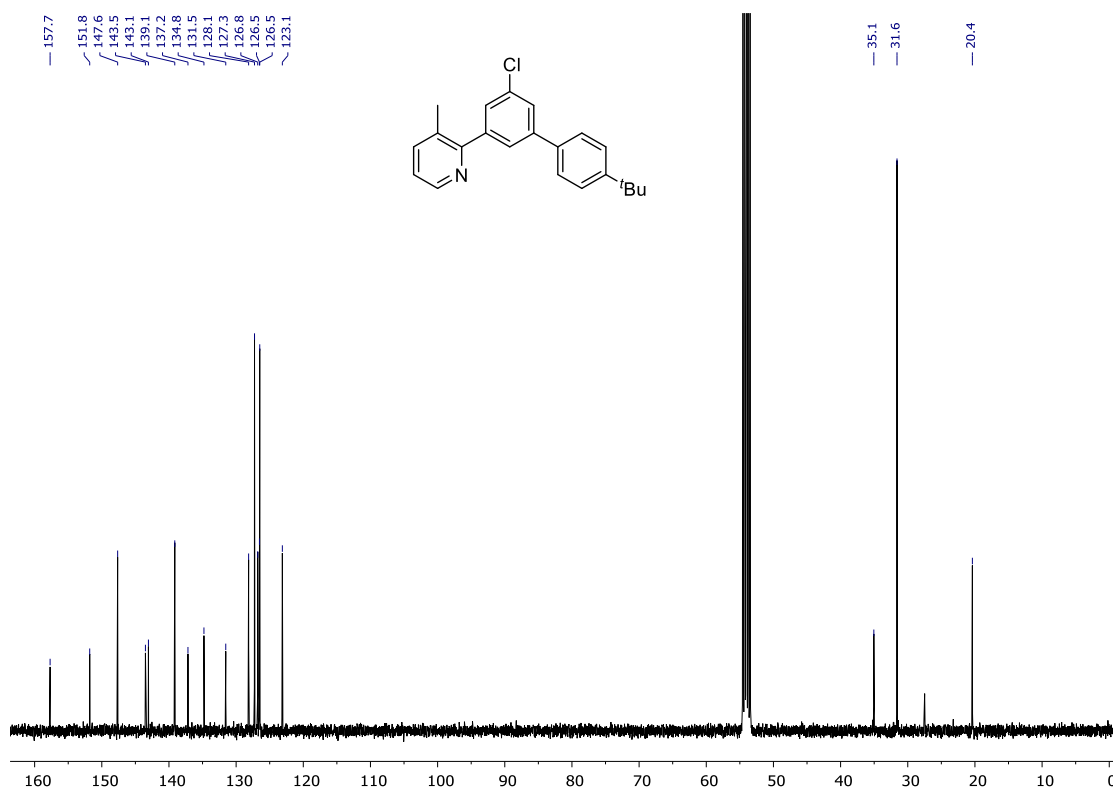


Figure 9. $^{13}\text{C}\{^1\text{H}\}$ NMR (101MHz, 298K) of 2-(4-(*tert*-butyl)-5-chloro-[1,1'-biphenyl]-3-yl)-3-methylpyridine in CD_2Cl_2 .

21_neQEx_1568 #65-71 RT: 0.63-0.68 AV: 4 SB: 25 0.03-0.24 , 0.70-0.94 NL: 2.44E8
T: FTMS + p ESI Full ms [100.0000-1500.0000]

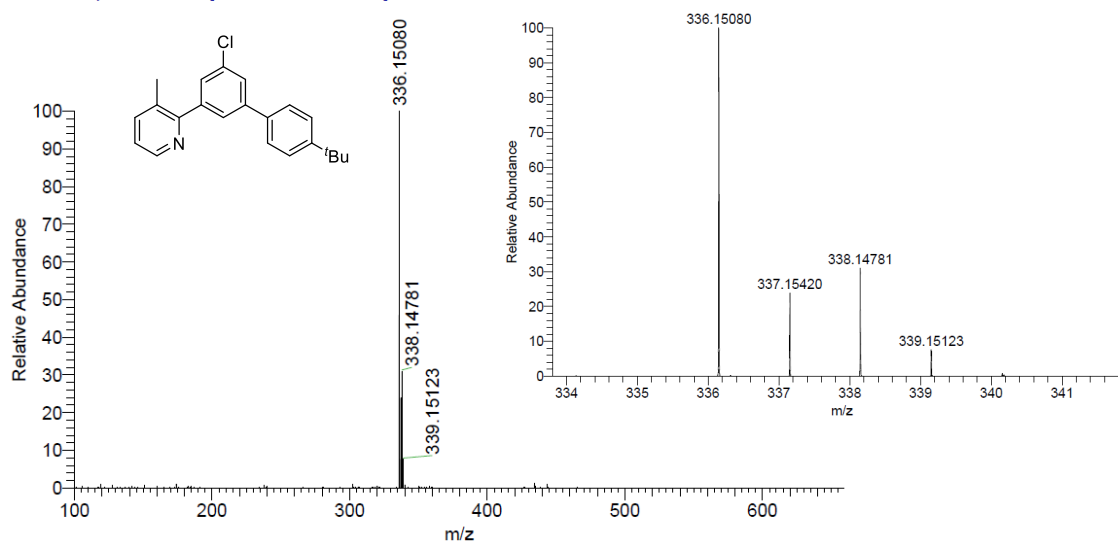


Figure 10. HRMS-ESI(+) of 2-(4-(*tert*-butyl)-5-chloro-[1,1'-biphenyl]-3-yl)-3-methylpyridine.

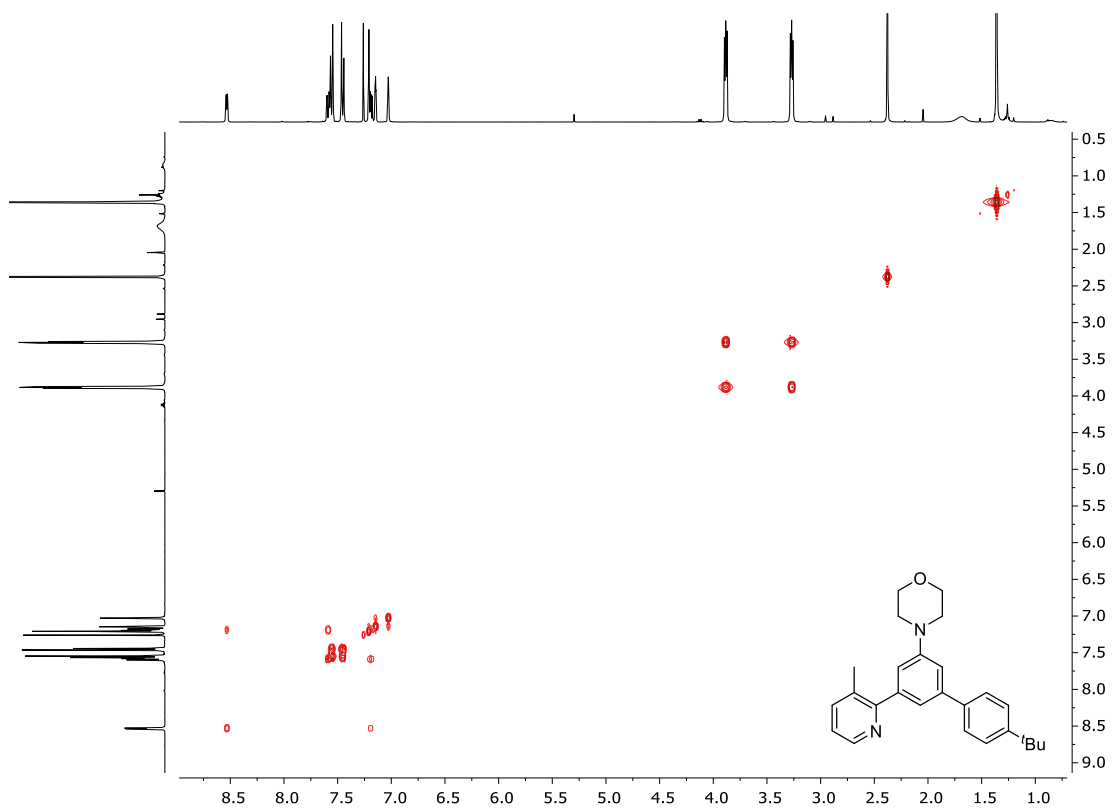


Figure 13. $^1\text{H}, ^1\text{H}$ -COSY NMR (400MHz, 298K) of compound 2^{H} in CDCl_3 .

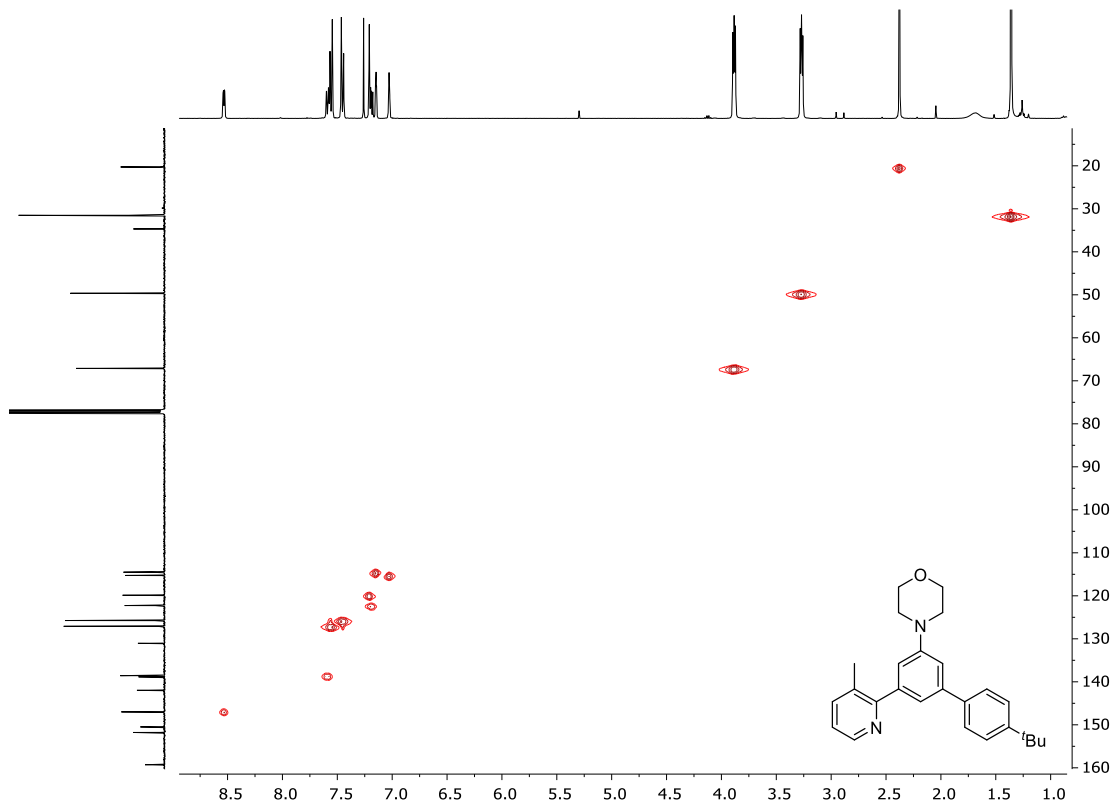


Figure 14. $^1\text{H}, ^{13}\text{C}$ -HSQC NMR (400MHz, 298K) of compound 2^{H} in CDCl_3 .

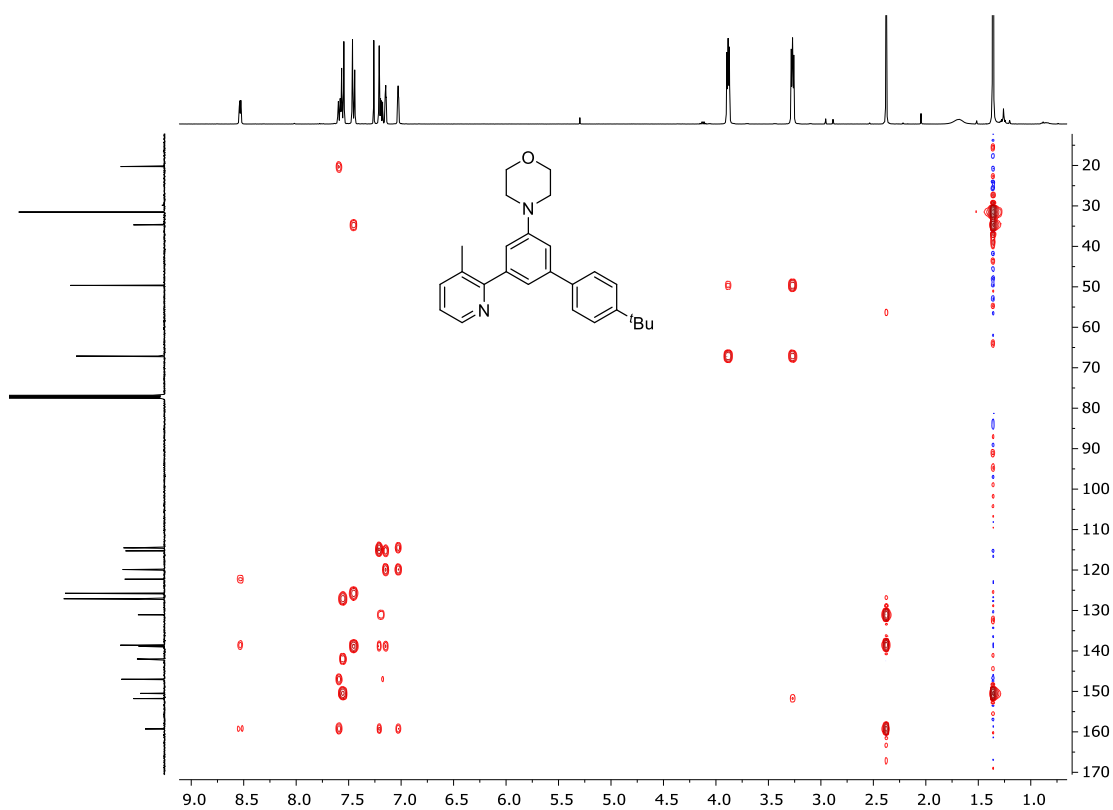


Figure 15. $^1\text{H},^{13}\text{C}$ -HMBC NMR (400MHz, 298K) of compound 2^{H} in CDCl_3 .

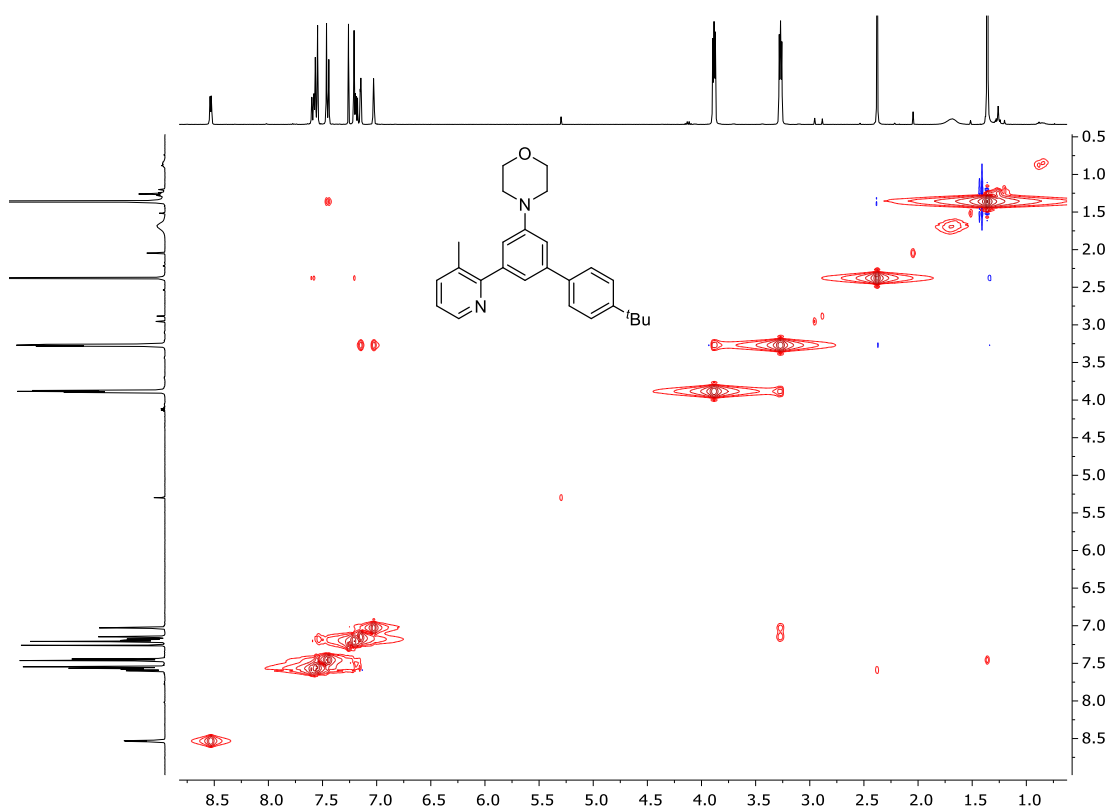


Figure 16. $^1\text{H},^1\text{H}$ -NOESY NMR (400MHz, 298K) of compound 2^{H} in CDCl_3 .

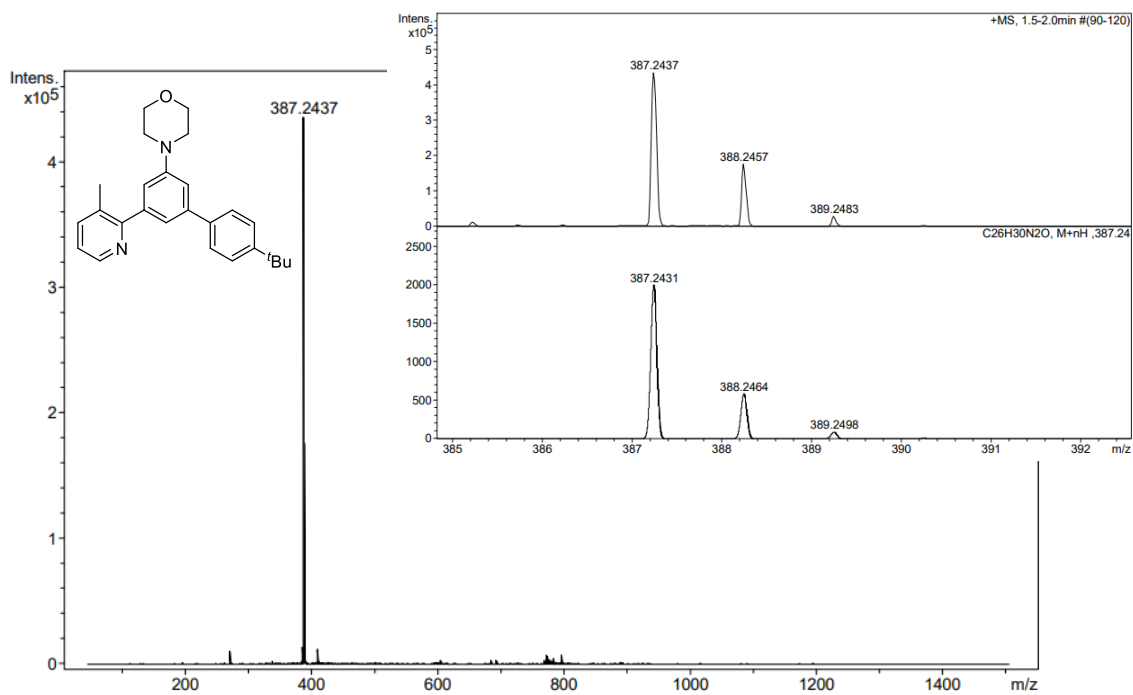


Figure 17. HRMS-ESI(+) of compound **2^H**.

3.6. Compound **2^{Br}**

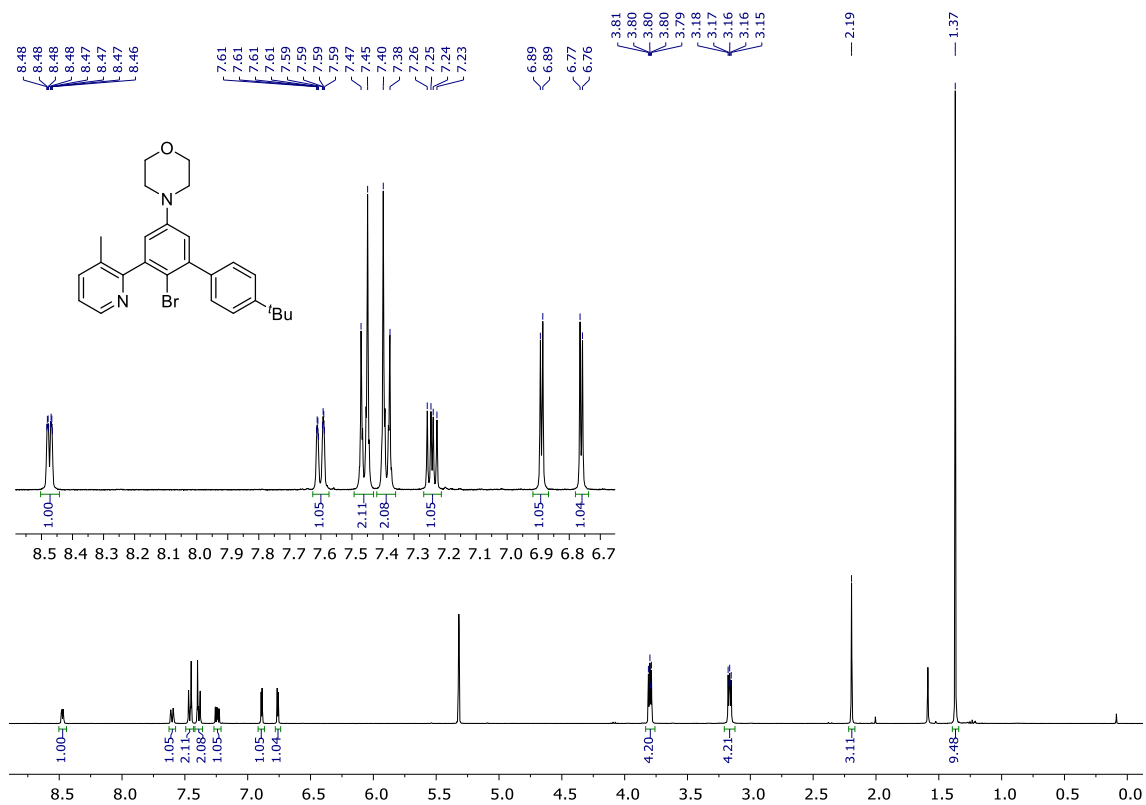


Figure 18. ¹H NMR (400MHz, 298K) of compound **2^{Br}** in CD₂Cl₂.

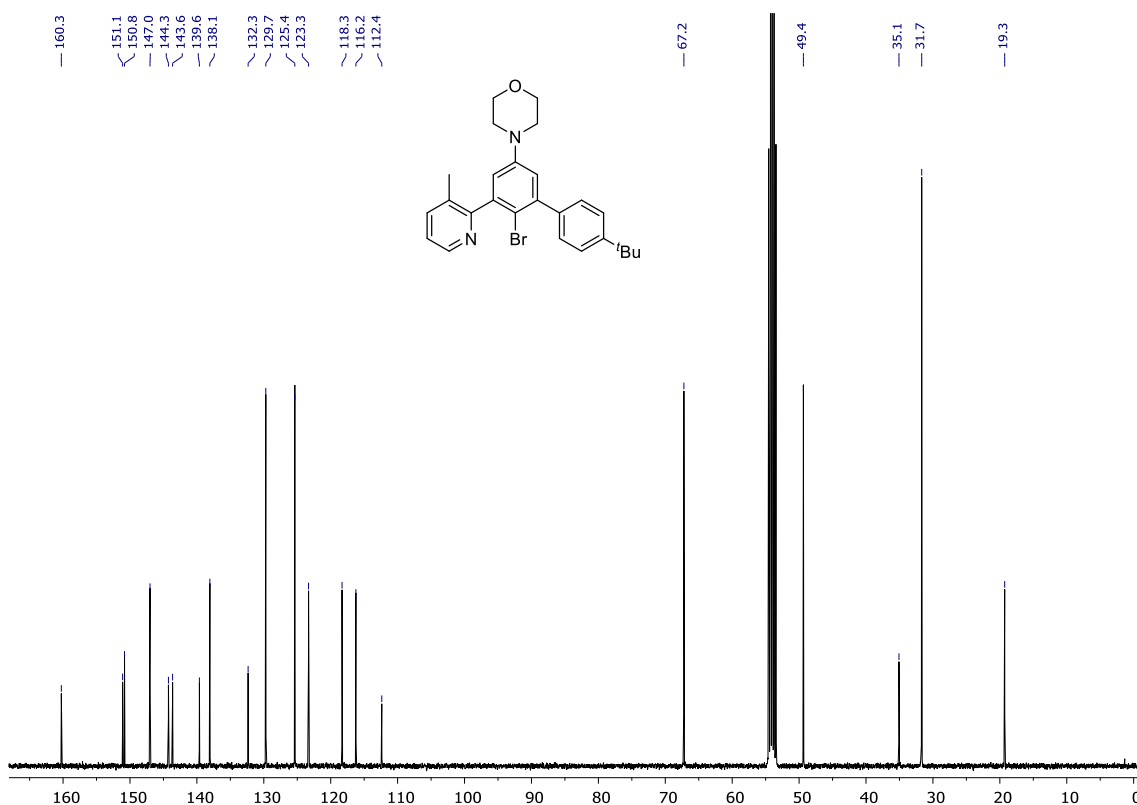


Figure 19. ¹³C{¹H} NMR (101MHz, 298K) of compound **2^{Br}** in CD₂Cl₂.

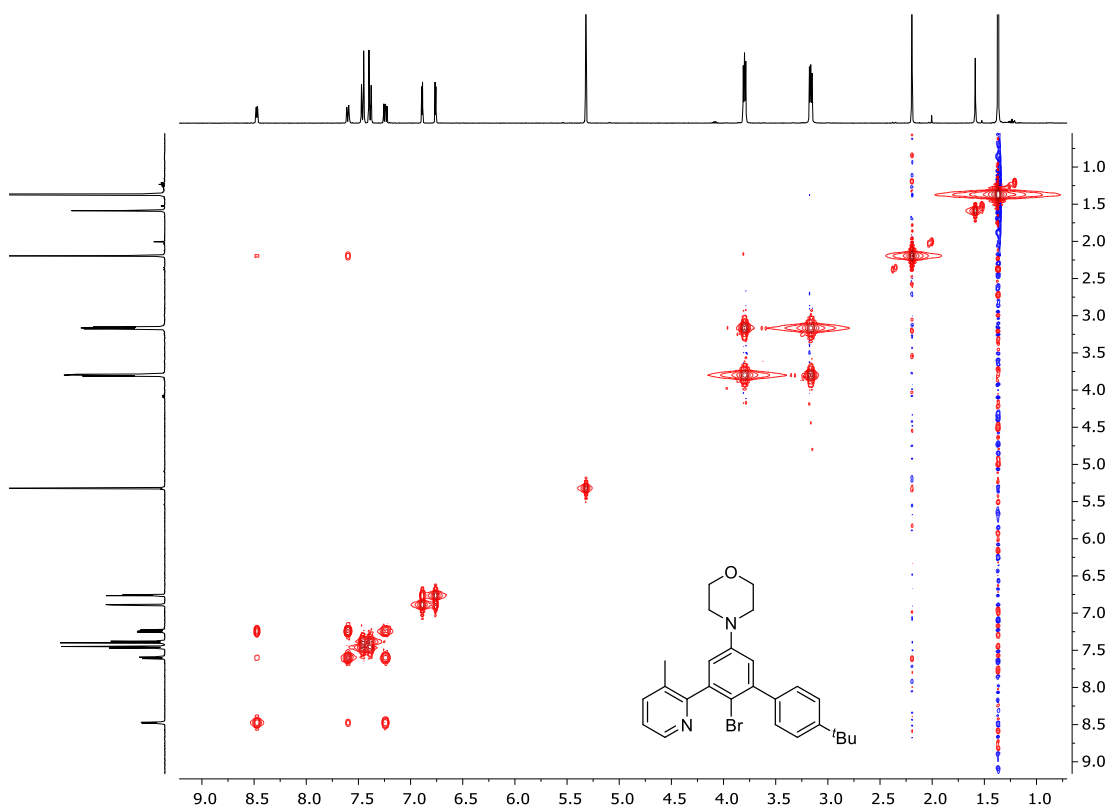


Figure 20. ¹H,¹H-COSY NMR (400MHz, 298K) of compound **2^{Br}** in CD₂Cl₂.

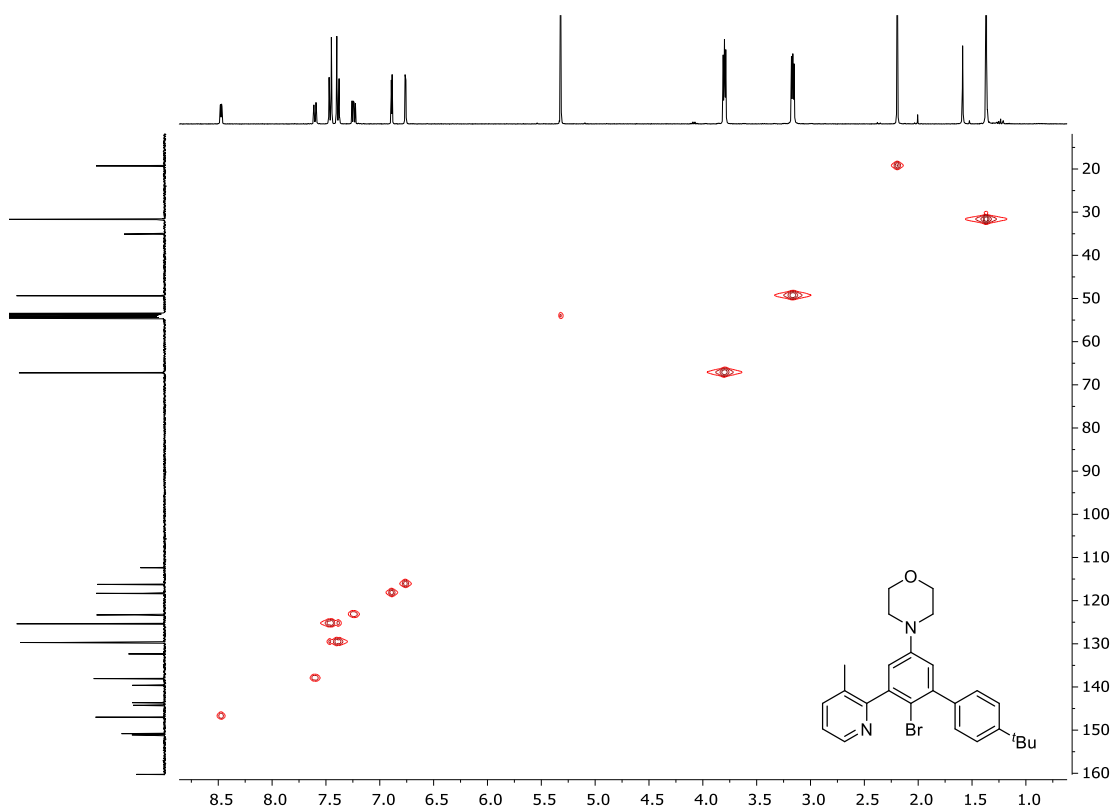


Figure 21. ^1H , ^{13}C -HSQC NMR (400MHz, 298K) of compound **2^{Br}** in CD_2Cl_2 .

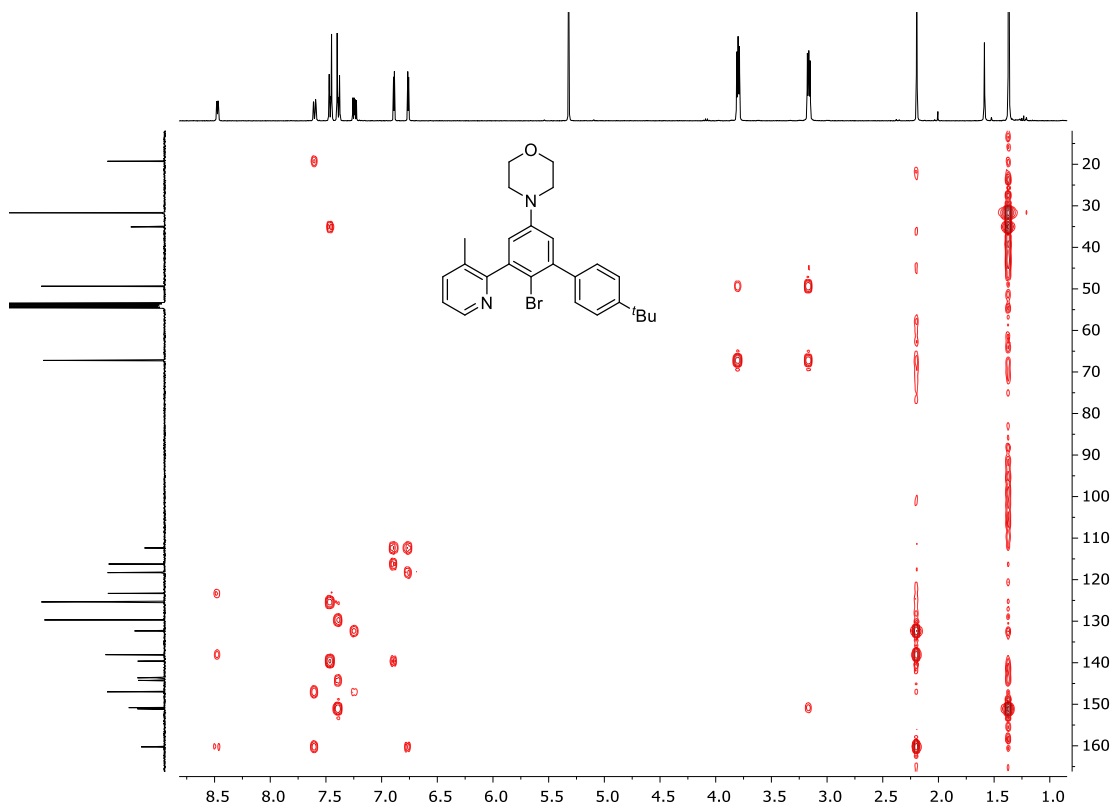


Figure 22. ^1H , ^{13}C -HMBC NMR (400MHz, 298K) of compound **2^{Br}** in CD_2Cl_2 .

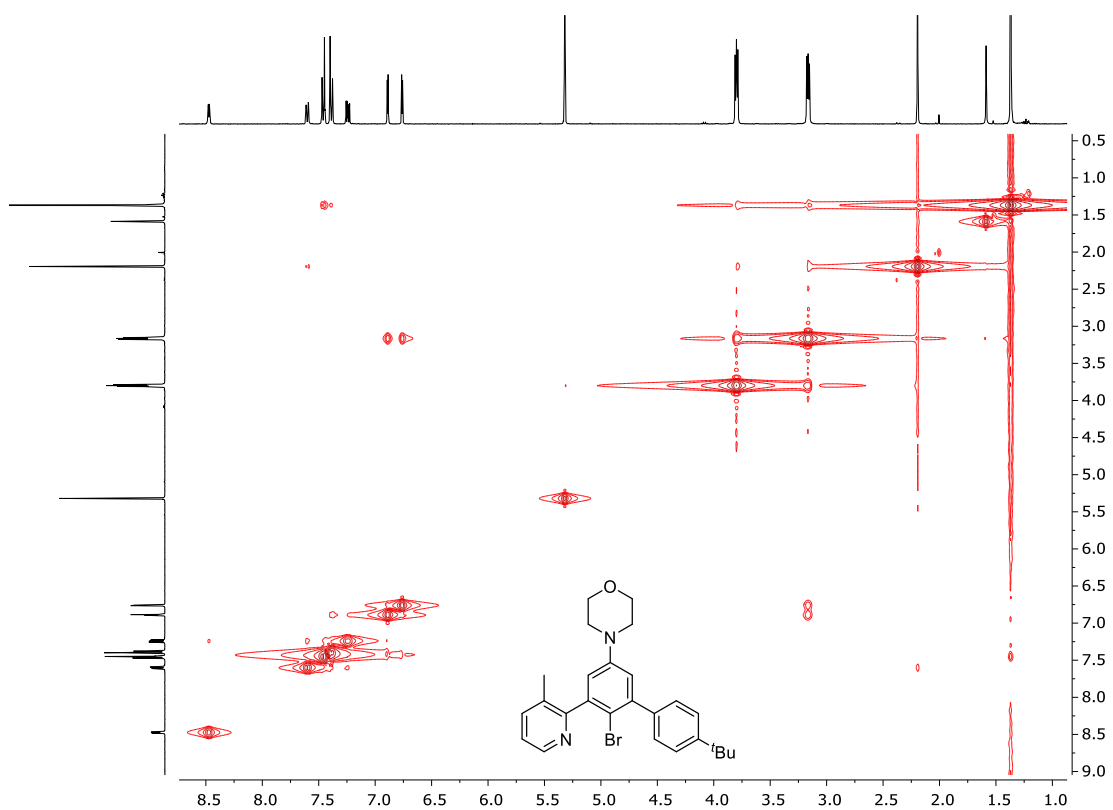


Figure 23. $^1\text{H}, ^1\text{H}$ -NOESY NMR (400MHz, 298K) of compound 2^{Br} in CD_2Cl_2 .

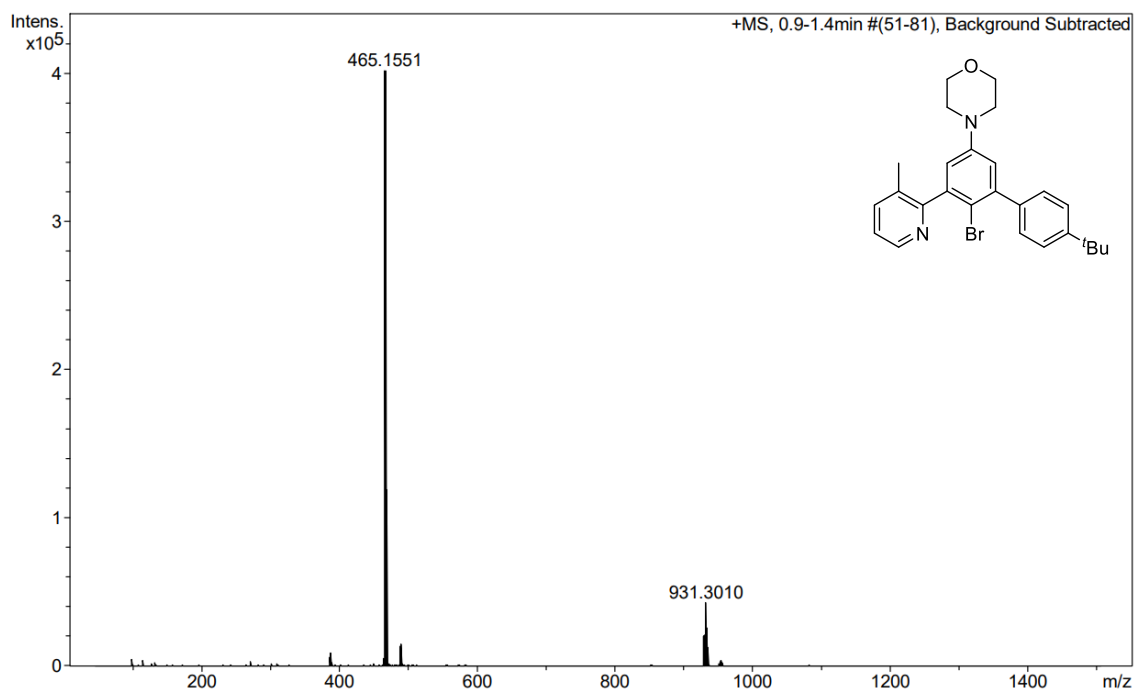


Figure 24. HRMS-ESI(+) of compound 2^{Br} .

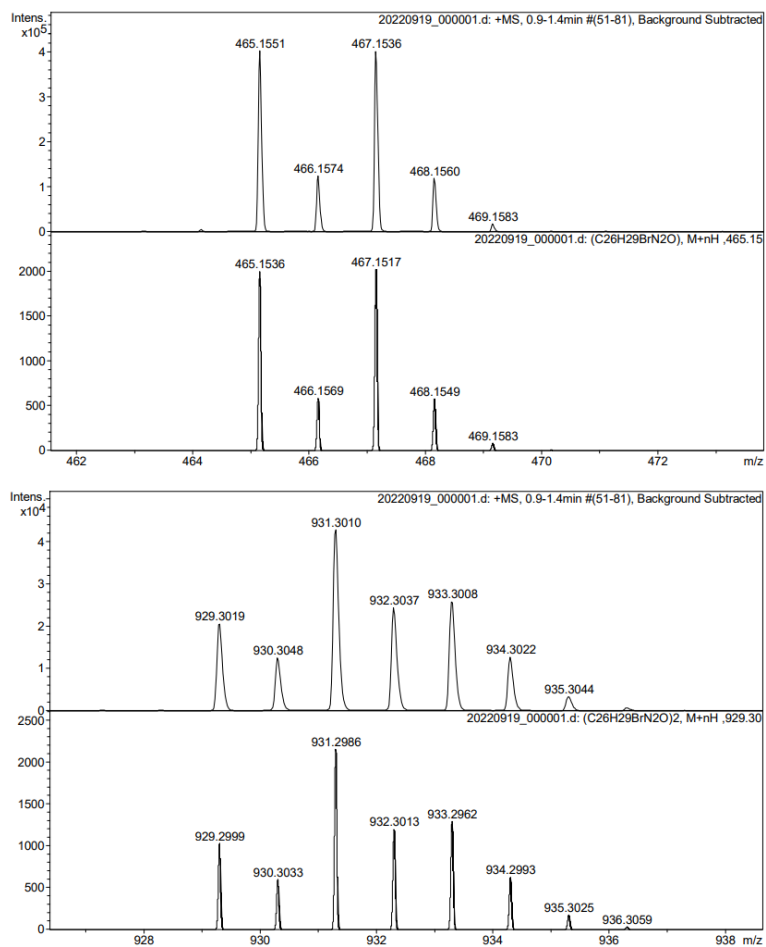


Figure 25. Experimental and simulated peaks for $[M+H]^+$ (top) and $[2M+H]^+$ (bottom) species of compound 2^{Br} , by HRMS-ESI(+).

3.7. Compound 2^{Bpin}

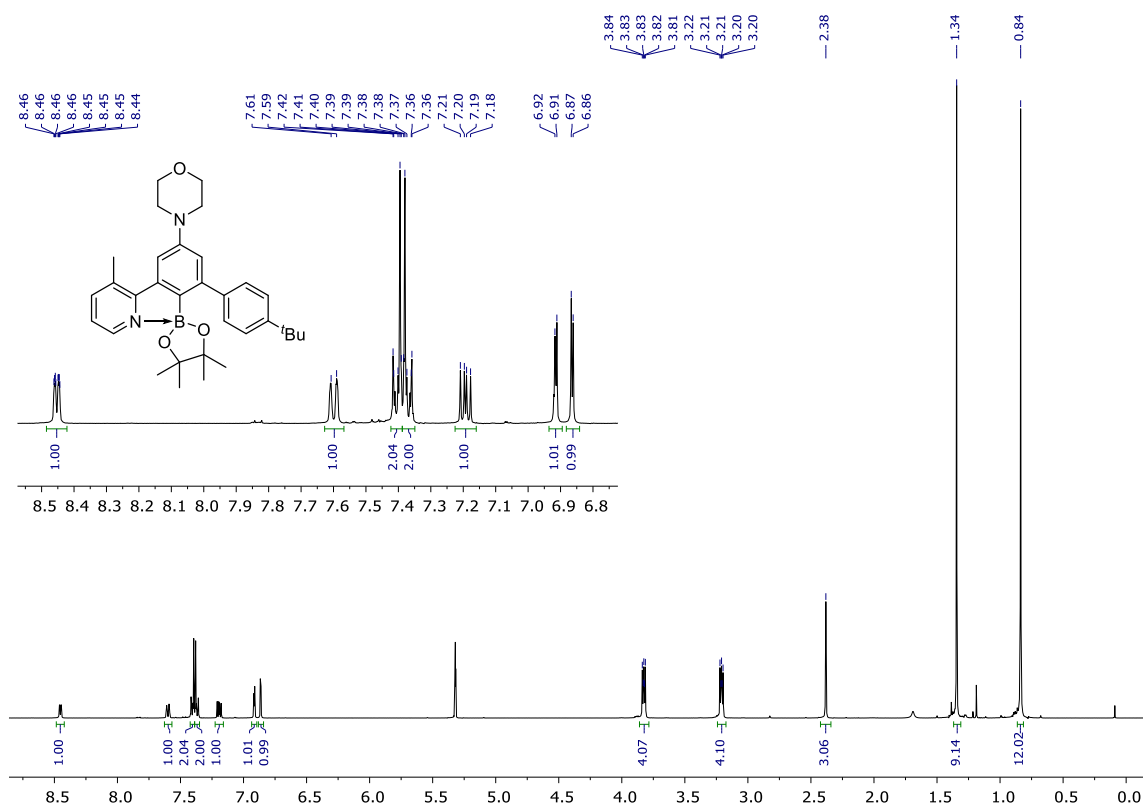


Figure 26. ¹H NMR (400MHz, 298K) of compound 2^{Bpin} in CD₂Cl₂.

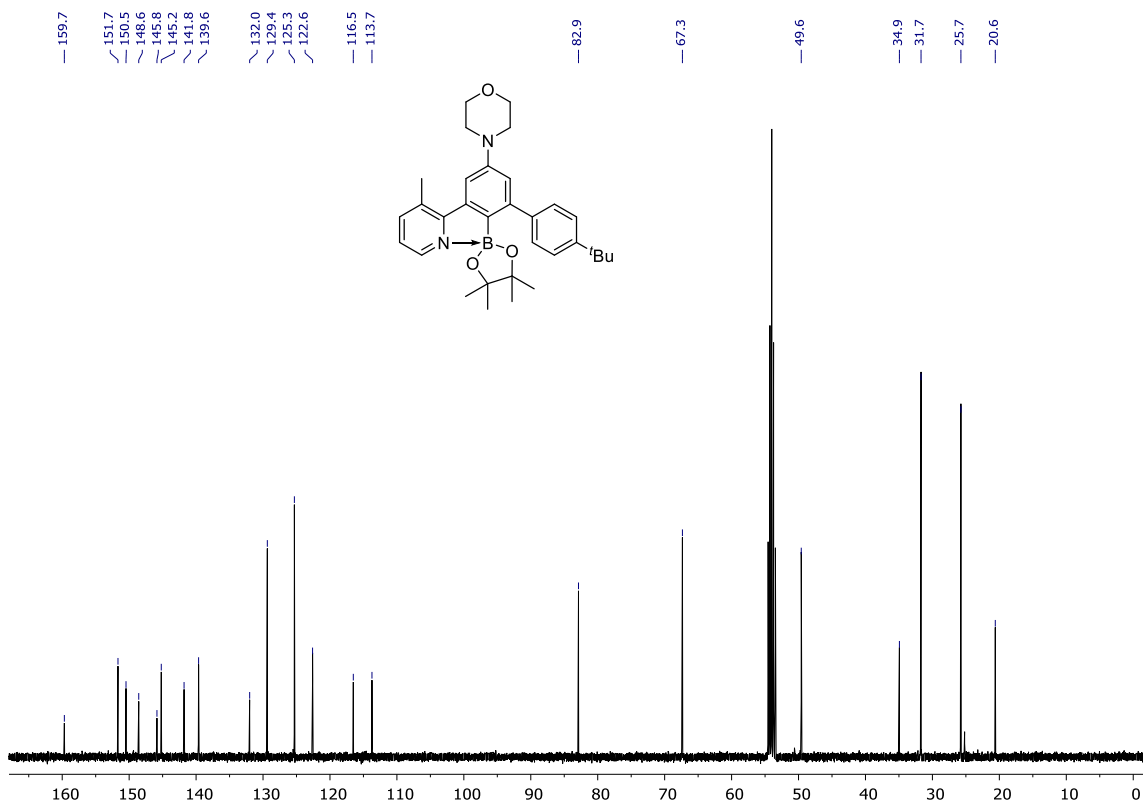


Figure 27. ¹³C{¹H} NMR (101MHz, 298K) of compound 2^{Bpin} in CD₂Cl₂.

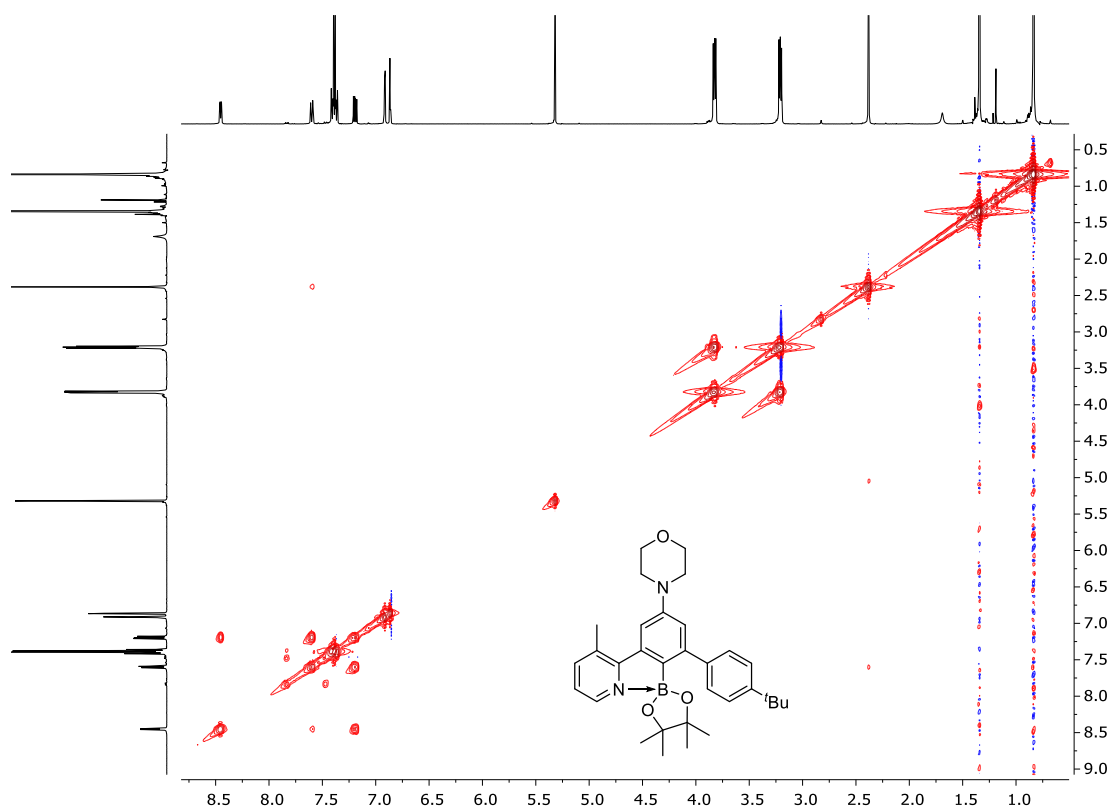


Figure 28. ^1H , ^1H -COSY NMR (400MHz, 298K) of compound **2^{Bpin}** in CD_2Cl_2 .

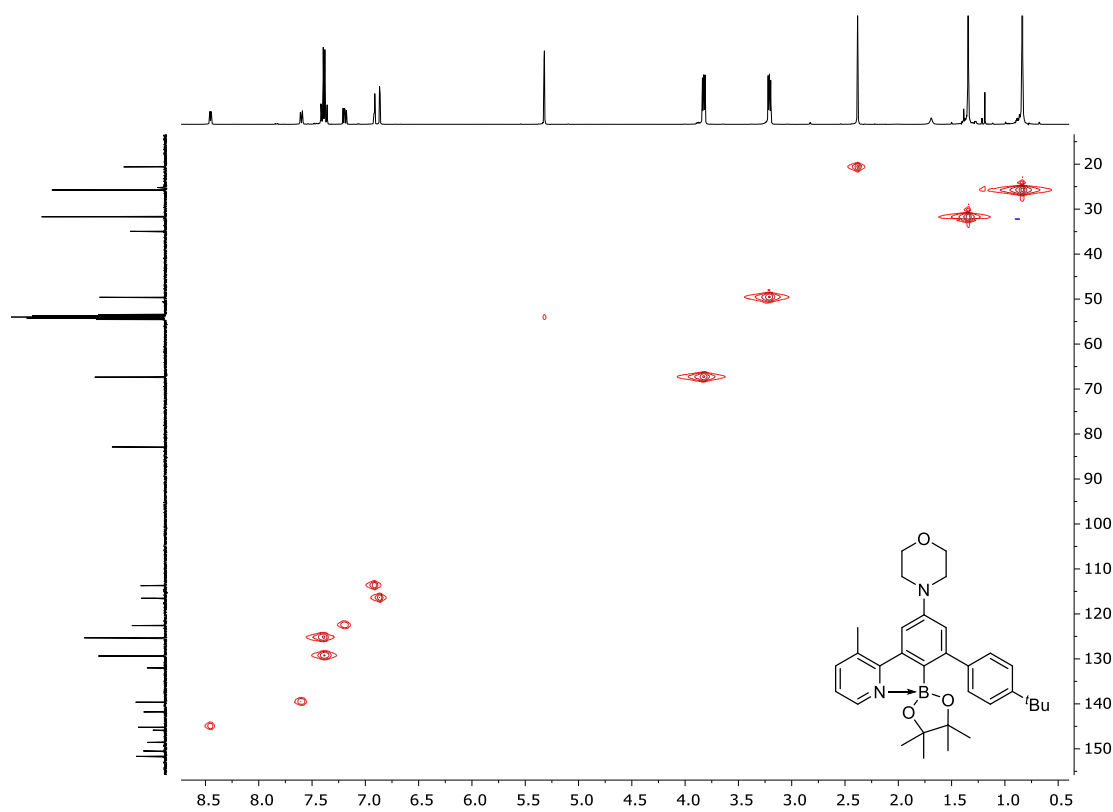


Figure 29. ^1H , ^{13}C -HSQC NMR (400MHz, 298K) of compound **2^{Bpin}** in CD_2Cl_2 .

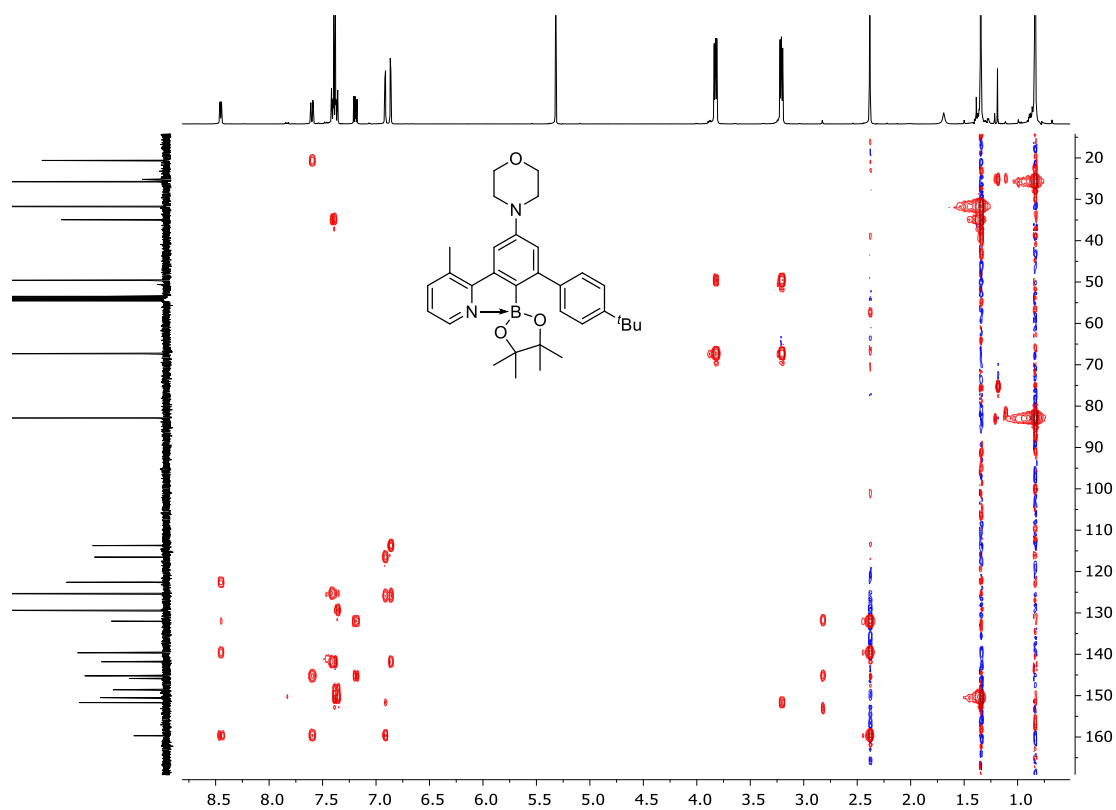


Figure 30. $^1\text{H}, ^{13}\text{C}$ -HMBC NMR (400MHz, 298K) of compound 2^{Bpin} in CD_2Cl_2 .

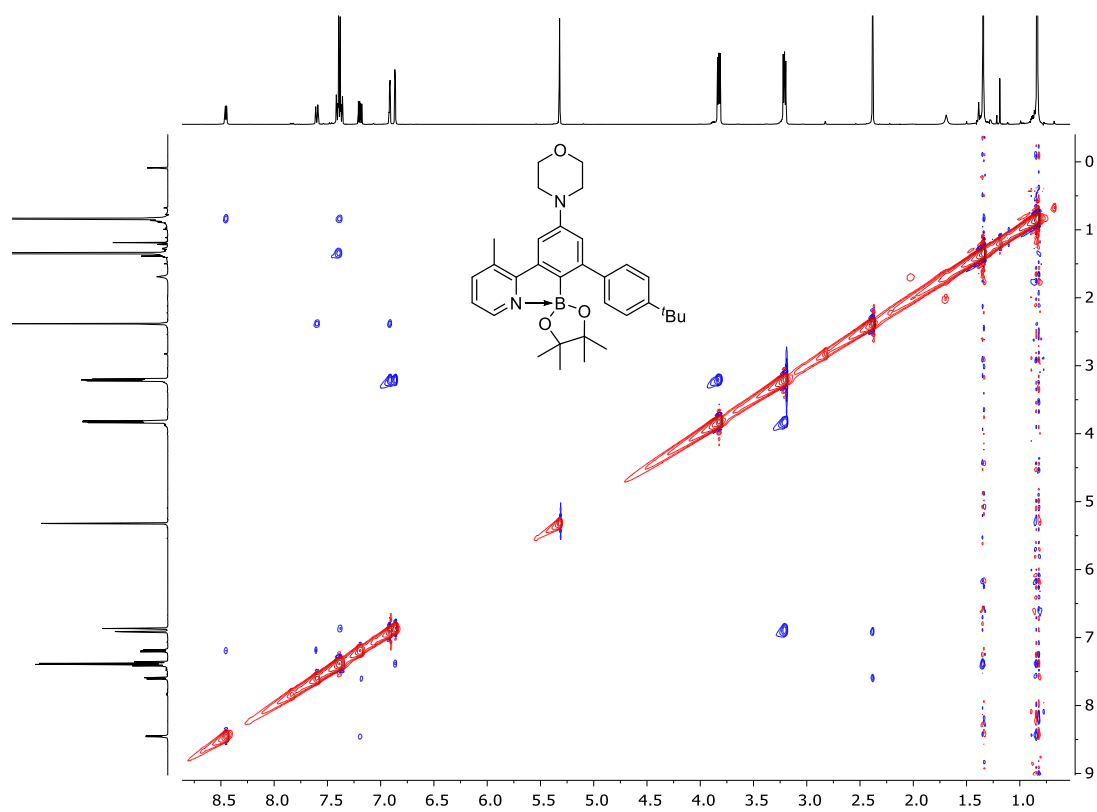


Figure 31. $^1\text{H}, ^1\text{H}$ -NOESY NMR (400MHz, 298K) of compound 2^{Bpin} in CD_2Cl_2 .

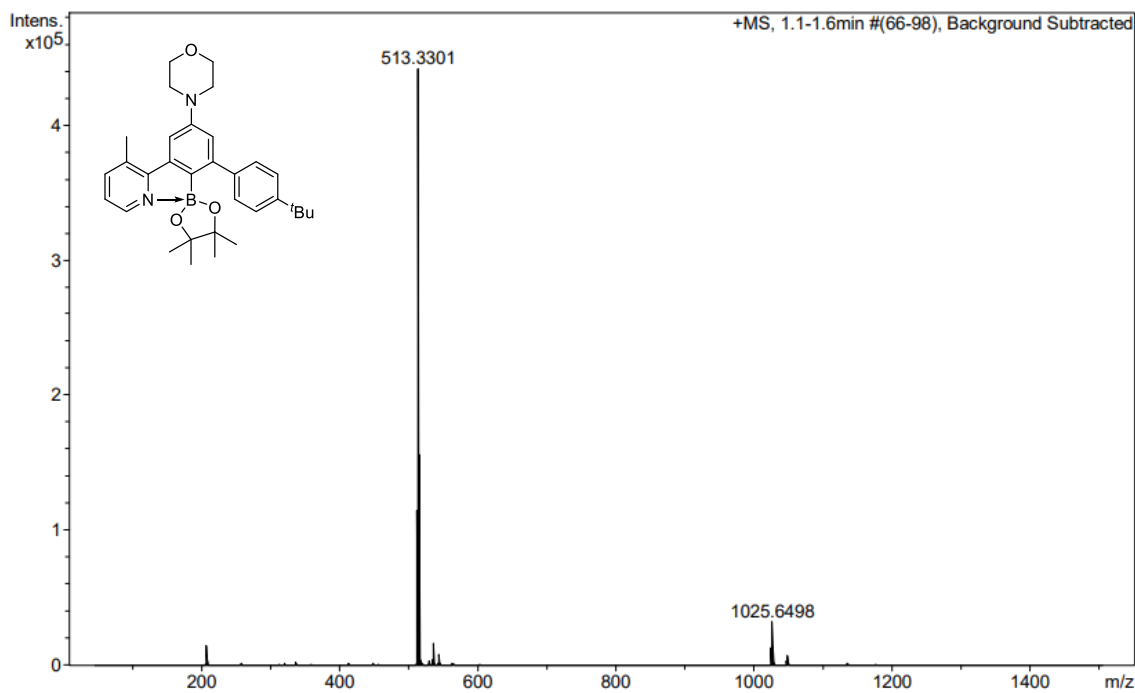


Figure 32. HRMS-ESI(+) of compound **2^{Bpin}**.

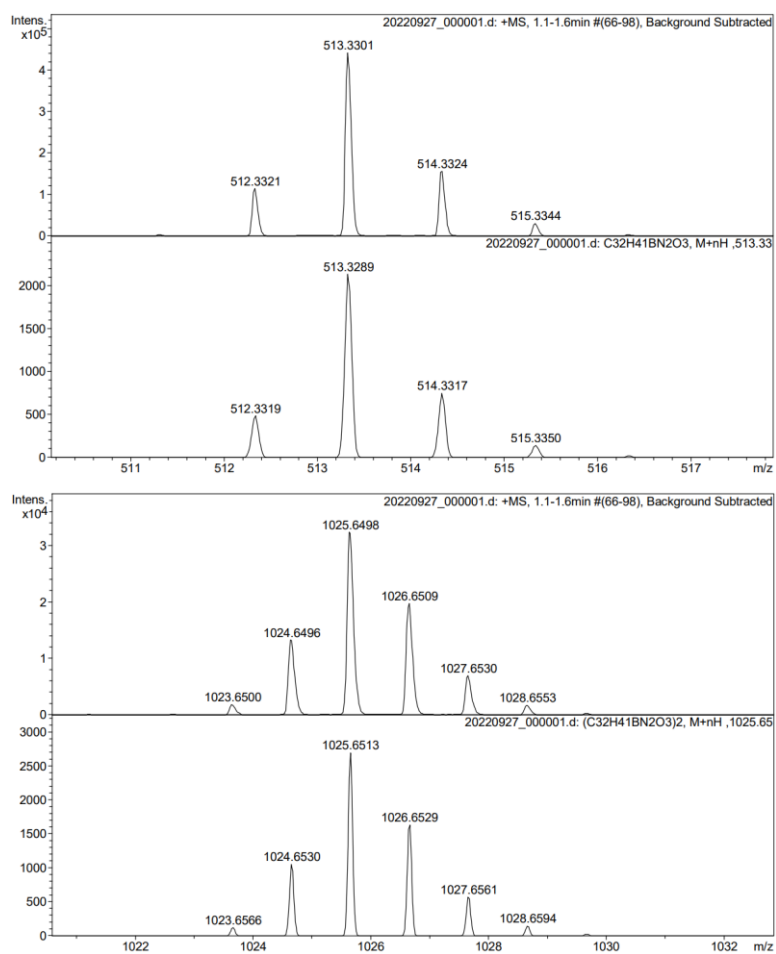


Figure 33. Experimental and simulated peaks for $[M+H]^+$ (top) and $[2M+H]^+$ (bottom) species of compound **2^{Bpin}**, by HRMS-ESI(+).

3.8. Complex 2AuCl

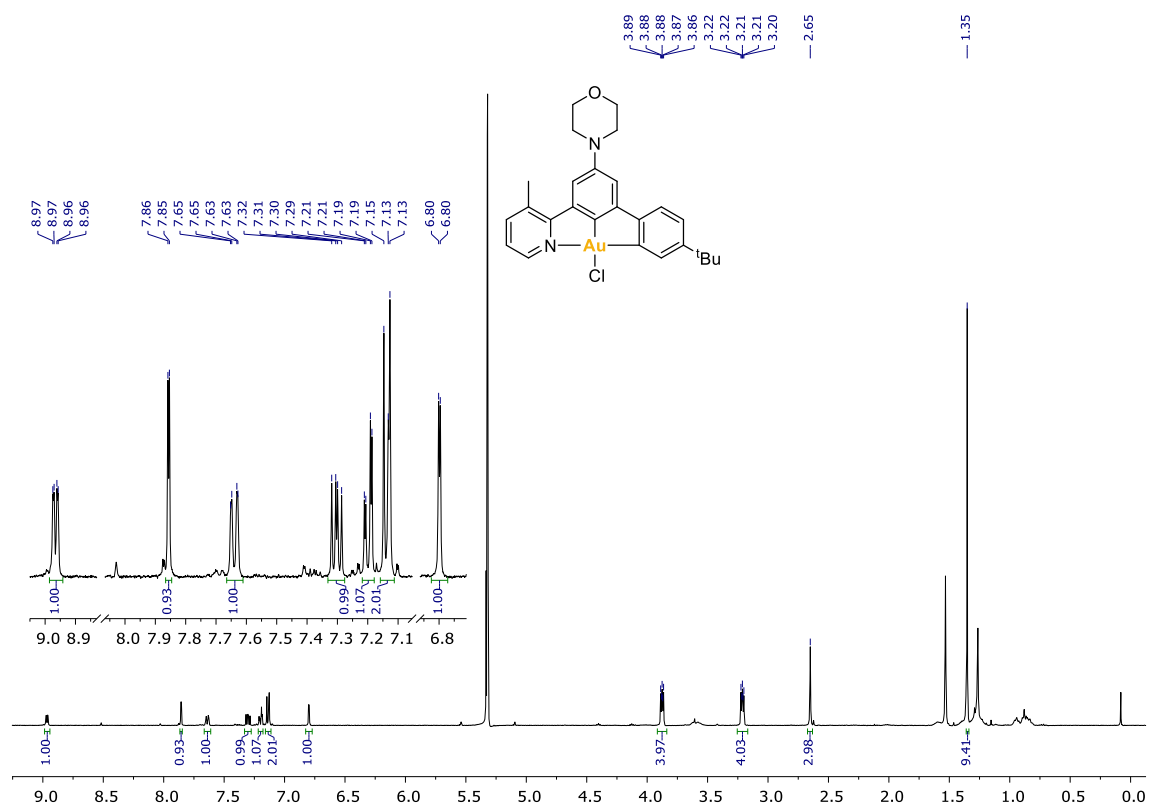


Figure 34. ¹H NMR (400MHz, 298K) of complex 2AuCl in CD₂Cl₂.

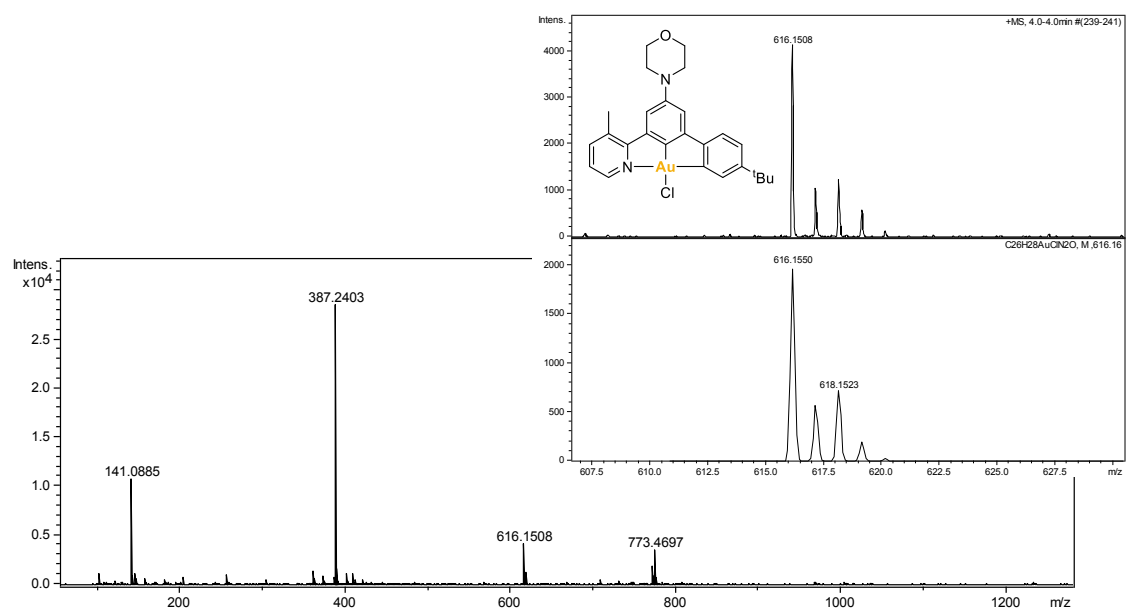


Figure 35. HRMS-ESI(+) of complex 2AuCl.

4. XRD analysis

4.1. Compound 1^{Bpin}

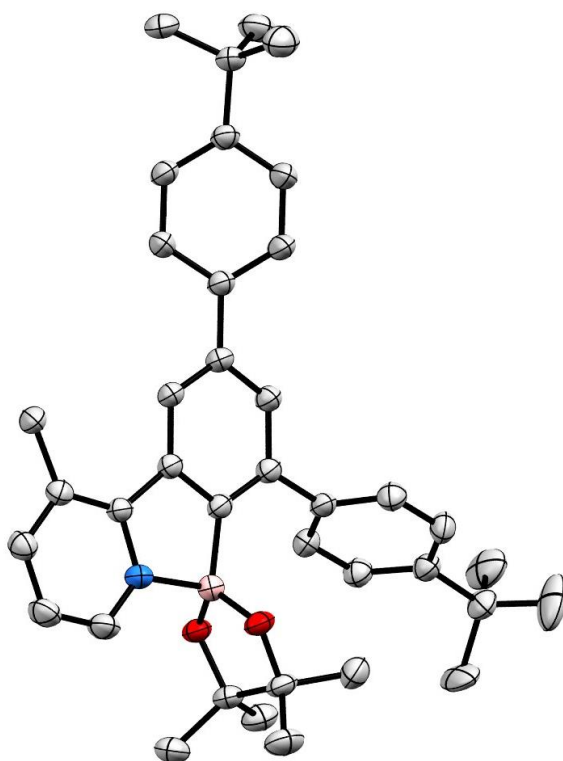


Figure 36. Crystal structure of compound 1^{Bpin}. Ellipsoids set at 50% probability; H atoms omitted for clarity.

Table 3. Crystallographic parameters for compound 1^{Bpin}.

Chemical formula	C ₃₈ H ₄₆ BNO ₂	
Formula weight	559.57 g/mol	
Temperature	160(1) K	
Wavelength	1.54184 Å	
Crystal size	0.05 x 0.06 x 0.14 mm	
Crystal system	Triclinic	
Space group	P -1	
Unit cell dimensions	a = 10.6280(5) Å	α = 105.901(3)°
	b = 11.5783(4) Å	β = 106.382(4)°
	c = 14.6803(6) Å	γ = 100.828(3)°
Volume	1596.52(12) Å ³	
Density (calculated)	1.164 g/cm ³	
Absorption coefficient	0.535 mm ⁻¹	
Final R indices	R(F)[I > 2σ(I)]	0.0602
	wR(F ²) (all data)	0.1692

A colorless, needle-like specimen of $C_{38}H_{46}BNO_2$ was mounted on a cryo-loop and used for a low-temperature X-ray structure determination. All measurements were made on a *Rigaku Oxford Diffraction SuperNova* area-detector diffractometer using Cu $K\alpha$ radiation ($\lambda = 1.54184$ Å) from a micro-focus X-ray source and an *Oxford Instruments Cryojet XL* cooler. The unit cell constants and an orientation matrix for data collection were obtained from a least-squares refinement of the setting angles of 7685 reflections in the range $6^\circ < 2\theta < 142^\circ$. A total of 3104 frames were collected using ω scans with κ offsets, 7.5-15.0 seconds exposure time and a rotation angle of 1.0° per frame, and a crystal-detector distance of 65.0 mm.

4.2. Compound 2^{Bpin}

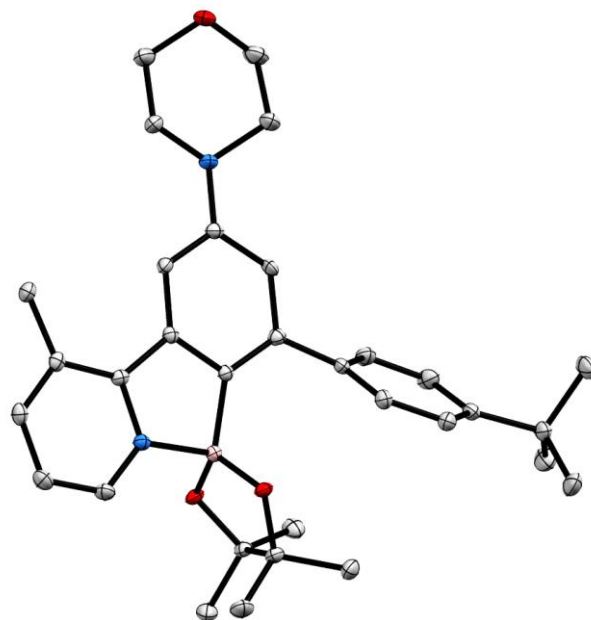


Figure 37. Crystal structure of compound 2^{Bpin} . Ellipsoids set at 50% probability; H atoms omitted for clarity.

Table 4. Crystallographic parameters for compound **2^{Bpin}**.

Chemical formula	C ₃₂ H ₄₁ BN ₂ O ₃
Formula weight	512.48 g/mol
Temperature	100(2) K
Wavelength	0.71073 Å
Crystal size	0.030 x 0.100 x 0.400 mm
Crystal system	Triclinic
Space group	P -1
Unit cell dimensions	a = 7.1734(10) Å α = 64.478(4)° b = 13.9355(17) Å β = 84.203(4)° c = 15.568(2) Å γ = 84.741(5)°
Volume	1395.2(3) Å ³
Density (calculated)	1.220 g/cm ³
Absorption coefficient	0.077 mm ⁻¹
Final R indices	5763 data; I>2σ(I) R1 = 0.0647, wR2 = 0.1479 All data R1 = 0.0753, wR2 = 0.1537

A colorless, needle-like specimen of C₃₂H₄₁BN₂O₃, approximate dimensions 0.030 mm x 0.100 mm x 0.400 mm, was used for the X-ray crystallographic analysis. The X-ray intensity data were measured on a D8 QUEST ECO three-circle diffractometer system equipped with a Ceramic x-ray tube (Mo Kα, λ = 0.71073 Å) and a doubly curved silicon crystal Bruker Triumph monochromator.

A total of 1952 frames were collected. The total exposure time was 9.89 hours. The frames were integrated with the Bruker SAINT software package using a narrow-frame algorithm. The integration of the data using a triclinic unit cell yielded a total of 37442 reflections to a maximum θ angle of 28.37° (0.75 Å resolution), of which 6701 were independent (average redundancy 5.588, completeness = 95.8%, R_{int} = 3.97%, R_{sig} = 3.07%) and 5763 (86.00%) were greater than 2σ(F²). The final cell constants of *a* = 7.1734(10) Å, *b* = 13.9355(17) Å, *c* = 15.568(2) Å, α = 64.478(4)°, β = 84.203(4)°, γ = 84.741(5)°, volume = 1395.2(3) Å³, are based upon the refinement of the XYZ-centroids of 9930 reflections above 20 σ(I) with 5.316° < 2θ < 56.73°. Data were corrected for absorption effects using the Multi-Scan method (SADABS). The ratio of minimum to maximum apparent transmission was 0.874. The calculated minimum and maximum transmission coefficients (based on crystal size) are 0.9700 and 0.9980.

The structure was solved and refined using the Bruker SHELXTL Software Package, using the space group P -1, with Z = 2 for the formula unit, C₃₂H₄₁BN₂O₃. The final anisotropic

full-matrix least-squares refinement on F^2 with 507 variables converged at $R1 = 6.47\%$, for the observed data and $wR2 = 15.37\%$ for all data. The goodness-of-fit was 1.160. The largest peak in the final difference electron density synthesis was $0.381 \text{ e}^-/\text{\AA}^3$ and the largest hole was $-0.339 \text{ e}^-/\text{\AA}^3$ with an RMS deviation of $0.063 \text{ e}^-/\text{\AA}^3$. On the basis of the final model, the calculated density was 1.220 g/cm^3 and $F(000)$, 552 e^- .

5. References

1. R. Kumar, A. Linden and C. Nevado, *Angew. Chem. Int. Ed.*, 2015, **54**, 14287-14290.
2. Z.-J. Du, L.-X. Gao, Y.-J. Lin and F.-S. Han, *ChemCatChem*, 2014, **6**, 123-126.
3. A. Klapars and S. L. Buchwald, *J. Am. Chem. Soc.*, 2002, **124**, 14844-14845.
4. D. R. Manke, J. A. Golen, C. R. Stennett, M. Naeem, D. R. Javier-Jimenez and P. P. Power, *Polyhedron*, 2022, **222**, 115947.

